

# Keyword Index

1,2-BIS(CHLOROMERCURIO) TETRAFLUOR...	CRYSTAL STRUCTURE.....	LEWIS ACIDES.....	TP210
16S RRNA.....	METHYLTRANSFERASE.....		MP029
2,3-DIOXYGENASE.....	UBIQUITIN-LIKE PROTEIN.....	SALICYLIC ACID-BINDING PROTEIN.....	01.06.06
2-OXOGLUTARATE.....	PROLYL HYDROXYLASE.....	HYPOXIA INDUCIBLE FACTOR.....	SP026
2D ASSEMBLY.....	2D ORDER.....	GISAXS.....	13.03.04
2D CRYSTAL.....	X-RAY.....	BREWSTER-ANGLE MICROSCOPY.....	MP160
2D ORDER.....	GISAXS.....	2D ASSEMBLY.....	13.03.04
4-OT HOMOLOGUE.....	TAUTOMERASE.....	CORYNEBACTERIUM GLUTAMICUM.....	SP031
A6 T CELL RECEPTOR.....	HAPTENATED TAX PEPTIDES.....	CROSS-REACTIVITY.....	TP107
AB INITIO.....	STRUCTURE PREDICTION.....	PHASING.....	01.07.06
AB INITIO.....	POWDER.....	TRIMELLITATE.....	07.01.04
AB INITIO CALCULATIONS.....	HIGH PRESSURE.....	PHASE TRANSITION.....	AW.01.04
ABC-TYPE TRANSPORTER SYSTEM.....	ZINC.....	SOLUTE-BINDING PROTEIN.....	SP012
ABSOLUTE STRUCTURE.....	ANOMALOUS DIFFRACTION.....	RESONANT SCATTERING.....	10.02.07
ABSORPTION.....	GISAXS.....	VIRUS.....	09.03.05
ACETYL-COA CARBOXYLASE.....	DIMERIZATION.....	BIOTIN CABOXYLASE.....	SP121
ACOSTATIN.....	RGD LOOP.....	DISINTEGRIN.....	01.08.04
ACT DOMAIN.....	PREPHENATE DEHYDRATASE.....	PROTEIN CRYSTALLIZATION DEVICE.....	SP041
ACTA CRYSTALLOGRAPHICA.....	QUALITY CRITERIA.....	CRYSTALLOGRAPHIC PUBLISHING.....	WK.02.04
ACTINIDES.....	SYNCHROTRON.....	SMALL-MOLECULE.....	MP227
ACTIVATING ENZYME.....	S-ADENOSYLMETHIONINE RADIA.....	PYRUVATE-FORMATE LYASE.....	SP017
ACTIVE PHARMCEUTICAL INGREDIENTS.....	CRYSTAL ENGINEERING.....	CO-CRYSTALS.....	SP206
ACYL-COA DEHYDROGENASE.....	FATTY ACID OXIDATION.....	MEMBRANE PROTEIN.....	01.04.05
ACYLASE.....	AUTOPROTEOLYSIS.....	THREE CHEMISTRY.....	TP176
ADENO-ASSOCIATED VIRUS.....	GENE THERAPY.....	PARVOVIRIDAE.....	SP039
ADENOSINE KINASE.....	NUCLEOSIDE ANALOGS.....	DRUG TARGET.....	MP033
ADENYLATE-FORMING ENZYMES.....	DOMAIN ALTERNATION.....		AW.03.08
AEROGEL.....	USAXS.....	USANS.....	TP190
AFM.....	DISSOLUTION.....	SIMULATION.....	AW.01.05
AGOSTIC EFFECT.....	CHARGE DENSITY.....	DISORDER.....	AW.03.04
ALDOSE REDUCTASE.....	PHENIX.....	JOINT X-RAY AND NEUTRON REFINE.....	06.01.02
ALDOSE REDUCTASE.....	PROTEIN-LIGAND COMPLEX.....	DRUG DESIGN.....	TP110
ALIX.....	GAG.....	HIV.....	SP042
ALLOSTERIC.....	ANTICOOPERATIVE.....	MUTAGENESIS.....	SP.01.05
ALLOSTERIC REGULATION.....	SAXS.....	LACI REPRESSOR.....	MP250
ALLOSTERY.....	HEMOGLOBIN.....		01.08.01
ALLOY.....	PHASE TRANSFORMATION.....		05.01.01
$\alpha$ -AMYLASE INHIBITORS.....	INHIBITOR SCREENING.....	NATURAL PRODUCT EXTRACTS.....	TP102
$\alpha$ -GLYCEROPHOSPHATE.....	FLAVOPROTEIN.....	$\alpha$ -GLYCEROPHOSPHATE OXIDASE.....	SP020
$\alpha$ -GLYCEROPHOSPHATE OXIDASE.....	A-GLYCEROPHOSPHATE.....	FLAVOPROTEIN.....	SP020
A/BETA KNOT.....	UNKNOWN FUNCTION.....	PF04013.....	MP247
ALTERNATIVE SPLICING.....	STRUCTURAL GENOMICS.....	HYPOTHETICAL PROTEINS.....	01.06.05
AMINOPEPTIDASE.....			SP023
AMYLASE.....	CARBOHYDRATES.....	ENZYME.....	SP.01.04
AMYLOID.....	PEPTIDE STRUCTURES.....	MICROFOCUS BEAMLIN.....	13.01.03
AMYLOID.....	PRION.....	MICROCRYSTALS.....	13.08.01
AMYLOID.....	MICROCRYSTAL.....	FIBER.....	10.04.02
AMYLOID.....	ANTIBODY.....	SPR.....	MP007
AMYLOID CONGENERS.....	SELF ASSEMBLY.....	SUPRAMOLECULAR STRUCTURE.....	MP162
ANAEROBIC CRYSTALLIZATION.....	UROPORPHYRINOGEN DECARBOX.....	HEME.....	01.02.03
ANION TRANSPORT.....	MEMBRANE PROTEIN.....		01.04.03
ANOMALOUS DIFFRACTION.....	RESONANT SCATTERING.....	ABSOLUTE STRUCTURE.....	10.02.07
ANOMALOUS GISAXS.....	NANOCATALYSIS.....	GISAXS.....	09.02.03
ANOMALOUS SCATTERING.....	SHELX.....	PHASING.....	WK.01.10
ANTI-DIABETIC INHIBITORS.....	IODIDE PHASING.....	FAMILY 31 GLYCOSIDE HYDROLASE.....	MP004
ANTI-HIV.....	PREGANE X RECEPTOR.....	PNU-142721.....	SP060
ANTIBIOTIC DEVELOPMENT.....	METABOLIC ENZYME.....	CATALYTIC MECHANISM.....	TP131
ANTIBIOTIC RESISTANT.....	LYASE.....	ENZYME MECHANISM.....	SP027
ANTIBODY.....	VACCINE.....	HIV-1.....	13.05.06
ANTIBODY.....	SPR.....	AMYLOID.....	MP007
ANTICOOPERATIVE.....	MUTAGENESIS.....	ALLOSTERIC.....	SP.01.05
APICOMPLEXA.....	MALARIA.....	CELL INVASION MACHINERY.....	MP165
ARCHAEAL EXOSOME.....	RNA PROCESSING.....	X-RAY STRUCTURE.....	TP118
AROMATASE/CYCLASE.....	POLYKETIDE.....	TETRACENOMYCIN.....	MP057
AROMATIC COMPOUND CATABOLISM.....	JOINT CENTER FOR STRUCTURAL.....	PHENYLACETIC ACID DEGRADATIO.....	SP248
ART.....	MICROSCOPE.....	PICTURES.....	SP244

# Keyword Index

ASPARTATE TRANSCARBAMOYLASE.....	THERMOSTABILITY.....	MUTATIONS.....	TP145
ASPARTATE TRANSCARBAMOYLASE.....	THERMOPHILIC.....	NEW STRUCTURE.....	TP153
ASPARTYL ISOMERIZATION.....	THIAMIN PYROPHOSPHOKINASE.....	SUCCINIMIDYL FORMATION.....	TP106
ASPHERICAL ATOM DATABANK.....	ELECTROSTATIC INTERACTIONS.....	INFLUENZA NEURAMINIDASE.....	TP114
ASSEMBLY.....	STRUCTURE.....	ORIENTATING METALLOMACROCYC.....	SP216
ATGRXCP PROTEIN.....	CYSTALLIZATION.....	X-RAY ANALYSIS.....	TP093
ATOM RESOLUTION.....	REFINEMENT.....	ESTIMATED STANDARD DEVIATIONS..	WK.01.04
ATOM RESOLUTION.....	REFINEMENT.....	ESTIMATED STANDARD DEVIATIONS..	WK.01.09
ATOMIC RESOLUTION.....	CYSTEINE OXIDATION.....	DJ-1.....	SP137
ATOMIC RESOLUTION.....	COUNTER-DIFFUSION.....	MICROGRAVITY.....	SP064
ATP-BINDING PROTEIN.....	“SECSG,”.....	STRUCTURAL GENOMICS.....	MP044
ATTRITION RATE.....	STRUCTURAL GENOMICS.....	CRYSTALLIZATION STRATEGY.....	SP075
AUOPHILIC INTERACTIONS.....	COORDINATION POLYMER.....		10.04.05
AUTOMATED CRYSTAL CENTERING.....	COMPUTER VISION.....	HIGH-THROUGHPUT CR.....	TP225
AUTOMATIC.....	CRYSTAL.....	CENTRING.....	SP233
AUTOMATION.....	SOFTWARE.....	CCD.....	03.01.06
AUTOMATION.....	HIGH THROUGHPUT.....	AUTOMOUNTER.....	MP230
AUTOMATION.....	SOFTWARE.....	FRAGMENT SCREENING.....	04.01.06
AUTOMATION.....	CRYSTALLIZATION.....	LIQUID HANDLING.....	SP073
AUTOMATION.....	ROBOTICS.....	SYNCHROTRON.....	TP222
AUTOMOUNTER.....	AUTOMATION.....	HIGH THROUGHPUT.....	MP230
AUTOPROTEOLYSIS.....	THREE CHEMISTRY.....	ACYLASE.....	TP176
AVIRULENCE PROTEIN.....	PLANT DISEASE RESISTANCE.....	CO2+ SAD PHASING.....	SP052
AXIOM.....	PHOTON-COUNTING.....	DETECTOR.....	MP236
AZIDE.....	REACTION.....	PHOTOLYSIS.....	10.01.02
AZIDO-BRIDGED.....	CRYSTAL STRUCTURE.....	COPPER COMPLEX.....	10.04.03
B CELL DEVELOPMENT.....	IMMUNOLOGY.....	SURROGATE LIGHT CHAIN.....	SP226
BACTERIAL.....	REDUCTASE.....	ISOPRENOIDS.....	SP011
BACTERIAL PILUS.....	X-RAY CRYSTALLOGRAPHY.....	STREPTOCOCCUS PYOGENES.....	SP022
BACTERICIDAL MECHANISM.....	INNATE IMMUNITY.....	PEPTIDOGLYCAN RECOGNITION PR.....	TP119
BEAMLINE.....	PROTEIN.....	CRYSTALLOGRAPHY.....	MP229
BENCHMARK.....	DOMAIN.....	DECOMPOSITION.....	01.05.04
BENZYLIDENEANILINE.....	ISOMERISM.....	ISOSTRUCTURALISM.....	10.04.04
BHLH.....	DNA.....	E-BOX.....	MP015
BI6(FE0.68BI0.32)P2O15.5.....	BI6(NI0.46BI0.54)P2O15.2.....	BI6ZNP2O15.....	05.02.07
BI6(NI0.46BI0.54)P2O15.2.....	BI6ZNP2O15.....	BI6(FE0.68BI0.32)P2O15.5.....	05.02.07
BI6ZNP2O15.....	BI6(FE0.68BI0.32)P2O15.5.....	BI6(NI0.46BI0.54)P2O15.2.....	05.02.07
BIFEO3.....	GISAXS.....	NUCLEATION.....	13.07.07
BIOINFORMATICS.....	SUBSTRATE IDENTIFICATION.....		TP092
BIOLOGICAL MOLECULES.....	STRUCTURE DETERMINATION.....	X-RAY SCATTERING.....	TR.01.06
BIOMEDICAL MATERIALS.....	USAXS.....	USANS.....	09.01.06
BIOMOLECULAR COMPLEXES.....	NEUTRON CONTRAST VARIATION.....	SMALL-ANGLE SCATTERING.....	13.03.06
BIOMOLECULES.....	LOW RESOLUTION STRUCTURE.....	SAXS.....	13.03.01
BIOTIN CARBOXYLASE.....	ACETYL-COA CARBOXYLASE.....	DIMERIZATION.....	SP121
BIS-CHELATE.....	PYRAZOLE.....	SUPRAMOLECULAR.....	AW.03.03
BLOCK COPOLYMER.....	NANOCOMPOSITES.....	SAXD.....	13.07.03
BLOCK COPOLYMER.....	LIQUID CRYSTAL.....	POLYMER THIN FILMS.....	09.02.05
BLOCK COPOLYMERS.....	COLLOIDS.....	GLASSES.....	09.01.08
BONDING.....	CHARGE-DENSITY.....		10.01.14
BONSE-HART TECHNIQUE.....	THEORETICAL LIMIT.....	SENSITIVITY.....	09.01.02
BOVINE.....	LIPOYL-AMP.....	SAD.....	MP034
BOVINE TRYPSIN.....	MELLITIC ACID.....	CO-CRYSTALLIZATION.....	SP066
BRAIN DEVELOPMENT.....	RECEPTOR-LIGAND INTERACTION.....	REELIN.....	TP146
BRANCHED.....	RELAXATION.....	SANS.....	13.04.02
BREWSTER-ANGLE MICROSCOPY.....	2D CRYSTAL.....	X-RAY.....	MP160
BRILLIANCE.....	MULTILAYER.....	OPTIC.....	MP228
BROAD SPECIFICITY.....	AMINOPEPTIDASE.....		SP023
C-REACTIVE PROTEIN.....	COMPLEX STRUCTURE.....	FC GAMMA RECEPTOR.....	MP166
CAFFEINE.....	CARBOXYLIC ACIDS.....	PHARMACEUTICAL COCRYSTALS.....	TP220
CALCIUM MESSENGER.....	MECHANISM OF CATALYSIS.....	HUMAN CD38.....	SP099
CALIXARENES.....	NANOPARTICLES.....	SELF-ASSEMBLY.....	13.07.05
CAMBRIDGE STRUCTURAL DATABASE.....	PROTEIN DATA BANK.....	DATA MINING.....	01.05.03
CANCER.....	CHK1.....	STRUCTURE-BASED DRUG DESIGN.....	04.01.01
CANCER.....	CATALYTIC MECHANISM.....	GLYCOBIOLOGY.....	AW.03.06
CANCER.....	SIGNAL TRANSDUCTION.....	X-RAY CRYSTALLOGRAPHY.....	SP047
CAPILLARIES.....	CRYOPRESERVATION.....	CRYOCRYSTALLOGRAPHY.....	MP081

# Keyword Index

CAPILLARY.....	MICROCRYSTALLOGRAPHY .....	HELIUM.....	13.08.06
CAPILLARY CRYOPROTECTION .....	SAD PHASING.....	HIGH PRESSURE CRYOCOOLING .....	13.01.06
CARBOHYDRATES.....	ENZYME.....	AMYLASE .....	SP01.04
CARBONIC ANHYDRASE.....	PROTON TRANSFER.....	KINETICS.....	TP132
CARBOXYLESTERASE .....	PROTEIN DESIGN.....	NERVE AGENTS .....	AW.03.05
CARBOXYLIC ACIDS.....	PHARMACEUTICAL COCRYSTALS.....	CAFFEINE.....	TP220
CARM1.....	PRMT .....	METHYLTRANSFERASE .....	MP243
CATALYSIS .....	NEUTRON DIFFRACTION.....	HYDROGEN STORAGE.....	13.06.04
CATALYSIS.....	SUPRAMOLECULAR.....	CLUSTER.....	SP218
CATALYSIS.....	GAS ABSORPTION.....	METAL-ORGANIC FRAMEWORK .....	MP195
CATALYSTS.....	HIGH-ENERGY.....	IN SITU .....	13.04.04
CATALYTIC MECHANISM.....	GLYCOBIOLOGY .....	CANCER.....	AW.03.06
CATALYTIC MECHANISM.....	PROTEIN DEUTERATION.....	HALOALKANE DEHALOGENASE .....	SP187
CATALYTIC MECHANISM.....	ANTIBIOTIC DEVELOPMENT.....	METABOLIC ENZYME .....	TP131
CATION ORDERING .....	KUTNAHORITE.....	CRYSTAL STRUCTURE.....	MP193
CAVITAND.....	COCRYSTALS.....	SUPRAMOLECULAR CHEMISTRY .....	SP207
CCD.....	AUTOMATION.....	SOFTWARE.....	03.01.06
CCD.....	DETECTORS .....	IMAGING PLATE .....	MP234
CCD DETECTORS.....	POINT SPREAD.....	DATA CORRECTION.....	MP237
CDK9.....	CYCLIN T1 .....	TAT.....	SP058
CELL CYCLE REGULATION .....	KINASE.....	TRANSCRIPTIONAL REGULATION .....	SP002
CELL INVASION MACHINERY.....	APICOMPLEXA.....	MALARIA .....	MP165
CENTRING.....	AUTOMATIC.....	CRYSTAL .....	SP233
CH.....	PROTEIN FOLDING.....		TP088
CHALCONES.....	PHARMACOLOGICAL TESTS.....	X-RAY STRUCTURE.....	10.01.09
CHALLENGING PROJECTS.....	STRUCTURAL GENOMICS .....	HIGH-THROUGHPUT PIPELINE .....	TP156
CHARGE DENSITY .....	DISORDER.....	AGOSTIC EFFECT .....	AW.03.04
CHARGE-DENSITY .....	BONDING .....		10.01.14
CHECKCIF.....	PLATON.....	VALIDATION.....	WK.01.07
CHEMICAL_BONDING.....	ENERGETIC_MATERIALS.....	TRANSANNULAR_INTERACTION.....	MP194
CHEMOTAXIS .....	DOMAIN SWAP.....	PAS SENSOR WITH C-TYPE HEME.....	TP115
CHK1 .....	STRUCTURE-BASED DRUG DESIG .....	CANCER.....	04.01.01
CHROMIUM RADIATION.....	SAD.....	SULFUR SAD PHASING .....	01.03.04
CIF.....	PUBLICATION.....	DATA VALIDATION.....	WK.01.06
CLATHRATE II STRUCTURE.....	THERMOELECTRIC MATERIAL .....	NA1-XGE3+Z .....	TP221
CLAY MIMICS .....	INTERCALATION.....		10.03.11
CLAY MIMICS .....	TRANSMISSION ELECTRON MICRO .....	INTERCALATION .....	SP213
CLOSED-CONFORMATION STABILIZATION .....	TRYPTOPHANYL-TRNA SYNTHETA .....	LIGAND FRAGMENT.....	TP155
CLUSTER.....	CATALYSIS.....	SUPRAMOLECULAR .....	SP218
CMOS FLAT PANEL DETECTOR .....	CONTINUOUS ROTATION METHOD .....	PROTEIN CRYSTALLOGRAPHY.....	13.02.03
CMP-NEU5AC.....	X-RAY CRYSTALLOGRAPHY .....	SIALYLTRANSFERASE.....	MP054
CO NANOSTRUCTURES .....	GISAXS.....	SELF-ORGANIZED GROWTH.....	09.02.04
CO(III) COMPLEXES.....	OXIME-AND-AMIDE LIGAND.....	SMALL CRYSTALLOGRAPHY .....	MP196
CO-CRYSTALLIZATION .....	BOVINE TRYPSIN.....	MELLITIC ACID.....	SP066
CO-CRYSTALS.....	ACTIVE PHARMCEUTICAL INGRE .....	CRYSTAL ENGINEERING.....	SP206
CO-CRYSTALS.....	MOLECULAR RECOGNITION.....	HYDROGEN BONDS .....	10.03.03
CO2+ SAD PHASING.....	AVIRULENCE PROTEIN.....	PLANT DISEASE RESISTANCE.....	SP052
COARSENING.....	USAXS.....	WASPALOY .....	09.01.10
COCKTAIL CRYSTALLOGRAPHY.....	STRUCTURAL GENOMICS .....	STRUCTURE-BASED DRUG DESIGN .....	MP163
COCRYSTALLIZATION.....	CRYSTAL ENGINEERING.....	MOLECULAR RECOGNITION.....	10.01.01
COCRYSTALS.....	SUPRAMOLECULAR CHEMISTRY .....	CAVITAND.....	SP207
COENZYME A.....	PYRIDINE NUCLEOTIDES .....	COENZYME A-DISULFIDE REDUCTA.....	AW.03.07
COENZYME A-DISULFIDE REDUCTASE.....	COENZYME A .....	PYRIDINE NUCLEOTIDES .....	AW.03.07
COHERENT IMAGING .....	FEMTOSECON.....	FREE-ELECTRON LASER .....	09.03.03
COLLECTIVE MOTION.....	PHONON .....	PROTEIN CRYSTALLOGRAPHY.....	TR.01.05
COLLOIDS .....	GLASSES .....	BLOCK COPOLYMERS.....	09.01.08
COMMENSURATELY MODULATED SUPERS .....	POLYMORPHIC SYSTEM .....	REVERSIBLE SOLID-SOLID PHASE .....	10.04.01
COMPARISON.....	PHENOLATE.....	STRUCTURE.....	SP01.03
COMPARISON.....	SELF-ASSEMBLY .....	STRUCTURE.....	TP202
COMPLEX.....	HOXA9 PBX DNA.....	TRANSCRIPTION FACTOR.....	SP009
COMPLEX.....	RNA.....	IRP1.....	01.01.01
COMPLEX.....	FRAMEWORK.....	POROUS .....	10.03.09
COMPLEX STRUCTURE .....	FC GAMMA RECEPTOR.....	C-REACTIVE PROTEIN.....	MP166
COMPOSITE CRYSTAL.....	INCLUSION COMPOUND.....	NMR CRYSTALLOGRAPHY.....	10.02.06
COMPOSITE CRYSTALS .....	MIXED CRYSTALS .....	CRYSTAL ENGINEERING.....	SP211
COMPUTATIONAL TOOLS .....	PLATON.....	SERVICE CRYSTALLOGRAPHY .....	10.02.04

# Keyword Index

COMPUTER VISION .....	HIGH-THROUGHPUT CR.....	AUTOMATED CRYSTAL CENTERING.....	TP225
COMPUTING.....	CRYSTAL STRUCTURE DETERMIN.....	SHELX .....	WK.01.01
COMPUTING.....	CRYSTAL STRUCTURE DETERMIN.....	SHELX .....	WK.01.08
COMPUTING.....	CRYSTAL STRUCTURE DETERMIN.....	SHELX .....	WK.01.11
COMPUTING.....	EXPERIMENTAL PHASING.....	DENSITY MODIFICATION.....	01.03.06
CONFORMATION.....	SANS.....	THERMO-SENSITIVE COMB LIKE PO.....	13.07.04
CONFORMATIONAL TRANSITIONS.....	DYNAMICS.....	SIGNALING.....	01.05.06
CONGO.....	RED.....	DOCKING.....	TP148
CONJUGATIVE DNA TRANSFER.....	MACROMOLECULAR CR.....	TRAI RELAXOSOME PROTEIN.....	01.01.04
CONTINUOUS ROTATION METHOD.....	PROTEIN CRYSTALLOGRAPHY.....	CMOS FLAT PANEL DETECTOR.....	13.02.03
CONTRAST MECHANISM.....	USAXS.....	IMAGING.....	09.01.09
CONTROL DROP SHAPE POSITION.....	CRYSTALLIZATION REPRODUCIBIL.....	IMAGE ANALYSIS.....	SP068
CONVERSION BY T CONTROL.....	NON-MEROHEDRAL TWIN.....	PSEUDO-MEROHEDRAL TWIN.....	SP201
COORDINATION COMPLEXES.....	CRYSTAL ENGINEERING.....	HYDROGEN BONDING.....	10.03.08
COORDINATION POLYMER.....	AUOPHILIC INTERACTIONS.....		10.04.05
COORDINATION POLYMERS.....	PORPHYRIN ASSEMBLIES.....	FRAMEWORK SOLIDS.....	10.01.03
COORDINATION POLYMERS.....	CRYSTAL ENGINEERING.....	MOLECULAR RECOGNITION.....	10.03.02
COORDINATION POLYMERS.....	HETEROMETALLIC COMPLEXES.....	SYNTHESIS & GROWTH.....	SP209
COOT.....	INTERFACES.....	SHELXL.....	WK.01.12
COPPER BROMIDE.....	THERMAL DISORDER.....	TEMPERATURE DEPENDENCE.....	05.01.04
COPPER COMPLEX.....	AZIDO-BRIDGED.....	CRYSTAL STRUCTURE.....	10.04.03
“CORDES, WALLY”.....	TEACHING.....		13.09.01
CORRELATED MOTION.....	PROTEIN DISORDER.....	DIFFUSE SCATTER.....	MP170
CORRELATED VARIATIONS.....	MOLECULAR ASSEMBLIES.....	NON-BRAGG DIFFRACTION.....	TR.01.04
CORROSION.....	SILANE.....	WATER-BARRIER.....	09.02.01
CORYNEBACTERIUM GLUTAMICUM.....	4-OT HOMOLOGUE.....	TAUTOMERASE.....	SP031
COUNTER DIFFUSION.....	DIFFUSION COEFFICIENT.....	PRECIPITANT.....	SP065
COUNTER-DIFFUSION.....	MICROGRAVITY.....	ATOMIC-RESOLUTION.....	SP064
COUNTER-DIFFUSION METHOD.....	PROTEIN CRYSTALLIZATION DEVICE.....		SP072
CROSS-REACTIVITY.....	A6 T CELL RECEPTOR.....	HAPTENATED TAX PEPTIDES.....	TP107
CRYATALLOGRAPHY.....	DIFFRACTOMETER.....	SMALL MOLECULE.....	MP241
CRYOCRYSTALLOGRAPHY.....	FLASH COOLING.....	CRYOPRESERVATION.....	MP080
CRYOCRYSTALLOGRAPHY.....	CAPILLARIES.....	CRYOPRESERVATION.....	MP081
CRYOLOOP ALIGNMENT.....	SYNCHROTRON BEAMLINES.....	CRYSTAL AUTOCENTERING.....	SP224
CRYOPRESERVATION.....	CRYOCRYSTALLOGRAPHY.....	FLASH COOLING.....	MP080
CRYOPRESERVATION.....	CRYOCRYSTALLOGRAPHY.....	CAPILLARIES.....	MP081
CRYOPROTECTANT.....	GLASS TRANSITION.....	FLASH COOLING.....	SP069
CRYOPROTECTANTS.....	CRYSTALLIZATION.....	SOLUBILITY ENHANCERS.....	SP067
CRYSTAL.....	CENTRING.....	AUTOMATIC.....	SP233
CRYSTAL AUTOCENTERING.....	CRYOLOOP ALIGNMENT.....	SYNCHROTRON BEAMLINES.....	SP224
CRYSTAL DECAY.....	SULFUR SAD.....		01.03.07
CRYSTAL DISORDER.....	DIFFUSE SCATTERING.....	PROTEIN DYNAMICS.....	TR.01.03
CRYSTAL ENGINEERING.....	MOLECULAR RECOGNITION.....	COCRYSTALLIZATION.....	10.01.01
CRYSTAL ENGINEERING.....	HYDROGEN BONDING.....	COORDINATION COMPLEXES.....	10.03.08
CRYSTAL ENGINEERING.....	HYDROGEN BOND.....	SUPRAMOLECULAR SYNTHON.....	AW.02.02
CRYSTAL ENGINEERING.....	CO-CRYSTALS.....	ACTIVE PHARMCEUTICAL INGREDI.....	SP206
CRYSTAL ENGINEERING.....	COMPOSITE CRYSTALS.....	MIXED CRYSTALS.....	SP211
CRYSTAL ENGINEERING.....	MOLECULAR RECOGNITION.....	COORDINATION POLYMERS.....	10.03.02
CRYSTAL ENGINEERING.....	SUPRAMOLECULAR CHEMISTRY.....	POWDER XRD.....	10.03.06
CRYSTAL ENGINEERING.....	POROSITY.....	GAS SORPTION.....	10.03.10
CRYSTAL ENGINEERING.....	POLAR CRYSTAL.....	DIPOLE ALLIGNMENT.....	10.03.12
CRYSTAL ENGINEERING.....	SUPRAMOLECULAR.....	HYDROGEN BOND.....	TP214
CRYSTAL LATTICE INTERACTIONS.....	PURIFICATION TAG.....	STRUCTURAL GENOMICS.....	01.02.06
CRYSTAL MOUNTING.....	LONGER WAVELENGTH.....	SAD METHOD.....	01.03.02
CRYSTAL PACKING.....	HYPERACID SALT.....	PROTONATED WATER.....	10.01.07
CRYSTAL PREPARATION.....	RADIATION DAMAGE.....	SCAVENGERS.....	13.10.05
CRYSTAL PREPARATION.....	RELATIVE HUMIDITY.....	DIFFRACTION IMPROVEMENT.....	MP082
CRYSTAL QUALITY.....	IN-SITU.....	MICROSCOPE.....	MP084
CRYSTAL STRUCTURE.....	SYMMETRY.....	DISORDER.....	10.02.05
CRYSTAL STRUCTURE.....	OUTER MEMBRANE PROTEIN.....	FATTY ACID TRANSPORT.....	SP085
CRYSTAL STRUCTURE.....	METAL HYDRIDE.....	MEMORY SHAPE MATERIAL.....	13.06.03
CRYSTAL STRUCTURE.....	HETEROMETALLIC COMPLEX.....	SUPRAMOLECULAR CHEMISTRY.....	SP204
CRYSTAL STRUCTURE.....	LEWIS ACIDES.....	1,2-BIS(CHLOROMERCURIO) TETRAF... TP210	
CRYSTAL STRUCTURE.....	COPPER COMPLEX.....	AZIDO-BRIDGED.....	10.04.03
CRYSTAL STRUCTURE.....	CATION ORDERING.....	KUTNAHORITE.....	MP193
CRYSTAL STRUCTURE.....	STEROSPECIFICITY.....	VESITONE REDUCTASE.....	SP046

# Keyword Index

CRYSTAL STRUCTURE.....	FMS1.....	POLYAMINE OXIDASE.....	SP103
CRYSTAL STRUCTURE.....	ISOTOPES.....	LABELED MATERIALS.....	SP199
CRYSTAL STRUCTURE DETERMINATION.....	SHELX.....	COMPUTING.....	WK.01.01
CRYSTAL STRUCTURE DETERMINATION.....	SHELX.....	COMPUTING.....	WK.01.08
CRYSTAL STRUCTURE DETERMINATION.....	SHELX.....	COMPUTING.....	WK.01.11
CRYSTAL STRUCTURE PREDICTION.....	POLYMORPHISM.....	MODELLING.....	AW.01.02
CRYSTAL STRUCTURE.....	TELOMERE BINDING PROTEIN.....	DNA COMPLEX.....	MP055
CRYSTALLIZATION.....	METASTABLE PHASES.....	SHAPE SELECTIVE SYNTHESIS.....	10.03.04
CRYSTALLIZATION.....	SOLUBILITY ENHANCERS.....	CRYOPROTECTANTS.....	SP067
CRYSTALLIZATION.....	LIQUID HANDLING.....	AUTOMATION.....	SP073
CRYSTALLIZATION.....	SURFACE ENTROPY REDUCTION.....	PSI-2 SPECIALIZED CENTER.....	SP074
CRYSTALLIZATION.....	METAL DEPENDENT.....	PHOHPHOLIPASE.....	SP076
CRYSTALLIZATION REPRODUCIBILITY.....	IMAGE ANALYSIS.....	CONTROL DROP SHAPE POSITION.....	SP068
CRYSTALLIZATION STRATEGY.....	ATTRITION RATE.....	STRUCTURAL GENIOMICS.....	SP075
CRYSTALLOGRAPHIC COMPUTING.....	INTERMOLECULAR INTERACTION.....	MOLECULAR DYNAMICS.....	AW.01.01
CRYSTALLOGRAPHIC EDUCATION.....	TEACHING INITIATIVE.....	UNDERGRADUATE STUDIES.....	SP.01.02
CRYSTALLOGRAPHIC ORBIFOLDS.....	RIEMANN-FINSLER GEOMETRY.....	HIGHER-ORDER THERMAL MOTION.....	03.02.03
CRYSTALLOGRAPHIC PUBLISHING.....	ACTA CRYSTALLOGRAPHICA.....	QUALITY CRITERIA.....	WK.02.04
CRYSTALLOGRAPHY.....	HIGH-THROUGHPUT SCREENING.....	PROTEIN CRYSTAL.....	03.01.03
CRYSTALLOGRAPHY.....	INDUSTRY.....	PROTEIN.....	04.01.04
CRYSTALLOGRAPHY.....	BEAMLINE.....	PROTEIN.....	MP229
CRYSTALLOGRAPHY.....	SYNCHROTRON.....	REMOTE.....	MP231
CUEO.....	MULTICOPPER.....	OXIDASE.....	SP109
CURACIN.....	DECARBOXYLASE.....		SP053
CYCLIN T1.....	TAT.....	CDK9.....	SP058
CYSTALLIZATION.....	X-RAY ANALYSIS.....	ATGRXCP PROTEIN.....	TP093
CYSTEINE BIOSYNTHESIS.....	SULFUR TRANSFER.....	MYCOBACTERIUM TUBERCULOSIS.....	SP014
CYSTEINE OXIDATION.....	DJ-1.....	ATOMIC RESOLUTION.....	SP137
CYTOCHROME.....	HEME P460.....		01.01.02
DASATINIB.....	PROCESS CONTROL.....	PHARMACEUTICAL.....	04.01.05
DATA COLLECTION STRATEGY.....	MLFSOM.....	TRAY GONIOMETER.....	13.01.05
DATA CORRECTION.....	CCD DETECTORS.....	POINT SPREAD.....	MP237
DATA DEPOSITION.....	NMR.....	STRUCTURE.....	WK.02.03
DATA MINING.....	CAMBRIDGE STRUCTURAL DATAB.....	PROTEIN DATA BANK.....	01.05.03
DATA PROCESSING.....	TWIN.....	NON-MEROHEDRAL.....	03.02.01
DATA QUALITY.....	ELECTRON DENSITY.....		10.01.15
DATA QUALITY.....	LOW NOISE.....	X-RAY SOURCE.....	MP079
DATA VALIDATION.....	CIF.....	PUBLICATION.....	WK.01.06
DATABASE.....	HIGH-RESOLUTION X-RAY CR.....	ELECTROSTATIC INTERACTION ENE.....	TP149
DATABASE INTEGRATION.....	UNIFORM CURATION.....	PROTEIN STRUCTURE.....	TP087
DCOH.....	ERH.....	HNF1A.....	SP035
DECARBOXYLASE.....	CURACIN.....		SP053
DECOMPOSITION.....	BENCHMARK.....	DOMAIN.....	01.05.04
DEFECTS.....	X-RAY AND NEUTRON SCATTERIN.....	DIFFUSE SCATTERING.....	TR.01.02
DENSITY BASIN.....	RNA QUADRUPLEX.....	MOLECULAR REPLACEMENT.....	SP246
DENSITY FUNCTIONS.....	MAXIMUM ENTROPY.....	POWDER DIFFRACTION.....	07.01.03
DENSITY MODIFICATION.....	COMPUTING.....	EXPERIMENTAL PHASING.....	01.03.06
DETECTOR.....	AXIOM.....	PHOTON-COUNTING.....	MP236
DETECTOR.....	MICRO-CRYSTALS.....	HOME LAB.....	TP240
DETECTORS.....	DIFFRACTION IMAGE STATISTICS.....	ESTIMATION INTEGRATED INTENSI.....	13.02.04
DETECTORS.....	IMAGING PLATE.....	CCD.....	MP234
DETERGENT.....	SAXS.....	PSI.....	MP161
DETERGENT MICELLES.....	SAXS.....	MEMBRANE PROTEINS.....	13.03.03
DFT, ABINITIO.....	THERMODYNAMICS, QUASI HAR.....	INELASTIC NEUTRON SCATTERING.....	13.06.01
DIAMONDS FROM AQUEOUS SOLUTIONS.....	RETROSYNTHETIC DIAMOND GR.....	DIAMONDS IN HYPERCRYTICAL WA.....	TP180
DIAMONDS IN HYPERCRYTICAL WATER.....	DIAMONDS FROM AQUEOUS SOL.....	RETROSYNTHETIC DIAMOND GROW.....	TP180
DIFFRACTION DEMONSTRATION.....	PATTERSON DEMONSTRATION.....	TEACHING GADGETS.....	13.09.02
DIFFRACTION IMAGE STATISTICS.....	ESTIMATION OF INTEGRATED INT.....	DETECTORS.....	13.02.04
DIFFRACTION IMPROVEMENT.....	CRYSTAL PREPARATION.....	RELATIVE HUMIDITY.....	MP082
DIFFRACTOMETER.....	SMALL MOLECULE.....	CRYATALLOGRAPHY.....	MP241
DIFFUSE.....	DISORDER.....	LAMELLAR DOMAINS.....	TR.01.07
DIFFUSE.....	VISUALIZATION.....	RECIPROCAL.....	TR.01.10
DIFFUSE SCATTER.....	CORRELATED MOTION.....	PROTEIN DISORDER.....	MP170
DIFFUSE SCATTERING.....	DISORDER.....	PSEUDO-SYMMETRY.....	MP169
DIFFUSE SCATTERING.....	DISORDER.....	POLYMORPHISM.....	SP168
DIFFUSE SCATTERING.....	DISORDER.....	NANOSCALE STRUCTURE.....	TR.01.01

# Keyword Index

DIFFUSE SCATTERING.....	ORDER-DISORDER .....	MODULATIONS.....	TR.01.11
DIFFUSE SCATTERING.....	DEFECTS .....	X-RAY AND NEUTRON SCATTERING.....	TR.01.02
DIFFUSE SCATTERING.....	PROTEIN DYNAMICS.....	CRYSTAL DISORDER.....	TR.01.03
DIFFUSE SCATTERING.....	PAIR DISTRIBUTION FUNCTION.....	NANOSTRUCTURE.....	TR.01.09
DIFFUSE SCATTERING.....	LIQUID CRYSTAL .....	ELASTOMER .....	TR.01.12
DIFFUSION.....	PLATE.....	VAPOUR.....	MP177
DIFFUSION COEFFICIENT.....	PRECIPITANT.....	COUNTER DIFFUSION .....	SP065
DIHYDROFOLATE REDUCTASE.....	QUINAZOLINES .....		TP120
DIMENSIONALITY REDUCTION .....	PATTERN MATCHING.....	MULTI-SCALE MODELING.....	01.05.05
DIMERIZATION.....	BIOTIN CABOXYLASE .....	ACETYL-COA CARBOXYLASE.....	SP121
DIOXYGENASE.....	HYDROXYMANDELATE.....		TP141
DIPOLE ALLIGNMENT.....	CRYSTAL ENGINEERING.....	POLAR CRYSTAL.....	10.03.12
DIRECT METHODS.....	PHASE RELATIONSHIPS.....	TEACHING AIDS .....	13.09.05
DIRECT SYNTHESIS.....	HETEROMETALLIC COMPLEXES.....	REINECKES SALT .....	TP203
DIRUTHENIUM COMPOUNDS.....	VARIABLE TEMP CR.....	ELECTRONIC STRUCTURE.....	10.01.13
DISAGGREGATION.....	NANOEMULSION .....	RHEO-SANS .....	13.04.03
DISINTEGRIN .....	ACOSTATIN .....	RGD LOOP .....	01.08.04
DISORDER.....	CRYSTAL STRUCTURE.....	SYMMETRY.....	10.02.05
DISORDER.....	SOLID STATE REACTION.....	TWINNING .....	10.03.01
DISORDER.....	PSEUDO-SYMMETRY.....	DIFFUSE SCATTERING.....	MP169
DISORDER.....	POLYMORPHISM.....	DIFFUSE SCATTERING.....	SP168
DISORDER.....	NANOSCALE STRUCTURE.....	DIFFUSE SCATTERING.....	TR.01.01
DISORDER.....	LAMELLAR DOMAINS .....	DIFFUSE.....	TR.01.07
DISORDER.....	SHELXL.....	REFINEMENT.....	WK.01.02
DISORDER.....	NEUTRON POWDER DIFFRACTION .....	LOW-TEMPERATURE CR .....	10.01.06
DISORDER.....	AGOSTIC EFFECT.....	CHARGE DENSITY.....	AW.03.04
DISORDERED PROTEINS .....	SOLUTION STRUCTURE.....	SMALL ANGLE SCATTERING.....	13.03.05
DISORDERED SOLVENT.....	MAXIMUM ENTROPY.....	X-RAY POWDER DIFFRACTION .....	07.01.11
DISSOLUTION.....	SIMULATION.....	AFM.....	AW.01.05
DJ-1 .....	ATOMIC RESOLUTION .....	CYSTEINE OXIDATION.....	SP137
DNA.....	E-BOX.....	BHLH.....	MP015
DNA.....	HOMEODOMAIN .....	NKX2.5.....	MP040
DNA.....	TREX1.....	POLY-PROLINE .....	SP062
DNA COMPLEX.....	CRYSTAL STRUCUTURE.....	TELOMERE BINDING PROTEIN.....	MP055
DNA DAMAGE.....	MUTAGENESIS.....	DNA REPLICATION .....	MP019
DNA MISMATCH REPAIR.....	HEAVY ATOM CLUSTER .....	TLS REFINEMENT .....	TP154
DNA MTASE.....	PROTEIN-PROTEIN COMPLEX.....		01.01.08
DNA REPLICATION.....	DNA DAMAGE.....	MUTAGENESIS .....	MP019
DNA-BINDING DOMAIN.....	PHOP.....	RESPONSE REGULATOR .....	TP116
DOCKING.....	SUPRAMOLECULAR .....	TELLURIUM(IV).....	TP215
DOCKING.....	CONGO.....	RED.....	TP148
DOMAIN.....	DECOMPOSITION.....	BENCHMARK.....	01.05.04
DOMAIN ALTERNATION .....	ADENYLATE-FORMING ENZYMES.....		AW.03.08
DOMAIN SWAP.....	PAS SENSOR WITH C-TYPE HEME .....	CHEMOTAXIS .....	TP115
DOMAINS .....	LEAST-SQUARES SUPERPOSITION.....	R.M.S.D.....	TP089
DOSE LIMIT .....	RADICAL SCAVENGERS .....	MICROSPECTROPHOTOMETRY.....	13.10.01
DOUBLE RING DNA HELICASE .....	ROTHMUND-THOMSON SYNDROME.....	HRECQL4.....	SP127
DRUG DESIGN .....	PROTEIN CRYSTALLOGRAPHY .....		SP104
DRUG DESIGN.....	PROTEASE INHIBITORS.....	HIV PROTEASE.....	TP112
DRUG DESIGN.....	ALDOSE REDUCTASE.....	PROTEIN-LIGAND COMPLEX .....	TP110
DRUG DISCOVERY.....	IMPACT.....	INDUSTRY.....	04.01.08
DRUG DISCOVERY.....	LIQUID HANDLING .....	PROTEIN CRYSTALS.....	MP179
DRUG TARGET.....	ADENOSINE KINASE.....	NUCLEOSIDE ANALOGS.....	MP033
DRUG TARGET.....	FATTY ACID SYNTHESIS.....	TULAREMIA.....	SP037
DSRNA CLEAVAGE.....	MECHANISM.....	RIBONUCLEASE III .....	MP021
DUAL CONFORMATION.....	PROTEIN SYNTHESIS.....	TRYPTOPHANYL-TRNA SYNTHETAS .....	MP049
DYNAMICS .....	ROTATION.....	SUPRAMOLECULAR .....	10.03.07
DYNAMICS .....	SIGNALING.....	CONFORMATIONAL TRANSITIONS .....	01.05.06
E-BOX.....	BHLH.....	DNA.....	MP015
E/Z-PHOTOISOMERIZATIONS.....	SINGLE-CRYSTAL-TO-SINGLE-CR .....	HOST-GUEST SYSTEMS.....	AW.03.02
ELASTOMER.....	DIFFUSE SCATTERING .....	LIQUID CRYSTAL.....	TR.01.12
ELECTRON DENSITY.....	METASTABLE STATES .....	PHASE TRANSITION.....	05.01.03
ELECTRON DENSITY.....	DATA QUALITY.....		10.01.15
ELECTRONIC STRUCTURE.....	DIRUTHENIUM COMPOUNDS .....	VARIABLE TEMP CR.....	10.01.13
ELECTROSTATIC INTERACTION ENERGY .....	DATABASE.....	HIGH-RESOLUTION X-RAY CR .....	TP149
ELECTROSTATIC INTERACTIONS .....	INFLUENZA NEURAMINIDASE.....	ASPHERICAL ATOM DATABANK .....	TP114

# Keyword Index

ELEMENT-SPECIFIC SUBSTRUCTURE	RESONANT ANOMALOUS X-RAY R	SURFACE AND INTERFACE	09.02.02
ENAMINONES	PHARMACOLOGICAL ACTIVITY	X-RAY DIFFRACTION	SP200
ENCAPSULANT	MORPHOLOGY	TEMPERATURE RESPONSIVE	09.01.03
ENDOTHAPEPSIN	NEUTRON PROTEIN CR	JOINT REFINEMENT	06.01.07
ENERGETIC MATERIALS	TRANSANNULAR INTERACTION	CHEMICAL BONDING	MP194
ENOLASES AMIDOHYDROLASES	STRUCTURAL GENOMICS	PROTEIN PHOSPHATASES	01.06.03
ENSEMBLE REFINEMENT	REFINEMENT METHODS	PROTEIN DYNAMICS	01.07.04
ENVIRONMENTAL	GISAXS	IRON OXIDE NANOPARTICLES	09.02.06
ENZYMATIC MECHANISM	PROTON	NEUTRON CRYSTALLOGRAPHY	06.01.06
ENZYME	NEUTRON	MECHANISM	06.01.01
ENZYME	AMYLASE	CARBOHYDRATES	SP01.04
ENZYME	GLYCOSYLATION	GLYCOSYLTRANSFERASE	TP135
ENZYME INHIBITORS	TROPICAL DISEASES	SCHISTOSOMIASIS	SP091
ENZYME MECHANISM	GTP CYCLOHYDROLASE		MP010
ENZYME MECHANISM	ANTIBIOTIC RESISTANT	LYASE	SP027
ENZYME MECHANISM	SUBSTRATE SPECIFICITY	GLYCOSYLTRANSFERASE	TP100
ENZYME MECHANISMS	FLAVOENZYME	FAD N5-ADDUCT	TP175
EPHRIN	RECEPTOR TYROSINE KINASE		SP025
ERH	HNFI A	DCOH	SP035
ESTIMATED STANDARD DEVIATIONS	ATOM RESOLUTION	REFINEMENT	WK.01.04
ESTIMATED STANDARD DEVIATIONS	ATOM RESOLUTION	REFINEMENT	WK.01.09
ESTIMATION OF INTEGRATED INTENSITIE	DETECTORS	DIFFRACTION IMAGE STATISTICS	13.02.04
ETTER'S RULE	INTRAMOLECULAR HYDROGEN B	O-H...O RINGS	MP197
EUDESMANES	VERBESINA TURBACENSIS	NATURAL PRODUCTS	SP191
EVOLUTION	STRUCTURE	NUCLEAR RECEPTOR	TP108
EXOSOME	MULTI-SUBUNIT	RNA	01.08.02
EXPERIMENTAL PHASING	DENSITY MODIFICATION	COMPUTING	01.03.06
EXTREME CONDITIONS	HIGH PRESSURE/TEMPERATURE	MINERALOGY/CRYSTALLOGRAPHY	05.02.01
FABG	SHORT-CHAIN OXIDOREDUCTASE		TP125
FAD N5 ADDUCTS	FLAVOPROTEIN	FAD-C4A-OXYGEN INTERMEDIATES	01.01.06
FAD N5-ADDUCT	ENZYME MECHANISMS	FLAVOENZYME	TP175
FAD-C4A-OXYGEN INTERMEDIATES	FAD N5 ADDUCTS	FLAVOPROTEIN	01.01.06
FAMILY 31 GLYCOSIDE HYDROLASE	ANTI-DIABETIC INHIBITORS	IODIDE PHASING	MP004
FATTY ACID OXIDATION	MEMBRANE PROTEIN	ACYL-COA DEHYDROGENASE	01.04.05
FATTY ACID SYNTHESIS	TULAREMIA	DRUG TARGET	SP037
FATTY ACID TRANSPORT	CRYSTAL STRUCTURE	OUTER MEMBRANE PROTEIN	SP085
FC GAMMA RECEPTOR	C-REACTIVE PROTEIN	COMPLEX STRUCTURE	MP166
FEMTOSECOND	FREE-ELECTRON LASER	COHERENT IMAGING	09.03.03
FIBER	AMYLOID	MICROCRYSTAL	10.04.02
FINGER	Y-FAMILY	POLYMERASE	SP096
FLASH COOLING	CRYOPRESERVATION	CRYOCRYSTALLOGRAPHY	MP080
FLASH COOLING	CRYOPROTECTANT	GLASS TRANSITION	SP069
FLAVOENZYME	FAD N5-ADDUCT	ENZYME MECHANISMS	TP175
FLAVONE	SMALL MOLECULE	P450 INHIBITORS	MP192
FLAVOPROTEIN	FAD-C4A-OXYGEN INTERMEDIATE	FAD N5 ADDUCTS	01.01.06
FLAVOPROTEIN	A-GLYCEROPHOSPHATE OXIDASE	A-GLYCEROPHOSPHATE	SP020
FMS1	POLYAMINE OXIDASE	CRYSTAL STRUCTURE	SP103
FRAGMENT CRYSTALLOGRAPHY	STRUCTURE BASED DRUG DESIG	LEAD IDENTIFICATION	04.01.03
FRAGMENT LIBRARY	FRAGMENT SCREENING	HSP90	MP178
FRAGMENT SCREENING	HSP90	FRAGMENT LIBRARY	MP178
FRAGMENT SCREENING	AUTOMATION	SOFTWARE	04.01.06
FRAGMENTS	SBDD	HSP90	04.01.02
FRAMEWORK	POROUS	COMPLEX	10.03.09
FRAMEWORK SOLIDS	COORDINATION POLYMERS	PORPHYRIN ASSEMBLIES	10.01.03
FREE RADICAL SCAVENGERS	RADIATION PROTECTION	RADIATION DAMAGE	13.10.06
FREE-ELECTRON LASER	COHERENT IMAGING	FEMTOSECOND	09.03.03
FUNCTION	STRUCTURAL GENOMICS		01.06.04
FUNCTION	PFAM	STRUCTURAL GENOMICS	TP128
FUNCTION FROM STRUCTURE	GO SLIMS	STRUCTURAL GENOMICS	01.06.02
FUNCTION PREDICTION	STRUCTURAL GENOMICS	PROTEIN SURFACE	01.06.07
FUNCTIONAL ASSOCIATION	REDUNDANT DATA-BASE	STRUCTURAL VARIATION	TP090
FUNCTIONAL MOTIF	RAF KINASE INHIBITOR PROTEIN	STRUCTURAL GENOMICS	TP124
FURIN	PROTEASE	PROPROTEIN CONVERTASE	TP143
GAG	HIV	ALIX	SP042
GAS ABSORPTION	METAL-ORGANIC FRAMEWORK	CATALYSIS	MP195
GAS SORPTION	CRYSTAL ENGINEERING	POROSITY	10.03.10

# Keyword Index

GENE REGULATION.....	SMALL ANGLE SCATTERING.....	SIGNAL TRANSDUCTION.....	13.03.02
GENE SYNTHESIS.....	WORKFLOW.....	PROTEIN EXPRESSION.....	TP094
GENE THERAPY.....	PARVOVIRIDAE.....	ADENO-ASSOCIATED VIRUS.....	SP039
GEOMETRIC EFFECTS.....	GRANDIDERITE.....	OMINELITE.....	05.02.04
GEOMETRIC PARAMETERS.....	HETEROMOLECULES.....	TOPOLOGY AND PARAMETER.....	03.01.04
GISAXS.....	ANOMALOUS GISAXS.....	NANOCATALYSIS.....	09.02.03
GISAXS.....	SELF-ORGANIZED GROWTH.....	CO NANOSTRUCTURES.....	09.02.04
GISAXS.....	IRON OXIDE NANOPARTICLES.....	ENVIRONMENTAL.....	09.02.06
GISAXS.....	VIRUS.....	ABSORPTION.....	09.03.05
GISAXS.....	2D ASSEMBLY.....	2D ORDER.....	13.03.04
GISAXS.....	NUCLEATION.....	BIFEO3.....	13.07.07
GLASS TRANSITION.....	FLASH COOLING.....	CRYOPROTECTANT.....	SP069
GLASSES.....	BLOCK COPOLYMERS.....	COLLOIDS.....	09.01.08
GLOBAL OPTIMIZATION.....	SIMULATED ANNEALING.....	X-RAY POWDER DIFFRACTION.....	TP189
GLYCOBIOLOGY.....	CANCER.....	CATALYTIC MECHANISM.....	AW.03.06
GLYCOSYLATION.....	GLYCOSYLTRANSFERASE.....	ENZYME.....	TP135
GLYCOSYL HYDROLASE.....			MP032
GLYCOSYLTRANSFERASE.....	MAMMALIAN EXPRESSION.....	SECRETORY PATHWAY.....	SP038
GLYCOSYLTRANSFERASE.....	ENZYME MECHANISM.....	SUBSTRATE SPECIFICITY.....	TP100
GLYCOSYLTRANSFERASE.....	ENZYME.....	GLYCOSYLATION.....	TP135
GO SLIMS.....	STRUCTURAL GENOMICS.....	FUNCTION FROM STRUCTURE.....	01.06.02
GRANDIDERITE.....	OMINELITE.....	GEOMETRIC EFFECTS.....	05.02.04
GRAZING INCIDENCE.....	LIPID MEMBRANES.....		MP158
GREEN FLUORESCENT PROTEIN.....	PRECRYSTALLIZATION SCREENIN.....	MEMBRANE PROTEIN.....	01.02.01
GRID COMPUTING.....	POWDER DIFFRACTION.....	STRUCTURE SOLUTION.....	07.01.02
GRID STRUCTURE.....	SCHIFF BASE LIGAND.....	TETRANUCLEAR CLUSTER.....	TP205
GTP CYCLOHYDROLASE.....	ENZYME MECHANISM.....		MP010
GYRASE.....	TOPOIV.....	TYPE IIA DNA TOPOISOMERASE.....	SP130
HALOALKANE DEHALOGENASE.....	CATALYTIC MECHANISM.....	PROTEIN DEUTERATION.....	SP187
HAPTENATED TAX PEPTIDES.....	CROSS-REACTIVITY.....	A6 T CELL RECEPTOR.....	TP107
HEAVY ATOM CLUSTER.....	TLS REFINEMENT.....	DNA MISMATCH REPAIR.....	TP154
HEAVY-ATOM SEARCH.....	PARALLEL.....	SHELXD.....	TP151
HELIUM.....	HIGH RESOLUTION.....	NEUTRON DIFFRACTION.....	13.01.02
HELIUM.....	CAPILLARY.....	MICROCRYSTALLOGRAPHY.....	13.08.06
HEME.....	ANAEROBIC CRYSTALLIZATION.....	UROPORPHYRINOGEN DECARBOXY.....	01.02.03
HEME P460.....	CYTOCHROME.....		01.01.02
HEME SENSOR.....	SOLUBLE GUANYLYL CYCLASE.....	NITRIC OXIDE RECEPTOR.....	03.01.02
HEMOGLOBIN.....	ALLOSTERY.....		01.08.01
HEMOLYSIN.....	VIRULENCE FACTOR.....	SPHINGOMYELINASE.....	SP123
HEPARIN.....	NEUROFILIN.....	VEGF.....	MP013
HETEROMETALLIC COMPLEX.....	SUPRAMOLECULAR CHEMISTRY.....	CRYSTAL STRUCTURE.....	SP204
HETEROMETALLIC COMPLEXES.....	REINECKES SALT.....	DIRECT SYNTHESIS.....	TP203
HETEROMETALLIC COMPLEXES.....	SYNTHESIS & GROWTH.....	COORDINATION POLYMERS.....	SP209
HETEROMOLECULES.....	SEVRER FOR TOPOLOGY AND PA.....	GEOMETRIC PARAMETERS.....	03.01.04
HIGH PRESSURE.....	X-RAY.....	WATER.....	05.02.03
HIGH PRESSURE.....	PHASE TRANSITION.....	AB INITIO CALCULATIONS.....	AW.01.04
HIGH PRESSURE.....	POWDER DIFFRACTION.....	VARIABLE TEMPERATURE.....	AW.03.01
HIGH PRESSURE CRYOCOOLING.....	CAPILLARY CRYOPROTECTION.....	SAD PHASING.....	13.01.06
HIGH PRESSURE/TEMPERATURE.....	MINERALOGY/CRYSTALLOGRAPH.....	EXTREME CONDITIONS.....	05.02.01
HIGH RESOLUTION.....	NEUTRON DIFFRACTION.....	HELIUM.....	13.01.02
HIGH THROUGHPUT.....	AUTOMOUNTER.....	AUTOMATION.....	MP230
HIGH-ENERGY.....	IN SITU.....	CATALYSTS.....	13.04.04
HIGH-RESOLUTION.....	TAKA-AMYLASE A.....	MICROGRAVITY.....	SP071
HIGH-RESOLUTION X-RAY CR.....	ELECTROSTATIC INTERACTION EN.....	DATABASE.....	TP149
HIGH-TEMPERATURE.....	STEELS.....	PRECIPITATION.....	09.01.05
HIGH-THROUGHPUT CRYSTALLOGRAPHY.....	AUTOMATED CRYSTAL CENTERIN.....	COMPUTER VISION.....	TP225
HIGH-THROUGHPUT PIPELINE.....	CHALLENGING PROJECTS.....	STRUCTURAL GENOMICS.....	TP156
HIGH-THROUGHPUT SCREENING.....	PROTEIN CRYSTAL.....	CRYSTALLOGRAPHY.....	03.01.03
HIGHER-ORDER THERMAL MOTION.....	CRYSTALLOGRAPHIC ORBIFOLDS.....	RIEMANN-FINSLER GEOMETRY.....	03.02.03
HIRSHFELD SURFACES.....	POLYMORPHISM.....	PHARMACEUTICALS.....	10.04.06
HIV.....	ALIX.....	GAG.....	SP042
HIV PROTEASE.....	DRUG DESIGN.....	PROTEASE INHIBITORS.....	TP112
HIV-1.....	ANTIBODY.....	VACCINE.....	13.05.06
HIV-1.....	PROTEASE.....	PIP6 SUBSTRATE.....	TP113
HNF1A.....	DCOH.....	ERH.....	SP035
HOME LAB.....	DETECTOR.....	MICRO-CRYSTALS.....	TP240

# Keyword Index

HOMEODOMAIN.....	NKX2.5.....	DNA.....	MP040
HOMOGENEOUS REACTIONS.....	PHOTOCHEMISTRY.....	HOST-GUEST COMPLEXES.....	AW.03.09
HOST SPECIFICITY.....	RATIONAL DESIGN.....		MP167
HOST-GUEST COMPLEXES.....	HOMOGENEOUS REACTIONS.....	PHOTOCHEMISTRY.....	AW.03.09
HOST-GUEST SYSTEMS.....	E/Z-PHOTOISOMERIZATIONS.....	SINGLE-CRYSTAL-TO-SINGLE-CRY.....	AW.03.02
HOXA9 PBX DNA.....	TRANSCRIPTION FACTOR.....	COMPLEX.....	SP009
HRECQL4.....	DOUBLE RING DNA HELICASE.....	ROTHMUND-THOMSON SYNDROME.....	SP127
HSP90.....	FRAGMENT LIBRARY.....	FRAGMENT SCREENING.....	MP178
HSP90.....	FRAGMENTS.....	SBDD.....	04.01.02
HUMAN CD38.....	CALCIUM MESSENGER.....	MECHANISM OF CATALYSIS.....	SP099
HXLR DOMAIN.....	TRANSCRIPTIONAL REGULATOR.....	WINGED HELIX-TURN-HELIX.....	MP043
HYALURONIDASE 1.....			MP024
HYDROGEN.....	NEUTRON DIFFRACTION.....	PROTEIN.....	06.01.04
HYDROGEN.....	REFINEMENT.....	RESTRAINTS.....	TP152
HYDROGEN BOND.....	SUPRAMOLECULAR SYNTHON.....	CRYSTAL ENGINEERING.....	AW.02.02
HYDROGEN BOND.....	PHOTOACTIVE YELLOW PROTEIN.....		06.01.03
HYDROGEN BOND.....	CRYSTAL ENGINEERING.....	SUPRAMOLECULAR.....	TP214
HYDROGEN BONDING.....	COORDINATION COMPLEXES.....	CRYSTAL ENGINEERING.....	10.03.08
HYDROGEN BONDING.....	MYOGLOBIN.....	LIGAND DISCRIMINATION.....	TP105
HYDROGEN BONDS.....	CO-CRYSTALS.....	MOLECULAR RECOGNITION.....	10.03.03
HYDROGEN STORAGE.....	CATALYSIS.....	NEUTRON DIFFRACTION.....	13.06.04
HYDROGEN STORAGE.....	TIME RESOLVED.....	NEUTRON DIFFRACTION.....	13.04.06
HYDROGEN STORAGE.....	POWDER DIFFRACTION.....	RIETVELD METHOD.....	13.06.06
HYDROGEN/DEUTERIUM.....	MACROMOLECULAR.....	NEUTRON LAUE DIFFRACTION.....	TP186
HYDROTHERMAL SYNTHESIS.....	MIXED LIGAND COMPLEXES.....	ITACONIC ACID.....	TP217
HYDROXYMANDELATE.....	HYDROXYMANDELATE.....	DIOXYGENASE.....	TP141
HYPERACID SALT.....	PROTONATED WATER.....	CRYSTAL PACKING.....	10.01.07
HYPOTHETICAL PROTEINS.....	ALTERNATIVE SPLICING.....	STRUCTURAL GENOMICS.....	01.06.05
HYPOXIA INDUCIBLE FACTOR.....	2-OXOGLUTARATE.....	PROLYL HYDROXYLASE.....	SP026
IMAGE ANALYSIS.....	CONTROL DROP SHAPE POSITION.....	CRYSTALLIZATION REPRODUCIBILI.....	SP068
IMAGING.....	CONTRAST MECHANISM.....	USAXS.....	09.01.09
IMAGING PLATE.....	CCD.....	DETECTORS.....	MP234
IMGCIF.....	MAPS.....	RASMOL.....	TP174
IMMUNOLOGY.....	SURROGATE LIGHT CHAIN.....	B CELL DEVELOPMENT.....	SP226
IMPACT.....	INDUSTRY.....	DRUG DISCOVERY.....	04.01.08
IN SITU.....	CATALYSTS.....	HIGH-ENERGY.....	13.04.04
IN SITU RAMAN SPECTROSCOPY.....	NON-AMBIENT CONDITIONS.....	IN SITU XRPD.....	05.01.02
IN SITU XRPD.....	IN SITU RAMAN SPECTROSCOPY.....	NON-AMBIENT CONDITIONS.....	05.01.02
IN-SITU.....	MICROSCOPE.....	CRYSTAL QUALITY.....	MP084
IN-SITU EXPERIMENTS.....	POWDER DIFFRACTION.....	MAGNETOSTRUCTURAL TRANSITIO.....	13.04.05
INCLUSION COMPOUND.....	NMR CRYSTALLOGRAPHY.....	COMPOSITE CRYSTAL.....	10.02.06
INCLUSION COMPOUNDS.....	L-LEUCYL-L-LEUCYL-L-LEUCINE.....	LAYERED STRUCTURE.....	10.03.05
INDUSTRY.....	DRUG DISCOVERY.....	IMPACT.....	04.01.08
INDUSTRY.....	PROTEIN.....	CRYSTALLOGRAPHY.....	04.01.04
INELASTIC NEUTRON SCATTERING.....	DFT, ABINITIO.....	THERMODYNAMICS, QUASI HARMO.....	13.06.01
INFLUENZA.....	VIRUS.....	NUCLEOPROTEIN.....	13.05.02
INFLUENZA NEURAMINIDASE.....	ASPHERICAL ATOM DATABANK.....	ELECTROSTATIC INTERACTIONS.....	TP114
INHIBITOR.....	RECEPTOR.....	PHEROMONE.....	TP098
INHIBITOR PROTEIN.....	PROTEIN PHOSPHATASE.....	INTRINSIC DISORDER.....	MP056
INHIBITOR SCREENING.....	NATURAL PRODUCT EXTRACTS.....	A-AMYLASE INHIBITORS.....	TP102
INNATE IMMUNITY.....	PEPTIDOGLYCAN RECOGNITION P.....	BACTERICIDAL MECHANISM.....	TP119
INORGANIC-ORGANIC PEROVSKITE.....	SONICATION.....	INTERCALATION.....	SP212
INOSITOL.....	PHOSPHATASE.....	PHYTASE.....	SP050
INOSITOL MULTIKINASE.....	IPK2.....	INOSITOL POLYPHOSPHATES.....	SP008
INOSITOL POLYPHOSPHATES.....	INOSITOL MULTIKINASE.....	IPK2.....	SP008
INSTRUMENTATION.....	NEUTRON.....	POWDER.....	07.01.10
INSULIN RECEPTOR.....	KRLB.....	IRS.....	TP122
INTERACTOME.....	STRUCTURAL GENOMICS.....		01.05.02
INTERCALATION.....	CLAY MIMICS.....		10.03.11
INTERCALATION.....	INORGANIC-ORGANIC PEROVSKIT.....	SONICATION.....	SP212
INTERCALATION.....	CLAY MIMICS.....	TRANSMISSION ELECTRON MICROS.....	SP213
INTERFACE.....	VISUALIZATION.....	MOTIF.....	SP01.06
INTERFACES.....	SHELXL.....	COOT.....	WK.01.12
INTERGROWTH.....	SYMMETRY.....	PHASE TRANSFORMATION.....	10.02.02
INTERMOLECULAR INTERACTIONS.....	MOLECULAR DYNAMICS.....	CRYSTALLOGRAPHIC COMPUTING.....	AW.01.01
INTERNAL RIBOSOME ENTRY SITE.....	VIRAL RNA.....	RNA STRUCTURE.....	13.05.01

# Keyword Index

INTRAMEMBRANE PROTEOLYSIS.....	RHOMBOID PROTEASE.....	MEMBRANE PROTEIN.....	01.01.05
INTRAMOLECULAR HYDROGEN BONDS.....	O-H...O RINGS.....	ETTER'S RULE.....	MP197
INTRINSIC DISORDER.....	INHIBITOR PROTEIN.....	PROTEIN PHOSPHATASE.....	MP056
INTRINSICALLY UNFOLDED PROTEIN.....	PARKINSON'S DISEASE.....	-SYNUCLEIN.....	MP030
IODIDE PHASING.....	FAMILY 31 GLYCOSIDE HYDROLA.....	ANTI-DIABETIC INHIBITORS.....	MP004
IP3.....	SMALL-ANGLE SCATTERING.....		MP159
IPK2.....	INOSITOL POLYPHOSPHATES.....	INOSITOL MULTIKINASE.....	SP008
IRON OXIDE NANOPARTICLES.....	ENVIRONMENTAL.....	GISAXS.....	09.02.06
IRP1.....	COMPLEX.....	RNA.....	01.01.01
IRS.....	INSULIN RECEPTOR.....	KRLB.....	TP122
ISOMERISM.....	ISOSTRUCTURALISM.....	BENZYLIDENEANILINE.....	10.04.04
ISOPRENIDS.....	BACTERIAL.....	REDUCTASE.....	SP011
ISOSTRUCTURALISM.....	BENZYLIDENEANILINE.....	ISOMERISM.....	10.04.04
ISOTOPES.....	LABELED MATERIALS.....	CRYSTAL STRUCTURE.....	SP199
ITACONIC ACID.....	HYDROTHERMAL SYNTHESIS.....	MIXED LIGAND COMPLEXES.....	TP217
JOINT CENTER FOR STRUCTURAL GENOMI.....	PHENYLACETIC ACID DEGRADATI.....	AROMATIC COMPOUND CATABOLIS.....	SP248
JOINT REFINEMENT.....	ENDOTHAPEPSIN.....	NEUTRON PROTEIN CR.....	06.01.07
JOINT X-RAY AND NEUTRON REFINEMENT.....	ALDOSE REDUCTASE.....	PHENIX.....	06.01.02
KINASE.....	TRANSCRIPTIONAL REGULATION.....	CELL CYCLE REGULATION.....	SP002
KINETICS.....	CARBONIC ANHYDRASE.....	PROTON TRANSFER.....	TP132
KRLB.....	IRS.....	INSULIN RECEPTOR.....	TP122
KUTNAHORITE.....	CRYSTAL STRUCTURE.....	CATION ORDERING.....	MP193
L-LEUCYL-L-LEUCYL-L-LEUCINE.....	LAYERED STRUCTURE.....	INCLUSION COMPOUNDS.....	10.03.05
LABELED MATERIALS.....	CRYSTAL STRUCTURE.....	ISOTOPES.....	SP199
LACI REPRESSOR.....	ALLOSTERIC REGULATION.....	SAXS.....	MP250
LAMELLAR DOMAINS.....	DIFFUSE.....	DISORDER.....	TR.01.07
LANGUAGE.....	VISUALIZATION.....	SCRIPTING.....	TP172
LARGE PROTEIN.....	TRANSCRIPTION.....	RNA POLYMERASE II.....	13.01.01
LAUE DIFFRACTION.....	TIME-RESOLVED.....	SYNCHROTRON.....	05.01.06
LAYERED STRUCTURE.....	INCLUSION COMPOUNDS.....	L-LEUCYL-L-LEUCYL-L-LEUCINE.....	10.03.05
LDL-BOUND.....	PHOSPHOLIPASEA2.....	PPAFAH.....	TP086
LEAD IDENTIFICATION.....	FRAGMENT CRYSTALLOGRAPHY.....	STRUCTURE BASED DRUG DESIGN.....	04.01.03
LEAST-SQUARES SUPERPOSITION.....	R.M.S.D.....	DOMAINS.....	TP089
LEWIS ACIDES.....	1,2-BIS(CHLOROMERCURIO) TETR.....	CRYSTAL STRUCTURE.....	TP210
LI6Y(BO3)3.....	SCINTILLATOR.....	NEUTRON DETECTOR.....	MP235
LIGAND DISCRIMINATION.....	HYDROGEN BONDING.....	MYOGLOBIN.....	TP105
LIGAND FRAGMENT.....	CLOSED-CONFORMATION STABILI.....	TRYPTOPHANYL-TRNA SYNTHETAS.....	TP155
LIGANDS.....	VALIDATIO.....	PROTEIN CRYSTALLOGRAPHY.....	01.05.01
LINEAR M-H-M BOND.....	NEUTRON DIFFRACTION.....	METAL HYDRIDE.....	MP198
LIPID MEMBRANES.....	GRAZING INCIDENCE.....		MP158
LIPOPROTEIN.....	TREPONEMA PALLIDUM.....	STRUCTURE-FUNCTION.....	TP140
LIPOYL-AMP.....	SAD.....	BOVINE.....	MP034
LIQUID CRYSTAL.....	POLYMER THIN FILMS.....	BLOCK COPOLYMER.....	09.02.05
LIQUID CRYSTAL.....	ELASTOMER.....	DIFFUSE SCATTERING.....	TR.01.12
LIQUID HANDLING.....	AUTOMATION.....	CRYSTALLIZATION.....	SP073
LIQUID HANDLING.....	PROTEIN CRYSTALS.....	DRUG DISCOVERY.....	MP179
LONG WAVELENGTH.....	SUBSTRUCTURE.....		01.03.03
LONG WAVELENGTH.....	MULTILAYER OPTICS.....	SAD PHASING.....	MP077
LONG WAVELENGTH FROM CR ANODE.....	SULFUR SAD.....	SULFUR PHASING.....	01.03.08
LONG WAVELENGTH PHASING.....	SULFUR-SAD.....	STRUCTURE VALIDATION.....	MP078
LONG WAVELWENGTH.....	RADIATION DAMAGE.....	PHASING.....	01.03.05
LONGER WAVELENGTH.....	SAD METHOD.....	CRYSTAL MOUNTING.....	01.03.02
LOV2 DOMAIN.....	STRUCTURAL CHANGES.....	PHOTOTROPINI.....	TP142
LOW NOISE.....	X-RAY SOURCE.....	DATA QUALITY.....	MP079
LOW RESOLUTION.....	NEUTRON DIFFRACTION.....	SIR PHASING.....	TP185
LOW RESOLUTION STRUCTURE.....	SAXS.....	BIOMOLECULES.....	13.03.01
LOW-TEMPERATURE CRYSTALLOGRAPHY.....	DISORDER.....	NEUTRON POWDER DIFFRACTION.....	10.01.06
LYASE.....	ENZYME MECHANISM.....	ANTIBIOTIC RESISTANT.....	SP027
MACA.....	MEMBRANE FUSION.....	MULTIDRUG EFFLUX TRANSPORTER.....	MP048
MACROMOLECULAR.....	NEUTRON LAUE DIFFRACTION.....	HYDROGEN/DEUTERIUM.....	TP186
MACROMOLECULAR CRYSTALLOGRAPHY.....	TRA I RELAXOSOME PROTEIN.....	CONJUGATIVE DNA TRANSFER.....	01.01.04
MACROMOLECULAR CRYSTALLOGRAPHY.....	RADIATION DAMAGE.....	MAD AND SAD PHASING.....	13.10.07
MACROMOLECULES.....	SYNCHROTRON RADIATION.....	USER FACILITIES.....	MP083
MAD.....	PROSTACYCLIN SYNTHASE.....	PGIS.....	SP036
MAD AND SAD PHASING.....	MACROMOLECULAR CR.....	RADIATION DAMAGE.....	13.10.07
MAGNET.....	PRUSSIAN BLUE.....		10.01.11

# Keyword Index

MAGNETIC SCATTERING .....	SOFT X-RAYS .....	RESONANT SCATTERING .....	09.03.01
MAGNETIC STRUCTURE .....	NANOPARTILES .....		13.07.09
MAGNETIC STRUCTURE .....	POLARIZED SINGLE CRYSTAL NEU .....	SPINEL .....	TP184
MAGNETISM .....	POWDER .....	SYNCHROTRON .....	07.01.06
MAGNETOSTRUCTURAL TRANSITIONS .....	IN-SITU EXPERIMENTS .....	POWDER DIFFRACTION .....	13.04.05
MAIL-IN CRYSTALLOGRAPHY .....	REMOTE DATA COLLECTION .....	SYNCHROTRON .....	MP232
MALARIA .....	CELL INVASION MACHINERY .....	APICOMPLEXA .....	MP165
MAMMALIAN EXPRESSION .....	SECRETORY PATHWAY .....	GLYCOSYLTRANSFERASE .....	SP038
MAPS .....	RASMOL .....	IMGCIF .....	TP174
MATERIALS SCIENCE .....	USAXS .....	SMALL ANGLE SCATTERING .....	09.01.01
MAXIMUM ENTROPY .....	X-RAY POWDER DIFFRACTION .....	DISORDERED SOLVENT .....	07.01.11
MAXIMUM ENTROPY .....	POWDER DIFFRACTION .....	DENSITY FUNCTIONS .....	07.01.03
MAXIMUM ENTROPY METHOD .....	MONTE CARLO METHOD .....	NUCLEAR/ELECTRON DENSITY DIST .....	03.02.02
MECHANISM .....	RIBONUCLEASE III .....	DSRNA CLEAVAGE .....	MP021
MECHANISM .....	ENZYME .....	NEUTRON .....	06.01.01
MECHANISM OF CATALYSIS .....	HUMAN CD38 .....	CALCIUM MESSENGER .....	SP099
MELLITIC ACID .....	CO-CRYSTALLIZATION .....	BOVINE TRYPSIN .....	SP066
MEMBRANE FUSION .....	VIRUS ENTRY .....		13.05.05
MEMBRANE FUSION .....	MULTIDRUG EFFLUX TRANSPORT .....	MACA .....	MP048
MEMBRANE PROTEIN .....	INTRAMEMBRANE PROTEOLYSIS .....	RHOMBOID PROTEASE .....	01.01.05
MEMBRANE PROTEIN .....	GREEN FLUORESCENT PROTEIN .....	PRECRYSTALLIZATION SCREENING .....	01.02.01
MEMBRANE PROTEIN .....	TONB .....	TRANSPORT .....	01.04.02
MEMBRANE PROTEIN .....	ANION TRANSPORT .....		01.04.03
MEMBRANE PROTEIN .....	ACYL-COA DEHYDROGENASE .....	FATTY ACID OXIDATION .....	01.04.05
MEMBRANE PROTEINS .....	MICROFLUIDICS .....	MESOPHASE .....	01.02.04
MEMBRANE PROTEINS .....	DETERGENT MICELLES .....	SAXS .....	13.03.03
MEMORY SHAPE MATERIAL .....	CRYSTAL STRUCTURE .....	METAL HYDRIDE .....	13.06.03
MESOPHASE .....	MEMBRANE PROTEINS .....	MICROFLUIDICS .....	01.02.04
METABOLIC ENZYME .....	CATALYTIC MECHANISM .....	ANTIBIOTIC DEVELOPMENT .....	TP131
METAL DEPENDENT .....	PHOHPHOLIPASE .....	CRYSTALLIZATION .....	SP076
METAL DEPENDENT PHOSPHODIESTERAS .....	THERMOPHILIC EUKARYOTE .....	STRUCTURAL GENOMICS .....	TP126
METAL HYDRIDE .....	X-RAY DIFFRACTION .....	TEXTURE ANALYSIS .....	13.06.02
METAL HYDRIDE .....	MEMORY SHAPE MATERIAL .....	CRYSTAL STRUCTURE .....	13.06.03
METAL HYDRIDE .....	LINEAR M-H-M BOND .....	NEUTRON DIFFRACTION .....	MP198
METAL HYDRIDES .....	POWDER X-RAY DIFFRACTION .....	RIETVELD METHOD .....	13.06.05
METAL IONS .....	RNA STRUCTURE .....	RIBOSWITCH .....	MP059
METAL-ORGANIC FRAMEWORK .....	CATALYSIS .....	GAS ABSORPTION .....	MP195
METAL-ORGANIC FRAMEWORKS .....			SP219
METALLOEZYME .....	STRUCTURE-FUNCTION .....	SPECTROSCOPY .....	SP138
METASTABLE PHASES .....	SHAPE SELECTIVE SYNTHESIS .....	CRYSTALLIZATION .....	10.03.04
METASTABLE STATES .....	PHASE TRANSITION .....	ELECTRON DENSITY .....	05.01.03
METHODOLOGY .....	SPACE GROUPS .....	SYMMETRY .....	13.09.04
METHODS .....	PROGRAMS .....	POWDERS .....	07.01.01
METHYLTRANSFERASE .....	CARM1 .....	PRMT .....	MP243
METHYLTRANSFERASE .....	16S RRNA .....		MP029
MICRO-BEAM .....	MICRO-CRYSTAL .....	SYNCHROTRON .....	TP239
MICRO-CRYSTAL .....	SYNCHROTRON .....	MICRO-BEAM .....	TP239
MICRO-CRYSTALS .....	MINI-BEAM .....	SIGNAL-TO-NOISE .....	13.08.03
MICRO-CRYSTALS .....	POLYHEDRIN .....	SR-INSTRUMENTATION .....	13.08.02
MICRO-CRYSTALS .....	HOME LAB .....	DETECTOR .....	TP240
MICROCRYSTAL .....	MICRODIFFRACTION .....	SYNCHROTRON .....	13.08.04
MICROCRYSTAL .....	FIBER .....	AMYLOID .....	10.04.02
MICROCRYSTALLOGRAPHY .....	HELIUM .....	CAPILLARY .....	13.08.06
MICROCRYSTALS .....	AMYLOID .....	PRION .....	13.08.01
MICRODIFFRACTION .....	SYNCHROTRON .....	MICROCRYSTAL .....	13.08.04
MICROFLUIDICS .....	MESOPHASE .....	MEMBRANE PROTEINS .....	01.02.04
MICROFOCUS BEAMLINE .....	AMYLOID .....	PEPTIDE STRUCTURES .....	13.01.03
MICROFOCUS BEAMLINE .....	SYNCHROTRON .....	PROTEIN CRYSTALLOGRAPHY .....	13.08.05
MICROFOCUS SOURCE .....	MULTILAYER .....	X-RAY OPTICS .....	03.01.05
MICROGRAVITY .....	HIGH-RESOLUTION .....	TAKA-AMYLASE A .....	SP071
MICROGRAVITY .....	ATOMIC-RESOLUTION .....	COUNTER-DIFFUSION .....	SP064
MICROSCOPE .....	CRYSTAL QUALITY .....	IN-SITU .....	MP084
MICROSCOPE .....	PICTURES .....	ART .....	SP244
MICROSPECTROPHOTOMETRY .....	DOSE LIMIT .....	RADICAL SCAVENGERS .....	13.10.01
MINERALOGY .....	QUANTUM OPTIMIZATION .....	SIMULATED ANNEALING .....	07.01.05
MINERALOGY .....	POWDER DIFFRACTION .....	RELATIVE HUMIDITY .....	05.02.02

# Keyword Index

MINERALOGY/CRYSTALLOGRAPHY.....	EXTREME CONDITIONS .....	HIGH PRESSURE/TEMPERATURE .....	05.02.01
MINI-BEAM.....	SIGNAL-TO-NOISE .....	MICRO-CRYSTALS .....	13.08.03
MIXED CRYSTALS.....	CRYSTAL ENGINEERING.....	COMPOSITE CRYSTALS .....	SP211
MIXED LIGAND COMPLEXES.....	ITACONIC ACID.....	HYDROTHERMAL SYNTHESIS.....	TP217
MLFSOM.....	TRAY GONIOMETER .....	DATA COLLECTION STRATEGY .....	13.01.05
MODELLING.....	CRYSTAL STRUCTURE PREDICTIO.....	POLYMORPHISM .....	AW.01.02
MODULATIONS.....	DIFFUSE SCATTERING .....	ORDER-DISORDER.....	TR.01.11
MOLECULAR ASSEMBLIES.....	NON-BRAGG DIFFRACTION.....	CORRELATED VARIATIONS.....	TR.01.04
MOLECULAR DYNAMICS.....	CRYSTALLOGRAPHIC COMPUTING .....	INTERMOLECULAR INTERACTIONS .....	AW.01.01
MOLECULAR RECOGNITION.....	COCRYSTALLIZATION .....	CRYSTAL ENGINEERING.....	10.01.01
MOLECULAR RECOGNITION.....	COORDINATION POLYMERS.....	CRYSTAL ENGINEERING.....	10.03.02
MOLECULAR RECOGNITION.....	HYDROGEN BONDS .....	CO-CRYSTALS .....	10.03.03
MOLECULAR REPLACEMENT.....	DENSITY BASIN.....	RNA QUADRUPLEX.....	SP246
MONTE CARLO METHOD.....	NUCLEAR/ELECTRON DENSITY DI.....	MAXIMUM ENTROPY METHOD .....	03.02.02
MORPHOLOGY.....	TEMPERATURE RESPONSIVE.....	ENCAPSULANT.....	09.01.03
MOTIF.....	INTERFACE.....	VISUALIZATION.....	SP.01.06
MRNA.....	RIBOSOME.....	TRNA.....	01.08.05
MULTI-SCALE MODELING.....	DIMENSIONALITY REDUCTION.....	PATTERN MATCHING.....	01.05.05
MULTI-SUBUNIT.....	RNA.....	EXOSOME .....	01.08.02
MULTICOPPER.....	OXIDASE.....	CUEO.....	SP109
MULTIDRUG EFFLUX TRANSPORTER.....	MACA.....	MEMBRANE FUSION.....	MP048
MULTILAYER.....	X-RAY OPTICS.....	MICROFOCUS SOURCE.....	03.01.05
MULTILAYER.....	OPTIC.....	BRILLIANCE.....	MP228
MULTILAYER OPTICS.....	SAD PHASING.....	LONG WAVELENGTH.....	MP077
MUTAGENESIS.....	DNA REPLICATION.....	DNA DAMAGE.....	MP019
MUTAGENESIS.....	ALLOSTERIC.....	ANTICOOPERATIVE.....	SP.01.05
MUTATIONS.....	ASPARTATE TRANSCARBAMOYL.....	THERMOSTABILITY .....	TP145
MYCOBACTERIUM TUBERCULOSIS.....	CYSTEINE BIOSYNTHESIS.....	SULFUR TRANSFER.....	SP014
MYOGLOBIN.....	LIGAND DISCRIMINATION.....	HYDROGEN BONDING.....	TP105
NA1-XGE3+Z.....	CLATHRATE II STRUCTURE.....	THERMOELECTRIC MATERIAL.....	TP221
NANO PORES.....	NUCLEATION.....	PROTEIN CRYSTALLIZATION .....	01.02.02
NANOCAPSULE.....	VAULT.....	RIBONUCLEOPROTEIN.....	01.08.03
NANOCATALYSIS.....	GISAXS.....	ANOMALOUS GISAXS.....	09.02.03
NANOCOMPOSITES.....	SAXD.....	BLOCK COPOLYMER .....	13.07.03
NANOCRYSTAL.....	SUPERLATTICE.....	SELF-ASSEMBLY .....	13.07.01
NANOCRYSTALS.....	SELF-ASSEMBLY .....	SURFACTANTS .....	13.07.02
NANOEMULSION.....	RHEO-SANS.....	DISAGGREGATION .....	13.04.03
NANOPARTICLES.....	SELF-ASSEMBLY .....	CALIXARENES .....	13.07.05
NANOPARTILES.....	MAGNETIC STRUCTURE.....		13.07.09
NANOSCALE STRUCTURE.....	DIFFUSE SCATTERING .....	DISORDER.....	TR.01.01
NANOSTRUCTURE.....	DIFFUSE SCATTERING .....	PAIR DISTRIBUTION FUNCTION.....	TR.01.09
NATURAL PRODUCT EXTRACTS.....	A-AMYLASE INHIBITORS.....	INHIBITOR SCREENING.....	TP102
NATURAL PRODUCTS.....	EUDESMANES.....	VERBESINA TURBACENSIS.....	SP191
NE-CAT.....	SYNCHROTRON.....	UNDULATOR.....	TP223
NEEDLE PROTEIN.....	TYPE III SECRETION SYSTEM.....	STRUCTURE.....	SP045
NEGATIVE THERMAL EXPANSION.....	X-RAY POWDER DIFFRACTION.....	NEUTRON DIFFRACTION.....	05.01.05
NERVE AGENTS.....	CARBOXYLESTERASE.....	PROTEIN DESIGN.....	AW.03.05
NEUROPILIN.....	VEGF.....	HEPARIN.....	MP013
NEUTRON.....	MECHANISM.....	ENZYME.....	06.01.01
NEUTRON.....	POWDER.....	INSTRUMENTATION.....	07.01.10
NEUTRON & SYNCHROTRON X-RAYS.....	POWDER DIFFRACTION.....	PEROVSKITE MANGANITES.....	TP188
NEUTRON CONTRAST VARIATION.....	SMALL-ANGLE SCATTERING.....	BIOMOLECULAR COMPLEXES.....	13.03.06
NEUTRON CONTRAST VARIATION.....	SMALL-ANGLE SOLUTION SCATTE.....	PROTEIN CONFORMATION.....	13.03.07
NEUTRON CRYSTALLOGRAPHY.....	ENZYMATIC MECHANISM.....	PROTON.....	06.01.06
NEUTRON DETECTOR.....	LI6Y(BO3)3.....	SCINTILLATOR.....	MP235
NEUTRON DIFFRACTION.....	NEGATIVE THERMAL EXPANSION.....	X-RAY POWDER DIFFRACTION.....	05.01.05
NEUTRON DIFFRACTION.....	PROTEIN.....	HYDROGEN.....	06.01.04
NEUTRON DIFFRACTION.....	PGSE NMR.....	SMALL MOLECULES.....	10.01.05
NEUTRON DIFFRACTION.....	HYDROGEN STORAGE.....	TIME RESOLVED.....	13.04.06
NEUTRON DIFFRACTION.....	HYDROGEN STORAGE.....	CATALYSIS.....	13.06.04
NEUTRON DIFFRACTION.....	SYNCHROTRON X-RAY DIFFRACTI.....	NICKEL HYDROXIDE.....	05.02.05
NEUTRON DIFFRACTION.....	SMALL MOLECULES.....	SINGLE CRYSTAL.....	10.01.10
NEUTRON DIFFRACTION.....	HELIUM.....	HIGH RESOLUTION.....	13.01.02
NEUTRON DIFFRACTION.....	METAL HYDRIDE.....	LINEAR M-H-M BOND.....	MP198
NEUTRON DIFFRACTION.....	SIR PHASING.....	LOW RESOLUTION.....	TP185
NEUTRON LAUE DIFFRACTION.....	HYDROGEN/DEUTERIUM.....	MACROMOLECULAR.....	TP186

# Keyword Index

NEUTRON POWDER DIFFRACTION	LOW-TEMPERATURE CR	DISORDER	10.01.06
NEUTRON PROTEIN CRYSTALLOGRAPHY	JOINT REFINEMENT	ENDOTHAPEPSIN	06.01.07
NEUTRON SCATTERING	SMALL-ANGLE SCATTERING	USER FACILITY	13.03.08
NEW STRUCTURE	ASPARTATE TRANSCARBAMOYL	THERMOPHILIC	TP153
NICKEL HYDROXIDE	NEUTRON DIFFRACTION	SYNCHROTRON X-RAY DIFFRACTION	05.02.05
NITRIC OXIDE	S-NITROSOTHIOLS		SP242
NITRIC OXIDE	NITROPHORIN	S-NITROSCYSTEINE	TP117
NITRIC OXIDE RECEPTOR	HEME SENSOR	SOLUBLE GUANYLYL CYCLASE	03.01.02
NITROPHORIN	S-NITROSCYSTEINE	NITRIC OXIDE	TP117
NKX2.5	DNA	HOMEODOMAIN	MP040
NMR	STRUCTURE	DATA DEPOSITION	WK.02.03
NMR CRYSTALLOGRAPHY	COMPOSITE CRYSTAL	INCLUSION COMPOUND	10.02.06
NMR STRUCTURAL DATA	NMR TASK FORCE	STANDARDS	WK.02.02
NMR TASK FORCE	STANDARDS	NMR STRUCTURAL DATA	WK.02.02
NON-AMBIENT CONDITIONS	IN SITU XRPD	IN SITU RAMAN SPECTROSCOPY	05.01.02
NON-BRAGG DIFFRACTION	CORRELATED VARIATIONS	MOLECULAR ASSEMBLIES	TR.01.04
NON-MEROHEDRAL	DATA PROCESSING	TWIN	03.02.01
NON-MEROHEDRAL TWIN	PSEUDO-MEROHEDRAL TWIN	CONVERSION BY T CONTROL	SP201
NUCLEAR	RECEPTORS	ORPHAN	TP111
NUCLEAR RECEPTOR	EVOLUTION	STRUCTURE	TP108
NUCLEAR/ELECTRON DENSITY DISTRIBUTION	MAXIMUM ENTROPY METHOD	MONTE CARLO METHOD	03.02.02
NUCLEATION	PROTEIN CRYSTALLIZATION	NANO PORES	01.02.02
NUCLEATION	BIFE03	GISAXS	13.07.07
NUCLEIC ACID CRYSTALLOGRAPHY	PHASING AND CRYSTALLIZATION	SELENIUM DERIVATIZATION	TP171
NUCLEOCAPSID	VIRUS REPLICATION	NUCLEOPROTEIN-RNA	13.05.03
NUCLEOPROTEIN	INFLUENZA	VIRUS	13.05.02
NUCLEOPROTEIN-RNA	NUCLEOCAPSID	VIRUS REPLICATION	13.05.03
NUCLEOSIDE ANALOGS	DRUG TARGET	ADENOSINE KINASE	MP033
O-H...O RINGS	ETTER'S RULE	INTRAMOLECULAR HYDROGEN BO	MP197
OMINELITE	GEOMETRIC EFFECTS	GRANDIDERITE	05.02.04
OPTIC	BRILLIANCE	MULTILAYER	MP228
OPTIMIZATION	VAPOR PRESSURE CONTROL	SCREENING	SP070
ORDER-DISORDER	MODULATIONS	DIFFUSE SCATTERING	TR.01.11
ORIENTATING METALLOMACROCYCLE	ASSEMBLY	STRUCTURE	SP216
ORIGIN OF LIFE	RIBOZYME	RNA	01.01.03
ORPHAN	NUCLEAR	RECEPTORS	TP111
OUTER MEMBRANE PROTEIN	FATTY ACID TRANSPORT	CRYSTAL STRUCTURE	SP085
OUTER MEMBRANE PROTEIN	XENOBIOTICS	TRANSPORTER	01.04.01
OXIDASE	CUEO	MULTICOPPER	SP109
OXIME-AND-AMIDE LIGAND	SMALL CRYSTALLOGRAPHY	CO(III) COMPLEXES	MP196
P1P6 SUBSTRATE	HIV-1	PROTEASE	TP113
P450 INHIBITORS	FLAVONE	SMALL MOLECULE	MP192
PAIR DISTRIBUTION FUNCTION	STRUCTURE DETERMINATION		07.01.12
PAIR DISTRIBUTION FUNCTION	NANOSTRUCTURE	DIFFUSE SCATTERING	TR.01.09
PARALLEL	SHELXD	HEAVY-ATOM SEARCH	TP151
PARKINSON'S DISEASE	-SYNUCLEIN	INTRINSICALLY UNFOLDED PROTEIN	MP030
PARVOVIRIDAE	ADENO-ASSOCIATED VIRUS	GENE THERAPY	SP039
PAS PROTEINS			SP063
PAS SENSOR WITH C-TYPE HEME	CHEMOTAXIS	DOMAIN SWAP	TP115
PATTERN MATCHING	MULTI-SCALE MODELING	DIMENSIONALITY REDUCTION	01.05.05
PATTERSON DEMONSTRATION	TEACHING GADGETS	DIFFRACTION DEMONSTRATION	13.09.02
PDF (PAIR DISTRIBUTION FUNCTION)	URANIUM ALLOY	RIETVELD	TP181
PDT DOMAIN	ACT DOMAIN	PREPHENATE DEHYDRATASE	SP041
PENTACENE AND ANTHRACENE	TCNQ CHARGE STATES	STRUCTURE PRECISION	AW.02.01
PEPTIDE STRUCTURES	MICROFOCUS BEAMLINE	AMYLOID	13.01.03
PEPTIDOGLYCAN RECOGNITION PROTEIN	BACTERICIDAL MECHANISM	INNATE IMMUNITY	TP119
PEROVSKITE MANGANITES	NEUTRON & SYNCHROTRON X-RAY	POWDER DIFFRACTION	TP188
PF04013	A/BETA KNOT	UNKNOWN FUNCTION	MP247
PFAM	STRUCTURAL GENOMICS	FUNCTION	TP128
PGIS	MAD	PROSTACYCLIN SYNTHASE	SP036
PGSE NMR	SMALL MOLECULES	NEUTRON DIFFRACTION	10.01.05
PHARMACEUTICAL	DASATINIB	PROCESS CONTROL	04.01.05
PHARMACEUTICAL COCRYSTALS	CAFFEINE	CARBOXYLIC ACIDS	TP220
PHARMACEUTICALS	HIRSHFELD SURFACES	POLYMORPHISM	10.04.06
PHARMACOLOGICAL ACTIVITY	X-RAY DIFFRACTION	ENAMINONES	SP200
PHARMACOLOGICAL TESTS	X-RAY STRUCTURE	CHALCONES	10.01.09

# Keyword Index

PHASE RELATIONSHIPS.....	TEACHING AIDS.....	DIRECT METHODS.....	13.09.05
PHASE TRANSFORMATION.....	ALLOY.....		05.01.01
PHASE TRANSFORMATION.....	INTERGROWTH.....	SYMMETRY.....	10.02.02
PHASE TRANSITION.....	PORPHYRIN.....		03.02.05
PHASE TRANSITION.....	ELECTRON DENSITY.....	METASTABLE STATES.....	05.01.03
PHASE TRANSITION.....	AB INITIO CALCULATIONS.....	HIGH PRESSURE.....	AW.01.04
PHASE TRANSITION.....			AW.02.03
PHASE TRANSITIONS.....	POWDER DIFFRACTION.....	POLYMORPHISM.....	AW.02.04
PHASING.....	LONG WAVELENGTH.....	RADIATION DAMAGE.....	01.03.05
PHASING.....	AB INITIO.....	STRUCTURE PREDICTION.....	01.07.06
PHASING.....	ANOMALOUS SCATTERING.....	SHELX.....	WK.01.10
PHASING AND CRYSTALLIZATION.....	SELENIUM DERIVATIZATION.....	NUCLEIC ACID CRYSTALLOGRAPHY.....	TP171
PHENIX.....	JOINT X-RAY AND NEUTRON REFI.....	ALDOSE REDUCTASE.....	06.01.02
PHENIX.....	REFINEMENT.....	TWINNING.....	TP150
PHENIX.....	REFINEMENT.....	TWINNING.....	01.07.07
PHENOLATE.....	STRUCTURE.....	COMPARISON.....	SP.01.03
PHENYLACETIC ACID DEGRADATION.....	AROMATIC COMPOUND CATABOL.....	CTR FOR STRUCTURAL GENOMICS.....	SP248
PEROMONE.....	INHIBITOR.....	RECEPTOR.....	TP098
PHOSPHOLIPASE.....	CRYSTALLIZATION.....	METAL DEPENDENT.....	SP076
PHONON.....	PROTEIN CRYSTALLOGRAPHY.....	COLLECTIVE MOTION.....	TR.01.05
PHOP.....	RESPONSE REGULATOR.....	DNA-BINDING DOMAIN.....	TP116
PHOSPHATASE.....	PHYTASE.....	INOSITOL.....	SP050
PHOSPHOLIPASEA2.....	PPAFAH.....	LDL-BOUND.....	TP086
PHOTOACTIVE YELLOW PROTEIN.....	HYDROGEN BOND.....		06.01.03
PHOTOCHEMISTRY.....	HOST-GUEST COMPLEXES.....	HOMOGENEOUS REACTIONS.....	AW.03.09
PHOTOLYSIS.....	AZIDE.....	REACTION.....	10.01.02
PHOTON-COUNTING.....	DETECTOR.....	AXIOM.....	MP236
PHOTOTROPIN1.....	LOV2 DOMAIN.....	STRUCTURAL CHANGES.....	TP142
PHYTASE.....	INOSITOL.....	PHOSPHATASE.....	SP050
PICTURES.....	ART.....	MICROSCOPE.....	SP244
PLANT DISEASE RESISTANCE.....	CO2+ SAD PHASING.....	AVIRULENCE PROTEIN.....	SP052
PLATE.....	VAPOUR.....	DIFFUSION.....	MP177
PLATON.....	SERVICE CRYSTALLOGRAPHY.....	COMPUTATIONAL TOOLS.....	10.02.04
PLATON.....	VALIDATION.....	CHECKCIF.....	WK.01.07
PNU-142721.....	ANTI-HIV.....	PREGANE X RECEPTOR.....	SP060
POINT SPREAD.....	DATA CORRECTION.....	CCD DETECTORS.....	MP237
POLAR CRYSTAL.....	DIPOLE ALIGNMENT.....	CRYSTAL ENGINEERING.....	10.03.12
POLARIZED NEUTRON DIFFRACTION.....	SPINEL STRUCTURE.....	SPIN DENSITY.....	TP183
POLARIZED SINGLE CRYSTAL NEUTRON.....	SPINEL.....	MAGNETIC STRUCTURE.....	TP184
POLY-PROLINE.....	DNA.....	TREX1.....	SP062
POLYAMINE OXIDASE.....	CRYSTAL STRUCTURE.....	FMS1.....	SP103
POLYHEDRIN.....	SR-INSTRUMENTATION.....	MICRO-CRYSTALS.....	13.08.02
POLYKETIDE.....	TETRACENOMYCIN.....	AROMATASE/CYCLASE.....	MP057
POLYMER THIN FILMS.....	BLOCK COPOLYMER.....	LIQUID CRYSTAL.....	09.02.05
POLYMERASE.....	FINGER.....	Y-FAMILY.....	SP096
POLYMORPH.....	PRECISION.....		TP173
POLYMORPH MOLECULAR COMPLEXES.....	SINGLE CRYSTAL NEUTRON DIFF.....	PROTON DISORDER AND TRANSFER.....	10.01.04
POLYMORPHIC SYSTEM.....	REVERSIBLE SOLID-SOLID PHASE.....	COMMENSURATELY MODULATED.....	10.04.01
POLYMORPHISM.....	POWDER DIFFRACTION.....	STRUCTURE SOLUTION.....	07.01.08
POLYMORPHISM.....	PHARMACEUTICALS.....	HIRSHFELD SURFACES.....	10.04.06
POLYMORPHISM.....	DIFFUSE SCATTERING.....	DISORDER.....	SP168
POLYMORPHISM.....	MODELLING.....	CRYSTAL STRUCTURE PREDICTION.....	AW.01.02
POLYMORPHISM.....	PHASE TRANSITIONS.....	POWDER DIFFRACTION.....	AW.02.04
POROSITY.....	GAS SORPTION.....	CRYSTAL ENGINEERING.....	10.03.10
POROUS.....	COMPLEX.....	FRAMEWORK.....	10.03.09
PORPHYRIN.....	PHASE TRANSITION.....		03.02.05
PORPHYRIN ASSEMBLIES.....	FRAMEWORK SOLIDS.....	COORDINATION POLYMERS.....	10.01.03
POST-TRANSLATIONAL MODIFICATION.....	X-RAY CRYSTALLOGRAHPY.....	TRIMETHYLTRANSFERASE.....	01.01.07
POST-TRANSLATIONAL MODIFICATION.....	X-RAY CRYSTALLOGRAHPY.....	TRIMETHYLTRANSFERASE.....	SP003
POWDER.....	SYNCHROTRON.....	MAGNETISM.....	07.01.06
POWDER.....	TRIMELLITATE.....	AB INITIO.....	07.01.04
POWDER.....	INSTRUMENTATION.....	NEUTRON.....	07.01.10
POWDER DIFFRACTION.....	STRUCTURE SOLUTION.....	POLYMORPHISM.....	07.01.08
POWDER DIFFRACTION.....	DENSITY FUNCTIONS.....	MAXIMUM ENTROPY.....	07.01.03
POWDER DIFFRACTION.....	PEROVSKITE MANGANITES.....	NEUTRON & SYNCHROTRON X-RAY.....	TP188
POWDER DIFFRACTION.....	RELATIVE HUMIDITY.....	MINERALOGY.....	05.02.02

# Keyword Index

POWDER DIFFRACTION.....	STRUCTURE SOLUTION.....	GRID COMPUTING.....	07.01.02
POWDER DIFFRACTION.....	PROTEIN.....	RIETVELD REFINEMENT.....	07.01.09
POWDER DIFFRACTION.....	MAGNETOSTRUCTURAL TRANSITI.....	IN-SITU EXPERIMENTS.....	13.04.05
POWDER DIFFRACTION.....	RIETVELD METHOD.....	HYDROGEN STORAGE.....	13.06.06
POWDER DIFFRACTION.....	POLYMORPHISM.....	PHASE TRANSITIONS.....	AW.02.04
POWDER DIFFRACTION.....	VARIABLE TEMPERATURE.....	HIGH PRESSURE.....	AW.03.01
POWDER X-RAY DIFFRACTION.....	RIETVELD METHOD.....	METAL HYDRIDES.....	13.06.05
POWDER XRD.....	CRYSTAL ENGINEERING.....	SUPRAMOLECULAR CHEMISTRY.....	10.03.06
POWDERS.....	METHODS.....	PROGRAMS.....	07.01.01
PPAFAH.....	LDL-BOUND.....	PHOSPHOLIPASEA2.....	TP086
PRECIPITANT.....	COUNTER DIFFUSION.....	DIFFUSION COEFFICIENT.....	SP065
PRECIPITATION.....	HIGH-TEMPERATURE.....	STEELS.....	09.01.05
PRECISION.....	POLYMORPH.....		TP173
PRECRYSTALLIZATION SCREENING.....	MEMBRANE PROTEIN.....	GREEN FLUORESCENT PROTEIN.....	01.02.01
PREGANE X RECEPTOR.....	PNU-142721.....	ANTI-HIV.....	SP060
PREPHENATE DEHYDRATASE.....	PDT DOMAIN.....	ACT DOMAIN.....	SP041
PRIMOSOME.....	REPLICATION.....	RECOMBINATION.....	TP249
PRION.....	MICROCRYSTALS.....	AMYLOID.....	13.08.01
PRMT.....	METHYLTRANSFERASE.....	CARM1.....	MP243
PROBLEM STRUCTURES.....	TWIN-DISORDER.....	PSEUDO-SYMMETRY.....	10.01.08
PROCEDURES.....	SMALL MOLECULE.....	SCIENCE.....	10.02.01
PROCESS CONTROL.....	PHARMACEUTICAL.....	DASATINIB.....	04.01.05
PROGRAMS.....	POWDERS.....	METHODS.....	07.01.01
PROLYL HYDROXYLASE.....	HYPOXIA INDUCIBLE FACTOR.....	2-OXOGLUTARATE.....	SP026
PROPROTEIN CONVERTASE.....	FURIN.....	PROTEASE.....	TP143
PROSTACYCLIN SYNTHASE.....	PGIS.....	MAD.....	SP036
PROTEASE.....	PIP6 SUBSTRATE.....	HIV-1.....	TP113
PROTEASE.....	PROPROTEIN CONVERTASE.....	FURIN.....	TP143
PROTEASE INHIBITOR.....	PROTEIN-PROTEIN COMPLEX.....	SERINE PROTEASE.....	SP139
PROTEASE INHIBITORS.....	HIV PROTEASE.....	DRUG DESIGN.....	TP112
PROTEASOME.....	VINYL-SULFONE INHIBITOR.....	PROTEIN DEGRADATION.....	SP001
PROTEASOME ACTIVATOR BLM10.....			TP097
PROTEIN.....	HYDROGEN.....	NEUTRON DIFFRACTION.....	06.01.04
PROTEIN.....	CRYSTALLOGRAPHY.....	INDUSTRY.....	04.01.04
PROTEIN.....	RIETVELD REFINEMENT.....	POWDER DIFFRACTION.....	07.01.09
PROTEIN.....	CRYSTALLOGRAPHY.....	BEAMLINE.....	MP229
PROTEIN CONFORMATION.....	NEUTRON CONTRAST VARIATION.....	SM-ANGLE SOLUTION SCATTERING.....	13.03.07
PROTEIN CRYSTAL.....	CRYSTALLOGRAPHY.....	HIGH-THROUGHPUT SCREENING.....	03.01.03
PROTEIN CRYSTALLIZATION.....	STRUCTURAL GENOMICS.....		01.02.05
PROTEIN CRYSTALLIZATION.....	NANO PORES.....	NUCLEATION.....	01.02.02
PROTEIN CRYSTALLIZATION DEVICE.....			SP072
PROTEIN CRYSTALLOGRAPHY.....	LIGANDS.....	VALIDATIO.....	01.05.01
PROTEIN CRYSTALLOGRAPHY.....	CMOS FLAT PANEL DETECTOR.....	CONTINUOUS ROTATION METHOD.....	13.02.03
PROTEIN CRYSTALLOGRAPHY.....	MICROFOCUS BEAMLINE.....	SYNCHROTRON.....	13.08.05
PROTEIN CRYSTALLOGRAPHY.....			SP104
PROTEIN CRYSTALLOGRAPHY.....	COLLECTIVE MOTION.....	PHONON.....	TR.01.05
PROTEIN CRYSTALS.....	DRUG DISCOVERY.....	LIQUID HANDLING.....	MP179
PROTEIN DATA BANK.....	DATA MINING.....	CAMBRIDGE STRUCTURAL DATABA.....	01.05.03
PROTEIN DEGRADATION.....	PROTEASOME.....	VINYL-SULFONE INHIBITOR.....	SP001
PROTEIN DESIGN.....	NERVE AGENTS.....	CARBOXYLESTERASE.....	AW.03.05
PROTEIN DEUTERATION.....	HALOALKANE DEHALOGENASE.....	CATALYTIC MECHANISM.....	SP187
PROTEIN DISORDER.....	DIFFUSE SCATTER.....	CORRELATED MOTION.....	MP170
PROTEIN DYNAMICS.....	ENSEMBLE REFINEMENT.....	REFINEMENT METHODS.....	01.07.04
PROTEIN DYNAMICS.....	CRYSTAL DISORDER.....	DIFFUSE SCATTERING.....	TR.01.03
PROTEIN EXPRESSION.....	GENE SYNTHESIS.....	WORKFLOW.....	TP094
PROTEIN FOLDING.....	CH.....		TP088
PROTEIN NUCLEAR MAGNETIC RESONAN.....	STRUCTURE QUALITY ASSESSME.....	STRUCTURAL GENOMICS.....	WK.02.05
PROTEIN PHOSPHATASE.....	INTRINSIC DISORDER.....	INHIBITOR PROTEIN.....	MP056
PROTEIN PHOSPHATASES.....	ENOLASES AMIDOHYDROLASES.....	STRUCTURAL GENOMICS.....	01.06.03
PROTEIN SOLUTION STRUCTURES.....	SAXS.....		01.07.02
PROTEIN STRUCTURE.....	DATABASE INTEGRATION.....	UNIFORM CURATION.....	TP087
PROTEIN STRUCTURE.....	SANS.....	SAXS.....	MP157
PROTEIN STRUCTURE UNIVERSE.....	STRUCTURAL GENOMICS.....	STRUCTURE-BASED FUNCTION.....	01.06.01
PROTEIN SURFACE.....	FUNCTION PREDICTION.....	STRUCTURAL GENOMICS.....	01.06.07
PROTEIN SYNTHESIS.....	TRYPTOPHANYL-TRNA SYNTHETA.....	DUAL CONFORMATION.....	MP049
PROTEIN-LIGAND COMPLEX.....	DRUG DESIGN.....	ALDOSE REDUCTASE.....	TP110

# Keyword Index

PROTEIN-PROTEIN COMPLEX.....	DNA MTASE.....		01.01.08
PROTEIN-PROTEIN COMPLEX.....	SERINE PROTEASE.....	PROTEASE INHIBITOR.....	SP139
PROTON.....	NEUTRON CRYSTALLOGRAPHY.....	ENZYMATIC MECHANISM.....	06.01.06
PROTON DISORDER AND TRANSFER.....	POLYMORPH MOLECULAR COMPL.....	SINGLE CRYSTAL NEUTRON DIFFRA.....	10.01.04
PROTON TRANSFER.....	KINETICS.....	CARBONIC ANHYDRASE.....	TP132
PROTONATED WATER.....	CRYSTAL PACKING.....	HYPERACID SALT.....	10.01.07
PRUSSIAN BLUE.....	MAGNET.....		10.01.11
PSEUDO-MEROHEDRAL TWIN.....	CONVERSION BY T CONTROL.....	NON-MEROHEDRAL TWIN.....	SP201
PSEUDO-SYMMETRY.....	PROBLEM STRUCTURES.....	TWIN-DISORDER.....	10.01.08
PSEUDO-SYMMETRY.....	DIFFUSE SCATTERING.....	DISORDER.....	MP169
PSI.....	DETERGENT.....	SAXS.....	MP161
PSI-2 SPECIALIZED CENTER.....	CRYSTALLIZATION.....	SURFACE ENTROPY REDUCTION.....	SP074
PUBLICATION.....	DATA VALIDATION.....	CIF.....	WK.01.06
PUBLICATION STANDARDS.....	STRUCTURAL BIOLOGY.....		WK.02.01
PUF.....	RNA.....	PUMILIO.....	MP061
PUMILIO.....	PUF.....	RNA.....	MP061
PURIFICATION TAG.....	STRUCTURAL GENOMICS.....	CRYSTAL LATTICE INTERACTIONS.....	01.02.06
PYRAZOLE.....	SUPRAMOLECULAR.....	BIS-CHELATE.....	AW.03.03
PYRIDINE NUCLEOTIDES.....	COENZYME A-DISULFIDE REDUCT ..	COENZYME A.....	AW.03.07
PYRUVATE DEHYDROGENASE.....	THIAMIN DIPHOSPHATE.....	VARIANT.....	TP134
PYRUVATE-FORMATE LYASE.....	ACTIVATING ENZYME.....	S-ADENOSYLMETHIONINE RADICAL.....	SP017
QUALITY CRITERIA.....	CRYSTALLOGRAPHIC PUBLISHING.....	ACTA CRYSTALLOGRAPHICA.....	WK.02.04
QUANTUM OPTIMIZATION.....	SIMULATED ANNEALING.....	MINERALOGY.....	07.01.05
QUINAZOLINES.....	DIHYDROFOLATE REDUCTASE.....		TP120
R.M.S.D.....	DOMAINS.....	LEAST-SQUARES SUPERPOSITION.....	TP089
RADIATION DAMAGE.....	PHASING.....	LONG WAVELENGTH.....	01.03.05
RADIATION DAMAGE.....	UV.....	RIP.....	13.01.04
RADIATION DAMAGE.....	SYNCHROTON.....	TEMPERATURE.....	13.10.03
RADIATION DAMAGE.....	SCAVENGERS.....	CRYSTAL PREPARATION.....	13.10.05
RADIATION DAMAGE.....	FREE RADICAL SCAVENGERS.....	RADIATION PROTECTION.....	13.10.06
RADIATION DAMAGE.....	MAD AND SAD PHASING.....	MACROMOLECULAR CR.....	13.10.07
RADIATION PROTECTION.....	RADIATION DAMAGE.....	FREE RADICAL SCAVENGERS.....	13.10.06
RADICAL SCAVENGERS.....	MICROSPECTROPHOTOMETRY.....	DOSE LIMIT.....	13.10.01
RAF KINASE INHIBITOR PROTEIN.....	STRUCTURAL GENOMICS.....	FUNCTIONAL MOTIF.....	TP124
RASMOL.....	IMGCIF.....	MAPS.....	TP174
RATIONAL DESIGN.....	HOST SPECIFICITY.....		MP167
REACTION.....	PHOTOLYSIS.....	AZIDE.....	10.01.02
RECEPTOR.....	PEROMONE.....	INHIBITOR.....	TP098
RECEPTOR TYROSINE KINASE.....	EPHRIN.....		SP025
RECEPTOR-LIGAND INTERACTION.....	REELIN.....	BRAIN DEVELOPMENT.....	TP146
RECEPTORS.....	ORPHAN.....	NUCLEAR.....	TP111
RECIPROCAL.....	DIFFUSE.....	VISUALIZATION.....	TR.01.10
RECIPROCAL SPACE.....	VISUALIZATION.....	SOFTWARE.....	13.09.03
RECOMBINATION.....	PRIMOSOME.....	REPLICATION.....	TP249
RED.....	DOCKING.....	CONGO.....	TP148
REDUCTASE.....	ISOPRENOIDS.....	BACTERIAL.....	SP011
REDUNDANT DATA-BASE.....	STRUCTURAL VARIATION.....	FUNCTIONAL ASSOCIATION.....	TP090
REELIN.....	BRAIN DEVELOPMENT.....	RECEPTOR-LIGAND INTERACTION.....	TP146
REFINEMENT.....	TWINNING.....	PHENIX.....	01.07.07
REFINEMENT.....	TWINNING.....	PHENIX.....	TP150
REFINEMENT.....	DISORDER.....	SHELXL.....	WK.01.02
REFINEMENT.....	TWIN.....	SHELXL.....	WK.01.03
REFINEMENT.....	ESTIMATED STANDARD DEVIATIO.....	ATOM RESOLUTION.....	WK.01.04
REFINEMENT.....	ESTIMATED STANDARD DEVIATIO.....	ATOM RESOLUTION.....	WK.01.09
REFINEMENT.....	TLS.....		01.07.05
REFINEMENT.....	TWINNING.....		10.02.03
REFINEMENT.....	RESTRAINTS.....	HYDROGEN.....	TP152
REFINEMENT METHODS.....	PROTEIN DYNAMICS.....	ENSEMBLE REFINEMENT.....	01.07.04
REINECKES SALT.....	DIRECT SYNTHESIS.....	HETEROMETALLIC COMPLEXES.....	TP203
REINFORCING FILLERS.....	SMALL-ANGLE SCATTERING.....		09.01.07
RELATIONSHIP.....	STRUCTURE.....	SEQUENCE.....	TP095
RELATIVE HUMIDITY.....	MINERALOGY.....	POWDER DIFFRACTION.....	05.02.02
RELATIVE HUMIDITY.....	DIFFRACTION IMPROVEMENT.....	CRYSTAL PREPARATION.....	MP082
RELAXATION.....	SANS.....	BRANCHED.....	13.04.02
REMOTE.....	CRYSTALLOGRAPHY.....	SYNCHROTRON.....	MP231
REMOTE ACCESS.....	UNDERGRADUATE.....	TEACHING AND EDUCATION.....	SP.01.01

# Keyword Index

REMOTE ACCESS AND CONTROL.....	VIRTUAL INSTRUMENT.....	WEB SERVICES.....	03.01.07
REMOTE DATA COLLECTION.....	SYNCHROTRON.....	MAIL-IN CRYSTALLOGRAPHY.....	MP232
REPLICATION.....	RECOMBINATION.....	PRIMOSOME.....	TP249
RESONANT ANOMALOUS X-RAY REFLECTI...	SURFACE AND INTERFACE.....	ELEMENT-SPECIFIC SUBSTRUCTURE...	09.02.02
RESONANT SCATTERING.....	ABSOLUTE STRUCTURE.....	ANOMALOUS DIFFRACTION.....	10.02.07
RESONANT SCATTERING.....	MAGNETIC SCATTERING.....	SOFT X-RAYS.....	09.03.01
RESPONSE REGULATOR.....	DNA-BINDING DOMAIN.....	PHOP.....	TP116
RESTRAINTS.....	HYDROGEN.....	REFINEMENT.....	TP152
RETROSYNTHETIC DIAMOND GROWTH.....	DIAMONDS IN HYPERCRYTICAL.....	DIAMONDS AQUEOUS SOLUTIONS.....	TP180
REVERSIBLE SOLID-SOLID PHASE TRANSIT..	COMMENSURATELY MODULATED.....	POLYMORPHIC SYSTEM.....	10.04.01
RGD LOOP.....	DISINTEGRIN.....	ACOSTATIN.....	01.08.04
RHEO-SANS.....	DISAGGREGATION.....	NANOEMULSION.....	13.04.03
RHOMBOID PROTEASE.....	MEMBRANE PROTEIN.....	INTRAMEMBRANE PROTEOLYSIS.....	01.01.05
RIBONUCLEASE III.....	DSRNA CLEAVAGE.....	MECHANISM.....	MP021
RIBONUCLEOPROTEIN.....	NANOCAPSULE.....	VAULT.....	01.08.03
RIBOSOME.....	TRNA.....	MRNA.....	01.08.05
RIBOSWITCH.....	METAL IONS.....	RNA STRUCTURE.....	MP059
RIBOZYME.....	RNA.....	ORIGIN OF LIFE.....	01.01.03
RIEMANN-FINSLER GEOMETRY.....	HIGHER-ORDER THERMAL MOTIO...	CRYSTALLOGRAPHIC ORBIFOLDS.....	03.02.03
RIETVELD.....	PAIR DISTRIBUTION FUNCTION.....	URANIUM ALLOY.....	TP181
RIETVELD METHOD.....	METAL HYDRIDES.....	POWDER X-RAY DIFFRACTION.....	13.06.05
RIETVELD METHOD.....	HYDROGEN STORAGE.....	POWDER DIFFRACTION.....	13.06.06
RIETVELD REFINEMENT.....	POWDER DIFFRACTION.....	PROTEIN.....	07.01.09
RIP.....	RADIATION DAMAGE.....	UV.....	13.01.04
RNA.....	IRP1.....	COMPLEX.....	01.01.01
RNA.....	ORIGIN OF LIFE.....	RIBOZYME.....	01.01.03
RNA.....	EXOSOME.....	MULTI-SUBUNIT.....	01.08.02
RNA.....	PUMILIO.....	PUF.....	MP061
RNA POLYMERASE II.....	LARGE PROTEIN.....	TRANSCRIPTION.....	13.01.01
RNA PROCESSING.....	X-RAY STRUCTURE.....	ARCHAEAL EXOSOME.....	TP118
RNA QUADRUPLEX.....	MOLECULAR REPLACEMENT.....	DENSITY BASIN.....	SP246
RNA STRUCTURE.....	INTERNAL RIBOSOME ENTRY SITE...	VIRAL RNA.....	13.05.01
RNA STRUCTURE.....	RIBOSWITCH.....	METAL IONS.....	MP059
ROBOTICS.....	SYNCHROTRON.....	AUTOMATION.....	TP222
ROTATION.....	SUPRAMOLECULAR.....	DYNAMICS.....	10.03.07
ROTHMUND-THOMSON SYNDROME.....	HRECQL4.....	DOUBLE RING DNA HELICASE.....	SP127
S-ADENOSYLMETHIONINE RADICAL.....	PYRUVATE-FORMATE LYASE.....	ACTIVATING ENZYME.....	SP017
S-NITROSCYSTEINE.....	NITRIC OXIDE.....	NITROPHORIN.....	TP117
S-NITROSOTHIOLS.....	NITRIC OXIDE.....		SP242
SAD.....	SULFUR SAD PHASING.....	CHROMIUM RADIATION.....	01.03.04
SAD.....	BOVINE.....	LIPOYL-AMP.....	MP034
SAD METHOD.....	CRYSTAL MOUNTING.....	LONGER WAVELENGTH.....	01.03.02
SAD PHASING.....	HIGH PRESSURE CRYOCOOLING.....	CAPILLARY CRYOPROTECTION.....	13.01.06
SAD PHASING.....	LONG WAVELENGTH.....	MULTILAYER OPTICS.....	MP077
SALICYLIC ACID-BINDING PROTEIN.....	2,3-DIOXYGENASE.....	UBIQUITIN-LIKE PROTEIN.....	01.06.06
SAMPLE HEATING.....	SYNCHROTRON.....	THERMAL IMAGING.....	13.10.02
SANS.....	BRANCHED.....	RELAXATION.....	13.04.02
SANS.....	THERMO-SENSITIVE COMB LIKE P...	CONFORMATION.....	13.07.04
SANS.....	SAXS.....	PROTEIN STRUCTURE.....	MP157
SAXD.....	BLOCK COPOLYMER.....	NANOCOMPOSITES.....	13.07.03
SAXS.....	PROTEIN SOLUTION STRUCTURES.....		01.07.02
SAXS.....	BIOMOLECULES.....	LOW RESOLUTION STRUCTURE.....	13.03.01
SAXS.....	MEMBRANE PROTEINS.....	DETERGENT MICELLES.....	13.03.03
SAXS.....	PROTEIN STRUCTURE.....	SANS.....	MP157
SAXS.....	PSI.....	DETERGENT.....	MP161
SAXS.....	LACI REPRESSOR.....	ALLOSTERICAL REGULATION.....	MP250
SBDD.....	HSP90.....	FRAGMENTS.....	04.01.02
SCAVENGERS.....	CRYSTAL PREPARATION.....	RADIATION DAMAGE.....	13.10.05
SCHIFF BASE LIGAND.....	TETRANUCLEAR CLUSTER.....	GRID STRUCTURE.....	TP205
SCHISTOSOMIASIS.....	ENZYME INHIBITORS.....	TROPICAL DISEASES.....	SP091
SCIENCE.....	PROCEDURES.....	SMALL MOLECULE.....	10.02.01
SCINTILLATOR.....	NEUTRON DETECTOR.....	Li6Y(BO3)3.....	MP235
SCREENING.....	OPTIMIZATION.....	VAPOR PRESSURE CONTROL.....	SP070
SCRIPTING.....	LANGUAGE.....	VISUALIZATION.....	TP172
SECRETORY PATHWAY.....	GLYCOSYLTRANSFERASE.....	MAMMALIAN EXPRESSION.....	SP038
SECSG.....	STRUCTURAL GENOMICS.....	ATP-BINDING PROTEIN.....	MP044

# Keyword Index

SELENIUM DERIVATIZATION.....	NUCLEIC ACID CR.....	PHASING AND CRYSTALLIZATION.....	TP171
SELF ASSEMBLY.....	SUPRAMOLECULAR STRUCTURE.....	AMYLOID CONGENERS.....	MP162
SELF-ASSEMBLY.....	SURFACTANTS.....	NANOCRYSTALS.....	13.07.02
SELF-ASSEMBLY.....	STRUCTURE.....	COMPARISON.....	TP202
SELF-ASSEMBLY.....	NANOCRYSTAL.....	SUPERLATTICE.....	13.07.01
SELF-ASSEMBLY.....	CALIXARENES.....	NANOPARTICLES.....	13.07.05
SELF-ORGANIZED GROWTH.....	CO NANOSTRUCTURES.....	GISAXS.....	09.02.04
SENSITIVITY.....	BONSE-HART TECHNIQUE.....	THEORETICAL LIMIT.....	09.01.02
SEQUENCE.....	RELATIONSHIP.....	STRUCTURE.....	TP095
SERINE PROTEASE.....	PROTEASE INHIBITOR.....	PROTEIN-PROTEIN COMPLEX.....	SP139
SERVICE CRYSTALLOGRAPHY.....	COMPUTATIONAL TOOLS.....	PLATON.....	10.02.04
SEVRER TOPOLOGY AND PARAMETER.....	GEOMETRIC PARAMETERS.....	HETEROMOLECULES.....	03.01.04
SGNH HYDROLASE.....			04.01.07
SHAPE SELECTIVE SYNTHESIS.....	CRYSTALLIZATION.....	METASTABLE PHASES.....	10.03.04
SHELX.....	COMPUTING.....	CR STRUCTURE DETERMINATION.....	WK.01.01
SHELX.....	COMPUTING.....	CR STRUCTURE DETERMINATION.....	WK.01.08
SHELX.....	PHASING.....	ANOMALOUS SCATTERING.....	WK.01.10
SHELX.....	COMPUTING.....	CR STRUCTURE DETERMINATION.....	WK.01.11
SHELXD.....	HEAVY-ATOM SEARCH.....	PARALLEL.....	TP151
SHELXL.....	REFINEMENT.....	DISORDER.....	WK.01.02
SHELXL.....	REFINEMENT.....	TWIN.....	WK.01.03
SHELXL.....	COOT.....	INTERFACES.....	WK.01.12
SHORT-CHAIN OXIDOREDUCTASE.....	FABG.....		TP125
SIALYLTRANSFERASE.....	CMP-NEU5AC.....	X-RAY CRYSTALLOGRAPHY.....	MP054
SIGNAL TRANSDUCTION.....	GENE REGULATION.....	SMALL ANGLE SCATTERING.....	13.03.02
SIGNAL TRANSDUCTION.....	X-RAY CRYSTALLOGRAPHY.....	CANCER.....	SP047
SIGNAL-TO-NOISE.....	MICRO-CRYSTALS.....	MINI-BEAM.....	13.08.03
SIGNALING.....	CONFORMATIONAL TRANSITIONS.....	DYNAMICS.....	01.05.06
SILANE.....	WATER-BARRIER.....	CORROSION.....	09.02.01
SILICON PIXEL ARRAY DETECTOR.....	X-RAY DETECTOR.....	SYNCHROTRON SCIENCE.....	13.02.02
SIMULATED ANNEALING.....	MINERALOGY.....	QUANTUM OPTIMIZATION.....	07.01.05
SIMULATED ANNEALING.....	X-RAY POWDER DIFFRACTION.....	GLOBAL OPTIMIZATION.....	TP189
SIMULATION.....	AFM.....	DISSOLUTION.....	AW.01.05
SINGLE CRYSTAL.....	NEUTRON DIFFRACTION.....	SMALL MOLECULES.....	10.01.10
SINGLE CRYSTAL NEUTRON DIFFRACTION.....	PROTON DISORDER AND TRANSFER.....	POLYMORPH MOLECULAR COMPLEX.....	10.01.04
SINGLE-CRYSTAL-TO-SINGLE-CRYSTAL TRANSFER.....	HOST-GUEST SYSTEMS.....	E/Z-PHOTOISOMERIZATIONS.....	AW.03.02
SIR PHASING.....	LOW RESOLUTION.....	NEUTRON DIFFRACTION.....	TP185
SMALL ANGLE NEUTRON SCATTERING.....	SUPERCONDUCTIVITY.....	VORTEX LATTICE.....	13.04.01
SMALL ANGLE SCATTERING.....	MATERIALS SCIENCE.....	USAXS.....	09.01.01
SMALL ANGLE SCATTERING.....	SIGNAL TRANSDUCTION.....	GENE REGULATION.....	13.03.02
SMALL ANGLE SCATTERING.....	DISORDERED PROTEINS.....	SOLUTION STRUCTURE.....	13.03.05
SMALL CRYSTALLOGRAPHY.....	CO(III) COMPLEXES.....	OXIME-AND-AMIDE LIGAND.....	MP196
SMALL MOLECULE.....	SCIENCE.....	PROCEDURES.....	10.02.01
SMALL MOLECULE.....	P450 INHIBITORS.....	FLAVONE.....	MP192
SMALL MOLECULE.....	CRYSTALLOGRAPHY.....	DIFFRACTOMETER.....	MP241
SMALL MOLECULES.....	NEUTRON DIFFRACTION.....	PGSE NMR.....	10.01.05
SMALL MOLECULES.....	SINGLE CRYSTAL.....	NEUTRON DIFFRACTION.....	10.01.10
SMALL-ANGLE SCATTERING.....	REINFORCING FILLERS.....		09.01.07
SMALL-ANGLE SCATTERING.....	IP3.....		MP159
SMALL-ANGLE SCATTERING.....	BIOMOLECULAR COMPLEXES.....	NEUTRON CONTRAST VARIATION.....	13.03.06
SMALL-ANGLE SCATTERING.....	USER FACILITY.....	NEUTRON SCATTERING.....	13.03.08
SMALL-ANGLE SOLUTION SCATTERING.....	PROTEIN CONFORMATION.....	NEUTRON CONTRAST VARIATION.....	13.03.07
SMALL-MOLECULE.....	ACTINIDES.....	SYNCHROTRON.....	MP227
SOFT X-RAY PHASING.....	SULFUR PHASING.....	SYNCHROTRON BEAMLINE OPTIMIZATION.....	01.03.01
SOFT X-RAYS.....	RESONANT SCATTERING.....	MAGNETIC SCATTERING.....	09.03.01
SOFTWARE.....	CCD.....	AUTOMATION.....	03.01.06
SOFTWARE.....	RECIPROCAL SPACE.....	VISUALIZATION.....	13.09.03
SOFTWARE.....	FRAGMENT SCREENING.....	AUTOMATION.....	04.01.06
SOLID STATE REACTION.....	TWINNING.....	DISORDER.....	10.03.01
SOLUBILITY ENHANCERS.....	CRYOPROTECTANTS.....	CRYSTALLIZATION.....	SP067
SOLUBLE GUANYLYL CYCLASE (SGC).....	NITRIC OXIDE (NO) RECEPTOR.....	HEME SENSOR.....	03.01.02
SOLUTE-BINDING PROTEIN.....	ABC-TYPE TRANSPORTER SYSTEM.....	ZINC.....	SP012
SOLUTION STRUCTURE.....	SMALL ANGLE SCATTERING.....	DISORDERED PROTEINS.....	13.03.05
SONICATION.....	INTERCALATION.....	INORGANIC-ORGANIC PEROVSKITE.....	SP212
SPACE GROUPS.....	SYMMETRY.....	METHODOLOGY.....	13.09.04
SPECTROSCOPY.....	METALLOENZYME.....	STRUCTURE-FUNCTION.....	SP138

# Keyword Index

SPHINGOMYELINASE.....	HEMOLYSIS .....	VIRULENCE FACTOR .....	SP123
SPIN DENSITY .....	POLARIZED NEUTRON DIFFRACTI.....	SPINEL STRUCTURE.....	TP183
SPINEL.....	MAGNETIC STRUCTURE.....	POLARIZED SINGLE CRYSTAL NEU D...	TP184
SPINEL STRUCTURE.....	SPIN DENSITY.....	POLARIZED NEUTRON DIFFRACTIO .....	TP183
SPR.....	AMYLOID.....	ANTIBODY.....	MP007
SR-INSTRUMENTATION .....	MICRO-CRYSTALS .....	POLYHEDRIN .....	13.08.02
STANDARDS.....	NMR STRUCTURAL DATA.....	NMR TASK FORCE.....	WK.02.02
STEELS .....	PRECIPITATION.....	HIGH-TEMPERATURE.....	09.01.05
STEROSPECIFICITY .....	VESTITONE REDUCTASE.....	CRYSTAL STRUCTURE.....	SP046
STREPTOCOCCUS PYOGENES.....	BACTERIAL PILUS .....	X-RAY CRYSTALLOGRAPHY.....	SP022
STRUCTURAL BIOLOGY.....	PUBLICATION STANDARDS .....		WK.02.01
STRUCTURAL CHANGES.....	PHOTOTROPIN1 .....	LOV2 DOMAIN .....	TP142
STRUCTURAL GENIOMICS .....	CRYSTALLIZATION STRATEGY .....	ATTRITION RATE.....	SP075
STRUCTURAL GENIOMICS.....	PROTEIN CRYSTALLIZATION .....		01.02.05
STRUCTURAL GENIOMICS.....	INTERACTOME.....		01.05.02
STRUCTURAL GENIOMICS.....	FUNCTION FROM STRUCTURE.....	GO SLIMS .....	01.06.02
STRUCTURAL GENIOMICS.....	PROTEIN PHOSPHATASES.....	ENOLASES AMIDOHYDROLASES .....	01.06.03
STRUCTURAL GENIOMICS.....	PROTEIN SURFACE.....	FUNCTION PREDICTION.....	01.06.07
STRUCTURAL GENIOMICS.....	METAL DEPENDENT PHOSPHODIES .....	THERMOPHILIC EUKARYOTE.....	TP126
STRUCTURAL GENIOMICS.....	PROTEIN NUCLEAR MAGNETIC RE .....	STRUCTURE QUALITY ASSESSMEN.....	WK.02.05
STRUCTURAL GENIOMICS.....	CRYSTAL LATTICE INTERACTIONS .....	PURIFICATION TAG .....	01.02.06
STRUCTURAL GENIOMICS.....	ATP-BINDING PROTEIN.....	SECSG.....	MP044
STRUCTURAL GENIOMICS.....	HIGH-THROUGHPUT PIPELINE.....	CHALLENGING PROJECTS.....	TP156
STRUCTURAL GENIOMICS.....	STRUCTURE-BASED FUNCTION .....	PROTEIN STRUCTURE UNIVERSE .....	01.06.01
STRUCTURAL GENIOMICS.....	FUNCTION .....		01.06.04
STRUCTURAL GENIOMICS.....	HYPOTHETICAL PROTEINS.....	ALTERNATIVE SPLICING.....	01.06.05
STRUCTURAL GENIOMICS.....	STRUCTURE-BASED DRUG DESIGN .....	COCKTAIL CRYSTALLOGRAPHY .....	MP163
STRUCTURAL GENIOMICS.....	FUNCTIONAL MOTIF .....	RAF KINASE INHIBITOR PROTEIN.....	TP124
STRUCTURAL GENIOMICS.....	FUNCTION .....	PFAM.....	TP128
STRUCTURAL VARIATION .....	FUNCTIONAL ASSOCIATION.....	REDUNDANT DATA-BASE.....	TP090
STRUCTURE.....	COMPARISON .....	PHENOLATE .....	SP.01.03
STRUCTURE.....	ORIENTATING METALLOMACROC .....	ASSEMBLY.....	SP216
STRUCTURE.....	NUCLEAR RECEPTOR.....	EVOLUTION .....	TP108
STRUCTURE.....	COMPARISON .....	SELF-ASSEMBLY .....	TP202
STRUCTURE.....	NEEDLE PROTEIN.....	TYPE III SECRETION SYSTEM.....	SP045
STRUCTURE.....	SEQUENCE.....	RELATIONSHIP .....	TP095
STRUCTURE.....	DATA DEPOSITION.....	NMR .....	WK.02.03
STRUCTURE BASED DRUG DESIGN .....	LEAD IDENTIFICATION.....	FRAGMENT CRYSTALLOGRAPHY .....	04.01.03
STRUCTURE DETERMINATION .....	X-RAY SCATTERING.....	BIOLOGICAL MOLECULES .....	TR.01.06
STRUCTURE DETERMINATION.....	PAIR DISTRIBUTION FUNCTION.....		07.01.12
STRUCTURE PRECISION.....	PENTACENE AND ANTHRACENE.....	TCNQ CHARGE STATES.....	AW.02.01
STRUCTURE PREDICTION.....	PHASING .....	AB INITIO .....	01.07.06
STRUCTURE QUALITY ASSESSMENT .....	STRUCTURAL GENIOMICS .....	PROTEIN NUCLEAR MAGNETIC RES.....	WK.02.05
STRUCTURE SOLUTION.....	POLYMORPHISM.....	POWDER DIFFRACTION .....	07.01.08
STRUCTURE SOLUTION.....	GRID COMPUTING.....	POWDER DIFFRACTION .....	07.01.02
STRUCTURE VALIDATION.....	LONG WAVELENGTH PHASING.....	SULFUR-SAD.....	MP078
STRUCTURE-BASED DRUG DESIGN .....	CANCER.....	CHK1 .....	04.01.01
STRUCTURE-BASED DRUG DESIGN .....	COCKTAIL CRYSTALLOGRAPHY .....	STRUCTURAL GENIOMICS .....	MP163
STRUCTURE-BASED FUNCTION.....	PROTEIN STRUCTURE UNIVERSE.....	STRUCTURAL GENIOMICS .....	01.06.01
STRUCTURE-FUNCTION.....	SPECTROSCOPY .....	METALLOEZYME.....	SP138
STRUCTURE-FUNCTION.....	LIPOPROTEIN .....	TREPONEMA PALLIDUM.....	TP140
SUBSTRATE IDENTIFICATION .....	BIOINFORMATICS .....		TP092
SUBSTRATE SPECIFICITY.....	GLYCOSYLTRANSFERASE.....	ENZYME MECHANISM.....	TP100
SUBSTRUCTURE.....	LONG WAVELENGTH.....	LONG WAVELENGTH.....	01.03.03
SUCCINIMIDYL FORMATION .....	ASPARTYL ISOMERIZATION .....	THIAMIN PYROPHOSPHOKINASE .....	TP106
SULFUR PHASING .....	LONG WAVELENGTH FROM CR AN.....	SULFUR SAD .....	01.03.08
SULFUR PHASING .....	SYNCHROTRON BEAMLINE OPTIM.....	SOFT X-RAY PHASING .....	01.03.01
SULFUR SAD.....	CRYSTAL DECAY.....		01.03.07
SULFUR SAD.....	SULFUR PHASING.....	LONG WAVELENGTH FROM CR ANO.....	01.03.08
SULFUR SAD PHASING.....	CHROMIUM RADIATION .....	SAD.....	01.03.04
SULFUR TRANSFER.....	MYCOBACTERIUM TUBERCULOSI.....	CYSTEINE BIOSYNTHESIS.....	SP014
SULFUR-SAD.....	STRUCTURE VALIDATION .....	LONG WAVELENGTH PHASING .....	MP078
SUPERANTIGEN.....			TP129
SUPERCONDUCTIVITY.....	VORTEX LATTICE .....	SM ANGLE NEUTRON SCATTERING .....	13.04.01
SUPERLATTICE.....	SELF-ASSEMBLY .....	NANOCRYSTAL.....	13.07.01
SUPRAMOLECULAR.....	DYNAMICS.....	ROTATION .....	10.03.07

# Keyword Index

SUPRAMOLECULAR.....	BIS-CHELATE.....	PYRAZOLE.....	AW.03.03
SUPRAMOLECULAR.....	CLUSTER.....	CATALYSIS.....	SP218
SUPRAMOLECULAR.....	TELLURIUM(IV).....	DOCKING.....	TP215
SUPRAMOLECULAR.....	HYDROGEN BOND.....	CRYSTAL ENGINEERING.....	TP214
SUPRAMOLECULAR CHEMISTRY.....	CAVITAND.....	COCRYSTALS.....	SP207
SUPRAMOLECULAR CHEMISTRY.....	CRYSTAL STRUCTURE.....	HETEROMETALLIC COMPLEX.....	SP204
SUPRAMOLECULAR CHEMISTRY.....	POWDER XRD.....	CRYSTAL ENGINEERING.....	10.03.06
SUPRAMOLECULAR STRUCTURE.....	AMYLOID CONGENERS.....	SELF ASSEMBLY.....	MP162
SUPRAMOLECULAR SYNTHON.....	CRYSTAL ENGINEERING.....	HYDROGEN BOND.....	AW.02.02
SURFACE AND INTERFACE.....	ELEMENT-SPECIFIC SUBSTRUCTU.....	RESONANT ANOMALOUS X-RAY REF... ..	09.02.02
SURFACE ENTROPY REDUCTION.....	PSI-2 SPECIALIZED CENTER.....	CRYSTALLIZATION.....	SP074
SURFACTANTS.....	NANOCRYSTALS.....	SELF-ASSEMBLY.....	13.07.02
SURROGATE LIGHT CHAIN.....	B CELL DEVELOPMENT.....	IMMUNOLOGY.....	SP226
SYMMETRY.....	DISORDER.....	CRYSTAL STRUCTURE.....	10.02.05
SYMMETRY.....	METHODOLOGY.....	SPACE GROUPS.....	13.09.04
SYMMETRY.....	PHASE TRANSFORMATION.....	INTERGROWTH.....	10.02.02
SYNCHROTON.....	TEMPERATURE.....	RADIATION DAMAGE.....	13.10.03
SYNCHROTRON.....	LAUE DIFFRACTION.....	TIME-RESOLVED.....	05.01.06
SYNCHROTRON.....	MAGNETISM.....	POWDER.....	07.01.06
SYNCHROTRON.....	MICROCRYSTAL.....	MICRODIFFRACTION.....	13.08.04
SYNCHROTRON.....	PROTEIN CRYSTALLOGRAPHY.....	MICROFOCUS BEAMLINE.....	13.08.05
SYNCHROTRON.....	THERMAL IMAGING.....	SAMPLE HEATING.....	13.10.02
SYNCHROTRON.....	SMALL-MOLECULE.....	ACTINIDES.....	MP227
SYNCHROTRON.....	MAIL-IN CRYSTALLOGRAPHY.....	REMOTE DATA COLLECTION.....	MP232
SYNCHROTRON.....	MICRO-BEAM.....	MICRO-CRYSTAL.....	TP239
SYNCHROTRON.....	REMOTE.....	CRYSTALLOGRAPHY.....	MP231
SYNCHROTRON.....	AUTOMATION.....	ROBOTICS.....	TP222
SYNCHROTRON.....	UNDULATOR.....	NE-CAT.....	TP223
SYNCHROTRON BEAMLINE OPTIMIZATIO.....	SOFT X-RAY PHASING.....	SULFUR PHASING.....	01.03.01
SYNCHROTRON BEAMLINES.....	CRYSTAL AUTOCENTERING.....	CRYOLOOP ALIGNMENT.....	SP224
SYNCHROTRON RADIATION.....	USER FACILITIES.....	MACROMOLECULES.....	MP083
SYNCHROTRON SCIENCE.....	SILICON PIXEL ARRAY DETECTOR.....	X-RAY DETECTOR.....	13.02.02
SYNCHROTRON X-RAY DIFFRACTION.....	NICKEL HYDROXIDE.....	NEUTRON DIFFRACTION.....	05.02.05
SYNTHESIS & GROWTH.....	COORDINATION POLYMERS.....	HETEROMETALLIC COMPLEXES.....	SP209
TAKA-AMYLASE A.....	MICROGRAVITY.....	HIGH-RESOLUTION.....	SP071
TAT.....	CDK9.....	CYCLIN T1.....	SP058
TATB.....	USAXS.....		09.01.04
TAUTOMERASE.....	CORYNEBACTERIUM GLUTAMICU.....	4-OT HOMOLOGUE.....	SP031
TCNQ CHARGE STATES.....	STRUCTURE PRECISION.....	PENTACENE AND ANTHRACENE.....	AW.02.01
TEACHING.....	CORDES, WALLY.....		13.09.01
TEACHING AIDS.....	DIRECT METHODS.....	PHASE RELATIONSHIPS.....	13.09.05
TEACHING AND EDUCATION.....	REMOTE ACCESS.....	UNDERGRADUATE.....	SP01.01
TEACHING GADGETS.....	DIFFRACTION DEMONSTRATION.....	PATTERSON DEMONSTRATION.....	13.09.02
TEACHING INITIATIVE.....	UNDERGRADUATE STUDIES.....	CRYSTALLOGRAPHIC EDUCATION.....	SP01.02
TELLURIUM(IV).....	DOCKING.....	SUPRAMOLECULAR.....	TP215
TELOMERE BINDING PROTEIN.....	DNA COMPLEX.....	CRYSTAL STRUCUTURE.....	MP055
TEMPERATURE.....	RADIATION DAMAGE.....	SYNCHROTON.....	13.10.03
TEMPERATURE DEPENDENCE.....	COPPER BROMIDE.....	THERMAL DISORDER.....	05.01.04
TERMPERATURE RESPONSIVE.....	ENCAPSULANT.....	MORPHOLOGY.....	09.01.03
TETRACENOMYCIN.....	AROMATASE/CYCLASE.....	POLYKETIDE.....	MP057
TETRANUCLEAR CLUSTER.....	GRID STRUCTURE.....	SCHIFF BASE LIGAND.....	TP205
TEXTURE ANALYSIS.....	METAL HYDRIDE.....	X-RAY DIFFRACTION.....	13.06.02
THEORETICAL LIMIT.....	SENSITIVITY.....	BONSE-HART TECHNIQUE.....	09.01.02
THERMAL DISORDER.....	TEMPERATURE DEPENDENCE.....	COPPER BROMIDE.....	05.01.04
THERMAL IMAGING.....	SAMPLE HEATING.....	SYNCHROTRON.....	13.10.02
THERMO-SENSITIVE COMB LIKE POLYME.....	CONFORMATION.....	SANS.....	13.07.04
THERMODYNAMICS,QUASI HARMONIC.....	INELASTIC NEUTRON SCATTERING.....	DFT, ABINITIO.....	13.06.01
THERMOELECTRIC MATERIAL.....	NA1-XGE3+Z.....	CLATHRATE II STRUCTURE.....	TP221
THERMOPHILIC.....	NEW STRUCTURE.....	ASPARTATE TRANSCARBAMOYLASE... ..	TP153
THERMOPHILIC EUKARYOTE.....	STRUCTURAL GENOMICS.....	METAL DEPENDENT PHOSPHODIESTE.....	TP126
THERMOSTABILITY.....	MUTATIONS.....	ASPARTATE TRANSCARBAMOYLASE... ..	TP145
THIAMIN DIPHOSPHATE.....	VARIANT.....	PYRUVATE DEHYDROGENASE.....	TP134
THIAMIN PYROPHOSPHOKINASE.....	SUCCINIMIDYL FORMATION.....	ASPARTYL ISOMERIZATION.....	TP106
THREE CHEMISTRY.....	ACYLASE.....	AUTOPROTEOLYSIS.....	TP176
TIME RESOLVED.....	NEUTRON DIFFRACTION.....	HYDROGEN STORAGE.....	13.04.06
TIME-RESOLVED.....	SYNCHROTRON.....	LAUE DIFFRACTION.....	05.01.06

# Keyword Index

TLS.....	REFINEMENT.....	01.07.05
TLS REFINEMENT.....	DNA MISMATCH REPAIR.....	TP154
TONB.....	TRANSPORT.....	MEMBRANE PROTEIN.....
TOPOIV.....	TYPE IIA DNA TOPOISOMERASE.....	GYRASE.....
TRA I RELAXOSOME PROTEIN.....	CONJUGATIVE DNA TRANSFER.....	MACROMOLECULAR CR.....
TRANSANNULAR INTERACTION.....	CHEMICAL BONDING.....	ENERGETIC MATERIALS.....
TRANSCRIPTION.....	RNA POLYMERASE II.....	LARGE PROTEIN.....
TRANSCRIPTION FACTOR.....	COMPLEX.....	HOXA9 PBX DNA.....
TRANSCRIPTIONAL REGULATION.....	CELL CYCLE REGULATION.....	KINASE.....
TRANSCRIPTIONAL REGULATORY.....	WINGED HELIX-TURN-HELIX.....	HXLR DOMAIN.....
TRANSLESION SYNTHESIS.....		SP016
TRANSMISSION ELECTRON MICROSCOPY.....	INTERCALATION.....	CLAY MIMICS.....
TRANSPORT.....	MEMBRANE PROTEIN.....	TONB.....
TRANSPORTER.....	OUTER MEMBRANE PROTEIN.....	XENOBIOTICS.....
TRAY GONIOMETER.....	DATA COLLECTION STRATEGY.....	MLFSOM.....
TREPONEMA PALLIDUM.....	STRUCTURE-FUNCTION.....	LIPOPROTEIN.....
TREX1.....	POLY-PROLINE.....	DNA.....
TRIMELLITATE.....	AB INITIO.....	POWDER.....
TRIMETHYLTRANSFERASE.....	POST-TRANSLATIONAL MODIFICA.....	X-RAY CRYSTALLOGRAHPY.....
TRIMETHYLTRANSFERASE.....	POST-TRANSLATIONAL MODIFICA.....	X-RAY CRYSTALLOGRAHPY.....
TRNA.....	MRNA.....	RIBOSOME.....
TROPICAL DISEASES.....	SCHISTOSOMIASIS.....	ENZYME INHIBITORS.....
TRYPTOPHANYL-TRNA SYNTHETASE.....	LIGAND FRAGMENT.....	CLOSED-CONFORMATION STABILIZ.....
TRYPTOPHANYL-TRNA SYNTHETASE/TRN.....	DUAL CONFORMATION.....	PROTEIN SYNTHESIS.....
TULAREMIA.....	DRUG TARGET.....	FATTY ACID SYNTHESIS.....
TWIN.....	SHELXL.....	REFINEMENT.....
TWIN.....	NON-MEROHEDRAL.....	DATA PROCESSING.....
TWIN-DISORDER.....	PSEUDO-SYMMETRY.....	PROBLEM STRUCTURES.....
TWINNING.....	PHENIX.....	REFINEMENT.....
TWINNING.....	DISORDER.....	SOLID STATE REACTION.....
TWINNING.....	PHENIX.....	REFINEMENT.....
TWINNING.....	REFINEMENT.....	10.02.03
TYPE IIA DNA TOPOISOMERASE.....	GYRASE.....	TOPOIV.....
TYPE III SECRETION SYSTEM.....	STRUCTURE.....	NEEDLE PROTEIN.....
UBIQUITIN-LIKE PROTEIN.....	SALICYLIC ACID-BINDING PROTEI.....	2,3-DIOXYGENASE.....
UNDERGRADUATE.....	TEACHING AND EDUCATION.....	REMOTE ACCESS.....
UNDERGRADUATE STUDIES.....	CRYSTALLOGRAPHIC EDUCATION.....	TEACHING INITIATIVE.....
UNDULATOR.....	NE-CAT.....	SYNCHROTRON.....
UNIFORM CURATION.....	PROTEIN STRUCTURE.....	DATABASE INTEGRATION.....
UNKNOWN FUNCTION.....	PF04013.....	A/BETA KNOT.....
URANIUM ALLOY.....	RIETVELD.....	PAIR DISTRIBUTION FUNCTION.....
UROPORPHYRINOGEN DECARBOXYLASE.....	HEME.....	ANAEROBIC CRYSTALLIZATION.....
USANS.....	BIOMEDICAL MATERIALS.....	USAXS.....
USANS.....	AEROGEL.....	USAXS.....
USAXS.....	SMALL ANGLE SCATTERING.....	MATERIALS SCIENCE.....
USAXS.....	TATB.....	09.01.04
USAXS.....	USANS.....	BIOMEDICAL MATERIALS.....
USAXS.....	IMAGING.....	CONTRAST MECHANISM.....
USAXS.....	WASPALOY.....	COARSENING.....
USAXS.....	USANS.....	AEROGEL.....
USER FACILITIES.....	MACROMOLECULES.....	SYNCHROTRON RADIATION.....
USER FACILITY.....	NEUTRON SCATTERING.....	SMALL-ANGLE SCATTERING.....
UV.....	RIP.....	RADIATION DAMAGE.....
VACCINE.....	HIV-1.....	ANTIBODY.....
VALIDATIO.....	PROTEIN CRYSTALLOGRAPHY.....	LIGANDS.....
VALIDATION.....	CHECKCIF.....	PLATON.....
VAPOR PRESSURE CONTROL.....	SCREENING.....	OPTIMIZATION.....
VAPOUR.....	DIFFUSION.....	PLATE.....
VARIABLE TEMP CRYSTALLOGRAPHY.....	ELECTRONIC STRUCTURE.....	DIRUTHENIUM COMPOUNDS.....
VARIABLE TEMPERATURE.....	HIGH PRESSURE.....	POWDER DIFFRACTION.....
VARIANT.....	PYRUVATE DEHYDROGENASE.....	THIAMIN DIPHOSPHATE.....
VAULT.....	RIBONUCLEOPROTEIN.....	NANOCAPSULE.....
VEGF.....	HEPARIN.....	NEUROPILIN.....
VERBESINA TURBACENSIS.....	NATURAL PRODUCTS.....	EUDESMANES.....
VESITONE REDUCTASE.....	CRYSTAL STRUCTURE.....	STEROSPECIFICITY.....
VINYL-SULFONE INHIBITOR.....	PROTEIN DEGRADATION.....	PROTEASOME.....

# Keyword Index

VIRAL RNA.....	RNA STRUCTURE.....	INTERNAL RIBOSOME ENTRY SITE .....	13.05.01
VIRTUAL INSTRUMENT .....	WEB SERVICES .....	REMOTE ACCESS AND CONTROL.....	03.01.07
VIRULENCE FACTOR .....	SPHINGOMYELINASE .....	HEMOLYSIN .....	SP123
VIRUS.....	ABSORPTION .....	GISAXS.....	09.03.05
VIRUS.....	NUCLEOPROTEIN .....	INFLUENZA .....	13.05.02
VIRUS ENTRY.....	MEMBRANE FUSION .....		13.05.05
VIRUS REPLICATION.....	NUCLEOPROTEIN-RNA.....	NUCLEOCAPSID .....	13.05.03
VISUALIZATION.....	SOFTWARE .....	RECIPROCAL SPACE.....	13.09.03
VISUALIZATION.....	MOTIF.....	INTERFACE.....	SP.01.06
VISUALIZATION.....	SCRIPTING.....	LANGUAGE .....	TP172
VISUALIZATION.....	RECIPROCAL .....	DIFFUSE.....	TR.01.10
VORTEX LATTICE.....	SM ANGLE NEUTRON SCATTERIN .....	SUPERCONDUCTIVITY .....	13.04.01
WASPALLOY .....	COARSENING .....	USAXS .....	09.01.10
WATER.....	HIGH PRESSURE .....	X-RAY .....	05.02.03
WATER-BARRIER.....	CORROSION .....	SILANE .....	09.02.01
WEB SERVICES.....	REMOTE ACCESS AND CONTROL.....	VIRTUAL INSTRUMENT .....	03.01.07
WINGED HELIX-TURN-HELIX .....	HXLR DOMAIN .....	TRANSCRIPTIONAL REGULATOR .....	MP043
WORKFLOW.....	PROTEIN EXPRESSION.....	GENE SYNTHESIS.....	TP094
X-RAY .....	BREWSTER-ANGLE MICROSCOPY.....	2D CRYSTAL .....	MP160
X-RAY .....	WATER.....	HIGH PRESSURE .....	05.02.03
X-RAY ANALYSIS.....	ATGRXCP PROTEIN .....	CYSTALLIZATION .....	TP093
X-RAY AND NEUTRON SCATTERING .....	DIFFUSE SCATTERING .....	DEFECTS.....	TR.01.02
X-RAY CRYSTALLOGRAHPY.....	TRIMETHYLTRANSFERASE .....	POST-TRANSLATIONAL MODIFICATI.....	01.01.07
X-RAY CRYSTALLOGRAHPY.....	TRIMETHYLTRANSFERASE .....	POST-TRANSLATIONAL MODIFICATI.....	SP003
X-RAY CRYSTALLOGRAPHY.....	SIALYLTRANSFERASE .....	CMP-NEU5AC.....	MP054
X-RAY CRYSTALLOGRAPHY.....	STREPTOCOCCUS PYOGENES .....	BACTERIAL PILUS .....	SP022
X-RAY CRYSTALLOGRAPHY.....	CANCER.....	SIGNAL TRANSDUCTION.....	SP047
X-RAY DETECTOR.....	SYNCHROTRON SCIENCE.....	SILICON PIXEL ARRAY DETECTOR .....	13.02.02
X-RAY DIFFRACTION.....	ENAMINONES .....	PHARMACOLOGICAL ACTIVITY.....	SP200
X-RAY DIFFRACTION.....	TEXTURE ANALYSIS.....	METAL HYDRIDE .....	13.06.02
X-RAY OPTICS.....	MICROFOCUS SOURCE.....	MULTILAYER .....	03.01.05
X-RAY POWDER DIFFRACTION .....	NEUTRON DIFFRACTION.....	NEGATIVE THERMAL EXPANSION .....	05.01.05
X-RAY POWDER DIFFRACTION .....	DISORDERED SOLVENT .....	MAXIMUM ENTROPY .....	07.01.11
X-RAY POWDER DIFFRACTION .....	GLOBAL OPTIMIZATION .....	SIMULATED ANNEALING.....	TP189
X-RAY SCATTERING.....	BIOLOGICAL MOLECULES.....	STRUCTURE DETERMINATION.....	TR.01.06
X-RAY SOURCE.....	DATA QUALITY .....	LOW NOISE.....	MP079
X-RAY STRUCTURE.....	CHALCONES .....	PHARMACOLOGICAL TESTS .....	10.01.09
X-RAY STRUCTURE.....	ARCHAEOAL EXOSOME.....	RNA PROCESSING .....	TP118
XENOBIOTICS.....	TRANSPORTER.....	OUTER MEMBRANE PROTEIN.....	01.04.01
Y-FAMILY.....	POLYMERASE.....	FINGER .....	SP096
Y-FAMILY POLYMERASE .....	TRANSLESION SYNTHESIS .....		SP016
ZINC .....	SOLUTE-BINDING PROTEIN.....	ABC-TYPE TRANSPORTER SYSTEM.....	SP012
-SYNUCLEIN.....	INTRINSICALLY UNFOLDED PROT.....	PARKINSON'S DISEASE.....	MP030

# Author Index

Aakeröy, Christer	10.01.01	Arakaki, Tracy	MP163	Beekman, M.	TP221
Aakeröy, Christer	10.03.03	Arakaki, Tracy	TP124	Beese, Lorena	TP154
Aakeröy, Christer	10.03.08	Arjunan, Palaniappa	TP134	Begley, Tadhg	SP014
Aakeröy, Christer	AW.03.03	Arnoux, Pascal	SP038	Begum, Anjuman	SP.01.04
Aakeröy, Christer	SP206	Aronson, Meigan	13.07.09	Bell, Jeffrey	TP152
Aakeröy, Christer	SP207	Arumugam, N.	05.02.07	Bellamy, Henry	13.10.02
Abashidze, M.	01.06.06	Arvai, Andrew	MP237	Bellamy, Henry	MP013
Acharya, Priyamvada	13.05.06	Asani, Ernest	SP199	Belman, Nataly	13.07.02
Achnine, Lahoucine	TP135	Ashish, (fnu)	13.03.07	Benavente, A.M.	TP189
Acton, Thomas	01.06.06	Asiamah, I. Awuah	TP172	Bendeif, El-Eulmi	TP149
Adachi, Shin-Ichi	05.01.06	Aspesi, Anthony	TP132	Benning, Matthew	MP236
Adams, Michael W.W.	MP044	Athay, Russ	04.01.06	Benson, Ronald	MP241
Adam, Martin	MP079	Atkinson, Ian	03.01.07	Berejnov, Viatcheslav	MP080
Adams, Paul	01.07.07	Austin, Brian P.	SP045	Berejnov, Viatcheslav	SP068
Adams, Paul	06.01.02	Awuah Asiamah, Isaac	TP174	Berghuis, Albert M.	SP027
Adams, Paul	TP150	Axelrod, Herbert	01.06.04	Bergman, Lawrence	MP165
Adjei, Araba	SP136	Babnigg, Y.-c.	SP075	Bergonia, Hector	01.02.03
Afonine, Pavel	01.07.07	Bache, Chris	MP197	Berman, H.M.	TP087
Afonine, Pavel	06.01.02	Badgandi, Hemant	TP117	Bernstein, Herbert J.	TP172
Agamalian, Michael	09.01.02	Badger, John	04.01.06	Bernstein, Herbert J.	TP174
Agamalian, Michael	09.01.05	Badger, John	MP178	Berry, Robert	TP117
Agaskar, Pradyat	MP169	Bae, Hansol	MP055	Bethel, Christopher	SP051
Agbandje-McKenna, Mavis	SP039	Bah, Alaji	SP252	Bettis, Stephanie E.	SP.01.03
Agbandje-McKenna, Mavis	TP132	Bahnson, Brian	TP086	Beuve, Annie	03.01.02
Agbandje-McKenna, Mavis	TP133	Bailey, Mark S.	13.04.06	Bezjak, Jana	05.02.06
Akerley, Brian	MP164	Bailey, Suzanna	SP062	Bhat, Divya	01.07.06
Akiba, Etsuo	13.06.06	Bains, Manjeet	01.04.03	Bhatia, Surita R.	09.01.08
Albertini, Aurelie	13.05.03	Bajpayee, Lisa	SP070	Bhattacharya, Aneerban	WK.02.05
Albinati, Alberto	10.01.05	Baker, Brian	TP107	Bigelow, Lance	SP075
Ali, Akbar	TP112	Baker, David	01.07.06	Bikzhanova, Galina A.	TP173
Ali, Maruf M.U.	01.04.02	Baker, Edward N.	SP022	Bilderback, Don	13.08.06
Ali Bahsas, B.	TP217	Baker, Thomas	TP105	Bilderback, Don	MP077
Alkire, Randy	MP083	Balasubramanian, Ramjee	13.07.05	Billinge, Simon	TR.01.09
Allaire, Marc	01.08.04	Balbirnie, Melinda	13.01.03	Billinge, Simon	07.01.12
Allen, Andrew J.	09.01.01	Balcewich, Misty	SP104	Bingeli, Nadia	09.03.04
Allen, Andrew J.	09.01.06	Baleja, Jim	SP226	Bingman, Craig	01.02.05
Almo, Steven	01.06.03	Balidemaj, B.	10.04.04	Bingman, Craig	TP126
Almo, Steven	TP101	Bandara, Nilantha	10.03.06	Binkowski, T. Andrew	01.06.07
Altarelli, Massimo	09.03.04	Bandara, Nilantha	SP212	Binkowski, T. Andrew	TP156
Altman, Michael	TP112	Bandaranayake, Rajintha	TP113	Binz, Thomas	13.05.04
Altomare, Angela	07.01.01	Bandarian, V.	MP010	Birmanns, Stefan	01.05.05
Amani, S.M.	TP189	Baraban, Joshua H.	AW.01.05	Bischof, Jaone	TP108
Amaro Luis, Juan Manuel	SP191	Barbour, Len	10.03.10	Bismayer, Ulli	TR.01.11
Ames, Brian	MP057	Barker, John	04.01.02	Bitto, Eduard	TP126
Anand, Kanchan	SP058	Barnard, Travis J.	01.04.02	Black, K.D.	TP150
Ananias, Sandra R.	10.04.03	Barty, Anton	09.03.03	Blackstock, Silas C.	10.03.12
Andersen, Raymond	TP102	Bau, Robert	01.08.04	Blake, Chris	07.01.05
Anderson, Carolyn S.	TP202	Bauer, Bill	SP009	Blakeley, Mathew	06.01.02
Anderson, Daniel	01.08.03	Bauer, Cary	MP079	Blakeley, Mathew	13.01.02
Anderson, S.	06.01.03	Bauer, Jacob	MP019	Blakeley, Mathew	TP186
Anderson, Thomas	MP198	Baughman, Russell G.	TP202	Blandin, Stephanie	TP245
Anderson, Wayne	01.02.06	Baumann, Ted	TP190	Blevins, John	TP140
Anderson, Wayne	TP106	Baxter, Richard	TP245	Blount, Jack	TP135
Andrade, Carlos	10.01.09	Beachy, Philip	MP028	Blum, Marc-Michael	06.01.01
Andrade, Fabiana C.	10.04.03	Beale, Thomas	09.03.04	Boccaleri, Enrico	05.01.02
Andrejasic, Miha	03.01.04	Beasley, A.G.	SP168	Boere, Clemens	13.09.03
Andricopulo, Adriano	SP091	Beasley, A.G.	TR.01.01	Boffa-Ballaran, Tiziana	TR.01.11
Angel, Ross J.	MP169	Beatty, Alicia	10.03.06	Bogan, Michael	09.03.03
Angel, Ross J.	TR.01.11	Beatty, Alicia	10.03.11	Bogdanov, A.A.	MP029
Anreso, T.	04.01.03	Beatty, Alicia	SP212	Bohm, Andrew	SP226
Antao, Sytle	MP193	Beatty, Alicia	SP213	Bonanno, Jeff	01.06.03
Antipin, Mikhail Yu.	TP210	Beatty, Alicia	TP214	Bonomo, Robert	SP051
Apostol, Marcin	10.04.02	Beavers, Christine M.	10.04.05	Borbulevych, Oleg	TP107
Apostol, Marcin	13.08.01	Becker, Michael	13.08.03	Borchardt, Thomas B.	TP251
Apostol, Marcin	13.01.03	Becker, Stefan	13.05.03	Borchers, Julie	13.07.09

## Author Index

- Bosanac, Ivan .....MP159  
 Bosch, Joergen .....MP163  
 Bosch, Juergen .....MP165  
 Bose, Sucharita .....SP011  
 Bott, Richard .....04.01.07  
 Boulee, Pascal .....MP228  
 Bourne, Philip .....01.05.04  
 Boutet, Sebastien .....09.03.03  
 Boycheva, D. ....TP172  
 Brailey, Jacquie .....SP242  
 Brannetti, Barbara .....TP089  
 Brastianos, Harry .....TP102  
 Brautigam, Chad A. ....TP140  
 Brayer, Gary .....SP01.02  
 Brayer, Gary .....SP01.04  
 Brayer, Gary .....TP102  
 Breidenbach, Mark .....13.05.04  
 Brettschneider, Susanne .....SP242  
 Bria, Lauren .....10.01.02  
 Bricogne, Gerard .....13.02.04  
 Bridgham, Jamie .....TP108  
 Britten, James F. ....13.09.03  
 Britten, James F. ....TR.01.10  
 Brock, Carolyn P. ....10.04.01  
 Brock, Carolyn P. ....AW.02.03  
 Brockhauser, Sandor .....MP237  
 Broderick, Joan .....SP017  
 Brower, Darren .....10.02.06  
 Brown, C. Kent .....SP138  
 Browner, Michelle .....MP179  
 Brownie, Edward .....MP018  
 Brownlee, June .....TP141  
 Brunger, Axel T. ....13.05.04  
 Bruno Colmenarez, Julia .....SP191  
 Brunzelle, Joseph .....01.02.06  
 Brzozowski, A. Marek .....MP177  
 Bucar, Dejan-Kresimir .....TP220  
 Bucar, Dejan-Kresimir .....TP251  
 Buchanan, Susan K. ....01.04.02  
 Buckner, Fred .....MP163  
 Buffey, Steve .....SP233  
 Buono, Rick .....MP231  
 Burchell, Tara .....10.03.05  
 Burgin, Alex .....04.01.03  
 Burgin, Alex .....TP094  
 Burk, David .....SP138  
 Burley, Stephen .....01.06.03  
 Burns, Kristin .....SP014  
 Buscaglia, Carlos .....MP165  
 Bush-Pelc, Leslie A. ....SP252  
 Bushnell, David .....13.01.01  
 Butler-Cole, Christine .....SP025  
 Byun, Jung-Sue .....MP055  
 Cachau, Raul .....06.01.02  
 Cagnon, Laurent .....13.06.03  
 Cai, Fei .....03.01.01  
 Calero, Guillermo .....13.01.01  
 Caliendo, Rocco .....07.01.01  
 Calo, Joseph .....09.02.03  
 Camalli, Mercedes .....07.01.01  
 Camargo, Ademir .....10.01.09  
 Cameron, Stanley .....10.01.14  
 Campana, Charles F. ....TP173  
 Campbell, Branton J. ....TR.01.02  
 Cannon, Gordon C. ....03.01.01  
 Cao, Hong .....TP112  
 Cao, Yixiang .....TP152  
 Capel, Malcolm .....13.08.04  
 Capel, Malcolm .....TP223  
 Capitani, Guido .....SP147  
 Caracelli, Ignez .....TP215  
 Carlucci-Dayton, Mary .....MP230  
 Carniato, Fabio .....05.01.02  
 Carpenter, Graham .....07.01.05  
 Carpenter, Jack .....09.01.02  
 Carrasco, Nicolas .....TP171  
 Carter Jr, Charles W. ....TP155  
 Casati, Nicola .....AW.01.04  
 Case, N. ....TP133  
 Caspar, Donald L. D. ....TR.01.04  
 Catanzariti, Ann-Maree .....SP052  
 Celestian, Aaron J. ....07.01.07  
 Cenda, Dan .....MP228  
 Cerasoli, Doug .....AW.03.05  
 Cetin, Anil .....AW.03.04  
 Chakoumakos, Bryan .....05.02.03  
 Chakoumakos, Bryan .....MP235  
 Chan, Jenny .....MP159  
 Chan, Nei-Li .....SP036  
 Chan, Nei-Li .....SP130  
 Chance, Mark .....01.06.03  
 Chandonia, John-Marc .....01.05.02  
 Chandra, Dhanesh .....13.04.06  
 Chandrasekhar, Krishnamoorthy .....TP134  
 Chang, C.B. ....13.04.03  
 Chang, Changsoo .....MP083  
 Chang, Changsoo .....TP156  
 Chang, Chung-I .....TP245  
 Chang, Gu-Gang .....SP121  
 Chang, Hsun-Tang .....SP130  
 Chang, Zhenzhan .....TP135  
 Changela, Anita .....TP154  
 Chao, Kinlin .....MP024  
 Chapman, Henry .....09.03.03  
 Charbonnier, Jean .....13.06.02  
 Chayen, Naomi .....01.02.02  
 Chee, Clinton .....03.01.07  
 Chellappan, Sripriya .....TP112  
 Chelliah, Yogarany .....TP245  
 Chen, Baoyu .....13.03.02  
 Chen, Julian .....06.01.01  
 Chen, L. ....TP087  
 Chen, Lei .....13.05.06  
 Chen, Lirong .....01.03.01  
 Chen, Lirong .....MP044  
 Chen, Ping .....04.01.01  
 Chen, Qianhong .....MP229  
 Chen, W.C. ....TP184  
 Chen, Xiaoyan .....SP047  
 Chen, Y. ....01.06.06  
 Chen, Zhiwei .....SP252  
 Cheng, Gang .....13.07.04  
 Cheng, Ninghui .....TP093  
 Cheng, Xiaodong .....01.01.08  
 Cheng, Yuan .....SP060  
 Cheung, Eugene .....07.01.08  
 Chiang, Chia-Wang .....SP036  
 Childers, Seth W. ....MP162  
 Chinte, Umesh N. ....13.10.03  
 Chiu, Elaine .....13.08.02  
 Chiu, Kenneth .....03.01.07  
 Cho, Hyun-Soo .....MP054  
 Cho, Hyun-Soo .....MP055  
 Cho, Ki Joon .....TP176  
 Cho, Sangwoo .....TP119  
 Cho, So-Hye .....MP195  
 Cho, Tae H. ....13.09.04  
 Choi, In-Geol .....01.06.01  
 Choi, Won-Chon .....SP074  
 Chou, Chi-Yuan .....SP121  
 Choudhury, Sumana .....SP062  
 Chowdhury, Rasheduzzaman .....SP026  
 Chrzas, John .....01.03.01  
 Chrzas, John .....MP232  
 Chrzas, John .....TP151  
 Chrzas, John .....TP222  
 Chu, Zhaolian .....SP216  
 Chupas, Peter .....13.04.04  
 Cioci, G. ....MP237  
 Claiborne, Al .....AW.03.07  
 Claiborne, Al .....SP020  
 Clearfield, Abraham .....07.01.07  
 Coates, Leighton .....06.01.05  
 Coates, Leighton .....06.01.07  
 Cody, Vivian .....TP120  
 Coetzee, Anita .....MP079  
 Colaneri, Michael .....TP153  
 Collins, Paul .....04.01.06  
 Collyer, Charles .....MP032  
 Columbus, Linda .....13.03.03  
 Colussi, Timothy .....SP020  
 Comasseto, Joao .....TP215  
 Comoletti, Davide .....13.03.06  
 Connare, S. ....TP088  
 Connor, Denise .....04.01.03  
 Contreras, Jines .....TP217  
 Cook, Mike .....13.08.06  
 Cooper, David .....SP074  
 Cooper, Jon .....06.01.07  
 Coppens, Philip .....05.01.06  
 Coppens, Philip .....AW.03.02  
 Coppens, Philip .....AW.03.04  
 Coppens, Philip .....TP114  
 Cornaby, Sterling .....13.08.06  
 Cort, John .....01.06.06  
 Cortese, Marc .....MP056  
 Costantino, David .....13.05.01  
 Costin-Hogan, Christina .....SP213  
 Coulibaly, Fasseli .....13.08.02  
 Coulibaly, Fasseli .....SP022  
 Court, Donald .....MP021  
 Cousido, Alexandra .....06.01.02  
 Covic, Nermina .....TP145  
 Cowan, John .....10.01.10  
 Cowan, John .....MP198  
 Cowan, John .....SP233  
 Cowan, Matt .....MP231  
 Craig, Paul .....SP01.06  
 Craig, P.A. ....TP172  
 Croce, Gianluca .....05.01.02  
 Crotty, Justin .....SP242  
 Crow, Lowell .....MP235  
 Cubitt, Robert .....13.04.01  
 Cudney, Robert .....SP066  
 Cuff, Marianne .....MP083

# Author Index

Cuff, Marianne .....	SP037	Dice, Lezlee .....	MP007	Edwards, A. ....	MP029
Cuff, Marianne .....	TP156	Dietz Rago, Nancy L. ....	09.03.05	Egami, Takeshi .....	13.07.08
Cunha, Rodrigo .....	TP215	Dietz Rago, Nancy L. ....	13.07.03	Ehlers, G. ....	TP184
Cunha, Silvio .....	SP200	Digre, Jeff .....	SP138	Ehm, Lars .....	05.02.03
Cuocci, Corrado .....	07.01.01	Dillard, Bret D. ....	MP044	Eidam, Oliv .....	SP147
Curtis, Joseph .....	13.03.05	DiMarco, John .....	04.01.05	Einspahr, Howard .....	WK.02.01
Custelcean, Radu .....	10.03.02	DiMarco, John .....	10.01.07	Eisenberg, David .....	01.08.03
Cutler, Paul .....	MP235	Dimitropoulos, D. ....	TP087	Eisenberg, David .....	10.04.02
Cymborowski, Marcin .....	TP156	Dix, Ina .....	03.02.01	Eisenberg, David .....	13.08.01
Dabrowski, Bogadn .....	TP188	Dix, Ina .....	TP240	Eisenberg, David .....	SP074
Daemen, Luke .....	05.02.05	Dixon, Richard A. ....	SP046	Eisenberg, E. ....	13.01.03
Dahbi, Louisa .....	13.04.02	Dixon, Richard A. ....	TP135	Ellis, Jeffrey .....	SP052
Dahlberg, Albert E. ....	01.01.07	Dmowski, Wojtek .....	13.07.08	Elmore, Bradley .....	01.01.02
Dahlberg, Albert E. ....	SP003	Dobrzanska, Liliana .....	10.03.10	Emerich, Hermann .....	05.01.02
Dai, Sheng .....	13.07.08	Dodds, Peter .....	SP052	Emsley, Paul .....	WK.01.12
Daily, Abigail .....	SP023	Domasevitch, Konstantin .....	SP209	Engebretson, J.E. ....	10.04.04
Daniels, Lee .....	10.01.14	Dominiak, Paula .....	TP114	Englich, Ulrich .....	13.10.06
Daniels, Lee .....	MP234	Domsic, John .....	TP132	Englich, Ulrich .....	MP077
Daniels, Lee .....	MP241	Dong, Aiping .....	01.03.08	Enright, Gary .....	10.02.06
Dann, Charles E., III .....	MP059	Dong, Huaze .....	SP216	Enright, Gary .....	10.03.05
Darakev, Georgi .....	TP172	Doniach, Sebastian .....	13.03.03	Erilov, Denis .....	SP147
Darakev, Georgi .....	TP174	Dontsova, O.A. ....	MP029	Escamilla-Trevino, Luis L. ....	TP135
Darakev, N. ....	TP172	Dorelejers, J. ....	TP087	Escuyer, Vincent .....	MP033
Das, Debanu .....	SP248	Dorelejers, Jurgan .....	WK.02.03	Escuyer, Vincent .....	SP037
Das, Rhiju .....	01.07.06	Dorset, Douglas .....	07.01.03	Esser, Lothar .....	01.04.02
Dauter, Zbigniew .....	01.03.05	Doucleff, Michaelleen .....	13.03.02	Evans, Colin .....	TP105
David, William .....	07.01.02	Dougan, Brenda .....	TP183	Ewalt, Karla .....	MP049
David, William .....	AW.02.04	Dowell, A.L. ....	MP082	Fabbiani, Francesca .....	10.04.06
Davies, Doug .....	04.01.03	Doxsee, Kenneth .....	10.03.04	Fait, James .....	01.03.01
Davis, Tara L. ....	SP025	Dragos, Vizitiu .....	TP100	Fait, James .....	MP232
Day, Graeme M. ....	AW.01.02	Dravid, Vinayak .....	13.07.07	Fait, James .....	TP222
Day, John .....	SP066	Drennan, Catherine .....	SP017	Falvello, Larry R. ....	10.01.12
De Carlo, Sacha .....	13.03.02	du Boulay, Douglas .....	03.01.07	Falvello, Larry R. ....	10.02.02
de Rango, Patricia .....	13.06.02	Du Clos, Terry W. ....	MP166	Falvello, Larry R. ....	MP169
de Silva, Udesh .....	SP062	Duax, W.L. ....	TP125	Fan, Erkang .....	MP163
Deacon, Ashley .....	01.06.04	Duax, W.L. ....	TP088	Fan, Erkang .....	TP124
Deacon, Ashley .....	SP248	Duax, W.L. ....	TP092	Fan, Fan .....	01.01.06
Deacon, Ashley .....	TP128	Duerst, Richard W. ....	TP251	Fanwick, Phillip .....	10.02.01
Deal, T.K. ....	10.04.04	Duggan, Erica .....	SP075	Farh, Lynn .....	SP130
Dealwis, Chris .....	MP007	Duke, Gerald .....	MP243	Faust, Annette .....	13.10.05
Debreczeni, Judit E. ....	WK.01.10	Duke, Norma .....	MP083	Fedorov, Alexander .....	TP101
Decker, Bjorn .....	13.07.05	Duke, Norma .....	MP247	Fedorov, Elena .....	TP101
Deisenhofer, Johann .....	TP245	Duke, Norma .....	TP115	Feng, Qiping .....	SP136
Deka, Ranjit K. ....	TP140	Duke, Norma .....	TP156	Feng, Z. ....	TP087
Delgado, Jose Miguel .....	TP217	Dunaway-Mariano, Debra .....	AW.03.08	Fenter, Paul A. ....	09.02.02
Delgado, Paulino .....	SP191	Duncan, J. Richard .....	10.03.12	Ferrara, Joseph D. ....	01.01.02
Demirci, Hasan .....	01.01.07	Dunham, Christine .....	01.08.05	Ferrara, Joseph D. ....	01.03.04
Demirci, Hasan .....	SP003	Dunin-Borkowski, Rafal .....	13.07.05	Ferrara, Joseph D. ....	10.01.14
DePaoli-Roach, Anna .....	MP056	Dunitz, Jack D. ....	AW.01.03	Ferrara, Joseph D. ....	MP082
Derewenda, Urszula .....	SP074	Dunker, A. Keith .....	MP056	Ferrara, Joseph D. ....	MP234
Derewenda, Zygmunt .....	SP074	Dunny, Gary M. ....	TP098	Ferrara, Joseph D. ....	MP241
Deschamps, J. ....	TR.01.12	Dunten, P. ....	SP246	Ferreira, Jailton .....	SP200
Desiraju, Gautam R. ....	AW.02.02	Durfee, William S. ....	AW.03.04	Ferreira, Janaina G. ....	10.04.03
Desper, John .....	10.01.01	Durst, Roger .....	MP236	Ferrell, Katherine .....	TP097
Desper, John .....	10.03.08	Dutta, S. ....	TP087	Fischetti, Robert .....	13.08.03
Desper, John .....	AW.03.03	Duxbury, Phillip M. ....	07.01.12	Field, Robert .....	TP181
Desper, John .....	SP206	Dworkowski, Florian .....	SP147	Fiser, Andras .....	01.06.03
Desper, John .....	SP207	Dyakonenko, Victoria .....	TP203	Fisher, Rob .....	SP042
Dewhurst, Charles .....	13.04.01	Dzikowski, Tashia .....	05.02.04	Fisher, S. Zoe .....	TP132
DeWitt, Kenneth J. ....	SP069	Ealick, Steven .....	13.08.04	Fisher, Suzanne .....	06.01.03
Dhe-Paganon, Sirano .....	SP025	Ealick, Steven .....	SP014	Fitzpatrick, Paul .....	01.01.06
Di Cera, Enrico .....	SP252	Ealick, Steven .....	TP223	Fitzpatrick, Paul F. ....	TP175
Diawara, Yacouba .....	MP236	Earart, Cathleen. A. ....	SP123	Fleming, Chris .....	AW.03.05
Diaz de Delgado, Graciela .....	SP191	Earhart, Cathleen A. ....	SP138	Flippen-Anderson, J. ....	TP087
Diaz de Delgado, Graciela .....	TP217	Earhart, Cathleen A. ....	TP098	Florence, Alastair .....	10.04.06

## Author Index

Flot, David .....	13.08.05	Gillilan, Richard .....	13.08.06	Gu, Zu Yi .....	SP138
Flynn, Galen .....	TP150	Gilliland, Gary .....	01.06.05	Guan, Weiguang .....	TR.01.10
Focia, Pamela .....	SP047	Gilmore, Chris .....	07.01.03	Guanga, Gerald .....	MP015
Fontes, Ernie .....	MP077	Gilson, Michael .....	TP112	Guelker, Megan .....	SP127
Forbes, Safiyyah .....	SP206	Gindhart, Amy .....	05.01.05	Guijarro, M. ....	13.08.05
Formosa, Timothy .....	TP097	Gindhart, Amy .....	AW.03.01	Guillot, Benot .....	TP149
Forouhar, Farhad .....	01.06.06	Ginell, Stephan.....	06.01.02	Guimaraes, Beatriz .....	TP118
Forster, A. ....	SP001	Ginell, Stephan .....	13.01.02	Gulick, Andrew .....	AW.03.08
Forwood, Jade .....	SP052	Ginell, Stephan .....	MP083	Guncar, Gregor .....	SP052
Fournier, Bertrand .....	TP149	Ginell, Stephan .....	SP224	Guo, Liang .....	13.03.02
Fox, Stephen .....	SP201	Girard, Gregory .....	13.06.02	Guo, Yi .....	TP129
Foxman, Bruce M. ....	10.03.01	Gleason, William .....	TP148	Guo, Youzhong .....	SP031
Foxman, Bruce M. ....	13.09.04	Gletting, Wayne .....	MP229	Guogas, Laura .....	01.01.04
Frank, Matthias .....	09.03.03	Glockshuber, Rudi .....	SP147	Gurda Whitaker, Brittney .....	SP039
Franke, Sylvia .....	SP109	Glusker, Jenny .....	13.09.02	Gurney, Mark .....	04.01.03
Franklin, Rosalind .....	TP141	Gniadek, Thomas J. ....	AW.01.05	Guss, Mitchell .....	MP032
Fraser, Marie .....	MP018	Godzik, Adam .....	01.06.04	Guss, Mitchell .....	MP157
Frey, Friedrich .....	TR.01.07	Godzik, Adam .....	TP090	Gutierrez, Aldo .....	13.03.01
Fritsky, Igor .....	MP196	Gofron, Kazimierz .....	SP224	Gutmann, Sascha .....	13.08.02
Fritsky, Igor .....	TP205	Golan, Yuval .....	13.07.02	Guzei, Ilia A. ....	TP173
Fronczek, Frank .....	SP201	Goldberg, Israel .....	10.01.03	Guzei, Ilia A. ....	WK.01.06
Fruchart, Daniel .....	13.06.02	Goldschmidt, Lukasz .....	13.08.01	Ha, Nam-Chul .....	MP048
Fruchart, Daniel .....	13.06.03	Goldschmidt, Lukasz .....	SP074	Ha, Ya .....	01.01.05
Fu, Zheng-Qing .....	01.03.01	Gonczy, John .....	01.03.01	Hackenberg, Robert .....	TP181
Fu, Zheng-Qing .....	MP232	Gonczy, John .....	MP232	Hackert, Marvin .....	SP031
Fu, Zheng-Qing .....	TP151	Gonczy, John .....	TP222	Hackley, Vincent A. ....	09.01.06
Fu, Zheng-Qing .....	TP222	Gonzalez, A.M. ....	TP189	Haddad, Salim .....	05.01.04
Fujiwara, Kazuko .....	MP034	Gonzalez, Ana .....	13.10.07	Haebel, Peter W. ....	13.08.02
Fukuto, Masafumi .....	13.03.04	Goodbread, Michele .....	TP105	Habel, J. ....	MP044
Fukuto, Masfaumi .....	MP160	Goodwin, Kristie .....	MP056	Haemig, Heather A. ....	TP098
Funk, Russell J. ....	TP208	Goossens, D.J. ....	TR.01.01	Haertlein, Michael .....	06.01.02
Furey, William .....	TP134	Gordon, Roni .....	TP100	Hagman, Kayla .....	TP140
Furubayashi, Naoki .....	SP065	Gosavi, Rajendrakumar .....	SP067	Hajdu, Janos .....	09.03.03
Fyfe, A. ....	SP246	Gou, Shaohua .....	SP216	Halavaty, Andrei .....	TP142
Gadda, Giovanni .....	01.01.06	Gouaux, Eric .....	01.02.01	Hall, Traci .....	MP061
Galella, Michael .....	04.01.05	Gougoutas, Jack .....	04.01.05	Hamada, Kensaku .....	SP072
Galella, Michael .....	10.01.07	Gougoutas, Jack .....	10.01.07	Hammes, Katherine .....	MP081
Gallegos, Jose H. ....	TP210	Govindasamy, L. ....	TP133	Hammouda, Boualem .....	MP157
Gambino, L. ....	TP125	Govindasamy, Lakshmanan .....	TP132	Hancock, Robert .....	01.04.03
Gan, Jianhua .....	MP021	Grabowski, Marek .....	TP095	Handly, Jeff .....	09.01.04
Garcia-Garibay, Miguel A. ....	10.03.07	Graeff, Richard .....	SP099	Hang, Dehva .....	WK.02.05
Gardberg, Anna .....	MP007	Graf, Jorgen .....	03.01.05	Hanley, Tracey .....	MP157
Garman, Elspeth .....	13.10.01	Gray, Lester T. ....	10.03.12	Hanse, E. ....	04.01.03
Garratt-Reed, Anthony .....	05.01.01	Green, Katherine .....	13.07.09	Hanson, B. ....	TP172
Garvey, Hugh .....	MP234	Greenbaum, Elis .....	MP161	Hanson, Brett .....	SP.01.06
Gates, Stacy .....	AW.03.01	Gregory, Steven T. ....	01.01.07	Hanson, Brian E. ....	MP169
Gatta, G. Diego .....	TR.01.11	Gregory, Steven T. ....	SP003	Hanson, Bryant L. ....	13.10.03
Gavezzotti, A. ....	AW.01.01	Greimann, Jaclyn .....	01.08.02	Hanson, Bryant L. ....	SP069
Geders, Todd .....	SP053	Grew, Edward .....	05.02.04	Hanson, Jonathan .....	13.04.04
Geisbrecht, Brian .....	MP028	Grice, Joel .....	07.01.05	Hanson, Leif .....	06.01.05
Geiser, Urs .....	TP208	Grice, Rena .....	TP094	Hanson, Leif .....	SP187
Gembicky, Milan .....	05.01.06	Grieving, Matthew .....	SP242	Hansson, Henrik .....	01.05.01
Gembicky, Milan .....	AW.03.02	Grishaev, Alexander .....	13.03.06	Hao, Quan .....	01.07.01
Genis, C. ....	TP133	Grizot, Sylvestre .....	01.04.02	Hao, Quan .....	13.01.06
Gentile, T.R. ....	TP184	Groat, Lee .....	05.02.04	Hao, Quan .....	MP077
George, Sumod .....	10.01.03	Grosse-Kunstleve, Ralf .....	01.07.07	Hao, Quan .....	SP099
Gerhardt, Rosario .....	09.01.10	Grossmann, J.G. ....	13.03.01	Hao, Quan .....	SP103
Gerlt, John .....	TP101	Gruber, Achim .....	MP167	Haq, O. ....	TP087
German-Acacio, Juan Manuel .....	10.03.08	Gruner, Sol M. ....	13.01.06	Harris, Julie .....	SP244
Gerwe, Brian .....	MP044	Gruner, Sol M. ....	MP077	Harris, Mark .....	01.05.01
Geyer, Matthias .....	SP058	Gruninger, Robert J. ....	SP050	Harris, Seth .....	MP179
Ghate, Manjiri .....	MP179	Grutter, Markus G. ....	SP147	Harrison, David .....	TP141
Ghirlando, Rodolfo .....	01.04.02	Gu, Liangcai .....	SP053	Hart, Darren J. ....	SP147
Ghirlando, Rodolfo .....	MP028	Gu, Minyi .....	MP247	Hartl, Monika .....	05.02.05
Giacovazzo, Carmelo .....	07.01.01	Gu, Minyi .....	SP041	Hartlieb, Bettina .....	13.05.03

# Author Index

Harty, Derek	MP032	Hodges, Jason	07.01.10	Inaka, Koji	SP065
Harvey, Scott	SP062	Hodges, Jason	MP235	Inaka, Koji	SP071
Hasegawa, Kazuya	13.02.03	Hoeft, Rebecca	SP138	Inderhees, Sue	13.07.09
Hasegawa, Kazuya	TP239	Hoffmann, Christian	03.01.05	Ionides, J.	TP087
Hasegawa, Tomokazu	SP072	Hoffmann, Christina	10.01.10	Irwin, Jeffrey	13.07.02
Hassan, Ishmael	MP193	Hoffmann, Christina	TP183	Isenegger, Andreas	MP229
Hassani, Abdellah	SP025	Hoffmann, Christina	TP184	Israelachvili, Jacob N.	13.07.02
Hatton, Peter	09.03.04	Hogan, Greg A.	10.03.06	Ito, Jennifer	MP159
Hatzos, Cathy	SP075	Hogan, Greg A.	10.03.11	Ivanova, Magdalena	10.04.02
Haukka, Matti	MP196	Hoghoj, Peter	MP228	Ivanova, Magdalena	13.01.03
Haukka, Matti	TP205	Hol, Wim	MP163	Iwasaki, Kenji	TP146
Hauptman, Herbert	TP185	Hol, Wim	MP165	Jackson, Michael R.	SP076
Hawley, Marilyn	09.03.02	Hol, Wim	TP124	Jacobs, Tia	10.03.10
Hayakawa, Koto	MP018	Holland, Timothy	01.05.04	Jacobsen, Steve	TR.01.11
Hazemann, Isabelle	06.01.02	Hollis, Thomas	SP062	Jacques, David	MP157
Hazemann, Isabelle	13.01.02	Holmes, William	SP008	Jain, Anubhav	TP225
Hazzard, James	TP117	Holton, James M.	13.01.05	Jakes, Karen S.	01.04.02
He, Miao	01.04.05	Holyoak, Todd	TP143	James, Rini	TP100
He, Panqing	TP141	Homrichhausen, Tanja	01.02.01	Jančar, Bötjan	05.02.06
He, Xianzhi	TP135	Hong, Kunlun	13.07.04	Jardetzky, Theodore	13.05.05
He, Xiaolin	SP047	Honndorf, Valerie	TP110	Jasinski, Jerry P.	13.09.04
Hedl, Matija	SP011	Hooft, Rob	10.02.07	Jasti, Jaysankar	01.02.01
Heerdegen, A.P.	TR.01.01	Hooft, Rob	MP079	Jeffries, Cy	MP159
Hegazy, Hussein	TP182	Hooper, Alan	01.01.02	Jelsch, Christian	TP149
Heine, Andreas	TP110	Hoover, Timothy	13.03.02	Jemian, Peter	09.01.01
Heinekey, D. Michael	13.06.04	Horton, Nancy	TP144	Jemian, Pete	09.01.05
Heinhorst, Sabine	03.01.01	Hosaka, Harumi	MP034	Jemian, Pete	09.01.09
Heinz, Dirk	MP167	Hou, Jingtong	01.06.01	Jemilawon, John	TP172
Heitfeld, Kevin A.	09.01.03	Howard, Andrew	01.06.05	Jemilawon, John	TP174
Heller, William T.	13.03.08	Howard, Andy	TP222	Jenkins, Joby	MP177
Heller, William T.	MP161	Hsiao, Chwan-Deng	TP249	Jenny, F.E.	MP044
Helmbrecht, Elizabeth	MP007	Hsieh, Tung-Ju	SP130	Jerina, Donald	MP019
Helton, Katherine E.	MP161	Hsu, Che-Hsiung	TP249	Jerzy, Osipiuk	MP043
Hemmert, Andrew	AW.03.05	Hua, Fengjun	13.07.04	Ji, Xinhua	MP021
Hennessy, Daniel	MP030	Huang, Cheng-yang	TP249	Jia, Da	01.01.08
Hennessy, Daniel	SP070	Huang, Hector	13.03.02	Jia, N.	TP172
Henning, R.	06.01.03	Huang, Q.	TP221	Jiang, Jiansheng	TP171
Henrick, K.	TP087	Huang, Qingqiu	SP103	Jin, Rongsheng	13.05.04
Henry, Rodger F.	TP251	Huang, Shu-Yun	SP130	Jin, Zhongmin	01.03.01
Her, Jae-Hyuk	07.01.11	Huang, Zhen	TP171	Jin, Zhongmin	MP232
Herbst-Irmer, Regine	03.02.01	Hubbard, Stevan	TP122	Jin, Zhongmin	TP222
Herbst-Irmer, Regine	WK.01.03	Huether, Robert	TP088	Joachimiak, Andrzej	01.06.07
Herbstein, Frank H.	AW.02.01	Huether, Robert	TP092	Joachimiak, Andrzej	06.01.02
Hernandez-Ortega, Simon	10.03.08	Huether, Robert	TP125	Joachimiak, Andrzej	13.01.02
Hèroux, Annie	01.01.06	Hults, William	TP181	Joachimiak, Andrzej	MP029
Hèroux, Annie	TP175	Hunt, John	01.06.06	Joachimiak, Andrzej	MP043
Hèroux, Luke	13.04.06	Hunter, Abigail V.	TP202	Joachimiak, Andrzej	MP083
Hersh, Louis	SP023	Hunter, Neil	13.03.01	Joachimiak, Andrzej	MP247
Herzberg, Osnat	01.06.05	Hupp, Joseph T.	MP195	Joachimiak, Andrzej	SP041
Herzberg, Osnat	MP024	Huq, Ashfia	07.01.10	Joachimiak, Andrzej	SP075
Heyman, Benjamin M.	10.03.01	Huq, Ashfia	13.04.06	Joachimiak, Andrzej	SP224
Heyman, Jeremy B.	10.03.01	Hura, Greg	01.07.02	Joachimiak, Andrzej	TP156
Hickmott, Donald	05.02.05	Hurley, Thomas	MP056	Joachimiak, Grazyna	SP075
Higashiura, Akifumi	SP071	Huseby, Medora	SP123	Jogl, Gerwald	01.01.07
Higgin, Joshua	MP061	Husseini, Naji	MP080	Jogl, Gerwald	SP003
Hill, Christopher	01.02.03	Ibberson, R.M.	10.01.06	Jogl, Gerwald	SP008
Hill, Christopher	SP001	Ikura, Mitsuhiko	MP159	Jogl, Gerwald	SP012
Hill, Christopher	TP097	Ilavsky, Jan	09.01.01	Johnson, A.R.	SP01.01
Hill, John	09.03.04	Ilavsky, Jan	09.01.04	Johnson, Carroll	03.02.03
Hirata, Kunio	13.02.03	Ilavsky, Jan	09.01.05	Johnson, John E.	01.07.03
Hirata, Kunio	TP239	Ilavsky, Jan	09.01.06	Johnson, William	SP031
Hirota, Erika	SP064	Ilavsky, Jan	09.01.09	Johnston, Andrea	10.04.06
Hjelm, Rex	09.03.02	Ilavsky, Jan	TP190	Jones, Gary	07.01.05
Hobbs, Linn	05.01.01	Imker, Heidi	TP101	Jones, G.L.	TP184
Hockla, Alexandra	SP139	Inaka, Koji	SP064	Jordan, Frank	TP134

# Author Index

Jorgensen, James D. ....	TP188	Kim, Man-Ho .....	09.01.05	Kumasaka, Takashi .....	TP239
Judge, Russel .....	06.01.06	Kim, Seulki .....	MP048	Kuntz, D.A. ....	AW.03.06
Juhas, Pavol .....	07.01.12	Kim, Sung-Hou .....	01.06.01	Kushner, James .....	01.02.03
Jun, Se-Ran .....	01.06.01	Kim, Woo Taek .....	MP055	Kwon, Young D. ....	13.05.06
Jun, Sung-Hoon .....	MP055	Kim, Youngchang .....	MP043	Kwong, Peter .....	13.05.06
Jun, Young-Shin .....	09.02.06	Kim, Youngchang .....	MP083	Kyser, Laura T. ....	10.03.12
Jurgenson, Christopher .....	SP014	Kim, Youngchang .....	TP156	Lager, George .....	05.02.01
Jusino, Manuel .....	MP013	Kinder, Steve .....	SP233	Lagoutte, Angèlique .....	TP149
Kaduk, James .....	TP221	King, Glenn .....	MP157	Lai, Thomas .....	MP044
Kaduk, James .....	07.01.04	King, Tristan .....	03.01.07	Lakshmanan, Govindasamy .....	SP039
Kaercher, Joerg .....	03.01.06	Kinney, John .....	09.01.04	Lakshminarasimhan, M.....	SP137
Kaercher, Joerg .....	13.09.03	Kinney, John .....	TP190	Lamb, Robert .....	13.05.05
Kaftory, Menahem .....	AW.03.09	Kinnibrugh, Tiffany L. ....	SP219	Lamzin, Victor .....	13.10.05
Kahr, Bart .....	AW.02.05	Kinnibrugh, Tiffany L. ....	TP173	Lander, Gerry .....	09.03.04
Kakizawa, Junko .....	TP113	Kirillova, Olga .....	TP095	Langan, Paul .....	06.01.01
Kale, Sachin .....	TP134	Kirouac, Kevin .....	SP096	Langan, Paul .....	06.01.03
Kalinin, Yevgeniy .....	SP068	Kiryukhina, O. ....	TP106	Langan, Paul .....	06.01.05
Kalt, Herbert .....	MP229	Kish, Kevin .....	MP243	Langan, Paul .....	06.01.07
Kamburov, Petko .....	TP172	Kissinger-Kane, Marie .....	13.07.06	Langan, Paul .....	SP187
Kamburov, Petko .....	TP174	Kitao, Tomoe .....	TP146	Langley, David .....	MP032
Kaminsky, Werner .....	MP084	Kiyanagi, Ryoji .....	03.02.02	Langley, David .....	MP157
Kang, HaeJoo .....	SP022	Klebe, Gerhard .....	TP110	Langs, David .....	TP185
Kantardjieff, K.A. ....	SP01.01	Klei, Herbert .....	MP243	Laowanapiban, Poramaet .....	TP155
Kantrowitz, Evan .....	TP153	Klein Stevens, Cheryl .....	MP192	Large, Andrew .....	13.03.01
Kapon, Moshe .....	AW.02.01	Kleywegt, Gerard J. ....	01.05.01	Lariucci, Carlito .....	10.01.09
Kaptein, Robert .....	WK.02.02	Klueh, Ron .....	09.01.05	Lariucci, Carlito .....	SP200
Karlen, Steven D. ....	10.03.07	Klug, Dennis .....	05.02.03	Larson, Eric .....	MP163
Karplus, P. Andrew .....	01.03.07	Kmetko, Jan .....	13.10.06	Larson, Eric .....	TP124
Karplus, P. Andrew .....	SP020	Ko, Jan .....	MP007	Larson, Steven .....	SP066
Kasahara, Hideko .....	MP040	Kobayashi, Tomoyuki .....	SP064	Laskowski, Roman .....	01.06.02
Kasama, Takeshi .....	13.07.05	Kobayashi, Tomoyuki .....	SP065	Lavy, Tali .....	AW.03.09
Katsube, Yukiteru .....	SP072	Kobayashi, Tomoyuki .....	SP071	Lawson, Andrew .....	TP181
Kauffmann, Brice .....	13.10.05	Kobayashi, Tomoyuki .....	SP072	Lawson, C. ....	TP087
Kawamoto, Masahide .....	TP239	Kobe, Bostjan .....	SP052	Lazarski, Krzysztof .....	MP083
Kawate, Toshimitsu .....	01.02.01	Kocsis, Jessica .....	SP009	Lazarski, Krzysztof .....	SP224
Kazimierz, Gofron .....	MP083	Koetzle, Thomas F. ....	10.01.10	Lazzari, Remi .....	09.02.04
Kazimirov, Alex .....	MP077	Koetzle, Thomas F. ....	13.06.04	Le Page, Yvon .....	07.01.05
Ke, Wei .....	SP051	Kohls, Doug .....	09.01.07	Le Trong, Isolde .....	MP163
Keel, Amanda .....	13.05.01	Kohrer, Caroline .....	MP049	Le Trong, Isolde .....	TP124
Kelekanjeri, V. Siva Kumar G. ....	09.01.10	Kokozay, Vladimir .....	TP203	Leahy, Daniel .....	MP013
Kelley, Laura-Lee Clancy .....	MP044	Kokozay, Volodymyr .....	SP204	Leahy, Daniel .....	MP028
Kelley, M. ....	TP189	Kondrashkina, Elena .....	13.03.02	Lecomte, Claude .....	05.01.03
Kelly, Ann .....	TP181	Kondrashov, Dmitry .....	01.07.04	Lecomte, Claude .....	TP149
Kenis, Paul .....	01.02.04	Kong, Leopold .....	13.05.06	Lee, Byeongdu .....	09.02.03
Kennedy, Michael .....	01.06.06	Konnert, John .....	TR.01.12	Lee, Byeongdu .....	09.02.06
Kenney, Christopher .....	13.02.02	Korczynska, Magdalena .....	SP027	Lee, Byeongdu .....	09.03.05
Kerfeld, Cheryl A. ....	03.01.01	Korman, Tyler .....	MP057	Lee, Byeongdu .....	13.07.03
Kerfeld, Cheryl A. ....	MP006	Kornberg, Roger .....	13.01.01	Lee, D. ....	MP044
Keyzers, Robert .....	TP102	Kornberg, Roger .....	SP.02.01	Lee, Hon Cheung .....	SP099
Khayat, Reza .....	01.07.03	Kortright, Jeff .....	09.03.01	Lee, Ji-Hye .....	TP176
Khazins, David .....	MP236	Kortright, Jeffrey .....	09.03.02	Lee, Jon .....	09.01.04
Khrustalev, Victor .....	SP199	Kosada, T. ....	TP087	Lee, Lisa S. ....	10.03.09
Khrustalev, Vlvtor .....	SP219	Koshihara, Shin-Ya .....	05.01.06	Lee, Sungsik .....	09.02.03
Kickhoefer, Valerie .....	01.08.03	Kouranov, A. ....	TP087	Lee, Ung .....	SP242
Kieft, Jeffrey .....	13.05.01	Kourinov, Igor .....	TP223	Lee, W.T. ....	TP184
Kienker, Paul S. ....	01.04.02	Kraabel, Brett .....	MP228	Lee, Weontae .....	MP055
Kim, Beomseok .....	13.07.05	Kretschmer, Jennifer .....	TP111	Lee, Yong Joo .....	MP054
Kim, Chae Un .....	13.01.06	Kriksunov, Irina .....	SP099	Leech, Charlotte .....	10.04.06
Kim, Chae Un .....	MP077	Krueger, Joanna .....	13.03.07	Legendre, Alexandre O. ....	10.04.03
Kim, Dong-Uk .....	MP054	Krueger, Susan .....	13.03.05	Lengeling, Andreas .....	MP167
Kim, Hidong .....	04.01.03	Krug, Robert .....	13.05.02	Leo, Stephen .....	03.01.06
Kim, Jin Kwang .....	TP176	Krumm, Brian .....	MP165	Leonard, Arah .....	03.01.06
Kim, Jung-Ja .....	01.04.05	Krumm, Brian .....	TP124	Leonard, Gordon .....	MP237
Kim, Kwan Soo .....	MP054	Kruse, Schoen .....	TP111	Leory, Frederic .....	09.02.04
Kim, Kyung Hyun .....	TP176	Kuglstatter, Andreas .....	MP179	Lesley, Scott A. ....	01.06.04

# Author Index

Lesley, Scott A. ....	13.03.03	Lystad, K.M. ....	10.04.04	McLellan, Jason .....	MP028
Lesnyak, D.V. ....	MP029	Ma, Baoqing .....	MP195	McMullen, Donald .....	03.01.07
Letoublon, Antoine .....	09.02.04	Ma, Dengbo .....	TP100	McPherson, Alexander .....	SP066
Levin, Elena .....	01.07.04	Ma, Xiaolei .....	03.01.02	McRee, Duncan .....	04.01.06
Levashin, Elena .....	TP245	Macchi, Piero .....	AW.01.04	McRee, Duncan .....	MP049
Levine, Lyle .....	09.01.09	MacDonald, John .....	10.03.09	McRee, Duncan .....	MP178
Li, Chunmin .....	TP102	MacGillivray, Leonard R. ....	TP220	McSweeney, Sean .....	13.08.05
Li, Hongmin .....	TP129	MacGillivray, Leonard R. ....	TP251	McSweeney, Sean .....	MP237
Li, Hua .....	SP012	Machius, Mischa .....	TP140	Medvedev, Dimitri .....	07.01.07
Li, Hue .....	SP075	Mackay, Joel .....	SP052	Meigs, George .....	13.01.05
Li, Hui .....	SP041	MacKnight, Kamrin .....	04.01.07	Meilleur, Flora .....	06.01.02
Li, Lenong .....	TP093	Maddry, Joseph .....	MP033	Meilleur, Flora .....	06.01.06
Li, Lenong .....	TP135	Mading, Steve .....	WK.02.03	Meilleur, Flora .....	13.01.02
Li, Meng .....	SP017	Madsen, Anders .....	10.04.02	Meinhold, Lars .....	TR.01.05
Li, Rongbao .....	MP033	Madsen, Anders .....	13.08.01	Melnichenko, Yuri .....	13.07.04
Li, Rongbao .....	SP037	Madsen, A.Ø. ....	13.01.03	Merritt, Ethan .....	01.07.05
Li, Xuefa .....	09.02.05	Mairs, T. ....	13.08.05	Merritt, Ethan .....	MP163
Li, Xuefa .....	13.07.07	Majeed, Shahzad .....	13.05.06	Merritt, Ethan .....	TP124
Li, Youli .....	13.07.02	Mal, Tapas .....	MP159	Meske, Louise .....	01.02.05
Li, Zhong .....	TP129	Mallett, T. Conn .....	AW.03.07	Messerschmidt, Marc .....	05.01.06
Liang, Yan .....	MP162	Mallett, T. Conn .....	SP020	Messerschmidt, Marc .....	TP114
Lima, Christopher .....	01.08.02	Malley, Mary .....	10.01.07	Metcalf, Peter .....	13.08.02
Lin, Jundong .....	WK.02.03	Mamat, Bjorn .....	04.01.03	Metz, Adrian .....	TP094
Lin, Te-Sheng .....	SP130	Mang, Joseph .....	09.03.02	Michaelsen, Carsten .....	03.01.05
Lin, Xiao-Min .....	13.07.01	Mao, Qilong .....	TP088	Michikawa, Takayuki .....	MP159
Lind, Cora .....	05.01.05	Mao, Qilong .....	TP092	Mihailova, Boriana .....	TR.01.11
Lind, Cora .....	AW.03.01	Mao, Qilong .....	TP125	Mikoshiba, Katsuhiko .....	MP159
Ling, Hong .....	MP019	Marchesini, Stefano .....	09.03.03	Milanesio, Marco .....	05.01.02
Ling, Hong .....	SP016	Marin-Garcia, Maria Liliana .....	SP211	Miller, Edward B. ....	SP039
Ling, Hong .....	SP096	Mariuzza, Roy .....	TP119	Miller, Joel .....	10.01.11
Lipfert, Jan .....	13.03.03	Mark, Brian .....	SP104	Miller, M.E. ....	TP184
Lipstman, Sophia .....	10.01.03	Markley, John .....	WK.02.03	Miller, Matthew .....	MP061
Littrell, Ken .....	09.01.02	Markley, J. ....	TP087	Miller, Mitchell .....	SP248
Liu, Gaohua .....	01.06.06	Marnell, Lorrain L. ....	MP166	Miller, Mitchell .....	TP128
Liu, Heli .....	SP047	Martick, M.M. ....	SP246	Milligan, Rory .....	SP075
Liu, J. ....	01.06.06	Martin, Kenneth L. ....	SP.01.03	Minasov, George .....	01.02.06
Liu, James .....	SP035	Martin, Kenneth L. ....	TP202	Minasov, George .....	TP106
Liu, Jianming .....	MP049	Martinez, Rodolfo .....	SP199	Minor, Wladek .....	TP095
Liu, Peng .....	MP162	Mason, T.G. ....	13.04.03	Minor, Wladek .....	TP156
Liu, Quansheng .....	01.08.02	Masters, E.I. ....	SP001	Miraglia, Salvatore .....	13.06.02
Liu, Qun .....	SP099	Mathews, F. Scott .....	SP252	Mishra, Rama .....	04.01.03
Liu, Xuying .....	SP187	Matsuda, Makoto .....	MP034	Mitchell, E. ....	13.08.05
Liu, Zhi-Jie .....	MP044	Matsuoka, Takeshi .....	SP020	Mitschler, Andre .....	06.01.02
Lo, Chieh-Tsung .....	09.03.05	Mattay, Jochen .....	13.07.05	Mitschler, Andre .....	13.01.02
Lo, Chieh-Tsung .....	13.07.03	Matthews, Kathleen .....	MP250	Mixon, Mark .....	MP084
Londer, Yuri .....	TP115	Mauro, Antonio E. ....	10.04.03	Mixon, Mark .....	TP094
Long, Gabrielle G. ....	09.01.01	Maurus, Robert .....	SP.01.04	Mo, Yiming .....	13.03.08
Long, Gabrielle G. ....	09.01.09	Maxey, Evan R. ....	13.04.06	Modolo, Luzia .....	TP135
Longo, Antonella .....	MP015	Maynard, James .....	SP244	Modrich, Paul .....	TP154
Lorimer, Don .....	TP094	Mays, Jimmy .....	13.07.04	Moffat, Keith .....	06.01.03
Lou, Xiaochun .....	TP251	Maziuk, Dimitri .....	WK.02.03	Moffat, Keith .....	TP142
Lountos, George .....	01.01.06	McAndrew, Ryan .....	01.04.05	Mohsen, Al-Walid A. ....	01.04.05
Lu, Jinghua .....	MP166	McBride, J. Michael .....	AW.01.05	Moiseeva, Natalia .....	01.08.04
Lu, Kun .....	MP162	McCarthy, Andrew .....	MP237	Mold, Carolyn .....	MP166
Luisi, Brian S. ....	10.03.09	McCarthy, Grace .....	MP231	Moliterni, Anna Grazia G. ....	07.01.01
Lukacik, Petra .....	01.04.02	McColester, Sarah .....	TP105	Molitsky, Mike .....	SP224
Lumpkins, Sara B. ....	TP140	McCoy, Jason .....	01.02.05	Montelione, Gaetano T. ....	01.06.06
Lund, Peter .....	13.03.01	McCoy, Jason .....	TP126	Montelione, Gaetano T. ....	WK.02.05
Lundy, Matthew .....	SP073	Mccoy, Airlie .....	01.07.06	Montfort, William .....	SP109
Luo, J. ....	SP219	McDonough, Michael A. ....	SP026	Montfort, William .....	SP242
Luo, T.-J. Mark .....	10.03.09	McFarlane, Heather .....	13.01.03	Montfort, William .....	TP117
Lynch, Ed .....	TP223	Mcintyre, Garry .....	TP183	Moore, Elizabeth .....	SP244
Lynch, V. ....	05.02.07	McKenna, Robert .....	SP039	Moore, John .....	SP244
Lynn, David G. ....	MP162	McKenna, Robert .....	TP132	Moraes, Trevor .....	01.04.03
Lynn, Gary .....	13.03.08	McKenna, Robert .....	TP133	Moran, Graham .....	TP141

## Author Index

Moreno-Carcamo, Abel .....	SP211	Nguyen, SonBinh T. ....	MP195	Pan, Guirong .....	09.02.01
Mori, Hajime .....	13.08.02	Nichol, Gary .....	SP218	Pan, Xioakang .....	01.02.05
Morokuma, Keiji .....	01.01.06	Nicolazzi, William .....	05.01.03	Pancera, Marie .....	13.05.06
Moroz, Iurii .....	TP205	Nielsen, Christopher .....	13.02.04	Panepucci, Ezequiel .....	MP229
Morrison, Shane D. ....	MP010	Nielsen, Christopher .....	MP237	Panizales, Christia .....	SP01.05
Morstadt, Lucia .....	SP226	Nienaber, Vicki .....	MP178	Panjikar, Santosh .....	01.03.03
Mosca, Roberto .....	TP089	Niimura, Nobuo .....	06.01.04	Panjikar, Santosh .....	MP078
Mosimann, Steven .....	SP050	Nikitina, Vitalina .....	TP203	Parise, John B.....	05.02.03
Moss, Lewis .....	09.01.10	Nisawa, Atsushi .....	TP239	Parise, John B. ....	07.01.07
Motohara, Moritoshi .....	SP072	Nishiyama, Mireille .....	SP147	Parish, David .....	TP092
Motokawa, Yutaro .....	MP034	Nixon, B. Tracy .....	13.03.02	Park, Changyong .....	09.02.02
Mottarella, S. ....	TP172	Nocek, Boguslaw .....	TP156	Park, Heeyoung .....	MP055
Moudrakovski, Igor .....	10.02.06	Nogales, Eva .....	13.03.02	Parker, Sherwood .....	13.02.02
Moult, John .....	01.06.05	Nogi, Terukazu .....	TP146	Parker, William .....	MP033
Moulton, Brian .....	10.03.09	Nolas, G. ....	TP221	Parkin, Sean .....	10.04.01
Mowers, Jonathan .....	SP053	Noll, Bruce C. ....	03.02.05	Parkin, Sean .....	AW.02.03
Moyer, Bruce .....	10.03.02	Nollert, Peter .....	MP084	Parsonage, Derek .....	SP020
Mueller, Peter .....	13.09.01	Nollert, Peter .....	TP094	Parsons, S. ....	10.01.06
Mueller, Peter .....	WK.01.02	Norgard, Michael V. ....	TP140	Pasche, Bastian .....	MP167
Mueller-Dieckmann, Christoph .....	01.03.03	Novotny, Marian .....	01.05.01	Patel, Dimki .....	SP085
Mueller-Dieckmann, Christoph .....	MP078	Nowell, Harriott .....	10.04.06	Paterson, Reay .....	13.05.05
Mueser, Timothy .....	SP067	Nunes, Rafael .....	SP200	Patterson, Paul .....	MP007
Mukhtar, Tariq A. ....	SP027	Nuñez, Jose E. ....	10.03.07	Pearson, Arwen .....	01.01.02
Mulfort, Karen L. ....	MP195	Nurizzo, D. ....	13.08.05	Pease, Brian .....	04.01.03
Muller-Diekmann, C. ....	MP237	Nurizzo, D. ....	MP237	Pecharsky, Vitalij .....	13.04.05
Muniappan, Sankar .....	10.01.03	Nussenzweig, Victor .....	MP165	Peng, Yi .....	SP136
Munshi, Cyrus .....	SP099	O'Brien, Zachary .....	10.03.07	Perez, Ruth G. ....	MP030
Muralidharan, Govindarajan .....	09.01.05	O'Neill, Hugh .....	MP161	Perman, Benjamin .....	MP013
Murillo, Carlos .....	10.01.13	Oeko, Benjamin .....	MP160	Perrino, Fred .....	SP062
Murphy, Frank .....	01.08.05	Ofek, Gilad .....	13.05.06	Perry, Sarah .....	01.02.04
Musaev, Djmaladdin .....	01.01.06	Ohlendorf, Douglas H. ....	SP123	Peschar, Rene .....	03.02.04
Mustyakimov, Marat .....	06.01.05	Ohlendorf, Douglas H. ....	SP138	Peterson, Matthew .....	07.01.08
Muthukumar, Lavanya .....	MP024	Ohlendorf, Douglas H. ....	TP098	Peterson, Ron .....	05.02.02
Muthusamy, Mylrajan .....	SP233	Ojala, W.H. ....	10.04.04	Petry, Sabine .....	01.08.05
Muziol, Tadeusz .....	13.05.03	Okamura-Ikeda, Kazuko .....	MP034	Pfingsten, Jennifer .....	13.05.01
Muzyczka, Nicholas .....	SP039	Olekhovitch, Natalya .....	SP074	Pflugrath, James W. ....	01.03.04
Myles, Dean .....	06.01.02	Oliva, Glaucius .....	SP091	Pflugrath, James W. ....	MP082
Myles, Dean .....	06.01.06	Oliveira, Carla .....	TP118	Pflugrath, James W. ....	MP234
Myles, Dean .....	13.01.02	Olmstead, Marilyn M. ....	03.02.05	Pham, Oanh .....	AW.03.02
Myles, Dean .....	13.03.08	Olmstead, Marilyn M. ....	10.01.02	Phillips, George N., Jr. ....	01.02.05
Myszka, David .....	MP007	Olmstead, Marilyn M. ....	10.04.05	Phillips, George N., Jr. ....	01.07.04
Naciri, J. ....	TR.01.12	Olsen, Bradley .....	09.02.05	Phillips, George N., Jr. ....	MP170
Nagarajan, Venugopalan .....	13.08.03	Orban, John .....	01.06.05	Phillips, George N., Jr. ....	TP126
Nagpal, Akanksha .....	TP175	Orler, Bruce .....	09.03.02	Phillips, George N., Jr. ....	TR.01.03
Nakagawa, Atsushi .....	MP034	Ornoff, Doug .....	TP108	Phillips, John D. ....	01.02.03
Nakagawa, Atsushi .....	SP065	Ortlund, Eric .....	TP108	Piao, Shunfu .....	MP048
Nakagawa, Atsushi .....	SP071	Orto, Peter .....	SP218	Piccoli, Paula M.B. ....	10.01.10
Nakamura, Yumiko .....	13.06.06	Orville, Allen M. ....	01.01.06	Piccoli, Paula M.B. ....	13.06.04
Nakamura, H. ....	TP087	Orville, Allen M. ....	TP175	Piccoli, Paula M.B. ....	MP198
Nalam, Madhavi .....	TP112	Ory, J. ....	TP087	Piccoli, Paula M.B. ....	TP184
Nam, Hyun-Joo .....	MP040	Osipiuk, Jerzy .....	MP029	Pichon-Pesme, Virginie .....	TP149
Nanao, Max .....	13.01.04	Osipiuk, Jerzy .....	TP156	Pickett, Austin .....	10.03.06
Napolitano, Hamilton .....	10.01.09	Osipiuk, Jerzy .....	MP083	Pickett, Austin .....	TP214
Narayanan, Beena .....	MP030	Otero, Francella .....	MP049	Pillet, Sebastien .....	05.01.03
Narayanan, Beena .....	SP070	Otwinowski, Z. ....	TP156	Pingali, Sai Venkatesh .....	MP162
Navarro, Marcos .....	TP118	Ou, Susan .....	MP007	Pinkerton, Alan A. ....	10.01.15
Nave, Colin .....	SP233	Ourmazd, Abbas .....	TR.01.06	Pinkerton, Alan A. ....	13.10.03
Neau, David .....	MP013	Ouyang, X. ....	SP01.01	Pinkerton, Alan A. ....	MP194
Neely, Helen .....	TP124	Overbury, Steven H. ....	13.07.08	Pint, Bruce .....	05.01.01
Neil, L. ....	TP140	Overturf, George .....	09.01.04	Pitak, Mateusz .....	05.01.06
Nelson, Rebecca .....	13.01.03	Pace, Jim B. ....	TP120	Pletnev, V.Z. ....	TP088
Nemeria, Natalia .....	TP134	Pagola, S. ....	TP189	Pletnev, V.Z. ....	TP125
Nesterova, Oksana .....	SP204	Paige, Carleitta .....	AW.03.07	Plotnikov, Liza .....	05.01.01
Neubert, Thomas .....	TP122	Pak, John .....	SP038	Podjarny, Alberto .....	06.01.02
Newton, M. Gary .....	MP044	Palmore, G. Tayhas R. ....	10.03.09	Podjarny, Alberto .....	13.01.02

# Author Index

Pohlhaus, Timothy	TP154	Riekel, Christian	10.04.02	Sabino, J. Ricardo	SP200
Pokkuluri, P. Raj	TP115	Riekel, Christian	13.01.03	Sack, John	MP243
Pommier, Carolyn	04.01.05	Riekel, Christian	13.08.01	Sadre-Bazzaz, Kianoush	TP097
Porcar, L.	13.04.03	Rife, Christopher	TP128	Safinya, Cyrus R.	13.07.02
Post, Kai	TP094	Rini, James	SP038	Salameh, Mohammed	SP139
Postigo, Matheus	SP091	Ripmeester, John	10.02.06	Salavaggione, Oreste	SP136
Potter, Phil	AW.03.05	Ripmeester, John	10.03.05	Saldin, Dilano	TR.01.06
Prabhakar, Rajeev	01.01.06	Rivera-Hernandez, Margarita	SP211	Sali, Andrej	01.06.03
Prabu-Jeyabalan, Moses	TP113	Rizzi, Rosanna	07.01.01	Samanta, Uttamkumar	TP086
Pradervand, Claude	13.08.02	Roach, Claudia	MP165	Sambashivan, Shilpa	10.04.02
Pradervand, Claude	MP229	Roberts, Andrew	07.01.05	Sambashivan, Shilpa	13.01.03
Prasad, B.V.L.S.	TP090	Roberts, Gordon	13.03.01	Sampath, Sowmya	SP023
Price, Sally	10.04.06	Roberts, Griffin	01.02.04	Sanchez, D.	SP147
Proft, Thomas	SP022	Roberts, Mary F.	SP01.05	Sandanayaka, V.	04.01.03
Proffen, Thomas	TP181	Roberts, Sue A.	MP010	Sanishvili, Ruslan	13.08.03
Puorger, Chasper	SP147	Roberts, Sue A.	SP109	Sankaran, Banuamthi	TP150
Pyckhout-Hintzen, Wim	13.04.02	Robertson, B.A.	SP031	Sano, Satoshi	SP064
Qian, Bin	01.07.06	Robertson, Michael	01.01.03	Sano, Satoshi	SP065
Qu, Zhican	MP033	Robinson, Howard	MP230	Sano, Satoshi	SP071
Quick, Rebekah	SP109	Robinson, Howard	MP231	Sano, Satoshi	SP072
Quilici, Roman	03.01.07	Robinson, Howard	TP097	Santella, Michael	09.01.05
Radisky, Evette	SP139	Robson, Cody	01.02.05	Santos, Regina H.A.	10.04.03
Rae, A. David	10.01.08	Rochon, Maïke	MP167	Saper, Mark	MP164
Raghavan, Aravinda	13.03.08	Rodgers, David	SP023	Sarma, Ganapathy	01.03.07
Rajashankar, Kanagalaghatta	13.08.04	Rodriguez, Jose	13.04.04	Sasaki, Katsunari	MP234
Rajashankar, Kanagalaghatta	TP223	Rodriguez, Mark	TP181	Satcher, Joe	TP190
Rajbanshi, Arbin	SP207	Rodwell, Victor	SP011	Satkunarajah, Malathy	SP038
RajBhandary, Uttam	MP049	Roger, Vincent	MP228	Satkunarajah, Malathy	TP100
Ramakrishnan, Venki	01.08.05	Rohner, Urs	09.03.03	Sato, Masaru	SP064
Ramirez, Irama	SP191	Romano, E.	TP189	Sato, Masaru	SP065
Ramirez-Cuesta, Anibal	13.06.01	Rome, Leonard	01.08.03	Sato, Masaru	SP071
Rana, Tariq	TP112	Ronnebro, Ewa	13.06.05	Sato, Masaru	SP072
Raschi, A. B.	TP189	Rosconi, Michael	01.02.01	Savchenko, A.	MP029
Ratna, B.	TR.01.12	Rose, David R.	AW.03.06	Saw, Cheng	TP190
Ravelli, Raimond	13.01.04	Rose, David R.	MP004	Sawaya, Michael R.	03.01.01
Ravelli, Raimond	13.05.03	Rose, John	01.03.01	Sawaya, Michael R.	10.04.02
Ravelli, Raimond	MP237	Rose, John	MP232	Sawaya, Michael R.	13.01.03
Ravich, Gil	03.01.03	Rose, John	TP151	Sawaya, Michael R.	13.08.01
Rawn, Claudia	MP235	Rose, John	TP222	Sawaya, Michael R.	MP006
Raymond, K.N.	MP227	Rose, John	MP044	Sayed, Nazish	03.01.02
Raza, Ashraf	SP137	Rose, Robert	SP002	Sayer, Jane	MP019
Read, Randy	01.07.06	Rose, Robert	MP015	Scapin, Giovanna	04.01.08
Reddy, Kiran	TP112	Rose, Robert	SP035	Scaringe, Raymond	04.01.05
Redinbo, Matthew	01.01.04	Rose, Robert	SP063	Schaefer, Dale W.	09.01.07
Redinbo, Matthew	AW.03.05	Rosenbaum, Gerd	13.10.02	Schaefer, Dale W.	09.01.03
Redinbo, Matthew	SP060	Rosenbaum, Gerd	MP083	Schaefer, Dale W.	09.02.01
Redinbo, Matthew	TP108	Rosenberg, John	MP030	Schall, Constance A.	13.10.03
Rees, Leigh	TR.01.11	Rosenberg, John	SP070	Schall, Constance A.	SP067
Reger, Albert S.	AW.03.08	Rosenfeld, Robin	04.01.06	Schall, Constance A.	SP069
Ren, Weiju	09.01.05	Rosenfeld, Robin	MP178	Scheffzek, Klaus	SP058
Ren, Zhong	06.01.06	Rosenkranz, Stephan	TR.01.08	Scheidt, W. Robert	03.02.05
Renaud, Gilles	09.02.04	Rosowsky, Andre	TP120	Schenk, Henk	03.02.04
Rensing, Christopher	SP109	Rost, Burkhard	01.06.06	Schenk, Henk	13.09.05
Rey, V.	13.08.05	Rotella, Frank J.	MP083	Schierbeek, Bram	MP079
Reynolds, Ross	TP111	Rotella, Frank J.	TP156	Schierbeek, Bram	MP236
Rho, Helen	SP002	Royer, William	01.08.01	Schiffer, Celia	TP112
Riccardi, Demian	MP170	Ruble, John	01.03.01	Schiffer, Celia	TP113
Rich, Rebecca	MP007	Ruf, Michael	03.01.06	Schiffer, Marianne	TP115
Richardson, D.	MP044	Ruf, Michael	13.09.03	Schimmel, Paul	MP049
Richardson, J.	MP044	Ruigrok, Rob	13.05.03	Schlievert, Patrick M.	SP123
Roccamante, Mauro	MP229	Ruiying, Wu	MP043	Schlueter, John A.	TP208
Richardson, James W.	03.02.02	Ruiz, Federico	06.01.02	Schmidt, Andrea	13.10.05
Richardson, James W.	09.01.02	Rummel, Andreas	13.05.04	Schneider, Dieter	MP230
Richardson, James W.	13.04.06	Rumsey, Michael	07.01.05	Schneider, Dieter	MP231
Richter, Dieter	13.04.02	Rydel, Timothy	04.01.04	Schneider, Roman	13.08.02

# Author Index

Schneider, Roman	MP229	Shi, Ke	SP138	Spillmann, C.	TR.01.12
Schneider, Thomas R.	TP089	Shi, Ke	TP098	Stanislavskaja, Valentina	MP081
Schneider, Thomas R.	WK.01.04	Shimizu, Nobutaka	TP239	Stanley, Chris	07.01.05
Schneider, Thomas R.	WK.01.09	Shin, Hye Jeong	TP176	Stauffer, Cynthia	SP011
Schoehn, Guy	13.05.03	Shindyalov, Ilya	01.05.04	Stec, Boguslaw	TP090
Schoenborn, Benno	06.01.01	Shingledecker, John	09.01.05	Steinfink, H.	05.02.07
Schofield, Christopher J.	SP026	Shinozaki, Shinichi	SP064	Stengl, Bernhard	TP110
Schubert, Wolf-Dieter	MP167	Shishkin, Oleg	TP203	Stenkamp, Ronald	01.07.05
Schulte, Antje	SP058	Shiu, Moy	MP043	Stephen, Withers	TP100
Schulte, Christopher	WK.02.03	Shneerson, Valentin	TR.01.06	Stephens, Peter	07.01.06
Schultz, Arthur	06.01.03	Shuvalova, Ludmilla	01.02.06	Stephens, Peter	07.01.11
Schultz, Arthur	10.01.10	Shuvalova, Ludmilla	TP106	Stephens, Peter	TP189
Schultz, Arthur	13.06.04	Siegler, Maxime A.	10.04.01	Steuber, Holger	TP110
Schultz, Arthur	MP198	Siegler, Maxime A.	AW.02.03	Steussy, Calvin	SP011
Schultz, Arthur	TP184	Sieling, Cecelia L.	MP059	Stevens, Edwin D.	SP.01.03
Schulz, Charles E.	03.02.05	Sievers, Stuart A.	01.08.03	Stewart, Lance	04.01.03
Schulze-Briese, Clemens	13.08.02	Sievers, Stuart A.	10.04.02	Stewart, Lance	TP094
Schulze-Briese, Clemens	MP229	Sievers, Stuart A.	13.01.03	Stieglitz, Kimberly A.	SP.01.05
Schwalbe, Carl	MP197	Silva, Wender	10.01.09	Stirling, John	07.01.05
Scone, Peyton	MP040	Silverman, David	TP132	Stojanoff, Vivian	TP225
Scott, Benjamin	AW.03.03	Silverman, David	TP133	Stojic, Natasa	09.03.04
Scott, William G.	SP246	Silvermail, Nathan J.	03.02.05	Stolken, J.	TP190
Scott, William G.	01.01.03	Sim, Lyann	MP004	Stollar, David	SP226
Seaver, Sean	06.01.05	Sim, Nigel	03.01.07	Straka, Derek	TP148
See, Ronald	TP105	Sims, Gregory	01.06.01	Straube, Ekkehard	13.04.02
Seetharaman, J.	01.06.06	Sines, Matthew	TP132	Straver, Leo	10.02.07
Segalman, Rachel	09.02.05	Singh, Jasbir	04.01.03	Strombergsson, Helena	01.05.01
Seibert, Marvin	09.03.03	Singh, Satish	SP109	Stroud, Robert	01.04.04
Seidel, S. Russell	TP202	Singh, Sumer	05.01.01	Strycker, Glenn	13.07.09
Seifert, Soenke	09.02.03	Siorek, Margo	TP148	Strynadka, Natalie	01.04.03
Selby, Tom L.	SP076	Sironi, Angelo	AW.01.04	Stubbs, Keith	SP104
Selezneva, Anna	01.01.01	Sivarajah, Prashanth	SP038	Stuckey, J.	13.05.06
Selinger, L. Brent	SP050	Sivarajah, Prashanth	TP100	Subramanian, Krishna	01.06.04
Sellin, Vincent	10.03.02	Skarina, T.	MP029	Suescun, Leopoldo	TP188
Selmer, Maria	01.08.05	Skelton, Brian	SP204	Sugar, F.	MP044
Selyakov, Aleksander	13.06.03	Skene, Robert	MP049	Sugiura, Wataru	TP113
Sergiev, P.V.	MP029	Skinner, John	MP231	Sugiyama, S.	SP071
Serrano, Hector	SP031	Skryabina, Nataliya	13.06.02	Sukumar, Narayanasami	TP223
Sevvana, Madhumati	03.02.01	Skryabina, Nataliya	13.06.03	Sun, J.	TP087
Shaffer, Paul	01.02.01	Slatest, Len	SP01.06	Sun, Kai	13.07.09
Shah, Anita	13.05.06	Slebodnick, Carla	MP169	Sun, Peter D.	MP166
Shah, Binal N.	13.10.03	Slebodnick, Carla	TR.01.11	Sun, Ping	SP045
Shah, Binal N.	SP069	Smilgies, Detlef	13.08.06	Sun, Tao	13.07.07
Shah, Niket	AW.03.06	Smith, Bradley	04.01.06	Sun, Yuh-Ju	TP249
Shamoo, Yousif	SP127	Smith, Janet	13.08.03	Suvorov, Danilo	05.02.06
Shankland, Kenneth	07.01.02	Smith, Janet	SP053	Suzuki, Mamoru	MP034
Shankland, Kenneth	10.04.06	Smith, Jeremy C.	TR.01.05	Suzuki, Mamoru	SP071
Shankland, Norman	10.04.06	Smith, Michelle	10.01.01	Swairjo, Manal	MP049
Shao, Hui	SP046	Smith, Peter	MP057	Swaminathan, Chitoor	TP119
Shao, Hui	TP135	Snell, Edward	06.01.06	Swaminathan, S.	01.06.03
Shapiro, A.	TP221	Snell, Edward	13.10.02	Sweet, Robert	MP230
Shaw, Gary	MP021	Snow, M.	TP184	Sweet, Robert	MP231
Sheats, Emily	MP235	Soares, Alexei	MP230	Swindell II, James	01.03.01
Sheldrick, George M.	01.03.06	Soares, Alexei	MP231	Swint-Kruse, Liskin	MP250
Sheldrick, George M.	03.02.01	Soares, Alexei	SP139	Szyperski, Thomas	01.06.06
Sheldrick, George M.	TP151	Sobolevsky, Alexander	01.02.01	Szebenyi, Thomas	13.08.06
Sheldrick, George M.	WK.01.01	Soldatov, Dima	10.03.05	Takagi, Junichi	TP146
Sheldrick, George M.	WK.01.05	Soler, Tatiana	MP169	Takahashi, Sachiko	SP064
Sheldrick, George M.	WK.01.08	Soriano-Giles, Gabriela	SP211	Takahashi, Sachiko	SP065
Sheldrick, George M.	WK.01.11	Spahr, Henrik	13.01.01	Takahashi, Sachiko	SP071
Shen, Yang	SP121	Spanos, Lykourgos	MP228	Tan, Kemin	MP083
Sheng, Jia	TP171	Speakman, Scott	05.01.01	Tan, Kemin	SP041
Sherman, David	SP053	Spek, Anthony	10.02.04	Tan, Kemin	TP156
Shevchenko, Denys	TP203	Spek, Anthony	10.02.07	Tanaka, Hiroaki	SP064
Shi, Ke	SP123	Spek, Anthony	WK.01.07	Tanaka, Hiroaki	SP065

## Author Index

Tanaka, Hiroaki .....	SP071	Trewhella, Jill .....	MP157	Vey, Jessica .....	SP017
Tanaka, Shiho .....	MP006	Trewhella, Jill .....	MP159	Vicic, David .....	MP198
Tanaka, Tetsuo .....	SP064	Trewhella, Jill .....	MP250	Vierling, Elizabeth .....	SP242
Tanaka, Tetsuo .....	SP065	Tripathi, Akhilesh .....	07.01.07	Vijayalakshmi, J. ....	MP164
Tanaka, Tetsuo .....	SP071	Tripp, Steven .....	13.07.05	Villasenor, Armando .....	MP179
Tanaka, Tetsuo .....	SP072	Trofymluk, Olga .....	03.02.05	Viney, Joanne .....	13.03.01
Tang, Liang .....	01.07.03	Tropea, Joseph E. ....	MP021	Viola, Ronald .....	SP187
Tang, Yi .....	MP057	Tropea, Joseph E. ....	SP045	Viola, Ronald .....	TP131
Taniguchi, Hisaaki .....	MP034	Tsai, Shiou-Chuan .....	MP057	Vitali, Jacqueline .....	TP145
Tao, Yizhi Jane .....	13.05.02	Tsai, Yingssu .....	03.01.01	Vitali, Jacqueline .....	TP153
Tao, Yuefei .....	09.02.05	Tsigelny, Igor .....	13.03.06	Viterbo, Davide .....	05.01.02
Taraban, Marc .....	MP250	Tu, Chingkuang .....	TP133	Vocadlo, David .....	SP104
Tarendeau, Franck .....	SP147	Tu, Chingkuang .....	TP132	Vockley, Jerry .....	01.04.05
Tarling, Chris .....	TP100	Tu, Xiaoyan .....	SP218	Volkart, Lour .....	SP075
Tarling, Chris .....	TP102	Tucker, Paul A. ....	01.03.03	Volkov, Anatoliy .....	TP114
Tate, Mark .....	13.02.01	Tucker, Paul A. ....	MP078	Volz, Heather .....	TP181
Taylor, Palmer .....	13.03.06	Tucker, Paul A. ....	MP078	Volz, Karl .....	01.01.01
Taylor, Robin .....	01.05.03	Tulk, Chris .....	05.02.03	Von Dreele, Robert .....	07.01.09
Teat, S.J. ....	MP227	Turk, Dusan .....	03.01.04	Vorontsov, Ivan .....	01.02.06
Tejero, Roberto .....	WK.02.05	Turley, Stewart .....	MP165	Vorontsov, Ivan .....	TP106
Telling, M.T.F. ....	10.01.06	Turner, Peter .....	03.01.07	Vranken, W. ....	TP087
Tempel, Wolfram .....	MP044	Twamley, Brendan .....	05.01.04	Vreshch, Olesya .....	SP204
Tempel, Wolfram .....	SP035	Tyree, William .....	MP198	Vreshch, Volodymyr .....	SP209
Terni, Marcela .....	SP091	Udachin, Konstantin .....	10.02.06	Vu, Thanh .....	MP057
Tesh, Kris F. ....	MP082	Udovic, Boris .....	TP180	Wakeman, Catherine A. ....	MP059
Teter, David .....	TP181	Ueno, Go .....	TP239	Walchli, John .....	TP094
Theil, Elizabeth .....	01.01.01	Ulrich, Eldon .....	TP087	Walden, William .....	01.01.01
Thiyagarajan, P. ....	06.01.03	Ulrich, Eldon .....	WK.02.03	Walker, Ann .....	TP117
Thiyagarajan, P. ....	09.03.05	Umland, T.C. ....	SP009	Walker, John R. ....	SP025
Thiyagarajan, P. ....	13.07.03	Umland, T.C. ....	TP088	Wallen, Jamie .....	AW.03.07
Thiyagarajan, P. ....	MP162	Umland, T.C. ....	TP125	Wan, Cheng .....	SP035
Thoma, Dan .....	TP181	Unik, John P. ....	TP223	Wang, Anderson .....	SP052
Thomas, J. ....	TP125	Urban, Volker S. ....	13.03.08	Wang, Bi-Cheng .....	01.03.01
Thompson, Albert .....	13.02.02	Urban, Volker S. ....	MP161	Wang, Bi-Cheng .....	MP044
Thompson, Michael J. ....	13.01.03	Vaidya, Akhil .....	MP165	Wang, Bi-Cheng .....	MP232
Thompson, Michael J. ....	13.08.01	Vajda, Stefan .....	09.02.03	Wang, Bi-Cheng .....	SP035
Thomson, Jodi .....	SP051	Valdes-Martinez, Jesus .....	10.03.08	Wang, Bi-Cheng .....	TP151
Thorne, Robert E. ....	13.10.06	Valdes-Martinez, Jesus .....	SP211	Wang, Bi-Cheng .....	TP222
Thorne, Robert E. ....	MP080	Valley, Michael P. ....	TP175	Wang, Dong .....	13.01.01
Thorne, Robert E. ....	MP081	van Beek, Wouter .....	05.01.02	Wang, Dongli .....	SP063
Thorne, Robert E. ....	SP068	van Buuren, Tony .....	09.01.04	Wang, Honghao .....	MP197
Thornton, Janet .....	01.06.02	van Buuren, Tony .....	TP190	Wang, Jin .....	09.02.05
Thornton, Joseph .....	TP108	van den Akker, Focco .....	03.01.02	Wang, Jin .....	13.07.07
Tice, Josh .....	01.02.04	van den Akker, Focco .....	SP051	Wang, Lee-Ho .....	SP036
Tidor, Bruce .....	TP112	van den Berg, Bert .....	01.04.01	Wang, Meitian .....	MP229
Timofeeva, Tatiana V. ....	SP199	van den Berg, Bert .....	SP085	Wang, Peng .....	09.02.01
Timofeeva, Tatiana V. ....	SP219	van den Heuvel, Joop .....	MP167	Wang, Qian .....	TP119
Timofeeva, Tatiana V. ....	TP173	van der Woerd, Mark .....	06.01.06	Wang, Shuishu .....	TP116
Timofeeva, Tatiana V. ....	TP210	van der Woerd, Mark .....	13.10.02	Wang, Suntao .....	13.03.04
Todorov, G. ....	TP172	Van Mechelen, Jan .....	03.02.04	Wang, Suntao .....	MP160
Tollin, Gordon .....	TP117	Van Voorhis, Wesley .....	MP163	Wang, Tan .....	SP037
Tolmie, David .....	WK.02.03	Vande Velde, Christophe .....	AW.03.02	Wang, Xianqin .....	13.04.04
Tomanicek, Steve J. ....	SP069	Vande Velde, Christophe .....	AW.03.04	Wang, Xiaoping .....	10.01.16
Tomchick, Diana R. ....	TP140	Vander Kooi, Craig .....	MP013	Wang, Xiaoping .....	10.02.05
Tomizaki, Takashi .....	13.08.02	VanVranken, Sandra J. ....	TP129	Wang, Xiaoqiang .....	SP046
Tomizaki, Takashi .....	MP229	Vega-Tejido, Mauricio .....	TP215	Wang, Xiaoqiang .....	TP093
Tomson, F.L. ....	TP140	Vela, Michael J. ....	13.09.04	Wang, Xiaoqiang .....	TP135
Tomyn, Stefaniya .....	MP196	Velankar, S. ....	TP087	Wang, Yimin .....	09.02.01
Tong, Liang .....	01.06.06	Vencato, Ivo .....	10.01.09	Wang, Yimin .....	MP033
Tong, Liang .....	SP121	Vencato, Ivo .....	SP200	Wang, Yimin .....	SP037
Tong, X. ....	TP184	Ventura, Oscar .....	06.01.02	Wang, Yongcheng .....	01.01.05
Tracanna, M.I. ....	TP189	Veretnik, Stella .....	01.05.04	Wang, Yu .....	10.03.09
Tran, Vu .....	03.01.03	Verlinde, Christophe .....	MP163	Wang, Yudong .....	01.04.05
Trewhella, Jill .....	13.03.06	Verlinde, Christophe .....	TP124	Wang, Yuejian .....	05.02.05
Trewhella, Jill .....	MP032	Vetsch, M. ....	SP147	Warby, Christy .....	01.02.03

## Author Index

- Ward, Laurelin ..... TP094  
Ward, Patrick ..... TP140  
Warkentin, Matthew ..... 13.10.06  
Warkentin, Matthew ..... MP080  
Warkentin, Matthew ..... MP081  
Warren, Joshua ..... TP154  
Watanabe, Nobuhisa ..... 01.03.02  
Watson, James ..... 01.06.02  
Waugh, David S. .... MP021  
Waugh, David S. .... SP045  
Waychunas, Glenn ..... 09.02.06  
Weekes, Dana ..... 01.06.04  
Weeks, Brandon ..... 09.01.04  
Weeks, C.M. .... TP088  
Wei, Alexander ..... 13.07.05  
Weichsel, Andrzej ..... SP109  
Weichsel, Andrzej ..... SP242  
Weichsel, Andrzej ..... TP117  
Weik, Martin ..... 13.10.04  
Weinshilbourn, Richard ..... SP136  
Weiss, Kevin ..... 13.03.08  
Weiss, Manfred S. .... 01.03.03  
Weiss, Manfred S. .... 13.10.05  
Weiss, Manfred S. .... MP078  
Weiss, Thomas M. .... MP158  
Weiss, Manfred S. .... WK.02.04  
Weissenhorn, Winfried ..... 13.05.03  
Weixlbaumer, Albert ..... 01.08.05  
Welberry, T.R. .... SP168  
Welberry, T.R. .... TR.01.01  
Welch, Cynthia ..... 09.03.02  
Wemmer, David ..... 13.03.02  
Wen, Wen ..... 13.04.04  
Wen, Xiaolin ..... 13.05.05  
Wenjun, Zhang ..... MP057  
Wernimont, Amy ..... 13.05.03  
Wesenberg, Gary ..... 01.02.05  
Wesenberg, Gary ..... 01.07.04  
Wesenberg, Gary ..... TP126  
Westbrook, Edwin ..... 13.02.02  
Westbrook, J. .... TP087  
Westin, Charles ..... TP172  
Westin, Charles ..... SP.01.06  
Westover, Ken ..... 13.01.01  
Wetzel, Ronald ..... MP007  
Wheatley, Joshua ..... TP143  
Whitby, Frank ..... 01.02.03  
Whitby, Frank ..... TP097  
Whitfield, Pamela ..... 07.01.05  
Whitman, Chris ..... SP031  
Whitten, Andrew ..... 13.03.06  
Whitten, Andrew ..... MP157  
Whitten, Andrew ..... MP159  
Wiesmann, Joerg ..... 03.01.05  
Wignall, George ..... 13.07.04  
Wildner, Guenter ..... SP242  
Wilk, Dennis ..... SP136  
Wilking, J.N. .... 13.04.03  
Wilkins, Stuart ..... 09.03.04  
Willett, Roger ..... 05.01.04  
Willey, Trevor ..... 09.01.04  
Willey, Trevor ..... TP190  
Williams, Eric B. .... 03.01.01  
Williams, Leslie ..... SP.01.04  
Williams, Wilton ..... TP132  
Willis, Michael ..... SP073  
Wilmot, Carrie ..... 01.01.02  
Wilson, Chick ..... 10.01.04  
Wilson, Ian ..... 01.06.04  
Wilson, Kristen S. .... 09.01.06  
Wilson, Mark ..... SP137  
Wiltzius, Jed J.W. .... 13.01.03  
Winans, Randall ..... 09.02.03  
Winans, Randall ..... 09.03.05  
Winans, Randall ..... 13.07.03  
Winger, J. .... 04.01.03  
Winkler, Wade C. .... MP059  
Withers, Stephen ..... SP.01.04  
Withers, Stephen ..... TP102  
Withrow, James ..... TP223  
Witt, Anna ..... SP137  
Wojcik, John ..... TP142  
Womack, Thomas ..... 13.02.04  
Wollert, Thomas ..... MP167  
Wong, April ..... MP179  
Wong, Jimson ..... SP016  
Wong-Ng, Winnie ..... TP221  
Wood, Stephen ..... TP115  
Woods, Bruce ..... 09.03.03  
Woods, Kate ..... TP102  
Wriggers, Willy ..... 01.05.05  
Wright, Gerard D. .... SP027  
Wroblecki, Debra ..... 09.03.02  
Wu, Huey-Nan ..... TP249  
Wu, Jinhua ..... TP122  
Wu, Rui ..... AW.03.08  
Wu, Ruiying ..... SP075  
Wyatt, Mathew ..... 03.01.07  
Xia, Yiping ..... MP084  
Xiao, Liren ..... TP124  
Xiao, R. .... 01.06.06  
Xie, Dianlin ..... MP243  
Xing, Guanxin ..... MP019  
Xing, Xuekun ..... SP038  
Xu, ChongFeng ..... TP122  
Xu, Eric ..... TP111  
Xu, Hongliang ..... TP185  
Xu, Hongwu ..... 05.02.05  
Xu, Jian ..... SP073  
Xu, Qingping ..... SP248  
Xu, Shenglan ..... 13.08.03  
Xu, Yongbin ..... MP048  
Xue, Ziling (Ben) ..... TP183  
Xuong, Ng. h. .... MP237  
Yagi, Haruhiko ..... MP019  
Yakovenko, Andrey A. .... TP210  
Yamamoto, Masaki ..... 13.02.03  
Yamamoto, Masaki ..... TP239  
Yamanaka, Mari ..... SP064  
Yamanaka, Mari ..... SP065  
Yamanaka, Mari ..... SP071  
Yan, H.Y. .... TP184  
Yang, Cheng ..... 01.01.02  
Yang, Cheng ..... 01.03.04  
Yang, Cheng ..... MP234  
Yang, H. .... TP087  
Yang, In Seok ..... TP176  
Yang, Jian ..... SP017  
Yang, Jie ..... MP056  
Yang, Lin ..... 13.03.04  
Yang, Lin ..... MP160  
Yang, X.F. .... TP140  
Yang, Xiang-Lei ..... MP049  
Yang, Z. .... TP221  
Yaniga, Bradley S. .... 13.10.03  
Yao, Hongyang ..... WK.02.03  
Yao, Shenqin ..... MP028  
Yasui, Norihisa ..... TP146  
Ye, Qiaozhen ..... 13.05.02  
Yeates, Todd O. .... 03.01.01  
Yeates, Todd O. .... MP006  
Yee, Vivien ..... SP136  
Yeh, Hui-Chun ..... SP036  
Yigit, Mehmet V. .... 10.03.09  
Yin, Hsien-sheng ..... 13.05.05  
Yoder, Derek ..... 13.08.03  
Yoo, Ji-Ho ..... MP054  
Young, Mark ..... 01.07.03  
Young, Matthew ..... 01.05.06  
Young, Victor ..... 10.02.03  
Yousufuddin, M. .... TP087  
Yuan, Ping ..... 13.05.05  
Yuksel, Deniz ..... SP226  
Zagotta, William ..... TP150  
Zanchin, Nilson ..... TP118  
Zembower, D. .... 04.01.03  
Zhai, Qianting ..... SP042  
Zhan, Hongli ..... MP250  
Zhang, Fan ..... 09.01.01  
Zhang, Fan ..... 09.01.09  
Zhang, Geoff G.Z. .... TP251  
Zhang, Jianzhong ..... 05.02.05  
Zhang, Lili ..... MP056  
Zhang, Qizhi ..... SP075  
Zhang, Ran ..... TP102  
Zhang, Rongguang ..... MP083  
Zhang, Rongguang ..... SP041  
Zhang, Rongguang ..... SP075  
Zhang, Rongguang ..... TP156  
Zhang, Ying ..... TP090  
Zhang, Yingjiu ..... 01.01.05  
Zhao, Jing ..... TR.01.11  
Zhao, Yusheng ..... 05.02.05  
Zheng, Meiyang ..... SP074  
Zheng, Shao-Liang ..... AW.03.02  
Zheng, Xiaoyan ..... MP028  
Zheng, Zhiping ..... SP218  
Zhou, Min ..... MP247  
Zhou, Min ..... SP075  
Zhou, Sihong ..... SP038  
Zhou, Tongqing ..... 13.05.06  
Zhu, Haibin ..... SP216  
Zhu, Naijue ..... MP192  
Zhurov, Vladimir ..... MP194  
Zhurova, Elizabeth ..... MP194  
Ziegler, Christopher J. .... AW.03.04  
Zolnai, Zsolt ..... 01.02.05  
Zolotukhin, Sergei ..... SP039  
Zou, Qin ..... MP056  
Zukerman-Schpector, Julio ..... TP215  
Zwart, Peter ..... 01.07.07  
Zwart, Peter ..... TP150

## 01.01 New Structures

**01.01.01 Structure of a Eukaryotic Repressor:mRNA Complex: IRP1:IRE Ferritin H.** Karl Volz<sup>1</sup>, Anna I. Selezneva<sup>1</sup>, Elizabeth C. Theil<sup>2</sup>, William E. Walden<sup>1</sup>, <sup>1</sup>Dept. of Microbiology and Immunology, Univ. of Illinois at Chicago, Chicago, IL, 60612, <sup>2</sup>Children's Hospital Oakland Research Inst., Oakland, CA, 94609.

Iron homeostasis in animal cells is maintained by two RNA binding proteins called iron regulatory proteins (IRP1 and IRP2). IRPs bind to specific RNA stem-loop structures known as iron responsive elements (IREs) located in the non-coding region of mRNAs for proteins involved in iron metabolism to regulate the translation. IRP1 (889 residues, 99 kDa) is a bifunctional protein that acts either as a RNA-binding translational regulator or an iron-sulfur cluster-containing cytosolic (c-)aconitase, depending upon cellular iron levels.

The structure of IRP1 in complex with a ferritin mRNA IRE (30 nt) has been solved to 2.8 Å resolution<sup>1</sup>. Comparison of IRE-bound IRP1 to the c-aconitase form reveals radical structural transformations that explain the regulation of the functional interconversion. In the complex, IRP1 assumes an open conformation that enables two-point binding of both the stem and loop of the IRE. The invariant, unpaired C8 of the IRE stem is bound by the C-terminal domain of IRP1, while the exposed AGU bases of the apical loop are bound in a cavity resulting from the remodelled iron-sulfur cluster region of the bifunctional protein.

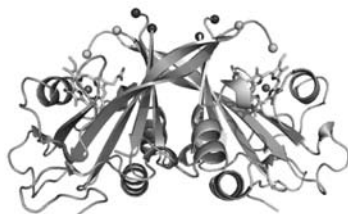
In addition, the structure of IRP1 in complex with a ΔU6 mutant ferritin IRE (29 nt) has been solved to 2.6 Å resolution. The mutated IRE represents the non-ferritin class of IREs that bind to IRPs with lower affinity. The ΔU6 mutation reduces the bend in the IRE stem, subtly changing some of the protein-RNA contacts. These results demonstrate the complexity of IRP1:IRE selectivity.

Funding in part by GM47522 (KV), NIH-DK 20251 (ECT), and DK 47281 (WEW). Data collected at SER-CAT of APS, ANL.

<sup>1</sup>Walden, *et al. Science* 314, 1903 (2006).

**01.01.02 The Crystal Structure of Cytochrome P460 of *Nitrosomonas europaea* Reveals a Novel Cytochrome Fold and Heme-protein Cross-link.** C.M. Wilmot\*, A.R. Pearson\*, B.O. Elmore\*, C. Yang#, J.D. Ferrara#, A.B. Hooper\*, Univ. of Minnesota, Minneapolis, MN 55455, Rigaku Americas Corp., The Woodlands, TX 77381.

We have determined the 1.8 Å X-ray crystal structure of a mono-heme c-type cytochrome, cytochrome P460, from *Nitrosomonas europaea*. The chromophore possesses unusual spectral properties analogous to those of the catalytic heme P460 of hydroxylamine oxidoreductase (HAO), the only known heme in biology to withdraw electrons from substrate coordinated to the iron. The structure was solved by S-SAD using 2.29 Å wavelength X-rays. The analysis reveals a homodimeric structure and elucidates a new c-type cytochrome fold that is predominantly β-sheet. In addition to the two cysteine thioether links to the porphyrin typical of c-type hemes, there is a third proteinaceous link involving a conserved lysine. The covalent bond is between the lysine side-chain nitrogen and the 13'-*meso* carbon of the heme, which following cross-link formation is sp<sup>3</sup> hybridized demonstrating loss of conjugation at



this position within the porphyrin. The protein underwent oxidation during crystallization, confirmed by mass spectrometry, leading to the presence of a hydroxyl group at the 5'-*meso* carbon of the heme. During X-ray data collection the hydroxyl group was lost in a dose dependent manner. Two structures were refined; the physiological structure using high dose data, and the structure with the additional hydroxyl using low dose data. The structure has implications for the analogous tyrosine-heme *meso* carbon cross-link observed in HAO.

This work was funded by NIH GM-66569 (CMW), NSF MCB 0093447 (ABH) and DOE DE-FG02-95ER20191A009 (ABH). Some data were collected at beam-line 4.2.2 at the Advanced Light Source, LBNL, Berkeley, CA.

**01.01.03 The Structural Basis for Ribozyme-Catalyzed RNA Assembly and its Implications for a Pre-Biotic RNA World.** William G. Scott, Michael P. Robertson, Center for the Molecular Biology of RNA, Univ. of California - Santa Cruz, Santa Cruz, CA.

Life originated, according to the RNA World hypothesis, from self-replicating ribozymes that catalyzed ligation of RNA fragments. We have solved the 2.6 Å crystal structure of a ligase ribozyme that catalyzes regio-specific formation of a 5' to 3' phosphodiester bond between the 5'-triphosphate and the 3'-hydroxyl termini of two RNA fragments. Invariant residues form tertiary contacts that stabilize a flexible stem of the ribozyme at the ligation site, where an essential magnesium ion coordinates three phosphates. The structure of the active site permits us to suggest how transition-state stabilization and a general base may catalyze the ligation reaction required for pre-biotic RNA assembly.

**01.01.04 The Structure of the TraI C-terminal Domain Reveals a Novel Fold: Implications for Assembly of the Multi-protein Relaxosome Conjugative DNA Transfer Complex.** Laura M. Guogas, Matthew R. Redinbo, Dept. of Chemistry, Univ. of North Carolina at Chapel Hill, Chapel Hill, NC 27599.

The multi-protein relaxosome complex is responsible for the conjugative DNA transfer (CDT) of DNA directly from donor to recipient cells. This process is a central driving force for horizontal transfer of genetic material and for the propagation of antibiotic resistance genes in bacteria. We report the structure of the C-terminal domain of the large, multifunctional *E. coli* F-plasmid TraI protein (TraI-CT). This multifunctional protein is involved in the nicking and unwinding of donor plasmid DNA. Recent genetic complementation and biochemical data suggest that TraI-CT may interact with TraM, another member of the relaxosome complex, to stimulate DNA nicking and initiate efficient DNA transfer. We solved the structure of TraI-CT to 2.1 Å using selenomethionine MAD phasing methods. The structure reveals that the majority of the domain folds into a novel, compact β-sheet core, while the N-terminal segment folds into a series of α-helices connected by loop regions. The extreme C-terminal residues were not ordered in the structure, indicating that the compact core, which is highly conserved amongst TraI proteins, is flanked by flexible regions that are less conserved. Additionally, TraI-CT packs as a tetramer in the crystal lattice, wherein one of the α-helices from one monomer domain-swaps into the β-sheet core of another. This novel oligomeric state suggests a highly dynamic role for the TraI-CT in relaxosome assembly and function.

**01.01.05 Crystal Structure of Rhomboid Intramembrane Protease GlpG.** Y. Ha, Y. Wang, Y. Zhang, Dept. of Pharmacology, Yale Univ. School of Medicine, New Haven, CT 06520 USA.

Rhomboid proteases are integral membrane proteins. They catalyze proteolysis of membrane-embedded peptide bonds. We

have solved the crystal structure of rhomboid protease GlpG, which represents the first for this class of enzyme structures. GlpG contains six

transmembrane helices. A Ser-His catalytic dyad (Ser-201 and His-254), and several water molecules, are found at the protein interior below the membrane surface, thus explaining its unusual activity within cell membranes. By lifting a surface loop (L5) that previously caps the active site, the closed protease becomes accessible by membrane-spanning peptide substrates from the side through a gap between two transmembrane helices (S2 and S5). The principles of intramembrane proteolysis learned from GlpG structure may be applicable to other membrane proteases such as gamma-secretase whose malfunction causes Alzheimer's disease.

We thank BNL-NSLS for access to beamlines X6A, X25, X26C and X29A. This research is supported by Yale University, Ellison Medical Foundation, and Neuroscience Education and Research Foundation.

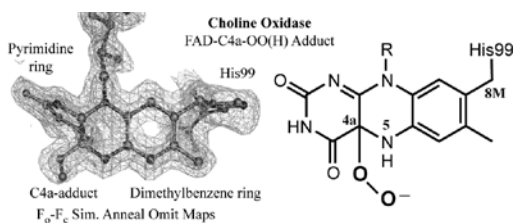
1. Wang, Y., Zhang, Y. & Ha, Y. (2006) Nature 444, 179-183.
2. Wang, Y. & Ha, Y. (2007) PNAS 104, 2098-2102.

**01.01.06 Mechanistic Insights into Flavoenzyme Oxidases from Structures of Trapped Reaction Intermediates.** Allen M. Orville, Annie Héroux, George T. Lountos, Paul F. Fitzpatrick, Fan Fan, Giovanni Gadda, Rajeev Prabhakar, Djameladdin G. Musaev, Keiji Morokuma, Biology Dept., Brookhaven National Laboratory, Upton, NY 11973.

Approximately 2-4% of all proteins are flavoproteins. Their ubiquity derives from the chemical versatility of the flavin isoalloxazine ring. It can act as an electrophile, a nucleophile, or form covalent adducts at the C4a, N5, C6, and C8M positions. We present results on two FAD-dependent

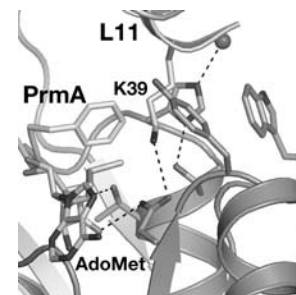
enzymes: nitroalkane oxidase (NAO) and choline oxidase (CHO). Several FAD-N5 adducts can

be trapped at low temperature during NAO turnover of nitroalkanes. We have determined crystal structures for oxidized NAO, the N5-nitrobutyl adduct, as well as several active site mutants and ligand complexes. These correlate with the carbanion-based reaction mechanism for the NAO reductive half-reaction. The oxidative half-reaction of many flavoenzymes include  $O_2$  and a C4a-OO(H) intermediate, which is only occasionally detected by transient kinetics and spectroscopy. However, a flavin-C4a- $O_2$  adduct has not been observed in any of the over 800 flavoprotein structures deposited in the PDB. The electron density maps for the FAD in aerobic CHO (1.8 Å resolution, 100 K) reveals the presence of a unique adduct. The C4a atom is  $sp^3$  hybridized and a C4a-OO(H) adduct fits the electron density well. Density functional theory calculations (B3LYP/6-31G(d,p)) probe the electronic structure of the flavin adduct, and estimate the contributions of the residues that stabilize the structure. We propose that the C4a-OO(H) adduct is generated *in situ* through FAD photoreduction, followed by reaction with  $O_2$  from within the aerobic crystal. Cryogenic conditions trap the flavin-oxygen adduct and fail to establish the proper  $H^+$  inventory on the surrounding residues required to yield  $H_2O_2$ .



**01.01.07 Recognition and Catalysis of Ribosomal Protein L11 by the Protein Trimethyltransferase PrmA.** Hasan Demirci, Steven T. Gregory, Albert E. Dahlberg, Gerwald Jogl, Dept. of Molecular Biology, Cell Biology and Biochemistry, Brown Univ., Providence, RI, USA.

Bacterial ribosomal protein L11 is post-translationally trimethylated at multiple residues by a dedicated methyltransferase, PrmA. Here, we describe multiple apo-enzyme structures and enzyme-substrate complexes of PrmA from the thermophile *T. thermophilus*. We have determined two apo-PrmA structures at 1.59 and 2.3 Å and two structures with bound cofactor AdoMet at 1.75 and 3.1 Å resolution. A PrmA-L11 enzyme-substrate complex structure at 2.4 Å resolution illustrates the highly specific interaction of the PrmA N-terminal domain with its substrate and places the L11 ε-amino group of Lys39 in the active site in a pre-catalytic state.



Two other complex structures at 1.75 and 2.56 Å resolution show the trimethylated α-amino group of Met1 and AdoHcy in the post-catalytic state. In addition, we have determined the structures of two active site mutants H104A and T106Y complexed with L11 at 2.1 and 3.2 Å resolution. A structure of the truncated PrmA substrate recognition domain complexed with the L11 N-terminal domain at 1.37 Å suggests that a single recognition mode is sufficient to place all substrate side chains in the active site. All structures of PrmA exhibit distinct relative positions of the substrate recognition and catalytic domains, revealing how the remarkable plasticity of PrmA can position the L11 substrate for multiple, consecutive side-chain methylation reactions. The presence of a unique flexible loop in the cofactor-binding site suggests how exchange of AdoMet with the reaction product AdoHcy can occur without necessitating the dissociation of PrmA from L11. Finally, the mode of interaction of PrmA with L11 explains its preference for L11 as substrate before its assembly into the 50S ribosomal subunit.

**01.01.08 Structure of Mammalian DNA Methyltransferase Dnmt3a Catalytic Domain in Complex with its Regulator DNMT3L.** Da Jia, Xiaodong Cheng, Dept. of Biochemistry, Emory Univ. School of Medicine, 1510 Clifton Rd., Atlanta, GA 30033.

Active DNA methyltransferase 3a (Dnmt3a) and its regulatory factor, DNA methyltransferase 3-like protein (Dnmt3L), are both required for *de novo* DNA methylation of most imprinted genes in mammalian germ cells. We used a co-expression and co-purification system to generate a homogeneous complex of Dnmt3L and Dnmt3a, yielded a stable complex at 1:1 stoichiometry. We have determined a structure of C-terminal domain of Dnmt3L in complex with the catalytic domain of active Dnmt3a, at a resolution of 2.9 Å in the presence of methyl donor analog S-adenosyl-L-homocysteine. The complex was crystallized in space group H3 with cell dimensions of  $a=b=400$  Å and  $c=50$  Å. The crystals usually took a few weeks to two months to reach a maximum size of approximately 0.05 x 0.05 x 0.4 mm. X-ray diffraction data were collected at SER-CAT beamline at the Advanced Photon Source, Argonne National Laboratory. The complex structure was solved by combined approaches of molecular replacement by PHASER, Se-MAD and NCS averaging by SOLVE and RESOLVE. The complex structure showed that the heterodimer of Dnmt3a-3L further dimerizes through Dnmt3a-3a interaction, forming a tetrameric enzyme complex with two active sites. The crystallographic asymmetric unit contains two tetramers. Substitution of key residues in the Dnmt3a-3L interface or Dnmt3a-

3a interface eliminated enzymatic activity. Molecular modeling of a DNA-Dnmt3a dimer suggested that the two active sites are separated by approximately one DNA helical turn. The functional implication of molecular architecture of the Dnmt3a-Dnmt3L tetramer with two active sites will be discussed.

## 01.02 Strategies for Crystallization Challenged Macromolecules

**01.02.01 Fluorescence-detection Size Exclusion Chromatography for Precrystallization Screening of Integral Membrane Proteins.** Toshimitsu Kawate<sup>1</sup>, Jaysankar Jasti<sup>1</sup>, Michael Rosconi<sup>1</sup>, Paul Shaffer<sup>1</sup>, Alexander Sobolevsky<sup>1</sup>, Tanja Homrichhausen<sup>1</sup>, Eric Gouaux<sup>1,2</sup>, <sup>1</sup>The Vollum Inst. at Oregon Health and Science Univ., 3181 SW Sam Jackson Park Rd, Portland, OR 97239, <sup>2</sup>Howard Hughes Medical Inst., kawatet@ohsu.edu.

Formation of well ordered crystals of membrane proteins is a bottleneck for structure determination by x-ray crystallography. Nevertheless, one can increase the probability of successful crystallization by precrystallization screening, a process by which one analyzes the monodispersity and stability of the protein-detergent complex. Traditionally, this has required microgram to milligram quantities of purified protein and a concomitant investment of time and resources. Here we show a rapid and efficient precrystallization screening strategy in which the target protein is covalently fused to green fluorescent protein (GFP) and the resulting unpurified protein is analyzed by fluorescent-detection size exclusion chromatography (FSEC). This strategy requires only nanogram quantities of unpurified protein and allows one to evaluate localization and expression level, degree of monodispersity, and approximate molecular mass. We have applied this screening strategy to six different integral membrane proteins and found promising target proteins for crystallization. We find that the probability of obtaining a well-behaved protein is about one in twenty, and most importantly, all of such “hits” have been successfully crystallized. In this talk, I show the application of this precrystallization screening to integral membrane proteins derived from prokaryotic or eukaryotic organisms.

**01.02.02 Advances Towards the Design of a ‘Universal’ Nucleant for Protein Crystallization.** Naomi E. Chayen, Div. of Biomedical Sciences, Faculty of Medicine, Imperial College London SW7 2AZ, UK .

Excessive nucleation leads to the formation of showers of useless crystals. The aim is to find substances (nucleants) that will induce efficient heterogeneous nucleation, thus leading to the production of single high-quality crystals. This talk will evaluate the use of nucleants for protein crystallization and will present the developments in the quest to develop a ‘universal’ nucleant. It will highlight a new nucleant with nano pores that has induced the crystallization of the largest number of proteins ever crystallized using a single nucleant [1] and present recent results obtained after the publication of reference [1].

[1]Chayen N.E., Saridakis, E., Sear, R.P. (2006). *Proc. Natl. Acad. Sci. USA*. 103: 597-601.

**01.02.03 Uroporphyrinogen Decarboxylase-Substrate Complex – Coping with an Unusual, Oxygen-Sensitive Substrate.** Frank G. Whitby, John D. Phillips, Hector Bergonia, Christy Warby, James P. Kushner, Christopher P. Hill, Univ. of Utah School of Medicine, 50 N. Medical Dr., Salt Lake City, UT 84132.

Uroporphyrinogen Decarboxylase (URO-D) is an essential enzyme of heme biosynthesis that carries out the four successive

decarboxylations required to convert uroporphyrinogen to coproporphyrinogen. URO-D is a two-fold symmetric homo-dimer with two identical enzyme active sites that act independently on the initial and three intermediate substrates. This unusual enzymatic activity requires no additional cofactors.

We have previously reported structures of the apo enzyme and enzyme-product complexes. Determination of the product-bound structure was possible only by crystallization of URO-D with concomitant enzymatic production of the highly oxygen-sensitive substrate under anaerobic conditions. Despite efforts aimed at reducing URO-D enzymatic activity through site-directed mutagenesis, URO-D remained active during the course of co-crystallization in all cases, resulting only in enzyme-product complexes.

Determination of a URO-D-substrate complex, required development of new methods for soaking crystals. This required a method to produce stable reduced substrate in which a crystal could be soaked. In answer to this problem, we developed a Palladium-Carbon reduction system in Hydrogen atmosphere that allowed us to produce substrate at neutral pH in a buffer amenable to crystal soaking. The structure of the URO-D-substrate complex reveals details of substrate binding. Comparison with enzyme-product complexes has suggested new insights into ligand binding and enzyme mechanism.

**01.02.04 Microfluidic Platforms for Membrane Protein Crystallization.** P.J.A. Kenis, S.L. Perry, J.D. Tice, G.W. Roberts, Dept. of Chemical & Biomolecular Engineering, Univ. of Illinois at Urbana-Champaign, 600 S. Mathews Ave., Urbana, IL 61801.

The crystallization of membrane-type proteins remains more art than science. Numerous factors such as protein amphiphilicity, limited quantity, and non-rigid conformations increase the difficulty of determining suitable crystallization conditions. The *in-surf* method utilizes detergents to solubilize membrane proteins. In prior work we have shown that kinetic control over crystal growth can be achieved by variation of the evaporation rate. Here we will report the successful use of the *in-surf* method in combination with controlled dehydration. The success of the *in-surf* method, however, has been limited, in part due to the fact that the detergent used does not appropriately mimic a lipid membrane. The *in-meso* method allows for the crystallization of membrane proteins without their removal from a membrane-like environment, alleviating concerns for both the solubilization and the loss of the functional protein conformation. *In-meso* crystallization requires the homogeneous mixing of two materials with viscosities differing by two orders of magnitude, which has proven to be challenging at the small scales needed for high throughput sparse matrix screening methods. Moreover, membrane proteins often are only available in minute quantities, eliminating the use of traditional crystallization screening tools as an option. Using the membrane protein bacteriorhodopsin (bR) as our test case, we will report on the successful design, fabrication, and testing of a microfluidic device designed for the on-chip formation and screening of *in-meso* crystallization conditions for membrane-type proteins on the nanoliter scale.

**01.02.05 High-Throughput Crystallization Pipeline at the Center for Eukaryotic Structural Genomics.** C.A. Bingman, C.J. Robson, L.M. Meske, X. Pan, G.E. Wesenberg, J.M. McCoy, Z. Zolnai, G.N. Phillips, Jr., Univ. of Wisconsin, 433 Babcock Dr., Madison, WI, 53706, <http://www.uwstructuralgenomics.org>.

The Center for Eukaryotic Structural Genomics (CESG) is one of five specialized centers funded through Phase-2 of Protein Structure Initiative (PSI) (National Institute of General Medical Sciences.)

During Phase-1 and into Phase-2 of PSI, CESG has evaluated hundreds of protein samples in thousands of high-throughput crystallization screens. Here we review the technical details of the high-throughput crystallomics pipeline at CESG, and summarize our aggregate experience in obtaining diffraction quality crystals of protein samples.

CESG conducts crystallization trials in a database-centric, automation-rich environment. Sesame, the project LIMS is the hub, storing all solution conditions: writes robot worklists for the construction of custom screens from stocks on a Tecan Genesis™ liquid handling robot, generates grid screens based on conditions giving screening hits, and writes custom barcodes for plate identification in our two CrystalFarm™ automated plate handling/imaging robots. Images of crystallization experiments and scores are stored in two MySQL databases on the CrystalFarm™ systems. Software under development in the Phillips lab further enhances user interactions with the image/score data on the CrystalFarm™ systems. We have named this system WHITE ICE (Wisconsin High Throughput Extensible Integrated Crystallization Environment.)

We will report a detailed statistical analysis of the results of over a quarter million individual crystallization experiments conducted at CESG.

The work of the entire CEGS staff is acknowledged. Supported by NIH Protein Structure Initiative grants P50 GM64598 and U54 GM074901 (John. L. Markley, PI).

**01.02.06 Role of the Purification Tag in Crystal Lattice Interactions.** L. Shuvalova, G. Minasov, I.I. Vorontsov, J.S. Brunzelle\*, W.F. Anderson, Midwest Center for Structural Genomics, Dept. of Molecular Pharmacology and Biological Chemistry, Northwestern Univ. Feinberg School of Medicine, Chicago, IL, \*Life Sciences Collaborative Access Team, Advanced Photon Source, Argonne National Laboratory, Argonne, IL.

Purification tags used by the Midwest Center for Structural Genomics are commonly removed by proteolysis because the tag increases the number of disordered residues resulting in crystals of poorer quality. However, for some proteins the tag can be important for obtaining crystals at all. The success of histidine purification tags with a wide variety of proteins indicates that they remain highly accessible and are not affected by the nature of the protein fused to them. Similarly, for tag sequences that include protease recognition sites, that site should be highly accessible and able to be bound by the protease. Consequently it is somewhat surprising when the tag residues are ordered in a crystal. Using proteins that failed to give diffraction quality crystals in a standard protocol with the tag removed we have examined the role of the tag sequence in those cases where the tagged fusion protein yielded diffraction quality crystals. Improved solubility of the fusion protein appears to be a factor in many cases and the tag residues are usually disordered in the crystal. But in some cases parts of the tag are ordered and make lattice interactions that appear to improve crystal quality. The structure of the purification tag depends upon the environment it is located in. The identical sequence adopts different conformation in different protein crystals. The pMCSG7 purification tag includes a TEV protease recognition site and it is this portion of the tag that is most frequently observed to be structured.

## 01.03 Experimental Phasing with Longer Wavelength X-rays

**01.03.01 Progress Towards Routine Soft X-ray Structure Determination at UGA and SER-CAT.** John P. Rose<sup>1,2</sup>, John Ruble<sup>2</sup>, John Chrzas<sup>1,2</sup>, John Gonczy<sup>1,2</sup>, James T. Swindell II<sup>2</sup>, Lirong Chen<sup>2</sup>, James Fait<sup>1,2</sup>, Zheng-Qing (Albert) Fu<sup>1,2</sup>, Zhongmin Jin<sup>1,2</sup>, Bi-Cheng Wang<sup>1,2</sup>, <sup>1</sup>Southeast Regional Collaborative Access Team, Advanced Photon Source, Argonne National Laboratory, Argonne, IL 60439, <sup>2</sup>Dept. of Biochemistry and Molecular Biology, Univ. of Georgia, Athens GA 30602.

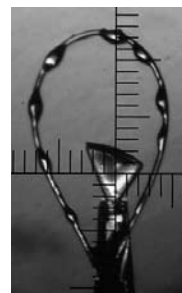
The SER-CAT beamlines were designed and optimized for collecting multiwavelength anomalous dispersion (MAD) data on crystals of seleno-methionyl derivatized protein at the selenium X-ray absorption edge (~12 keV). However, single-wavelength anomalous scattering (SAS) methods have opened up the possibility of structure determination from native crystals based on the weak sulfur anomalous scattering signal enhanced by data collection using soft (6-8 keV) X-rays.

Over the past two years, SER-CAT has embarked on a program of soft X-ray beamline optimization focused on identifying and correcting instabilities in the system at low energies which can significantly contribute to noise level in the SAS data produced. This is important to the success of sulfur-SAS structure determination since although the SAS signal is enhanced at longer wavelengths the strength of the signal at ~6 keV is still only about one-third of that produced by selenium at its absorption edge.

Progress on the optimization of both the SER-CAT undulator and bending magnet beamlines for routine, high quality soft X-ray data collection will be presented.

**01.03.02 On the Use of a New Crystal Mounting Method for the Longer X-Ray S-SAD Phasing.** Nobuhisa Watanabe, Faculty of Advanced Life Science, Hokkaido Univ., Sapporo, Japan.

Using longer wavelength X-ray for the SAD method is one of the hottest trends in macromolecular crystallography. In the laboratory, using longer wavelength of Cr  $K\alpha$  X-rays (2.29 Å) might be an optimal choice, where the anomalous intensity difference or the Bijvoet ratio of almost all sulfur containing protein crystals becomes about 1% of total reflection intensity, because the  $f'$  value of sulfur becomes 1.14 e<sup>-</sup> as compared to 0.56 e<sup>-</sup> at Cu  $K\alpha$ . But the Bijvoet difference is still small and highly accurate data collection is essential. One of the experimental difficulties using Cr  $K\alpha$  X-rays is the increased absorption. Especially, in standard protein crystallography where the crystal is freeze-mounted in a cryoloop with cryo-buffer, X-ray absorption by these materials sometimes prevents the detection of tiny anomalous signals. Therefore we have developed a novel crystal mounting technique to eliminate absorption by the frozen cryo-buffer and cryoloop [1]. This technique increases the precision of the measured anomalous differences between the Bijvoet mates, and makes the S-SAD phasing method with a Cr  $K\alpha$  X-ray source a very useful tool for high-throughput structure determination. The practical applicability of the mounting method was examined using several novel proteins. Proteins from 9.6 kDa to 84 kDa have been solved using this method without any derivatization. In most cases, more than 90% of all the structures were constructed automatically with side chains by use of the SAD phasing method.



This study was supported in part by a research grant from the National Project on

Protein Structural and Functional Analysis from the Ministry of Education, Culture, Sports, Science and Technology of Japan.

[1] Kitago, Y., Watanabe, N. and Tanaka, I. (2005), *Acta Cryst.*, D61(8), 1013-1021.

**01.03.03 Determination of a Protein's Anomalous Scattering Substructure Using Longer X-ray Wavelengths.** Christoph Mueller-Dieckmann, Santosh Panjikar, Paul A. Tucker, Manfred S. Weiss, ESRF, F-38043 Grenoble, France.

The small, but significant, signals provided by the anomalous scattering properties of innate sulfur (in protein), phosphorous (in DNA/RNA) or other light atoms (Ca, K, Cl, etc.) using longer X-ray wavelengths can, in principle, be used to solve the phase problem in macromolecular crystallography.

An additional positive side effect of using longer X-rays wavelengths is that anomalous difference fourier syntheses ( $\Delta F_{\text{obs}}$ ,  $\alpha=90^\circ$ ) will allow a more exact determination of the anomalous substructure of a protein crystal including low Z-elements such as potassium, calcium, chloride as well as sulfate-ions. Given the fact that many protein crystallisation set-ups contain NaCl, KCl or  $\text{Na}_2\text{SO}_4$  only 10-15% of all PDB depositions contain these ions. A careful examination of the substructures of 23 different protein crystals revealed in all but two cases the presence of additionally bound ions to the protein. These findings suggest that a data set collected at longer X-ray wavelengths is necessary in order to completely describe a protein structure<sup>[1]</sup>.

[1] C. Mueller-Dieckmann *et al.* (2007). *Acta Cryst.* D63, 366-380.

**01.03.04 Taking the Edge Off: The Softer Side of In-house SAD Phasing.** Cheng Yang, James W. Pflugrath, Joseph D. Ferrara, Rigaku Americas Corporation, The Woodlands, TX, USA.

The phase problem in macromolecular crystallography has been mitigated dramatically in recent years by advances in methodology and instrumentation. SAD phasing has now become the primary *de novo* phasing method. A search of the PDB of structures released in 2006 reveals the number of structures solved by SAD phasing exceeds those solved by MAD for the first time. A number of these examples of successful S-SAD and Se-SAD phasing used Cr radiation ( $\lambda = 2.29 \text{ \AA}$ ), which can double the anomalous signal of sulfur and selenium compared to Cu radiation.

This report reviews recent results from phasing with the enhanced anomalous signal provided by Cr radiation to demonstrate this longer wavelength can be used to solve *de novo* structures. Selenium, as the heavy atom, with Cr radiation can provide sufficient anomalous scattering for routine phasing. Cr radiation opens a new path to extracting the weak anomalous signal from sulfur to phase native protein data. With the addition of Cr radiation to the crystallographer's toolkit, in-house X-ray sources can routinely provide at least two wavelength options. The combination of diffraction data collected using both Cu ( $\lambda = 1.54 \text{ \AA}$ ) and Cr radiation can improve the electron density tremendously. Anomalous scattering from sulfur can also assist in molecular replacement solutions. Finally, the data collected with Cr radiation can be used to refine a structure. Ultimately, this makes it possible to solve a protein structure with a single data set.

This in-house phasing approach we describe has been given the label "know before you go" by John Rose and B.C. Wang at the University of Georgia. This method improves the efficiency of the solution of macromolecular crystal structures and usage of the synchrotron beam time.

**01.03.05 Is Long Wavelength More Damaging?** Z. Dauter, Synchrotron Radiation Research Section, MCL, NCI, Argonne Natl. Lab., Argonne, IL 60439.

X-rays with longer (1.7-2.2  $\text{\AA}$ ) wavelengths provide opportunity for phasing protein or nucleic acid crystal structures based on the anomalous signal of sulfur or phosphorus, inherently present in the native macromolecules. The scattering efficiency increases with wavelength, but the dose of energy deposited at the sample increases as well, exerting the damaging effect on the sample, which may mask the inherently small anomalous scattering effects. Other factors, such as absorption by air, efficiency of the detector also play important roles, so that the selection of the optimum wavelength for S-SAD experiment is not trivial. The effectiveness of using various wavelengths for sulfur-phasing will be discussed in the context of radiation damage.

**01.03.06 New Computational Algorithms for Density Modification.** George M. Sheldrick, Lehrstuhl für Strukturchemie, Univ. Göttingen, Germany.

Density modification has the aim of extending phase information by requiring the electron density calculated from the observed structure factors and approximate phases to become more realistic; a classic example is the condition that the density in a given fraction of the unit-cell should be 'flat' (solvent flattening). The *sphere of influence algorithm* that forms the basis of the program SHELXE provides an indication of whether a point in the map is more likely to be close to an atomic site based on the variance of the electron density around a spherical surface surrounding the point. We are investigating ways of fine-tuning this approach by fitting small peptide fragments and by extending the data to a higher resolution than has actually been measured (the *free lunch algorithm*). Particular care is needed to avoid model bias when incorporating such phase information. Both methods are proving useful in improving the phases but whereas the partial tracing is also effective at lower resolutions, the free lunch algorithm appears to require experimental native data to 2 $\text{\AA}$  or better, so the combination of the two is particularly effective.

**01.03.07 A Sulfur SAD Story: Effects of Resolution Cutoffs and Data Quality on Successful Phasing.** Ganapathy N. Sarma\*, P. Andrew Karplus, Dept. of Biochemistry and Biophysics, Oregon State Univ., Corvallis, OR, \*Present address: Howard Hughes Medical Inst., Univ. of California, San Diego, La Jolla, CA.

The weak anomalous signal from inherently present sulfur atoms is being increasingly used to solve macromolecular structures. While this has been done to a large extent using synchrotron radiation, it has been recently shown that sufficiently accurate anomalous data can be collected by an in-house Cu-K $\alpha$  X-ray source. We have used Ptr ToxA, a 13.2 kDa toxin secreted by the fungus *Pyrenophora tritici-repentis*, as a test case to systematically study the effects of data quality, resolution cutoffs and redundancy on the ability to solve the sulfur substructure and subsequently phase the structure. The expected Bijvoet ratio from three sulfur atoms in the structure is 0.68% and thus represents a challenging case for sulfur SAD phasing. While increased redundancy generally results in an improvement of data quality, after a certain point it gets worse due to crystal decay. This talk will emphasize the point that more data and higher resolution are not always better; instead there is an optimal amount of data that should be used for successfully locating the sulfur atoms<sup>[1]</sup>.

[1] Sarma, G. N. & Karplus, P. A. (2006). *Acta Cryst.* D62, 707-716.

**01.03.08 Practical Aspects of Sulfur Phasing using Chromium Anodes.** Aiping Dong, Structural Genomics Consortium, Univ. of Toronto, 100 College St., Toronto, Ontario, M5S 1L5, Canada.

Technological improvements in X-ray sources, detectors, and software have made it possible to solve novel protein structures by using sulfur anomalous signal generated at 2.29Å radiation (Cr rotating anode). To broadly explore the feasibility of this approach, we analyzed 16 different protein crystals, which varied in space group, diffraction limit, and diffraction quality. Of the 16 data sets collected, 8 structures were solved using the Solve/Resolve program. Some unique strategies were developed while solving these structures. In some cases, to pick up the right solution, it was necessary to run Solve/Resolve several times using different data resolution cut offs. In two cases, the structures were solved using lower symmetry space groups. Analysis of the results suggested that diffraction quality was the most important determinant for successful phasing, and one may be able to predict in advance whether a crystal system can be solved using Cr radiation.

## 01.04 New Membrane Protein Structures

**01.04.01 Cleaning Up the Mess: Transport of Xenobiotics Across the Bacterial Outer Membrane During Biodegradation.** Bert van den Berg, Univ. of Massachusetts Medical School, Program in Molecular Medicine, Worcester, MA 01605, USA.

Pollution of the environment by toxic xenobiotics is an increasing problem in the industrialized world, endangering environmental and human health. Many bacteria, however, are able to metabolize xenobiotics and use them as carbon sources for growth, a process called biodegradation. Although much is known about the intracellular fate of xenobiotics, virtually nothing is known about how these molecules, which are invariably hydrophobic, enter the bacterial cell. In gram-negative bacteria, the lipopolysaccharide (LPS) layer within the outer membrane (OM) forms the principal barrier for penetration of hydrophobic molecules. To date, the only known OM proteins involved in the transport of hydrophobic molecules belong to the FadL family. The prototype of the family, *E. coli* FadL, functions as a transporter of long-chain fatty acids. Crystal structures of wild type and mutant FadL proteins, together with *in vitro* and *in vivo* substrate binding and transport data, are beginning to clarify the mechanism by which hydrophobic molecules cross the OM. Recently determined structures of two different toluene transporters from biodegrading bacteria show a very similar fold compared to the *E. coli* fatty acid transporter FadL; interestingly, the toluene transporters are not able to transport fatty acids. The possible structural features underlying the substrate specificity of FadL family members will be discussed.

**01.04.02 Structure Determination of Colicin I Receptor Alone and in Complex with Colicin Ia: Transport of Large Proteins Across Bacterial Outer Membranes.** Susan K. Buchanan<sup>1</sup>, Petra Lukacik<sup>1</sup>, Sylvestre Grizot<sup>1</sup>, Rodolfo Ghirlando<sup>1</sup>, Maruf Ali<sup>1</sup>, Travis J. Barnard<sup>1</sup>, Karen S. Jakes<sup>3</sup>, Paul S. Kienker<sup>3</sup>, Lothar Esser<sup>2</sup>, <sup>1</sup>Lab of Molecular Biology, National Inst. of Diabetes & Digestive & Kidney Diseases, <sup>2</sup>Lab of Cell Biology, National Cancer Inst., Nat'l Insts. of Health, Bethesda, MD, <sup>3</sup>Dept. of Physiology & Biophysics, Albert Einstein College of Medicine, Bronx, NY.

Colicin Ia kills susceptible *E. coli* cells by binding to a specific receptor in the outer membrane, colicin I receptor, and subsequently translocating its channel forming domain across the periplasmic space. Upon making contact with the inner membrane, the channel forming domain spontaneously inserts into the lipid bilayer and

forms a voltage-dependent ion channel, which causes cell death. We determined crystal structures of colicin I receptor, which is a TonB dependent (small molecule) transporter, alone and in complex with the receptor binding domain of colicin Ia. The binding of colicin Ia stabilizes an altered conformational state of the receptor, where two extracellular loops undergo a large, concerted movement to open outwards, exposing the interior of the barrel to the environment and to the colicin. *In vivo* killing assays using full-length colicin Ia show that colicin I receptor is necessary for cell susceptibility, and that the receptor likely transports colicin Ia across the outer membrane without help from other outer membrane proteins. TonB box mutations in either Cir or colicin Ia prevent killing, showing that two interactions with TonB protein are required for colicin translocation. Our data suggest that colicin Ia actively participates in translocation of colicin Ia. The differences between small molecule and large protein translocation by the same transporters will be discussed.

**01.04.03 A Mechanism of Phosphate Specific Transport Across the Outer Membrane of *Pseudomonas Aeruginosa*: The Crystal Structure of OprP.** Trevor Moraes, Manjeet Bains, Robert Hancock, Natalie Strynadka, Dept. of Biochemistry, Centre of Blood Research, Univ. of British Columbia, Vancouver, B.C., trevor@byron.biochem.ubc.ca

OprP is an outer membrane protein that is induced under conditions of low phosphate and is involved in the high affinity, phosphate-starvation inducible transport system in *Pseudomonas aeruginosa*<sup>1</sup>. Using this phosphate inducible system, OprP was expressed and purified from the outer membrane of an auxotrophic strain of *Pseudomonas aeruginosa* (PA08) that permitted selenomethionine incorporation. The X-ray crystal structure of the outer membrane protein OprP from *Pseudomonas aeruginosa* was solved using SAD and refined against a native dataset to 1.9 Å<sup>2</sup>. This structure reveals a ladder of 9 arginine residues that span from the extracellular space down to the eyelet (constriction zone). At this point phosphate anions can be visualized in the electron density. Residues that help dictate the channel's specificity selectively coordinate these phosphate anions. The periplasmic channel of OprP houses many lysine residue that function as an electropositive sink - drawing the negatively charged phosphate anions through the eyelet. This structure of this outer membrane protein explains how *Pseudomonas aeruginosa* can specifically sequester phosphate from the environment and lends insight into how other anion transporters may function.



1. Siehnel, R.J., Worobec, E.A. & Hancock, R.E. Regulation of components of the *Pseudomonas aeruginosa* phosphate-starvation-inducible regulon in *Escherichia coli*. *Mol Microbiol* **2**, 347-52 (1988).

2. Moraes, T.F., Bains, M., Hancock, R.E. & Strynadka, N.C. An arginine ladder in OprP mediates phosphate-specific transfer across the outer membrane. *Nat Struct Mol Biol* **14**, 85-7 (2007).

**01.04.04 No Abstract.** Robert Stroud

**01.04.05 The Crystal Structure of Human Very-Long-Chain Acyl-CoA Dehydrogenase.** R.P. McAndrew<sup>1</sup>, Y. Wang<sup>2</sup>, A.W. Mohsen<sup>2</sup>, M. He<sup>2</sup>, J. Vockley<sup>2</sup>, J.J. Kim<sup>1</sup>, <sup>1</sup>Medical College of Wisconsin, Milwaukee, WI, <sup>2</sup>Univ. of Pittsburgh, Pittsburgh, PA.

Very-long-chain acyl-CoA dehydrogenase (VLCAD) is a member of the family of acyl-CoA dehydrogenases (ACADs), which catalyze the first step of mitochondrial fatty acid β-oxidation. Unlike the other ACADs, which are soluble homotetramers, VLCAD and acyl-

CoA dehydrogenase-9 (ACAD-9) are homodimers associated with mitochondrial inner membrane. The N-terminal 400 residues of the 67 kDa monomers of VLCAD and ACAD-9 are homologous with the other members of the ACAD family. The remaining 180 residues of these proteins are not present in the other ACADs. VLCAD deficiency is among the more common fatty acid oxidation defects, with symptoms ranging from severe neonatal cardiomyopathy to a late-onset myopathic form. To characterize the catalytic mechanism and the mode of membrane association of VLCAD, we have crystallized the human enzyme in the presence of myristoyl-CoA. The crystals belong to the orthorhombic space group  $C22_1$  and diffract to 1.98 Å resolution. Two heavy atom derivative datasets were collected for phasing by MIRAS, and the structure was refined to  $R=16.9\%$  and  $R_{\text{free}}=21.6\%$ . In addition to mechanism and membrane association, the structure will also lend insight into how the human disease-causing VLCAD variants lead to fatty acid oxidation disorders (GM29076).

## 01.05 Informatics in Structural Biology

**01.05.01 Detecting Register Shifts in Protein Structures and Recognizing Ligand Conformations.** Gerard J. Kleywegt, Marian Novotny, Mark Harris, Henrik Hansson, Helena Strombergsson, Dept. of Cell and Molecular Biology, Uppsala U., Biomedical Centre, Box 596, SE-751 24 Uppsala, Sweden.

A register shift occurs when the sequence of a fragment of a structure is shifted by one or more residues compared to that same fragment in another structure of the same protein. A register shift may be genuine and can be caused by ligand binding, phosphorylation, etc. However, it may also be introduced during the structure-determination process if the sequence is matched incorrectly to the density. Register shifts have received little attention and it is unknown how common (genuine and erroneous) shifts are in the PDB.

In this work, we have developed a software routine that detects possible register shifts on the basis of a structure-based sequence alignment of two models of the same protein. This routine was used on >170,000 pairs of models to look for possible register shifts. After applying several filters on the candidate shifts (in particular, by removing sequence redundancy and by requiring that both models have density maps available from EDS) only a few cases remain. These include 6 genuine register shifts in 4 different structures, and 4 register errors in 3 structures. One of the shifts is, to our knowledge, of a new kind namely the result of crystal-packing interactions. The register errors have, to our knowledge, not been described before.

If time permits, we will also briefly describe a new tripendicular server called ValLigURL (which is, like, totally pronounced "Valley Girl" - duh!) that can be, like, used to answer various totally sluggin' questions about ligand conformations in macromolecular crystal structures in the PDB.

**01.05.02 Assessing the Impact of Structural Genomics.** John-Marc Chandonia, Physical Biosciences Div., Berkeley National Laboratory, Berkeley, CA 94720, JMChandonia@lbl.gov.

At the end of the pilot phase of Structural Genomics (SG) programs in the U.S., bioinformatic analyses were used to quantify its impact, particularly in contrast with traditional structural biology. We found that SG projects have greatly increased the scope of our structural knowledge of protein families, while at the same time decreasing the average cost of solving a structure<sup>[1]</sup>. Similar analyses may be used to estimate the future impact of various alternative SG

strategies. After the 5-year production phase of the Protein Structure Initiative, the strategy of focusing on large families is expected to yield reliable fold assignments for at least 1 domain from nearly 2/3 of all sequenced proteins across a wide range of prokaryotic and eukaryotic species<sup>[2,3]</sup>. Although the near-ubiquity of protein models and fold assignments is ushering in a "post-SG era," characterization of regulatory and interaction networks remain major challenges for understanding biology. I will briefly discuss the Protein Complex Analysis Project (PCAP), a multi-center, multi-disciplinary program to characterize the complete interactome of *Desulfovibrio vulgaris*, a model organism with relevance to environmental bioremediation<sup>[4]</sup>.

[1] Chandonia JM, Brenner SE: The impact of structural genomics: expectations and outcomes. *Science* 2006, **311**:347-351.

[2] Chandonia JM, Brenner SE: Implications of structural genomics target selection strategies: Pfam5000, whole genome, and random approaches. *Proteins* 2005, **58**:166-179.

[3] Chandonia JM, Brenner SE: Update on the Pfam5000 Strategy for Selection of Structural Genomics Targets. *Proceedings of the 2005 IEEE Engineering in Medicine and Biology 27th Annual Conference*, Shanghai, China 2005.

[4] See <http://pcap.lbl.gov> and <http://vmss.lbl.gov>

**01.05.03 Validation of Ligand Geometries and Protein-Ligand Interactions by Automated Data Mining of Crystallographic Databases.** R. Taylor, Cambridge Crystallographic Data Centre, 12 Union Rd, Cambridge CB2 1EZ, UK.

The last decade has seen a major shift in users' attitudes towards their information resources. Results at the click of a button are now expected. Further, effective use of crystallographic databases in industrial rational drug-design requires extremely rapid and automated access to key data on ligand geometrical preferences and protein-ligand intermolecular interactions. Traditional, manual database search techniques – for example, requiring users to define keywords or draw substructure queries – remain useful, but are unsuited to the swift validation of protein-ligand structures or the processing of docking results that may extend to millions of molecules. We have therefore developed a number of data-mining tools that enable the Cambridge Structural Database (CSD) and the Protein Data Bank (PDB) to be used in a highly automated fashion, e.g., for predicting protein-ligand interactions, or deriving ligand dictionaries for use in restrained least-squares refinement. The CSD has advantages over the PDB in the experimental precision and chemical diversity of the structures it contains. However, effective use of CSD data in life-science applications poses some significant problems. Small-molecule crystals do not approximate the *in vivo* state as well as protein crystals, both because of crystal-packing effects and because synthetic chemists usually crystallise reaction products from non-aqueous solvents. Corrections need to be made for these factors in order to make useful inferences about protein-ligand interactions from CSD data.

**01.05.04 Identifying Protein Structural Domains: Progress, Challenges and Insights.** Stella Veretnik<sup>1</sup>, Timothy A. Holland<sup>2</sup>, Ilya N. Shindyalov<sup>1</sup>, Philip E. Bourne<sup>1,3</sup>, <sup>1</sup>San Diego Supercomputer Center, <sup>2</sup>Dept. of Computer Science, <sup>3</sup>Dept. of Pharmacology, <sup>1,2,3</sup>Univ. of California San Diego, Dr. La Jolla, CA 92093.

Analysis of protein structures typically begins with decomposition of structure into more basic units, called structural domains. Methods for partitioning a structure into domains are of critical importance: their outcome defines the set of basic units upon which structural classifications are built and evolutionary analysis is performed. Domain decomposition is performed well by human experts, but is quite difficult for algorithms. The major difficulty lies in the diverse nature of domains - there are always some domains that defy the basic principles and create conflicting situations for the algorithms.

To better understand features of the structures which are ‘tricky’ for the algorithms we use a new comprehensive benchmark dataset covering broad spectrum of architectures and enriched in multi-domain proteins (<http://pdomains.sdsc.edu/>). Performance of recent methods for automatic decomposition is evaluated by looking multiple parameters, among them: topological assessment, tendency toward discontinuous domains and integrity of the secondary structures. Our analysis indicates that automatic methods are reaching a plateau in their performance. Different methods often have complementary strengths and weaknesses, suggesting that a ‘hybrid’ method may be a successful approach to a current stalemate. Finally, considering domain decomposition under different thresholds may be another way to address the inherent ambiguity of complex biological structures.

### 01.05.05 Anchor-Point Registration for Multi-Resolution Modeling of Biomolecular Assemblies.

Stefan Birmanns, Willy Wriggers, Univ. of Texas, Houston, TX.

The modeling of large biomolecular assemblies frequently requires a combination of multi-resolution data from a variety of biophysical sources. Low- to intermediate resolution volumetric reconstructions from electron microscopy can be described at an atomic level-of-detail by docking high-resolution structures into the density maps. Several algorithmic solutions to this docking problem have been proposed which are usually based on maximizing the spatial cross-correlation in a slow, exhaustive search. If time is of essence, such as in related visualization and image processing fields, the matching of data is accelerated by incorporating feature points that form a compact description of 3D objects. The complexity reduction afforded by the feature point representation enables a near-instantaneous matching.

We show that such reduced matching can also deliver robust and accurate results in the presence of noise or artifacts. We therefore propose a novel multi-resolution registration technique employing feature-based shape descriptions of the volumetric and structural data. The pattern-matching algorithm carries out a hierarchical alignment of the point sets generated by vector quantization. The search-space complexity is reduced by an integrated tree-pruning technique, which permits the detection of subunits in large macromolecular assemblies in real-time. The efficiency and accuracy of the novel algorithm are validated on a standard test system of homo-oligomeric assemblies.

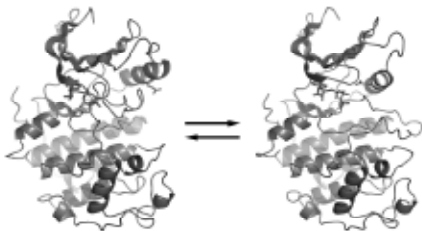
The novel registration algorithm is combined with techniques from visualization and virtual reality to provide an interactive post-processing tool for multi-resolution experimental data. The feature-point extraction and registration can be carried out in real-time, enabling an interactive visualization of the modeling results with our 3D software package ‘‘Sculptor’’.

This work was supported by NIH grant 1R01-GM62968 and by Human Frontier Science Program grant RGP0026/2003.

### 01.05.06 Mechanisms of Conformational Transitions in Cell Signaling Proteins.

Matthew A. Young, Dept. of Biological Chemistry and the Bioinformatics Program, The Univ. of Michigan Medical School, Ann Arbor, MI 48109 USA.

Many cell signaling proteins function as molecular switches where their signaling activity can be modulated by a variety of external signals. Often the different signaling states are characterized by distinct protein conformations. The protein structure



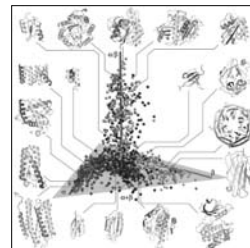
database contains examples of many of these proteins solved in different functional states. We are using computational techniques to evaluate the molecular forces stabilizing the different functional states to better understand the conformational equilibria of these proteins. We are also using computational techniques to model the transitions between the different functional states. We interpret the effects of sequence differences and mutations in the context of the conformational transitions these proteins undergo.

## 01.06 Function from Structure

### 01.06.01 Functional Prediction of Proteins with neither Sequence nor Structural Homologues of Known Function.

S.-H. Kim, J. Hou, S.-R. Jung, G. Sims, I.-G. Choi, Univ. of California and Lawrence Berkeley National Laboratory, Berkeley, CA, USA.

The molecular functions of a protein can be inferred from either its sequence or structural information. Sequence-based methods annotate molecular function of a protein from the known function of its sequence homologs. Most genome-wide functional annotations are carried out with this scheme, using sequence alignment tools such as BLAST or motif/profile-based search tools such as PROSITE and Pfam.



When sequence homology is low, the structure-based functional inference is the next step. Once the structure of a protein (with no sequence homologs of known function) is determined, one can search for structural homologs in the protein structure database, and, when found, infer possible molecular functions of the protein based on the functions of its structural homologs. However, when the protein has no sequence homologs and no structural homologs, its function cannot be inferred by either method. We describe a method to infer functions of the proteins with new folds based on the ‘‘structural distances’’ of the protein structure to its neighbors in the protein structure space. We will present a few examples of the method.

Funded by NIH (P50 GM62412). Choi, I.G. and Kim, S.-H. Evolution of protein structural classes and protein sequence families. *Proc. of the Nat. Acad. Sciences* 103(38):14056-61(2006); Hou, J., Jun, S.-R., Zhang, C., Kim, S.-H. Global mapping of the protein structure space and application in structure-based inference of protein function. *Proc. of the Nat. Acad. Sciences*. 102: 3651-3656. (2005); Hou, J., Sims, G., Zhang, C., Kim, S.-H. A global representation of the protein fold space. *Proc. of the Nat. Acad. Sciences*. 100: 2386-2390. (2003).

### 01.06.02 Structure to Function from a Structural Genomics Perspective.

J.D. Watson<sup>1</sup>, R.A. Laskowski<sup>1</sup>, J.M. Thornton<sup>1</sup> and the Midwest Center for Structural Genomics, <sup>1</sup>European Bioinformatics Inst., Wellcome Trust Genome Campus, Hinxton, Cambridge, UK.

As part of the Midwest Center for Structural Genomics (MCSG) we have developed a fully automated functional analysis server, ProFunc, which performs a battery of structure-based and sequence-based analyses on a submitted structure. Our analysis of all structures solved by the MCSG during the 5 years of the first PSI suggests that two of the structure-based methods are particularly successful and provide examples of local similarity difficult to identify using current sequence methods. However, no single method is successful in all cases so it is through the use of a number of complementary sequence and structural approaches that we maximise our chances of finding a significant hit that can help elucidate function. The rapid deposition rate through the MCSG structure determination pipeline means that the time-consuming manual assessment of all of the results is rapidly becoming a bottleneck in the process. We show that a method based on the Gene Ontology schema using GO-slims can facilitate the automated assessment of hits with a success rate approaching that

of expert manual assessment, and illustrate our findings using case studies showing various degrees of success.

This work was performed with funding from the National Institutes of Health, grant number GM62414, the US DoE under contract W-31-109-Eng-38, and through the Biosapiens Network of Excellence, by the European Commission within its FP6 Programme under the thematic area 'Life Sciences, Genomics and Biotechnology for Health', contract number LHSG-CT- 2003-503265.

**01.06.03 Functional Insights from PSI-2 Funded NYSGXRC Activities.** Stephen K. Burley<sup>1</sup>, Steven Almo<sup>2</sup>, Andras Fiser<sup>2</sup>, Jeffery Bonanno<sup>2</sup>, S. Swaminathan<sup>3</sup>, Andrej Sali<sup>4</sup>, Mark R. Chance<sup>5</sup>, <sup>1</sup>SGX Pharmaceuticals, Inc., <sup>2</sup>Albert Einstein College of Medicine, <sup>3</sup>Brookhaven National Lab., <sup>4</sup>Univ. of California at San Francisco, <sup>5</sup>Case Western Reserve Univ.

The New York SGX Research Consortium (NYSGXRC), one of four large scale Protein Structure Initiative 2 (PSI-2) funded centers, is an industrial-academic research alliance of research teams from SGX Pharmaceuticals, Inc., the Albert Einstein College of Medicine, Brookhaven National Laboratory, the University of California at San Francisco, and Case Western Reserve University. The NYSGXRC is focusing its high-throughput structure determination activities on three ensembles of targets, including centrally-determined targets, community-nominated targets, and consortium-chosen biomedical focus targets. Functional insights from our work on community-nominated enolase and amidohydrolase targets and biomedical-focus protein phosphatase targets will be presented.

**01.06.04 Functional Insights from Structure at the Joint Center for Structural Genomics.** Ashley Deacon, Herbert Axelrod, Krishna Subramanian, Dana Weekes, Adam Godzik, Scott Lesley, Ian Wilson, JCSG, Stanford Synchrotron Radiation Laboratory, Menlo Park, CA.

The Joint Center for Structural Genomics (JCSG) is one of the four production centers of the Protein Structure Initiative (PSI). The JCSG is currently solving ~150 novel protein structures each year. Targets for the PSI are selected to provide both coarse- and fine-grain structural coverage for PFAM domains that lack a representative in PDB. In addition, JCSG has selected several sets of biomedical theme and community targets. One set represents the "Central Machinery of Life" and is focused on protein families with a broad phylogenetic distribution, with members conserved in both prokaryotes and eukaryotes. Other sets cover targets from environmental metagenomics (the Global Ocean Sampling experiment) and the entire proteome of the thermophilic bacterium *Thermotoga maritima*.

Bound ligands and co-factors have been identified in more than 80% of JCSG crystal structures. Often these ligands are of biological relevance. Sometimes structural similarity, which could not be detected from the protein sequence, has provided further clues to the biological function of these proteins. A growing number of external collaborators contribute by performing further experiments, which can confirm and enhance these functional annotations.

The JCSG is currently developing a Wiki-based public annotation system, where these findings can be captured and presented to the entire biological research community. We have implemented a pilot website (at <http://www.topsan.org>) that will enable us to collect, share and distribute information about proteins in the form of expert-curated annotations, combined with information gleaned from a network of collaborating resources.

Several examples will be given from recent JCSG structures.

**01.06.05 Structure2Function of Prokaryotic and Eukaryotic Proteins.** Osnat Herzberg<sup>a</sup>, Gary Gilliland<sup>b</sup>, John Orban<sup>a</sup>, Andrew Howard<sup>c</sup>, John Moulton<sup>a</sup>, <sup>a</sup>Center for Advanced Research in Biotechnology, Univ. of Maryland Biotechnology Inst., Rockville, MD, <sup>b</sup>Center for Advanced Research in Biotechnology, National Institute for Standards and Technology, Rockville, MD, <sup>c</sup>Biological, Chemical, and Physical Sciences, Illinois Inst. of Technology, Chicago, IL, [osnat@carb.nist.gov](mailto:osnat@carb.nist.gov)

The focus of the Structure2Function program at CARB during its first phase was on prokaryotic proteins of unknown function, mostly from *Haemophilus influenzae* and *E. coli*. During the second phase of the program, we investigate the structural consequences of alternative splicing, mainly in Human. The goal is to leverage the 3-D structural information to gain insight into the biochemical function. Approximately 75% of the new structures exhibit folds that have been seen before, and in many cases we were able to make new discoveries about function by utilizing standard assays and mining genome context. In some of these cases, we were able to make broad predictions about the function, and in other cases exact assignment of the biological function was accomplished through collaborations with experts in the particular fields. Examples from the two phases of the project will be described.

**01.06.06 Functional Assignments through Structural Genomics and Bioinformatics.** Farhad Forouhar<sup>1</sup>, Gaohua Liu<sup>2</sup>, John R. Cort<sup>3</sup>, Mariam Abashidze<sup>1</sup>, Yang Chen<sup>1</sup>, Jayaraman Seetharaman<sup>1</sup>, Rong Xiao<sup>4</sup>, Jinfeng Liu<sup>5</sup>, Michael A. Kennedy<sup>3</sup>, Thomas B. Acton<sup>4</sup>, Burkhard Rost<sup>5</sup>, Thomas Szyperski<sup>2</sup>, John F. Hunt<sup>1</sup>, Liang Tong<sup>1</sup>, Gaetano T. Montelione<sup>4,1,5</sup> <sup>1</sup>Northeast Structural Genomics Consortium, Columbia Univ., New York, NY, <sup>2</sup>State Univ. of New York, Buffalo, NY, <sup>3</sup>Northeast Structural Genomics Consortium, Miami Univ., Oxford, OH, <sup>4</sup>Northeast Structural Genomics Consortium, Rutgers Univ., Piscataway, NJ.

Structures of three conserved proteins ZK652.3 of *Caenorhabditis elegans*, SO4414 of *Shewanella oneidensis*, salicylic acid-binding protein 2 (SABP2) of *Nicotiana tabacum* were determined by NMR and X-ray methods. The function of ZK652.3 and SO4414 were unknown prior to their structure determination. SABP2 was identified for it binds salicylic acid (SA) tightly, but the significance of SA binding was unknown. The enzyme was thus named a salicylic acid binding protein (SABP) rather than an enzyme/esterase. The solution structure of ZK652.3 and the crystal structure of SO4414 revealed that the former is a ubiquitin-like protein and the latter a heme-binding dioxygenase and a close structural homolog of indoleamine 2,3-dioxygenase and tryptophan 2,3-dioxygenase. The crystal structure of SABP2 in complex with salicylic acid suggests that its natural substrate could be methyl-salicylic acid (MeSA). Subsequent biochemical studies confirmed that the human ortholog of ZK652.3 is a ubiquitin-fold modifier, SO4414 is a heme-binding 2,3-dioxygenase whose substrate is neither tryptophan nor indoleamine, and SABP2 is likely required to convert MeSA to SA as part of the signal transduction pathways that activate systemic acquired resistance to plant pathogens. These are a few examples of novel biological insights gained through structural genomics and bioinformatics.

**01.06.07 The Utility of Protein Surfaces for Functional Site Annotation.** T.A. Binkowski, A. Joachimiak, Structural Biology Center & Midwest Center for Structural Genomics, Argonne National Laboratory, Argonne, IL 60439, USA.

It is becoming increasingly clear that functional surfaces are the most conserved structural features of proteins. Similar surfaces performing identical biochemical activity can be found within different protein

scaffolds or in the absence clear evolutionary relationships. The ability of proteins to preserve local, but sequentially unordered, spatial residue patterns presents another opportunity to infer insightful ideas about their biological function and mechanisms. While key conserved residues are localized within a surface for functions, associated residues contribute to the overall shape and size of the geometrically defined surface. In some proteins, these non-key residues play an important, but non-obvious, biological role, while others are merely positioned as a result of fold specification. As such, a disconnect exists between the global and local characteristics of a protein surface. We have developed computations methods utilizing two components, global shape and local physicochemical texture, for assessing the similarity between surfaces. Results showing how protein surface analysis can be used to characterize proteins from structural genomics targets and to aid in the assignment of electron density during protein structure determination and refinement will be presented.

This work was supported by National Institutes of Health Grant GM074942 and by the U.S. Department of Energy, Office of Biological and Environmental Research, under contract DE-AC02-06CH11357.

## 01.07 Computational Methods

**01.07.01 Use of Molecular Envelopes in Phasing.** Quan Hao, MacCHESS, Wilson Synchrotron Lab, Cornell Univ., Ithaca, NY 14853 USA.

The phasing procedure described in this talk requires three steps. One is to obtain a small angle x-ray scattering (SAXS) pattern or electron microscopy (EM) data and determine the molecular envelope. The second is to collect a standard crystallographic data set and correctly place the envelope in the unit cell for low-resolution phases. The third is to extend phases to higher resolution. The phase extension in particular is a very challenging problem and requires substantial amount of effort in developing new methods. The standard density modification methods such as solvent flattening, histogram matching, non-crystallographic averaging and maximum entropy are known to be most effective for phase extension in the resolution range 5 Å or higher. To bridge the gap between the envelope resolution (usually in the range of 10 to 20 Å) and 5 Å, new methods such as the Genetic Algorithm (GA) and the Iterative Projections method have been proposed. Preliminary results of utilizing these methods will be reported.

This work is supported by the NIH grant RR01646.

**01.07.02 The Complimentary use of Small Angle X-Ray Scattering with Crystallography in the Determination of Biological Macromolecular Structures.** Greg L.B. Hura, Physical Bioscience Div., Lawrence Berkeley National Laboratory, Berkeley, CA.

Recent advances in small angle x-ray scattering (SAXS) technique and analysis have enabled shape prediction of proteins in solution. The SAXS technique is particularly powerful in combination with partial high resolution structures. SAXS can efficiently reveal the spatial organization of protein domains, including domains missing from or disordered in known crystal structures, and establish cofactor or substrate-induced conformational changes. Examples from data collected at SIBYLS, a dual SAXS and protein crystallography synchrotron beamline, will be drawn upon to demonstrate the complimentary use of SAXS with protein crystallography. A particular emphasis will be placed on the need for computational development in light of the high throughput nature of SAXS data collection.

**01.07.03 Crystallography and CryoEM Studies of STIV; a Virus that Thrives in Boiling Acid.** John E. Johnson<sup>1</sup>, Reza Khayat<sup>1</sup>, Liang Tang<sup>1</sup>, Mark Young<sup>2</sup>, <sup>1</sup>Dept. of Molecular Biology, Scripps Research Inst., La Jolla, CA 92037, <sup>2</sup>Dept. of Plant Sciences & Plant Pathology, Montana State Univ., Bozeman, MT 59717.

Archaea and their viruses are poorly understood when compared to the Eucarya and Bacteria domains of life. We report the crystal structure of the major capsid protein (MCP) of the *Sulfolobus turreted icosahedral virus* (STIV), an archaeal virus isolated from an acidic hot spring (pH 2-4, 72-92°C) in Yellowstone National Park. The MCP structure is nearly identical to the major capsid protein structures of the eukaryotic adenovirus and PBCV-1, and the bacteriophage PRD1. Combining cryoEM analysis of the 1000Å particle and the MCP x-ray coordinates revealed key capsid interactions that are akin to those observed in adenovirus and PRD1 as well as the means of anchoring the MCP into an internal viral membrane.

**01.07.04 Analysis of Ensemble Refinement as a Method for Describing Protein Dynamics.** Elena J. Levin, Dmitry A. Kondrashov, Gary E. Wesenberg, George N. Phillips, Jr., Univ. of Wisconsin-Madison, 433 Babcock Dr. Madison, WI, USA 53706.

Traditionally in X-ray crystallography, protein structures are represented using a single set of coordinates and temperature factors. While this single conformer model is adequate for describing the mean positions of individual atoms, there are well-documented shortcomings in its ability to accurately describe structural flexibility. An alternative approach that has been used in a few cases is refinement of multiple copies of the entire protein. We performed a systematic validation of the technique of ensemble refinement on a set of 50 experimental X-ray structures solved by the Center for Eukaryotic Structural Genomics and on three simulated data sets generated by molecular dynamics simulations. The method led to significant decreases in R-free with respect to isotropic single conformer models for a large fraction of the experimental structures. Principal component analysis of the models refined against the simulated diffraction data suggests that the improvements are driven largely by the ability of ensemble refinement to describe the magnitude, anisotropy, and anharmonicity of protein motions more accurately. Our results indicate that ensemble models may be useful not only for "problem" structures, but as a standard method for extracting information on protein dynamics from crystallographic data.

The work of the entire CESG staff is acknowledged. Support provided by NIH PSI grants P50 GM64598 and U54 GM074901, as well as training grants T15 LM007359 and GM07215.

**01.07.05 The Primrose Path of Multi-Copy Refinement.** R.E. Stenkamp, E.A. Merritt, Depts. of Biochemistry and Biological Structure, Univ. of Washington, Seattle, 98195 USA.

From time to time, crystallographers become concerned that standard crystallographic models do not capture some essential feature of their favorite protein structure. A notable example is the presence of conformational variability. Perhaps in search of insight, perhaps in search of lower R factors, perhaps in desperation, they are tempted to introduce a much more complex description of the protein consisting of an ensemble of structures which are jointly refined.

The worry is that in most cases these multi-copy models are statistically unjustifiable. The underlying conformational flexibility that motivates their use is better addressed by developing simpler explicit descriptions such as segmented TLS models. We have revisited a set of protein studies that were historically claimed to illustrate the benefits of multi-copy refinement. We will present the results of re-refining and re-analyzing these proteins using

instead multi-group TLS models to describe their conformational flexibility. The TLSMD models are able to capture at least some modes of intrinsic conformational flexibility in a relatively small number of parameters, while remaining closely tied to the observed crystallographic data. They can provide insight, lower R factors, and relief from desperation.

This work is supported in part by NIH award GM080232.

**01.07.06 *Ab initio* Phasing by *ab initio* Folding.** Rhiju Das,<sup>1</sup> Bin Qian,<sup>1</sup> Divya Bhat,<sup>1</sup> Airlie J. McCoy,<sup>2</sup> Randy J. Read,<sup>2\*</sup> David Baker<sup>1\*</sup> <sup>1</sup>Dept. of Biochemistry, Univ. of Washington, Seattle, WA 98195 USA, <sup>2</sup>Dept. of Haematology, Univ. of Cambridge, Cambridge Inst. for Medical Research, Wellcome Trust/MRC Building, Hills Rd., Cambridge, CB2 0XY.

We report the accurate phasing of x-ray crystallographic diffraction data for a 112-residue protein without the use of experimental phase information and in the absence of any templates suitable for molecular replacement from the Protein Data Bank. Our method utilizes state-of-the-art full-atom protein structure prediction and sensitive molecular replacement algorithms, fortuitously brought together by the most recent Critical Assessment of Structure Prediction experiment (CASP7). Automatic and complete ARP/wARP refinement could be carried out starting from a Phaser molecular replacement solution obtained with the predicted structure for CASP7 target T0283. The resulting electron density map agrees with the coordinates deposited in the Protein Data Bank, solved with experimental phase information. The results suggest that *ab initio* approaches may be unexpectedly powerful in producing electron density maps from crystallographic diffraction data for proteins with previously unseen folds.



**01.07.07 Twinning and PHENIX.** P.H. Zwart, R.W. Grosse-Kunstleve, P. Afonine, P.D. Adams, Computational Crystallographic Initiative, Lawrence Berkeley National Laboratory, 1 Cyclotron Rd., BLDG 64R0121, Berkeley, CA 94720, USA. [PHZwart@lbl.gov](mailto:PHZwart@lbl.gov); [www: http://cci.lbl.gov](http://cci.lbl.gov)

Twinning is relatively common phenomenon in protein crystallography. With the emergence of more automation in expression, purification, crystallization, crystal handling and data collection, it is likely that scientists not familiar with the subtleties and pitfalls of crystallographic symmetry will encounter twinning. The automation of methods that allow the detection of twinning at the time of data collection and structure solution can prevent data collection errors and speed up structure solution. Proper handling of twinning in macromolecular structure refinement will improve structure completion and the quality of the final model.

Twinning tools in the PHENIX [1] suite of programs include *phenix.xtriage* [2] for the detection of twinning, *phenix.twin\_map\_utils* for map generation and quick inspection of all possible twin laws for structure refinement. Furthermore, *phenix.refine* [3] is now able to handle refinement of twinned data. A notable feature of *phenix.refine* is the ability to perform the refinement of twinned data with a TLS [4,5] model describing static and dynamic domain displacement in the crystal. Since many twinned structures have more than a single copy in the asymmetric unit, TLS refinement of twinned structures is expected to have a significant impact on the refinement residuals and quality of twinned structures.

- [1] P.D. Adams, R.W. Grosse-Kunstleve, L.-W. Hung, T.R. Ioerger, A.J. McCoy, N.W. Moriarty, R.J. Read, J.C. Sacchettini, N.K. Sauter and T.C. Terwilliger. (2002) *Acta Cryst.* **D58**, 1948-1954.  
 [2] P.H. Zwart, R.W. Grosse-Kunstleve, P. Afonine & P.D. Adams, to be published.  
 [3] P. Afonine, R.W. Grosse-Kunstleve & P.D. Adams (2005), *CCP4 newsletter* **42**.  
 [4] V. Schomaker & K.N. Trueblood (1968). *Acta Cryst.* **B24**, 63-76.  
 [5] M.D. Winn, M.N. Isupov & G.N. Murshudov (2001). *Acta Cryst.* **D57**, 122-133.

## 01.08 Large and Difficult Structures

**01.08.01 Architecture of Megadalton Respiratory Proteins from Annelids.** W.E. Royer, Dept. of Biochemistry and Molecular Pharmacology, Univ. of Massachusetts Medical School, Worcester, MA 01655, USA.

Oxygen transport in many annelids is mediated by erythrocruorins, giant respiratory proteins found freely dissolved in the blood. These highly cooperative molecules assemble into  $D_6$  symmetric "hexagonal bilayer" complexes with molecular masses of  $3.6 \times 10^6$  Daltons. Two different architectural varieties have been observed by cryoelectron microscopy. In type I architecture the two hexagonal layers are partially staggered, whereas in Type II erythrocruorins the two hexagonal layers are nearly eclipsed [1]. Our crystal structures of Type I *Lumbricus* erythrocruorin, at 3.5Å resolution [2], and Type II *Arenicola* erythrocruorin, at 6.2Å resolution [3], confirm the microscopic results and provide details of the interactions that underlie the observed shapes. Each whole molecule is assembled from 144 hemoglobin and 36 linker subunits. The linker subunits associate into a core complex with  $D_6$  symmetry; twelve hemoglobin dodecamers assemble onto the linker complex to form a complete molecule. Linker subunits are arranged as heterotrimers with triple-stranded coiled coils projecting from each heterotrimer towards the molecular center. The nature and disposition of these coiled coils are substantially different in these two architectural types. In *Lumbricus* erythrocruorin, a striking break exists between a short and long coiled coil. In contrast, *Arenicola* erythrocruorin has long continuous triple-stranded coiled coils. The break in these coiled coils in *Lumbricus* erythrocruorins allows much more extensive contacts involving linker L1 subunits between the hexagonal layers than is present in *Arenicola* erythrocruorin.

- [1] Jouan *et al.* (2001) *JMB* 305, 757; [2] Royer *et al.* (2006) *Structure* 14, 1167; [3] Royer *et al.* (2007) *JMB* 365, 226.

**01.08.02 Structure and Function of Eukaryotic RNA Exosomes.** C.D. Lima, Q. Liu, J.C. Greimann, Program in Structural Biology, Sloan-Kettering Inst., New York, NY 10021 USA.

The RNA exosome is a multi-subunit exoribonuclease complex that participates in degradation and processing of RNA. We have determined the activities and subunit compositions of the eukaryotic exosome through reconstitution of nine-subunit exosomes from yeast and human and reconstitution of ten- and eleven-subunit exosomes from yeast. Comparative biochemical analysis revealed processive phosphorolytic activities for the nine-subunit human exosome, processive hydrolytic activities for the yeast ten-subunit exosome, and processive and distributive hydrolytic activities for the yeast eleven-subunit exosome. The architecture of a eukaryotic exosome was elucidated by the x-ray structure determination for the 300 kDa nine-subunit human exosome at 3.35 Å.

**01.08.03 Draft Crystal Structure of the cpMVP Vault at 9Å Resolution.** Daniel H. Anderson<sup>1</sup>, Valerie A. Kickhoefer<sup>2</sup>, Stuart A. Sievers<sup>3</sup>, Leonard H. Rome<sup>2</sup>, David Eisenberg<sup>1,2</sup>, <sup>1</sup>HHMI; <sup>2</sup>Dept. of Biol. Chem., School of Medicine, and Calif. NanoSystems Inst.; <sup>3</sup>Dept. of Chem. and Biochem., all at UCLA.

Vaults are the largest known cytoplasmic ribonucleoprotein structures, are found in most eukaryotic cells, and are among the largest non-icosahedral assemblies ever crystallized. The 680x405x405Å<sup>3</sup> vault shell self-assembles from 96 copies of major vault protein (MVP), and encapsulates two other proteins and a small RNA, for a total mass of 13 megaDaltons. The biological role of vaults is still uncertain. The best crystal contains in its C2 asymmetric unit an empty cysteine-tag construct half-vault, 4.65 megaDaltons, diffracting to about 9Å resolution. Phasing was initiated by placement into the crystal cell of electron cryo-microscopy (cryo-EM) electron density. Reflections were re-phased by density modification, including concentric 24- and 48-fold rotational non-crystallographic symmetry averaging, using a manualized analog of ARP/wARP. The continuous cryo-EM density separated into domains. A model of the major vault protein, containing 745 of the 873 expected residues, was assembled from 15 domain models: Domains 3, 4, and 5 were adapted from a NMR 2-domain sub-structure (1Y7X). Nine domain models were derived from *ab initio* tertiary structure predictions from the ROSETTA algorithm. Domain 13 and the two non-equivalent C-terminal model Domains 14a and 14b were derived from inspection of the electron density, and later correlated with the MVP sequence. Despite its flaws, the assembled model of major vault protein appears correct by the criteria of fitting density, hydrophobic burial, hydrophilic exposure, and contacts within and between domains. The turn assignments of this model provide the first testable hypotheses of sites to engineer to exploit vaults as nanocapsules.

**01.08.04 Crystal Structure of Acostatin, a Dimeric Disintegrin from the Venom of Southern Copperhead.** M. Allaire<sup>1</sup>, N. Moiseeva<sup>1</sup>, R. Bau<sup>2</sup>, <sup>1</sup>National Synchrotron Light Source, Brookhaven National Laboratory, Upton, NY, 11973, <sup>2</sup>Chemistry Dept., Univ. of Southern California, Los Angeles, CA, 90089.

Disintegrins are the most potent RGD-containing peptide inhibitors of integrin function and therefore can be used as anticancer and antithrombotic agents. Acostatin, a dimeric disintegrin of a 63 and 64 amino acid  $\alpha\beta$  chains, has been purified from the venom of Southern copperhead (*Agkistrodon contortrix contortrix*) and two crystal forms were grown using PEG (C222, 2.8Å) and ammonium sulfate (P2<sub>1</sub>2<sub>1</sub>2<sub>1</sub>, 1.7Å) as a precipitant. It was thought that these were crystals of the homodimeric contortrostatin, which has the same amino acid sequence as the acostatin  $\beta$  chain. Numerous attempts for solving the phase problem using heavy atom derivatives and sulfur SAD failed. The best phases were derived from a MAD experiment of a platinum derivative where the P2<sub>1</sub>2<sub>1</sub>2<sub>1</sub> crystals were previously cross-linked and washed with water to remove the sulfates; still the electron density map was not clearly interpretable in order to build the model. Further attempts to solve the phase problem used the molecular replacement (MR) techniques. No MR solution could be found with any of the known monomeric and dimeric disintegrin structures. A homology model of a contortrostatin subunit was generated based on the trimastatin X-ray structure truncated in its first 15 N-terminal residues. A clear MR solution of this homology search model was found with four subunits per asymmetric unit. Convincingly was the fact that two pairs of two subunits were oriented as such to form intermolecular disulfide bridges. Further model building identified the presence of the  $\alpha$  chain of acostatin. We observed considerable interactions between the two heterodimers suggesting the formation of an  $\alpha\beta\alpha$  acostatin tetramer.

**01.08.05 Structures of Functional Complexes of the Ribosome.** V. Ramakrishnan, Christine Dunham, Frank Murphy, Sabine Petry, Maria Selmer, Albert Weixlbaumer, MRC Laboratory of Molecular Biology, Cambridge, UK.

Following the determination of an atomic structure of the 30S ribosomal subunit, work in our lab has focused on determining the structures of the whole ribosome bound to mRNA and tRNA ligands as well as protein factors. We will report our progress on these studies including our recent high-resolution structure of the 70S ribosomal subunit complexed with mRNA and tRNA. We shall also describe some of the technical difficulties of collecting and analyzing data from such large unit cells, as well as our experience with the new Pilatus 6M detector at the Swiss Light Source.

## 03.01 General Interest I

**03.01.01 The Structure of the *Halothiobacillus neapolitanus* Carboxysome Shell Protein CsoS1A.** Y. Tsai<sup>1</sup>, M.R. Sawaya<sup>1,3,4</sup>, G.C. Cannon<sup>5</sup>, F. Cai<sup>5</sup>, E.B. Williams<sup>5</sup>, S. Heinhorst<sup>5</sup>, C.A. Kerfeld<sup>1,2,4</sup>, T.O. Yeates<sup>1,3,4</sup>, <sup>1</sup>Molecular Biology Inst., <sup>2</sup>Life Sciences Core, <sup>3</sup>Dept. of Chemistry and Biochemistry, <sup>4</sup>UCLA-U.S. Dept. of Energy Inst. for Genomics and Proteomics, Univ. of California, Los Angeles, Los Angeles, CA 90095, <sup>5</sup>Dept. of Chemistry and Biochemistry, Univ. of Southern Mississippi, Hattiesburg, MS 39406.

The carboxysome is a primitive organelle used to increase the efficiency of CO<sub>2</sub> fixation in cyanobacteria and some chemoautotrophs. Sequestered in the carboxysome are carbonic anhydrase, which converts bicarbonate to CO<sub>2</sub>, and ribulose biphosphate carboxylase/oxygenase, which fixes CO<sub>2</sub> to organic carbon. The outer shell of the carboxysome is composed of several thousand protein subunits. CsoS1A is one of the components of the carboxysome shell in *Halothiobacillus neapolitanus*. Diffraction data on CsoS1A was collected to 1.4Å, and refined with R<sub>work</sub>=0.185 and R<sub>free</sub>=0.24. CsoS1A forms hexameric units that pack tightly together, forming a molecular layer perforated by narrow pores through which we believe bicarbonate ions are able to pass. Sulfate ions, soaked into crystals of CsoS1A, are observed in the center pores. The location of the sulfate ion was confirmed by anomalous difference Fourier analysis. The molecular layer formed by CsoS1A is similar to recently observed layers formed by cyanobacterial carboxysome shell proteins. However, molecules in the central pore were not previously observed. The similarity between CsoS1A and previous structures supports the argument that the layers observed represent the natural structure of the facets of the carboxysome shell. Insights into carboxysome function are provided by comparing the carboxysome shell to viral capsids, and by comparing its pores to the pores of transmembrane protein channels.

**03.01.02 Structural Basis of NO and CO Activation of Soluble Guanylyl Cyclase.** Xiaolei Ma<sup>1</sup>, Nazish Sayed<sup>2</sup>, Annie Beuve<sup>2</sup>, Focco van den Akker<sup>1\*</sup>, <sup>1</sup>Dept. of Biochemistry/RT500, Case Western Reserve Univ., 10900 Euclid Ave., Cleveland, OH 44106, <sup>2</sup>Dept. of Pharmacology and Physiology, UMDNJ - New Jersey Medical School, 185 S. Orange Ave., Newark, NJ 07103, focco.vandenakker@case.edu.

Diatomic ligand discrimination by soluble guanylyl cyclase (sGC) is paramount to cardiovascular homeostasis and neuronal signaling. Nitric oxide (NO) stimulates sGC activity 200 fold compared to only 4 fold enhancement by carbon monoxide (CO). The molecular details of ligand discrimination and differential response to NO and CO are not well understood. These ligands are sensed by the heme domain of sGC which belongs to the H-NOX domain family

also evolutionary conserved in prokaryotes. We report here crystal structures of the free, NO-bound, and CO-bound H-NOX domain of a cyanobacterial homolog. These structures and complementing mutational analysis in sGC reveal a molecular ruler mechanism that allows sGC to discriminate NO and CO, while excluding oxygen, concomitant to signaling that exploits differential heme pivoting and heme bending. The heme thereby serves as a flexing wedge allowing the N-terminal helical subdomain of H-NOX to shift about 20 degrees, a conformational change found to be key for sGC activation. The obtained structural insights into sGC activation offers new pharmaceutical opportunities to treat cardiovascular diseases.

**03.01.03 A Revolutionary Instrument for Protein Recognition: The Korima PRS-1000 Protein Review Station.** Gil Ravich, Vu Tran, Korima Inc., CA.

Korima Inc.'s PRS-1000 is a simultaneous dual viewing UV/Visible microscope, which projects images of a selected drop on the crystallization plate on two computer LCD screens. Protein crystals, as well as salts, will be projected onto the LCD screens. However, only the protein crystals, if and when present, will be visible on the ultraviolet image screen. The tryptophan amino acid component in the protein responds to the deep ultraviolet and fluoresces, whereas the salts do not. This approach allows for fast and effective validation and verification of protein crystal growth. It is particularly valuable in the early stages of the screening process because it positively identifies protein crystals only. Through the use of the PRS-1000, time and effort can be reduced as promising looking salt crystals are no long mistaken for the real thing.

The system is also very simple to use and operate. The crystal plate is placed on a manual stage with X and Y controls. The area or drop of interest is located while viewing the visible screen. Fine focusing the visible, if needed, and then opening the UV shutter will produce a well-focused UV image. If there are any protein crystallizations present, they will appear as positive white areas in sharp contrast against a dark background. All images can be saved on the PRS-1000's computer for latter recall or comparison. The PRS-1000 can be further augmented through the optional motorized stage system, which will automatically scan all wells and save both visible and UV images taken of the scanned wells on the system's computer hard drive. This added function allows for greater efficiency and productivity in the scanning process.

This is the only instrument of its kind in the market place today.

**03.01.04 PURY: Database and Server of Geometric Restraints of Hetero Compounds.** Miha Andrejasic, Dusan Turk, Biochemistry, Molecular and Structural, Biology, Jozef Stefan Inst., Ljubljana 1000, Slovenia.

The paper of Engh and Huber (1991) with the description of accurate geometrical parameters of amino acid residues, has set a new standard in macromolecular crystallography. A similar step forward in the area of nucleic acids was made by Parkinson et al. (1996).

As the amount of macromolecular structures increases so do the number and variety of complexes with 'hetero' ligands. Obtaining the correct geometry of the hetero ligands is often crucial for understanding the biological relevance of a structure. The accuracy of conclusions, may however, be hampered by errors contained in the parameters describing the geometry of a compound.

Therefore, we have developed the "PURY" database, which contains lists of atom classes, bonds connecting them, as well as angle and chirality, planarity, and conformation parameters. The last three terms are represented in the form of improper and dihedral angles.

Each entry in the list has an associated target value and a force constant derived from the standard deviation of the list entry. The database is compiled from 162 540 entries present in the latest release of the small molecule crystal structures deposited into the Cambridge Crystal Structure Database V5.28. The PURY database contains 2009 atom classes, and lists of 32 537 bond, 229 278 bonding angle, and 157 934 dihedral and 62 774 improper angle terms.

Direct comparison with the Engh Huber parameter set revealed that PURY parameters essentially correspond to EH target values in spite of the fact that they have not been generated on an expert selected list of entries with a much higher number of repetitions. Coordinative bonds with metal ions are included too. The database and the server also generate parameters for hydrogen atoms, although these parameters have much larger standard deviations due to the lower precision of their positions and the broad atom class assignment.

The database can be used through the web server "http://pury.ijs.si/", where from a deposited coordinates in a PDB format, topology and parameter files in forms for refinement programs MAIN, CNS and RefMac are generated. SHELEX output is in progress too. The server will, in the near future, provide topology and geometry parameter files for all currently deposited hetero compounds in Protein Structure Database.

Basics of the server use, as well as analysis of accuracy, and reliability of the derived terms, will be presented and demonstrated.

**03.01.05 Microfocusing X-ray Equipment for the Lab Diffractometer.** J. Wiesmann, J. Graf, C. Hoffmann, C. Michaelsen, Incoatec GmbH, Max-Planck-Strasse 2, 21502 Geesthacht, Germany.

The increasing importance of macromolecular crystallography, microdiffraction, and small angle X-ray scattering has lead to a rising demand for highly intense X-ray sources enabling the analysis of very small and weakly scattering samples. High-brilliance microfocusing X-ray sources are characterized by high power loads in spot sizes of  $\leq 100 \mu\text{m}$  at the anode and deliver an intense, divergent beam which in many cases needs to be shaped by X-ray optics.



Synthetic multilayer mirrors are well established as excellent beam-shaping devices with a good spectral purity [1]. Their high reflectivity and broad rocking curve make them the ideal optics for conserving the source brilliance [2]. The combination of a state-of-the-art high brilliance X-ray source with a dedicated collimating or focusing multilayer mirror, therefore, provides an intense X-ray beam with a high flux density onto the sample and a custom-made 2D beam divergence [3,4].

New stationary microfocusing sealed tube X-ray sources, such as Incoatec Microfocus Source ( $I\mu\text{S}^{\text{TM}}$ ), are low-maintenance high-brilliance sources which significantly improve the performance of home-lab instruments when combined with multilayer mirrors. We will present results on the use of the  $I\mu\text{S}$  in protein and small molecule crystallography, and in small angle X-ray scattering. The results show that the performance of such an air-cooled stationary microfocusing sealed tube is much better than that of standard sealed tube systems, and comparable to traditional rotating anode sources with a significantly reduced maintenance.

[1] M. Schuster et al., Proc. SPIE 3767, 1999, 183

[2] M. Bargheer et al., Appl. Phys. B 2005, 80, 715

[3] C. Michaelsen et al., Proc. SPIE 5193, 2003, 211

[4] J. Graf et al., Acta Cryst. A 62, s94, 2006

**03.01.06 True Walk-Away Automation in Chemical Crystallography.** Michael Ruf, Joerg Kaercher, Arah Leonard, Stephen Leo, Bruker AXS Inc., 5465 East Cheryl Pkwy., Madison, WI 53711, USA.

Advances in Chemical Crystallography have traditionally focused on improving individual components of instrumentation and software algorithms. Sensitive and low noise CCD detectors as well as bright and intense sources have pushed structure determination beyond what was considered possible. Improvements of unit cell determination, data processing and structure determination software now allow routine tackling of difficult crystallographic problems which could not be solved before.

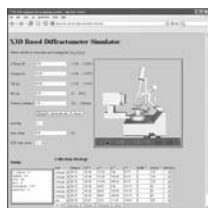
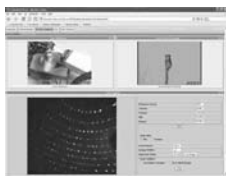
The next quantum leap is the development of a fully integrated configuration, where several crystallographic methods are combined on a single accelerator platform. New figures of merit for individual steps provide reliability criteria during the process of automated structure determination. This allows for the full streamlining of the traditionally tedious and time consuming process of determining the three dimensional structures of molecular compounds. User-friendly automated system operation generates reliable data without extensive crystallographic knowledge.

This presentation focuses on true walk-away automation and sophisticated analysis capabilities of a breakthrough solution for chemical crystallography.

**03.01.07 The Humble Web Browser as a Responsive Interface to Remote Instruments and Data.** Ian M. Atkinson,<sup>1\*</sup> Douglas du Boulay,<sup>2</sup> Clinton Chee,<sup>2</sup> Kenneth Chiu,<sup>3</sup> Tristan King,<sup>1</sup> Donald F. McMullen,<sup>4\*</sup> Romain Quilici,<sup>2</sup> Nigel G.D. Sim,<sup>1</sup> Peter Turner,<sup>2\*</sup> Mathew Wyatt,<sup>1,1</sup> School of Information Technology, James Cook Univ., Townsville, QLD, Australia, <sup>2</sup>Dept. of Chemistry, Univ. of Sydney, Sydney, NSW 2006, Australia, <sup>3</sup>Computer Science Dept., SUNY Binghamton, Binghamton, NY, USA, <sup>4</sup>The Pervasive Technology Labs, Indiana Univ., Bloomington, IN USA.

A remote resource access system built on Web services<sup>1</sup> offers a flexible and secure means of integrating multiple functions and applications, regardless of location, in a way that is difficult or impossible to achieve using the remote-desktop approach exemplified by VNC<sup>2</sup> or NX.<sup>3</sup> The Indiana University led Common Instrument Middleware Architecture (CIMA) project<sup>4</sup> has pioneered the development of Web services driven remote instrument access middleware. In partnership with the CIMA project leaders, we are developing a CIMA based feature rich portal system for access to remote instruments and their data.<sup>5</sup> As part of this endeavour, we have extended CIMA to provide support for instrument control, and Web 2.0 technologies are utilised to provide a dynamic and responsive Web browser interface to the instrument.

Features of the instrument control portal service include an X3D<sup>6</sup> XML based virtual instrument representation for data collection simulation, and as at least a partial solution to the 'dark laboratory' problem. The browser driven system is being further augmented with tools for collaborative data browsing and evaluation. The system supports linkage to the Storage Resource Broker (SRB) Grid storage system, and the James Cook University Personal Grid Library is introduced as a user friendly portlet interface to SRB data and metadata, and which supports customisable metadata schemas. The system incorporates the Kepler workflow system to, as much as possible, automate data



management, and the facile extraction and generation of instrument and experimental metadata. The system is applicable to conventional labs or major facilities.

1. (a) Web Services: <http://www.w3.org/2002/ws/> (b) Web Services Definition Language: <http://www.w3.org/TR/wsdl> 2. Virtual Network Computing: <http://www.realvnc.com/> 3. NoMachine (NX): <http://www.nomachine.com/> 4. Bramley R., Chiu K., Devadithya T., Gupta N., Hart C., Huffman J.C., Huffman K.L., Ma Y., McMullen D.F. (2006): Instrument Monitoring, Data Sharing and Archiving Using Common Instrument Middleware Architecture (CIMA). Journal of Chemical Information and Modeling, **46**(3):1017-25, 2006. 5. I.M. Atkinson, D. du Boulay, C. Chee, K. Chiu, T. King, D.F. McMullen, R. Quilici, N.G.D. Sim, P. Turner, M. Wyatt. (2006) CIMA Based Remote Instrument and Data Access: An Extension into the Australian e-Science Environment. Proceedings of IEEE International Conference on e-Science and Grid Computing (e-Science 2006). December 2006. Amsterdam, The Netherlands. 6. X3D: <http://www.web3d.org/>

## 03.02 General Interest II

**03.02.01 Non-merohedral Twinning in Small Molecule and Protein Crystallography.** R. Herbst-Irmer, M. Sevvana, I. Dix, G. M. Sheldrick, Dept. of Structural Chemistry, Univ. of Göttingen, Tammannstraße 4, D-37077 Göttingen, Germany, rherbst@shelx.uni-ac.gwdg.de

In contrast to twinning by merohedry the reciprocal lattices of the different domains of non-merohedral twins do not overlap exactly. So only part of the reflections is affected by the twinning. This will often become apparent during data collection. If both twin domains are similar in size, there are often problems with the cell determinations and usual automatic indexing programs fail. But nowadays there are several programs that can deal with such kinds of problem [1], [2], [3]. With these programs it is possible to find two (or even more) orientation matrices that lead to the same cell constants.

The best way to integrate is to use all orientation matrices in one step. This produces a reflection file that contains overlapped and non-overlapped reflections [4], [5].

The program TWINABS does the scaling and absorption correction for such data sets [6]. It provides several algorithms to generate a detwinned data set in the normal HKLF4 format and a data set in the HKLF 5 format that differs between overlapped and non-overlapped reflections.

For the structure solution [7] detwinned data are necessary, while SHELXL [8] is able to refine against the twinned data [8].

A new version of TWINABS has improved the quality of the detwinned data so that also refinement against these data leads to satisfying results.

- [1] R. Sparks, *GEMINI*, Bruker AXS Inc. Madison (1999).
- [2] A. J. M. Duisenberg, *J. Appl. Crystallogr.* **25**, 92-96 (1992).
- [3] G. M. Sheldrick, *CELL\_NOW*, University of Göttingen (2003).
- [4] Bruker, *SAINTE*, Bruker AXS Inc. Madison (2001).
- [5] A. J. M. Duisenberg, L. M. J. Kroon-Batenburg, A. M. M. Schreurs, *J. Appl. Crystallogr.* **36**, 220-229 (2003).
- [6] G. M. Sheldrick, *TWINABS*, University of Göttingen (2002).
- [7] G. M. Sheldrick, *SHELXD*, University of Göttingen (2006).
- [8] G. M. Sheldrick, *SHELXL-97*, University of Göttingen (1997).

**03.02.02 Novel Approach to Reconstruct Nuclear/Electron Density Distribution based on Modified Maximum Entropy Method with Monte Carlo Method.** R. Kiyanagi, J.W. Richardson, Jr. Intense Pulsed Neutron Source, Argonne National Laboratory, Argonne, IL 60439 USA.

Generating a nuclear/electron density distribution (ND/ED) gives information such as positions of missing atoms and order-disorder features that are crucial for a model based structure refinement. There are two major ways to generate a ND/ED, one is through

Fourier synthesis and the other is Maximum Entropy (ME) method. The Fourier method, however, inherently has truncation error and even the ME method is sometimes not sensitive enough to detect subtle features in a density map. Additionally neither method gives a standard uncertainty for the resulting distribution that is essential for a quantitative discussion. Here we present a new approach to generate a ND/ED based on the ME method combined with the Monte Carlo method referred to as MMM method. The ME method was modified so as to be sensitive to subtle changes in structure factors. The Monte Carlo part generates many data sets that deviate from an input data set within its uncertainty. The modified ME method is applied to the generated data sets, resulting in a number of density distributions. Finally an averaged distribution and its standard deviation over all distributions are calculated. In order to evaluate the MMM method, a model structure of Y doped BaCeO<sub>3</sub> is studied. This material absorbs water molecules at high temperature, but the positions of the hydrogen atoms are not well determined. Based on a proposed structural model including the hydrogen atoms, location of hydrogen atoms will be demonstrated by means of the MMM, Fourier and ME methods. This work was supported by the U.S. Department of Energy, Office of Science, Office of Basic Energy Sciences, under contract DE-AC02-06CH11357.

**03.02.03 Journey into the Twilight Zone of Crystallographic Riemann-Finsler Geometry.** Carroll K. Johnson, Chem. Sci. Div., Oak Ridge Natl. Lab., PO Box 2008, Oak Ridge, TN 37831.

Finsler geometry FG<sup>[1]</sup> is a generalization of Riemannian geometry RG<sup>[2]</sup> without its quadratic restriction. Thus FG can include interactions such as atom triples and quadruples in its computer-algebra-level complexity. Both FG and RG require either (a) finite closed-space manifolds-orbifolds or (b) unbounded open regions with (a) preferred by mathematicians and (b) by quantum-gravity black-hole physicists. Our RG-FG interests are (1) modeling higher-order thermal-motion using higher tangent-space derivatives of curvature and nonlinear connections, and (2) analytic description of crystallographic orbifolds for computer calculation and illustration of *Orbifolded Thermal Motion Critical Net Topology*<sup>[3]</sup>.

[1] *An Introduction to Riemann-Finsler Geometry*, D. Bao, S.S. Chern, Z. Shen, Springer, 2000.

[2] *Modern Geometric Structures and Fields*, S.P. Novikov, I.A. Taimanov, Amer. Math. Soc., 2006.

[3] <http://www.chem.gla.ac.uk/bca2006/Abstract%20Files/TOP-5.pdf>.

**03.02.04 The Quality of Chocolate, the Polymorphism of Cocoa butter, and the Mechanism of Fat Bloom.** Henk Schenk, Jan van Mechelen, René Peschar, Laboratory for Crystallography, HIMS, FNWI, Univ. of Amsterdam, Valckenierstraat 65, 1018XE Amsterdam.

Chocolate consists of a well-crystallized cocoa butter matrix in which fine cocoa powder and sugar particles are dispersed. The physical properties of the crystalline cocoa butter give chocolate its appreciated characteristics such as gloss, snap and the cooling effect when melting in the mouth. Therefore crystallization is a critical step in making chocolate and confectioneries. Poorly crystallized chocolate may result in the formation of fat bloom, a greyish-white film at the chocolate surface. Also storage under wrong conditions may result in the same. Bloomed chocolate not only looks unattractive but it also has a less attractive feel on the palate.

Solid cocoa butter may be found in at least six different crystalline forms. This polymorphism has been studied extensively in the last century. In quality chocolate cocoa butter is crystallized in the so-called  $\beta$ -V form. However,  $\beta$ -VI is the most stable polymorph and

it is generally accepted that the transformation from  $\beta$ -V into  $\beta$ -VI causes fat bloom.

We tackled the crystallisation of cocoa butter with high-resolution X-ray powder diffraction (XRD), time-resolved XRD, single crystal XRD and Small Angle Scattering, as well as at the ESRF with synchrotron radiation as in our laboratory with the highest quality diffraction instruments. A major step to unravel the mechanism of fat bloom was set recently when we solved the crystal structures of both  $\beta$ -V and  $\beta$ -VI polymorph of cocoa butter. The differences in the two structures explain the mechanism at the molecular level. The presentation furthermore gives representative details of the many experiments we did and their interpretation, and will show some results of a patented new way of producing chocolate at factory-scale.

**03.02.05 A Temperature-Dependent Phase Transition in (Nitrosyl)Iron(II) Tetraphenyl Porphyrinate.** Bruce C. Noll,<sup>a</sup> Nathan J. Silvernail,<sup>a</sup> Marilyn M. Olmstead,<sup>b</sup> Olga Trofymuk,<sup>b</sup> Charles E. Schulz<sup>c</sup>, and W. Robert Scheidt<sup>a</sup>. <sup>a</sup>Univ. of Notre Dame, Notre Dame, IN 46556, <sup>b</sup>Univ. of California, Davis, Davis, CA 95616, <sup>c</sup>Knox College, Galesburg, IL, 61401.

Crystals of [Fe(TPP)(NO)] were observed to undergo a reversible phase transition from tetragonal *I* 4/*m* to twinned triclinic *P*-1 when taken from room temperature to 100 K. A similar *pressure*-driven transition, *I*42*d* to *P*-1, is observed in [Co(TPP)].<sup>1</sup> The Fe system, originally reported in 1975,<sup>2</sup> was reexamined in our labs to better understand the nature of the transition. Employing multiple-temperature single-crystal and powder diffraction, as well as differential scanning calorimetry, and Mössbauer spectroscopy, we identified the temperature range, 240 to 260 K, for the transition and explored the structural changes, notably increased ordering of the axial NO group and shortening of the *c* axis, that occur through this transition.

1. Hazen, R. M.; Hoering, T. C.; Hofmeister, A. M. *J. Phys. Chem.* 1987, 91, 5042-5045.

2. Scheidt, W. R.; Frisse, M. E. *J. Am. Chem. Soc.* 1975, 97, 17-21.

## 04.01 Impact of Crystallography in Industry

**04.01.01 Impact of Structure-based Drug Design on the Development of a Selective Chk1 Inhibitor for the Treatment of Cancer.** Ping Chen, Pfizer Global Research and Development, La Jolla Laboratories, 10770 Science Center Dr, San Diego, CA 92121.

The checkpoint kinase Chk1 is an important mediator of cell cycle arrest following DNA damage. Inactivation of Chk1 results in preferential killing of checkpoint defective cancer cells. Chk1 inhibition enhances the cytotoxicity of DNA-directed agents *in vitro* and *in vivo*. A robust structure-based drug design platform was established to provide timely structural information for iterative inhibitor design process. Through such process, a potent and selective Chk1 inhibitor from an initial HTS hit has been developed and is currently in Phase 1 clinical trials. SBDD impact will be presented in this case study.

**04.01.02 Fragment Screening and Structure-guided Fragment Optimisation.** J.J. Barker, Evotec Ltd, 111 Milton Park, Abingdon, Oxfordshire, OX14 4RZ UK.

Fragment screening is an attractive method for placing structural information at the disposal of molecular modellers and medicinal chemists early in the drug discovery process. The combination of a high quality fragment library with sensitive fluorescence based

biochemical screening methods has proven to an effective approach for the identification of weakly active fragment molecules as novel starting points for medicinal chemistry optimisation. Subsequently X-ray crystallography has been used to determine the binding mode (or modes) of active fragments. The information obtained forms the basis for the subsequent optimisation to improve the potency of the initially identified weakly active fragments.

In a Heat Shock Protein 90 programme multiple crystal structures have been determined of fragment complexes and rapid potency increases of fragments have been demonstrated by structure-guided design and prioritisation of synthetic candidates.

**04.01.03 Fragments of Life™ (FOL) for Lead Identification and Optimization.** Doug Davies, Lance Stewart, Bjorn Mamat, Vincent Sandanayaka, Denise Connor, Rama Mishra, Brian Pease, Erik Hansen, Jennifer Winger, Thorkell Andresson, Jasbir Singh, David Zembower, Alex Burgin, Mark Gurney, deCODE biostructures, Bainbridge Island, WA 98110.

Small molecules of life carry natural born information content, and through co-evolution with proteins they are likely to have high ligand efficiency for protein binding. Inspired by this concept, we have developed a novel Fragments of Life™ library for lead identification and optimization in conjunction with protein X-ray crystallography. The Fragments of Life™ library includes molecules of life, secondary metabolites, and hetero-functional derivatives thereof, each selected for pharmaceutic properties, water solubility, and potential for chemical elaboration to facilitate medicinal chemistry efforts. We have used the Fragments of Life™ technology to rapidly expand our understanding of the structure activity relationships for inhibitors of leukotriene A4 hydrolase (LTA4H). This allowed us to carry out chemotype switching experiments in two synthetic cycles, converting a ~350 uM potent fragment to a ~10 nM potent back-up compound to a clinical candidate, as measured in human whole blood cell assays.

**04.01.04 The Benefits of Protein Crystallography to Monsanto's Ag Biotech R&D.** T.J. Rydel, Monsanto Company, Chesterfield, MO.

Monsanto is a global agricultural company dedicated to providing innovative products to farmers and growers in the areas of seeds, genomics, and agricultural productivity. Monsanto's seeds and genomic traits focus on large acre crops, such as corn, cotton, soybeans, and canola, as well as small acre crops, such as vegetables. The seed-based genomic traits can provide benefits to farmers (i.e., insect resistance, herbicide tolerance), processors (i.e., improved animal feed & corn hybrids for ethanol), and consumers (i.e., healthier oils). Monsanto's non-seed agricultural productivity products include crop protection and animal ag offerings.

Protein crystallography has made noteworthy contributions to Monsanto's ag biotech R&D in four key areas: (a) delivering novel protein structures, (b) aiding protein design, (c) revealing key binding interactions, and (d) facilitating regulatory submissions. This talk will review specific Monsanto examples from these four impact categories.

**04.01.05 The Importance of Single Crystal Studies of Process Relevant Pharmaceutical Crystal Forms.** John DiMarco, Michael Galella, Raymond Scaringe, Carolyn Pommier, Jack Gougoutas, Solid State Chemistry, Bristol-Myers Squibb Pharmaceutical Research Inst., Route 206 & Province Line Rd, Princeton, NJ 08543.

Ideally, the active pharmaceutical ingredient (API) in a drug product should have a well characterized and relatively stable crystal structure. However, complications can arise for molecules that crystallize in several solvated and/or neat forms which may de-solvate/transform and/or interconvert during the manufacturing process. Single crystal studies of these forms define their structure/composition and moreover allow predictions/simulations of spectra (PXRD, Raman, etc.) which can be used to improve process control. Some recent examples will be presented, with emphasis on process relevant forms of dasatinib.

**04.01.06 From Images to Co-crystal Structures in a Single Automated Process.** J. Badger<sup>1</sup>, P. Collins<sup>1</sup>, R. Rosenfeld<sup>1</sup>, B. Smith<sup>1</sup>, R. Athay<sup>2</sup>, D.E. McRee<sup>1</sup>, <sup>1</sup>ActiveSight, 4045 Sorrento Valley Blvd., San Diego CA 92121, <sup>2</sup>Rigaku Americas Corporation, 491 S. Orem Blvd., Orem, UT 84058.

A major focus for protein crystallography in the commercial sector is the rapid determination of large numbers of protein:ligand structures for lead compound optimization. X-ray crystallography now also contributes directly to lead discovery through fragment screening methodologies and our experience with the ActiveSight fragment library ([http://www.active-sight.com/products\\_screening.htm](http://www.active-sight.com/products_screening.htm)) is that fragment-based screening projects typically requires the examination of 100-200 electron density maps.

To assist the protein crystallographer analyze these volumes of data we have recently extended our previous automated structure determination application (<http://mi.active-sight.com/MIAutoStructure.html>) to include image data processing and various options for ligand placement. Neither the image data processing step (d\*TREK v97 or MOSFLM) nor the structure determination steps (CCP4/MOLREP and CCP4/REFMAC5) managed by this application occupy more than a few minutes on a modern laptop computer. For this reason the structure solution GUIs and underlying Python script system are designed to conveniently support the processing of *multiple* related data sets within a single job and maintain convenient logs of the structure solution tasks. Amongst the outputs from this application is a session file for convenient loading of models and maps into the MIFit software. The MIFit program allows for the independent but simultaneous display of models and maps from multiple data sets.

We have used this software to analyze many hundreds of data sets across several fragment screening projects.

**04.01.07 The Value of Tertiary Structure in Intellectual Property.** Richard Bott, Kamrin MacKnight, Protein Science, Genencor a Danisco Div., 925 Page Mill Rd, Palo Alto, CA 94304.

Proteins useful as drug targets and/or other products can be highly valuable proprietary assets. Obtaining patent claims that cover sites within linear protein sequences is a common means of gaining protection for proteins. However, the practice of utilizing the entire three-dimensional structure of proteins to develop patent claims is a fairly new approach.

Indeed, for industrial enzymes, most patents include claims that are directed toward critical sites for mutagenesis. This has provided protection for variant enzymes with improved performance and other desirable characteristics. One example where this approach has been very successful is the subtilisin family of enzymes.

In contrast, in the approach described herein, the three-dimensional structure of an SGNH hydrolase was used in the development of patent claims. The structure of this enzyme deviates from all other

known SGNH hydrolases and provides an indication of useful changes for the production of enzyme variants with commercial benefits.

**04.01.08 Industrial Macromolecular Crystallography in the 21<sup>st</sup> Century: One Technique, Multiple Roles.** Giovanna Scapin, Depts. of Medicinal Chemistry Merck Research Laboratories, PO Box 2000, Rahway, NJ, 07065.

In the past few years macromolecular crystallography has become a standard technique used by many pharmaceutical and biotechnology companies. Thanks to the recent technological innovations such as high-throughput crystallization, high performance synchrotron beamlines, and new computational methods, structural data have become increasingly available. The large numbers of ligand-receptor structures produced within an industrial setting has allowed for structure-based information to expand from simple protein-ligand interaction analysis to include other aspects of the drug discovery process that used to be almost the exclusive property of biology and chemistry. Structural information that we provided have been used to support current stages of a program as well as to steer it into a new direction or to provide the basis for a timely go/no-go decision, which could be extremely valuable in today's drug market. Examples, including work done on the phosphatase PTP1b, the peptidase DPP-4 and the kinase p38, will be presented to elucidate the different roles that macromolecular crystallography can play today in the pharmaceutical industry.

## 05.01 Non-Ambient Crystallography

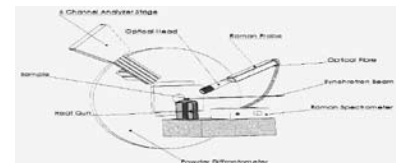
**05.01.01 *In-situ* Diffraction Study of the High Temperature Behavior of Ni-Al-Pt-Hf Alloys.** Sumer Singh, Linn W. Hobbs, Scott A. Speakman, Anthony Garratt-Reed, Liza Plotnikov, Bruce A. Pint.

Cast alloys of (Ni,Pt)-Al were made with Al content between 32.5 to 37.5 at.%, Pt content between 0 to 5 at.%, and Hf doping from 0.05 to 0.4 at.%. As cast, these alloys contained a mixture of  $\beta$ -NiAl and  $\gamma$ -Ni<sub>3</sub>Al. Near 1150°C, the two-phase alloy system transformed into a single  $\beta$ -NiAl phase. The volume change associated with this phase transformation may be a factor in the observed macroscopic deformation which ultimately leads to failure in coatings made with this material.

*In-situ* X-ray diffraction was used to study the phase transformations in these alloys. For some samples, the initial *in-situ* XRD yielded fruitful results; yet for other samples the quantitative analysis of HTXRD data was not self-consistent. Subsequent research attempted to identify and isolate the effects of large grains and texture by comparing the results of *in-situ* data collected with point detectors, linear position sensitive detectors, and 2-dimensional area detectors. Large grain size, particularly when the samples partially recrystallized at higher temperatures, often compromised the ability to execute accurate quantitative analysis. Extensive *in-situ* XRD, particularly that collected with a 2-dimensional area detector, allowed much of the phase transformation to be more accurately monitored and correlated to mechanical and microscopic data for the Ni-Al alloy system. The effect of Pt alloying and Hf doping on the phase transformation was also better able to be quantified.

**05.01.02 *In situ* Simultaneous Raman and High-Resolution X-ray Powder Diffraction X-ray Powder Diffraction Study of Transformations Occurring in Materials at Non-Ambient Conditions.** D. Viterbo<sup>a</sup>, E. Boccaleri<sup>a</sup>, M. Milanesio<sup>a</sup>, F. Carniato<sup>a</sup>, G. Croce<sup>a</sup>, W. van Beek<sup>b</sup>, H. Emerich<sup>b</sup>, <sup>a</sup>DISTA, Univ. del Piemonte Orientale, Alessandria, Italy, <sup>b</sup>Swiss-Norwegian Beamlines, ESRF, Grenoble Cedex, France.

Materials containing disordered moieties and/or amorphous or liquid-like phases or showing surface- or defect-related phenomena constitute a



problem for their characterization using X-ray powder diffraction (XRPD), and Raman spectroscopy can provide useful complementary information. We have designed and realized a novel experimental set-up for simultaneous *in situ* Raman/<High-resolution XRPD> experiments, to take full advantage of the complementarities of the two techniques in investigating solid-state transformations at non-ambient conditions. The invaluable added value of the proposed experiment is the perfect synchronization of the two probes with the reaction coordinate and the elimination of possible bias caused by different sample holders and conditioning modes used in “*in situ* but separate” approaches. The set-up was developed by the Swiss-Norwegian Beamline at the European Synchrotron Radiation Facility in Grenoble and tested on three solid-state transformations: *i*) the kinetics of the solid-state synthesis of the charge-transfer complex fluorene:TCNQ, *ii*) the thermal swelling of stearate-hydroxalcite nanocomposites, *iii*) the photoinduced 2+2 cyclization of (E)-furylideneoxindole. The reported experiments demonstrated that, even though the simultaneous Raman/XRPD experiment is more challenging than the separated ones, high-resolution XRPD and Raman data could be collected. A gas blower allows studies from RT to 700K and 100K can be reached using a nitrogen cryostream. The experimental setup flexibility allows the addition of ancillary devices, such as the UV-lamp used to study photoreactivity.

**05.01.03 Photocrystallography and Application to the Phase Transitions Occurring in Magnetic Molecular Materials: Domain Formation and Electron Density Studies.** William Nicolazzi,<sup>a</sup> Claude Lecomte<sup>a</sup>, Sébastien Pillet<sup>a</sup>, <sup>a</sup>LCM3B, UMR CNRS 7036, Univ. Henri Poincaré, BP 239, 54506 Vandoeuvre les Nancy Cédex, France, [claudie.lecomte@lcm3b.uhp-nancy.fr](mailto:claudie.lecomte@lcm3b.uhp-nancy.fr)

It is well accepted that the characteristics of solid state spin transitions, abrupt, gradual, with or without hysteresis, are highly dependent on the cooperativity of the molecular lattice. Several comparative crystallographic studies have been performed in order to correlate the microscopic structural properties to the spin transition characteristics. It is well accepted that the thermally induced and light induced spin transition mechanisms have some similarities but exhibits also fundamental differences. It is for instance still controversial whether the light induced HS metastable, thermally quenched HS metastable and room temperature HS states can be considered as structurally identical. Detailed and accurate structural analyses as a function of temperature and light excitation are therefore highly relevant for a clear understanding of the spin transition phenomenon. We have undertaken such a complete study on the spin crossover material Fe(btr)<sub>2</sub>(NCS)<sub>2</sub>·H<sub>2</sub>O [1]. From high resolution x-ray diffraction measurements, we have analyzed the electron density redistribution related to the LS to HS transition: 3d orbital electron populations, electrostatic potential [2]. We have also shown that the thermally and light induced transitions occur through nucleation and growth of like spin domains and follow an Avrami model. In the case of

the light induced transition, a specific mechanism of light induced structural reorganization has been pointed out (domain coarsening) [3]. Several models have been proposed to describe the lattice local interaction: inter- and intra- molecular lattice vibration (Ising-like model...), elastic interaction and cooperative Jahn-Teller type of interaction; most of these have been frequently solved analytically in the mean field approximation and studied numerically at the thermodynamic equilibrium. However, the nucleation and growth of spin-like domains have been seldom considered. In this direction, we are developing new models of spin transitions and solving them by Monte Carlo simulations. During the presentation, the synergy between experimental x-ray diffraction measurements and simulations will illustrate all these aspects on the archetype of highly cooperative spin transitions system  $\text{Fe}(\text{btr})_2(\text{NCS})_2 \cdot \text{H}_2\text{O}$ .

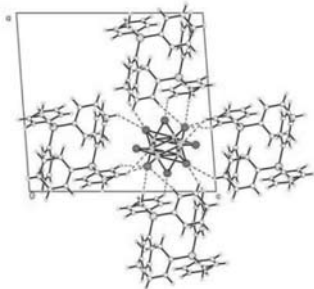
[1] S. Pillet, J. Hubsch and C. Lecomte, *Eur. Phys. J.*, 2004, **B 38**, 541.

[2] V. Legrand S. Pillet M. Souhassou, N. Lugan & C. Lecomte, *J. Am. Chem. Soc.*, (2006), **128**, 13931.

[3] S. Pillet, V. Legrand, M. Souhassou & C. Lecomte, *Phys. Rev. B*, (2006), **74**, 140101.

**05.01.04 Thermally Induced Disorder of Cu Ions in  $[(\text{C}_6\text{H}_5)_3\text{CH}_2\text{P}]\text{Cu}_3\text{Br}_4$ .** Roger D. Willett, Dept. of Chemistry, Washington State Univ., Pullman, WA 99164, Salim F. Haddad, Dept. of Chemistry, Univ. of Jordan, 11942 Amman, Jordan, Brendan Twamley, Univ. Research Office, Univ. of Idaho, Moscow, ID 88434.

The title compound crystallizes in the space group  $P2_1/n$  and undergoes a continuous order-disorder transition between 90 K and room temperature, retaining the  $P2_1/n$  space group throughout the temperature regime. The structure consists of stacks of the organic cations and  $(\text{Cu}_3\text{Br}_4)_n$  columns, held together by C-H...Br interactions. The stacks are stabilized by edge-facial interactions between phenyl groups. The bromide ions form an outer layer on the columns, with the copper ions occupying coordination sites within the interior of the columns. Multiple sites exist, with the occupancy of these varying as a function of temperature. In the low temperature regime, all three independent Cu atoms have trigonal planar  $\text{CuBr}_3$  coordination spheres. Cu-Br-Cu bridges, with acute angles, link the Cu ions together, forcing short Cu-Cu contacts of 2.6-3.0 Å. In addition, a short H-Cu1 contact exists (2.8 Å). As the temperature is increased, other sites begin to be occupied by Cu1, in order to eliminate the short H-Cu contact. This induces very short Cu-Cu contacts with the other Cu atoms which, in turn, cause the other Cu atoms to occupy multiple sites. In spite of this, the Br atoms do not undergo major reorganization.



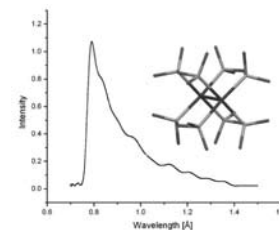
**05.01.05 Variable Temperature Neutron and X-ray Diffraction Studies of the  $\text{A}^{2+}\text{A}^{7+}\text{W}_3\text{O}_{12}$  Family.** Amy Gindhart, Cora Lind, Dept. of Chemistry, Univ. of Toledo, Toledo, OH 43606.

Negative thermal expansion (NTE) materials have been of interest because of the observed reduction in the overall expansion when they are incorporated into composites. Previous work in the  $\text{A}^{3+}\text{W}_3\text{O}_{12}$  system showed that the thermal expansion is dependent on the identity of the  $\text{A}^{3+}$  cation. Crystallization studies showed that this family undergoes a transition from a monoclinic to an orthorhombic phase upon heating. NTE has only been observed in the orthorhombic phase. The A site has also been substituted with a mixture of  $\text{Hf}^{4+}$  and  $\text{Mg}^{2+}$ .

The systems of interest in this paper involve previously unknown compounds in the  $\text{AA}'\text{W}_3\text{O}_{12}$  family ( $\text{A}=\text{Mg}^{2+}, \text{Zn}^{2+}$ ;  $\text{A}'=\text{Zr}^{4+}, \text{Hf}^{4+}$ ). Several possible pathways were explored for the preparation of these materials. The desired phases were obtained by high energy ball-milling and subsequent calcinations of the samples. Crystallization studies as a function of temperature were performed on the samples to establish what phases were preferentially formed. Variable temperature X-ray and neutron diffraction experiments were carried out on  $\text{AA}'\text{W}_3\text{O}_{12}$  to determine thermal expansion and phase transition behavior. Both monoclinic and orthorhombic phases were observed. The monoclinic phase could be fitted in  $P2_1/a$ , which is a known structure for  $\text{A}^{3+}\text{W}_3\text{O}_{12}$ . In contrast, the orthorhombic phase could not be fitted in  $\text{Pnca}$ , which is the common phase that displays NTE for  $\text{A}^{3+}\text{W}_3\text{O}_{12}$ . From indexing and systematic absences the space group  $\text{Pnma}$  was established as the highest possible symmetry. There were some inconsistencies between the X-ray and neutron diffraction data for  $\text{MgZrW}_3\text{O}_{12}$ , which were addressed by simultaneous Rietveld refinement of the X-ray and neutron data.

**05.01.06 Small Molecule Laue Diffraction for Time Resolved Experiments.** M. Gembicky, M. Pitak, M. Messerschmidt, P. Coppens, Dept. of Chemistry, SUNY Buffalo, NY, 14260, USA, S-I Adachi, Inst. of Materials Structure Science, KEK & ERATO, JST, 1-1 Oho, Tsukuba, Ibaraki 305-0801, Japan, S. Koshihara, FCRC & Dept. of Materials Science, Tokyo Inst. of Technology, 2-12-1 Oh-okayama, Meguro-ku., Tokyo 152-8551, Japan.

As a prerequisite of our study of transient species in confined environments, pink-beam Laue data on ground state structures were collected and analyzed. Experiments were performed at the NW14 beamline at PF-AR, KEK with accumulated exposure times of 1-5ns per CCD frame. Data were processed with the PRECOGNITION™ software, which derives a  $\lambda$ -curve by fitting to Chebyshev polynomials. Data refinement on  $\text{Cu}(\text{I})(\text{dmp})_2$  tosylate,  $n$ -butyl[Pt<sub>2</sub>(pop)<sub>4</sub>], tris(bis-trifluoromethyl Cu(I)pyrazolate) and dihydroxybenzophenone/diazacrownether led to  $R_F$ -factors of 5-6%, which is slightly better than agreements achieved in earlier work.<sup>2</sup> For the first two cases parallel stroboscopic pump-probe experiments were performed using pulsed 355 and 400 nm laser irradiation. With the Laue technique response ratios, defined as fractional changes in the observed intensities on irradiation, can be evaluated from the raw spot intensities and from the integrated intensities after scaling. The two sets of values will be compared and the choice of optimal analysis will be discussed.



Research funded by the US Department of Energy (DEFG02-02ER15372). This work was performed under the approval of the Photon Factory Program Advisory Committee (Proposal No. 2004S1-001).

1. Ren, Precognition™ (5.0), Renz Research, Inc. 2006

2. Helliwell et al. *J. App. Cryst.* (1989), 22, 483-497; Helliwell et al. *Acta Cryst.* (1989), B45, 591-596; Gomez de Anderez et al., *Acta Cryst.* (1989), B45, 482-488; Snell et al. *J. Synchrotron Rad.* (1995), 2, 22-26

## 05.02 Mineralogy and Crystallography Real Crystals, Extreme Conditions

**05.02.01 Crystallography of Earth Materials at Extreme Conditions from Experimental and Computational Studies.** G.A. Lager, Dept. of Geography & Geosciences, Univ. of Louisville, Louisville, KY 40292 USA.

Knowledge of the crystal structure of materials in the Earth's interior is fundamental to our understanding of surface processes and the development of models to interpret physical and chemical processes at depth. The range of possible structures that can exist in the interior is constrained by the density and composition of the Earth as well as by seismological models, which provide information on the variation of seismic wave velocities. The synergistic relationship between experimental and computational studies has been instrumental in identifying and characterizing many of these structures. This talk will explore the crystallography of earth materials at high  $P$ - $T$  as we descend from the crust to the core. In the crust and upper mantle, many of the phases of interest are complex silicates that contain significant amounts of structurally incorporated "water" in the form of  $H_2O$  and/or  $OH$ . In these cases, the behavior of hydrogen bonds at non-ambient conditions can dramatically affect both the properties and the stability of the structure. Examples include lawsonite, hydrous magnesium silicates, and layered structures, such as chlorite and the 10 Å-phase. Earth models are consistent with a lower mantle composed primarily of silicate perovskite, and the recently discovered post-perovskite phase, which has the  $CaIrO_3$ -type structure. The latter, which is a layered structure even at these extreme pressures, may be responsible for the seismic discontinuity at the top of the D'' layer (mantle/core boundary). Another possible phase in the lower mantle is Fe-bearing periclase (magnesiowüstite), which undergoes a high-spin to low-spin ( $Fe^{2+}$ ) transition at high pressure. The stable phase under the conditions of the inner core is most likely hexagonal closest-packed Fe.

**05.02.02 Hydration-Dehydration Reactions under Extreme Conditions: Experimental Methods and Results.** R.C. Peterson, Dept. of Geological Sciences and Geological Engineering, Queen's Univ., Kingston, Ontario, Canada, K7L 3N6.

Some materials change hydration state with changes in temperature and relative humidity. These changes may be very rapid or quite sluggish. These transformations may or may not be reversible. Often the transformations are limited by diffusion of water vapour through the solid. Crystallographic study of these reactions may be effectively investigated using modern powder diffractometry techniques and experimental apparatus that control the temperature and relative humidity. In nature, metal sulfates such as melanterite ( $FeSO_4 \cdot 7H_2O$ ) and epsomite ( $MgSO_4 \cdot 7H_2O$ ) commonly form from solution and then subsequently dehydrate to lower hydration states as the system dries. Understanding these processes is important in deciphering the role of minerals in the environmental impact of mine waste as these phases attenuate and then release metals as they crystallize, dehydrate, or dissolve throughout the seasons of the year.

Metal sulfates are thought to exist on the surface of Mars. This is based on the chemical analysis by the MER rovers on trenches made by tracks in the Martian regolith. As a result of these discoveries there is a renewed interest in the relative stabilities of these phases, under the extreme conditions of the Martian surface. Experimental results using in-situ X-ray diffraction at controlled temperature and relative humidity will be discussed. The design and application of various apparatus to study these reactions will be highlighted.

**05.02.03 High Energy X-ray Diffraction Studies of Str II and Str H Noble Gas Clathrate Hydrates.** Chris Tulk,<sup>1</sup> Dennis D. Klug,<sup>2</sup> Bryan C. Chakoumakos,<sup>1</sup> Lars Ehm<sup>3</sup>, John B. Parise<sup>3</sup>, <sup>1</sup>Oak Ridge National Laboratory, <sup>2</sup>National Research Council Canada, <sup>3</sup>Stony Brook Univ.

At low pressure, water and noble gases such as Kr can form structure II clathrate hydrate, while larger Xe atoms form structure I clathrate hydrate. Upon applying pressure in the 10-20 kbar range, these structures transform into much higher density crystalline form whose large cages are likely multiply occupied, and where the overall structure is known to be hexagonal. Furthermore, disorder of the guest atoms within these cages is not well understood. High energy x-ray data (0.137 angstroms) has been collected over a wide momentum transfer range and this data has been used to determine the radial distribution functions (rdf) of both forms. These rdf functions show correlations between atoms over the local and intermediate radial distance from 0 to 20 angstroms. It is clear that some intercage guest - guest correlations are evident, but only for the small cages where the location of the guest atom is more spatially confined. The intercage guest-guest correlations for the large cages are diffuse, or even absent, from the rdf data. Current structural models do not exhibit this behavior and show clear evidence for the large intercage guest guest correlations. The same scattering data was used to perform rietveld refinements using the best models currently available and to subsequently produce Fourier difference maps. The density maps clearly indicate the complicated spatial extent of guest atom disorder within the cages. For example, the Kr atom in the structure II large cage shows a 'shell' of density with roughly tetrahedral geometry, with no evidence of any density at the cage center, as is often modeled. These new locations for the guest atoms were then used to further refine the overall structural model.

**05.02.04 The Geometric Effects of  $^{56}Fe^{2+}$  for  $^{56}Mg$  Substitution on the Crystal Structures of the Grandidierite-Ominelite Series.** L.A. Groat, T.J. Dzikowski, Dept. of Earth and Ocean Sciences, Univ. of British Columbia, Vancouver, BC V6T 1Z4, Canada, E.S. Grew, Dept. of Geological Sciences, Univ. of Maine, Orono, ME 04469-5790, USA.

The electron microprobe compositions and crystal structure of seven members of the grandidierite-ominelite ( $MgAl_3BSiO_9 - Fe^{2+}Al_3BSiO_9$ ) series with  $X = (Fe^{2+} + Mn + Zn)/(Fe^{2+} + Mn + Zn + Mg)$  ranging from 0.00 to 0.52 were studied to determine the geometric effects of Fe substitution for Mg on the crystal structures. Calculating  $Fe^{3+}$  from the electron microprobe analyses gave 0.04-0.06  $Fe^{3+}$  apfu, but such small amounts at the Al sites could not be detected in the refinements. Regression equations derived from single-crystal X-ray diffraction data show that  $b$  increases by 0.18 from  $X = 0$ -1. The crystal structure refinements show that the most significant changes involve the  $(Mg, Fe^{2+})O_5$  polyhedron, which increases in volume by  $0.36 \text{ \AA}^3$  (5.0%), largely as a result of expansion of the  $MgFe-O5$ ,  $-O2$ , and  $-O6$  ( $\times 2$ ) bond distances, which increase by 0.09 (4.4%), 0.06, and 0.04 Å, respectively. Other significant changes include increasing  $O1-MgFe-O2$  ( $3.44^\circ$ ) and  $-Al3-O5a$  angles ( $1.9^\circ$ ) and a decreasing  $O6-MgFe-O6b$  ( $-2.20^\circ$ ) angle. Significant increases are also seen in the lengths of the  $O1-O2$  (0.13 Å) and  $O6-O5a$  ( $\times 2$ ) (0.09 Å) edges. The  $SiO_4$  tetrahedra appear to respond to changes in the surrounding polyhedra by changing  $O-Si-O$  angles such that the tetrahedral angle variance and mean tetrahedral quadratic elongation increase with  $X$ . The  $BO_3$  triangles appear to behave as relatively invariant units in the crystal structure. Regression equations obtained from the  $MgFe-O$  bond distances were used to determine a radius for  $^{56}Fe^{2+}$  of 0.70 Å.

**05.02.05 High-P/T Neutron and Synchrotron X-ray Diffraction Study of Ni(OD)<sub>2</sub>.** H. Xu, Y. Zhao, J. Zhang, Y. Wang, D.D. Hickmott, L.L. Daemen, M.A. Hartl, Los Alamos National Laboratory, Los Alamos, NM 87545.

Nickel hydroxide is of considerable interest due to its use as a cathode material in Ni-based alkaline secondary cells. As a member of the CdI<sub>2</sub>-type, layered hydroxide family M(OH)<sub>2</sub> (M = Mg, Ca, Ni, Co, etc.), this compound is also interesting from the crystal-chemical viewpoint, since it provides a model structure for studying hydrogen-mediated interatomic interactions. In this study, using time-of-flight neutron and energy-dispersive synchrotron X-ray diffraction, we have examined the structure and stability of deuterated Ni(OD)<sub>2</sub> at pressures up to 8 GPa and temperatures up to 623 K. Rietveld analysis of the data allowed determination of its elastic properties such as coefficients of thermal expansion and bulk moduli. Moreover, the atomic positions and displacement parameters, particularly of D, have been obtained, and the role of D-related interactions in the mechanisms of Ni(OD)<sub>2</sub> compression and thermal expansion are discussed.

**05.02.06 Synthesis and Crystal-structure Refinement of Ba<sub>4</sub>Nb<sub>2</sub>O<sub>9</sub>.** J. Bezjak, B. Jančar, D. Suvorov, Advanced Materials Dept. K - 9, Jozef Stefan Inst., Jamova 39, SI-1000 Ljubljana, Slovenia.

An investigation of the hexagonal perovskites within the BaO-WO<sub>3</sub>-Nb<sub>2</sub>O<sub>5</sub> system revealed similarities in the X-ray diffraction spectra between the ternary compound Ba<sub>6</sub>WNb<sub>2</sub>O<sub>14</sub> and the binary compound Ba<sub>4</sub>Nb<sub>2</sub>O<sub>9</sub>. Furthermore, preliminary investigations indicate the existence of a broad compositional region where hexagonal perovskite-related structures form. In order to understand the crystal chemistry governing the formation of hexagonal perovskites in the BaO-WO<sub>3</sub>-Nb<sub>2</sub>O<sub>5</sub> system we first looked at the binary compound Ba<sub>4</sub>Nb<sub>2</sub>O<sub>9</sub>. We applied a conventional solid-state reaction for the synthesis and carried out investigations with X-ray diffraction combined with transmission and scanning electron microscopy. X-ray diffraction revealed at least three phase transitions below 1400°C. This observation is, however, in disagreement with previously reported results. Therefore, the aim of the present work was to precisely establish the sequence of structural phase transitions and refine the crystal structure of Ba<sub>4</sub>Nb<sub>2</sub>O<sub>9</sub>.

**05.02.07 The Crystal Chemistry of Bi<sub>6</sub>TP<sub>2</sub>O<sub>15+x</sub>, T = Fe, Ni, Zn. Isomorphism and Polymorphism, Structural Relationship to Bi<sub>6</sub>TiP<sub>2</sub>O<sub>16</sub>.** N. Arumugam, V. Lynch, H. Steinfink. Texas Materials Inst., Univ. of Texas, 1 Univ. Sta, C0400, Austin, TX 78712.

The crystal structures of compounds with nominal compositions Bi<sub>6</sub>FeP<sub>2</sub>O<sub>15+x</sub> (I), Bi<sub>6</sub>NiP<sub>2</sub>O<sub>15+x</sub> (II) and Bi<sub>6</sub>ZnP<sub>2</sub>O<sub>15+x</sub> (III) were determined from single-crystal X-ray diffraction data. They are monoclinic, space group *I*2, *Z* = 2. The lattice parameters for (I) are *a* = 11.2644(7) Å, *b* = 5.4380(3) Å, *c* = 11.1440(5) Å, β = 96.154(4)°; for (II) *a* = 11.259(7) Å, *b* = 5.461(4) Å, *c* = 11.109(7) Å, β = 96.65(1)°; for (III) *a* = 19.7271(5) Å, *b* = 5.4376(2) Å, *c* = 16.9730(6) Å, β = 131.932(1)°. Least squares refinements on *F*<sup>2</sup> converged for (I) to *R*1 = 0.0554, *wR*2 = 0.1408; for (II) *R*1 = 0.0647, *wR*2 = 0.1697; for (III) *R*1 = 0.0385, *wR*2 = 0.1023. The crystals are complexly twinned by 2-fold rotation about [1 0 -1], by inversion and by mirror reflection. The structures consist of edge-sharing articulations of OBi<sub>4</sub> tetrahedra forming layers in the *a* - *c* plane that then continue by edge-sharing parallel to the *b* axis. The three-dimensional networks are bridged by Fe and Ni octahedra in (I) and (II) and by Zn trigonal bipyramids in (III) as well as by oxygen atoms of the PO<sub>4</sub> moieties. Bi also randomly occupies the octahedral sites. Oxygen vacancies exist in the structures of the three compounds due to required charge

balances and they occur in the octahedral coordination polyhedron of the transition metal. In compound (III) no positional disorder in atomic sites is present. The Bi - O coordination polyhedra are trigonal prisms with one, two or three faces capped. Magnetic susceptibility data for compound (I) were obtained between 4.2 - 350 K. Between 4.2 - 250 K it is paramagnetic, μ<sub>eff</sub> = 6.1 μ<sub>B</sub>; a magnetic transition occurs above 250 K.

## 06.01 Neutron Macromolecular Crystallography

**06.01.01 Neutron Structure of DFPase: Insights into the Phosphotriesterase Mechanism.** Marc-Michael Blum, Benno Schoenborn, Paul Langan, Julian C.-H. Chen, Inst. of Biophysical Chemistry, J.W. Goethe Univ. Frankfurt, Frankfurt, Germany.

Diisopropyl fluorophosphatase (DFPase) is capable of degrading a wide range of toxic organophosphorus compounds, such as Sarin, Soman, Cyclosarin, and Tabun. As such, it is a prime candidate for the enzymatic decontamination of existing nerve agent stocks. The mechanism of DFPase has been clarified through a number of recent structural and enzymological studies. To better understand the mechanism of DFPase, we have collected neutron diffraction data from the spallation source at Los Alamos, and have determined its structure at 2.2 Å resolution. Implications for the mechanism of this and related proteins such as regucalcin and paraoxonase, are discussed.

**06.01.02 Joint X-ray and Neutron Study of Aldose Reductase: Observation of Enzymatic Proton Networks.** Pavel V. Afonine\*, Mathew Blakeley, Federico Ruiz, Raul Cachau, Isabelle Hazemann, Flora Meilleur, Andre Mitschler, Steve Ginell, Oscar Ventura, Alexandra Cousido, Michael Haertlein, Andrzej Joachimiak, Dean Myles, Paul D. Adams, Alberto Podjamy, \*Physical Biosciences Div., Lawrence Berkeley National Laboratory, Berkeley, CA.

We present the first study of an enzyme, human Aldose Reductase (AR), combining neutron scattering data (perdeuterated sample, 0.15 mm<sup>3</sup>, 2.2 Å resolution), ultra-cold X-ray scattering data at sub-angstrom resolution (0.82 Å), room temperature (RT) X-Ray data at 1.8 Å and quantum mechanical modeling. The RT structure was refined using jointly the X-Ray and neutron data. Analysis of the observed electron density and neutron scattering density maps with those obtained quantum-mechanically allows their detailed interpretation in the context of the enzymatic mechanism. The combined power of the techniques employed results in a view of the enzyme structure with high level of details revealing the internal organization of the hydrogen bond network that define the properties of the enzyme catalytic engine. Extended proton wires are observed, tightly coupling multiple sites, revealing the structural motifs underpinning the enzymatic mechanism. The very detailed experimental maps obtained, reveal the nature of the proton mobility along an extended proton pathway, providing the structural evidence to support a new catalytic mechanism, in which the proton transfer follows hydride donation as a nearly barrierless process, as it has been previously suggested. This demonstrates the combined power of ultra-high resolution X-ray diffraction and neutron scattering to be higher than either one of them separately, highlighting the importance of neutron scattering for this type of studies. The joint X-ray and neutron structure refinement and completion were performed using the new general purpose crystallographic software package PHENIX [1], with neutron specific tools developed by the Macromolecular Neutron Crystallography (MNC) consortium [2].

[1] PHENIX: building new software for automated crystallographic structure determination. P. D. Adams, R. W. Grosse-Kunstleve, L.-W. Hung, T. R. Ioerger,

A. J. McCoy, N. W. Moriarty, R. J. Read, J. C. Sacchettini, N. K. Sauter and T. C. Terwilliger. *Acta Cryst.* (2002). D58, 1948-1954; (<http://phenix-online.org/>)  
[2] MNC is an NIH-NIGMS funded consortium (1R01GM071939) between Los Alamos National Laboratory and Lawrence Berkeley National Laboratory.

**06.01.03 Structural Studies of the Short Hydrogen Bonds in Photoactive Yellow Protein (PYP).** Fisher, S.Z., Anderson, S., Henning, R., Moffat, K., Thiagarajan, P., Langan, P., Schultz, A., BioScience Div., Los Alamos National Lab, Los Alamos, NM.

Photoactive yellow protein (PYP) from *Halorhodospira halophila* is a cytosolic 14 kDa blue-light photoreceptor that belongs to the PAS-domain superfamily. PYP absorbs blue light via its para-coumaric acid chromophore (pCA), covalently attached to Cys69, and has been implicated in the negative phototactic response to blue light of *Halorhodospira halophila*. Photoactivated PYP undergoes a reversible photocycle, with the transduction of photon energy causing a functional structural change in the pCA binding region. Numerous high-resolution X-ray crystal structures of PYP in the ground state revealed that pCA is stabilized by two unusually short hydrogen bonds to the protein. The phenolate oxygen of pCA is hydrogen bonded to Tyr42 and Glu46 with distances of 2.49 and 2.58 Å, respectively. Site-directed mutagenesis and structure determination of E46Q PYP showed that the length of the hydrogen bond to residue 46 increased to ~2.9 Å and was observed to cause changes in the photocycle. Thus, the length and strength of these hydrogen bonds to pCA are important for the normal functioning of PYP. In order to fully characterize the short, strong hydrogen bonds in PYP, we are carrying out neutron crystallographic studies on the PCS at Los Alamos National Laboratory. We shall present the joint X-ray and neutron structure of PYP and discuss insights into whether these bonds are high barrier vs. low barrier hydrogen bonds and the implications of our results for understanding the functional mechanism of PYP.

**06.01.04 A Neutron Crystallographic Analysis of a Cubic Insulin at pD 6.6 and Ribonuclease A.** N. Niimura, Dept. of Applied Beam Science, Graduate School of Ibaraki Univ., Naka-Narusawa, 4-12-1, Hitachi, Ibaraki, 316-8511, Japan.

A neutron diffraction study has been recently carried out 1) at 2.7Å resolution on cubic porcine insulin at pD 6.6 (Cubic insulin) and 2) at 1.5 Å on ribonuclease A (RNase A) using the BIX-4 single crystal diffractometer at the JRR-3 reactor of the JAEA by our group.<sup>1,2)</sup>

Cubic insulin: The ionization states of several amino acids in porcine insulin have been obtained at pD 6.6. A large single crystal of 2.7 mm<sup>3</sup> (= 2.0 x 1.7 x 0.8 mm) was obtained by dialysis. The structure refinement was carried out using the program CNS. The resulting R-factor is 21.3% and the free R is 29.3% at a resolution of 2.7Å. Protonation and deprotonation of various ionizable amino acid residues were observed and discussed on the basis of the charged states estimated by the pK<sub>a</sub> values of the amino acid residues. In the case of HisB5 and HisB10, both Nπ and Nτ of an imidazole ring are protonated at pD 6.6.

RNase A: High resolution neutron diffraction experiment of bovine pancreatic ribonuclease has been carried out not only to understand the details of the catalytic mechanism and but also to integrate the fine knowledge of structural chemistry in biology. A large single crystal of 6.0 mm<sup>3</sup> (= 3.0 x 2.0 x 1.0 mm) was obtained. 15,039 unique reflections were collected. The structure refinement is under way.

<sup>1)</sup> T.Ishikawa et al: To be submitted. <sup>2)</sup> D.Yagi et al: To be submitted

**06.01.05 X-ray and Neutron Structure of Low pH, Polyamine-free, Z-DNA.** Marat Mustyakimov<sup>a</sup>, Sean Seaver<sup>b</sup>, Leif Hanson<sup>b</sup>, Paul Langan<sup>a,c</sup>, Leighton Coates<sup>a</sup>, <sup>a</sup>Bioscience Div., Los Alamos National Laboratory, Los Alamos NM 87545, <sup>b</sup>Arts and Sciences Instrumentation Center, Univ. of Toledo, Toledo OH 53606, <sup>c</sup>Chemistry Dept., Univ. of Toledo, Toledo, OH 53606.

In X-ray crystallographic studies of DNA hydration, water in the protein-binding major groove of the Z-form is obscured by the presence of crystallizing agents such as polyamines. We have crystallized the oligonucleotide d(CGCGCG) in the Z-form at low pH without the presence of polyamines.<sup>[1]</sup> X-ray and neutron data were collected at room temperature using the ASI center at Toledo University and the PCS<sup>[2]</sup> at Los Alamos National Laboratory (1.5 Å resolution; P2<sub>1</sub>2<sub>1</sub>2<sub>1</sub>; a=17.95Å, b=30.87Å, c=44.74Å). A joint X-ray and neutron (X-N) structure was refined using new software, referred to here as nCNS, developed by the Macromolecular Neutron Crystallography (MNC) consortium.<sup>[3]</sup> nCNS is a patch for the structure solution program Crystallography & NMR System (CNS).<sup>[4]</sup> By combining global X-ray, neutron and energy refinement with cross-validated maximum likelihood simulated annealing refinement, nCNS provides a more accurate structure than either X-ray or neutron refinement on its own. In particular we found water molecules much easier to locate and orient using joint X-N maps. The structure reveals, for the first time, an extended network of ordered water molecules in the major groove of the Z-DNA double helix. The significance of these results to our understanding of the factors that determine DNA structure will be discussed.

[1] Langan et al. *Acta Cryst.* F62, 2006, 62, 453-456

[2] The PCS is funded by the Office of Science and the Office of Biological and Environmental Research of the US Department of Energy

[3] MNC is an NIH-NIGMS funded consortium (1R01GM071939-01) between Los Alamos National Laboratory and Lawrence Berkeley National Laboratory.

[4] Brunger et al. *Acta Cryst.* D54, 1998, 905-921.

**06.01.06 The Enzymatic Mechanism of Xylose Isomerase Revealed by Neutron Protein Crystallography.** Flora Meilleur<sup>1,2</sup>, Zhong Ren<sup>3</sup>, Edward H. Snell<sup>4</sup>, Mark J. van der Woerd<sup>5</sup>, Russell A Judge<sup>6</sup>, Dean A. A. Myles<sup>2</sup>, <sup>1</sup>North Carolina State Univ., Raleigh, NC 27695, <sup>2</sup>Oak Ridge National Laboratory, Oak Ridge, TN 37831, <sup>3</sup>Renz Research, PO Box 605, Westmont, IL 60559, <sup>4</sup>Hauptman-Woodward Inst., Buffalo, NY 14203, <sup>5</sup>Colorado State Univ., Fort Collins, CO 80523, <sup>6</sup>Abbott Laboratories, Abbott Park, IL 60064.

D-xylose isomerase catalyses the first reaction in the catabolism of D-xylose and is also able to convert D-glucose to D-fructose. Linearization and isomerization of the substrate rely upon a complex hydrogen transfer. The available X-ray and biochemical data do not allow a full understanding of the enzymatic mechanism involved in this hydrogen transfer. In particular, the role of the catalytic metal ion remains unclear and the protonation state of catalytic residues remain unknown.

We collected neutron crystallographic data on a substrate-free D-xylose isomerase crystal using the LADI instrument at the Institut Laue Langevin with the objective to provide further insight into the enzymatic mechanism. The neutron structure shows unambiguously that the active site residue His-53 is doubly protonated (Meilleur et al. (2006) EBJ 35:601-609). This is the first report of direct observation of double protonation of His 53 and the first validation of the ring opening mechanism at the active site of D-xylose isomerase. Subsequently, we have collected LADI data sets at 2.2 Å on substrate bound and inhibitor bound enzyme crystals. Data were processed with the new program Precognition (Renz Research, Inc), adapted to process quasi-Laue neutron data.

We will present the three neutron structures and show how

neutron crystallography has provided complementary and unique information to further characterize the enzymatic mechanism of D-xlose isomerase.

### 06.01.07 Joint Refinement of Neutron and Room Temperature X-ray Diffraction Data from Endothiapepsin.

Leighton Coates<sup>1</sup>, Paul Langan<sup>2</sup>, Jon Cooper<sup>3</sup>, <sup>1</sup>Spallation Neutron Source, Oak Ridge National Laboratory, Oak Ridge, TN, 37831, USA, <sup>2</sup> Bioscience Div., Los Alamos National Laboratory, Los Alamos, NM, 87544, USA, <sup>3</sup>Div. of Biochemistry and Molecular Biology, School of Biological Sciences, Univ. of Southampton, Bassett Crescent East, Southampton, SO16 7PX, England.

The neutron diffraction structure of endothiapepsin co-complexed with a transition state analogue inhibitor (H261) was published in 2001. With the data being collected on the LADI instrument at the Institut Laue Langevin. This data set has been used in the testing and development of neutron enabled CNS[2]. Improvements in refinement residuals and map quality and their origins will be discussed.

Due to the large number of atoms modeled in the refinement of a protein neutron diffraction structure great care has to be taken to ensure that the data to parameter is maintained at a sensible level. Room temperature X-ray data is used to locate and refine the positions of Carbon, Nitrogen and Oxygen atoms. With the neutron diffraction data being the main driver for the location of deuterium atoms within the structure. Neutron and X-ray maps produced from a joint refinement are complementary giving information on the location of most of the atoms within the protein structure. Several neutron diffraction structures collected at the Protein Crystallography Station in Los Alamos [3] are being used in testing the joint X-ray neutron refinement.

[1] Coates *et al* 2001 *Biochemistry* (2001) **40** 13149-13157.

[2] MNC is an NIH-NIGMS funded consortium (IR01GM071939-01) between Los Alamos National Laboratory and Lawrence Berkeley National Laboratory.

[3] The PCS is funded by the Office of Science and the Office of Biological and Environmental Research of the US Department of Energy.

## 07.01 SDPD (Structure Determination from Powder Diffraction): Getting Better and Better

### 07.01.01 EXPO2007: A Tool for Crystal Structure Solution and Refinement from Powder Data.

C. Giacovazzo<sup>1</sup>, A. Altomare<sup>1</sup>, R. Caliandro<sup>1</sup>, M. Camalli<sup>2</sup>, C. Cuocci<sup>1</sup>, A.G.G. Moliterni<sup>1</sup>, R. Rizzi<sup>1</sup>, <sup>1</sup>CNR-Istituto di Cristallografia, Via Amendola 122/O, 70126 Bari, Italy, <sup>2</sup>CNR-Istituto di Cristallografia, Area della Ricerca di Roma 1, 00016 Monterotondo Stazione (Roma), Italy.

In EXPO2007 all the traditional steps for the *ab-initio* crystal structure solution from powder data are automatically carried out: indexing, space group determination, decomposition of the pattern for extracting the observed structure factor moduli, structure solution by Direct Methods or Patterson techniques, model refinement by non-Rietveld and Rietveld procedures.

Special emphasis will be given to:

a) a new technique for the automatic determination of the extinction symbol. It is based on a statistical analysis of the integrated reflection intensities and on the automatic inspection of the intensities eventually violating the candidate extinction symbol.

b) an efficient least squares procedure for improving the structural

model, which uses integrated intensities of the reflections and proper weights to take into account the peak overlapping.

c) the procedure POLPO. It is particularly useful for inorganic or metallorganic compounds. The heavy atoms are located by Direct or Patterson methods. The crystal structure completion is performed by application of Montecarlo techniques which exploits some low level available information on molecular geometry (e.g., cation coordination, cation-anion distances, etc.).

d) The procedure REDI, particularly useful for organic structures. It combines Direct and Montecarlo techniques: the peaks in the electron density map provided by Direct Methods are used as pivots for the structural search. All the user interventions are made easy by a powerful graphic.

### 07.01.02 Structure Solution from Powder Diffraction Data – Tackling the Bottlenecks.

K. Shankland, W.I.F. David, ISIS Facility, Rutherford Appleton Laboratory, Chilton, OX110QX, U.K.

The use of global optimisation methods has increased the size and complexity of molecular organic structures that can now be solved directly from powder diffraction data. However, these methods require many repeat runs to be performed in order to confirm the location of the global minimum in parameter space. This is particularly true of very complex structures, where success rates in locating the minimum may fall to only a few percent. Fortunately, these multiple runs can be performed independently of each other and as such, they are ideally suited to the notion of grid-type computing. We have recently adapted the DASH structure determination package to run under the United Devices GRIDMP system, which is widely used in pharmaceutical industry, mainly in the context of virtual screening. The current setup allows over one hundred DASH runs to be executed in parallel on existing desktop computing resources. The first half of this presentation will focus on results obtained using the DASH and HMC structure determination programs running under GRIDMP. These show not only impressive performance gains but also indicate that new computational routes that were previously closed to us due to their compute-intensive requirements are now open. The second half of the talk will focus on the solution of inorganic structures from powder diffraction data. While these structures are usually much smaller in terms of atoms within the asymmetric unit than their molecular counterparts, the problem associated with multiple topological possibilities is a major bottleneck in the determination of the correct crystal structure. These issues will be discussed within the context of the massive parallelisation available with grid-type computing.

### 07.01.03 Solving Structures from Powder Data Using Density Building Functions and Histogram Matching.

Chris Gilmore<sup>1</sup>, Douglas Dorset<sup>2</sup>, <sup>1</sup>WESTCHEM, Dept. of Chemistry, Univ. of Glasgow, Glasgow G128QQ, UK, <sup>2</sup>Advanced Characterization, ExxonMobil Research & Engineering Co., Annandale, NJ 08801 USA.

Recently we have applied techniques that use density building functions and density histogram matching methods coupled with entropy maximisation and likelihood analysis to solve a number of structures *ab initio* using electron diffraction data in 2- and 3-dimensions. The same methodology can be used with powder diffraction:

A low resolution structure is generated using non-overlapped low resolution structure factors combined with the origin defining rules of direct methods [1].

New reflections are given permuted phase angles (and intensities if

overlapped) and analysed using density building functions [2].

The optimal phase sets are subjected to entropy maximisation [3].

Likelihood and density histograms are used to select the optimal phase set.

Applications to a number of varied inorganic systems will be presented.

[1] Rogers, D. (1980) *Theory and Practice of Direct Methods in Crystallography* edited by M.F.C. Ladd & R.A. Palmer pp. 23-92. New York: Plenum Press.

[2] Gilmore, C.J., Bricogne, G & Bannister, C. (1990). *Acta Cryst.* A46, 297-308.

[3] Bricogne, G & Gilmore, C.J. (1990). *Acta Cryst.* A46, 284-297.

**07.01.04 Aromatic Carboxylates. Trimellitates.** James A. Kaduk, INEOS Technologies, P.O. Box 3011 MC F-9, Naperville IL 60563 USA.

Trimellitic acid (1,2,4-benzenetricarboxylic acid,  $\text{H}_3\text{C}_9\text{H}_3\text{O}_6$ ) is of interest as a ligand in the preparation of nanoporous metal organic frameworks (MOFs). It is also an impurity in the commercial synthesis of terephthalic acid and other aromatic acids. The crystal structures of several new trimellitates have been determined using powder diffraction data, and the bonding has been examined using quantum chemical calculations.  $(\text{NH}_4)_2\text{HC}_9\text{H}_3\text{O}_6$  was prepared by recrystallizing the hygroscopic solid obtained by the reaction of ammonia vapor and trimellitic acid from water. It crystallizes in  $P2_1/a$ , with  $a = 13.8644(10)$ ,  $b = 20.0654(12)$ ,  $c = 3.7344(2)$  Å,  $\beta = 96.947(6)^\circ$ ,  $V = 1031.27(12)$  Å<sup>3</sup>,  $Z = 4$ , and  $\rho = 1.573$  g/mL. There is a very strong intramolecular hydrogen bond between the 1- and 2-carboxyl groups, and an extensive network of intermolecular hydrogen bonds.

The new compound  $\text{Ca}(\text{HC}_9\text{H}_3\text{O}_6)_2\text{H}_2\text{O}$  was prepared by reaction of aqueous solutions of trimellitic acid and calcium acetate monohydrate. It crystallizes in  $P-1$ , with  $a = 6.9418(2)$ ,  $b = 7.0404(2)$ ,  $c = 10.4125(3)$  Å,  $\alpha = 86.884(3)$ ,  $\beta = 82.418(2)$ ,  $\gamma = 69.531(1)^\circ$ , and  $V = 472.58(3)$  Å<sup>3</sup>. The complete synthesis, solution, and refinement was carried out in under one day!  $\text{Ce}(\text{C}_9\text{H}_3\text{O}_6)(\text{H}_2\text{O})_4$  crystallizes in  $P2_12_12_1$  with  $a = 6.1541(12)$ ,  $b = 9.7258(20)$ ,  $c = 20.311(4)$  Å, and  $V = 1215.7(4)$  Å<sup>3</sup>. It is isostructural to known Nd and Er analogs.

The structure of the new compound  $[\text{Mn}(\text{HC}_9\text{H}_3\text{O}_6)(\text{H}_2\text{O})]\text{H}_2\text{O}$  was solved and refined using synchrotron powder data. It crystallizes in  $P-1$  with  $a = 6.41805(8)$ ,  $b = 7.35044(7)$ ,  $c = 10.87662(11)$  Å,  $\alpha = 92.2118(9)$ ,  $\beta = 100.9500(13)$ ,  $\gamma = 99.9543(10)^\circ$ , and  $V = 494.829(10)$  Å<sup>3</sup>. The 1- and 2-carboxylate groups are rotated significantly out of the ring plane. One water molecule bridges two Mn, and the other lies in a channel along the  $a$ -axis, and is hydrogen bonded to the 4-carboxyl group, the 2-carboxylate group, and the coordinated water molecule.

$[\text{M}(\text{H}_2\text{C}_9\text{H}_3\text{O}_6)(\text{H}_2\text{O})_4](\text{H}_2\text{O})_2$ ,  $\text{M} = \text{Co}$  and  $\text{Ni}$  are isostructural to the known Mn complex.  $[\text{M}(\text{HC}_9\text{H}_3\text{O}_6)(\text{H}_2\text{O})](\text{H}_2\text{O})_2$ ,  $\text{M} = \text{Mg}$  and  $\text{Co}$  are isostructural to the known Fe complex. The hydrogen bonding in these compounds and in  $[\text{Cu}(\text{HC}_9\text{H}_3\text{O}_6)(\text{H}_2\text{O})_{1.5}](\text{H}_2\text{O})$  have been quantified using quantum calculations.

**07.01.05 Novel Mineral Structure of  $\text{LiNaSiB}_3\text{O}_7(\text{OH})$  from Lab Powder Diffraction Data and *Ab-Initio* Quantum Optimization.** P.S. Whitfield<sup>1</sup>, Y. Le Page<sup>1</sup>, J.D. Grice<sup>2</sup>, C.J. Stanley<sup>3</sup>, G.C. Jones<sup>3</sup>, M.S. Rumsey<sup>3</sup>, C. Blake<sup>4</sup>, A.C. Roberts<sup>5</sup>, J.A.R. Stirling<sup>5</sup>, G.J.C. Carpenter<sup>6</sup>, <sup>1</sup>ICPET, National Research Council, Ottawa, Canada, <sup>2</sup>Canadian Museum of Nature, Ottawa, Canada, <sup>3</sup>Dept. of Mineralogy, Natural History Museum, London, UK, <sup>4</sup>Rio Tinto, Somerset, UK, <sup>5</sup>Geological Survey of Canada, Ottawa, Canada, <sup>6</sup>Materials Technologies Laboratories, Natural Resources Canada,

Ottawa, Canada.

Agglomerates of crystals smaller than 5  $\mu\text{m}$  of a new mineral (IMA 2006-36) with the title composition were discovered in a drill core from the Jadar Basin in Serbia. The crystals are too small for standard laboratory single crystal X-ray diffractometry, so structure solution from laboratory X-ray powder diffraction data was attempted.

The structure was solved by simulated annealing in TOPAS (Bruker-AXS) from capillary X-ray data indexed by singular value decomposition algorithm. A mixture of z-matrices and soft bond-length constraints were used in the structure solution step, but removed for final refinement except the O-H bond length. Obtaining neutron diffraction data of this material is problematic due to high boron content, so VASP *ab-initio* optimization in the *Materials Toolkit* framework was used to validate the structure and to better localize the H atom.

The unit cell is monoclinic ( $P2_1/c$ ) with  $a = 6.7620(1)$  Å,  $b = 13.8016(3)$  Å,  $c = 7.6878(2)$  Å, and  $\beta = 124.0894(9)^\circ$ . The structure contains a layer of corner-sharing, tetrahedrally coordinated Li, Si and B, decorated with triangular  $\text{BO}_3$  groups. The H forms a weak intra-layer hydrogen bond, whilst the Na is situated between the layers in a distorted octahedral site. The structure appears to be unique and has no known direct structural analogues.

**07.01.06 Use of Powder Diffraction in Molecule-Based Magnets.\*** P.W. Stephens, Dept. of Physics and Astronomy, State Univ. of New York, Stony Brook, NY 11794.

Much of our understanding of the properties of materials comes from analysis of crystal structures. This is an essentially routine procedure if single crystals can be grown, but many interesting materials are available only in polycrystalline form. It has become possible to solve rather complex crystal structures from powder data, even in cases where the correct composition or stoichiometry is not known.

We have recently been studying magnetic salts of transition or alkali metals and TCNE (tetracyanoethylene,  $\text{C}_2(\text{CN})_4$ ). Structural insights from powder diffraction have made important contributions to the understanding of these materials. For example, we have discovered the first two compounds with direct bonding between Fe(II) and  $\mu_4$ -[TCNE]<sup>•-</sup>, which exist as ruffled sheets. These all have ferromagnetic transitions around 100K. Their structures suggest a similar local bonding pattern for the intriguing room temperature magnet based on  $\text{V}[\text{TCNE}]_2$ .

We have also determined structures of polycrystalline samples of several materials based on  $\text{Ru}_2(\text{CO}_3)_4$  and  $\text{Ru}_2(\text{O}_2\text{CCH}_3)_4$ . Again, the structures are important for understanding the magnetic behavior.

Work performed in part at the National Synchrotron Light Source, Brookhaven National Laboratory, which is supported by the U.S. Department of Energy, Office of Basic Energy Sciences, under Contract No. DE-AC02-98CH10886.

\* Research in collaboration with J.H. Her, J.D. Bagnato, M. Bonner, K.I. Pokhodnya, B. S. Kennon, and J.S. Miller.

**07.01.07 An *in-situ* Crystallographic Study of Crystal Growth and Ion Exchange in Titanium Silicates.** Abraham Clearfield, Aaron J. Celestian, Akhilesh Tripathi, Dimitri Medvedev, John B. Parise, Chemistry Dept., Texas A&M Univ., College Station, TX 77843, Dept. of Chemistry, Stony Brook Univ., Stony Brook, NY, 11794.

One of the vexing environmental problems involves the remediation and disposal of large volumes of nuclear waste that has accumulated from the U. S. nuclear weapons program. In particular isotopes Cs-

137, Sr-90 and actinides such as Pu and Np need to be sequestered and immobilized. A particular titanium silicate  $\text{Na}_2\text{Ti}_2\text{O}_3(\text{SiO}_4)\cdot 2\text{H}_2\text{O}$  is highly selective for the removal of  $\text{Cs}^+$  and  $\text{Sr}^{2+}$  from the waste systems. We will describe how the use of powder X-ray and neutron diffraction has revealed the structural origin of the selectivity and the use of *in-situ* X-ray methods has elucidated the mechanism of the exchange reaction. This knowledge is now being applied to the pharmacosiderite phases such as  $\text{K}_4\text{Ti}_4\text{O}_4(\text{SiO}_4)_3\cdot 8\text{H}_2\text{O}$  for removal of addition highly radioactive species.

**07.01.08 Polymorphic Discoveries using Power X-Diffraction – Discoveries during Pharmaceutical Development.** Eugene Y. Cheung, Matthew L. Peterson, TransForm Pharmaceuticals, 29 Hartwell Ave., Lexington, KY, USA.

Amides have been studied extensively in the solid for their hydrogen bonding capabilities for many years.<sup>1</sup> The capacity to form hydrogen bonds in a specific manner is often counter-balanced by non-directional intermolecular forces which promote different types of crystal forms.<sup>2</sup> In recent years, the study of polymorphism has become increasingly important in scientific and industrial settings, with the commercial value of form and formulation studies acquiring a significant presence during the development timeline.<sup>3</sup> Sophisticated techniques are often used to monitor for polymorphs during the screening of a pharmaceutical compound,<sup>4</sup> but from a fundamental point of view, there is much insight to be gained by investigating the structural aspects of amides. It has been found that even compounds which are well known in the chemical literature offer many surprises when they are studied using modern X-ray diffraction equipment. Advances in powder X-ray diffraction, in particular, give researchers the opportunity to make new discoveries even for “old” compounds.

<sup>1</sup>Leiserowitz, L.; Tuval, M. *Acta Crystallogr.* **1978**, *B34*, 1230.

<sup>2</sup>Caira, M.R. In *Design of Organic Solids*; Weber, E., Ed.; Topics in Current Chemistry; Springer-Verlag: Berlin, 1998; pp.163–208.

<sup>3</sup>Bauer, J.; Spanton, S.; Henry, R.; Quick, J.; Dziki, W.; Porter, W.; Morris, J. *Pharm. Res.* **2001**, *18*, 859.

<sup>4</sup>Peterson, M.L.; Morissette, S.L.; McNulty, C.; Goldsweig, A.; Shaw, P.; LeQuesne, M.; Monagle, J.; Encina, N.; Marchionna, J.; Johnson, A.; Gonzalez-Zugasti, J.; Lemmo, A.V.; Ellis, S.J.; Cima, M.J.; Almarsson, Ö. *J. Am. Chem. Soc.* **2002**, *124*, 10958.

**07.01.09 Reaching for High Resolution in Protein Powder Diffraction.** R.B. Von Dreele, APS/IPNS Argonne National Laboratory, Argonne, IL USA 60439.

The central problem in using powder diffraction data for the solution and refinement of crystal structures is that the diffraction information is severely limited relative to that obtained from a single crystal covering the same region of reciprocal space. The scattering from a single crystal is represented in reciprocal space by an array of slightly broadened delta functions; their intensity measurement is a simple integration of the peak intensity above background. For a powder diffraction experiment, the reciprocal space picture is of a nested series of spherical shells broadened by sample and instrumental effects; the density of these shells increases quadratically with distance from the reciprocal space origin. Their intensity corresponds to that of the structure factor responsible for the shell and its multiplicity. Use of the individual structure factor intensities that form the powder pattern is then compromised by the increasing overlap of these shells. This is particularly acute for proteins as the diffraction patterns are made from a very large number of reflections. However, the unprecedented sharpness of protein powder pattern peaks and their position sensitivity to sample environment provides a means of overcoming this loss of information. This talk will present some

recent results on the improvement possible from using combinations of protein powder patterns for Rietveld refinement.

Supported by US DOE/OS/BES under Contract No. DE-AC-02-06CH11357.

**07.01.10 POWGEN3: A New Neutron Powder Diffractometer Suitable for *Ab-Initio* Crystal Structure Determination.** J.P. Hodges, A. Huq, Neutron Scattering Science Div., Oak Ridge National Lab., P.O. Box 2008, TN 37830, hodgesj@ornl.gov.

POWGEN3 is a fundamental departure from previous designs for a time-of-flight powder diffractometer at a spallation neutron source and may be considered a third-generation design. The instrument is optimized for both parametric studies of materials under a wide range of conditions (T, P, H, flowing gases, etc) and *ab-initio* crystal structure determinations of complex solid-state materials with asymmetric unit-cells of the order  $\sim 15,00 \text{ \AA}^3$ . The geometric design of the instrument allows for all detected scattered neutrons to be focused onto a single diffraction profile yielding high count rate while preserving good resolution  $\Delta d/d = 0.0015$  at  $d = 1 \text{ \AA}$ . The new time-event mode for data acquisition will permit stroboscopic experiments and filtering of the incoming data, neutron by neutron, allowing very high resolution diffraction profiles to be generated with  $\Delta d/d \sim 0.0007$  at  $d = 1 \text{ \AA}$ . ORNL/SNS is managed by UT-Battelle, LLC, for the U.S. Department of Energy under contract DE-AC05-00OR22725.

**07.01.11 Maximum Entropy Crystal Structure Reconstruction using X-ray Powder Diffraction Data.** Jae-Hyuk Her, Peter W. Stephens, Physics and Astronomy, Stony Brook Univ., Stony Brook, NY.

Under the process of crystal structure determination, it is quite often to meet disordered or otherwise difficult to model structural features. Most crystallographic analysis is based on the presence of discrete atoms in a sample, but sometimes that is not applicable. In order to treat such problems, solvent scattering was suggested and implemented (e.g. SQUEEZE).

Modeling of this solvent scattering is a particularly difficult problem in powder diffraction, where there is much less redundancy in the data available to produce a structural model. The use of a maximum entropy map instead of a Fourier map is attractive because it is relatively insensitive to truncation errors and is theoretically less sensitive to bias by unknown features which might exist in the prior structure model. We have extended previous techniques to include appropriate treatment of partially overlapping peaks via the correlation coefficients of nearby reflections, as opposed to simply summing intensities in clusters of peaks.

We have written a Maximum Entropy Program for Powder Diffraction (MEPPD) to implement the idea and have used it against several problems. We will show results from molecular magnet materials,  $\text{Fe}[\text{TCNE}]_2$  and  $(\text{NEt}_4)_2\text{Mn}_3(\text{CN})_8$ , containing disordered solvent molecules.

**07.01.12 Distance Puzzle - Structure Mining from Pair Distribution Function.** Pavol Juhas, Phillip M. Duxbury, Simon J.L. Billinge, Physics and Astronomy, Michigan State Univ., East Lansing, MI.

A vast majority of known structures has been found using reciprocal-space methods, which assume periodic long-range order in the material. However, for many important systems, such as nanomaterials or non-crystallized molecules, the periodic order is not present and they cannot be solved using conventional crystallographic methods. The

analysis of the atomic Pair Distribution Function (PDF) is not limited by periodic order and it has yielded important atomic scale information on nanomaterials. The experimental PDF provides probability of pair distances scaled by scattering factors of the contributing atoms. We will demonstrate how to use this one-dimensional PDF information to determine structure of simple molecules and periodic systems with large supercells. The applications to periodic materials with local distortions will also be discussed.

## 09.01 USANS/USAXS

**09.01.01 USAXS Facility at Advanced Photon Source for Complex Microstructure Studies in Materials Science.** Jan Ilavsky, Peter R. Jemian, Gabrielle G. Long, Fan Zhang, APS, ANL, Argonne, IL 60439, Andrew J. Allen, NIST, Gaithersburg, MD.

Latest research is aimed at development of hierarchical functional microstructures. Understanding of these microstructures requires characterization methods that provide statistically representative information over many decades in size. Ultra small-angle X-ray Scattering (USAXS) is an invaluable tool addressing this need. The Advanced Photon Source (APS) USAXS facility at 32ID beamline (<http://usaxs.xor.aps.anl.gov>) uses Bense-Hart design. It has been developed into a robust and reliable instrument, with an intensity dynamic range of up to 9 decades, and a scattering vector ( $q$ ) range of 4 decades ( $0.0001$  to  $1 \text{ \AA}^{-1}$ ). This instrument is uniquely suited to many problems in materials science, chemistry, medicine, and biology, with its ability to characterize, in a single measurement, scattering features ranging in size from nanometers to micrometers. Among many advantages of this instrument are high  $q$ -resolution of  $0.0001 \text{ \AA}^{-1}$  which is independent of the absolute  $q$  value, standard-less absolute intensity calibration, and USAXS imaging capabilities. Flexible beam sizes from  $0.01 \text{ mm}^2$  to  $1.5 \text{ mm}^2$  allow characterization both of small samples (or gradient microstructures) and statistically representative volumes of up to few  $\text{mm}^3$ . Both slit-smeared and 2D-collimated (effective pinhole) configurations are available. For slit-smeared data, a robust numerical desmearing code is included within the data evaluation software package provided. The presentation will cover basic principles of this instrument, data reduction and analysis software packages, as well as examples of science for which this facility is uniquely suitable.

Use of the APS was supported by the U. S. Department of Energy, Office of Science, Office of Basic Energy Sciences, under Contract No. DE-AC02-06CH11357.

**09.01.02 Riching the Theoretical Limit of Sensitivity for the Bense-Hart Ultra-Small-Angle Neutron Scattering (USANS) Technique.** M. Agamalian<sup>1</sup>, J.M. Carpenter<sup>1, 2</sup>, K. Littrell<sup>1</sup>, J.W. Richardson<sup>2</sup>, <sup>1</sup>Oak Ridge National Laboratory, Spallation Neutron Source, Oak Ridge, TN 37831, <sup>2</sup>Argonne National Laboratory, Intense Pulsed Neutron Source, Argonne, IL 60439.

Bense-Hart Double-Crystal Diffractometers (DCD) using multi-bounce channel-cut crystals have been employed for small-angle X-ray scattering studies since 1965. Approximately twenty years later this technique was adopted successfully for small-angle neutron diffraction. The multi-bounce approach dramatically increases the sensitivity of a DCD, offering an opportunity to detect weak small-angle X-ray and neutron scattering in the range of very low transfer momentums that are not accessible in conventional SAS instruments. However, the sensitivity of the world's best USAXS and USANS diffractometers still remains several orders of magnitude less than the theoretical prediction.

Our recent measurements of the neutron diffraction from a Si(111)

triple-bounce channel-cut crystal conducted at the Intense Pulsed Neutron Source, Argonne National Laboratory have revealed a new source of the parasitic scattering, which very likely is the reason for the limitation in sensitivity. The mechanism of this background as well as the way of suppressing it is the main focus of the current presentation. The authors believe that the next generation of USANS instruments will more-closely approach the theoretical limit and that the sensitivity will be improved by additional two orders of magnitude.

**09.01.03 Morphological Considerations in the Design of Temperature Responsive Encapsulants.** Dale W. Schaefer, Kevin A. Heitfeld, Dept. of Chemical and Materials Engineering, Univ. of Cincinnati, Cincinnati, OH 45221.

Thermally responsive hydrogels (TRGs) undergo large volume changes in response to temperature. Gels exhibiting a lower critical solution temperature collapse at high temperature. Such gels are candidates for encapsulants with significantly reduced high temperature permeation compared to conventional gel encapsulants used in the food industry.

We used ultra small angle x-ray and neutron scattering to explore the relationship between barrier properties and microphase separation in modified hydroxy propyl cellulose gels. The scattering data reveal a cooperative effect between chemical modification and microphase separation, which leads to non-uniform crosslinking (topological fluctuations). On raising the temperature, these topological fluctuations lead to a heterogeneous collapsed state with poor barrier properties. By managing phase separation during gel synthesis, however, we achieved substantially improved high temperature barrier properties.

The improved encapsulants are suitable for control flavors in the food industry. Flavors often contain volatile compounds, so in the absence of encapsulation, they are vulnerable to premature release. Encapsulation also offers protection against environmental damage such as oxidation, light-induced reactions, etc.

**09.01.04 Void Distributions in Temperature Cycled Insensitive High Explosives.** Trevor M. Willey<sup>1</sup>, Jeff A. Handly<sup>1,a</sup>, Tony van Buuren<sup>1</sup>, Brandon L. Weeks<sup>1,b</sup>, Jon R.I. Lee<sup>1</sup>, Jan Ilavsky<sup>4</sup>, George E. Overturf<sup>1</sup>, John H. Kinney<sup>1</sup>, <sup>1</sup>Lawrence Livermore National Laboratory, Livermore, CA, <sup>2</sup>Advanced Photon Source, Argonne National Laboratory, Argonne, IL, <sup>3</sup>Current address: BWXT Pantex, Amarillo, TX, <sup>4</sup>Current address: Texas Tech. Univ., Lubbock, TX.

Collapse of small voids roughly 100 nm to 1 micron in size create so called hot-spots within an energetic material during detonation. These hot spots are ignition sites that grow in temperature, size, and pressure and sustain the reaction. Properties of the detonation depend on these hot-spots, and thus the distribution, number, and size of the voids within the material.

We are investigating polymer-blended systems containing the insensitive explosive triamino-trinitrobenzene (TATB). The volume of these explosives increases in a non-reversible manner when exposed to cycled temperatures. Such expansion could cause changes in void distributions of interest. Furthermore, several mechanisms for this non-reversible growth have been proposed and investigated modeling techniques, but none of the mechanisms have been experimentally verified.

Ultra-small Angle X-ray Scattering (USAXS) is used to investigate these void distributions in both freshly pressed specimens, and samples that have undergoing thermal cycling between  $-60 \text{ C}$  and  $74 \text{ C}$ . USAXS able to investigate scatters with sizes from a few

nanometers to a few microns. Differences in the small-angle scattering during temperature cycling occur at both of these size extremes, and show voids that are on average larger and more plentiful after thermal cycling. The USAXS also gives insight into the mechanism for the expansion. Finally, the derived size distributions provide empirical input to modeling the initiation and detonation physics of these explosives.

#### **09.01.05 Microstructural Characterization of Ferritic-Martensitic Steels using SANS/USANS/USAXS Techniques\*.**

G. Muralidharan, M. Agamalian, R.L. Klueh, Weijun Ren, J.P. Shingledecker, M.L. Santella, Oak Ridge National Laboratory, Man-Ho Kim, Dept. of MSE, Univ. of Maryland, College Park, MD, Jan Ilavsky, Pete Jemian, Advanced Photon Source, Argonne National Laboratory, Argonne, IL.

Ferritic/martensitic steels are candidate structural materials for use at elevated temperatures in various energy systems, including the Generation IV fission reactor concepts, Ultrasupercritical (USC) boilers, heat recovery steam generators, turbines, and fuel cells. Steel grades such as modified 9Cr-1Mo (Grade P91), and HCM12A (Grade P122) consist of about 9 and 12% Cr, respectively, with about 0.1 wt. % C along with varying levels of Mo, V, Nb, and W. These steels are typically used in the normalized-and-tempered or quenched-and-tempered condition. In this condition, their microstructure consists of a martensitic lath structure with a relatively high density of dislocations along with  $M_{23}C_6$  precipitates (60-150 nm in size) on the lath boundaries and prior austenite grain boundaries. With the addition of V and Nb, small (20-80 nm sized) MX carbides, nitrides, or carbonitrides are also present within the matrix. MX retards recovery and stabilizes the microstructure at high temperatures by pinning dislocations and lath boundaries, thus retaining strength. There is a need to understand the precipitation and growth of various types of carbides/carbonitrides and relate the microstructural evolution to the mechanical properties of these steels.

Small-angle neutron scattering (SANS) and Ultra-small-angle neutron scattering techniques (USANS) are sensitive to the variation of the neutron coherent scattering length density and both combined can be used in the study of internal inhomogeneities of size range 1 nm to 10 nm. We present the results of our initial SANS/USANS and complementary USAXS studies of advanced steels carried out at NIST and at the Advanced Photon Source at Argonne National Laboratory.

\* Research sponsored by the Laboratory Directed Research and Development Program of Oak Ridge National Laboratory (ORNL), managed by UT-Battelle, LLC for the U. S. Department of Energy under Contract No. DE-AC05-00OR22725.

#### **09.01.06 Application of Ultrasmall-angle Scattering Methods in Biomedical Materials Research.**

A.J. Allen, V.A. Hackley, K.S. Wilson, Materials Science and Engineering Laboratory, National Institute of Standards and Technology, Gaithersburg, MD 20899, J. Ilavsky, Advanced Photon Source, Argonne National Laboratory, Argonne, IL 60439.

Despite the current prominence of biological applications in crystallography, advances in biomedicine are frequently driven by materials science. While nanoscale structures and phenomena are of increasing interest in biomedical materials research, so also are the quantitative connections between phenomena or structures at the nano-scale level and those at the micro-scale level. When combined with conventionally collimated small-angle X-ray or neutron scattering (SAXS or SANS) methods, ultrasmall-angle scattering (USAXS or USANS) methods can provide the necessary quantitative microstructure characterization over the scale range from nanometers

to micrometers (USAXS) or tens of micrometers (USANS).

At a 3rd generation synchrotron, USAXS can access virtually all of the microstructure scale range. Furthermore, in the context of solution-mediated fabrication or assembly of nano-particulate suspensions, for example in a flow cell, USAXS can work with concentrations that frequently approach the dilution levels needed for bio-applications. While USANS must almost always be used in conjunction with SANS, it provides the Q range needed to account for the entire microstructure in many solid biomedical systems, e.g., dental nano-composites. USAXS and USANS studies of biomedically-relevant materials will be described with an emphasis on the critical information provided by data in the ultra-low Q regime, obtained contiguously with data in the more conventional SAS Q range.

#### **09.01.07 Small-Angle Scattering Studies on the Hierarchical Structure of Reinforcing Fillers.** Doug Kohls, Dale W. Schaefer, Univ. of Cincinnati, Cincinnati, OH 45221.

The hierarchical structure of reinforcing fillers is studied using small-angle scattering techniques. The fillers studied were a series of newly developed precipitated silica with a range of surface areas and DBP values. Small-angle light and ultra small-angle x-ray techniques are employed to study the structure of the particles from the nanometer to micron size scales. The data from both techniques are combined and analyzed using a unified approach to quantitatively describe the primary particle, aggregate, and agglomerate morphologies of the fillers. A new perspective on elastomer reinforcement is presented wherein the degree of aggregation and agglomeration, measured by small-angle scattering, are correlated with observed mechanical properties.

#### **09.01.08 Large-scale Structure of Block Polyelectrolyte Micelles: Analogies to Attractive Colloids.** Surita R. Bhatia, Dept. of Chemical Engineering, Univ. of Massachusetts Amherst, 686 North Pleasant St., Amherst, MA, 01003.

We present experimental USANS results on micellar gels of poly(styrene)-poly(acrylic acid). At low to moderate polymer concentrations (~2 wt%), these systems form translucent elastic gels. The critical concentration for gelation and the elastic modulus depend strongly on the charge density of the PAA block. The liquid-gel transition occurs at an effective micellar volume fraction of approximately 0.6 for all systems. In addition, the systems show interesting nonlinear rheology that is reminiscent of that observed in attractive colloidal gels, including strain-hardening and shear instabilities. Ultra-small angle neutron scattering shows the presence of large scale inhomogeneities in our gels, and fluorescence microscopy confirms the existence of micron-sized structures in these systems. We believe that some of the nonlinear rheology we observe may be due to rearrangement of these large-scale structures.

#### **09.01.09 Quantitative Characterization of Contrast Mechanism in Ultra-Small-Angle X-ray Imaging.** Fan Zhang, Gabrielle G. Long, Jan Ilavsky, Pete R. Jemian, Advanced Photon Source, Argonne National Laboratory, Argonne, IL, 60439, Lyle E. Levine, Materials Science and Engineering Laboratory, National Inst. of Standards and Technology, Gaithersburg, MD 20899.

Ultra-Small-Angle X-ray Scattering (USAXS) imaging has been developed recently to probe the morphology and three-dimensional arrangements of the small-angle scattering objects directly. It is a size sensitive imaging technique, where images acquired at different reciprocal scattering vectors can reveal different microstructural

features within the same sample volume. USAXS imaging has been proven useful in studies of metallurgical, biological and polymeric materials. Until now, the contrast mechanism has not been modeled.

In this work, we describe a quantitative characterization of contrast mechanism in USAXS imaging. Our treatment makes use of geometrical optical theory to trace the intensity distribution at the detector plane. We simulated USAXS images of a model system (polydispersed, micrometer-sized SiO<sub>2</sub> embedded in a polypropylene matrix) using X-ray refraction (Porod scattering) and reflection for a series of reciprocal scattering vectors and sample-to-detector distances. A comparison with experimental data shows good agreement with our numerical simulations. We also calculated the relative refracted and reflected intensities with our model and show the intensity discrepancy can be attributed to the intrinsic surface roughness in the model system.

**09.01.10 Coarsening Studies in Controlled Waspaloy Microstructures Based on SEM and USAXS Observations.** V. Siva Kumar G. Kelekanjeri, Lewis K. Moss, Rosario A. Gerhardt, School of Materials Science and Engineering, Georgia Inst. of Technology, Atlanta, GA, 30332, USA.

Nickel-base superalloys are an important class of high-temperature materials that find their use in land and air-based turbine engine components. Their excellent strength retention properties are attributed to the presence of the  $\gamma$  phase that precipitates coherently with the matrix ( $\gamma$ ) phase [1]. In this work, controlled microstructures of Waspaloy are produced via systematic heat-treatments with the objective of studying the coarsening kinetics in this alloy. Initial solutionizing treatments were conducted at 1045°C, 1090°C and 1145°C to vary the grain size of the matrix. The microstructures were then controlled in terms the  $\gamma$  precipitate size distribution by aging at 800°C for times ranging from 0.1 hrs to 100 hrs.

SEM observations revealed the progressive growth of  $\gamma$  precipitates upon continued aging at 800°C for specimens with all three prior solution-treatments. USAXS data were acquired at the 32 ID beam line at Argonne. The spectra clearly showed the presence of at least one Guinier region in the high  $q$  regime in all the specimens analyzed that corresponded to scattering from a distinct  $\gamma$  distribution. The mean precipitate radius- $\langle r \rangle$  obtained upon fitting the spectra was found to increase progressively with the aging time-  $t$  for all the three pre-solution-treatment cases, thus corroborating the SEM observations. A plot of  $\langle r \rangle^3$  vs  $t$  yielded reasonable linear fits for all three pre-solution-treatment cases, indicating LSW type volume-diffusion controlled coarsening [1].

The authors gratefully acknowledge the research funding from USDOE under grant DE-FG02-03-ER46035.

[1] J. W. Martin, R. D. Doherty and B. Cantor, *Stability of Microstructure in Metallic Systems*, Cambridge University Press, NY, 1997.

## 09.02 Characterization of Surfaces and Interfaces

**09.02.01 Water-Barrier Properties of Anticorrosion Coatings Based on Bridged Silanes.** Dale W. Schaefer, Yimin Wang, Guirong Pan, Peng Wang, Dept. of Chemical and Materials Engineering, Univ. of Cincinnati, Cincinnati, OH 45221 USA.

Silane coupling agents are known to improve the anti corrosion properties of many metals. Electrochemical impedance measurements show that the silanes improve the barrier properties of both neat films and silane-laced polymer coatings. This presentation focuses on the morphological characteristics and water-response of silane films determined by X-ray reflectivity, neutron reflectivity and grazing-incidence small-angle scattering. With few exceptions, we find that thin films of pure silanes, mixed silanes and silane-laced epoxy absorb water and swell. These results show that anticorrosion performance is not related to water-barrier properties of the bulk film.

Of particular interest are the properties of mixed films composed of two bridged silanes neither of which is particularly protective. The improved protective behavior of mixed films is related to the impact of one of the silanes on the cure chemistry of the other.

**09.02.02 Phasing Resonant Anomalous X-ray Reflectivity Data and Fourier Synthesis of Element-specific Density Profiles at Buried Interfaces.** C. Park, P.A. Fenter, Chemistry Div., Argonne National Laboratory, Argonne, IL 60439, USA.

The distribution of a specific element at buried interface is fundamental to understand many processes. Surface/interface x-ray reflectivity has been extensively used to probe interfacial structures as seen by the total interfacial density profile, but the interfacial distribution of a particular elemental-substructure can be obscured when its contribution to the total interfacial density is small. This approach also has no chemical sensitivity when measured at fixed photon energy. Resonant Anomalous X-ray Reflectivity (RAXR), i.e., x-ray reflectivity measured as function of incident photon energy near an absorption edge at fixed momentum transfer, can be used to overcome this limitation. In particular, density distribution of an element-specific sub-structure can be obtained with RAXR by exploiting its phase sensitivity. We discuss the underlying fundamentals of phasing RAXR data and illustrate the direct imaging of element-specific partial density profile by Fourier synthesis using the example of Rb<sup>+</sup> and Sr<sup>2+</sup> adsorbed at the mica-electrolyte interface (Park et al., Phys. Rev. Lett. 97, 016101). The RAXR spectra are also directly sensitive to the X-ray absorption near-edge structure (XANES) of the interfacial element, which is sensitive to the chemical state or local coordination structure of the interfacial species. The simultaneous determination of elemental profile and XANES using RAXR is illustrated with the example of aqueous platinum-tetra-ammine adsorbed complexes adsorbed on the quartz (100) surface (Park et al., Phys. Rev. Lett. 94, 0761040).

Work performed under the auspices of the US-DOE Office of Science, Office of Basic Energy Sciences, Geoscience Research Program, under contract number W-31-109-ENG-38.

**09.02.03 In situ GISAXS Studies of Metal Nanocluster Catalysis.** Randall E. Winans<sup>1,2</sup>, Stefan Vajda<sup>1</sup>, Byeongdu Lee<sup>2</sup>, Soenke Seifert<sup>2</sup>, Sungsik Lee<sup>1</sup>, Joseph M. Calo<sup>3</sup>, <sup>1</sup>Chemistry, <sup>2</sup>X-ray Science Divisions, Argonne National Laboratory, <sup>3</sup>Div. of Engineering, Brown Univ.

It has become clear that metal nanoparticles are very reactive for many heterogeneous catalytic reactions. However, sintering of

supported, catalytically active nanoparticles during chemical reaction at elevated temperatures, often leads to the loss of the catalytic activity and selectivity of these particles. The reactivity and thermal stability of atomic platinum, gold and silver clusters supported on  $\text{Al}_2\text{O}_3/\text{SiO}_2/\text{Si}(100)$  have been studied in hydrogen and in the partial oxidation of alkenes to alkene oxides. Grazing incidence SAXS was used to follow changes in particle shape and size during reaction. Reaction products were monitored simultaneously with mass spectrometry. In addition, "anomalous" GISAXS was shown to be very effective for observing very dilute coverages of particles ( $\sim 1\%$  monolayer coverage) on fairly rough surfaces where scattering from these surfaces is significant. Typically, these are small, size-selected clusters containing  $9 - 10 \pm 3$  atoms. Extremely high thermal stability of  $\text{Pt}_{7-10}$  clusters in vacuo, as well as in the presence of hydrogen, was observed on  $\text{SiO}_2/\text{Si}(100)$  coated with six cycles of  $\text{Al}_2\text{O}_3$  film prepared by an atomic layer deposition technique. Changes in nanocluster size and shape with alkene partial oxidation have been observed.

Work benefited from the use of the APS funded by DOE, BES under contract DE-AC02-06CH11357 to the UChicago Argonne, LLC.

**09.02.04 *In situ* GIXS and GISAXS Studies of the Self-organized Growth of Cobalt Nanostructures.** Frederic Leroy<sup>1</sup>, Gilles Renaud<sup>2</sup>, Antoine Létoublon<sup>3</sup>, Remi Lazzari<sup>4</sup>, <sup>1</sup>CRMCN-CNRS, UPR 7281, Marseille, France, <sup>2</sup>DRFMC-SP2M, CEA-Grenoble, Grenoble, France, <sup>3</sup>INSA Rennes, Foton UMR 6082 CNRS, Rennes, France, <sup>4</sup>INSP, UMR 7588 CNRS, Paris, France.

Ordered nanostructures deposited on a substrate may have fascinating new properties, which are of interest both for basic and applied research. A very promising method is the self-organized growth. A regular network of preferential nucleation sites can induce by material deposition an ordered lattice of nanostructures. In this context we show the potentialities of the *in situ* Grazing Incidence Small Angle X-ray Scattering (GISAXS) [1] technique to investigate the conditions of self-organized growth. It is applied to the growth of Co nanostructures on Au(111) as a model system and to the growth of Co nanostructures on a Ag(100) surface patterned by a dislocation network buried below the surface.

The sensitivity of this technique is first demonstrated on the growth of Co/Au(111) for an amount of Co deposited on the surface as small as 0.05 atomic monolayer. Then it is shown that the growth of Co nanostructures on a thin film of Ag on MgO(001) patterned by a buried dislocation network can be characterized thanks to the interferences between the waves scattered by the internal structure of the thin film made of a regular dislocation network and those scattered by the Co nanostructures [2]. The self-organization phenomenon is put in evidence and allows localizing the nucleation-growth site upon the dislocation core.

[1] G. Renaud, R. Lazzari, C. Revenant, A. Barbier, M. Noblet, O. Ulrich, F. Leroy, J. Jupille, Y. Borensztein, C. R. Henry, J.-P. Deville, F. Scheurer, J. Mane-Mane, O. Fruchart, *Science*, 300, 1416 (2003).

[2] F. Leroy, G. Renaud, A. Létoublon, R. Lazzari, C. Mottet, J. Goniakowski, *Phys. Rev. Lett.* **95**, 185501 (2005)

**09.02.05 Multidimensional Self-Assembly of Liquid Crystalline Rod-Coil Block Copolymers.** Rachel Segalman<sup>1</sup>, Brad Olsen<sup>1</sup>, Yuefei Tao<sup>1</sup>, Xuefa Li<sup>2</sup>, Jin Wang<sup>2</sup>, <sup>1</sup>UC Berkeley, Lawrence Berkeley National Labs, <sup>2</sup>Argonne National Labs.

Many applications of nanopatterned polymers require functional blocks, such as helical polypeptides or semiconducting polymers, that are rigid-rods. The thermodynamics of these materials is distinct from classical block copolymers due to liquid crystallinity.

We have recently developed a weakly segregated system (poly(2,5-diethylhexyloxy-phenylenevinylene-*b*-isoprene) (PPV-*b*-PI)) with large conformational asymmetry and thermally accessible phase transitions which allows us to probe the fundamental self-assembly behavior of liquid crystalline rod-coil systems. Self-assembly in classical block copolymer systems is controlled through the enthalpic benefit of separating the two blocks countered by an entropic penalty for stretching the chain across an interface. Liquid crystalline rod-coil block copolymers, however, are also influenced by rod-rod attractions and geometrical asymmetries of the rod and coil on opposite sides of an interface. The four dimensional phase diagram will be described during this talk.

The rod orientation and crystalline packing of the rodlike homopolymer (DEH-PPV) also affects the structure of the analogous block copolymer at low temperature. DEH-PPV, as studied using grazing incidence X-ray diffraction and electron diffraction, has a tetragonal unit cell with a 001 dimension of 0.665 nm and 100/010 dimensions of 1.348 nm. In the block copolymer, a greater extent of order is observed in the 001 direction due to the effect of microphase separation at aligning the rods. Grazing incidence X-ray scattering of the thin film reveals that the crystalline DEH-PPV phase influences the defect structures in the nanodomain structure of the block copolymer and ultimately results in unusual grain structures.

**09.02.06 Kinetic Study of Nucleation and Growth of Environmental Nanoparticles at Water-Mineral Interfaces using *in situ* Time-Resolved GISAXS.** Young-Shin Jun<sup>1,2</sup>, Glenn A. Waychunas<sup>2</sup>, Byeongdu Lee<sup>3</sup>, <sup>1</sup>Univ. of California, Berkeley, CA 94720, <sup>2</sup>Lawrence Berkeley National Laboratory, Berkeley, CA 94720, <sup>3</sup>Argonne National Laboratory, Argonne, IL 60439.

The nucleation and growth of metal oxide nanoparticles on mineral surfaces can markedly affect aqueous metal contaminant transport and other surface-controlled reactions. Recently, grazing incidence small angle x-ray scattering has been used to analyze the size, shape, and distribution of quantum dots and polymers on substrates. However, no work has been attempted using GISAXS for environmental applications, especially in aqueous systems.

In this work, we devised the first environmental application of GISAXS in aqueous systems and studied the kinetics of nucleation and growth of iron oxide nanoparticles at water-quartz interfaces using *in situ* time-resolved GISAXS. The changes in the sizes and shapes of nuclei and the interspacing between nuclei on quartz surfaces are determined as a function of exposure time and the direction of x-ray beam with respect to that of steps. The iron oxide nuclei started to grow close to steps rather than on terraces (diameter:  $5.3 \pm 0.5$  nm; height:  $1.9 \pm 0.2$  nm at 4 min reaction time with  $[\text{Fe}^{3+}] = 10^{-4}$  M). At 31 min, the nuclei began to coalesce with each other and form larger surface clusters. We found that the surface steps direct the iron oxide nucleation and affect the kinetics of nucleation and growth of iron oxide nanoparticles at water-quartz interfaces. For comparison, we generated simulations of the nanoparticle scattering and conducted measurements with AFM.

GISAXS can provide statistically improved morphological information of the early stage of environmental nanoparticle growth compared with AFM and SEM, and allow real-time geochemical kinetics analysis of nanoparticle growth and reactions.

## 09.03 X-ray Imaging and Resonant Scattering

**09.03.01 Resonant Soft X-ray Magnetic Scattering to Resolve Lateral and In-Depth Structure.** J.B. Kortright, Materials Sciences Div., Lawrence Berkeley National Lab, Berkeley, CA.

Understanding modern magnetic materials requires sensitivity to chemical and magnetic structure in small volumes and at short length scales. Tuning to soft x-ray core levels of magnetic transition metal and rare earth constituents yields large resonant enhancements in separate charge and magnetic contributions to the scattering factor. Combined with q-resolved scattering, these resonant effects enable us to resolve magnetic from chemical correlations in a broad range of systems. This talk will review general features and implications of the resonant scattering factors at relevant soft x-ray core levels, before presenting studies of specific systems. Applications can be broadly categorized as studies of lateral vs. depth-resolved structure in thin films and nanostructured systems.

In-plane correlations can be studied via diffuse scattering in transmission geometry. We can distinguish between magnetic and chemical correlations through their q, energy, and applied field dependence, and study question regarding magnetic memory with coherent scattering techniques. Such measurements have been applied to systems ranging from magnetic recording media to superparamagnetic nanoparticle assemblies.

Specular reflectivity provides depth-resolved information relevant to layered magnetic heterostructures. An example involves exchange-bias couples between ferromagnetic and antiferromagnetic layers. Modeling reflectivity features allows separation of the different magnetic contributions in both layers, and their depth distribution relative to the nominal chemical interfaces.

This research was done at LBNL's Advanced Light Source with many collaborators and was supported by the U. S. Dept. of Energy under Contract No. DE-AC03-76SF0098.

**09.03.02 Thin Polymer Film Structure using Resonant Soft X-ray Scattering and Reflectometry.** Cynthia F. Welch, Rex P. Hjelm, Joseph T. Mang, Marilyn E. Hawley, Debra A. Wroblewski, E. Bruce Orler, Jeffrey B. Kortright, Materials Science & Technology Div., Los Alamos National Lab, Los Alamos, NM.

Thin films of carbon-containing materials are found in a pervasive number of applications, ranging from well-established industrial binders and coatings to novel biomedical and optoelectronic devices based on recent advances in nanotechnology. Phase separation through self-assembly gives these films their desirable properties; thus, determining the film structure and understanding its formation are key to unravelling the structure-property relationships. However, determining the morphology of thin, carbon-based films via traditional x-ray and neutron scattering techniques is often difficult due to weak contrast between phases and small scattering volumes. Consequently, standard scattering techniques often require either heavy atom, for x-rays, or deuterium labelling, for neutrons, to locate the various chemical constituents in the structure. Here we develop soft x-ray scattering and reflectometry techniques that allow us to analyze the morphology of thin polymer films whose phase-separated domains are distinguishable without resorting to chemical modification or isotopic labelling. With these techniques, we achieve significant, x-ray energy-dependent contrast between carbon atoms in different chemical environments using soft x-ray resonance at the carbon edge. We demonstrate the use of this contrast mechanism on the phase-separated structure of a model thin polymer film. While the realization of these methods represents a significant advance in our ability to probe the morphology of thin polymer films, we expect that they will also find extensive use in the

analysis of other thin, carbon-containing films often found in biological systems and new nanocomposite devices.

**09.03.03 Coherent Diffraction Imaging using Free-Electron Lasers.** S. Boutet, M.J. Bogan, A. Barty, U. Rohner, B.W. Woods, M. Seibert, S. Marchesini, M. Frank, J. Hajdu, H.N. Chapman, Stanford Linear Accelerator Center, Menlo Park, CA, 94025.

Coherent beams of x-rays can and have been used to image, without the use of a lens and at diffraction limited resolution a variety of objects including thin films, small crystals and a variety of sub-micron objects. Such beams can be used in theory to image any isolated object. The technique of coherent diffraction imaging is interesting in its simplicity and wide ranging applications. I will introduce the concepts behind the technique and how in practice such measurements are performed. After a short review of past results in the field, I will discuss current work using coherent imaging at the new free-electron laser facilities. These new sources offer greatly increased brilliance and high coherence of the beam which make a host of new measurements possible. I will discuss our current progress toward imaging radiation sensitive objects beyond the radiation damage limit. Finally, I will discuss the current status of the project aimed at structural determination of single molecules and future steps needed to achieve that goal.

**09.03.04 X-ray Resonant Scattering from Novel Ordering in Strongly Correlated Materials.** Stuart B. Wilkins, Condensed Matter & Materials Science, Brookhaven National Lab, Upton, NY.

Transition metal oxides are typical strongly correlated electron systems in which interactions strongly determine the electronic properties. Colombic repulsion between the d-electrons of the transition metal ions tends to localize the electrons at atomic lattice sites whereas hybridization within the metal - oxygen bond to the oxygen 2p states tends to cause delocalization. These very subtle balances make transition metal oxides excellent candidates for studying metal-insulator transitions, orbital ordering, spin ordering and lattice effects. These charge, spin, lattice and orbital degrees of freedom produce complex phases and phenomena such as phase separation and pattern formation. Resonant X-ray scattering is an ideal technique for the studies of such novel orderings. Results will be presented on various systems which display long range spin and orbital ordering.

**09.03.05 Anomalous Small-Angle X-ray Scattering Characterization of Bulk Block Copolymer/Nanoparticle Composites.** Byeongdu Lee<sup>1</sup>, Chieh-Tsung Lo<sup>1</sup>, Nancy L. Dietz Rago<sup>2</sup>, Randall E. Winans<sup>1</sup>, P. Thiyagarajan<sup>3</sup>, <sup>1</sup>XSD, <sup>2</sup>CMT, <sup>3</sup>IPNS, Argonne National Lab, IL.

We demonstrate the versatility of anomalous small angle X-ray scattering (ASAXS) to investigate the morphology of multi-component bulk composites comprising poly(styrene-*b*-2 vinylpyridine) (PS-PVP) and Au nanoparticles. Contrast variation near the L<sub>3</sub> absorption edge of Au enables the separation of the partial scattering functions of the polymer and nanoparticle phases. Theoretical and experimental methods developed for the ASAXS analysis of the composites will be useful for the investigation of other such multi-component systems with heavy elements. At 8.8% loading, the Au nanoparticles remain well dispersed in the lamellar polymer matrix, while at 27.0% loading the polymer morphology transforms to a hexagonal packed cylinder phase and the concentrations of nanoparticles in PS domains fluctuate strongly to form aggregates with structures resembling fractal aggregates as evidenced by the power-law scattering at low *Q* and the liquid like peak at high *Q* region, indicating the inter-particle correlations between the nanoparticles in the aggregated domains.

Work benefited from the use of APS, CMT and IPNS funded by DOE, BES under contract DE-AC02-06CH11357 to the UChicago Argonne, LLC.

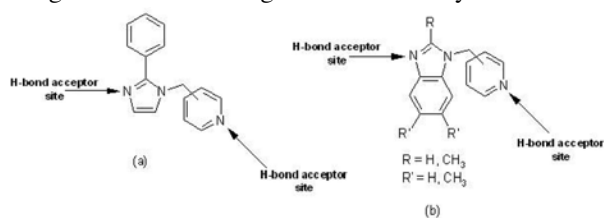
## 10.01 Important Science from Small Molecule Structures

**10.01.01 New Building Blocks for the Construction and Deconstruction of Ternary Supramolecules.** Michelle Smith, Christer Aakeroy, John Desper, Dept. of Chemistry, Kansas State Univ., Manhattan KS 66502.

In order to construct ternary supramolecules, several ditopic building blocks equipped with two different binding sites have been synthesized (Figure 1).

The binding sites differ with respect to their geometries and electrostatics. Systematic co-crystallization studies were conducted (complemented by electrostatic surface potential calculations) to establish whether a supramolecular reagent such as a carboxylic acid or cyanoxime can distinguish between, and preferentially bind to, the different sites.

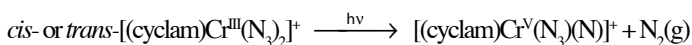
It has been found that whenever a 1:1 stoichiometric cocrystal between a building block outlined in Figure 1 and a carboxylic acid is formed,



the carboxylic acid preferentially binds to the pyridyl binding site of the ligand. Additionally, a 2:1 binary cocrystal formed between ligand (b) and the ditopic building block 4-carboxyphenylcyanoxime, containing both carboxylic acid and cyanoxime functionalities (Figure 2), yielded the same result with the carboxylic acid moiety opting for the pyridyl site, and the oxime proton preferentially binding to the imidazole nitrogen site. When the carboxyphenyl cyanoxime molecule is ‘deconstructed’ by positioning the oxime and carboxylic acid moieties on different molecular fragments, a ternary system is obtained.

**10.01.02 Snapshots of a Solid State Reaction: Photolysis of Coordinated Azide in Chromium(III) Complexes.** Marilyn M. Olmstead, Lauren E. Bria, Dept. of Chemistry, One Shields Ave., Univ. of California, Davis, Davis, CA 95616, USA.

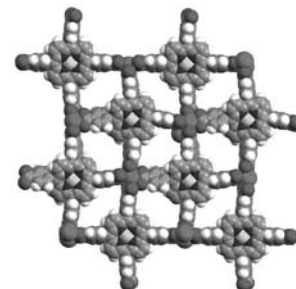
Recent results on our investigations into the inorganic solid state reaction



will be reported. The reaction proceeds slowly by photolysis and involves photochemical bond cleavage of the coordinated azido ligand. Two azido groups are present in the precursor molecule, but often only one will be affected by photolysis. The reaction yields a new complex with a coordinated nitride plus dinitrogen gas. There is an increase in the formal oxidation state of the metal center by two. Because the net charge on the complex and the coordination number of the Cr are conserved, only minor reorganization of the structure occurs in this process, and crystallinity is often retained. We are able to follow this reaction in a single crystal, and we aim to determine some of the influences of different microenvironments on the photodissociation process such as, presence or absence of hydrogen bonding, change in anion, and volume of the reaction cavity. Our preliminary results indicate that the reaction is strongly influenced by the ability of  $\text{N}_2(\text{g})$  to diffuse out of the crystal.

**10.01.03 Porphyrin-Based Framework Coordination Polymers Tailored with Lanthanide Bridging Reagents.** I. Goldberg, S. Lipstman, S. Muniappan, S. George, School of Chemistry, Sackler Faculty of Exact Sciences, Tel-Aviv Univ., 69978 Tel-Aviv, Israel.

The chemical and structural diversity of porphyrins allows us to reasonably control their self-assembly process and to alter systematically the composition, topology, porosity and functionality of the supramolecular arrays that form. This crystal-engineering approach represents an attractive “bottom-up” strategy to tailoring ordered lattice materials and organic zeolite analogs from suitably functionalised tetraarylporphyrin building blocks. Targeted synthesis of framework coordination polymers was achieved by reacting the *meso*-substituted (3-carboxyphenyl)-



and (4-carboxyphenyl)-porphyrin scaffolds with common salts of lanthanide metal ions [George, S.; Lipstman, S.; Goldberg, I., *Cryst. Growth Des.*, 2006, 6, 2651-2654]. The large size, high coordination numbers and strong affinity of the latter, combined with favourable hydrothermal conditions, allowed the formation of open 3D single-framework architectures by coordination polymerisation. In the polymeric arrays the tetra-dentate porphyrin units are inter-coordinated in 3D by multi-nuclear assemblies of the bridging metal ions. The latter serve as construction pillars of the supramolecular arrays, affording stable structures. These materials reveal several modes of polymerisation, which differ by the spatial functionality of the porphyrin building blocks, coordination patterns of the lanthanide-carboxylate assemblies and the topology of the resulting frameworks. All structures exhibit, however, periodically spaced channel voids that perforate the polymeric architectures and are accessible to other molecular components.

This work was supported by The Israel Science Foundation (Grant 254/04).

**10.01.04 High Throughput Single Crystal Neutron Diffraction – New Opportunities in Molecular Structure.** Chick C. Wilson, Dept. of Chemistry and WestCHEM Research School, Univ. of Glasgow, Glasgow G12 8QQ, UK.

Many of the areas recently advanced in single crystal studies of small molecule materials rely heavily on the ability to study structures on a shorter timescale, either to examine a series of samples or to study a single sample under a range of conditions. This “high throughput” approach has only recently become feasible for single crystal neutron diffraction as a result of a substantial revolution in the provision of instrumentation with massive detector arrays, which has allowed neutron chemical crystallography to respond in a highly successful fashion to modern trends in structural molecular science. This has extended the applications of neutron diffraction in the area of chemical crystallography and molecular materials; many of these exploit the power of neutron diffraction in determining accurately the hydrogen atom parameters in materials.

This high throughput capability allows the powerful information available from neutron diffraction to be harnessed, with complementary X-ray and computational input, to tackle more of the problems at which neutron diffraction excels, particularly those involving hydrogen atom location. These include prominent examples in hydrogen bonding including weaker hydrogen bonding interactions, in complementing charge density studies and in studying materials under conditions of variable temperature and variable pressure.

The potential of this new capability will be illustrated by a range of recent studies from the Glasgow Laboratory on proton migration, hydrogen atom disorder and transfer, polymorphism in molecular complexes, thermochromic materials and hydrogen-bonding interactions. The powerful complementary use of both X-ray and computational methods with neutron diffraction in these studies will also be highlighted.

**10.01.05 The Combined Use of X-ray Diffraction, Neutron Scattering and (PGSE) NMR Measurements in Coordination Chemistry.** Alberto Albinati, Univ. of Milan, Dept. of Structural Chemistry (DCSSI), 20133 Milan, Italy.

X-ray diffraction has always been of paramount importance in elucidating the solid-state structures of coordination compounds and in improving our understanding of chemical bonding. Moreover, combining solid-state structural data with solution NMR measurements has led to a deeper understanding of chemical reactivity, for example, showing how soluble chiral transition metal catalysts transfer their chirality to the substrate. The important role of the solvent and/or counter-ions, in these reactions, has been recently highlighted by (PGSE) NMR diffusion measurements, a technique that allows the study of molecular aggregation in solution. The relationships between the observed behaviour in solution and the solid-state structures will be discussed using examples from Pt(II) and Pd(II) chemistry.

When metal hydrides are involved, the use of neutron diffraction becomes essential to obtain accurate geometrical parameters for the "M-H" and "M-H<sub>2</sub>" moieties. However, discrepancies between bond distances obtained from neutron diffraction and NMR measurements are often observed. I will discuss how these two observations may be reconciled by a proper treatment of the molecular motions.

**10.01.06 Structure Determination and Glass Transition Behaviour of Cyclohexene.** R.M. Ibberson<sup>a</sup>, M.T.F. Telling<sup>a</sup>, S. Parsons<sup>b</sup>, <sup>a</sup>ISIS Facility, CCLRC - Rutherford Appleton Laboratory, Chilton, Didcot, Oxfordshire, OX11 0QX, U.K., <sup>b</sup>School of Chemistry, The Univ. of Edinburgh, King's Buildings, West Mains Rd, Edinburgh, EH9 3JJ, U.K.

Cyclohexene, C<sub>6</sub>H<sub>10</sub>, is one of the fundamental structures in the stereochemistry of organic compounds and is also of interest as one of the family of organic molecular crystals with mono-cyclic ring structures that often exhibit order-disorder phase transitions in the solid state. The crystal structures of the three low-temperature phases of cyclohexene have been solved and the complex phase behaviour characterised using complementary high-resolution neutron powder and single-crystal X-ray diffraction techniques. Phase II is the only orientationally ordered structure crystallising in the triclinic space group *P*1. Phases I and III exhibit orientational disorder corresponding to free uniaxial rotation and ring inversion of the molecule respectively. Phase I is cubic, space group *P*2<sub>1</sub>3, and the molecule is located on a 3-fold axis with *Z'*=1/3. Phase III is monoclinic, space group *P*2<sub>1</sub>/*c*, with pseudo-cubic character inherited from the phase I structure. In this phase the molecules are disordered and exhibit ring inversion which freezes at the glass transition temperature of 80 K. The energy difference between the two conformations is determined from the powder diffraction measurements. The low melting point and complex phase behaviour including first-order phase transitions of cyclohexene present particular technical difficulties for both powder and single-crystal diffraction techniques. However, the complementary use of both techniques has enabled a full and detailed structural study to be completed.

**10.01.07 The Role of Protonated Water Aggregates (H<sub>2n+1</sub>O<sub>n</sub>)<sup>+</sup> in the World of Crystalline Hyperacid Salts.** Michael A. Galella, Jack Z. Gougoutas, John D. DiMarco, Mary F. Malley, Solid State Chemistry, PRI, Bristol Myers Squibb Co., Princeton, NJ 08543.

Crystalline "hyperacid" salts contain excess acid which typically is assembled in the crystal structure as an ordered aqueous aggregate [(H<sub>2n+1</sub>O<sub>n</sub>)<sup>+</sup> • X<sup>-</sup>]. The excess acid clearly is not required stoichiometrically, and as such is simply another chemical component in the structure (e.g., like H<sub>2</sub>O in hydrates). Despite the characteristically short/strong intra and intermolecular H-bonds of the [(H<sub>2n+1</sub>O<sub>n</sub>)<sup>+</sup> • X<sup>-</sup>] ion pairs, crystalline hyperacid salts tend to be unstable during isolation. However, a number of surprisingly stable crystal structures have been observed and in some cases are key forms for the manufacturing process.

**10.01.08 Problem Structures: Attempts to Rationalize their Description and Refinement.** A. David Rae, Research School of Chemistry, Australian National Univ., Science Road, Canberra, ACT 0200 Australia.

The author is currently completing an update of his refinement program *RAELS* to refine problem crystal structures, prior to general release. The program's concept includes using a number of components to diffraction intensity, the combination of which is to be determined by modeling and refinement. The program is currently restricted to three *hkl* indices per component but a component can be an adjacent reflection, a substructure in the same cell or of a different orientation of the same cell or a different cell. Each component specifies a selection of cell, atoms, symmetry elements and reflection indices. This allows a most general description of twin-disorder, including stacking faults that combine different orientations and origins of a prototype (ideally ordered structure). It also allows the coexistence of polymorphic structures that interchange across a commensurate surface. Reflections can be monitored according to user set index conditions *h* = *g* + *m**q*. Often structures can be described as a modulation of a parent structure of higher symmetry corresponding to parent reflections *g* and identifies a twin-disorder mechanisms involving pseudo symmetry at an interface. This allows the construction of symmetrized components of the scattering density corresponding to particular combinations of pseudo-equivalent reflections per value of *m*, each with its own choice of systematic absences, global phase, scale and content. This identifies minor components of the scattering density and possible false minima. Sensible constraint-restraint procedures should restrict the minor components. Solved structures will be presented detailing relevant concepts.

**10.01.09 Crystal Structures of Seven Chalcones with Pharmacological Activity.** Hamilton Napolitano<sup>1</sup>, Ademir Camargo<sup>1</sup>, Ivo Vencato<sup>1</sup>, Carlito Lariucci<sup>2</sup>, Wender Silva<sup>3</sup>, Carlos Andrade<sup>3</sup>, <sup>1</sup>Ciências Exatas e Tecnológicas-UEG, <sup>2</sup>Instituto de Física-UFG, <sup>3</sup>LaQMOS-Instituto de Química-UnB, Brazil.

Chalcones or 1,3-diaryl-2-propen-1-ones have a wide biological activity spectrum, as anticancer, anti-herpes Simplex virus and anti-inflammatory. These compounds can occur naturally or be easily synthesized. The wide action spectrum has attracted our attention to synthesize and characterize different chalcones aiming to obtain pharmacologically active molecules. Crystal data collections were performed in a CAD4 diffractometer, CuK $\alpha$  radiation. The respective solutions, anisotropic refinements, geometrical calculations, molecular packing and drawings were done with the program package WINGX. (I): C<sub>16</sub>H<sub>12</sub>O<sub>3</sub>, *a* = 7.809(2), *b* = 11.1764(9), *c* = 28.601(2) Å, orthorhombic system, space group *P*cab, *R* = 0.0557; (II): C<sub>16</sub>H<sub>11</sub>O<sub>4</sub>Br, *a* = 4.160(3), *b* = 11.757(2), *c* = 27.598(7) Å,  $\beta$

= 92.87(4)°, monoclinic system, space group P2<sub>1</sub>/c, R = 0.0809; (III): C<sub>15</sub>H<sub>11</sub>N<sub>1</sub>O<sub>3</sub>, a = 4.7580(9), b = 6.096(1), c = 10.658(2) Å, α = 95.807(2)°, β = 90.482(2)°, γ = 96.397(2)°, triclinic system, space group P1, R = 0.0492; (IV): C<sub>13</sub>H<sub>10</sub>O<sub>3</sub>, a = 3.9530(9), b = 14.583(2), c = 17.893(5) Å, monoclinic, space group P2<sub>1</sub>/n, R = 0.0527; (V): C<sub>15</sub>H<sub>12</sub>O<sub>2</sub>, a = 12.641(1), b = 12.066(2), c = 7.813(1) Å, β = 101.278(9)°, monoclinic system, space group P2<sub>1</sub>/c, R = 0.0820; (VI): C<sub>15</sub>H<sub>12</sub>O<sub>2</sub>, a = 6.822(2), b = 10.474(4), c = 17.097(2) Å, α = 73.88(2), β = 84.29(2), γ = 87.66(3)°. Triclinic, space group P-1, R = 0.0701; (VII): C<sub>15</sub>H<sub>11</sub>NO<sub>3</sub>, a = 6.299(3), b = 13.226(3), c = 14.809 Å, β = 99.73(9)°, monoclinic system, space group P2<sub>1</sub>/c, R = 0.0660. The nature of the hydrogen bonds observed in the crystal structure was theoretically investigated using Gaussian03 suite of program.

This work was partially financed by CNPq, PrP/UEG and FUNAPE/UEG.

**10.01.10 Neutron Diffraction Characterization of Hydrogen in Transition Metal Complexes.** P.M.B. Piccoli<sup>a</sup>, J.A. Cowan<sup>a</sup>, A.J. Schultz<sup>a</sup>, T.F. Koetzle<sup>a</sup>, C. Hoffmann<sup>b</sup>, <sup>a</sup>IPNS, Argonne National Laboratory, Argonne, IL 60439, <sup>b</sup>SNS, Oak Ridge National Laboratory, Oak Ridge, TN 37831.

With the ability to accurately locate light atoms in the presence of heavy atoms, neutron diffraction is a unique tool for probing fundamental research questions involving the molecular structure of materials containing hydrogen. We will present recent results in which neutron diffraction has played a key role in determining the structure and bonding of hydrogen in transition metal coordination and cluster complexes. Data were obtained at the Intense Pulsed Neutron Source with the time-of-flight Laue single-crystal diffractometer with two position-sensitive area detectors. Materials studied include: dinickel hydride complexes with unsupported linear Ni–H–Ni bonds,<sup>1,2</sup> terminal mono-oxo platinum and gold complexes with polyoxo-tungstate ligands,<sup>3</sup> and a catalytic intermediate in the dehydrogenation of ammonia borane.<sup>4</sup> Additionally a new single crystal diffractometer with the capability to greatly impact future research, currently under construction at the Spallation Neutron Source at ORNL, will be described. This new instrument, named TOPAZ, will have multiple area detectors and will be capable of obtaining data from “X-ray size” crystals.

Work at ANL was supported by the DOE/OS/BES under contract DE-AC02-06CH11357.

(1) Vivic, D. A.; Anderson, T. J.; Cowan, J. A.; Schultz, A. J. *J. Am. Chem. Soc.* 2004, *126*, 8132.

(2) Tyree, W. S.; Vivic, D. A.; Piccoli, P. M. B.; Schultz, A. J. *Inorg. Chem.* 2006, *45*, 8853.

(3) Anderson, T. M.; Neiwert, W. A.; Kirk, M. L.; Piccoli, P. M. B.; Schultz, A. J.; Koetzle, T. F.; Musaev, D. G.; Morokuma, K.; Cao, R.; Hill, C. L. *Science* 2004, *306*, 2074.

(4) Denney, M. C.; Pons, V.; Hebden, T. J.; Heinekey, D. M.; Goldberg, K. I. *J. Am. Chem. Soc.* 2006, *128*, 12048.

**10.01.11 New Chemistry and New Magnets from Small-Molecule Structures.** Joel S. Miller, Dept. of Chemistry, Univ. of Utah, Salt Lake City, UT 84112-0850 USA.

Several examples where the results a single crystal structural determination has lead to new chemical insight and new chemistry will be discussed. Examples will include [(TPyA)Co(CA)Co(TPyA)]<sup>z+</sup> [z = 1+, 2+, 3+, 4+] where oxidation from z = 2+ to 3+ leads to the reduction of the CA<sup>2-</sup> bridging ligand to CA<sup>3-</sup> for this valance ambiguous compound. The perplexing photodecomposition reaction of [Mn<sup>IV</sup>(CN)<sub>6</sub>]<sup>2-</sup> lead to the formation of two compounds, whose identities could not be rationalized via spectroscopic analysis. Their structural determinations revealed most unexpectedly the organic species [C<sub>12</sub>N<sub>12</sub>]<sup>2-</sup> and the first and sub-hexacoordinate transition metal percyanide, namely, [Mn<sup>II</sup>(CN)<sub>4</sub>]<sup>2-</sup>. The latter led to a new type of Prussian blue structured materials with tetrahedral, not octahedral

metal sites. Here the strong-field CN<sup>-</sup> stabilizes high spin Mn<sup>II</sup>. Again structural determinations have led us identify species such as high spin [Cr<sup>II</sup>(CN)<sub>5</sub>]<sup>3-</sup> and another isomer of [C<sub>12</sub>N<sub>12</sub>]<sup>2-</sup> {and [C<sub>18</sub>H<sub>6</sub>N<sub>6</sub>]<sup>2-</sup>}. Structural determinations have also been essential in the area do developing and understanding molecule-based magnets, and several examples will be discussed. Finally, two examples where crystal structures revealed that our chemistry was wrong, and that we had to rethink and change course in our research will be discussed.

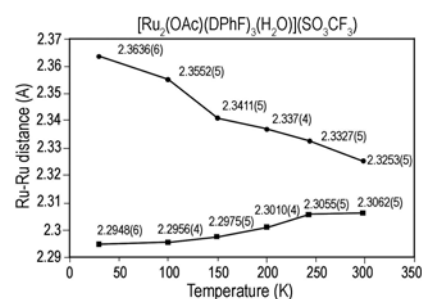
We thank the numerous crystallographers that have and continue to make major contributions to this work that include, A.M. Arif, J.C. Calabrese, R.L. Harlow, J.-H. Her, A.L. Rheingold, P.W. Stephens among others as well as the continued partial support by the DO DMS (Grant #DE-FG03-93ER45504 and #DE-FG02-01ER45931), the NSF (Grant #0553573), and the AFOSR (Grant No. F49620-03-1-0175).

**10.01.12 F. Albert Cotton (1930-2007) and the Development and use of Chemical Crystallography.** Larry R. Falvello.

**10.01.13 Electronic Structure from Changes in Metal-Metal Bond Distances Using Variable Temperature Crystallography.** Carlos A. Murillo, Texas A&M Univ., College Station, TX 77842.

Diruthenium paddlewheel compounds of the type Ru<sub>2</sub>(bridging ligand)<sub>4</sub>(L<sub>ax</sub>)<sub>m</sub>, where the number of axial ligands, L<sub>ax</sub>, could be 0, 1 or 2 which have Ru<sub>2</sub><sup>n+</sup> cores, n = 4, 5, 6, present a special challenge for the determination of the electronic structures, which cannot often be sorted out from magnetic measurements. For example, when n = 6, the core has a total of 10 electrons capable of participating in metal–metal bonding. Eight of the 10 electrons are in bonding molecular orbitals (MOs) occupying the σ<sup>2</sup>π<sup>4</sup>δ<sup>2</sup> core (Q<sup>8</sup>). The two additional electrons are in antibonding MOs. Because the δ\* and π\* MOs are usually close in energy determination of the ground state may be ambiguous even when the molecule is diamagnetic at low temperature which might appear to favor a Q<sup>8</sup>δ\*<sup>2</sup> configuration. Here we will show that variable temperature (VT) crystallography can be used to sort out changes in electronic configurations and the effect of zero-field splitting in this Ru<sub>2</sub> compounds.

Results will also be shown for Ru<sub>2</sub><sup>5+</sup> species whose electronic structures have been difficult to determine unambiguously. For these 11-electron species the variation of the Ru–Ru bond distances with changes in temperature allows unambiguous determination of the electronic structure.



Finally an example of a cationic species having two crystallographically independent molecules will be presented. These species have three bridging DPhF groups ((C<sub>6</sub>H<sub>6</sub>N)<sub>2</sub>CH<sup>-</sup>) and one carboxylate group and they differ by having minute differences in Ru–water<sub>ax</sub> distances. These two crystallographically independent, but chemically equivalent species at room temperature, exhibit a remarkable change in Ru–Ru bond distances between 298 and 27 K (see figure) which is consistent with a change in electronic structure as the temperature is varied.

**10.01.14 Non-traditional Bonding Interactions via Experimental Charge Density.** Lee M. Daniels<sup>1</sup>, T. Stanley Cameron<sup>2</sup>, Joseph D. Ferrara<sup>1</sup>, <sup>1</sup>Rigaku Americas Corp., 9009 New Trails Dr., The Woodlands, TX 77381 USA, <sup>2</sup>Dept. of Chemistry, Dalhousie Univ., Halifax, Nova Scotia, Canada B3H 4J3.

Years ago, crystallography revolutionized a lot of thought about Important Science, and provided perhaps the most powerful tool for the study of chemical bonding. Precise positional information giving exact bond distances became routine; more recently advances in charge density studies have provided extensive views of bonding once available only in theory. Direct observation of covalent bonding is now possible, and extension of the analysis provides detailed information about *intermolecular* interactions. Using the criteria proposed by Koch and Popelier, a “bond path” can be constructed between any two atoms or groups in a structure, allowing one to distinguish “bonding” interactions from van der Waals contacts. In this work interactions such as H-H bonding, F-F bonding, I-S bonding, P-N ring bonding, etc. are considered.

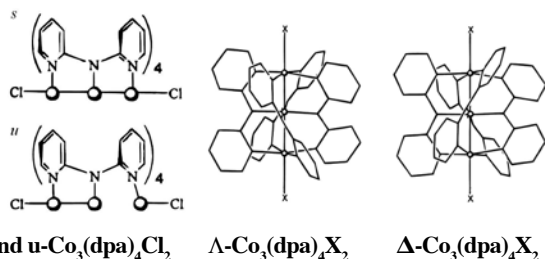
**10.01.15 Small Molecule Crystallography – Way More than Structure Determination.** A.A. Pinkerton, Dept. of Chemistry, Univ. of Toledo, Toledo, OH 43606 USA.

The advances made over the past few years in hardware and software for X-ray crystallography is impressive. By careful choice of hardware and software, it is possible to obtain diffraction data of a quality only previously dreamed of for anything other than the smallest of problems. An evaluation of the features of various hardware configurations and integration software will be provided. Examples will be given of electron density studies of “large” small molecules and of molecules with heavy elements. Evaluation of data quality based on the results of multipole refinements will be discussed.

This work is supported by the Office of Naval Research award N00014-07-1-0314.

**10.01.16 Finding Chiral Crystals in Racemic Mixtures – A Reflection on How to Get the Most From X-Ray Crystallography in the Laboratory for Molecular Structure and Bonding at Texas A&M University.** Xiaoping Wang, Dept. of Chemistry, Univ. of North Texas, Denton, TX 76203.

The tricobalt compound  $\text{Co}_3(\text{dpa})_4\text{Cl}_2$ , 1, (dpa = di(2-pyridyl)amide) can be isolated from the same solution as crystals in either symmetrical *s*- $\text{Co}_3(\text{dpa})_4\text{Cl}_2$  or unsymmetrical *u*- $\text{Co}_3(\text{dpa})_4\text{Cl}_2$  forms. An important feature in the class of  $\text{M}_3(\text{dpa})_4\text{X}_2$  compounds is their typical helical arrangement of the four dpa ligands about the  $\text{Co}_3$  unit. The isolated products usually consist of racemic mixtures of right- and left-handed species, and crystal structures have shown an equal number of molecules of each enantiomer. However, reaction of the linear tricobalt compound 1 with silver hexafluorophosphate in acetonitrile yields two polymorphs of  $[\text{Co}_3(\text{dpa})_4(\text{CH}_3\text{CN})_2][\text{PF}_6]_2$ , 2, namely, a monoclinic ( $P2_1$ ) form 2- $\text{CH}_3\text{CN}\cdot 2\text{Et}_2\text{O}$  and a triclinic ( $P\bar{1}$ ) form, 2- $3\text{CH}_3\text{CN}$ . Individual chiral crystals of either  $\Lambda$  or  $\Delta$  configurations in the monoclinic form were isolated by hand and their absolute structures were determined.[1] The results from X-ray



crystallography have made it possible to measure the CD spectra of both enantiomers and to assign each one to the correct enantiomers.

[1] Rodolphe Clerac, F. Albert Cotton, Kim R. Dunbar, Tongbu Lu, Carlos A. Murillo and Xiaoping Wang, *Inorg. Chem.* 2000, 39, 3065-3070.

## 10.02 Tricks of the Trade: Interpretation of Structural Results

**10.02.01 Is Small Molecule Crystallography Still Science?** Phillip Fanwick, Dept. of Chemistry, Purdue Univ., W. Lafayette, IN 47907-2084.

Since the first experiments, small molecule crystallography has been an important tool for chemical analysis and studies of the solid state. Today at 95 years old the technique is displaying all the signs of a mature science. Unfortunately, these include the use of preconceptions, past experiences, experts, and scholarship in accessing results and methods rather than a reliance on experimentation and science. This is having consequences on the use and growth of crystallography and the way procedures are carried out. In this presentation, hydrogen refinement, atomic displacement shapes and absorption correction will be used to illustrate the above statements.

**10.02.02 On the Correct Use of Incorrect Space Groups and Unit Cells.** Larry R. Falvello, Univ. of Zaragoza - C.S.I.C., Dept. of Inorganic Chemistry and Aragon Materials Science Inst., Plaza San Francisco s/n, E-50009 Zaragoza, Spain. falvello@unizar.es

Examples are given in which the use of space groups known to be incorrect is a decisive factor in structure solution or refinement. The use of a subgroup for initial structure solution, which occurs commonly, is shown to be useful for a high-symmetry, unknown structure with poorly defined lattice type and otherwise ambiguous systematic absences. Circumstances are described in which a structure is best refined and published using an incorrect space group, even though the correct space group can be established using diffraction data. Employing an incorrect unit cell -- incorrect and not just unconventional -- is shown to be useful in the context of the role of the unit cell as the crystal metric, in a case in which two different but related structures are being compared.

Research supported by the Ministry of Education and Science (Spain), Grant CTQ2005-03141.

**10.02.03 Multiple Component Twins: The Challenges of The Refinement of Problematic Data.** Victor G. Young, Jr., X-Ray Crystallographic Lab, Chemistry Dept., Univ. of Minnesota, 192C Kolthoff Hall, 207 Pleasant St. S.E., Minneapolis, MN 55455.

Non-merohedral twins involving two or more individuals pose numerous problems to the chemical crystallographer. The general perception is data taken from non-merohedrally twinned specimens is necessarily poorer than comparable data taken from single crystals. While it is generally more straightforward to process data taken from single crystals, ones usually pays little or no penalty for using data taken from twinned crystals when using modern software. There has been much discussion as to what data should be used for refinement of non-merohedral twins. This presentation will focus on the pitfalls chemical crystallographers face when confronted with these. The data one uses, whether it comes from the individual of largest mass or a sum of all individuals, affects the quality of the results. Data from reflections that are interfering, or partially overlapped with another individual, are the most problematic subclass. Consideration will be given to whether one should merge equivalent data or use data from

all individuals as independent data. The number of independent data used in least-squares refinement will affect the refinement residuals and standard uncertainties, so comparisons of these models will be made. Strategies for retaining the most significant data while assuring completeness will be presented.

**10.02.04 PLATON, A Set of Tools for the Interpretation of Structural Results.** A.L. Spek, National Single Crystal Service Facility, Bijvoet Center for Biomolecular Research, Utrecht Univ., The Netherlands. (<http://www.cryst.chem.uu.nl>)

The ideal world of a service crystallographer might look like: the diffractometer runs smoothly, the chemist knows what he has created, the (semi) automatic software produces a reasonably refined structure, leaving the analyst the task of checking and finishing off the details of the analysis, ready for publication. In the real world, a service crystallographer will have to address many, often time-consuming, issues such as poor crystal quality, real or artificial disorder, pseudo-symmetry, twinning, disordered solvents of unknown composition, large amounts of crystal water for which attached H-atom positions have to be found. The PLATON program incorporates numerous solutions for problems that we encountered over more than 35 years of experience in service crystallography. A number of recent examples will be presented.

**10.02.05 Elucidation of Disorder in a Crystal Structure.** Xiaoping Wang, Dept. of Chemistry, Univ. of North Texas, Denton, TX 76203.

The advances in instrumentation and crystallographic software have made it possible for a user to determine a crystal structure with minimum training in instrument and knowledge of crystallography. The user may then include the structural result in a publication after having it checked with the PLATON program.<sup>1</sup> Common mistakes in crystal structure determination such as missing symmetry can be detected directly with the available structural validation program and corrected with the highest possible symmetry.<sup>2</sup> What left for explanation in some cases is the molecules that are found disordered after high symmetry has been applied to the crystal structure. However, the appearance of disorder in a crystal structure may also be caused by an incorrect Bravais Lattice and by having the assigned symmetry too high. An example is given for the "disordered" structure of Ta(NMe<sub>2</sub>)<sub>5</sub>.<sup>3</sup> Analysis of this problematic structure will be presented.

[1] A.L. Spek, *J. Appl. Cryst.* 2003, 36, 7.

[2] R.E. Marsh, M. Kapon, S. Hu and F.H. Herbstein, *Acta Cryst.* B58, 2002, 62.

[3] A.S. Batsanov, A.V. Churakov, J.A.K. Howard, A.K. Hughes, A.L. Johnson, A.J. Kingsley, I.S. Neretin, K. Wade, *J. Chem. Soc., Dalton Trans.* 1999, 3867.

**10.02.06 Guest-induced Changes in Long-range and Local Order in Crystals of p-tert-butylcalix[4]arene.** G.D. Enright, D.H. Brouwer, I.L. Moudrakovski, K.A. Udachin, J.A. Ripmeester, Steacie Inst. for Molecular Sciences, National Research Council, Ottawa, ONT, Canada.

We use single crystal diffraction and NMR spectroscopy to follow the loading of xenon into p-tert-butylcalix[4]arene (tBC). Two distinct Xe-containing structures are identified and appear to coexist in separate domains of the same composite crystal. The loading of tBC can take a considerable length of time, however, crystal transformation continues long after the loading has finished. Hence the characterization results obtained for this material can be a function of time for weeks. The structures for the empty tBC lattice (**1**), a low-loaded (tBC:0.25Xe) inclusion (**2**) and a high-

loaded (tBC:0.50Xe) inclusion (**3**) have been determined. All the crystals examined had unit cells consistent with the same metrically-tetragonal unit cell. As with many tBC inclusions the structures were found to be best described in twinned monoclinic space groups. For **1** the structure was solved in space group P2<sub>1</sub>/n. Initial attempts at solving **2** and **3** in this space group were not satisfactory, particularly for crystals with increased guest occupancy, so recourse was taken to study the materials by <sup>129</sup>Xe and <sup>13</sup>C NMR spectroscopy. Novel double quantum filtered <sup>129</sup>Xe NMR spectroscopic techniques were used to reintroduce weak dipolar couplings between Xe guests in inequivalent sites in order to infer their relative separations in the different crystal environments. The dipolar coupling constants are among the smallest measured in molecular solids and were used to estimate intrapair Xe distances of ~ 6.5 – 8.5 Å. Based primarily on these results other possible space groups were examined for **2** and **3** and their structures were determined in the space group Pn with the additional complication of racemic twinning.

**10.02.07 Optimal Use of Measured Data to Determine the Absolute Configuration of Pharmaceutically Interesting Molecules.** Rob W.W. Hoofst<sup>a</sup>, Leo H. Straver<sup>a</sup>, Anthony L. Spek<sup>b</sup>. <sup>a</sup>Bruker AXS, PO Box 811, NL-2600 AV Delft, The Netherlands, <sup>b</sup>Bijvoet Center for Biomolecular Research, Utrecht Univ. Padualaan 8, NL-3584 CH Utrecht, The Netherlands.

To determine the absolute configuration of enantiopure compounds such as pharmaceuticals, most often the Flack *x* parameter [1] is refined in parallel with structural parameters. The obtained value and its standard deviation are subject of statistical analysis [2] to quantify the reliability of the absolute structure assignment.

We developed a more sensitive method to determine the absolute structure that assigns individual weights to each measured Bijvoet difference [3]. Our method includes a rigorous estimate of the reliability of the absolute structure assignment without assuming the Gaussian nature of the absolute structure parameter.

On all data sets we have used to test this method the standard uncertainty could be reduced by at least a factor of two relative to the standard uncertainty of the Flack *x* parameter. The validity of the smaller standard uncertainty was established by a statistical analysis. The smaller uncertainty makes reliable absolute structure assignments possible in cases where the Flack *x* analysis is not sufficient.

If good data can be measured, our method can be used to determine a trustworthy absolute structure using molybdenum K $\alpha$  radiation on structures containing only atoms not heavier than oxygen. A very reliable assignment was obtained from all tested data sets for equally light atom structures that were measured using copper K $\alpha$  radiation.

[1] Flack, H.D. (1983). *Acta Cryst.* A39, 876-881.

[2] Flack, H.D. & Bernardinelli, G. (2000). *J. Appl. Cryst.* 33, 1143-1148.

[3] Bijvoet, J.M., Peerdeman, A.F. & van Bommel, A.J., (1951) *Nature* 168, 271-272.

## 10.03 Supramolecular Chemistry

### 10.03.01 Solid-state Transformations of Metal Carboxylates.

Bruce M. Foxman, Benjamin M. Heyman, Jeremy B. Heyman, Dept. of Chemistry, Brandeis Univ., Waltham, MA 02454-9110.

Metal crotonate coordination compounds. (M = Li, Na, K, Rb, Mg, Ca) undergo chemo- and stereospecific solid-state reactions upon exposure to  $^{60}\text{Co}$   $\gamma$ -rays, resulting in formation of at least eight different products. The reactions include, but are not restricted to: linear dimerization and trimerization, cyclodimerization, thermal and radical ene dimerizations, and radiation-induced Michael additions. The Michael addition and cyclodimerization reactions appear to occur by the same mechanism. Using deuterium-labeled crotonic acid, we examined the direction of H atom transfer in the solid state. The presentation will review past work, including synthesis of different materials, the geometric aspects of H or D abstraction, and consistency (or apparent lack thereof) with topochemical ideas. With previous analyses in hand, we are in a position to study and analyze far more complex materials (e.g., potassium and rubidium acid salts) that produce mixtures of two, three or more products.

Very recently we have turned our attention to several long-standing problems in the crystallography of metal carboxylates. First, we have made excellent progress in uncovering the structures of the alkali metal acrylate and methacrylates that undergo solid-state polymerization upon  $^{60}\text{Co}$  irradiation. In the early 1960s, these materials were discovered by Herbert Morawetz and were among the early compounds used to formulate topochemical ideas for solid-state reactions. In particular, we note the unusual "magic" features of the structures of potassium carboxylates that help to promote solid-state reactivity. Second, we have solved the long-standing problem of disorder, polymorphism, phase transformations and radiation-induced annealing in diaquabis(2-hydroxy-2-methylpropionato)copper(II) first noted by Keith Prout in 1968. Finally, we have solved a decade-old problem in our own research: the radiation-induced twinning and solid-state reactivity of sodium hydrogen acetylenedicarboxylate dihydrate.

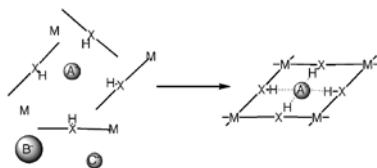
### 10.03.02 Coordination and Hydrogen-Bonded Frameworks for Anion Binding and Separation.

Radu Custelcean, Vincent Sellin, Bruce A. Moyer, Chemical Sciences Div., Oak Ridge National Laboratory, Oak Ridge, TN 37831 USA.

Design, synthesis, structural characterization, and anion separation properties of coordination and hydrogen-bonded frameworks functionalized with

hydrogen-bonding groups for selective anion binding will be presented. An important part of the presentation will focus on our recently articulated approach to anion separation, involving competitive crystallization of these functional solids from aqueous anionic mixtures. This process may result in selective inclusion of certain anions depending on their size, shape, or specific interactions with the crystalline frameworks. The key factors determining the anion selectivity in these supramolecular materials will be discussed.

This research was sponsored by the Division of Chemical Sciences, Geosciences, and Biosciences, Office of Basic Energy Sciences, U.S. Department of Energy, under contract number DE-AC05-00OR22725 with Oak Ridge National Laboratory, managed and operated by UT-Battelle, LLC.



### 10.03.03 Synthetic Protocols for the Assembly of Molecular Co-crystals.

Christer B. Aakeröy, Dept. of Chemistry, Kansas State Univ., Manhattan, KS, 66506, USA, aakeroy@ksu.edu

Recrystallization is an essential purification step carried out at some stage during a covalent synthetic procedure and is performed on a daily basis in almost every synthetic laboratory as a critical isolation step. Over 90% of all specialty chemicals – pharmaceuticals, agrochemicals, dyes, and sensor components – go through a recrystallization as part of their manufacture. Consequently, crystallization as a means of purification and isolation is crucial to synthesis and processing of a wide range of materials.

Within supramolecular chemistry, however, the very same event provides the practitioner with an opportunity to impart specific bulk physico-chemical properties to a crystalline material – a co-crystallization is a deliberate attempt at bringing together different molecular species within one periodic crystalline lattice without making or breaking covalent bonds. Co-crystals represent a hitherto untapped resource for new materials, but before such compounds reach maturity in terms of applications and devices, we need to develop reliable synthetic strategies for co-crystals and gain better control over the balance between re-crystallization and co-crystallization. It is important to note that co-crystallizations allow for synthesis to take place without making or even requiring any covalent changes to the participating species. This signifies a critical shift (from covalent to supramolecular) in terms of design and assembly of new functional materials and may offer new methods for optimizing bulk properties of any solid that derives its specific efficacy from a carefully, and often painstakingly, constructed molecular structure.

### 10.03.04 Phase- and Shape-Selective Synthesis and Crystallization of Solid-State Materials.

Kenneth M. Doxsee, Dept. of Chemistry, Univ. of Oregon, Eugene, OR 97403 USA.

Salt metathesis reactions represent a remarkably simple and versatile synthetic route to a wide variety of solid-state materials. Through the formation of soluble complexes, many salts serving as synthetic precursors for metal halides, chalcogenides, oxides, and carbonates, *inter alia*, may be brought into solution in nonaqueous solvents. Reaction crystallization with other salts results in the formation of solid-state materials, as in the case of aqueous metathesis reactions, but the effects of solvation and chelation on the morphology and phase of the crystalline products are often dramatic. Translation of salt metathesis reactions to the nonaqueous milieu through the intermediacy of soluble complexes offers promise for the facile preparation of metastable phases from simple precursors under ambient conditions.

### 10.03.05 The Ability of Lower Peptides to Form Co-crystals: Inclusion Compounds of the Tripeptide L-Leucyl-L-Leucyl-L-Leucine.

T.J. Burchell, D.V. Soldatov, G.D. Enright, J.A. Ripmeester, Steacie Inst. for Molecular Sciences, National Research Council Canada, Ottawa, Canada, K1A 0R6.

In recent years there has been growing interest in inclusion compounds of short oligopeptides (i.e. dipeptides or tripeptides) and many interesting helical or layered inclusions compounds have been obtained. This work focuses on the use of the tripeptide L-Leucyl-L-Leucyl-L-Leucine (LLL) as a host molecule for inclusion compounds. The LLL molecule is flexible and can adopt extended or helical conformations depending on the guest molecule or crystallization conditions. For example, when LLL is crystallized from water two polymorphs may be obtained depending on the rate of evaporation of water. One polymorph,  $\text{LLL} \cdot 1/2\text{H}_2\text{O}$ , has a double

helix structure while the other,  $LLL \cdot H_2O$ , forms an unusual twisted  $\beta$ -sheet structure with channels for the guest water molecules. Similar layered structures are formed with an alcohol-water mixture. LLL also forms layered inclusion compounds  $LLL \cdot P$  ( $P = Py, 2MePy, 3MePy, 4MePy$ ) with pyridine or methylpyridine as guest. In these compounds the LLL molecules form regular anti-parallel  $\beta$ -sheet structures with large channels that host the pyridine or methylpyridine guest molecules. Interestingly, crystals of the  $LLL \cdot P$  inclusions were invariably twinned and in most cases the host molecules (and sometimes guests) were also highly disordered.

**10.03.06 Insights into the Intercalation of Small Molecules into Hydrogen-bonded "Clay Mimics".** A.M. Beatty, Nilantha Bandara, Greg A. Hogan, Austin Pickett, Dept. of Chemistry, Mississippi State Univ., Mississippi State, MS 39762.

We have recently become interested in clay mimics because of their rich diversity of chemical applications. Clays, which are constructed from strong metal-oxide bonds, are known to intercalate or absorb gases, small molecules and ions, and thus serve as materials capable of storage, chemical separations, and catalysis. Our "clay mimics" comprise hydrogen-bonded organic and coordination complexes, and the sheet structure is maintained by (relatively weak) hydrogen bonds. We have been investigating the ability of these hydrogen-bonded layers to withstand the disruption caused by intercalation and/or loss of guest molecules, and we have some insights into how to achieve intercalation in hydrogen bonded solids.

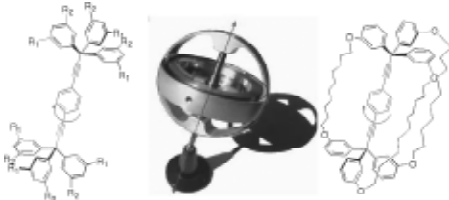
The synthesis and solid state structure of "clay mimics," both organic and inorganic, will be discussed. Results from intercalation studies for these hydrogen-bonded solids will also be shown in detail, with conclusions based on TGA and Powder XRD studies.

**10.03.07 Amphidynamic Materials: Steps Towards Controllable Inertial Motion in Crystalline Solids.** Miguel A. Garcia-Garibay, Steven D. Karlen, Jose E. Nuñez, Zachary O'Brien, Dept. of Chemistry & Biochemistry, U. of California, Los Angeles, CA.

Growing interest in the artificial molecular machinery<sup>1</sup> has recently led to the exploration and development of amphidynamic crystals,<sup>2</sup> a new class of functional materials with physical properties that may be modified by controlling their internal motion in the solid state.

Our contributions in this area have covered molecules with shapes and function analogous to those of macroscopic gyroscopes.<sup>1b,2</sup>

They consist of an intrinsically barrierless dialkynyl rotator that acts as the dynamic component, such as axially substituted 1,4-dialkynyl phenylenes (shown in red), and two triarylmethyl (trityl) or triptycyl groups that act as the stator (shown in blue). In our quest to design crystals with internal dynamics that approach gas phase frequencies and barriers, we have prepared and analyzed several molecular gyroscopes with novel high-symmetry rotators,<sup>3</sup> including structures with bicyclo[2.2.2]octanes, carboranes, cubanes and diamantanes, as well as structures with triply bridged and "exploded" stators.



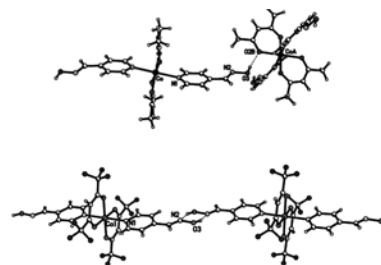
1. (a) Kottas, G. S.; Clarke, L. I.; Horinek, D.; Michl, J. *Chem. Rev.* 2005, 105, 1281. (b) Khuong, T.-A.; Nuñez, J. E.; Godinez, C. E.; Garcia-Garibay, M. A. *Acc. Chem. Res.* 2006, 39, 413.

2. (a) Garcia-Garibay, Miguel A. *Proc. Natl. Acad. Sci.* 2005, 102, 10771-10776; (b) Karlen, Steven D.; Garcia-Garibay, Miguel A. *Topics Curr. Chem.* 2006, 262, 179.

3. Karlen S. D.; Ortiz, R.; Chapman, O. L.; Garcia-Garibay, M. A. *J. Am. Chem. Soc.*, 2005, 127, 6554.

**10.03.08 Tuning Intermolecular Interactions in H-bonded Coordination Compound Networks.** J. Valdés-Martínez<sup>a</sup>, J. M. Germán-Acacio<sup>a</sup>, S. Hernández-Ortega<sup>a</sup>, Christer B. Aakeröy<sup>b</sup>, John Desper<sup>b</sup>, <sup>a</sup>Inst. de Química, Univ. Nacional Autónoma de México, México DF, 04510, México, <sup>b</sup>Dept. of Chemistry, Kansas State Univ., Manhattan, Kansas 66506, USA.

Crystal Engineering has focused mainly on the syntheses of extended organic networks or transition-metal based coordination polymers. The construction of inorganic-organic hybrid materials with intermolecular forces has been less studied. The synthetic tools available for the construction of such assemblies are non-covalent interactions, many of which are poorly understood and difficult to calculate and measure. Consequently, controlling the properties of a solid through precise control over its crystal structure or principal structural motifs is a formidable task. We have demonstrated that isonicotinamide is a very effective supramolecular reagent for the construction of infinite 1-D metal-containing motifs. While extending our studies to the analog 4-pyridinealdoxime coordinated to  $[M(acac)_2]$  complexes, with  $M = Ni(II)$  and  $Co(II)$ , we found that instead of the expected oxime...oxime interaction a H-bond between the oxime and the coordinated acac was favored. Nevertheless we were able, through electronic effects on the acac ligand, to favor the oxime...oxime interaction being able with this to tune the supramolecular interaction.



**10.03.09 Considerations for the Design of Complex Modular Solids.** John C. MacDonald<sup>1</sup>, Mehmet V. Yigit<sup>1</sup>, Yu Wang<sup>1</sup>, Lisa S. Lee<sup>1</sup>, G. Tayhas R. Palmore<sup>2</sup>, T.-J. Mark Luo<sup>3</sup>, Brian Moulton<sup>4</sup>, Brian S. Luisi<sup>4</sup>, Dept. of Chemistry & Biochemistry, Worcester Polytechnic Inst., Worcester, MA 01609<sup>1</sup>, Div. of Engineering, Brown Univ., Providence, RI 02913<sup>2</sup>, Materials Science & Engineering, North Carolina State Univ., Raleigh, NC 27695<sup>3</sup>, Dept. of Chemistry, Brown Univ., Providence, RI 02913<sup>4</sup>.

We are interested in molecular self-assembly as a means to fabricate open molecular frameworks with the goal of developing porous crystalline materials that feature interchangeable molecular components. Such modular solids offer structural advantages in that a given architecture can be achieved using a range of building blocks, as well as functional advantages whereby the properties of the material can be changed without significantly altering the crystal structure. Polyfunctional molecules that self-assemble both via coordination to metal ions and hydrogen bonding are attractive building blocks because they form frameworks with 1-D, 2-D and 3-D architectures that depend on the geometry and placement of functional groups. The design, structures and properties of crystalline solids prepared from carboxyimidazoles and carboxypyridines will be presented along with insights into the design of crystals with complex composition.

**10.03.10 Crystal Porosity: Discovery and Design.** L.J. Barbour, L. Dobrzańska, T. Jacobs, Dept. of Chemistry, Univ. of Stellenbosch, 7602 Stellenbosch, South Africa.

Over the past decade the study of porous crystalline solids has become highly topical, especially with regard to potentially important applications such as gas storage, separation and sensing. Well-known systems include zeolites and metal-organic frameworks and, to a lesser extent, organic molecular crystals. However, discrete metal complexes have received little attention as components of porous materials.

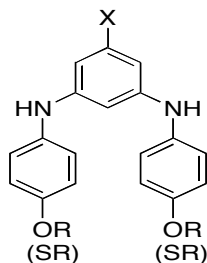
One of the basic tenets of the solid state is that molecules tend to pack closely, thus affording minimal free space at the molecular scale. We are attempting to overcome this tendency by designing simple complexes that cannot pack efficiently without including solvent molecules. Indeed, we are specifically interested in forming solvent-templated complexes that do not collapse upon subsequent solvent removal. We have recently discovered several systems that behave in this manner; some of these structures can be considered to be porous in the conventional sense, but we have also noted that conventional porosity is not a prerequisite for mass transport in the solid state. These systems have now been studied using a variety of complementary techniques, including X-ray diffraction, isothermal gas sorption and molecular modeling. Non-conventional use of these techniques has enabled us to gain a deep understanding of the relationship between structure and gas sorption dynamics.

**10.03.11 Do “Clay Mimics” Mimic Clays?** Greg A. Hogan, Alicia M. Beatty, Dept. of Chemistry, Mississippi State Univ., Mississippi State, MS 39762.

Clays and other layered materials are known to intercalate small molecules or ions. We have synthesized a series of layered hydrogen-bonded inorganic/organic hybrid material, and we now wish to determine if the hydrogen-bonded layers hold together during intercalation. In other words, can our “clay mimics” mimic clays? Our layered materials/hydrogen-bonded clay mimics are created from metal-containing dicarboxylic acid and organic amines. Varying the amine allows us to vary the interlayer spacing. The transition metal ion of our layer component contains two axial water ligands, which we predict can be replaced by various Lewis bases, such as pyridine. To study the ability of our material to intercalate, we sonicated our ionic solids in hydrocarbon solution containing the Lewis bases. To determine if the Lewis bases are transported into the solid and replace the axial water ligand, the samples will be characterized by TGA, IR, UV-Vis, and powder XRD.

**10.03.12 Polar Lattices of Aryl Diamines. A New Synthon for Dipolar Alignment in Organic Aryl Amine Crystals.** S.C. Blackstock, L.T. Gray, J.R. Duncan, L.T. Kyser, Dept. of Chemistry, Univ. of Alabama, Tuscaloosa, AL, 35487 USA.

Devising new methods for dipolar alignment in molecular crystals is an active area of crystal engineering. Special supramolecular forces are normally required to offset a general tendency for electronic cancellation of molecular dipoles in crystal packing. This presentation will describe a set of aryl diamines which assemble naturally into polar lattices. By altering various regions of the molecular structure, we have probed the molecular structure features which influence the dipolar alignment in the lattice and have tested the general viability of this synthon for polar assembly.



Hydrogen bonding between diamines plays an important role in the 2D molecular assembly process and the resultant electronic features of the crystal lattices. The X and OR groups may be varied to change the magnitude of the molecular dipole without significantly altering the molecular packing in the lattice.

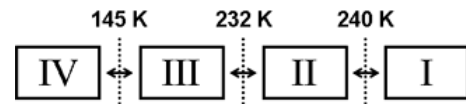
We thank the National Science Foundation (CHE and DMR) for support of this work.

## 10.04 Cool Structures

**10.04.01 [Ni(MeCN)(H<sub>2</sub>O)<sub>2</sub>(NO<sub>3</sub>)<sub>2</sub>](15-crown-5)·MeCN: Another Polymorphic System With an Intermediate, High-Z' Phase.** M.A. Siegler, S. Parkin, C.P. Brock, Dept. of Chemistry, Univ. of Kentucky, Lexington, KY, 40506 USA.

Previous studies<sup>1,2</sup> of the series of the compounds  $[M(H_2O)_2(15\text{-crown-5})(NO_3)_2]$ ,  $M = \text{Mg, Mn, Fe, Co, Cu}$  and  $\text{Zn}$  described a rich polymorphic system. In the course of synthesizing the analogous Ni complex, which took considerable effort to make, the compounds  $[Ni(H_2O)_6](NO_3)_2 \cdot (15\text{-crown-5}) \cdot 2H_2O$  and  $[Ni(MeCN)(H_2O)_2(NO_3)_2] \cdot (15\text{-crown-5}) \cdot MeCN$  were produced as well. Careful investigations have showed that the two latter compounds are similar polymorphic systems with an intermediate, high-Z' phase.

Four phases of  $[Ni(MeCN)(H_2O)_2(NO_3)_2] \cdot (15\text{-crown-5}) \cdot MeCN$  were found between 90 and 273 K: the ordered phase IV ( $P1$  bar,  $Z' = 2$ ) is stable below 145 K, the mostly ordered phase III ( $P2_1/c$ ,  $Z' = 1$ ) is stable between 145 and 232 K, the disordered phase II ( $B2_1$ ,  $Z' = 5$ ), which is a commensurately modulated structure, is stable between 232 and 240 K and the more disordered phase I ( $P2_1/m$ ,  $Z' = 1/2$ ) is stable above 240 K. All solid-solid phase transitions are reversible without any significant loss of crystallinity. The phase transition I  $\leftrightarrow$  III occurs with the intermediate phase II. The phase sequence was characterized by using differential scanning calorimetry, measuring the temperature dependence of the cell dimensions and inspecting the reconstructed reciprocal lattice slices near the temperatures of the phase transitions.



Comparisons in the phase sequence of the compounds  $[Ni(H_2O)_6](NO_3)_2 \cdot (15\text{-crown-5}) \cdot 2H_2O$  and  $[Ni(MeCN)(H_2O)_2(NO_3)_2] \cdot (15\text{-crown-5}) \cdot MeCN$  will be discussed.

- Hao, X.; Parkin, S.; Brock, C. P. *Acta Cryst.* 2005, *B61*, 675-688.
- Hao, X.; Siegler, M. A.; Parkin, S.; Brock, C. P. *Cryst. Growth Des.* 2005, *5*, 2225-2232.
- $[Ni(H_2O)_6](NO_3)_2 \cdot (15\text{-crown-5}) \cdot 2H_2O$ : An Uncommon Polymorphic System. M.A. Siegler, X. Hao, S. Parkin, C.P. Brock. ACA meeting, Honolulu, Hawaii, USA, 2006.

**10.04.02 Structures of Amyloid-like Fibrils Suggest Seven Distinct Classes of the Steric Zipper Motif.** M.R. Sawaya, S. Sambashivan, R. Nelson, M. Ivanova, S.A. Sievers, M.I. Apostol, M.J. Thompson, M. Balbirnie, J.J.W. Wiltzius, H. McFarlane, A. Ø. Madsen, C. Riek, D. Eisenberg. Univ. of California, Los Angeles, UCLA-DOE Laboratory of Structural Biology and Molecular Medicine, Box 951570 UCLA, Los Angeles, CA 90095-1570.

Extracellular protein fiber deposits are a characteristic feature of about 25 different human diseases known collectively as amyloid disease. Well known examples include Alzheimer's disease and type II diabetes. These fibers are composed predominantly of a single type of protein, the identity of which depends on the disease. Fiber diffraction studies reveal that regardless of their source, all amyloid fibers share a common cross- $\beta$  structure in which two or more  $\beta$ -sheets pack together with their strands running perpendicular to the fiber axis. Structural studies of amyloid fibers are only now beginning

to provide an understanding of their assembly and hopefully will ultimately lead to a means for obtaining their disassembly. One structural motif, the steric zipper, has recently been proposed to be a defining feature of amyloid fibers. The proposal is based on the crystal structure of a seven residue segment derived from the prion determining domain of yeast sup35. In this structure, two parallel  $\beta$ -sheets are packed face-to-face with their side chains tightly enmeshed, so that water is excluded from the sheet-sheet interface. Since this publication, over a dozen new peptide structures have been determined, derived from various amyloidogenic proteins. They have revealed four out of a total of seven possible geometrically distinct classes of steric zippers in which the sheets may be (1) either parallel or antiparallel, (2) either packed face-to-face or face-to-back, and (3) either packed with a relative up-down or up-up orientation.

**10.04.03 Influence of the Asymmetric Binding Modes of the Azido-bridged Cu(II) Compounds in the Crystals Structures.** J.G Ferreira<sup>1</sup>, R.H.A. Santos<sup>1</sup>, A.E. Mauro<sup>2</sup>, F.C. Andrade<sup>2</sup>, Legendre A.O.<sup>2</sup>, Ananias S.R.<sup>2</sup>, <sup>1</sup>IQSC-USP, São Carlos-S.P., Brazil, <sup>2</sup>IQ-UNESP, Araraquara-S.P., Brazil.

In an unique reaction were obtained two complexes of copper(II) azide with N,N- dimethylethylenediamine (N,N-dimen) as ligand have been characterized by X-ray crystallography. The crystal structure of di- $\mu$ (1,1)-azido-bis[azido(N,N-dimethylethylenediamine);copper(II)] (**1**) consists of centrosymmetric dimeric units, in which the Cu atom is penta-coordinated, using two nitrogen atoms of the N,N-dimen, two nitrogen atoms of two N<sub>3</sub> bridging ions and one nitrogen atom of another terminal azido ion. In the crystal structure of catena- $\mu$ (1,3)-azido- $\mu$ (1,1)-azido-bis[azido(N,N-dimethylethylenediamine);copper(II)] (**2**) the Cu(II) has a distorted square pyramidal coordination geometry, with [CuN<sub>3</sub>(N,N-dimen)]<sub>n</sub> moieties containing: terminal azido ligands in which the metal ion is alternatively bridge by end-to-end and end-on azido bridges, given rise to a one-dimensional polymer. Although the polyhedron coordination around the copper(II) ions can be considered quite similar, distorted square-planar, in both compounds, the binding features of the azido group are the major responsible for the formation of the dinuclear **1** and polinuclear **2** species.

The crystal packing of **1** and **2** showed the existence of intramolecular hydrogen bonds. It should be noted that in compound **1** the hydrogen-bonding interactions also play a vital role in the solid-state structure of this compound, in which, each terminal azide forms a hydrogen bond with the N,N-dimen of adjacent molecule, yielding a 2D supramolecular assembly. In compound **2** there are no specific direction of interactions between adjacent chains.

**10.04.04 A Solid-State Search for Structure-Organizing Halogen-Nitrile Contacts in "Bridge-Flipped" Isomeric Benzylideneanilines.** W.H. Ojala, K.M. Lystad, B. Balidemaj, T.K. Deal, J.E. Engebretson, Chemistry Dept., Univ. of St. Thomas, St. Paul, MN 55105 USA, C.R. Ojala, Chemistry Dept., Normandale Community College, Bloomington, MN 55431 USA.

We describe as "bridge-flipped isomers" those molecules that differ in structure only in the orientation of a bridge of atoms connecting two major portions of the molecule, as among the benzylideneanilines: Ar-CH=N-Ar' vs. Ar-N=CH-Ar' (Ar = aryl). Co-crystallization of isostructural isomers may yield solid solutions with properties that could be modified systematically by varying the proportions of co-crystallized compounds. Isostructuralism between isomeric benzylidene-anilines bearing both a nitrile group and a halogen atom might be encouraged by Lewis base-Lewis acid C $\equiv$ N:---X contacts linking molecules into similar chains. In earlier work we

determined the crystal structures of two pairs of bridge-flipped benzylideneanilines from the *ortho*-cyano-*para*-halogen series, the fluoro and chloro derivatives; we now have determined the crystal structures of the bromo isomers and of one of the iodo isomers. None of the bridge-flipped isomeric pairs are isostructural thus far. Significantly, in accord with the weakness of fluoro, chloro, and bromo substituents as Lewis acids, there are no close halogen-nitrile contacts in these structures; however, the iodo-nitrile benzylideneaniline we have examined does possess them. We are attempting to crystallize the remaining iodo-nitrile isomer to determine whether a similar contact in this last benzylideneaniline of the series would compel this compound to crystallize in a packing arrangement identical to that of its isomer.

Acknowledgment is made to the Donors of the American Chemical Society Petroleum Research Fund for support of this research.

**10.04.05 Gold Monomers, Dimers and Trimers; All in One Structure!** Christine M. Beavers, Marilyn M. Olmstead, Dept. of Chemistry, Univ. of California, Davis, CA 95616.

Aurophilic interactions are well known in linear gold(I) compounds. These interactions create interesting structural motifs such as extended linear chains, discrete dimers or trimers. They are much more common in cationic gold(I) complexes. Anionic gold(I) compounds are less likely to aggregate, due to Coulombic repulsion, and are usually surrounded by cations in the solid state. This trend can be altered if the anionic gold(I) center is [Au(CN)<sub>2</sub>]<sup>-</sup>. Dicyanoaurate is a versatile anion in that it can act as a ligand in the presence of transition metals and other cations, but it can also hydrogen bond. This enables the dicyanoaurate to form coordination polymers and, in the right circumstances, aurophilic interactions. In the structure of [Ba(diaza-18-crown-6)][Au(CN)<sub>2</sub>]<sub>2</sub>, monomers, dimers and trimers are all present within a three dimensional coordination polymer.

**10.04.06 Control, Prediction and Rationalization of Packing Motifs: Predicted and Observed Structures of Carbamazepine and Some of its Analogues.** F.P.A. Fabbiani,<sup>a\*</sup> A. Johnston,<sup>b</sup> A.J. Florence,<sup>b</sup> K. Shankland,<sup>a</sup> N. Shankland,<sup>b</sup> C.K. Leech,<sup>a</sup> H. Nowell<sup>c</sup>, S.L. Price<sup>d</sup> <sup>a</sup>ISIS Neutron Facility, STFC, UK, <sup>b</sup>Inst. of Pharmacy and Biomedical Sciences, Univ. of Strathclyde, UK; <sup>c</sup>Diamond Light Source Ltd, UK; <sup>d</sup>Dept. of Chemistry, Univ. College London, UK. F.P.A.Fabbiani@rl.ac.uk

The ultimate goal of research in the field of polymorphism is the ability to control and predict the occurrence of crystal structures, particularly in respect of the preparation of specific polymorphs of drug substances with desirable physicochemical properties.

We present here the results of an automated parallel crystallisation search for the physical forms of the antiepileptic drug carbamazepine.<sup>1</sup> We also illustrate how careful analysis of the packing motifs exhibited by the known polymorphs of the drug, in conjunction with structural information extracted from a computational search, have lead us to the discovery of the first catameric configuration of the molecule in a novel 1:1 solid solution of carbamazepine:dihydrocarbamazepine.<sup>2</sup> The subtle relationships between the structures of carbamazepine and some of its analogues are illustrated and rationalised using Hirshfeld surfaces and 2D fingerprint plots,<sup>[3]</sup> which are valuable tools for visualising and analysing intermolecular interactions in polymorphs, making the task of polymorph comparison easier and faster.<sup>3,4</sup>

<sup>1</sup>A.J. Florence, A. Johnston, S.L. Price, H. Nowell, A.R. Kennedy and N. Shankland, *J. Pharm. Sci.*, 2006, 95, 1918.

<sup>2</sup>A.J. Florence, C.K. Leech, N. Shankland, K. Shankland and A. Johnston, *CrystEngComm*, 2006, 8, 746.

<sup>3</sup>J.J. McKinnon, M.A. Spackman, A.S. Mitchell, *Acta Crystallogr., Sect B*, 60, 2004, 627-668.

<sup>4</sup>J.J. McKinnon, F.P.A. Fabbiani, M.A. Spackman, *Cryst. Growth Des.*, 2007, 7(4), 755-769.

## 13.01 Advances in Data Collection

**13.01.01 Tackling Large Proteins: Lessons Learned from a Decade of RNA Polymerase II Crystallography.** David A. Bushnell, Ken D. Westover, Dong Wang, Guillermo Calero, Henrik Spahr, Roger D. Kornberg, Structural Biology, Stanford Univ., Stanford, CA.

RNA polymerase II (Pol II) is a half megaDalton complex comprised of 12 subunits and more than 4500 amino acids. Over the course of more than a decade of effort Pol II diffraction improved from 20 angstroms to 2.3 angstroms, with more than 10 different unit cells ranging from a small of 123,223,379 Å I222 to a large of 212, 217,423 Å P222. Many of the obstacles overcome in this journey were not atypical of many protein crystallography projects, save in scope. Heterogeneity of purified complexes, crystal non-isomorphism, inadequate crystal size and of course phasing were just some of the problems faced. Improvements in computational methods, beamline intensities and crystals all contributed to the eventual solution of Pol II.

**13.01.02 Data Collection Strategies for Ultra-High Resolution X-rays at 15K and Neutron Diffraction at 293K: The Fully Deuterated *h*-Aldose Reductase Case.** A. Mitschler<sup>1</sup>, S. Ginell<sup>2</sup>, A. Joachimiak<sup>2</sup>, M. Blakeley<sup>3</sup>, F. Meilleur<sup>3\*</sup>, I. Hazemann<sup>3</sup>, D. Myles<sup>4\*</sup>, A. Podjarny<sup>1</sup>, IGBMC, CNRS, ULP, INSERM, Illkirch, France, <sup>2</sup>SBC, ANL, Argonne, IL, USA, <sup>3</sup>ILL, Grenoble, France, <sup>4</sup>EMBL Grenoble Outstation, ILL, Grenoble, France, \*Current address: ORNL, Oak Ridge, TN, USA.

The stringent experimental requirements needed for obtaining high quality X-ray diffraction data at subatomic resolutions (< 1Å) are described for 1) crystal quality, 2) state-of-the-art synchrotron beamline and 3) data collection strategy to minimize radiation-induced damage. The use of a Helium cryostat has proved to be a promising additional tool. As an example, we will describe how data collection of fully deuterated *h*-Aldose-Reductase crystals has met these requirements. This data collection was performed at SBC-APS (Temp:15K, resolution 0.8Å, mosaicity 0.2°, R-merge 2.3%, refinement R-Factor 11.5%). We shall also describe the neutron diffraction data collection at 2.2Å resolution with a radically small crystal (0.15 mm<sup>3</sup>) at ILL, Grenoble. Neutron diffraction provides a powerful tool for protonation analysis despite its specific difficulties (e.g., the need of large crystals), and has the advantage of the absence of any detectable radiation damage at room temperature.

The enzymatic mechanism of Human Aldose Reductase (*h*-AR) includes a hydride donation from the coenzyme NADPH and a proton donation from the enzyme. The X-Ray and neutron joint refinement, using the data described above, has enhanced the visibility of a mobile catalytic proton between Asp43 and Lys77 - Tyr48 and led to a new model of the catalytic reaction.

**13.01.03 Breakthrough in Amyloid-like Segment Structure Determination by using ESRF Microfocus Beamline.** Magdalena I. Ivanova<sup>1\*</sup>, M.R. Sawaya<sup>1\*</sup>, S. Sambashivan<sup>1\*</sup>, R. Nelson<sup>1\*</sup>, S.A. Sievers<sup>1</sup>, M.I. Apostol<sup>1</sup>, M.J. Thompson<sup>1</sup>, M. Balbirnie<sup>1</sup>, J.J.W. Wiltzius<sup>1</sup>, H. McFarlane<sup>1</sup>, A.Ø. Madsen<sup>2,3</sup>, C. Riekel<sup>3</sup>, D. Eisenberg<sup>1</sup>, <sup>1</sup>H. Hughes Medical Inst. UCLA-DOE Inst. of Genomics & Proteomics, Los Angeles, CA USA, <sup>2</sup>Centre for Crystallographic Studies, Dept. of Chemistry, Univ. of Copenhagen, Denmark, <sup>3</sup>European Synchrotron Radiation Facility, Grenoble, France, \*These authors have made equivalent contributions.

Many proteins aggregate into amyloid fibrils associated with diseases such as Alzheimer's, Parkinson's and prion diseases. These

depositions of different proteins share many similarities: elongated unbranched fibrils, Congo red and ThioflavinT binding and 'cross-β' X-ray diffraction patterns. Aided by bioinformatic algorithms, we characterized many peptide segments from disease-related proteins to be amyloid-like.

Structure determination of the amyloid-like segments was hindered by the size of the crystals. In concentrated solutions, most of these amyloid-like segments form mixtures of fibrils and needle-shaped microcrystals. The microcrystals grew to various lengths, but rarely exceeded 2x2µm in cross section. The breakthrough in data collection and structure determination became possible due to the availability ESRF microfocus beamline ID13 in France.

To date we have determined the structures of two dozen amyloid-like segments. It became evident that molecules of the amyloid-like segments are arranged in a pair of β-sheets interdigitating into a dry 'steric zipper'. Based on these structures, we also propose that the amyloid fibrils are formed by core residues which pack in a dry 'steric zipper' and the rest of the protein residues adopt either native-like or unfolded conformations. Thus, the knowledge of amyloid-like peptide structures can give us a better understanding of molecular mechanisms of many neurodegenerative diseases.

**13.01.04 Phasing Macromolecular Structures with UV-induced Structural Changes.** Max Nanao, Raimond Ravelli, Structural Biology, Exelixis, S. San Francisco, CA 94083.

Recently, it was demonstrated that intensity differences induced by X-ray radiation damage also contain phasing information, exploiting specific structural changes characteristic of X-ray damage. This method (RIP; radiation-damage induced phasing) has the advantage that it can be performed on a single crystal of the native macromolecule. However, it suffers from the fact that X-rays introduce a large number of generally small changes, which can be difficult to locate, model and refine. In this study, UV (ultra violet) radiation has been used to induce specific changes within macromolecules. Like X-ray RIP, the native macromolecular crystal can be used. However, it is shown that UV damage, in comparison to X-ray damage, leads to a larger contrast between radiation susceptible and non-susceptible sites, favoring subsequent phasing steps. Furthermore, unlike X-ray RIP, a UV-RIP experiment does not require the use of a synchrotron X-ray source. Data collected on a large series of macromolecules are presented: all structures could readily be solved using UV-induced structural changes.

**13.01.05 Optimizing the Success Rate of Structure Determination.** James M. Holton<sup>1,2</sup>, <sup>1</sup>Univ. of California San Francisco, George Meigs<sup>2</sup>, <sup>2</sup>Lawrence Berkeley National Laboratory, Berkeley, CA 94720.

The world's macromolecular crystal x-ray data collection capacity is approximately 100 times the number of structures published each year. Why is there such a large gap? What can be done to address it and increase the "success rate" of structure determination? To answer these questions, the workflow at the Advanced Light Source (ALS) beamline 8.3.1 was analyzed. It was found that the most significant component of the data-to-structure gap arises from problems with collection strategy. That is, many data sets are collected from crystals that cannot yield data of sufficient quality to solve the structure before radiation damage "sets in". Formulating better strategies requires a clear understanding of the rate of site-specific radiation damage as well as the data quality requirements of available structure-solving software. The rate of radiation damage to selenomethionine sites was measured and shown to be generally

unpredictable from crystal to crystal. However, the extent of damage can be measured before and after each data collection. The “threshold of solvability” was evaluated using a diffraction image simulator (called MLFSOM) to systematically vary parameters such as crystal size, heavy atom occupancy and detector performance. In general, an anomalous signal-to-noise ratio of 1 or greater is required to solve a structure. Improved methods for crystal “trriage” highlight the general problem of growing a crystal of sufficient quality to solve the structure. Addressing this problem requires more efficient crystal screening technology and rapid feedback of diffraction quality into crystallization trials. At ALS 8.3.1, the advantages of interactive crystal screening are maximized by allowing data collection runs to be deferred to the middle of the night, and a new “tray goniometer” is under development for screening crystallization trays for diffraction quality directly.

### 13.01.06 High Pressure Cryocooling for Capillary Sample Cryoprotection and Diffraction Phasing at Long Wavelengths.

Chae Un Kim<sup>1,2</sup>, Quan Hao<sup>2</sup>, Sol M. Gruner<sup>1,3,4</sup>, <sup>1</sup>Field of Biophysics, <sup>2</sup>MacCHESS, <sup>3</sup>Cornell High Energy Synchrotron Source (CHESS), <sup>4</sup>Physics Dept., Cornell Univ., Ithaca, NY 14853, USA.

Crystal cryocooling is usually employed to reduce radiation damage during x-ray crystallography. Recently a high-pressure cryocooling method has been developed which often results in better crystal diffraction than conventional cryocooling methods, even without the use of penetrative cryoprotectants. The method has been successfully extended to crystal diffraction phasing at a long wavelength (1.7 Å) and two recent results are presented here. First, xenon gas was incorporated in the high pressure cryocooling method and *de novo* Xe - SAD phasing was carried out on porcine pancreas elastase (PPE, 240 residues, 26 kDa). A single 0.70 occupied xenon site in a PPE gave an expected Bijvoet amplitude ratio ( $\langle \Delta F \rangle / \langle F \rangle$ ) of 2.8 %. The auto-model-building with the experimental phases was very straightforward: 97 % of total residues (232 out of 240) could be found and docked in the electron density at 1.8 Å resolution. Secondly, native sulfur SAD phasing was performed on a thaumatin crystal diffraction. Surprisingly, successful cryoprotection of the crystal was achieved in a thick-walled (300 μm) capillary without additional cryoprotectants other than the native mother liquor. All 17 sulfur atoms in thaumatin could be distinguished in the anomalous substructure and S - SAD phasing was successful at 1.9 Å resolution. These developments may be useful in structural solution of proteins without the need for seleno-methionine incorporation and in high-throughput crystallography.

## 13.02 Detectors

### 13.02.01 Recent Advances in X-ray Pixel Array Detectors.

Mark W. Tate, Lab. of Atomic and Solid State Physics, Cornell Univ., Ithaca, NY 14853 USA.

Pixel array detectors (PADs) are solid-state imaging devices with in-pixel processing of the associated x-ray signal. PADs are generally two layer devices with pixel-by-pixel connection of a diode detector array to an underlying pixel processing chip. The diode layer provides an efficient means of converting x-rays to charge with excellent spatial and energy resolution. The pixel-processing chip is fabricated using standard CMOS methods and the functionality of the in-pixel processing can be tailored to the imaging problem at hand. A variety of pixel architectures are currently being developed including Photon-counting PADs with x-ray energy discrimination circuitry, analog-integrating PADs with vastly increased count-rate abilities, PADs with extended dynamic range capability, PADs with

fast electronic shuttering with the ability to isolate single bunches within the synchrotron beam structure, and PADs with multi-frame storage to record transient events on microsecond timescales.

### 13.02.02 3DX: An X-ray Pixel Array Detector with Active Edges.

Edwin M. Westbrook, Christopher J. Kenney, Albert C. Thompson, Sherwood I. Parker, Molecular Biology Consortium, Chicago, IL 60612, USA.

The Molecular Biology Consortium is developing a prototype X-ray detection system, optimized for protein crystallography, which should also be ideal for many other types of synchrotron science. X rays are captured directly in thick, high-resistivity, single-crystal, silicon pixel sensors. 3DX sensors have “active edges” that are formed from electrodes in the third dimension, perpendicular to the top and bottom surfaces. Thus, a 3DX sensor is fully sensitive to within a micron of its physical border. Each sensor is a 64 x 64 two-dimensional array of 150 μm pixels, so its area is about 1 cm<sup>2</sup>. Our 0.5mm thick silicon sensors capture 12.66keV X rays (the selenium edge energy) with 87% efficiency.

Behind each sensor, a custom CMOS readout chip is bump-bonded to the sensor. It reads out the full array cyclically every 64 μs, with a dead time for each pixel of 1 μs. On three edges, it lies completely hidden behind the sensor. A 3mm wide region on the remaining edge of each CMOS chip contains readout circuits and connections. Here it protrudes beyond the sensor edge, but it can be covered by the active region of a neighboring sensor module, in an array similar to that of shingles on a roof. Sensor units can be easily arrayed to cover large areas.

So far, we have proven our sensors are active to within 1-2 μm of their edges, and that each pixel can count 12keV X-ray photons at rates up to 150,000Hz. The sensor design solves the problem of double-counting or under-counting X rays striking at boundaries between two pixels. 3DX detectors are inherently tolerant of X-radiation. We are currently upgrading our CMOS readout chip. By the end of 2007 we expect to be making large numbers of completely operational, full-scale devices.

This work is supported by NIH grant RR16230.

### 13.02.03 Diffraction Data Collection with Continuous Rotation Method using CMOS Flat Panel Detector.

M. Yamamoto<sup>a,b</sup>, K. Hasegawa<sup>b</sup>, K. Hirata<sup>a</sup>, <sup>a</sup>RIKEN SPring-8 Center, <sup>b</sup>SPring-8/JASRI, 1-1-1 Kouto, Sayo, Hyogo 679-5198 Japan.

Continuous rotation method is expected to be useful in protein crystallography, because fine sliced diffraction images can be recorded without incorporating error caused by jitter of synchronized motion of goniometer and shutter. But the development of a new detector with rapid read out speed is essential to reduce dead time during read out of image. We consider a CMOS flat panel detector as a promising candidate for continuous rotation method and have been developing it in collaboration with Hamamatsu Photonics KK. We examined the performance of the method using our latest version of CMOS detector at SPring-8 BL44B2.

The CMOS flat panel detector is Hamamatsu Photonics C10158DK, which is an active type CMOS detector using directly deposited crystalline CsI as scintillator. It is composed of a single CMOS image sensor and has effective pixel size and detector area of 2352 x 2352 pixels and 118x118mm<sup>2</sup>, respectively. Maximum frame rate of readout is 3Hz. Diffraction data of a tetragonal lysozyme crystal were recorded with the method using the spindle angular velocity of 0.1deg/sec and the frame rate of 1Hz. The result of data showed

$R_{\text{merge}}$  of 2.3% (outer shell 3.3%) up to  $2\text{\AA}$ , which is better than those obtained with the conventional oscillation method using CCD detector. We also collected the diffraction data of a Se-Met protein whose structure was not known, and successfully determined the structure by MAD data. Our result shows that the continuous rotation method with CMOS flat panel detector has a potential to substitute conventional oscillation method at synchrotron beamlines.

**13.02.04 Obtaining Better Data from Existing CCD Detectors.** G. Bricogne<sup>1</sup>, T. Womack<sup>1</sup>, C. Nielsen<sup>2</sup>, <sup>1</sup>Global Phasing Ltd., Sheraton House, Castle Park, Cambridge CB3 0AX, UK, <sup>2</sup>Area Detector Systems Corp., Poway CA 92064, USA.

Our goal has been to analyse the various factors which can prevent the correct estimation of the variances of individual intensity measurements, as shown by the fact that the scatter of measurements which should be equivalent is often much greater than would be predicted on the basis of those individual variances. Such factors are to be found at many levels, notably in the statistical techniques by which integrated intensities are estimated from diffraction images.

While pursuing this first line of investigation, we observed “corner effects” in some of the derived data we had calculated for 3x3 CCD detectors, which have provided the basis for a separate study of these effects, their characterisation and correction, from that presented by Arvai *et al.* in this same session.

We conclude that there remains much scope for obtaining improved data from the present CCD detectors through improved statistical treatment of the raw data and finer calibrations, while the capabilities of Pixel Array Detectors are being explored.

## 13.03 Biomolecular Assemblies and Biomembranes

**13.03.01 Biological Relevance of Protein Structures, Assemblies and Conformational Mobility Probed with Solution X-Ray Scattering.** J.G. Grossmann<sup>1</sup>, A. Large<sup>2</sup>, P. Lund<sup>2</sup>, J. Viney<sup>3</sup>, C.N. Hunter<sup>3</sup>, A. Gutierrez<sup>4</sup>, G.C.K. Roberts<sup>4</sup>, <sup>1</sup>Molecular Biophysics Group, CCLRC Daresbury Laboratory, Warrington WA4 4AD, UK, <sup>2</sup>School of Biosciences, Univ. of Birmingham, Birmingham B15 2TT, UK, <sup>3</sup>Dept. of Molecular Biology and Biotechnology, Univ. of Sheffield, Sheffield S10 2TN, UK; <sup>4</sup>Dept. of Biochemistry, Univ. of Leicester, Leicester LE1 9HN, UK.

Increasingly complex biological macromolecules are being investigated and consistently require a variety of methods to gain insights into their structure-function relationships. Small-angle scattering using X-rays (SAXS) or neutrons (SANS) is a well-known technique for studying the low resolution structure of non-crystalline systems such as biomolecules in solution with the advantage of exploring near physiological conditions. Enhanced data analysis and interpretation procedures allow the retrieval of significantly more structural information of direct biological interest than previously anticipated. Three examples of complex proteins (ranging in mass from 60 to 900 kD) will be discussed. (1) The group II chaperonin complex (CCT) from the extreme halophilic archaeon *Haloflex volcanii* has been purified as a hexadecamer. Like most halophile proteins, CCT requires 2M sodium or potassium chloride as a minimum salt requirement for stability. SAXS studies of this archaeal CCT were performed to investigate structural similarities with its eukaryotic counterparts. (2) *Synechocystis* Mg-chelatase is a key enzyme in the chlorophyll biosynthetic pathway and consists of three components (I, D and H subunits). Mg<sup>2+</sup> insertion is catalyzed in an ATP-dependent reaction. The first structural information for all

three subunits was obtained and their conformational characteristics probed and evaluated in the context of a complex. (3) Cytochrome P450 reductase (CPR) is a complex multidomain protein containing two flavin-binding domains (FAD/FMN) separated by a “hinge” domain, which is present as an insert in the FAD-domain. For electron transfer from NADPH to the P450 cytochrome partners, the FMN-domain would have to “swing” in and out in relation to the rest of the CPR molecule. SAXS studies of native and mutant CPR demonstrate that the differences between the crystal-structure and SAXS models are likely due to the conformational equilibrium being “distorted” by crystallization’s packing forces.

We thank CCLRC for the provision of SAXS beamtime at the Synchrotron Radiation Source at Daresbury Laboratory, UK.

**13.03.02 Signal Transduction and Transcription Activation by Bacterial Enhancer Binding Proteins.** B. Tracy Nixon,<sup>1</sup> Baoyu Chen,<sup>1</sup> Michaelleen Doucleff,<sup>2</sup> Sacha De Carlo,<sup>2</sup> Hector H. Huang,<sup>2</sup> David E. Wemmer,<sup>2</sup> Eva Nogales,<sup>2</sup> Timothy R. Hoover,<sup>3</sup> Elena Kondrashkina,<sup>4</sup> Liang Guo<sup>4</sup>, <sup>1</sup>Penn State, University Park, PA 16802, <sup>2</sup>Univ. of California, Berkeley, CA 94720, <sup>3</sup>Univ. of Georgia, Athens, GA 30602, <sup>4</sup>Argonne National Lab, Argonne, IL 60439.

AAA+ ATPases are important molecular motors in all kingdoms of life. We are still learning how their actions are controlled and how they perform mechanical work. Solution structures derived from small-angle and wide-angle scattering ( $q$  range 0.004 – 1.25 Å<sup>-1</sup>) provide us insight into both questions for AAA+ATPases that regulate transcription of genes by the  $\sigma$ 54-form of bacterial RNA polymerase. In one case, a regulatory domain adopts two homo-dimeric forms, alternately repressing or derepressing motor assembly by adjacent ATPase domains (Figure – top left); in another case, regulatory and ATPase domains cooperate to stabilize the assembled motor (Figure – bottom left). The latter structure is confirmed by reconstructions of negatively stained EM images, and reveals for the first time that the CT-DNA binding domain typical of these activators is located below the ring. Structures of ATPase in the presence of nucleotide analogs show subdomain reorientations that are coupled with conformational changes in the GAFTGA loop portion of the ring shaped motors to mediate interaction with the target protein,  $\sigma$ 54 (Figure – right). Coupled with molecular biology experiments, these results support a model whereby activation of ring assembly permits contact with RNA polymerase in the ATP ground and transition states, with remodeling and release of the polymerase to begin transcription occurring after hydrolysis.

Work funded by grants from the DOE and NIH. EN is a Howard Hughes Investigator, and the BioCAT is an NIH supported Research Center.

**13.03.03 Membrane Protein-Detergent Interactions and Protein-Detergent Complex Structure Studied by Small-Angle X-ray Scattering.** Jan Lipfert<sup>1</sup>, Linda Columbus<sup>2</sup>, Scott A. Lesley<sup>2,3</sup>, Sebastian Doniach<sup>4</sup>, <sup>1</sup>Depts. of Physics, <sup>4</sup>Applied Physics, Stanford Univ., <sup>2</sup>The Joint Center for Structural Genomics, The Scripps Research Inst., <sup>3</sup>Genomics Inst. of the Novartis Research Foundation.

We use small-angle X-ray scattering (SAXS) to probe protein-detergent complexes (PDCs) of membrane proteins solubilized by micelle forming detergents. Using the alpha-helical integral membrane protein TM0026 from *T. maritima* as a model system, we discuss how SAXS measurements give insight into the (low resolution) structure of PDCs and provide a framework for understanding protein-detergent interactions.

First, we discuss how SAXS can be used as a screening tool to determine the oligomerization state of the protein inside the PDC [1].

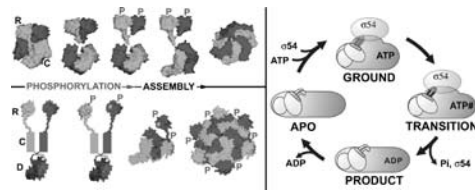
Furthermore, we show how the scattering signal from the PDC can be separated from that of “empty” detergent micelles in a protein-detergent mixture [2]. The scattering profiles from this analysis can be used in combination with NMR data to construct intermediate resolution models.

Finally, we present NMR and EPR spectroscopy data indicating that TM0026 populates different conformations in different detergents.

The observed trends can be rationalized in terms of a match (or mismatch) between the size of the protein and the characteristic micelle thickness.

The results suggest a

way to optimize micelle properties for membrane protein studies by mixing detergents and matching the thickness of the mixed micelle to the size of the protein (manuscript in preparation). The figure shows the characteristic micelle thickness determined by SAXS for a set of detergents commonly used to solubilize membrane proteins.



[1] Columbus, Lipfert, Klock, Millett, Doniach, and Lesley *Protein Sci.* 15:961-75 (2006)

[2] Lipfert, Columbus, Chu, and Doniach *J. Appl. Cryst.* 40 (2007)

**13.03.04 Monitoring Structural Ordering in Two-dimensional Assemblies of Proteins and Viruses.** Lin Yang, Masafumi Fukuto, Suntao Wang, National Synchrotron Light Source, Brookhaven National Laboratory, Upton, NY.

Two-dimensional protein crystals and ordered arrays of nanoparticles are of great scientific and technological interest. Creating these structures requires an understanding of structural ordering in two dimensions in general. Here, we utilize synchrotron-based grazing incidence x-ray scattering and optical microscopy to explore ordering of the proteins and viruses that adsorb to a lipid monolayer at the lipid-air interface as well as on a substrate supported bilayer. The lipid membrane provides the in-plane mobility that is essential for forming well ordered structures, while the liquid phase provides a means to control the inter-particle interactions. We report results on the effects of membrane charge density and liquid-phase additives on the development of structural order.

**13.03.05 Structure Modeling of Intrinsically Disordered Proteins using SANS and Computational Methods.** S. Krueger, J.E. Curtis, NIST, Center for Neutron Research, Gaithersburg, MD 20899 USA.

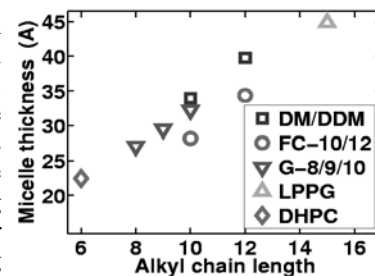
We are developing software tools to study the structure of intrinsically disordered proteins by comparison of theoretical predictions to experimental small-angle neutron scattering (SANS) data. Specifically, we are merging methodologies developed to search conformational space of small molecular pharmaceuticals with the conformational search problem posed by intrinsically disordered proteins and nucleic acids. This is achieved by generating an ensemble of macromolecular structures by varying sets of backbone dihedral angles and using energetics, importance sampling, and linear algebraic methods to rapidly determine structures that have small angle scattering spectra that are consistent with experiment. We are also developing methods to incorporate information from electron microscopy density plots into our model structures. We have used these tools to predict a set of structures for two nucleic acid-binding proteins, HIV-1 Gag and mini-chromosome maintenance complex, under physiologically relevant conditions. In both cases, only partial x-ray crystal structures are available for these proteins due to the inherent disorder in portions of their structures, which is

necessary for their function. The solution structures for these proteins in the absence and presence of nucleic acid will be discussed, along with the software methods under development.

**13.03.06 Small-angle X-ray Scattering and Neutron Contrast Variation Reveal the Arrangement of Synaptic Proteins Implicated in Autism.** J. Trehwella<sup>1</sup>, D. Comoletti<sup>2</sup>, A. Grishaev<sup>3</sup>, A. E. Whitten<sup>1,4</sup>, I. Tsingly<sup>2</sup>, P.W. Taylor<sup>2</sup>. <sup>1</sup>School of Molecular and Microbial Biosciences, Univ. of Sydney, <sup>2</sup>Dept. of Pharmacology, Skaggs School of Pharmacy and Pharmaceutical Sciences, Univ. of California, San Diego, La Jolla, CA 92093; <sup>3</sup>National Inst. of Diabetes and Digestive and Kidney Diseases, Bethesda, MD 20892; <sup>4</sup>Bragg Inst., Australian Nuclear Science and Technology Organization.

In the central nervous system, synapses allow neurons to form interconnected neural circuits that must be highly regulated to ensure the appropriate responses to different stimuli. Neuroligins are postsynaptic cell adhesion proteins that associate with their presynaptic partners, the neurexins. Different forms of these proteins (isoforms) are associated with different pathways. Using small angle solution scattering, we characterized a low-resolution structure of the extracellular region of neuroligin 1 and its complex with  $\beta$ -neurexin. We also show that the globular domains of several neuroligin isoforms dimerize via a four-

helix bundle and have an overall fold that is typical of the cholinesterases. The region connecting the globular neuroligin domains to the cell membrane appears elongated projecting radially from the globular domains. X-ray scattering and neutron contrast variation



experiments demonstrate that two neurexin monomers associate with a neuroligin dimer at symmetric locations such that the complex is  $\sim 20\text{\AA}$  longer than neuroligin alone. Our structure delineates the topological arrangements of the different neuroligin domains and the synaptic disposition of the partnering molecules. As mutations of neurexin and neuroligin genes appear linked to autism and mental retardation, these structures provide a framework for understanding altered structure and recognition function of these synaptic proteins in developmental disorders.

**13.03.07 Neutrons in Biology: SAS Solutions in Protein Structural Analysis.** Joanna K. Krueger\*, (fnu) Ashish, Chemistry Dept., UNC Charlotte, Charlotte, NC.

Proteins are the functional products of gene translation and as such, structural analysis of proteins will be a primary objective for researchers in this genome-enabled era. An important goal of such analysis is to discover how protein structures interact with one another to regulate specific cellular events. Techniques capable of providing information on the resultant large macromolecular complexes will be a central component of any structural biologists' toolbox. The techniques of small-angle X-ray and neutron scattering on macromolecular complexes complement other structural approaches, providing a low-resolution framework from which to begin assembling molecular-level details on individual proteins or protein subunits into their intact, functional units. Indeed, interpretation of small-angle scattering data is most effective when used as a complementary tool with other structural and biochemical information such as that obtained from selected-site mutagenesis, circular dichroism, NMR, crystallography or electron microscopy,

providing key pieces of information that complete a story. This seminar will provide some current examples on the biological application of small-angle scattering technologies. These technologies, particularly that of neutron scattering using contrast variation, is relatively new and not yet widely explored; however, they show great promise in providing structural information on protein:protein interactions that can be difficult to obtain otherwise.

**13.03.08 The Center for Structural Molecular Biology (CSMB) at Oak Ridge National Laboratory.** W.T. Heller<sup>1</sup>, G.W. Lynn<sup>1</sup>, A. N. Raghavan<sup>1</sup>, V. S. Urban, K.L. Weiss<sup>1</sup>, Y. Mo<sup>1</sup>, D.A.A. Myles<sup>1</sup>, <sup>1</sup>Chemical Sciences Div. ORNL, Oak Ridge, TN 37831.

The CSMB at ORNL is developing facilities and techniques for the characterization and analysis of biological systems at the High Flux Isotope Reactor (HFIR) and the Spallation Neutron Source (SNS). The cornerstone of the effort is a small angle neutron scattering instrument (Bio-SANS) currently under construction at HFIR that will be dedicated to the analysis of the structure, function and dynamics of complex biological systems. In support of this program, we are developing advanced computational tools for data analysis and modeling, alongside a supporting biophysical characterization and X-ray scattering infrastructure. Specifically, we established a Bio-Deuteration Laboratory for *in vivo* production of H/D labeled macromolecules that will permit selected parts of macromolecular structures to be highlighted and analyzed *in situ* using neutron scattering. The CSMB is also expanding our efforts to include the study of biomembranes by neutron reflectometry. These new facilities will make ORNL a world-leading scientific center and user facility for neutron-based studies of bio-molecular structure and function.

This work was supported by the Office of Biological and Environmental Research of the U.S. Dept. of Energy project KP1102010 and the Laboratory Directed Research and Development program of Oak Ridge National Laboratory, managed by UT-Batelle, LLC under contract No. DE-AC05-00OR22725 with Oak Ridge National Laboratory. The submitted manuscript has been authored by a contractor of the U.S. Government under Contract DE-AC05-00OR22725. Accordingly, the U.S. Government retains a nonexclusive royalty-free license to publish or reproduce the published form of this contribution, or allow others to do so, for U.S. Government purposes.

## 13.04 Time and Field Dependent Responses in Scattering Experiments

**13.04.01 Small Angle Neutron Scattering (SANS) Studies of the Vortex Lattice in Type II Superconductors.** C.D. Dewhurst, R. Cubitt, Inst. Laue Langevin, 38042 Grenoble, France.

The last fifteen years or so has seen a number of important published studies of the vortex lattice (VL) in type II superconductors. The complexity and diversity of this range of materials includes the high-temperature superconductors, multi-band, heavy-fermion and unconventional materials, non-local superconductors, as well as 'classic' materials such as Nb. Phenomena such as non-locality, order parameter symmetry, multi-component superconductivity, VL melting, static and dynamic response of the VL to driving forces and disorder are topical and continue to be investigated.

In the non-magnetic borocarbide materials [Y or Lu]Ni<sub>2</sub>B<sub>2</sub>C, V<sub>3</sub>Si, Ca<sub>3</sub>Rh<sub>4</sub>Sn<sub>13</sub> and heavy-fermion CeCoIn<sub>5</sub> non-local effects and Fermi surface anisotropy determine a range of VL structures, first- and second-order phase transitions from (almost) hexagonal at low fields to distorted rhombic and then square VL at higher fields. In MgB<sub>2</sub> the magnetic field dependent scattering from the VL confirms the picture of two-band superconductivity arising from both from one isotropic and one highly anisotropic sheet on the Fermi surface. The effects of an anisotropic *d*-wave order parameter in the high-Tc

materials YBa<sub>2</sub>Cu<sub>3</sub>O<sub>7-δ</sub>, La<sub>2-x</sub>Sr<sub>x</sub>CuO<sub>4+δ</sub> and Nd<sub>2-x</sub>Ce<sub>x</sub>CuO<sub>4+δ</sub> stabilises a square VL over much of the phase diagram. The VL can 'shaken' by an *ac* magnetic field to promote better order against material disordering influences or pinning forces. An applied transport current perpendicular to the applied field can create flowing ordered and disordered VL states while a current parallel to the applied field results in a complex 'force-free' configuration resulting in a helical vortex instability. We have performed the first imaging of the VL structure under these conditions.

**13.04.02 Quenched SANS for Studies of Polymer Relaxation.** W. Pyckhout-Hintzen<sup>a</sup>, L. Dahbi<sup>a</sup>, D. Richter<sup>a</sup>, E. Straube<sup>b</sup>, <sup>a</sup>Research Center Jülich, IFF, D-52425 Jülich, Germany, <sup>b</sup>Univ. of Halle, Dept. of Physics, D-06099 Halle, Germany.

Hierarchical relaxation in non-linearly stretched branched polymers with model architecture can be conveniently investigated by means of SANS in the quenched state. The increasing interest in their relaxation behaviour as well as the fast expanding number of the applications of such materials is mainly based on the different processing and the new time-dependencies they invoke through their branches. It represents a very active field of research both from scientific and technological point of view. Investigations therefore aim typically to couple rheology and neutron scattering and to provide a toolbox for the prediction of the processing properties of such new soft composites. Recent progress was triggered by advances in the tube model theory and the availability of model polymers. We will report on SANS studies of H-shaped as well as blends of hyperbranched model polymers with linear matrix under uniaxial strain as a function of time and discuss the underlying dynamics. The reference simple linear chain relaxes according to textbook expectations and was accessed for the first time. Further, the use of advanced random phase theory to account for elastic fluctuations and inhomogeneities will be illustrated.

**13.04.03 Shear-Induced Disaggregation of Droplets in Attractive Nanoemulsions Probed by Rheo-SANS.** T.G. Mason, J.N. Wilking, C.B. Chang, L. Porcar, Dept. of Chemistry and Biochemistry, Dept. of Physics and Astronomy, and California NanoSystems Inst., UCLA, Los Angeles, CA 90095 USA.

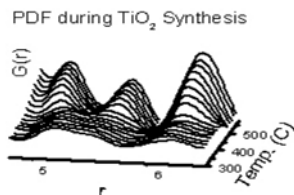
Using Rheological Small Angle Neutron Scattering (Rheo-SANS), we study how an applied steady shear alters the structure of nanoscale droplets in jammed networks of attractive nanoemulsions. Monodisperse silicone oil-in-water nanoemulsions, stabilized by the anionic surfactant sodium dodecylsulfate, are prepared by ultracentrifugal fractionation, yielding an average droplet radius of 40 nm. Relative to thermal energy, the interaction potential of the droplets is tuned from repulsive to attractive by adding up to 0.7 M NaCl. Attractive nanoemulsions at a droplet volume fraction of 0.44 can form elastic gels well below random close packing. In the absence of shear, we observe the hallmarks of slippery diffusion-limited aggregation: a strong fractal power-law rise in the intensity, *I*, toward low wavenumbers, *q*, and clear nearest-neighbor correlation peaks at high-*q*. However, when high shear stresses are applied, the emulsion's viscosity shear-thins, the scattering is anisotropic, and the low-*q* intensity drops significantly. These trends are interpreted in terms of shear-induced de-gelling of the attractively jammed networks through a limited degree of disaggregation of nanodroplets.

We thank NIST for providing access to the NG-7 beam line and for supporting rheo-SANS experiments.

**13.04.04 *In situ* Time-Resolved X-Ray Diffraction (TR-XRD) as a Tool for Characterizing Catalysts and Active Sites.** Jonathan Hanson, Xianqin Wang, Wen Wen, Jose Rodriguez, Chem. Dept., BNL, Upton NY 11973, Peter Chupas, APS, ANL, Argonne IL.

At the NSLS beam line X7B, we have put together a facility capable of conducting *in situ*, sub-minute TR-XRD experiments under a wide variety of temperature and pressure conditions (80 K < T < 1250 K; 1 Torr < P < 150 atm)[1] Current measurements also include control of gas flow and measurement of gas composition of the products with mass spectrometry and gas chromatography. Thus we are able to determine structures of active catalysts.

Using TR-XRD, one can obtain information about structural details, phase composition, kinetics of transformation, intermediate phases and crystal characteristics. Examples of problems studied to date with TR-XRD include: (1) Substrate binding of zeolites[2]; (2) reduction/oxidation of oxide catalysts[3]; (3) Water Gas Shift reaction with Copper[4] and Gold [5]supported on cerium oxide; (4) Synthesis of Manganese oxide[6] and titanium oxide catalyst. This talk will explore the use of profile refinement and PDF analysis using *in situ* data obtained with high energy X-ray powder patterns[7].



The work was supported through contract DE-AC02-98CH10086 (BNL) and Contract No. W-31-109-Eng-38.(ANL) by the US DOE, Office of Science, Office of Basic Energy Sciences.

1. Rodriguez, J.A. and J. Hanson. *Ciencia*, 2006. 14: p. 177-188. 2. Wang, X.Q., et al. *J Phys. Chem. B*, 2004. 108(43): p. 16613-16616. 3. Wang, X., et al. *J. Phys. Chem. B.*, 2004. 108(36): p. 13667-13673. 4. Wang, X., et al. *J Phys. Chem B.*, 2006. 110: p. 428-434. 5. Wang, X., et al. *J. Chem. Phys.*, 2005. 123: p. 221101. 6. Shen, X.-F., et al. *J. Am. Chem. Soc.*, 2006. 128(14): p. 4570-4571. 7. Chupas, P.J., et al. *J. Appl. Crystallography*, 2003. 36: p. 1342-1347.

**13.04.05 *In-situ* X-ray Diffraction Studies of the Magnetic Field Induced Structural Transformations.** V.K. Pecharsky, Ames Lab and Dept. of Materials Science and Engineering, Iowa State Univ., Ames, IA 50010-3020, USA.

By coupling a rotating anode powder diffractometer with a continuous-flow liquid helium-cooled cryostat and a split-coil superconducting magnet, Rietveld-quality powder diffraction data have been obtained between 5 and 315 K in magnetic fields reaching 4 T. A typical experiment quantifying both the phase composition and changes in the unit cell dimensions and phase volume(s) may be carried out in as little as ten to twenty minutes. A few hours long experiment is sufficient to provide detailed information about the individual atomic parameters. Both massive and subtle field-induced structural changes have been detected, providing structural data needed to develop a better understanding of structure-property relationships of solids.

This research was supported by the Division of Materials Science of the Office of Basic Energy Sciences of the US DOE under contract No. DE-AC02-07CH11358 with Iowa State University.

**13.04.06 Time Resolved Neutron Diffraction Studies of Defect Structure Formation in Lithium Imide During Hydrogenation and De-hydrogenation.** Ashfia Huq<sup>1</sup>, Luke Heroux<sup>1</sup>, James W. Richardson<sup>2</sup>, Evan R. Maxey<sup>2</sup>, Mark S. Bailey<sup>3</sup>, Dhanesh Chandra<sup>4</sup> <sup>1</sup>Spallation Neutron Source, Oak Ridge National Lab, Oak Ridge TN 37831, <sup>2</sup>Intense Pulsed Neutron Source and Material Science Div., Argonne National Lab, Argonne, IL 60439, <sup>4</sup>Metallurgical and Materials Engineering, Univ. of Nevada, Reno, Reno NV 89557.

Reversible hydrogen absorption and desorption properties of lithium imide to lithium amide at 250°C have generated a great interest in

this system. The structure of lithium amide is fairly well established where as there is significant debate about the structure of lithium imide. While there is general agreement about the position of the Li and N atoms which form an antifluorite structure, several types of hydrogen positions have been proposed. In all these models, however, a common theme is the disordered hydrogen. *In situ* neutron diffraction measurement revealing a variation in stoichiometry of cubic lithium imide during hydrogenation and dehydrogenation at 250°C will be presented.

ORNL/SNS is managed by UT-Battelle, LLC, for the U.S. Department of Energy under contract DE-AC05-00OR22725. Work at ANL supported by the U.S. DOE, Basic Energy Sciences--Materials Sciences, under Contract W-31-109-ENG-38.

## 13.05 Structural Mechanisms of Infectious Diseases

**13.05.01 The Structural Basis of Translation Initiation by a Viral Internal Ribosome Entry Site RNA.** J.S. Kieft, D.A. Costantino, A. Keel, J.S. Pflugsten, Dept. of Biochemistry and Molecular Genetics, Univ. of Colorado at Denver and Health Sciences Center, Aurora, CO 80045.

Many pathogenic viruses use internal ribosome entry sites (IRESs) as a critical part of their infection strategy, in some cases using these RNAs to elude the host cell's antiviral responses. IRES RNAs use an RNA structure-based mechanism to recruit, position, and activate the host cell's protein-making machinery without the use of a 5' cap or many of the canonical translation initiation factors in what has been called "molecular hijacking." Using a novel means of phasing RNA crystal data, we have solved the structures of both independent domains of a *Dicistroviridae* IRES RNA. This IRES drives translation initiation in the absence of any protein factors, operating as an all-RNA translation initiation apparatus necessary for viral infection. The two structures, when pieced together, are the first complete structure of an IRES RNA. The structure reveals a complex fold that positions conserved RNA bases in space to interact with both the 40S and 60S ribosomal subunits, and suggests a dynamic mechanism in which both the IRES RNA and the ribosome change conformation during the process of initiating translation. Our structures also show that the IRES RNA uses a novel form of tRNA mimicry to interact with the ribosome, potentially explaining the ability of the IRES to operate without initiator tRNA. Using mutagenesis and continued structural studies, we are testing our mechanistic hypotheses with the ultimate goal of understanding the general RNA structure-based rules of IRES function.



**13.05.02 The Influenza A Virus Nucleoprotein.** Qiaozhen Ye<sup>1</sup>, Robert Krug<sup>2</sup>, Yizhi Jane Tao<sup>1</sup>, <sup>1</sup>Dept. of Biochemistry and Cell Biology, Rice Univ., 6100 Main St., MS140, Houston, TX 7700, <sup>2</sup> Inst. for Cellular and Molecular Biology, Univ. of Texas at Austin, 2500 Speedway, Austin, TX 78712.

Influenza A viruses pose a serious threat to world public health, particularly the currently circulating avian H5N1 viruses. The influenza viral nucleoprotein, NP, forms the protein scaffold of the helical genomic ribonucleoprotein (RNP) complexes, and plays a critical role in viral RNA replication. Here we report a 3.2Å crystal structure of NP, the overall shape of which resembles a crescent

with a head and a body domain, with a protein fold different from that of the rhabdovirus nucleocapsid protein. NP oligomerization is mediated by a flexible tail loop that is inserted inside a neighboring molecule. This flexibility in the tail loop enables NP to form loose polymers as well as rigid helices, both of which are important for NP functions. Single residue mutations in the tail loop result in the complete loss of NP oligomerization. A RNA-binding groove, which is found between the NP head and body domains at the exterior of the NP oligomer, is lined with highly conserved basic residues widely distributed in the primary sequence. The NP structure shows that only one of two proposed nuclear localization signals are accessible, and suggests that the body domain of NP contains the binding site for the viral polymerase. Our results identify the tail loop binding pocket as a potential target for antiviral development.

NP diffraction data were collected at the Bookhaven National Synchrotron Light Source and the Cornell High-Energy Synchrotron Source. This work is supported by grants from the Welch Foundation, National Institutes of Health, and the Nanoscale Science and Engineering Initiative of the National Science Foundation.

**13.05.03 Negative Strand RNA Virus Nucleocapsid Structure and Function.** Winfried Weissenhorn<sup>1,2</sup>, Aurélie A.V. Albertini<sup>2</sup>, Amy K. Wernimont<sup>1</sup>, Tadeusz Muziol<sup>1</sup>, Raimond B.G. Ravelli<sup>1</sup>, Bettina Hartlieb<sup>3</sup>, Stephan Becker<sup>3</sup>, Guy Schoehn<sup>2</sup>, Rob W.H. Ruigrok<sup>2</sup>, <sup>1</sup>European Molecular Biology Lab., 38042 Grenoble, France, <sup>2</sup>Unit for Virus Host-Cell Interactions, Univ. Joseph Fourier, UMR 5233 UJF-EMBL-CNRS, 38042 Grenoble, France, <sup>3</sup>European Molecular Biology Lab., 38042 Grenoble, France, weissenhorn@embl.fr.

Negative strand RNA viruses condense their single stranded RNA genome into a helical nucleoprotein-RNA complex, the nucleocapsid, which is packed into virions and serves as a template for the RNA-dependent RNA polymerase complex. The crystal structure of a recombinant rabies virus nucleoprotein-RNA complex, organized in an undecameric ring, has been determined at 3.5 Å resolution. Polymerization of the nucleoprotein is achieved by domain exchange between protomers, with flexible hinges allowing nucleocapsid formation. The two core domains of the nucleoprotein clamp around the RNA at their interface in a sequence unspecific manner and shield it from the environment. RNA sequestering by nucleoproteins is likely a common mechanism employed by negative strand RNA viruses to protect their genomes from the innate immune response directed against viral RNA in human host cells at certain stages of an infectious cycle. Furthermore we discuss an electron microscopy reconstruction of the filovirus nucleocapsid and the 2.0 Å X-ray structure of its associated accessory factor VP30 and compare structural and functional aspects of both nucleocapsids to those of other negative strand RNA viruses.

**13.05.04 Structural Aspects of SNARE - Botulinum Neurotoxin Interactions.** Axel T. Brunger<sup>1</sup>, Mark Breidenbach<sup>1</sup>, Rongsheng Jin<sup>1</sup>, Thomas Binz<sup>2</sup>, Andreas Rummel<sup>3</sup>, <sup>1</sup>Howard Hughes Medical Inst. and Depts. of Molecular and Cellular Physiology, Neurology and Neurological Sciences, Structural Biology, and Stanford Synchrotron Radiation Lab., Stanford, CA 94305, <sup>2</sup>Inst. of Biochemistry, <sup>3</sup>Inst. of Toxicology, Medical School of Hannover, Carl-Neuberg-Strasse 1, 30625 Hannover, Germany.

Botulinum neurotoxins (BoNTs) impair neuronal exocytosis through specific proteolysis of essential proteins called SNAREs. BoNTs bind with high specificity at neuromuscular junctions and they impair exocytosis of synaptic vesicles containing acetylcholine through specific proteolysis of SNAREs which constitute part of the synaptic vesicle fusion machinery. We obtained the structure of a BoNT in complex with its protein receptor: the receptor binding domain of botulinum neurotoxin serotype B (BoNT/B) bound to the luminal

domain of synaptotagmin II, determined at 2.15 Å resolution. Upon binding a helix is induced in the luminal domain which binds to a saddle-shaped crevice on a distal tip of BoNT/B. This crevice is adjacent to the non-overlapping ganglioside binding site of BoNT/B. Site-specific SNARE hydrolysis is catalysed by the BoNT light chains, a unique group of zinc-dependent endopeptidases. SNARE assembly into a low-energy ternary complex is believed to catalyse membrane fusion, precipitating neurotransmitter release; this process is attenuated in response to SNARE proteolysis. We solved the first structure of a BoNT endopeptidase in complex with its target SNARE at a resolution of 2.1 Å: botulinum neurotoxin serotype A (BoNT/A) protease bound to human SNAP-25. The structure, together with enzyme kinetic data, revealed an array of exosites that determine substrate specificity. Substrate orientation is similar to that of the general zinc-dependent metalloprotease thermolysin. We observed significant structural changes near the toxin's catalytic pocket upon substrate binding, probably serving to render the protease competent for catalysis.

**13.05.05 Receptor Binding, Membrane Fusion and Virus Entry Mediated by the Paramyxovirus HN and F Proteins.** Theodore Jardetzky<sup>†</sup>, Hsien-sheng Yin<sup>†\*</sup>, Xiaolin Wen<sup>†</sup>, Ping Yuan<sup>†</sup>, Reay Paterson<sup>†\*</sup>, Robert A. Lamb<sup>\*\*†</sup>. <sup>†</sup>Dept. of Biochemistry, Molecular Biology & Cell Biology, <sup>\*</sup>Howard Hughes Medical Inst., Northwestern Univ., Evanston, IL.

The paramyxoviridae are enveloped viruses that include, among others, mumps virus, measles virus, Sendai virus, Newcastle disease virus (NDV), human respiratory syncytial virus (hRSV), parainfluenza virus 5 (SV5) and human parainfluenza viruses 1-4 (hPIV). Like other enveloped viruses, such as influenza and HIV, the paramyxoviruses require fusion of the viral and cellular membranes to enter a host cell. For many paramyxoviruses, the hemagglutinin-neuraminidase (HN) protein functions in virus attachment to cells, cleavage of sialic acid from oligosaccharides, and in stimulating membrane fusion during virus entry into cells. The mechanism by which HN activates virus entry remains to be fully understood. The fusion (F) protein catalyzes viral and cellular membrane merger and it has been postulated that F initially folds to a metastable conformation and subsequently undergoes complex refolding during this process. However, it has remained unclear to what extent the F pre- and post-fusion conformations differ and how these are linked to membrane fusion.

We have determined the crystal structures of SV5 HN and its complexes with sialic acid, the inhibitor DANA and the model receptor sialyllactose. SV5 HN shares common structural features with HN of NDV and hPIV3, but unlike previously determined HN structures, SV5 HN forms a tetramer in solution, which is thought to be the physiological oligomer. The sialyllactose complex reveals intact receptor within the active site, but no major conformational changes in the protein. The SV5 HN structures do not support previously proposed models for HN action in membrane fusion and suggest alternative mechanisms by which HN may activate F for membrane fusion and promote virus entry into cells.

We have also determined the crystal structures of the SV5 and hPIV3 F proteins, in the pre- and post-fusion conformations, respectively. For the hPIV3 F protein, we determined the structure of the uncleaved, secreted F ectodomain, truncated before the transmembrane (TM) domain. We made the unexpected finding that this structure contains a 6-helix bundle associated with the post-fusion conformation, indicating that the F TM domain and/or the cytoplasmic tail are important for the folding to or stability of the pre-fusion, metastable state. For the SV5 F protein, we have determined the crystal structure of the pre-fusion conformation, after stabilizing the metastable state by the addition of a C-terminal trimerization domain. The comparison of the SV5 and

hPIV3 F structures reveals major conformational differences between the pre- and post-fusion states, involving transformations in secondary and tertiary structure. The positions and structural rearrangements of key parts of the fusion machinery clarify how a novel metastable protein fold and its conformational transition to a more stable state can trigger membrane fusion.

**13.05.06 HIV-1 Mechanisms for Evading Antibody-Mediated Neutralization.** P.D. Kwong, P. Acharya, L. Chen, L. Kong, Y.D. Kwon, S. Majeed, G. Ofek, M. Pancera, A. Shah, J. Stuckey, T. Zhou, The Structural Biology Section, Vaccine Research Center, NIAID/NIH, Bethesda, MD 20892 USA.

Infection by HIV-1 elicits many anti-HIV-1 specific antibodies, but virtually all of these are ineffective at neutralizing virus. Although structural characterization remains to be carried out on the complete HIV-1 viral spike, analysis of a primary component, the HIV-1 exterior gp120 envelope glycoprotein, has revealed some of the structural mechanisms for this evasion. Extensive N-linked glycosylation cloaks most of the expected outer surface of the viral spike, conformational masking hides conserved functionally relevant surfaces from patrolling antibody, and immunodominant variable loops provide decoys and antigenic variation. Despite all of this, broadly neutralizing antibodies have been identified, which have the ability to neutralize diverse primary isolates of HIV-1. These antibodies provide clues on how to bypass HIV-1 mechanisms of humoral evasion. Here we present structures of human antibodies in complex with HIV-1 gp120, and discuss the impact of this structural information on the design of an effective HIV-1 vaccine.

This research is supported by the Intramural Research Program of the NIH, by the International AIDS Vaccine Initiative, and by a grant from the Bill and Melinda Gates Foundation Grand Challenges in Global Health Initiative. Use of SER-CAT at the Advanced Photon Source was supported by the US Department of Energy, Basic Energy Sciences, Office of Science.

## 13.06 Energy Storage and Conversion

**13.06.01 Some Applications of INS and DFT in Hydrogen Containing Materials, Thermodynamics Study of the Structural and Dynamical Properties.** Anibal J. Ramirez-Cuesta, ISIS Facility, Rutherford Appleton Laboratory, Chilton, Didcot, OX11 0QX, UK.

The neutron is an ideal probe for the study of hydrogenous materials [1]. Neutrons are scattered by atomic nuclei. All molecular vibrations are neutron-active because the nuclear interactions are not subject to dipole or polarisability selection rules. All vibrations are in principle, observable. Because the neutron has a mass, it also allows the sampling of the vibrations in the Brillouin zone. The intensity of the vibrational modes is proportional to the amplitude of motion of the atoms in the solid; this combined with the lack of selection rules makes the comparison of calculated spectra with experimental straightforward [2]. All these characteristics combined make INSS (Inelastic Neutron Scattering Spectroscopy) an ideal test bed for the applicability of quantum mechanical *ab initio* calculations.

In the solid it is possible to take into consideration quantum effects by means of the quasi-harmonic lattice dynamics approximation. The quantity to be minimised is the Helmholtz free energy, which includes the zero point motion as well as thermal effects. This approximation is considered to be valid over a wide range of temperatures, but it is especially valid up to room temperature [3].

We tested different functional in DFT calculations and found that in the case of the whole series of simple metal hydrides (LiH ... CsH) the better structural and dynamical agreement, for calculations including thermal effects was when using LDA functionals rather

that the most widely “trusted” GGA functionals. Further studies demonstrated that the same effect is observed on other systems, most notably in polyethylene [4].

In this talk I’ll address the capabilities of INS spectroscopy and the correspondence with *ab initio* dynamical calculations.

[1] Vibrational Spectroscopy with Neutrons; PCH Mitchell, SF Parker, AJ Ramirez-Cuesta and J Tomkinson, World Scientific, London 2005.

[2] Ramirez-Cuesta, A.J. *Computer Physics Communications* **2004**, *157* (3), 226-238.

[3] Barrera, G. D.; Colognesi, D.; Mitchell, P. C. H.; Ramirez-Cuesta, A. J. *Chemical Physics* **2005**, *317* (2-3), 119-129.

[4] Barrera, G. D.; Parker SF; Ramirez-Cuesta AJ; Mitchell P. C. H. *Macromolecules* **2006**, *39*, 2683-2690.

**13.06.02 Nanostructured and Catalysed MgH<sub>2</sub> Powders for Fast Reactions.** N.E. Skryabina, Dept of Physics, Perm State Univ., 15 Bukireva St, 614990 Perm, Russia, J. Charbonnier, P. de Rango, D. Fruchart, G. Girard, S. Miraglia, Dept. MCMF, Inst. Neel & CRETA, BP 166, 38042 Grenoble Cedex, France.

MgH<sub>2</sub> is of the most promising metal hydride able to store reversibly up to 7.6 w%. Also because Mg is abundant, cheap, easy to process, and environmental friendly element, in the past ten years many research activities have focused on processing and structural analysis of optimized MgH<sub>2</sub> powders. Two main conditions must be fulfilled to get high reaction rates for practical application: 1 - formation of nicely homogeneous nano-sized crystallites 2 - feeding Mg (MgH<sub>2</sub>) particles with a few at.% of so-called catalysts. X-ray and *in-situ* neutron diffraction experiments were undertaken to better understand the advancement of the activating procedure both in terms of diffraction profile analysis and progressive transformation of metal additive catalysts, after processing using energetic ball milling. Besides, HREM enables providing pictures of the of the well designed nanostructured crystallites when activated. Presently alternative metallurgy techniques such as cold rolling, ECAP, extrusion... are developed to deliver amounts of ideally structured Mg/MgH<sub>2</sub> powders. We finally report on the progressive modification of the crystal texture and particle size distribution by using XRD and texture analysis on ECAP processed ingots.

This research is supported by the EC research IP NessHy No: 518271 (SES6).

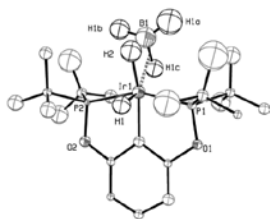
**13.06.03 Impact on the Crystallization Process of Shape Memory Alloys upon Hydrogen Insertion.** D. Fruchart, L. Cagnon, Institut Neel, BP 166, 38042 Grenoble Cedex, France, N.E. Skryabina, Dept of Physics, Perm State Univ., 15 Bukireva St, 614990 Perm, Russia, A. V. Shelyakov, Moscow Physical-Technical Engineering Inst., Kashirskoe sh.31, Moscow, 115409, Russia.

Generally peaking the shape memory alloys with TiNi or TiNi(Cu) formula exhibit typical types of successive structures that are known as B2 (CsCl type), rhombohedral (premartensite), B19 (martensite, orthorhombic), and B19' (martensite, monoclinic). The types of crystal structures are found in succeeding versus temperature on cooling down and reversely on heating up. Besides hydrogen electrodes have been proposed for a proton storage as based on such alloys. We have analyzed such type of materials starting from amorphous precursor alloys, as well as the corresponding materials after being submitted to an electrolytic process for hydrogenation. Systematically, X-ray and neutron diffraction patterns, DSC analyses, electrical resistance and SEM pictures were recorded on the different types of materials, in the initial state and as well as hydrogenated, therefore before and after applying specific thermal treatments. Cooling down reveals for the TiNi and TiNi<sub>0.50</sub>Cu<sub>0.50</sub> alloys the B2 to B19' and B2 to B19 transformations respectively, with similar trends in the thermal variations of the **a**, **b** and **c** cell parameters. For the second type of

alloy, hydrogenation of the B19 phase leads to similar tendency of cell parameter variation as described here above. The transformation of the binary TiNi alloy upon hydrogenation appears somewhat different with the precipitation of a tetragonal type of hydride. The various behaviors will be analyzed and compared for.

**13.06.04 Neutron Diffraction Study of the Dormant Form of a Catalyst for Ammonia Borane Dehydrogenation.** Thomas F. Koetzle,<sup>a</sup> D. Michael Heinekey,<sup>b</sup> Paula M.B. Piccoli,<sup>a</sup> Arthur J. Schultz<sup>a</sup>, <sup>a</sup>IPNS, Argonne National Laboratory, Argonne, IL 60439, <sup>b</sup>Dept. of Chemistry, Univ. of Washington, Seattle, WA 98195.

Ammonia borane (H<sub>3</sub>NBH<sub>3</sub>) is a promising candidate material for chemical hydrogen storage, due to its high hydrogen content and potential for reversible release of hydrogen. Heinekey and co-workers recently reported efficient catalysis of ammonia borane dehydrogenation by the iridium(IV) pincer complex (POCOP)Ir(H)<sub>2</sub> (POCOP)=[η<sup>3</sup>-1,3-(OPtBu)<sub>2</sub>2C<sub>6</sub>H<sub>3</sub>]. A dormant form of the catalyst resulting from B-N bond cleavage and addition of BH<sub>3</sub> to the iridium center is formed at long reaction times. This product reverts to the active species upon exposure to hydrogen. A low-temperature, single-crystal neutron diffraction study carried out at IPNS has now definitively established the structure of this product as (POCOP)Ir(H)<sub>2</sub>(BH<sub>3</sub>), see figure.



Work at ANL was supported by the DOE/OS/BES under contract DE-AC02-06CH11357.

<sup>1</sup>Denney, M.C.; Pons, V.; Hebden, T.J.; Heinekey, M.D.; Goldberg, K.I. *J. Am. Chem. Soc.* **2006**, *128*, 12048.

**13.06.05 Synthesis and Structural Characterization of New Metal Hydrides and Borohydrides.** Ewa Rönnebro, Sandia National Laboratories, 7011 East Ave., Livermore, CA 94551 USA.

Hydrogen storage is a key technology for realizing the hydrogen economy. It is a grand challenge to find new materials for onboard hydrogen storage that meets the performance targets of USA's DOE i.e. 6wt% hydrogen, 1.5kWh/liter, 2.0kWh/kg and 1000 cycles. However, with a future perspective, the solid state H-storage materials are more likely to be selected as appropriate candidates. We will here present recent results on synthesis and characterization of new metal hydride systems. At Sandia, we are using solid-state routes including ball milling and high-H<sub>2</sub> pressure sintering in autoclaves. In order to get clues to better understand the hydrogen diffusion process, we are using X-ray and neutron diffraction techniques to determine the crystal structures by the Rietveld method. If the metal atom matrix is composed of light-weight atoms, synchrotron sources, and even powder-XRD can be sufficient to determine the H-atom's positions. A newly discovered quaternary compound, K<sub>2</sub>LiAlH<sub>6</sub>, was synthesized and characterized by powder X-ray diffraction to be isostructural with K<sub>2</sub>LiAlF<sub>6</sub>. By using a unique technique, a hydrogen rich Mg-based transition metal hydride, Mg<sub>7</sub>TiH<sub>16</sub>, was prepared at 8GPa and 873K with a cubic anvil press at AIST, Osaka. It was investigated with high-energy X-ray synchrotron radiation data from the facility SPring-8, Japan and the structure was elucidated by Rietveld refinements revealing an atomic arrangement similar to Ca<sub>7</sub>Ge having a substructure corresponding to CaF<sub>2</sub>. Another recently investigated material at Sandia is Ca(BH<sub>4</sub>)<sub>2</sub>, which crystallizes in an orthorhombic space group. We recently showed that it can be rehydrided at 700 bar and 400°C and we are continuing exploring its potential for application as a 9.6wt% reversible hydrogen storage material.

**13.06.06 In situ Powder Diffraction Studies of Metal Hydrides for Hydrogen Storage.** Y. Nakamura, E. Akiba, National Inst. of Advanced Industrial Science and Technology, Tsukuba, Japan.

Metal hydrides are attractive materials for energy storage, e.g. hydrogen gas storage for a fuel cell, electric power storage with rechargeable batteries, etc. Hydrogen atoms in metal hydrides are located in interstitial sites of metal sublattice, stabilized by bonding with surrounding metal atoms. Powder diffraction is widely used for this kind of materials to determine the crystal structure and follow the phase relation during the reaction.

In this talk, we present our recent work on metal hydrides using *in situ* powder diffraction technique.

We have successfully performed *in situ* neutron diffraction for LaNi<sub>5</sub>-M<sub>x</sub>D<sub>x</sub> (M=Al, Sn) along the Pressure-Composition isotherms [1,2]. Positions and occupancies of hydrogen at various hydrogen contents were determined by Rietveld refinement. Only one site is fully occupied during the whole reaction. The other three sites, located closely with each other, are partially occupied and redistributed during desorption.

Line broadening is observed in diffraction pattern for a lot of hydrides during hydrogen absorption. Analysis of *in situ* X-ray diffraction data for LaNi<sub>5</sub>-based hydrides revealed that line broadening is caused by lattice strain, corresponding defects formation, rather than size effects [3]. This agrees with those observed by TEM and positron lifetime measurements. Two kinds of anisotropic lattice strain were observed depending on the composition of the materials.

The authors thank R.C. Bowman, Jr. for providing LaNi<sub>5</sub>-Sn<sub>x</sub> and valuable discussion. This work was financially supported by the Ministry of Economy Trade and Industry (METI) of Japan. [1] Y. Nakamura et al., *J. Alloys Compd.*, **384** (2004) 195. [2] Y. Nakamura, et al., *J. Alloys Compd.* in press. [3] Y. Nakamura, E. Akiba, *J. Alloys Compd.* **308** (2000) 309.

## 13.07 Nanostructures

**13.07.01 Structure and Dynamics of Nanocrystal Superlattices.** Xiao-Min Lin, Center for Nanoscale Materials, Argonne National Laboratory, Argonne, IL.

Most studies in the colloidal nanocrystals have so far focused on the properties of single particle. By comparison, only in recent year, we are beginning to explore assemblies of nanocrystals, i.e. nanocrystal superlattices. The exciting aspect of nanocrystal superlattices is that they are truly a new class of material, where the basic building blocks are nanocrystals instead of atoms in the traditional materials. So in principle, we can obtain many unique properties by changing the composition, the size, the shape of nanoscale building blocks and how strongly they are coupled in the assemblies.

Using *in-situ* small angle x-ray scattering and optical microscopy, we have studied the nanocrystal superlattice formation using both colloidal droplet evaporation and Langmuir trough. We have shown that the evaporation kinetics and the concentration of ligand play important roles on the dynamics and structure of superlattices. There are also distinct differences in long range spatial coherence for arrays formed using these two techniques. This is attributed to the different dynamics that leads to the array formation.

**13.07.02 Surfactant Assisted Assembly of Nanocrystals.** Y. Li<sup>1</sup>, N. Belman<sup>4</sup>, Y. Golan<sup>4</sup>, J. Irwin<sup>1</sup>, C.R. Safinya<sup>2</sup>, J.N. Israelachvili<sup>1,3</sup>, <sup>1</sup>Materials Research Laboratory, <sup>2</sup>Materials Dept., <sup>3</sup>Chemical Engineering Dept., Univ. of California, Santa Barbara, CA 93106 USA, <sup>4</sup>Dept. of Materials Engineering, Ben Gurion Univ. of

the Negev, Beer Sheva 84105 ISRAEL.

To ability to organize nanocrystals into two- and three-dimensional ordered structures is a pre-requisite to many technological applications. In the current work we used chain-crystalline surfactants to link nanocrystals into 2D and 3D ordered assemblies with well defined inter-particle distance as well as crystallographic orientation of the nanocrystals over long ranges. As an example, we present results of structural characterization of ZnS nanorods organized into stacked sheets with an in-plane 2D-crystalline superlattice as evidenced by transmission electron microscopy and x-ray diffraction data. We show that the unit cell of the nanorod superlattice (including type and dimensions) is directly templated from the crystal structures of the pure surfactants, and thus can be tuned predictably by varying the chain length of the surfactant. The methodology is non-specific with regard to the nanocrystals being assembled and therefore can be applied broadly.

Supported by ONR N00014-05-1-0540, DOE DE-FG02-06ER46314, NSF DMR-0503347, and by the US-Israel Binational Science Foundation Grant No. 2002059.

**13.07.03 Strategy for Better Ordering of Polymer Phase in Diblock Copolymer Based Nanocomposites.** P. Thiyagarajan<sup>1</sup>, Chieh-Tsung Lo<sup>2</sup>, Byeongdu Lee<sup>2</sup>, Nancy L. Dietz Rago<sup>3</sup>, Randall E. Winans<sup>2</sup>, <sup>1</sup>IPNS, <sup>2</sup>XSD, <sup>3</sup>CMT, Argonne National Lab, IL.

Advancements in nanotechnology require highly reliable synthetic routes for the fabrication of periodic hybrid nanocomposites. While block copolymers with their rich phase behavior offer as versatile platforms for dispersing nanoparticles it has been a challenge to create highly ordered periodic structures of block copolymer based nanocomposites. We demonstrate a novel method of using homopolymers that can selectively sequester in the same domain as the nanoparticles to synthesize composites with highly ordered lamellar structures as evidenced by SAXD. By tuning the molecular properties and the composition it would be possible to synthesize ordered nanocomposites with other morphologies. We provide a thermodynamic model to explain the phenomenon. The changes in the interfacial curvature by the swelling caused by the homopolymers facilitate phase transitions. The low MW homopolymers by increasing the conformational entropy swell the preferred domains and enable the nanoparticles to redistribute uniformly in it. This simple concept can be extended to synthesize highly ordered self-assembled block copolymer based composites with different morphologies. We believe that this approach will have high impact in the fabrication of composites for various nanotechnological applications.

Work benefited from the use of IPNS, CMT and APS funded by DOE, BES under contract DE-AC02-06CH11357 to the UChicago Argonne, LLC.

**13.07.04 Conformation of Oligo(ethylene glycol) Grafted Polystyrene in Aqueous Solutions.** Gang Cheng, Yuri. B. Melnichenko, George. D. Wignall, Neutron Scattering Science Div., Fengjun Hua, Kunlun Hong, Jimmy W. Mays, Chemical Science Div. and Center for Nanophase Materials Sciences, Oak Ridge National Laboratory, Oak Ridge, TN 37831

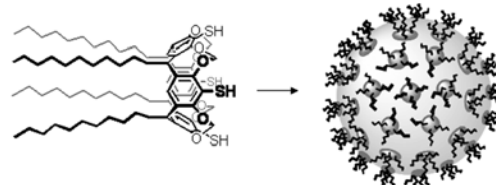
Understanding the fundamentals of the conformational changes of water soluble polymers during the phase transition is imperative for a variety of applications. Polystyrenes grafted with short ethylene glycol (EG) side chains (four EG monomer units) have been synthesized and are found to exhibit lower critical solution temperatures (LCSTs) in water. Temperature induced conformational changes of the polymers (Mw=9400 g/mol) in aqueous solutions were investigated by small angle neutron scattering (SANS), neutron transmission and dynamic light scattering (DLS). The measurements were made as a function of temperature in the range of 25-55°C for three polymer concentrations

(0.1, 0.3, and 1.8 wt %). The neutron transmission measurements were used to monitor the amount of polymer which precipitates or remains in solution above the cloud point  $T_{CP}$ . DLS revealed presence of large clusters in all solutions both below and above  $T_{CP}$  and SANS provided information on the structure and interactions between individual chains. It was found that in the homogeneous region below  $T_{CP}$  the shape of individual polymers is close to ellipsoidal with the dimensions  $R_a=37 \text{ \AA}$  and  $R_b=14 \text{ \AA}$ . The SANS data taken for the most concentrated solution studied (1.8 wt %) can be fitted to the model of ellipsoids with attractive interactions which were approximated by the Ornstein-Zernike function with a temperature-dependent correlation length in the range 24 – 49 Å. Above  $T_{CP}$  a collapse of individual polymers to spherical globules with the radius 15 Å was observed. The study of the influence of the backbone length on the conformation and phase behavior is currently underway.

**13.07.05 Calixarene-Encapsulated Nanoparticles: Self-Assembly into Functional Nanomaterials.** Alexander Wei,\* Beomseok Kim,\* Steven L. Tripp,\* R. Balasubramanian,\* Björn Decker,† Jochen Mattay,‡ Takeshi Kasama,†, Rafal Dunin-Borkowski†, \*Dept. of Chemistry, Purdue Univ., West Lafayette, IN, USA, †Dept. of Chemistry, Univ. of Bielefeld, 33501 Bielefeld, Germany, ‡Dept. of Materials Science, Univ. of Cambridge, Cambridge, UK.

Calixarenes are excellent dispersing agents for metal and inorganic nanoparticles (1). The headgroup can be tailored for strong chemisorption to nanoparticle surfaces, and the tailgroups are displayed in an

arrangement which enhances nanoparticle dispersion control. A variety of calixarenes have



been developed for encapsulating metal nanoparticles and promoting their self-assembly into well-defined ensembles. Examples includes two-dimensional arrays of colloidal Au particles with size-dependent plasmonic responses, and the self-assembly of ferromagnetic Co nanoparticle rings with chiral magnetic states. Nanoparticles within these ensembles are strongly coupled, giving rise to useful and possibly unique collective optical or magnetic properties. The gold nanoparticle arrays exhibit collective plasmon responses and produce electromagnetic field factors that vary strongly with particle size and interparticle spacing, with application to surface-enhanced spectroscopies and nonlinear optical phenomena. The magnetic nanoparticle rings support stable flux closure states at ambient temperatures despite their small size (less than 100 nm) and their polarizations can be reversed upon exposure to an out-of-plane magnetic pulse, with potential utility for nonvolatile data storage.

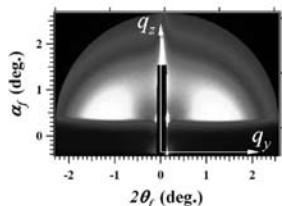
This work was supported by the National Science Foundation (CHE-0243496; ECS-0210445), DARPA (MDA972-02), and the Birk Nanotechnology Center.

(1) Wei, A. *ChemComm* 2006, 1581-91.

**13.07.06 New Methodologies for Formulation and Characterization of Polymer Nanocomposites.** Marie Kissinger-Kane.

**13.07.07 In-situ Investigation of Nucleation and Grain Growth of Sol-gel Derived BiFeO<sub>3</sub> Thin Films.** Tao Sun<sup>1,2</sup>, Xuefa Li<sup>2</sup>, Jin Wang<sup>2</sup>, Vinayak P. Dravid<sup>1</sup>, <sup>1</sup>Dept. of Materials Science and Engineering, Northwestern Univ., Evanston, IL 60208. <sup>2</sup>Advanced Photon Source, Argonne National Laboratory, Argonne, IL 60439.

Sol-gel processing is one of the most attractive techniques for fabricating oxide films, where desired microstructures can be achieved by controlling the nucleation and grain growth (NGG) behavior of films. In the present study, grazing-incidence small-angle x-ray scattering (GISAXS) was utilized to calculate the size, correlation distance and distribution of nuclei of multiferroic BiFeO<sub>3</sub> thin film. Complementary information in real space, as well as the phase and elemental characteristics of nuclei, was provided by transmission electron microscopy. Thermogravimetric analysis and Fourier transform infrared characterization were also carried out to elucidate the nucleation mechanism. By taking advantages of the high-intensity synchrotron x-ray beam at Advance Photon Source in Argonne National Laboratory, we are able to investigate the NGG process in real time from the very early stage when the nuclei are as small as 2 nm. For the first time, the thermodynamic analysis of NGG through fitting the nuclei size with Arrhenius equation yields activation energies for grain growth of BiFeO<sub>3</sub> at different temperature. Moreover, the GISAXS data can describe the distribution of nuclei in the direction normal to the thin films surfaces and interfaces. This study has convincingly demonstrated that GISAXS is the best suited technique for quantitative and in-situ study of the kinetics in NGG for sol-gel derived oxide thin films.



This GISAXS beamtime and use of APS facility is supported by DOE under Contract No. W-31-109-ENG-38. This work was also supported by NSF-NSEC under Contract No. EEC-0118025/003 and NSF-MRSEC under Contract No. DMR-0520513.

**13.07.08 Local Atomic Structure of Gold Nanoparticles on Oxide Support.** W. Dmowski<sup>1</sup>, T. Egami<sup>1,2</sup>, S. Dai, S.H. Overbury, <sup>1</sup>Dept. of Materials Science & Engineering, Univ. of Tennessee, Knoxville, TN 37996, <sup>2</sup>Oak Ridge National Lab, Oak Ridge, TN 37831.

Bulk metallic gold is chemically inert. However, its chemistry drastically changes when gold is deposited on metal oxides as nano-sized particles with diameters smaller than 5 nm. Oxide-supported gold catalysts have been shown to exhibit exceptional catalytic activity in many important reactions, for example oxidation of CO. However, many aspects of the interface structure and chemical nature of gold particles are not well known. It is observed that Au supported on reducible oxides, such as TiO<sub>2</sub>, has a less tendency to suffer deactivation compared to Au on irreducible oxides, such as MgO and SiO<sub>2</sub>. We have used atomic pair-density function (PDF) analysis to study the local-range atomic order of Au nanoparticles on titania and titania covered particles. The X-ray scattering was performed at high energy (86 keV) and at gold L<sub>3</sub> absorption edge. The results indicate that there are some definite correlations between nanocrystalline gold and the TiO<sub>2</sub> support. These extra bonding appear as the second nearest neighbors to Au atoms. Thus it may as well modify the chemical state of Au resulting in, for example, preferred binding of CO.

This work was supported by the National Science Foundation through grant DMR04-04781 and by the Office of Basic Energy Sciences, U.S. Department of Energy.

**13.07.09 Magnetic Structure of Co/CoO Core-Shell Nanoparticles: Implications for Exchange Bias.** Meigan Aronson, Brookhaven National Laboratory and Stony Brook Univ.

We will present the results of neutron diffraction studies on a powder of Co core/ CoO shell nanoparticles. Electron microscopy shows that the CO/CoO interface is highly directional, yielding a faceted core. Neutron diffraction measurements find that antiferromagnetic order in

the CoO shell develops below ~250 K. In addition to the conventional antiferromagnetic modulation of CoO, which is along (111), we find in addition strong magnetic diffraction at the wave vector  $2\pi/a$  (100), almost absent in bulk CoO. The relative magnitudes of both magnetic and purely nuclear peaks are adequately described using a simple model in which the Co O shells are tetragonally strained. As we will show, progressive oxidation leads to differing CoO shell thicknesses and differing degrees of strain. This tetragonal strain results in an uncompensated Co moment at the core-shell interface which we propose is responsible for the large exchange bias effect which is observed in these nanoparticles. Finally, we note that the exchange bias effect only occurs below ~200 K, which is well below the Neel temperature of the shell. Inelastic neutron scattering measurements indicate that the exchange bias effect requires dynamical matching between a rapidly fluctuating core and an initially stationary interface and shell.

## 13.08 Micro-crystals, Micro-beams, and Multiple Crystals

**13.08.01 Towards Understanding the Atomic Basis of Prion Amyloid.** Marcin I. Apostol, Michael R. Sawaya, Lukasz Goldshmidt, Michael J. Thompson, Anders O. Madsen, Christian Riek, David Eisenberg, Univ. of California, Los Angeles, CA.

An aberrant protein-protein interaction between prion molecules is hypothesized to be the cause of transmissible neurodegenerative diseases such as Creutzfeldt-Jakob in humans, Bovine Spongiform Encephalopathy in cows, and Chronic Wasting Disease in free-ranging elk. The self-seeding property of this interaction has a resemblance to amyloid formation and suggests how prion disease propagates among individuals and across species without the need for a nucleic acid component. To gain an understanding of the atomic nature of this interaction, we have solved the structures of a four six amino acid peptides predicted to form amyloid by a 3-D profile computational method. The structures show that the peptides form both parallel and anti-parallel beta-sheets that stack laterally with a tight packing of sidechains that entirely excludes water. This is known as the canonical cross-beta structure, a fundamental characteristic of amyloid. The peptide structures suggest that i) prion can utilize multiple peptide interfaces to form ordered aggregates, ii) the combinatorial assembly of a variety of peptide interfaces can be used to explain the phenomenon of amyloid strains, and iii) structural differences between peptides from disease prone species can explain susceptibility and transmission between species.

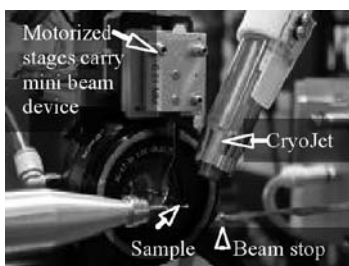
**13.08.02 Protein Micro-crystallography at the Swiss Light Source.** Clemens Schulze-Briese, Elaine Chiu, Sascha Gutmann, Peter W. Haebel, Peter Metcalf, Hajime Mori, Claude Pradervand, Roman Schneider, Takashi Tomizaki.

The undulator beamline X06SA at the Swiss Light Source was designed for the study of weakly diffracting, large unit cell crystals as well as biological micro-crystals. Correspondingly, the beamline is equipped with a dynamically focussing optical system, allowing the beam to be focussed either on the dedicated micro-diffractometer MD2 or on the sample, beamstop or detector position of the high resolution diffractometer.

The presentation will cover the beamline instrumentation as well as several recent highlights of micro-crystallography. The X-ray analysis of in vivo grown CPV polyhedra that allowed its structure to be determined at 2 ~ resolution from 5 - 12 microns crystals will be described in detail.

**13.08.03 Mini-beam for Macromolecules on GM/CA-CAT Beamlines at APS.** R. Sanishvili<sup>1</sup>, V. Nagarajan<sup>1</sup>, S. Xu<sup>1</sup>, M. Becker<sup>1</sup>, D. Yoder<sup>1</sup>, J.L. Smith<sup>1,2</sup>, R.F. Fischetti<sup>1</sup>, <sup>1</sup>GM/CA-CAT, Advanced Photon Source and Biosciences Div., Argonne National Laboratory, Argonne, IL 60439, <sup>2</sup>Life Sciences Inst., Dept. of Biological Chemistry, Univ. of Michigan, Ann Arbor, MI 48109.

Solving crystal structures of some of the most important and challenging biological macromolecules and complexes often stumbles upon an inability to grow crystals large enough or with sufficient order to produce useful diffraction data. While modern synchrotron beamlines have been essential for tackling many difficult projects, today's "standard" beam sizes (50-300  $\mu\text{m}$ ) are too large for sample crystals with sizes on the order of 10 microns. GM/CA-CAT has implemented a "mini beam" apparatus on the two undulator beamlines at the APS. Selected size pin holes and a focal spot of  $\sim 70 \times 20 \mu\text{m}^2$  close to the sample tailor the beam down to crystal size ( $6 \times 8 \mu\text{m}^2$  FWHM, with 10  $\mu\text{m}$  pinhole) without using additional optical elements. Flux at the sample is  $\sim 1 \times 10^{11}$  photons/sec. This apparatus allows data collection from samples of less than 10  $\mu\text{m}$  with excellent signal-to-noise. Overfilling an aperture with a somewhat larger incident beam contributes to overall beam stability. The mini-beam apparatus can be exchanged easily with a conventional scatter guard allowing fast transition between experiments with micro and larger crystals. In addition, larger crystals can be scanned with the mini beam to find high-quality regions for data collected. With the mini-beam apparatus, several useful data sets have been collected from micro-crystals of  $\sim 1 \times 10^{-6} \text{ mm}^3$  leading to good statistics for data processing and model refinement.



GM/CA CAT is supported by the NIGMS (Y1-GM-1104) and the NCI (Y1-CO-1020), NIH, U.S. Public Health Service. The APS is supported by the U.S. DoE, BES, Office of Science (W-31-109-ENG-38).

**13.08.04 Implementation of Microdiffraction Techniques at NorthEastern Collaborative Access Team APS Beamlines.** Malcolm Capel, Steven Ealick, Kanagalaghatta Rajashankar, North Eastern Cooperative Access Team, Advanced Photon Source, Dept Chemistry & Chemical Biology, Cornell Univ., Ithaca, NY.

North Eastern Collaborative Access Team (NECAT) has constructed and operates 2 undulator beam lines optimized for macromolecular microcrystal diffraction at the Advanced Photon Source, (APS) using the APS tandem offset undulator as the X-ray source and incorporating Kirkpatrick-Baez focusing. Our Phase I beam line is tunable over a spectral range of 5-25 KeV (focus spot size 60H x 20V microns, FWHH), while our Phase II beam line is a fixed energy beam line operating at 12.662 or 14.76 KeV (focus spot size 100H x 50V micron FWHH). Both beam lines produce very high flux density and use x,y mirror steering to dynamically stabilize the beam position at the spindle. A Maatel MD2 micro diffractometer has recently been installed on the Phase II beam line which provides shaped X-ray beams down to 10 microns and the ability to visualize and center 5-10 micron sample crystals. Hardware and software systems supporting microcrystallography techniques at NECAT are described, along with recent results. We also describe plans for improving the flux density and beam position stability of our beam lines intended to make data collection from microcrystals a low risk and routine endeavor.

**13.08.05 ID23-2 - The New MX-dedicated Microfocus Beamline at the ESRF.** D. Flot<sup>a</sup>, T. Mairs<sup>b</sup>, E. Mitchell<sup>b</sup>, M. Guisjarro<sup>b</sup>, V. Rey<sup>b</sup>, D. Nurizzo<sup>b</sup>, S. McSweeney<sup>b</sup>, <sup>a</sup>EMBL, Grenoble, France, <sup>b</sup>ESRF, Grenoble, France.

In the early 1990s, on the ID13 beamline at the ESRF, it was demonstrated that it was possible to collect diffraction data from crystals of micrometer size (microcrystal)<sup>1</sup>. Initially devoted to small molecule crystallography, pioneering work was carried out to see if it was possible to collect data from very small protein crystals<sup>2</sup>. Based on this experience, a new microfocus beamline (ID23-2), dedicated tool for studying protein microcrystal, has been built at the ESRF. ID23-2 is the second beamline built on a canted undulator straight section and in a fixed wavelength beamline using a single bounce Si[111] monochromator. The beam is focused down to 7.5  $\mu\text{m}$  horizontally by 5  $\mu\text{m}$  vertically (FWHM) by Pt-coated silicon mirrors in a Kirkpatrick-Baez (KB) geometry. The experimental setup is composed of a MD2M diffractometer (MAATEL, under an EMBL licence), a SC3 sample changer<sup>3</sup> and a MarMOSAIC 225 CCD detector.

The main challenge for ID23-2 was to provide to the MX user community a beamline with a beam size smaller than 10  $\mu\text{m}$  in diameter while keeping the same 'easy-to-use' environment and reliability as the other ESRF MX beamlines (ID14, ID23-1, ID29, BM14)<sup>4</sup>. The beamline has been open to the user community since mid-November 2005. The first year of user operation has demonstrated that the design was basically sound and that the beamline can be used by inexperienced users. Instrumentation developments, data collection strategies and first results will be presented and discussed.

[1] RB Neder *et al.*, *Z. Kristallogr.* (1996) **211**(11) 763-765. [2] Cusack S *et al.*, *Nat Struct Biol* 1998, **5**:634-637. [3] Cipriani *et al.*, *Acta Cryst.* (2006) **D62**, 1251-1259. [4] [http://www.esrf.fr/UsersAndScience/Experiments/MX/About\\_our\\_beamlines](http://www.esrf.fr/UsersAndScience/Experiments/MX/About_our_beamlines)

**13.08.06 Microcrystals and Microbeams at MacCHESS.** R.E. Gillilan, M.J. Cook, S. Cornaby, Detlef Smilgies, T.A. Szebenyi, D.H. Bilderback, Cornell High-Energy Synchrotron Source, Ithaca NY.

There are multiple advantages to using X-ray microbeams in protein crystallography. While such beams are naturally suited to microcrystals, sometimes one can obtain dramatically better diffraction from larger crystals which are inhomogeneous in quality by judicious positioning of the beam. Crystals growing in clusters that are difficult to separate are also not uncommon. In this case as well, microbeam positioning can make data collection possible. Unexpectedly, microbeam optics have also proven to be a very significant advantage on our weakest, flux-limited station. Users accustomed to using 150 micron diameter beams to achieve reasonable signal are now able to use 18 micron beams with essentially no degradation in signal. Beams 18 microns in diameter typically deliver a flux of  $1.4 \times 10^{10}$  photons/second at our brightest stations. Optical elements are housed in newly designed enclosures that minimize distortion and allow for easy interchange and reproducible alignment. Subject to the limitations of source size, focal length, and divergence permissible for protein crystallography, we have pushed our beam diameters as small as 5 microns. Optics producing the smallest beams require motorized focus and alignment procedures which are straightforward and mechanically stable. Capillaries are housed in newly designed enclosures that minimize possible deformation, yield reproducible alignment, and allow for easy interchange with conventional collimators. In this talk I will describe our complete protein microcrystallography setup, including an integrated helium enclosure for reducing background scatter that is compatible with ALS-style sample automounting. Several examples from recent MacCHESS users will be discussed, including our experience with collecting data on 1-2 micron diameter needle-shaped crystals.

Many thanks to the staff of MacCHESS and CHESS who are supported through NIH NCCR grant RR-01646 and NSF award DMR 0225180.

## 13.09 Teaching Gadgets and Educational Tools

**13.09.01 Are Teaching Gadgets Obsolete in Times of Computer Animations?** Peter Müller, MIT Dept. of Chemistry, 77 Massachusetts Av., 2-325, Cambridge, MA 02139, pmueller@mit.edu

The author of this presentation has used several teaching gadgets during a graduate level class on crystallography, taught once a year within the curriculum of the MIT Department of Chemistry. Some of these gadgets are re-dedicated dog toys from Trader Joe's, some were self-made by Wally Cordes, the Godfather of crystallographic teaching gadgets, and some were manufactured for the purpose of teaching and are commercially available (namely the diffraction grids sold by the Institute for Chemical Education at the UW-Madison). At the end of the term the students were asked their opinions about the usefulness of the teaching gadgets used in class. Their responses are going to be presented alongside the actual gadgets themselves (as far as they can be brought to Salt Lake City) and a comparison will be drawn between teaching the same class with and without the help of these tools.

**13.09.02 Crystallographic Teaching Tools for Beginners.** J.P. Glusker, Fox Chase Cancer Center, 333 Cottman Ave., Philadelphia, PA 19111 USA.

We live in a three-dimensional world and study the three-dimensional structures of crystals. Therefore I will show some three-dimensional methods of teaching about the basics of this branch of science. Models that beginning students can hold in their hands greatly help them understand the many new and complicated principles that are taught them. Such gadgets can be used in addition to the powerpoint-based descriptions and interactive computer programs currently used. Some of the gadgets I have used will be described here. They include ways of describing diffraction and interpreting diffraction patterns, demonstrating crystal symmetry, explaining direct methods and Patterson maps, and pointing out specific geometric properties in crystal structures. Finally some uses of three-dimensional models in probing enzyme mechanisms will be described. The aim is to encourage the student to appreciate the practical and three-dimensional aspects of X-ray crystallography.

**13.09.03 Walking the Reciprocal Space: Beyond Bragg & Co.** J. Kaercher<sup>1</sup>, J. F. Britten<sup>2</sup>, C. Boere<sup>3</sup>, M. Ruf<sup>1</sup>, <sup>1</sup>Bruker AXS Inc., Madison, WI, USA, <sup>2</sup>McMaster Univ., Hamilton Ontario, Canada, <sup>3</sup>Bruker AXS B.V., Delft, The Netherlands.

A new tool is presented that displays an interactive three-dimensional view of reciprocal space. The visualized information is derived directly from pixel data collected with two-dimensional detectors and preserves contour details on many orders of intensity magnitude. Unlike precession images or pseudo-precession images, no upfront knowledge of the sample orientation is required, which makes this method amenable to any kind of monochromatic diffraction data, e.g. from Bragg diffraction, diffuse scattering, or texture analysis. Controls exist to choose the color scale and contour level(s) at which to render the diffraction intensities. Other tools let the user select an arbitrary plane in reciprocal space or a resolution shell.

Examples will be presented that illustrate the usefulness of the tool and its application in education.

**13.09.04 PowerPoint Presentations as Warm, User-Friendly Teachers: New Tricks for an Old Dog.** Bruce M. Foxman, Jerry P. Jasinski, Michael J. Vela, Tae H. Cho, Dept. of Chemistry, Brandeis Univ., Waltham, MA, Dept. of Chemistry, Keene State College, Keene, NH, Concord-Carlisle Regional High School, Concord, MA, Sharon High School, Sharon, MA.

*Symmetry and Space Groups* is an interactive PowerPoint tutorial containing over 200 PowerPoint "slides", in five modules, arranged by crystal class; a sixth module covers special topics. The triclinic and monoclinic groups (2+13) are built from "scratch", and are derived from the Hermann-Mauguin symbol. Additional sections provide practice on many of the orthorhombic groups in crystal class 222 as well as on enantiomorphous space groups. In the tutorial, lattice points build iteratively & interactively with keyclick, and the coordinates of points "pop up" as the unit cell is filled. The tutorial features interactive questions and answers, occasional humor, sound bites, and photos and links to the biographies of some of the important figures in the field. (<http://people.brandeis.edu/~foxman/teaching/indexpr.html>)

A second tutorial, *Crystalline Insights*, was written for the advanced high school science student. Since most high school chemistry classes only briefly discuss aspects of crystal structure, the goal of *Crystalline Insights* is to provide a demonstration of the *practical operations* of X-ray diffraction and structure determination. The preferred use of the tutorial would have small groups of high school students, accompanied by their teachers, visit a local X-ray lab for a *field trip*. In preparation for the trip, students would complete part of the tutorial and grow crystals of citric acid or sucrose. A suitable crystal would be selected from the batch, mounted on the diffractometer, and solved in a few hours' time. The tutorial contains over 110 PowerPoint "slides", as well as many external links. (<http://people.brandeis.edu/~foxman/teaching/indexhs.html>)

**13.09.05 How to Teach the Phase Problem and the Basics of Direct Methods.** Henk Schenk, Laboratory for Crystallography, HIMS, FNWI, Univ. of Amsterdam, Valckenierstraat 65, 1018XE Amsterdam.

In the present machinery for structure determination from X-Ray diffraction data, the so called Direct Methods play a very important role in solving the phase problem. Although the theory behind Direct Methods is complicated and firmly based on mathematical theory, the basics of the methods can be easily explained from electron density considerations. Simple physical pictures such as these are attractive for teaching purposes (Schenk 1971, 1973, 1979, 1981).

The presentation will begin with introducing the phase problem using two dimensional electron density images on overhead foils. Then the phase relation between the three reflections  $h\ k\ l$ ,  $h_1\ k_1\ l_1$  and  $-h_1\ -k_1\ -l_1$  (to be referred to as  $H\ K\ H-K$ ) will be explained using the same foils, leading to the famous triplet relation holding for large structure factors of the reflections  $H$ ,  $K$ , and  $-H-K$

$$\phi_H + \phi_K + \phi_{-H-K} \approx 0$$

Also its probability character will be demonstrated. Starting from this relation also a simple Direct Method will be presented visually that solves a simple structure almost completely. If time permits, in the same easy way more complicated phase relations like the negative quartet relation will be introduced and a more modern way of presentation will be shown.

Schenk, H. (1971). *De Symbolische Additie Methode*. Programmed instruction (in Dutch). Schenk, H. (1973). *Acta Cryst.* A29, 480-481. Schenk, H. (1979). *J. Chem. Educ.* 56, 383-384. Schenk, H. (1981) *Acta Cryst.* A37, 573-578

## 13.10 Radiation Damage

**13.10.01 Radiation Damage in Macromolecular Cryocrystallography.** E.F. Garman, Dept. of Biochemistry, Univ. of Oxford, Rex Richards Bldg, Oxford OX1 3QU, UK.

Advances in dealing with radiation damage in macromolecular crystallography are intimately intertwined with the development of cryotechniques (100K) in the 1990s. The loop mounting innovation of Teng<sup>[1]</sup> made the method much more straightforward and gave impetus to many laboratories to experiment with it.

However, it was not long before high flux density synchrotron beams were observed to cause radiation damage even for cryocooled crystals. Researchers started to try to understand the physical and chemical processes involved in this damage (reviewed in [2]), which manifests itself in a number of different ways, including: changes in crystal colour, decreasing diffraction power with dose, noticeable first in decreasing values of  $I/\sigma(I)$  for the highest resolution reflections, a small linear increase in unit cell volume, and specific structural damage to covalent bonds in the protein in a reproducible order<sup>[3-5]</sup>. This specific damage can lead to incorrect conclusions on biological mechanisms being drawn from structures, especially as enzyme active sites and metal binding sites seem particularly sensitive to change by X-ray irradiation. Thus the issue of radiation damage has recently come to the fore as a concern for all structural biologists.

This contribution will summarise the current state of our understanding of radiation damage in macromolecular cryocrystallography, including putative mitigation strategies and the experimental determination of a dose limit of  $3 \times 10^7$  Gy<sup>[6]</sup>.

[1] Teng, T-Y (1990) *J Appl Cryst* 23, 387-391

[2] Ravelli RGB and Garman EF (2006) *Curr Opin Struct Bio*, 16, 624-629

[3] Weik M *et al.* (2000) *PNAS* 97, 623-628.

[4] Burmeister W.P (2000) *Acta Cryst.* D56, 328-341.

[5] Ravelli RGB and McSweeney S (2000) *Structure* 8, 315-328.

[6] Owen *et al.* (2006) *PNAS* 103, 4912-4917.

**13.10.02 Crystal Crystal Heating in a Third Generation Synchrotron X-ray Beam, a Significant Factor or Not?** E.H. Snell<sup>a</sup>, H.D. Bellamy<sup>b</sup>, G. Rosenbaum<sup>c</sup>, M.J. van der Woerd<sup>d</sup>, <sup>a</sup>Hauptman Woodward Medical Research Inst., Buffalo, NY 14203, <sup>b</sup>CAMD, Louisiana State Univ., Baton Rouge, LA 70806, <sup>c</sup>Dept. of Biochemistry, Univ. of Georgia, SERCAT at APS, Argonne, IL 60439, <sup>d</sup>Dept. of Biochemistry and Molecular Biology, Colorado State Univ., Fort Collins, CO 80523.

Cryocooling mitigates the effects of secondary radiation damage. However, the sample will be warmed by energy deposited from X-ray photons. How large is the temperature increase, does it reduce the effectiveness of cryocooling and enhance radiation damage effects? We measured beam heating using thermal imaging; specifically, the temperature rise of 1 mm and 2 mm glass spheres (sample surrogates) exposed to an intense synchrotron X-ray beam while cooled in a 100 K nitrogen gas stream. Calculations, validated by our measurements, show that the temperature rise is on the order of 1-10 K for macromolecular samples. Beam heating is not a significant factor for devitrification or enhancing free radical mobility under typical conditions.

However, microcrystals require more careful considerations. Model calculations show that the temperature rise is mainly proportional to the flux intercepted by the sample and only mildly dependent on the sample size; the temperature rise increases only by a factor of size<sup>-0.14</sup>. Increasing flux on the sample, instead of increasing exposure time to compensate for the smaller sample, may steer into dangerous

territory. The same caveat applies to radiation damage studies if maximum fluxes are used instead of just maximum flux densities. Beam heating in this case may bring the sample close to the onset of enhanced free-radical mobility (120-130 K) with associated consequences for radiation damage.

**13.10.03 A Statistical Measure of Mitigation of Radiation Damage to Protein Crystals.** B.N. Shah<sup>\*</sup>, B.S. Yaniga<sup>\*</sup>, U.N.Chinte<sup>†</sup>, A.A. Pinkerton<sup>‡</sup>, B.L. Hanson<sup>‡</sup>, C.A. Schall<sup>\*</sup>, <sup>\*</sup>Dept of Chemical & Environmental Engineering, <sup>‡</sup>Chemistry The Univ. of Toledo, Toledo, OH 43606, <sup>†</sup>School of Structural Biology, Univ. of Pittsburgh, PA 15217.

X-ray diffraction data collected at Bio-CARS on matched D-xylose isomerase crystals of different sizes at 15K and 100K have shown marked improvement in lifetime of the crystals cooled to 15 K (Chinte *et al.*, 2007). The diffraction data is further analyzed using Analysis of Variance (ANOVA) which gives a statistical level of significance associated with the sources of variation (size, temperature, cycle, resolution shell). It also takes into account effects due to interaction of factors (eg. interaction between size and temperature). ANOVA was done on all crystals for matching resolution shells and also on individual sets of small crystals and large crystals. The analysis shows that temperature does have a significant effect on diffraction. Additionally, differences in the diffraction data from crystals of XI grown in differing conditions and measured at 15K and 100K will also be described and compared, to better assess the contribution of solvent composition in diffraction lifetime.

Chinte, U., Shah, B., Chen, Y.-S., Pinkerton, A. A., Schall, C. A. & Hanson, B. L. (2007). *Acta Crystallogr., Sect D: Biol. Crystallogr.* **D63**, Accepted.

**13.10.04 No Abstract.** Martin Weik.

**13.10.05 Quick Soak for Long Life - Practical Radiation Damage Prevention.** Andrea Schmidt, Brice Kauffmann, Annette Faust, Manfred Weiss, Victor Lamzin, EMBL Hamburg, Notkestrasse 85, D-22607 Hamburg, Germany.

Radiation damage is caused by a cascade of ionization events and the formation of radicals, and can severely and irreversibly affect the quality of diffraction data from macromolecular crystals. Cryocrystallographic techniques have alleviated this problem but with third generation synchrotron sources, it has again become a hot topic.

We established an easy-to-apply scavenger quick-soaking (< 30 s) method to combat radiation damage in macromolecular crystals. Nicotinic acid, DTNB and oxidized glutathione were tried on crystals of hen egg-white lysozyme, porcine pancreatic elastase and thaumatin. We used a pairwise R factor ( $R_p$ ) as a function of distance in frame number to monitor global radiation damage on the data level. This always agreed with the reduction of strong features in difference maps. Significantly less damage occurred in the scavenger-treated crystals. Nicotinic acid appeared to be the most "universal" and effective compound, DTNB was equally powerful, but less effective in protecting disulphide bridges, and glutathione was least suitable. The protection effect seemed to depend on the chemical composition of the scavenger and the protein sample, suggesting different protection mechanisms.

Following on those results, screening for suitable compounds and addition of scavengers, most notably DTNB or nicotinic acid could become part of the preparation of crystals for X-ray data collection. Our current efforts thus aim at a better understanding of the mechanisms of radiation protection and the specificity of scavengers, as well as the quantification of the scavenger effects and the time

progress of radiation damage by spectrophotometric monitoring. An overview of the current studies and the latest findings will be given.

**13.10.06 Can Radiation Damage to Protein Crystals Be Reduced Using Small Molecule Compounds?** J. Kmetko<sup>1</sup>, M. Warkentin<sup>2</sup>, U. Englich<sup>3</sup>, R.E. Thorne<sup>2</sup>. <sup>1</sup>Physics Dept., Kenyon College, Gambier, OH 43022, <sup>2</sup>Physics Dept., Cornell Univ., Ithaca NY 14853, <sup>3</sup>MacCHESS, Cornell Univ., Ithaca NY 14853.

Our previous studies defined a data collection protocol and a metric that provide a robust measure of radiation damage to protein crystals, and confirmed that radiation damage at cryogenic temperatures is roughly independent of the crystal's mass-energy absorption coefficient [1]. Using this protocol and metric, we have screened 17 small-molecule compounds (introduced either by co-crystallization or soaking) for their ability to protect protein crystals from radiation damage. The compounds were selected based upon their ability to interact with radiolytic products (e.g., hydrated electrons, hydrogen, hydroxyl and perhydroxyl radicals) and/or their efficacy in protecting biological molecules from radiation damage in dilute aqueous solutions. At room temperature we find a varied response, from sensitizing to protecting, that depends upon the compound as well as on the protein crystal. At cryogenic temperatures, no compound provides additional protection against radiation damage. These results and possible underlying mechanisms will be discussed.

[1] J. Kmetko *et al.*, *Acta Cryst. D* 62, 1030–1038 (2006).

We thank CHESS for access to beam lines F3 and F1. This work was funded by the National Institute of Health (R01 GM65981).

**13.10.07 The Effects of Radiation Damage on Anomalous Dispersion Experiments.** Ana Gonzalez, SLAC, 2575 Sand Hill Rd., Menlo Park CA 94025.

Information obtained from crystal diffraction data can be seriously affected because of radiation damage of the sample. The documented effects of radiation damage under x-rays include: 1) gradual loss of reflections at high resolution; 2) expansion of the unit cell; 3) increase of the crystal mosaicity; 4) specific damage to individual atoms in the sample (breakage of disulfide bonds, decarboxylation of acidic side chains, reduction of intrinsic metals and heavy atoms).

These effects compromise SAD and MAD experiments in several ways: a) Loss of diffraction resolution affects map interpretability; b) the unit cell expansion and specific structural changes result in loss of isomorphism during the experiment that makes data scaling difficult and interferes with accurate measurement of the anomalous signal. Location of anomalous scatterers may become impossible, particularly for large substructures; c) Changes in the anomalous scatterer oxidation state complicates refinement of the site parameters and result in less accurate phases. In some cases, heavy atoms may become totally delocalized, and the anomalous signal decreases dramatically.

Although radiation damage cannot be eliminated, some of the effects listed above can be mitigated by adequate sample preparation, freezing and careful selection of the data collection parameters.

## AW.01 Kenneth Trueblood Award Symposium

**AW.01.01 Forty Years of Struggle with Computers Over Crystallography and Intermolecular Interactions.** A. Gavezzotti, Dipartimento di Chimica Strutturale e Stereochimica Inorganica, Univ. of Milano, Milano, Italy.

After an unavoidable but moderate excursion down memory lane, the lecture will present a survey of the development of computer techniques for the analysis, prediction and when possible, control of organic crystal structures, from early data processing, to thermal motion analysis, all the way to molecular packing analysis, intermolecular interactions and present-day massive techniques including dynamic simulation. The tone will be appropriate to an encomiastic occasion with little technicality and plenty of colourful examples.

**AW.01.02 *Ab initio* Prediction of Crystal Structures – Blind Tests and Recent Applications.** Graeme M. Day, Dept. of Chemistry, Univ. of Cambridge, Cambridge, UK.

The ambitious goal of predicting the crystal structure of a molecule, given only a molecular diagram, is a great challenge for the molecular modelling community. The pursuit of successful crystal structure prediction (CSP) methodologies has been a driving force for the development of a variety of methods, both for sampling the space of all possible close-packed crystal structures and for calculating crystal properties and energies used to assess which of the many possibilities are most likely to be observed. Both the reliability of CSP and recent applications of such calculations are discussed.

The “blind tests” have been organised by the Cambridge Crystallographic Data Centre as an objective evaluation of existing methodologies for CSP of organic molecules [1]. The organisation and results of these collaborations are presented and discussed in the context of other published studies. While overall success rates are low, some of the methods tested are becoming reliable; consistent failures for certain molecule types point to areas for future development.

These calculations are of particular interest in the pharmaceutical industry, where predictive tools to anticipate new crystal forms are desired. Examples from our recent efforts to apply CSP to polymorph and solvate formation in pharmaceutical systems are presented [2], demonstrating the power of current computational methods in understanding crystallization behavior.

[1] J. P. Lommerse *et al.*, *Acta Cryst.* (2000), B56, p.697; W. D. S. Motherwell *et al.*, *Acta Cryst.* (2002), B58, p.647; G. M. Day *et al.*, *Acta Cryst.* (2005), B61, p.511.

[2] A. J. Cruz Cabeza, G. M. Day, W. D. S. Motherwell and W. Jones, *Crystal Growth & Design* (2006), 6, p.1858; A. J. Cruz Cabeza, G. M. Day, W. D. S. Motherwell and W. Jones, *J. Amer. Chem. Soc.* (2006), 128, p.14466.

**AW.01.03 Fluorine- Odd Man Out<sup>1</sup>.** Jack D. Dunitz, Organic Chemistry Laboratory, Swiss Federal Inst. of Technology (E.T.H. Zurich) CH-8093 Zurich, Switzerland.

Introduction of fluorine into organic compounds changes their chemical and physical properties in many interesting and not completely understood ways. Here we deal mainly with condensed phases, especially crystal structures. For example, in contrast to early expectations, organic fluorine hardly ever forms hydrogen bonds. Examples of crystal structures of several organo-fluorine compounds will be described and discussed, sometimes with the help of intermolecular energy calculations. The main lesson to be learned is that in a molecular assembly containing fluorine atoms, these atoms have to go somewhere, and wherever they go you can make a nice story. Endnotes: <sup>1</sup>Odd man out: one that does not fit into a group

**AW.01.04 Thermodynamics of Molecular Crystals Under High Pressure From Quantum Chemistry: The Solid-Solid Phase Transitions of  $\text{Co}_2(\text{CO})_6(\text{XPh}_3)_2$  ( $\text{X}=\text{P}, \text{As}$ ).** Piero Macchi, Nicola Casati, Angelo Sironi, Dip. Di Chimica Strutturale e Stereochimica Inorganica, Univ. di Milano, Via Venezian 21, 20133 Milano, Italy.

Transition metal carbonyl clusters attracted chemists for their unusual features, stimulating experimental and theoretical works to explain the nature of metal-metal and metal-carbonyl bonds. However, little information was obtained by studying their structure at extreme conditions. A few spectroscopic investigations were carried out on  $\text{MM}'(\text{CO})_n$  species<sup>1</sup> ( $\text{M} = \text{Mn}$ ;  $\text{M}' = \text{Mn}, \text{Re}$ ) at high pressure, providing evidence of conformational changes about the metal-metal bond axis. Recently, we confirmed this hypothesis through X-ray diffraction experiments on single crystals of  $\text{Co}_2(\text{CO})_6(\text{PPh}_3)_2$  ( $\text{X} = \text{P}, \text{As}$ ) at high pressure and low temperature.<sup>2</sup> These metal carbonyl dimers transform the conformation of carbonyls about the Co-Co bond from staggered to eclipsed when the volume is reduced. Because a crystalline symmetry is broken, this rearrangement is always accompanied by a solid-solid phase transition. The experimental data available stimulated theoretical investigations to produce a comprehensive thermodynamic characterization of the solid state behaviour of  $\text{Co}_2(\text{CO})_6(\text{XPh}_3)_2$  under extreme conditions. Other significant changes of the molecular geometries, such as shrinking of metal-metal and metal-ligand bonds, require a quantum mechanical description instead of the more traditional molecular mechanics approach. In fact, the most significant variance to the free energy comes from the perturbation of soft intramolecular bonds, whereas the weak intermolecular interactions have only an indirect role.

<sup>1</sup>Adams, D. M.; Hatton, P. D.; Shaw, A. C. *Journal of Physics: Condensed Matter* 1991, 32, 6145.

<sup>2</sup>Casati, N.; Macchi, P.; Sironi, A. *Angew. Chem. Int. Ed.*, 2005, 44, 7736.

**AW.01.05 Is There a Mechanism for Crystal Growth and Dissolution? AFM & Computer Simulation for DL-Serine.** J. Michael McBride, Joshua H. Baraban, Thomas J. Gniadek, Dept. of Chemistry, Yale Univ., New Haven, CT 06520 USA.

For more than 300 years scientists have been fascinated by the intricate process of self-assembly involved in crystal growth and dissolution. Until quite recently they had to rely on phenomenological theories based on bulk observation. Now it is possible to observe the dynamics of monolayer patterns on growing and dissolving surfaces of molecular crystals using AFM and to apply this information toward developing a detailed structural theory of these processes. Recent work with the amino acid DL-serine will be used to illustrate an approach to this problem. Experimental evidence concerning critical sizes, the efficiency of damage repair, and the evolution of mesas and etch pits on enantiomeric monolayers will be presented. PIXEL calculations by Angelo Gavezzotti have provided a starting point for empirical kinetic studies aimed at using these AFM results together with Monte-Carlo simulation to identify factors that control the rate of addition to, or loss from, myriad individual surface sites.

The AFM instrument was obtained under support of ONR Grant N00014-97-1-1047

## AW.02 Isidor Fankuchen Award Symposium

**AW.02.01 What Can We Learn from the Multiple Crystal Structures Reported for Pentacene, and for the Anthracene and Tetracyanoquinodimethane (TCNQ) Molecules in Their Various Guises?** Frank H. Herbstein, Moshe Kapon, Schulich Faculty of Chemistry, Technion-Israel Inst. of Technology, Haifa, Israel.

Independent reports of the crystal structures of pentacene have been compared to assess their precision and dependence on crystalline environment. Bond lengths from four independent structure determinations (at 295, 293, 180 and 90 K) of pentacene agree well with each other and with calculated values. However, deviations from planarity (up to 0.13 Å) differ in detail in the two half-molecules of pentacene in the asymmetric unit, as does their temperature dependence. Analogous studies have been carried out for pristine anthracene and some of its molecular compounds—bond lengths are similar in different situations while deviations from planarity vary in detail from one crystalline environment to the next and are ascribed to intermolecular influences; agreement among different determinations is good. The results for TCNQ are less precise and more complicated; the neutral species and various salts have been studied. The three species—neutral  $\text{TCNQ}^0$ , mono-anionic dimeric  $(\text{TCNQ})_2^{-1}$  and mono-anionic  $\text{TCNQ}^{-1}$ —can often (but not always) be distinguished through their different bond-length patterns but deviations from planarity are ascribed to intermolecular influences. Infra-red and (especially) resonant Raman spectroscopy provide alternative ways of determining TCNQ charge states. These sometimes match those determined from diffraction and sometimes not, the discrepancies being ascribed to physical differences between the single crystals used for diffraction measurements and the powder samples used for spectroscopy. Unfortunately most materials have been investigated by either diffraction or spectroscopic techniques rather than by both.

**AW.02.02 Kinetic and Thermodynamic Crystals. Interactions and Close Packing.** Gautam R. Desiraju, School of Chemistry, Univ. of Hyderabad, Hyderabad 500 046, India.

The packing of organic molecular crystals may be considered from two viewpoints. In the geometrical approach, crystal structures are governed by close packing and no significant role is assigned to directional intermolecular interactions. Alternatively, a crystal may be considered on the basis of chemical factors, and a hierarchy of directional interactions is assumed to control crystal packing. Many examples have been cited which follow one or the other of these models, and also violations thereof. The problem with both descriptions is that they seek to relate a complex event, namely crystallization, in simple terms. In actuality, these models correspond to thermodynamic and kinetic outcomes of crystallization, and the differences between them are most starkly etched in polymorphic systems. The concept of the supramolecular synthon, which is a kinetic unit, is useful in describing the situations which lie between the kinetic and thermodynamic extremes. The synthon model is another form of structural simplification but one which admits to and incorporates the complexity of the prevailing situation. Therefore, generality is not compromised. It demands neither a scale of interaction energies as does the chemical model, nor a scale of crystal packing energies as does the geometrical model. It is concerned only with the frequencies of occurrence of representative patterns in crystal structures. If a pattern is seen often enough, it is kinetically favoured and is likely to recur. If a sufficiently large number of crystal structures are examined, any kind of molecule → crystal relationship may be predicted even if it is not understood entirely.

**AW.02.03 Detailed Studies of the Low-Temperature Phase Transitions in  $[\text{Ni}(\text{H}_2\text{O})_6](\text{NO}_3)_2 \cdot (15\text{-crown-5}) \cdot n\text{H}_2\text{O}$ ,  $n = 1$  and  $2$ .** Carolyn P. Brock, Maxime A. Siegler, Sean Parkin, Dept. of Chemistry, Univ. of Kentucky, Lexington, KY 40506-0055, USA.

Three related compounds have been found that go through reversible phase transitions between 300 K and 90 K without significant crystal damage. Two of the compounds each go through a sequence of three transitions during which the number of independent units first becomes quite large ( $Z' = 7$  and  $5$ ) and then becomes small again.



The three compounds can all be made easily and cheaply. All contain octahedrally coordinated  $\text{Ni}^{2+}$  ions and separate 15-crown-5 molecules; the complex ion and the crown are linked by H bonding to form infinite chains in which the cation and molecule alternate. The two compounds that will be discussed are  $[\text{Ni}(\text{H}_2\text{O})_6](\text{NO}_3)_2 \cdot (15\text{-crown-5}) \cdot n\text{H}_2\text{O}$ ,  $n = 1$  and  $2$ .

The phase transition in the  $n = 1$  compound is quite conventional. The space group above *ca.* 190-195 K is  $P2_1$  with  $Z' = 1$ ; below this temperature the space group is unchanged but  $Z' = 2$  and the atomic displacement parameters are smaller.

The phase sequence in the  $n = 2$  compound is much more unusual; during slow cooling  $Z'$  changes from  $\frac{1}{4} \rightarrow \frac{1}{2} \rightarrow 7 \rightarrow 1$  between room temperature and 90 K. All phases except the  $Z' = 1$  phase, which was already known (Steed *et al.*, 2001), are disordered. With cooling the disorder and the molar volume decrease as expected.

Studies of the phase transitions in these two compounds have included DSC measurements and analyses of single-crystal data sets measured at large numbers of different temperatures (22 for  $n = 1$  and 30 for  $n = 2$ ). Details of the transitions will be discussed in light of Herstein's (2006) review.

Steed, Sakellariou, Junk & Smith (2001). *Chem. Eur. J.* **7**, 1240-1247. Herstein (2006). *Acta Cryst.* **B62**, 341-383.

**AW.02.04 Phase Transitions, Polymorphism and Parametric Powder Diffraction.** W.I.F. David, ISIS Facility, Rutherford Appleton Laboratory, Chilton, OX11 0QX, U.K.

Powder diffraction is an excellent method for the rapid characterisation of structural phase transitions and polymorphism in molecular systems. Phase transition temperatures, crystal structures and structural order parameters may all be extracted from powder diffraction data. This talk will include a discussion of structural phase transitions in sulfur and pyridine performed on the high resolution neutron powder diffractometer, HRPD, at the ISIS spallation neutron source. As well as discussing the detailed structural information that has been obtained for these two materials, this talk will also highlight the experimental difficulties encountered in unravelling the true nature of the phase transitions in these compounds.

**AW.02.05 Eligio Perucca First Observed Induced Optical Activity in 1919.** Bart Kahr, Dept. of Chemistry, Univ. of Washington, Seattle, WA 98195.

It is widely acknowledged that first observation of induced activity in the service of the study of non-covalent interactions was made in 1959. Induced optical activity became a major area of inquiry during the 1960s when commercial polarization modulation spectropolarimeters were introduced. Here, we show that Torino

physics professor Eligio Perucca first observed induced optical activity while studying sodium chlorate crystallization in the presence of equilibrium mixtures of triarylmethane dyes. We reinvestigate his sodium chlorate crystals using a newly developed circular extinction imaging microscope and reveal what these findings suggest about crystal growth mechanisms. We show that Perucca appears unnamed in what the Royal Institution of London observer named as the "best science book ever written", *The Periodic Table*, by Primo Levi.

## AW.03 Margaret Etter Early Career Award Symposium

**AW.03.01 Negative Thermal Expansion Materials: X-ray and Neutron Diffraction Adventures under Non-ambient Conditions.** Cora Lind, Stacy D. Gates, Amy M. Gindhart, Dept. of Chemistry, The Univ. of Toledo, Toledo, OH 43606, USA.

Negative thermal expansion (NTE) materials have received considerable scientific attention due to their potential for use as fillers in controlled thermal expansion composites. Crystallographically, these compounds are interesting because their open framework structures are prone to undergo temperature and pressure induced phase transitions. In most cases, only one of the phases displays NTE. Diffraction experiments as a function of temperature and pressure can be used to investigate the occurrence and reversibility of phase transitions, with the ultimate goal of gaining an in-depth understanding of structural and stability relationships between different polymorphs. In addition, the intrinsic thermal expansion and compressibility behavior can be determined from variable temperature and pressure diffraction data in combination with Rietveld refinement. Full structural characterization of new polymorphs is challenging, as many NTE materials are metastable and can only be prepared as powders through synthetic approaches that use kinetic control. This is especially true for high-pressure experiments, where the small sample size and experimental setup limit data quality. In this talk, the synthesis of several new compounds belonging to the  $\text{A}_2\text{M}_3\text{O}_{12}$  family of NTE materials, as well as results from high-pressure *in situ* X-ray diffraction and variable temperature X-ray and neutron diffraction experiments will be presented.

We thank the Cornell High Energy Synchrotron Source and the NIST Center for Neutron Research for beamtime. This research is supported by the National Science Foundation through award DMR-0545517.

**AW.03.02 Single-Crystal-to-Single-Crystal *E/Z* Isomerization Studies of Molecules Embedded in Supramolecular Solids.** S.-L. Zheng, M. Gembicky, C. Vande Velde, O. Pham, P. Coppens, Dept. of Chemistry, State Univ. of New York at Buffalo, Buffalo, NY, 14260, USA.

What controls the selectivity of chemical reactions? Chemistry in solutions is, to a large extent, controlled by entropy and Brownian movement. There are many conformations which are present and, quite often, there are many reactions which are possible. Supramolecular solids are a largely untested medium for photocrystallographic research [1]. Yet, like widely applied rigid glasses they offer the prospect of molecular dilution but without the loss of 3-D periodicity and molecular orientation [2]. We have embedded a series of photoactive guests (*eg.* tiglic acid, cyclooctene) within the nanocavities of supramolecular framework and monitored the *E/Z* single-crystal-to-single-crystal reaction that proceeds in the fully ordered systems without side reactions and with full retention of the crystal lattice [3]. Among them, the asymmetric *E/Z* isomerization in a chiral framework shows a unique reaction selectivity, which is unlikely to be observed

in solution [4]. Developing time-resolved diffraction techniques will provide the way to elucidate the mechanism of chemical reactions.

Research supported by the National Science Foundation (CHE0236317) and the Petroleum Research Fund (#43594-AC4).

1. Coppens, *et al. CrystEngComm*, 2006, 9, 1.

2. Keating and Garcia-Garibay, *Photochemical solid-to-solid reactions in Organic and inorganic photochemistry* (Ed by Ramamurthy and Schanze) Marcel Dekker, Inc. New York, 1998; Toda, (Ed.) *Topics in Current Chemistry*, 254: *Organic Solid State Reactions* Springer, 2005, and references cited therein.

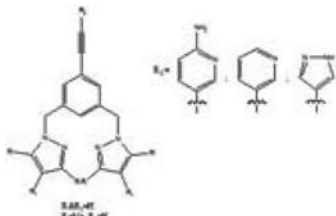
3. Zheng, and Coppens. In preparation.

4 Griesbeck and Meierhenrich *Angew. Chem. Int. Ed.* 2002, 41, 3147.

**AW03.03 Bis-pyrazole Based Ligands...Versatile Tools for Supramolecular Synthesis.** Benjamin M.T. Scott, Christer B. Aakeröy, John Desper, Kansas State Univ., Manhattan, KS, 66506.

Functionalised bis-pyrazole ligands can be utilized as 'building blocks' of extended metal-containing networks by combining the pyrazole moieties with a second binding site designed with a specific supramolecular intent, Scheme 1.

These compounds can form supramolecules via (1) hydrogen bonding to either the pyrazole or the second functionality and (2) metal coordination through one or more available nitrogen sites.



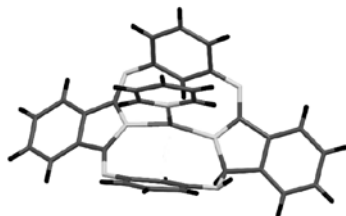
In the presence of a single metal ion, the bidentate chelating site comprising two pyrazole moieties would likely dominate, however, with the addition of a second coordination site, a level of competition is introduced which could allow for the chelating site to be partly abandoned. To reduce such competition, the bis-pyrazole moiety is 'locked' via the formation of a Pd-C covalent bond satisfying the pyrazole bis-chelate, leaving the second binding site 'free' for supramolecular assembly.

This contribution reports on the design and synthesis of several new ligands along with results from structural studies.

**AW03.04 When Chemistry Meets Charge Density, and Chemistry Wins ...** Christophe M.L. Vande Velde<sup>1,2</sup>, Anil Cetin<sup>3</sup>, William S. Durfee<sup>4</sup>, Christopher J. Ziegler<sup>3</sup>, Philip Coppens<sup>1</sup>, <sup>1</sup>State Univ. of New York at Buffalo, DOC, Buffalo, NY 14260, <sup>2</sup>Univ. of Antwerp, DOC, 2610 Antwerpen, Belgium, <sup>3</sup>Univ. of Akron, DOC, Akron, OH 44325, <sup>4</sup>Buffalo State College, DOC, Buffalo, NY 14222.

A number of metal-dicarbhemiporhyrazine complexes (see figure) were prepared, with the purpose of studying a possible agostic effect involving the metal atom. A charge density (CD) study would be the instrument of choice to see if any indications for its presence would show up.

Disordered solvent was present in the crystal, but the macrocycle itself seemed not badly affected. A CD quality dataset was collected for the best crystal (M=Fe), and the disorder was modeled to the maximum extent possible. With good data, it was also clear that one double bond of the macrocycle was hydrogenated, as the H-atoms could be easily localized. Another Fourier peak was modeled as a partial oxygen with 13% occupancy. The reason for the partial occupancy was assumed to be that not enough water was present for complete occupancy (drybox). At this stage of the spherical atom refinement



the largest Fourier peak was situated close to Fe, and we felt confident enough to proceed with a multipole refinement in XD. Initially, this led to promising results, and the deformation densities in the macrocycle seemed convincing. No sense could however be made of the results for the Fe atom. After rigorous checking and introducing all possible corrections, the final unraveling of the plot convincingly demonstrated that the crystallographer needs to keep an open mind towards all possibilities for the explanation of his/her observations, and not take anything for granted.

Support by NSF grant nr. che0236317 is gratefully acknowledged.

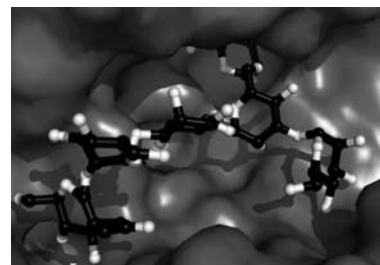
**AW.03.05 Structure-Guided Design of a Protein-Based Therapeutic for Nerve Agent Exposure.** A.C. Hemmert, C.D. Fleming, D.M. Cerasoli, P.M. Potter, M.R. Redinbo, Biochemistry and Biophysics, Univ. of North Carolina at Chapel Hill, NC.

The lethal nerve agents sarin, soman, tabun, and VX inhibit human acetylcholinesterase, eliminating the body's ability to degrade the acetylcholine neurotransmitter, resulting in asphyxiation due to diaphragm incapacitation. Current treatments offer limited protection. Thus, there is interest in developing protein-based prophylactics for the detoxification of nerve agents. Human carboxylesterase 1 (hCE1), a broad-spectrum serine hydrolase, is known to bind organophosphate nerve agents, but currently exhibits no hydrolase activity. We recently determined crystal structures of hCE1 in covalent complexes with the nerve agents soman and tabun bound in the active site. The enzyme is trapped in the acyl-enzyme intermediate state, apparently unable to catalyze the second, hydrolytic step to generate the acyl product. Based on these crystal structures, we are rationally designing active site mutations, to drive the catalytic cycle to completion. Two initial variants, L97H and V146H, resulted in the increased hydrolysis of o-nitrophenyl acetate, a conventional esterase substrate, relative to the wild type enzyme. These mutant forms of hCE1 are currently being tested by the US military with live nerve agents for novel hydrolysis activity. By using a combination of structural and functional data as a guide, our goal is to design a catalytically efficient form of hCE1 capable of protecting personnel at-risk for nerve agent exposure.

**AW.03.06 Structural Insights into an Enzyme Interacting with its Substrate: Golgi alpha-mannosidase II & G<sub>n</sub>Man<sub>5</sub>G<sub>n</sub><sub>2</sub>.** N. Shah<sup>1</sup>, D.A. Kuntz<sup>2</sup>, D.R. Rose<sup>1,2</sup>, <sup>1</sup>Dept. of Medical Biophysics, Univ. of Toronto, <sup>2</sup>Div. of Cancer Genomics & Proteomics, Ontario Cancer Inst., Univ. Health Network, Toronto, ON M5G1L7 Canada.

A feature typical of many cancerous cells is their altered cell surface glycosylation. Golgi alpha-mannosidase II (GMII, 125 kDa) catalyzes the committed step of complex N-glycan formation in the N-glycosylation pathway. Inhibition of GMII by small molecule inhibitors is known to reduce metastasis in cancer patients and generally improve clinical outcome. GMII catalyzes the hydrolysis of two different mannose-mannose bonds converting G<sub>n</sub>Man<sub>5</sub>G<sub>n</sub><sub>2</sub> to G<sub>n</sub>Man<sub>3</sub>G<sub>n</sub><sub>2</sub>. Its catalytic action is highly specific and unique.

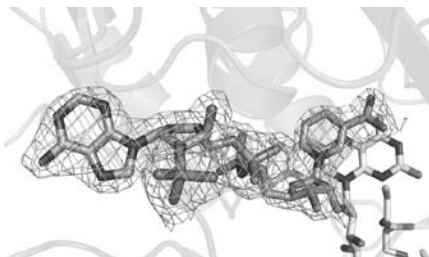
Our laboratory has previously solved the crystal structure of GMII from *Drosophila melanogaster* and has studied many potential inhibitors against this enzyme. Through current work,



we aim to gain insight into the catalytic mechanism of GMII. The objective of my work is to study the enzyme interacting with its natural substrate. Here we present the crystal structure of an inactive mutant of GMII interacting with its natural substrate,  $\text{GnMan}_5\text{Gn}_2$ . The mode of substrate binding reveals a great deal of information regarding the proposed catalytic mechanism of this enzyme. It is our hope that information from this crystal structure will allow for the design of highly specific inhibitors that may be used in the future as chemotherapeutics.

**AW.03.07 Crystallographic Analyses of Coenzyme A-Disulfide Reductase in Complex with Pyridine Nucleotides.** Jamie R. Wallen, Carleitta Paige, T. Conn Mallett, Al Claiborne, Center for Structural Biology, Wake Forest Univ. School of Medicine, Winston-Salem, NC, USA.

Coenzyme A-disulfide reductases (CoADRs) are flavoproteins which catalyze the NAD(P)H-dependent reduction of coenzyme A-disulfide (CoAD) to two CoASH. Whereas most CoADR enzymes are specific for either NADH or NADPH, the *Bacillus anthracis* CoADR (BACoADR) can use either pyridine nucleotide in turnover. We have solved and refined the oxidized BACoADR crystal structure at 2.30 Å resolution. Sequence analyses reveal that BACoADR conserves both Gly160 and Glu180, which confer NADH specificity, but BACoADR also contains Arg181, which is conserved in NADPH-specific enzymes and interacts with the 2'-phosphate of NADPH. Structural analyses indicate that a conformational change must occur to accommodate either pyridine nucleotide, a feature that is unique to BACoADR. To address how BACoADR interacts with the two pyridine nucleotides, oxidized BACoADR crystals were soaked with NADH and NADPH, respectively, and the crystal structures of substrate complexes have been solved and refined at 2.25-2.26



Å resolution. The structures reveal a novel 8 Å conformational change of an active-site loop which opens up a pocket to allow NAD(P)H binding. This loop contains both Glu180 and Arg181, and both residues interact with *both* NADH and NADPH. The 2'-phosphate of NADPH interacts with Arg181 and Asn182, and the protein pushes the additional phosphate group out toward solvent. In addition, the BACoADR Cys42-SSCoA redox-active disulfide is reduced, and the Cys42 side chain adopts a new conformation, interacting with Tyr367' and Tyr425'. These conformational changes between oxidized and NAD(P)H-bound BACoADR provide structural insights into the molecular basis for substrate recognition and the mechanism of CoAD reduction.

**AW.03.08 4-Chlorobenzoate CoA Ligase/Synthetase Utilizes a 140° C-terminal Domain Rotation to Perform Two Unique Half-Reactions.** Albert S. Reger<sup>1</sup>, Rui Wu<sup>2</sup>, Debra Dunaway-Mariano<sup>2</sup>, Andrew M. Gulick<sup>1</sup>, <sup>1</sup>SUNY, Dept. of Structural Biology, Hauptman-Woodward Medical Inst., Buffalo, NY 14203-1102, <sup>2</sup>Dept. of Chemistry, Univ. of New Mexico, Albuquerque, NM.

4-Chlorobenzoate CoA Ligase/Synthetase is part of the adenylate-forming family of enzymes. This family, which includes Acetyl-CoA Synthetase and the adenylation domains of Non-Ribosomal Peptide Synthetases, performs two half-reactions using a ping-pong mechanism. Structural and functional studies on members of this

family suggest that after the completion of the initial adenylate-forming reaction, the C-terminal domain of this enzyme rotates 140° to perform the second thioester-forming half-reaction. We have determined the structure of 4-Chlorobenzoate CoA Ligase/Synthetase in both the adenylate and thioester-forming conformation. The structure identifies a novel-binding pocket for the CoA nucleotide. A comparison of the original adenylate-forming structure and the new thioester-forming structure, along with kinetic analysis of the "hinge" mutant D402P, will be presented in support of the Domain Alternation hypothesis.

**AW.03.09 Photochemical Reactions in Inclusion Compounds.** T. Lavy, M. Kaftory, Shulich Faculty of Chemistry, Technion - Israel Inst. of Technology, Haifa, 32000, Israel.

In inclusion compounds the guest molecules occupy space formed by the host molecules. Carrying out photochemical reactions in inclusion compounds proved to be a unique method for the synthesis of a large variety of compounds. The research deals with unimolecular and bimolecular photochemical reactions in inclusion compounds. In a recent publication the effect of the reaction core on the homogeneity/heterogeneity of the reaction was studied[1]. A question arises from this recent study: what happens if the volume of the product is smaller than that of the reactant? Free volumes are not anticipated to exist. Therefore it is expected that the following possibilities will occur: either destruction of the crystal as a result of the collapse of the cavity's walls (heterogeneous reaction) or that some other molecules will occupy the free space. We have encountered for the first time few examples where a photochemical dimerization reaction is taking place in a single crystal of inclusion compound and at the end of the reaction water molecules penetrate into the free space without destruction the crystal lattice. Moreover, at the end of the dimerization, the orientation of the dimer with respect to the host molecules is different than that prior to the reaction. Evidently the dimer is rotating during or after the photoreaction[2].

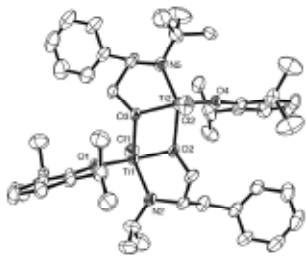
The aim of the unimolecular study is to examine to what extent the conformation adopted by N,N disubstituted- $\alpha$ -oxoamides determines its photochemical reaction. We have used different host molecules in order to control the conformation of the guest. It was found that indeed the N,N disubstituted- $\alpha$ -oxoamides show different photochemical behavior which depends on their conformation.

1. Tali Lavy, Yana Sheynin and Menahem Kaftory, *Eur. J. Org. Chem.*, 2004, 4802-4808.
2. Tali Lavy and Menahem Kaftory, *CrystEngComm.*, 2007. In press, DOI: 10.1039, paper number: b615032b

## SP.01 Undergraduate Research Showcase

**SP.01.01 Teaching Crystallography to Undergraduates through Distance Learning and Remote Access.** K.A. Kantardjieff<sup>1,2</sup>, A.R. Johnson<sup>3</sup>, X. Ouyang<sup>2</sup>, <sup>1</sup>Dept. of Chemistry and Biochemistry, <sup>2</sup>Keck Center for Molecular Structure, CSU Fullerton, <sup>3</sup>Dept. of Chemistry, Harvey Mudd College.

With the migration of academic crystallography from a research specialty to a technique employed by a wide community of users, inclusion of crystallography as a formal course in the undergraduate curriculum has diminished in the last decade. This has resulted in fewer students who are familiar with the research opportunities afforded by crystallography, and who appreciate the value of crystallographic information. In a collaboration between Harvey Mudd College and Cal State Fullerton, undergraduate students at both institutions are engaged in research and training at the Center for Molecular Structure that helps them to develop a sufficient working knowledge of the field, enabling them to answer specific research questions, to collaborate with those having greater expertise, and to utilize crystallographic results as the basis for or validation of their own work. Guided by ACA and USNC/Cr policies, we jointly offer a senior level course in both chemistry departments, in which lectures and demonstrations are delivered through interactive web conferencing software to the remote site. Students access instrumentation to initiate experiments and collect diffraction data via remote access. Independent single crystal structure-determination projects range from small organics to DNA. We will discuss the course content, the relative advantages and disadvantages of delivering such courses in remote modalities, and the pedagogical implications.



This project has been supported by a Mission and Goals Initiative at CSU Fullerton, an educational matching grant from iLinc Communications, and the National Science Foundation.

**SP.01.02 Passing the Torch: The Challenge of Teaching Biologists Protein Crystallography in an Increasingly Automated Environment.** Gary D. Brayer, Dept. of Biochemistry and Molecular Biology, Univ. of British Columbia, Vancouver, BC, Canada.

The use of X-ray crystallography is experiencing explosive growth, propelled by new protein expression methodologies, the emergence of genomic methods and accelerating automation. Conversely, the resources devoted to teaching crystallographic fundamentals, are in steep decline (or non-existent) at many teaching institutions. The basis for this latter trend would seem to be two-fold. First, the structural genomics process has attracted large numbers of crystallographic professionals to institutes and industry, where there is little opportunity to teach. Second, the sharply declining number of trained professionals remaining in university settings are beset by the demands of being competitive for research grants, leaving little time for new teaching initiatives. Particularly worrisome is the lack of educational resources for the myriad of new biological users of crystallography, who have no training in this technique at all. Without appropriate theoretical insight, this user group is particularly poorly equipped to solve high quality structures. The TORCH teaching initiative seeks to address this issue by laying a foundation of crystallographic methodology in senior biology

undergraduates through a compact 12 lecture segment of material that can be incorporated into any advanced course in proteins. The goal is to instill these aspiring biologists with sufficient background to be able to make wise decisions in either pursuing structural projects as part of future graduate research, or making use of structural data produced by others. To facilitate the widest possible usage, these teaching materials are being formulated to allow their presentation by faculty with or without a crystallographic background. Supported by NSERC.

**SP.01.03 A Comparison of Crystal Structures of the Tetramethylammonium and Sodium Salts of 3-Nitrophenolate.** Stephanie E. Bettis<sup>1</sup>, Kenneth L. Martin<sup>1</sup>, Edwin D. Stevens<sup>2</sup>, <sup>1</sup>Dept. of Chemistry, Berry College, Mount Berry, GA 30149, <sup>2</sup>Dept. of Chemistry, Univ. of New Orleans, New Orleans, LA 70148.

The stoichiometric addition of a solution of sodium hydroxide to 3-nitrophenol followed by slow evaporation led to orange-red crystalline needles of sodium 3-nitrophenolate. A similar procedure was performed for tetramethylammonium 3-nitrophenolate using tetramethylammonium hydroxide and 3-nitrophenol and led to orange-red crystalline plates. For the sodium 3-nitrophenolate crystals, 11707 Mo- $K_{\alpha}$  reflections were measured at 150 K via Bruker *SMART* 1-K CCD single-crystal diffractometer. The tetramethylammonium 3-nitrophenolate crystal structure had 12664 Mo- $K_{\alpha}$  reflections measured at 173 K via Bruker *SMART* 2-K CCD single-crystal diffractometer. The unit cell parameters for sodium 3-nitrophenolate are:  $a = 6.814(1) \text{ \AA}$ ,  $b = 6.5437(8) \text{ \AA}$ ,  $c = 18,206(4) \text{ \AA}$ ,  $\alpha = 90^{\circ}$ ,  $\beta = 94.46(3)^{\circ}$ ,  $\gamma = 90^{\circ}$ , and  $V = 809.4(3) \text{ \AA}^3$ . The tetramethylammonium salt's unit cell was found to have the following parameters:  $a = 23.543(4) \text{ \AA}$ ,  $b = 5.636(1) \text{ \AA}$ ,  $c = 16.387(3) \text{ \AA}$ ,  $\alpha = 90^{\circ}$ ,  $\beta = 128.513(3)^{\circ}$ ,  $\gamma = 90^{\circ}$ , and  $V = 1701.4(9) \text{ \AA}^3$ . The space group was determined to be  $P2_1/n$  for the sodium structure and  $C2/c$  for the tetramethylammonium salt. The structures were solved and refined by full-matrix least-squares method via *SHELXTL V 5.1*. The  $R$  factor calculated for the sodium salt was 0.0740 and was 0.0402 for the tetramethylammonium salt. The high  $R$  factor of the sodium salt led to the synthesis of the tetramethylammonium salt. A comparison of the two crystal structures revealed that the bond lengths of the 3-nitrophenolate moiety were statistically the same, which showed that it is not affected by the cation.

**SP.01.04 Characterizing the Catalytic Boost Provided by an Alternative Anion in Human Pancreatic Alpha-Amylase.** L.K. Williams, R. Maurus, A. Begum, S.G. Withers, G.D. Brayer, Depts. of Biochemistry and Molecular Biology, and Chemistry, Univ. of British Columbia, Vancouver, B.C., Canada.

Human pancreatic alpha-amylase (HPA) is an enzyme vital for the breakdown of starch in the diet; as such, it is a potential drug target for the development of treatments for diabetes and obesity. To reach maximal activity, HPA requires an activating anion that binds in a well defined pocket in the enzyme near the catalytic residues D197, E233 and D300. *In vivo*, HPA is activated by a chloride ion. When this chloride ion is replaced with nitrite *in vitro*, the catalytic rate and  $k_{\text{cat}}/K_m$  increase substantially. The effects of binding nitrite in the anion binding pocket are clearly demonstrated in two structure determinations of the nitrate activated enzyme: HPA in complex with nitrite, and HPA in complex with nitrite and the inhibitor/substrate acarbose. Enhancement of catalytic activity in nitrate substituted HPA appears to result from an alternative positioning of the catalytic residue D300 and the corresponding changes in hydrogen bonding that occur. Furthermore, nitrite binding significantly alters the electrostatic potential in the substrate binding cleft near the active

site. Interestingly, these two factors combine to produce a different product upon catalytic cleavage and transglycosylation of acarbose, suggesting anion binding is also a factor in substrate specificity and observed product profiles.

This research is supported by the Canadian Institutes of Health Research.

**SP.01.05 Characterization of Anti-cooperative Substrate and Metal Cofactor Binding.** C. Panizales<sup>1</sup>, M.F. Roberts<sup>2</sup>, K. Stieglitz<sup>1</sup>, <sup>1</sup>Chemistry Dept., Univ. of Massachusetts, Boston, MA 02169, <sup>2</sup>Dept. of Chemistry, Boston College, Chestnut Hill, MA 02467.

The hyperthermophile *Archeoglobus fulgidus* inositol monophosphatase (IMPase), pathway intermediate for generation of novel osmolyte dimyooinositol phosphate cleaves inositol-1-phosphate to myoinositol and inorganic phosphate. Structural studies are underway to characterize the details of the anticooperative substrate and metal cofactor binding. A thorough structural understanding of the anti-cooperative mechanism of these homodimeric bacterial enzymes may aid in our understanding of how this class of enzymes diverged to evolve as tetrameric allosterically regulated enzymes. An intrinsic fluorescent assay utilizing a Shimadzu RF 5000 V spectrofluorometer has been developed to track conformational changes of the enzyme subunits during substrate and metal cofactor binding. Differences in emission peak positions for hydrophobic residues have been observed as a function of the concentration of activating metal and inhibitory metal and substrate. These experiments have been performed at elevated temperature. The data suggests we may develop a novel assay to track the enzymes conformational changes as it binds metal cofactor in the absence or presence of substrate. Site directed mutagenesis along the subunit interfaces of the enzyme has been done to identify residues that promote conformational changes affecting the affinity of the enzyme for the substrate and metal cofactor. X-ray crystallographic experiments are in progress at elevated temperatures to identify which active site residues that may be linked to interfacial contacts to understand how the architecture of the active site may influence conformational changes of the subunits to prevent cooperative binding in the active site of the adjacent monomer.

**SP.01.06 ProMOL, Simplification and Increased Functionality of PyMOL.** Brett Hanson, Charles Westin, Len Slate, Paul Craig., Biological Sciences, Rochester Inst. of Technology, 85 Lomb Memorial Dr., Rochester, NY 14623 USA.

PyMol is a powerful open source molecular modeling tool. A complex user interface provides access to a wide range of features, but that necessary complexity can be daunting to novices. To help alleviate this problem, a new plugin for PyMOL called ProMOL was created. Numerous PyMOL functions were simplified and capabilities added, including electron density map importing and controls, Ramachandran plot fetcher, ray trace options, mouse modes, multiple perspective options, polar contacts, and roving functions. With the novice user in mind, buttons, sliders, and various other widgets were implemented to improve ease of use and efficiency. In addition, ProMOL contains tools to compare any PDB file against more than 30 known catalytic active site motifs. The motif prediction algorithms are based on the relative positions of the atoms in the catalytic residues in the active site of an enzyme. The predefined measurement range can be modified by the user. An additional plugin for PyMOL, Motif-Maker, was created to automate the process, allowing users to easily create their own precise motif definitions. The program measures the inter-atomic distances for the residues specified on the template and writes them to a script file which can then be compared to other protein structures to search for the presence

of the active site. Further improvements to ProMOL will include the implementation of functional algorithms for the prediction of ligand and protein docking, simplified sequence alignment, and a hydrogen bonding scheme. The new features of ProMOL are being linked to the SBEVSL (see related poster) script translation platform so that equivalent capabilities can be migrated to other graphics packages, including RasMol and Jmol. Work supported in part by NSF 0402408, NIGMS 1R15GM078077-01.

## SP.02 Plenary Lecture

**SP.02.01 Structural Basis of Transcription.** Roger Kornberg, Dept. of Structural Biology, Stanford Univ. Medical School, Stanford, CA 94305.

The structure of RNA polymerase II in the form of an actively transcribing complex has been extended in two directions. First, cocrystals with nucleoside triphosphates have revealed the basis of fidelity in transcription, at the level of both initial nucleotide selection and subsequent proofreading for error correction. Second, crystals of higher complexes, including general transcription factors, adding another 150 kD to the structure, have revealed principles of both promoter opening for the initiation of transcription and stabilization of the transcribing complex. In other work, we have sought to extend the resolution of cryo-EM for structure determination of the still larger complexes involved in the initiation and regulation of transcription. To this end, we have determined the structure of a gold nanoparticle at 1.2 Å resolution.

## TR.01 Diffuse Scattering for the Masses: Local Structural Correlations in Molecular, Macromolecular, and Inorganic Crystals

**TR.01.01 Diffuse Scattering as a Probe of Nanoscale Structure and Function.** T.R. Welberry, D.J. Goossens, A.G. Beasley, A.P. Heerdegen, Research School of Chemistry, Australian National Univ., Canberra, ACT 0200, Australia.

The strong sharp Bragg reflections that occur in diffraction patterns of all real crystals are used by conventional x-ray crystallography to deduce the average repetitive arrangements of atoms or molecules. Diffuse scattering, on the other hand, contains information about the deviations from the average (i.e., different types of disorder) and gives structural information on a scale that goes beyond that of the average unit cell and extends over a range of 1 Å<sup>-1</sup>–1000 Å<sup>-1</sup>. In many important materials, it is this extended range of structural information that is crucial in determining the unique or novel properties of the material, rather than the average unit cell structure. We review the development of our diffuse scattering methodology using a variety of examples taken from different fields to illustrate the kind of information that can be obtained by current day methods — information that is simply not available from the Bragg experiment.

Amongst these will be the zeolite mordenite, the organic pentachloronitrobenzene, which is one of a series of chloronitrobenzene compounds whose anomalous dielectric properties are thought to be related to their disorder, the relaxor ferroelectric PZN and finally examples of organic molecular crystals that exhibit polymorphism — a topic of crucial interest to the pharmaceutical industry.

We gratefully acknowledge the support of the Australian Research Council, the Australian Synchrotron Research Program, the Access to Major Research Facilities Program and the Australian Partnership for Advanced Computing.

**TR.01.02 Quantitative Three-dimensional Defect Structures.**

Branton J. Campbell, Dept. of Physics & Astronomy, Brigham Young Univ., Salt Lake City, UT.

Crystal defects contribute to the useful properties of many of our functional materials. Today, advanced sources and detectors, together with ever more powerful computers, make it possible to probe the diffuse scattering distributions that can reveal their fully three-dimensional local structures. While large contiguous volumes of reciprocal space can be mapped out with unprecedented speed, sensitivity, and resolution, the multi-gigabyte data sets that arise can be difficult to analyze. In contrast to average-structure determination problems, where only the Bragg peaks are integrated, one needs to simultaneously fit a structural model against every voxel in the dataset. Here, I will demonstrate several state-of-the-art methods and tools in the context of recent successes from the cuprate superconductors, relaxor piezoelectrics, and colossal magnetoresistive manganites.

**TR.01.03 Interpreting Diffuse X-ray Scattering Patterns from Crystals of Macromolecules.** George Phillips, Dept. of Biochemistry, Univ. of Wisconsin, Madison, WI.

Although most X-ray crystallography experiments do not have time components, it does not follow that the technique cannot sense fluctuations around the average structure. Displacement parameters, either isotropic or anisotropic, are the usual treatment to describe combinations of motion and displacement 'disorder.' Simple displacement parameters do not embody correlations of displacements (although TLS models can treat rigid-body motions of blocks of the structure). To learn about correlation properties of fluctuations, one should analyze, in addition to the mean Bragg Fourier spectrum, the diffuse variational components of the data. The study of the diffuse scattering from a crystal reveals aspects of higher moments in the statistical distribution of atomic locations in the molecule.

Whereas Bragg analysis yields the individual mean-square displacements, diffuse intensity contains information on all of the correlations among displacements in atomic coordinates. Another important point is that the damping of the number of photons in the Bragg reflections with respect to that from perfectly positioned atoms results in an increase in intensity between the Bragg spots. The effects can be separated into different classes of fluctuations, and this can help in qualitative interpretation of diffuse scattering features.

Protein and nucleic acid crystals show varying degree of complexity in their diffuse scattering, varying from independent atomic displacements to domain motions to long range lattice-coupled effects. Various examples will be presented and some practical guides for general interpretation given.

**TR.01.04 A Brief History of Variations in Regimented States of Living and Inanimate Matter Reflected in Reciprocal Space.**

Donald L.D. Caspar, Inst. of Molecular Biophysics, Florida State Univ., Tallahassee, FL.

Before X-ray crystallography was invented, Einstein (1908) tried unsuccessfully to explain the specific heat of diamond at low temperatures by postulating that the atoms would independently fluctuate about their equilibrium positions; Debye (1912) succeeded with this problem by representing the crystal energy levels by the normal modes of the elastically coupled atoms. When Debye (1914) proposed his temperature factor to explain the fall-off in intensity with increasing Bragg spacing of the recently discovered crystal X-ray reflections, he presumed that the intensity lost due to thermal fluctuations would appear as independent atomic scattering – as from an Einstein crystal. Assuming Debye's elastically coupled model for

thermal fluctuations in a crystal lattice, Waller (1923, 1925) showed that the thermal diffuse scatter should be concentrated in halos about the Bragg reflections; and Laval (1938) first measured the predicted shape of these halos. Lonsdale (1942) pioneered relating anisotropic elastic properties of molecular crystals to the shapes of the thermal diffuse halos about the Bragg reflections. When the diffuse scatter from a protein crystal was measured in my laboratory (1988), it was evident that the dominant features were due to liquid-like, short-range correlated fluctuations of the amino acid side chain positions. There are a great variety of biologically significant variations, both static and dynamic, in the structures of macromolecular crystals, fibrous proteins, membrane assemblies and virus particles, which are manifest in their diffraction patterns. A rich range of variations is also exhibited in diffraction from inanimate condensed matter. Variations I will discuss include: (a) An aperiodic hemoglobin crystal structure observed by Howells and Perutz, and explained by Bragg (1954) in which successive layers are randomly staggered up or down in two energetically equivalent packing arrangements; (b) The aperiodic decagonal quasicrystal structures represented by Penrose tilings (1979), in which conserved edge-to-edge pentagon contacts are randomly combined; (c) Short-range correlated fluctuations in segments of the fibrous tropomyosin molecule in a highly hydrated mesh-work crystal, as modeled by Phillips (1986); (d) Uncorrelated fluctuations, mapped by Sosinsky et al. (1990), in hexagonally arrayed connexons of a gap junction membrane lattice, which has a diverging autocorrelation function as for the colloidal, hard-core two-dimensional hexatic phase model; (e) Fluctuations in a swollen icosahedral plant virus, which Li and I (unpublished) characterized by solution scattering and crystal diffraction; (f) A periodic incommensurate perturbation of the helical structure of a strain of Tobacco Mosaic Virus, which Holmes and I (1968) analyzed by fiber diffraction; (g) The variable temperature-dependent transitional incommensurate phase of quartz, occurring between the alpha and beta phases, visualized by Heaney (1991); and (h) Confusion about amyloid fibril assemblies, which have an axially well-ordered cross-beta structure but are laterally inscrutably variable. Variations in regimented states of matter are usually referred to as defects or disorder, as if they were unwelcome insults to some perfect Platonic regimen. Variations manifest intrinsic properties of matter. For living matter, variation is the secret of life, as apprehended by Darwin. The technology of high-throughput protein crystallography has been developed to ignore how structural variations may be correlated. Looking at the shape and the space between the Bragg reflections of crystalline living molecules can reveal vital aspects of their structures.

**TR.01.05 From Diffuse Features to Precise Motions: An MD Approach.** Lars Meinhold<sup>1,2,\*</sup>, Jeremy C. Smith<sup>1,3</sup>, <sup>1</sup>Univ. Heidelberg -- IWR, D-69120 Heidelberg, Germany, <sup>2</sup>California Inst. of Technology, Pasadena, CA, USA, <sup>3</sup>Univ. of Tennessee/Oak Ridge National Lab, Oak Ridge, TN, USA, \*lars.meinhold@caltech.edu

Understanding X-ray crystallographic diffuse scattering is likely to improve our comprehension of equilibrium collective protein dynamics. The dynamical origin of the X-ray diffuse scattering by crystals of a protein, Staphylococcal nuclease, is determined using molecular dynamics simulation. The so-called solvent ring is shown to originate from equal contributions from correlations in nearest-neighbour water molecule dynamics and from internal protein motions. Intense, three-dimensional scattering features that originate from a very small number of slowly-varying (>10ns) collective motions are assigned to specific collective motions in the protein, and some of these explicitly involve potentially functional active-site deformations. Simplified models of correlated protein motion are also critically examined. Furthermore, all-atom lattice dynamical

calculations are presented for a crystalline protein, ribonuclease A. The sound velocities, density of states, heat capacity and thermal diffuse scattering are all consistent with available experimental data. In the vicinity of Bragg peaks, the inelastic scattering of X-rays by phonons is found to originate from acoustic mode scattering.

**TR.01.06 Crystallography without Crystals: Determining the Structure of Individual Biological Molecules.** Abbas Ourmazd, Dilano Saldin, Valentin Shneerson, Univ. of Wisconsin-Milwaukee.

Protein X-ray crystallography, is now the mainstay of biology, biochemistry, and the pharmaceutical industry. However, roughly 40% of biological molecules do not crystallize. And although the more than half a million proteins have been sequenced, the structure of less than 40,000 has been determined. By obviating the need for purification and crystallization, the ability to determine the structure of individual biological molecules would constitute a fundamental breakthrough. The confluence of four developments in has generated intense interest in achieving this by short-pulse X-ray scattering:

The advent of algorithms capable of “solving the phase problem” with practical demonstrations in astronomy, high-energy electron diffraction, and protein crystallography [1,2,3].

Development of sophisticated techniques for determining the relative orientation of electron microscope *images* of biological entities such as cells and large macromolecules [4].

Development of techniques for producing beams of hydrated proteins [3,5].

The promise of ultra-bright, short pulses of X-rays from X-ray Free Electron Lasers (XFELs) under construction in the US, Japan, and Europe.

I will describe how these and other key developments have brought the prospect of single-molecule structure determination “tantalizingly close,” perhaps even closer than generally realized in the literature. (See also [www.uwm.edu/~ourmazd](http://www.uwm.edu/~ourmazd))

[1] J. R. Fienup, Appl. Opt. 21, 2758 (1982).

[2] J. Miao et al. PNAS 98, 6641 (2001).

[3] J.C.H. Spence et al. Acta Cryst. A61, 237 (2005)

[4] J. Frank, *3-Dimensional Electron Microscopy of Macromolecular Assemblies* (OUP Press, '06)

[5] J.B. Fenn, J. Biomolecular Techniques 13, 101 (2002).

**TR.01.07 Disorder Diffuse Scattering— from Elementary to Exotic.** F. Frey, Dept. of Earth and Environment, LMU Univ. München, D 80333 München, Germany.

Diffuse scattering is due to departures of any kind from perfectly ordered periodic array of identical structural units in d-dimensional space. Crystals and quasicrystals refer to  $n=3$  and  $n > 3$ , respectively. Periodicity of aperiodically ordered quasicrystals is restored in hyper space ( $n>3$ ). The term “disorder” includes structural fluctuations such as chemical, displacive or domain-like fluctuations in crystals, and also phasonic type fluctuations in quasicrystals. Elementary analytical expressions of diffuse scattering are discussed for various simple types of disorder. A particularly important type of diffuse scattering relates to layer- or lamellar domain disordered crystals and quasicrystals. Examples of disordered extraterrestrial pyroxenes and decagonal quasicrystals are shortly discussed.

**TR.01.08 Probing Nanoscale Correlations in Crystalline Materials using Single Crystal Diffuse Scattering.** S. Rosenkranz, Materials Science Div., Argonne National Lab, Argonne, IL 60439.

Many emerging phenomena of high technological and scientific interest are governed by complex disorder and nanoscale self-organization in the form of stripes, phase separation, dimerization etc, resulting from the competition between interactions with incompatible order. Examples include high temperature superconductivity, colossal magnetoresistance, relaxor ferroelectricity, and negative thermal expansion. Single crystal diffuse neutron and X-ray scattering potentially provides a very powerful probe of such disorder in crystalline materials on the 1-10nm length scale, though there are still formidable difficulties both in obtaining and analyzing large volumes of data with sufficient momentum and energy resolution required for accurate modeling, as well as in obtaining physically meaningful models of complex local disorder from such data sets. Here, I will discuss diffuse scattering studies of manganese oxides and related compounds and how they impact our understanding colossal magnetoresistance. These examples also serve to discuss some of the difficulties often encountered in diffuse scattering studies, and I will discuss a proposal for new instrumentation that allows efficient measurement of single crystal diffuse neutrons scattering with energy discrimination.

Work supported by US DOE BES-DMS DE-AC02-06CH11357.

**TR.01.09 Local Structures from Powders: Recent Advances in Atomic Pair Distribution Function Methods and Modeling.** Simon J.L. Billinge, Dept. of Physics and Astronomy, Michigan State Univ., East Lansing, MI 48824, USA.

Information about nanoscale structure is contained not in the Bragg but the diffuse component of the x-ray, neutron or electron scattering: the topic of this symposium. How can we analyze this information when we have isotropic samples such as powders of small crystallites, disordered ensembles of nanoparticles or nanoparticles in solution? The information content is degraded in this case because the powder averaging results in a one-dimensional intensity distribution and angular information is lost. Nonetheless, the information that survives is rich in structural information and we can learn a great deal about local structure in this case. The experiments are generally straightforward and analyzing and modeling the data is now becoming more sophisticated with the development of new methods and programs. A useful approach in handling the data is to carry out a Fourier transformation from reciprocal space to real-space resulting in the atomic pair distribution function (PDF) and refining structures to this function.

In this talk I will concentrate on recent developments in collecting, analyzing and modeling powder data from interesting nanostructured materials using the PDF method. I will illustrate this with a number of different scientific examples from different classes of nanostructure materials.

**TR.01.10 Explorations of Reciprocal Space – Routine Observations of Diffuse Scattering.** Jim Britten, Weiguang Guan, McMaster Univ., Hamilton, ON, Canada

For several years many of us have been scanning single and polycrystalline samples using 2D detectors, and storing gigabytes of 3D data. We sample this data at Bragg allowed points or d-spacings, and ignore the rest. We now have the ability to view the continuous volume of reciprocal space. Texture (preferred orientation) of solids now can be seen clearly. Streaks on the frames of problem single crystals become a lot more interesting when you can view the true

shape and location of the diffuse scattering. The methods of modeling and predicting this diffuse scattering also become more interesting, and will be outlined by the experts throughout this symposium.

We will illustrate the relationship of the 2D data frames to 3D reciprocal space, and present videos of raw 3D volumes showing a variety of diffuse scattering events.

**TR.01.11 X-ray Diffuse Scattering.** R.J. Angel<sup>1</sup>, C. Slebodnick<sup>1</sup>, J. Zhao<sup>1</sup>, B. Mihailova<sup>2</sup>, U. Bismayer<sup>2</sup>, G.D. Gatta<sup>3</sup>, T. Boffa-Ballaran<sup>4</sup>, L. Rees<sup>5</sup>, S. Jacobsen<sup>6</sup>, <sup>1</sup>Virginia Tech Crystallography Laboratory, Virginia Tech, Blacksburg, VA, USA, <sup>2</sup>Mineralogisch-Petrographisches Inst. der Univ. Hamburg, Hamburg, Germany, <sup>3</sup>Dip. Scienze della Terra, Univ. degli Studi di Milano, Milano, Italy, <sup>4</sup>Bayerisches Geoinstitut, Univ. Bayreuth, Bayreuth, Germany, <sup>5</sup>Oxford Diffraction Ltd., Oxfordshire, UK, <sup>6</sup>Dept. of Earth and Planetary Sciences, Northwestern Univ., Evanston IL, USA.

The routine use of area detectors such as CCD's for service crystallography, and the continued improvement in detector sensitivity and the intensity of lab-based X-ray sources, means that diffuse scattering is seen on a regular basis. Often, the detection of diffuse scattering during crystal screening leads to rejection of the crystal. However, the correct interpretation of diffuse scattering patterns, even on a qualitative basis, can help in structure solution and in the development of an appropriate model of disorder for the structure refinement. In this presentation we will review the common types of diffuse scattering that are observed in molecular compounds, ceramics and minerals, and demonstrate some software tools for their characterization.

Single-crystal diffraction measurements under either varying temperature or pressure can provide further insights in to the structural cause of diffuse scattering. Changes with pressure or temperature in the intensity or pattern of diffuse scattering imply that the structural origin of the disorder is displacive or dynamic in nature (as in nepheline and some relaxor ferroelectric perovskites), whereas the persistence of the diffuse scattering points to an origin in atomic ordering (as in FeO).

**TR.01.12 Liquid Crystal Elastomers: Display and Analyses of Diffuse, 3D X-ray Scattering.** J. Konnert<sup>1</sup>, J.R. Deschamps<sup>1</sup>, C. Spillmann<sup>2</sup>, J. Naciri<sup>2</sup>, B. Ratna<sup>2</sup>, <sup>1</sup>Code 6030, <sup>2</sup>Code 6930, Naval Research Laboratory, 4555 Overlook Ave., Washington, DC 20375, konnert@nrl.navy.mil.

The use of liquid crystals is well known in electrooptics, yet their potential use in other areas of technology is ever increasing. For example, liquid crystals in the nematic phase have been incorporated into cross-linked polymer networks to form materials capable of reversible, uniaxial contraction for use as mechanical actuators<sup>[1,2]</sup>. In order to obtain the maximum possible structure information, 3D diffraction data is desired. These data are collected with one degree phi scans at several chi values. These data are then combined and stored on an arbitrary orthogonal grid of reciprocal space. Continuous one, two, and three dimensional regions of reciprocal space may then be viewed and analyzed. The 3D features in the data place considerably more constraints on the derived molecular model of the sample than would single wavelength data collected with a single sample orientation.

[1] Gleim, W. & Finkelmann, H. Thermoelastic and Photoelastic Properties of Cross-Linked Liquid-Crystalline Side-Chain Polymers. *Makromolekulare Chemie-Macromolecular Chemistry and Physics* **188**, 1489-1500 (1987).

[2] Thomsen, D. L., Keller, P., Naciri, J., Pink, R., Jeon, H., Shenoy, D. & Ratna, B. R. Liquid crystal elastomers with mechanical properties of a muscle. *Macromolecules* **34**, 5868-5875 (2001).

## WK.01 SHELX Workshop

**WK.01.01 Introduction to SHELXL Refinement: Restraints, Constraints and Esds.** George M. Sheldrick, Lehrstuhl für Strukturchemie, Univ. Göttingen, Germany.

The SHELXL program was originally intended for small-molecule refinement but can also be used for macromolecules given adequate resolution (better than 2Å). The program contains extensive facilities for refining disordered and twinned structures. This introductory talk is designed to provide an overview of concepts behind the program with the emphasis on the use of constraints and restraints to take chemical information into account during the refinement. Although the full-matrix approach to least-squares refinement is normally used for small molecules and the conjugate gradient solution of the least-squares normal equations for macromolecules, the latter can be used to speed up the refinement of larger small molecule structures and the former is useful for estimating individual esds in macromolecular refinement. There is now no sharp dividing line between small and macromolecules, and it is hoped that this workshop will bring together both groups of crystallographers, there is much we can learn from each other.

A separate short talk will describe the program SHELXPRO that was designed as an interface to SHELXL for protein applications.

**WK.01.02 Refinement of Disorder with SHELXL.** Peter Müller, MIT, Dept. of Chemistry, 77 Massachusetts Ave, 2-325, Cambridge, MA 02139, pmueller@mit.edu.

The structure determined from a diffraction pattern is the spatial average over the whole crystal. In the ideal crystal all unit cells are identical, with all molecules in exactly the same conformation, orientation and position as in the cells to its left, right, top, bottom, front and back. Sometimes, however, parts of molecules (and in some extreme cases even whole molecules) are found in more than one crystallographically independent orientation. One can distinguish three cases:

1. More than one molecule in the asymmetric unit
2. Twinning
3. Disorder

With disorder the orientations of some atoms differ randomly in the different unit cells of the crystal. In most cases it suffices to describe a disorder by formulating two different positions per disordered atom and, in addition, the ratio between the two alternative positions.

In this presentation, the parameterization of disorder will be illustrated, and, based on several examples, the refinement of disorder with the program SHELXL will be demonstrated. This will include a detailed description of how to use restraints and constraints in refinements of disorder.

**WK.01.03 Twinning.** R. Herbst-Irmer, Dept. of Structural Chemistry, U. of Göttingen, Tammannstraße 4, D-37077 Göttingen, Germany, rherbst@shelx.uni-ac.gwdg.de.

For the description of a twin two things are necessary: a description of the symmetry operator that transforms one orientation into each other (twin law) and the fractional contribution of each twin domain. The twin law can be expressed as a matrix that transforms the *hkl* indices of one species into the other.

In SHELXL<sup>[1]</sup> the twin refinement method of Pratt, Coyle and Ibers<sup>[2]</sup> and Jameson<sup>[3]</sup> has been implemented. The twin law must be given

in a single command or by editing the reflection file. The fractional contribution will be refined.

It will be discussed how the twinning can be detected, the twin law be derived and how the structures can be solved and refined. Examples of twinned small molecules and also macromolecule structures will be presented.

- [1] Sheldrick G. M. (1997). *SHELXL-97*, University of Göttingen.  
 [2] Pratt, C. S., Coyle, B. A. & Ibers J. A. (1971). *J. Chem. Soc., A*, 2146 - 2151.  
 [3] Jameson, G. B. (1982). *Acta Cryst. A* **38**, 817 - 820.

**WK.01.04 Protein Refinement at Atomic Resolution.** T.R. Schneider, EMBL c/o DESY, Notkestr. 85, 22603 Hamburg, Germany.

With continuing progress in crystal production, diffraction instrumentation and data evaluation software, diffraction data to atomic resolution (i.e. 1.1 Å or higher) can be extracted from more and more protein crystals. SHELXL offers a large repertoire of facilities that can be used for building the best structural model against such data.

The talk will describe how more complicated parameterizations than normally used in macromolecular crystallography can be introduced due to the increased number of unique reflections. We will discuss the refinement of anisotropic displacement parameters, the introduction of multiple discrete sites for certain atoms, and the inclusion of hydrogen atoms into macromolecular models.

Furthermore the determination of estimated standard deviations by inversion of the normal-matrix of the refinement and their interpretation will be described.

**WK.01.05 SHELXPRO.** George Sheldrick.

**WK.01.06 Preparing CIF's for Publication. Useful Programs and Common Errors.** Ilia A. Guzei, Chemistry Dept., Univ. of Wisconsin-Madison, Madison, WI, 53558, USA.

Program *publCIF* (beta version 1.0.2) released by the IUCr Editorial Office in 2006 has proven to be invaluable in data verification and manuscript preparation for *Acta Cryst. C* and *E*. This program allows easy on-line data validation which produces *PLATON*-like outputs with interactive pop-up windows. In *publCIF* the manuscript author and comment sections can be edited and formatted with both Wordpad style and CIF-notation windows and generation of additional tables is extremely facile. An important element of the program is its reference handling capability; it is now possible to conveniently sort the references in the alphabetical order and check for correspondence between the entries in the bibliography section and all citations in the Comment and crystallographic tables. These and other *publCIF* features will be shown in action. In my laboratory we use an in-house program *ModiCIFer* that resolves many default CIF entries set by *SHELXTL*. A CIF processed with *ModiCIFer* and subsequently checked with *publCIF* is usually sufficient for submission to a chemistry journal as supporting information. A number of common mistakes resulting from discounting the Notes for Authors in the papers submitted to *Acta Cryst. C* will be discussed.

**WK.01.07 Crystal Structure Validation with PLATON.** A.L. Spek, National Single Crystal Service Facility, Bijvoet Center for Biomolecular Research, Utrecht Univ., The Netherlands. (<http://www.cryst.chem.uu.nl>).

A crystal structure determination is not complete when not validated for completeness, consistency and correctness. The International

Union of Crystallography has developed a tool for this task called CheckCIF. This tool can be run using the IUCr webserver on the results of the structure analysis supplied in CIF format. Since the program *PLATON* forms part of CheckCIF, validation can also be done in-house with a locally implemented version of *PLATON*. Validation should not be postponed to the publication stage. Corrections might be impossible at that late stage. Automatic validation will produce a list of ALERTS (if any) on issues such as missing data, errors or unusual features. The last ones will require a close inspection of the issues raised. The expected response is either a correction or a satisfactory explanation of the issue when the associated ALERT does not go away. Important ALERTS include messages on missed higher symmetry, significant solvent accessible voids in a structure, problems with atom type assignments, problems with H-atoms and overlooked pseudo-merohedral twinning. Several examples will be discussed.

**WK.01.08 SHELXD for Large Small Molecules and SHELXC/D for Macromolecular Substructures.** George M. Sheldrick, Lehrstuhl für Strukturchemie, Univ. Göttingen, Germany.

The program SHELXD was originally designed for the solution of large equal-atom structures using the random omit algorithm combined with the tangent formula; it has been successful in the solution of structures with up to 1000 equal atoms (no atom heavier than oxygen). When heavier atoms are present, much larger structures can be solved, especially when Patterson seeding is employed. These techniques are also effective at solving for heavy-atom substructures at much lower resolution, e.g. to find the selenium atoms in a selenomethionine MAD experiment or the sulfur atoms in a sulfur-SAD experiment. The critical parameters in such experiments are how far it is necessary to truncate the resolution and running an adequate number of trials. The program SHELXC generates the  $F_A$  values and files necessary for substructure solution with SHELXD, and outputs various statistics to judge the quality of the data and where to truncate the resolution. These programs, together with SHELXE to generate phases from the substructure, are designed to be easy to call from a GUI or pipeline for macromolecular phasing.

**WK.01.09 HKL2MAP.** T.R. Schneider, EMBL c/o DESY, Notkestr. 85, 22603 Hamburg, Germany.

HKL2MAP is a graphical user interface for macromolecular phasing. It connects several programs from the SHELX suite of crystallographic programs and guides the user from the analysis of the diffraction data to the inspection of an electron density map. For every step of the structure solution process, the interface collects input parameters from the user, launches a SHELX job, and presents the result of the computations both in text and in graphical format. User input is kept minimal and where it is required, it is checked for plausibility. The communication between different programs via intermediate data files is fully transparent to the user. All figures generated by the program can be stored in publication quality in PostScript format.

HKL2MAP will be demonstrated with real-life examples. The program can be obtained from [thomas.schneider@embl-hamburg.de](mailto:thomas.schneider@embl-hamburg.de).

**WK.01.10 Practical Aspects of SAD and MAD.** Judit E. Debreczeni, AstraZeneca, Alderley Park, SK10 4TG, UK.

Techniques exploiting the anomalous scattering of heavy atoms (sulfur and above) are the most popular methods for *ab initio* structure solution of macromolecules. These all include equally

important steps of data collection, heavy atom substructure solution and subsequent phase calculation and improvement, each presenting a variety of potential pitfalls. Practical aspects and limitations of these techniques together with feasibility considerations will be presented and illustrated with real life cases. Infrequently used settings of SHELXD/E will be highlighted and their affect on success of structure solution will be discussed.

**WK.01.11 SHELXE: From Substructure to Structure.**

George M. Sheldrick, Lehrstuhl für Strukturchemie, Univ. Göttingen, Germany.

SHELXE applies the SAD, MAD, SIR or SIRAS methods to generate starting phases using the files from SHELXC and a successful substructure solution with SHELXD, and then refines these phases by density modification to obtain an electron density map. This program is still in a state of active development and it is hoped that it will be possible to present some improvements at the ACA Meeting. One innovation that is already proving very effective, given native data to better than 2Å, is the extrapolation of the phases to a resolution higher than has actually been measured (the *free lunch algorithm*).

**WK.01.12 Coot for SHELXL Users.** Paul Emsley, Univ. of York, York, UK.

Coot is a program for molecular model-building using X-ray data. Part of the remit is to facilitate the interaction with validation programs and refinement programs, such as SHELXL.

To this end, Coot is able to read and write the SHELX “.ins” file format including the ability to construct a space group description from a list of symmetry operators. Coot can also read the SHELXL output CIF data file (.fcf) containing phase information and use it to construct sigma-a and sigma-a difference maps.

Furthermore, Coot reads the output “.lst” file of SHELXL and uses it to generate a dialog to direct the attention of the crystallographer to features noted in that log file.

The combination of these features make it straightforward to find model errors, manipulate the model (adding waters, splitting residues and so on) and then run SHELXL refinement with (ideally) no hand-editing of the files.

Various aspects of Coot functionality will be demonstrated.

**WK.02 Standards for Publication of Macromolecular NMR Structures**

**WK.02.01 The Purpose of Publication Standards.** Howard Einspahr, Ph. D., Editor, *Acta Crystallographica* Section F, P. O. Box 6395, Lawrenceville NJ 08648-0395. hmeinspahr@yahoo.com

A brief discussion of the bases of standards governing scientific publication will be presented. Prominent among these bases is the requirement that a publication present sufficient detail to allow readers a reasonable chance to replicate the experiment and reproduce the published results. Because methods and technology evolve over time, these standards must be periodically reviewed and updated. This has become particularly evident for publication of structural biology results, crystallographic and NMR, in recent years.

**WK.02.02 The NMR Task Force of the World-wide PDB.**

Robert Kaptein, Bijvoet Center, Utrecht Univ., Padualaan 8, NL-3584 CH Utrecht, The Netherlands.

The NMR Task Force is an advisory body of the wwPDB representing the NMR structural biology community. It provides advice and recommendations to the PDB and the BioMagResBank (BMRB) on standards for submission of NMR derived biomolecular structures and supporting data.

The Task Force was rejuvenated in 2005. Its members come from both academia and industry and have a broad range of expertise in biomolecular NMR (e.g. spectroscopy, software development, structure validation, solution and solid state NMR).

An overview will be given of the recent activities of the Task Force and the recommendations it has produced. These deal with the representation of NMR structures in the PDB (including a description of coordinate uncertainty), the deposition of experimental NMR data, and the nomenclature for hydrogen atoms. Although the main mission of the Task Force is to advise the PDB and BMRB, ideas are also generated on standards for publication of NMR structures.

**WK.02.03 BioMagResBank (BMRB) Data Deposition and Entry Processing Requirements.**

Eldon L. Ulrich, Jurgen Doreleijers, Jundong Lin, Steve Mading, Dimitri Maziuk, Christopher Schulte, David Tolmie, John L. Markley, Dept. of Biochemistry, Univ. of Wisconsin-Madison, Madison, WI 53706 USA.

BioMagResBank (RCSB-BMRB), in collaboration with the RCSB-PDB, has developed the one-stop ADIT-NMR deposition system for the submission of NMR structures, restraints used to calculate the structures, and a wide variety of NMR experimental data. Deposition requirements are consistent with published IUPAC recommendations [Recommendations for the Presentation of NMR Structures of Proteins and Nucleic Acids, *Pure & Appl. Chem.* 70, 117-142 (1998)]. The issues addressed in developing the new ADIT-NMR deposition system and in the annotation of the data deposited will be discussed.

We acknowledge our many fruitful interactions with members of the scientific community, the wwPDB, the Collaborative Computational Program on NMR (CCPN), the European Bioinformatics Institute (EBI), and the Condor team. BMRB is supported by grant LM05799 from the US National Library of Medicine.

**WK.02.04 Standards for Crystallographic Publishing.**

Manfred S. Weiss, EMBL Hamburg Outstation, c/o DESY, D-22603 Hamburg, Germany.

Any scientific publication ought to contain (either in the main paper or as easily accessible supplementary material) sufficient information, so that the average consumer of the publication can be convinced that the answers to the questions posed are well supported by experimental evidence. Furthermore, it seems essential that the results published can easily be put in context to similar studies carried out by different authors.

The current evaluation criteria for publishing crystallographic results in IUCr journals (*Acta Crystallographica* Sections D and F) with respect to sample information, data collection and structure solution statistics, model generation and refinement and model validation have some time ago been assembled and are available on the web (<http://journals.iucr.org/d/services/evaluationcriteria/>). A somewhat extended list of criteria has resulted from the work geared towards mmCIF definition (<http://journals.iucr.org/f/services/structuralcommunications/requirements.html>) and it has been proposed that these items should be required for a structural communication.

The criteria laid down in the mentioned pages will be summarized and reviewed. Some experiences with author compliance along with some thoughts with respect to what should be the minimally acceptable standards will be presented. Furthermore, particular emphasis will be given to criteria, which have undergone re-evaluation over the past years and may need to be redefined.

[1] Notes for authors (2007). *Acta Cryst.* **D63**, 424-429.

**WK.02.05 Evaluating Protein Structures Determined by Structural Genomics Consortia.** Aneerban Bhattacharya, Dehua Hang, Roberto Tejero, Gaetano T. Montelione\*, Center for Advanced Biotechnology and Medicine, Northeast Structural Genomics Consortium, Rutgers Univ. and Robert Wood Johnson Medical School, Piscataway, NJ, 08854.

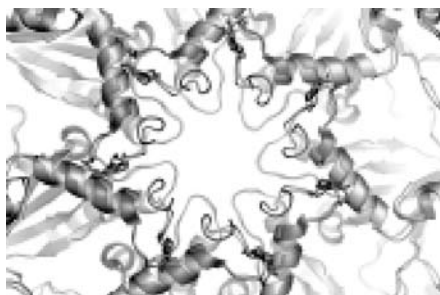
Structural genomics projects are providing large quantities of new 3D structural data for proteins. In order to monitor the quality of these data, we have developed the Protein Structure Validation Software suite (PSVS), for assessment of protein structures generated by NMR or X-ray crystallographic methods. PSVS is broadly applicable for structure quality assessment in structural biology projects. The software integrates under a single interface analyses from several widely-used structure quality evaluation tools, including PROCHECK (Laskowski RA, et al., *J Appl Crystallog* 1993; 26: 283 - 291), MolProbity (Lovell SC, et al., *PROTEINS* 2003; 50: 437-450), Verify3D (Luthy R, et al., *Nature* 1992; 356: 83-85), ProsaII (Sippl MJ, *PROTEINS* 1993; 17: 355-362), the PDB validation software, and various structure-validation tools developed in our own laboratory, including simple “NMR R factors”. PSVS provides standard constraint analyses, statistics on goodness-of-fit between structures and experimental data, and knowledge-based structure quality scores in standardized format suitable for database integration. The analysis provides both global and site-specific measures of protein structure quality. Global quality measures are reported as Z scores, based on calibration with a set of high-resolution X-ray crystal structures. PSVS is particularly useful in assessing protein structures determined by NMR methods, but is also valuable for assessing X-ray crystal structures or homology models. Using these tools, we assessed protein structures generated by the Northeast Structural Genomics Consortium and other international structural genomics projects, over the past several years. Protein structures produced from structural genomics projects exhibit

quality score distributions similar to those of structures produced in traditional structural biology projects during the same time period. However, while some NMR structures have structure quality scores similar to those seen in higher-resolution X-ray crystal structures, the majority of NMR structures have lower scores. Potential reasons for this “structure quality score gap” between NMR and X-ray crystal structures will be discussed



**SP001 Structural Studies of *T. Acidophilum* Proteasome: Implications for Proteasome Activation and Inhibition.** E.I. Masters, A. Förster, C.P. Hill, Dept. of Biochemistry, Univ. of Utah, Salt Lake City, UT.

The 20S proteasome is an essential, barrel-shaped enzyme possessing catalytic sites sequestered within a central chamber. Substrates and products must traverse gated axial pores in order to access the catalytic sites. Both an increase in pore diameter and conserved N-terminal residues are required to achieve a stable open gate<sup>[1]</sup>. We have solved a 2.5 Å crystal structure of *T. acidophilum* proteasome (Ta20S) which clarifies structural elements seen in a previous lower resolution structure<sup>[2]</sup> and supports our model of gate opening. The recently solved structure shows a pore diameter of 37.8 Å, consistent with a disordered, non-open gate conformation and less than the 40.1 Å diameter present in the open-gate 20S/11S complex structure<sup>[1]</sup>. The slight, outward rigid body motion of the alpha subunits of the open gate 20S/11S complex structure also becomes clearer when compared against the higher resolution unliganded Ta20S structure. In addition, a 2.8 Å crystal structure of Ta20S with a vinyl sulfone (VS) inhibitor bound has been solved. The Ta20S-VS structure shows an inhibitor covalently bound to the N-terminal catalytic threonine of the β subunit. The mode of binding and interaction of the inhibitor and catalytic site are consistent with predicted models.



[1] Förster, A., *et al.*, The 1.9 Å structure of a proteasome-11S activator complex and implications for proteasome-PAN/PA700 interactions. *Mol Cell*, 2005. **18**(5): p. 589-99.

[2] Lowe, J., *et al.*, Crystal structure of the 20S proteasome from the archaeon *T. acidophilum* at 3.4 Å resolution. *Science*, 1995. **268**(5210): p. 533-9.

**SP002 Crystallization of the Dyrk1B Kinase Domain.** H. Rho, R.B. Rose, Dept. of Molecular and Structural Biology, North Carolina State Univ., Raleigh, NC.

Mini-brain related kinase (Mirk) is an arginine-directed, tyrosine-regulated, dual specificity serine/threonine kinase. Mirk regulates the activity of the transcription factor hepatocyte nuclear factor-1 alpha (HNF-1α). HNF-1α regulates tissue specific gene expression in liver, pancreas, and intestine. Mutations in HNF-1α are associated with a familial form of diabetes. Mirk upregulation is correlated with a variety of cancers such as colon, lung, and ovarian cancers. Thus, Mirk is involved in the regulation of differentiation as well as the cell cycle.

Mirk is identical to Dyrk1B. There are currently no structures of the Dyrk family, which includes Dyrk1A (associated with Down's Syndrome). The closest related kinase structure is that of the MAPK, extracellular signal-regulated protein kinase 2 (ERK2). Mirk is unique because it is a dual specificity kinase. It autophosphorylates tyrosine in its activation loop and serine and threonine in substrates.

Our goal is to determine how Mirk recognizes its substrates. To accomplish this we have identified a minimal kinase domain that is soluble and active. This domain has been purified and crystallized.

**SP003 Structure Based Protein Engineering of Ribosomal Protein Trimethyltransferase PrmA.** Hasan Demirci, Steven T. Gregory, Albert E. Dahlberg, Gerwald Jogl, Dept. of Molecular Biology, Cell Biology and Biochemistry, Brown Univ., Providence, RI.

Bacterial ribosomal protein L11 trimethyltransferase, PrmA, is an unusual enzyme in its capability for highly specific recognition and flexible reorientation of its substrate during multiple trimethylation. Among trimethyltransferases, PrmA is uniquely capable of catalyzing the trimethylation of ε-amino groups of multiple lysine side chains and the α-amino group of the first methionine residue with high accuracy. There are no bulky residues present in the tunnel-like active site cavity that could restrict the rotational movement of either lysine side chains or the N-terminal α-amino group during catalysis as would be expected for a trimethyltransferase. Here we present the preliminary results of site-directed mutagenesis studies of the PrmA active site in an attempt to generate a mono- or dimethyltransferase from a trimethyltransferase by insertion of bulkier residues surrounding the active site cavity. In additional experiments to study the structural basis of enzymatic catalysis, we found that replacement of the strictly conserved His104 by alanine surprisingly results in a hyper-active trimethyltransferase. Further biophysical and biochemical studies are currently performed to investigate catalysis and specificity of the engineered versions of PrmA.

**MP004 Structural Investigations into the Role of Human Maltase-glucoamylase in Starch Digestion.** Lyann Sim<sup>1,2</sup>, David Rose<sup>1,2</sup>, <sup>1</sup>Dept. of Medical Biophysics, Univ. of Toronto, <sup>2</sup>Div. of Cancer Genomics and Proteomics, Ontario Cancer Inst., Toronto, ON.

Human starch digestion requires the sequential hydrolyzing activities of several key enzymes (including salivary and pancreatic α-amylases and two intestinal α-glucosidases) to release glucose from the long and branched glucose polymers that form starch. Maltase-glucoamylase (MGA) and sucrase-isomaltase (SIM) are intestinal Family 31 glycoside hydrolases (GH31) responsible for catalyzing the last glucose-releasing step in starch digestion. MGA and SIM have two catalytic domains, share high sequence similarities and are believed to have complementary activities as they share similar substrates but differ in their abundance and in their rates of hydrolysis. These starch-digesting enzymes are currently targeted for inhibition by α-glucosidase inhibitors as one of the treatments for Type II diabetes.

To gain a better understanding of the roles of the MGA and SI catalytic domains in relations to human starch digestion and to aid in the design of novel anti-diabetic inhibitors, our objective is to conduct structural and kinetic studies on the individual catalytic domains. Our laboratory has recently solved the crystal structure of the N-terminal catalytic domain of human MGA (100 kDa) to 2.0 Å. This entailed MGA expression in *Drosophila* S2 cells, crystallization with the help of reductive methylation and SAD phasing using the quick iodide soak approach. Here we present the crystal structure of the N-terminal domain of MGA, the structure in complex with alpha-glucosidase inhibitors and modeling studies of the MGA and SI catalytic domains.

**MP006 The Crystal Structure of Carboxysome Subunit CcmL Reveals a Pentameric Assembly Suggesting its Role as a Vertex in the Bacterial Microcompartment.** S. Tanaka, M.R. Sawaya, C.A. Kerfeld, T.O. Yeates, Dept. of Chem. and Biochem., Univ. of California, Los Angeles, CA.

We have determined the 2.7 Å X-ray crystal structure of a carboxy-

some subunit, CcmL, from *Synechocystis* sp. PCC 6803. The carboxysome is a poorly understood bacterial microcompartment, roughly 1000Å in diameter, that sequesters enzymes involved in carbon fixation. The shell is built from several thousand protein subunits and resembles a viral capsid. We have previously solved the crystal structures of hexameric carboxysome shell subunits, which suggest their roles in forming flat facets of the polyhedral shell (Kerfeld *et al.*). The CcmL subunit possesses a predominantly  $\beta$ -sheet structure and assembles as a pentamer. Its structure suggests a role in forming icosahedral vertices of the protein shell, according to principles common to many viral capsids.



The structure was solved by standard three wavelength anomalous dispersion on a selenomethionyl derivative. After three rounds of refinement, the five chains were essentially complete, but  $R_{\text{work}}$  and  $R_{\text{free}}$  stalled at 41.7% and 44.8%. Strong difference density could be found in the crystal interstices of the  $F_o - F_c$  maps, which appeared to result from the presence of two additional pentamers partially overlapping the current model. It was reasoned that this residual density could be explained by a lattice translocation disorder and that the structure factors could be corrected to remove the disorder by following the procedures outlined in Wang *et al.*, 2005.  $R_{\text{work}}$  and  $R_{\text{free}}$  for the two-pentamer-model immediately dropped to 32.0% and 34.9% after the structure factors were corrected. Current values of  $R_{\text{work}}$  and  $R_{\text{free}}$  are 24.7% and 30.7%.

Wang, J. *et al.* (2005). *Acta Cryst.* D61, 67-74.  
Kerfeld, C.A. *et al.* (2005). *Science.* 309, 936-8.

**MP007 Structures of the Immunogenic Region of A-beta Complexed with Anti-protofibril Antibodies.** Anna S. Gardberg<sup>1</sup>, Lezlee T. Dice<sup>2</sup>, Susan Ou<sup>3</sup>, Rebecca L. Rich<sup>4</sup>, Elizabeth Helmbrecht<sup>1</sup>, Jan Ko<sup>3</sup>, Ronald Wetzel<sup>5</sup>, David G. Myszka<sup>4</sup>, Paul H. Patterson<sup>3</sup>, Chris Dealwis<sup>1</sup>, <sup>1</sup>BCMB, Univ. of Tennessee, Knoxville, TN. <sup>2</sup>Graduate School of Medicine, Univ. of Tennessee, Knoxville, TN. <sup>3</sup>California Inst. of Technology, Pasadena, CA, <sup>4</sup>Univ. of Utah, Salt Lake City, UT, <sup>5</sup>Univ. of Pittsburgh, Pittsburgh, PA.

Amyloid aggregates of the A $\beta$  peptide are implicated in the pathology of Alzheimer's disease. Anti-A $\beta$  monoclonal antibodies (mAbs) have been shown to reduce amyloid plaques *in vitro* and in animal studies. Consequently, passive immunization is being considered for treating Alzheimer's, and anti-A $\beta$  mAbs are now in phase II trials. We report the isolation of two new mAbs (PFA1 and PFA2) that recognize A $\beta$  monomers, protofibrils, and fibrils, as well as the structures of their antigen binding fragments (Fabs) in complex with the A $\beta$ (1-8) peptide DAEFRHDS. The immunodominant EFRHD sequence forms salt-bridges, hydrogen-bonds, and hydrophobic contacts, including interactions with a striking WWDD motif of the Fabs. We also show that a similar sequence (AKFRHD) derived from the human protein GRIP1 is able to cross-react with both PFA1 and PFA2 and, when co-crystallized with PFA1, binds in an identical conformation to A $\beta$ (1-8). Since such cross-reactivity has implications for potential side effects of immunotherapy, our structures provide a template for designing derivative mAbs that target A $\beta$  with improved specificity and higher affinity.

**SP008 Crystal Structure of Inositol Polyphosphate Multikinase 2 with Substrate Kinetics Analysis.** William Holmes, Gerwald Jogl.

Inositol polyphosphates, such as inositol 1,4,5-trisphosphate (IP<sub>3</sub>), are

important small molecules that act as a second messenger in eukaryotic cells. Other inositol polyphosphates, such as IP<sub>6</sub>, have been associated with a variety of cellular processes such as mRNA export and DNA damage repair. Enzymes that synthesize these polyphosphates belong to the inositol phosphate superfamily, and are predicted to have a similar fold despite low sequence similarity. To investigate the structural basis for substrate specificity, we have determined the crystal structure of the inositol phosphate multi-kinase Ipk2 in the apo form and in a complex with ADP and Mn<sup>2+</sup> at up to 2.0 Å resolution. The three-dimensional structure revealed an overall similarity to the human IP<sub>3</sub> 3-kinase, with the inositol binding domain significantly smaller in Ipk2. Comparison with the human IP<sub>3</sub> 3-kinase, analysis of the active site suggested possible key residues in substrate binding. We performed site directed mutagenesis on these residues and analyzed the catalytic activity of each mutant. Replacement of critical side chains in the inositol binding site suggests how a modification of substrate recognition motifs might determine enzymatic substrate preference and catalysis.



**SP009 Elucidation of the First Crystal Structure of HoxA9 and Pbx Homeodomains Bound to an *In Vivo* Derived DNA Target.** W.J. Bauer<sup>1,2</sup>, J. Kocsis<sup>1</sup>, T.C. Umland<sup>1,2</sup>, <sup>1</sup>Hauptman Woodward Medical Research Inst., <sup>2</sup>State Univ. of New York at Buffalo, Buffalo, NY.

Homeobox (Hox) proteins have long been known to control the regulation of embryonic development and cell differentiation of all animals possessing bilateral symmetry. However, new evidence suggests that many Hox proteins may also play a role in post-embryonic transcriptional regulation within several pathways, such as hematopoiesis and many types of cancer. Despite these very crucial roles, relatively few *in vivo* transcriptional targets of Hox proteins have been identified. One of the few known examples of a true *in vivo* Hox target is a region found up stream of the mouse *Ren-1* gene known as the renin proximal promoter element (PPE). Several members of the Hox family, including HoxA9, and the cofactor Pbx have been shown to bind to the renin PPE and upregulate *renin* transcription. Renin is an aspartyl protease which participates in the regulation of blood pressure and electrolyte levels through the conversion of angiotensinogen to angiotensin I, which ultimately results in an increase in blood pressure. Revealing the exact mechanisms of recognition and binding would lead to a greater understanding of the underlying forces behind this important pathway and possibly lead to new treatments for hypertension. Here we present the first crystal structure of homeodomains of mouse Hox A9 and Pbx cofactor bound to an *in vivo* derived DNA sequence similar to that found in the renin PPE. The specific contacts and geometries discovered here will be compared to Hox structures bound to DNA derived from *in vitro* binding assays to draw conclusions on the importance of flanking nucleotides, specificity of binding and DNA recognition mechanisms.

**MP010 The Crystal Structure of GTP Cyclohydrolase III with Bound Substrate.** Sue A. Roberts, Shane D. Morrison, Vahe Bandarian, Dept. of Biochemistry and Molecular Biophysics and Dept. of Chemistry, Univ. of Arizona, Tucson, AZ.

GTP cyclohydrolase II (GCH II) is a zinc-containing protein that catalyzes the conversion of GTP to 2,5-diamino-6-ribosylamino-4(3H)-pyrimidinone 5'-phosphate (APy) or, in the case of a GCH II from *S. coelicolor*, 2-amino-5-formylamino-6-ribosylamino-4(3H)-py-

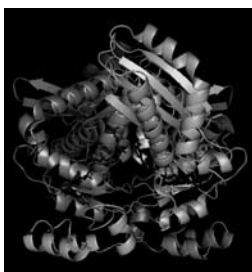
rimidinone 5'-phosphate (FAPy) (Spoonamore, *et.al.*, *Biochemistry*, 2006, 45, 12144-55). An enzyme from *M. jannaschii* that catalyzes the conversion of GTP to FAPy was described by White and coworkers (*Biochemistry*, 2002, 41, 15074-15084). Interestingly the enzyme does not appear to have sequence similarity to GCH II proteins, nor does it contain zinc. To determine if the protein has structural similarity to GCH II, we have determined its crystal structure. Se-methionine substituted protein was prepared and the protein co-crystallized with its GTP substrate. The complex crystallizes in space group I222 with unit cell parameters  $a=90.16 \text{ \AA}$ ,  $b=98.13 \text{ \AA}$ ,  $c=125.16 \text{ \AA}$ ,  $Z=2$ . The structure of the protein-GTP complex was solved from a 2.8 Å three-wavelength MAD data set collected at the Se edge. Twelve of sixteen Se atoms in the asymmetric unit were found using SOLVE. After density modification with RESOLVE, the entire protein chain, except residues near the C-terminus, were located. The structure was refined with Refmac5 and rebuilt using coot. The protein appears to have a new fold. The structure of the protein/GTP complex allows us to speculate on how the enzyme performs a GTP cyclohydrolase reaction without the usual catalytic zinc.

Data were measured at beam line 9-2, SSRL. This work is supported by NIH grant GM72523 (VB) and a Burroughs Wellcome Career Award in Biomedical Sciences (VB)

**SP011 Structural Studies on HMG-CoA Reductase from the Pathogenic Bacterium *Enterococcus faecalis*.** Sucharita Bose, C. Nicklaus Steussy, Matija Hedl, Victor W. Rodwell, Cynthia V. Stauffacher, Purdue Univ., IN.

*E. faecalis* is an opportunistic bacterium causing bacteremia, urinary tract infections and infective endocarditis. Acquisition of resistance to several antibiotics, has led to emergence of *E. faecalis* as a nosocomial pathogen posing considerable therapeutic challenge. *E. faecalis*, along with other gram-positive cocci, rely on the mevalonate pathway for isoprenoid biosynthesis critical for their survival. Thus the enzymes of the mevalonate pathway are considered to be potential candidates for drug targets.

HMG-CoA reductase catalyzes the NADPH-dependent reduction of HMG-CoA to mevalonate, the first committed step in the mevalonate pathway. Bacterial HMG-CoA reductase and its eukaryotic counterpart differ in regulation and sensitivity toward statins, which reflects an underlying structural difference that can be exploited to generate specific antibiotics targeted against *E. faecalis*. The structure of the *E. faecalis* enzyme has been solved at 2.25 Å by the molecular replacement method using the bacterial *P. mevalonii* enzyme as the search model. As for the other HMG-CoA reductases, this structure shows a dimer as the functional catalytic unit. Each monomer comprises a large domain known to bind HMG-CoA and a small cofactor binding domain. The structure shows close resemblance to the *P. mevalonii* enzyme in its active site while possessing the structural features determining its specificity towards NADP over NAD. Crystalline complexes of this protein have been produced with substrates and cofactors to investigate molecular basis of the NADP preference. Potential inhibitors have been identified from a high throughput screen that will also serve as the basis for future structure-based drug design.



**SP012 Crystal Structure of the Zinc-binding Transport Protein ZnuA from *Escherichia coli* Reveals an Unexpected Variation in Metal Coordination.** Hua Li, Gerwald Jögl, Dept. of Molecular Biology, Cell Biology and Biochemistry, Brown Univ., Providence, RI.

Bacteria maintain metal homeostasis by high- and low-affinity metal import systems. The metal transporters they use for zinc and manganese ions belong to the cluster 9 family of high-affinity ATP-binding cassette (ABC) transport systems. ABC-type metal ion transport systems consist of three proteins: a solute-binding protein (SBP), a transmembrane permease and a nucleotide-binding protein. We determined the structure of the zinc-specific SBP, ZnuA from *E. coli* with bound zinc at 1.75 Å resolution.

The overall structure of ZnuA is similar to other SBP structures. The bound zinc ion is coordinated by three histidine residues (His78, His161 and His225) and one glutamate residue (Glu77). Compare to previously determined solute-binding proteins, the structure of *E. coli* ZnuA shows an unexpected metal coordinating glutamate residue (Glu 77). To better understand



this variation in metal coordinating sites of ZnuA and other SBPs, 42 homologous sequences from different organisms were chosen from a BLAST database search to perform structure-based sequence alignment. Based on available structures and results of structure-based sequence alignment, we found that for four coordination sites of the metal ion, two histidine residues (His78 and His161 in ZnuA<sub>ec</sub>) are strictly conserved in all proteins. The third coordination site can either be a histidine residue in the zinc-specific SBPs or a glutamate residue in the manganese-specific SBPs. The fourth coordination site is occupied by either a solvent water molecule or a glutamate or aspartate residue in the zinc-specific SBPs and an aspartate residue in the manganese-specific SBPs.

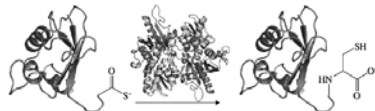
**MP013 Structural Basis for Ligand and Heparin Binding to Neuropilin B Domains.** Craig Vander Kooi, Manuel Jusino, Benjamin Perman, David Neau, Henry Bellamy, Daniel Leahy, Dept. of Biophysics and Biophysical Chemistry, Johns Hopkins Univ. School of Medicine, Baltimore, MD, Center for Advanced Microstructures and Devices, Louisiana State Univ., Baton Rouge, LA.

Neuropilin (Nrp) is a cell surface receptor with essential roles in angiogenesis and axon guidance. Interactions between Nrp and the positively-charged C-termini of its ligands, vascular endothelial growth factor (VEGF) and semaphorin, are mediated by Nrp domains b1 and b2, which share homology to coagulation factor domains. We have determined the crystal structure of the tandem b1 and b2 domains of Nrp-1 (N1b1b2) and show that they form a single structural unit. CocrySTALLIZATION of N1b1b2 with Tuftsin, a peptide mimic of the VEGF C-terminus, reveals the site of interaction with the basic tail of VEGF on the b1 domain. We also show that heparin promotes N1b1b2 dimerization and map the heparin binding site on N1b1b2. These results provide a detailed picture of interactions at the core of the Nrp signaling complex and establish a molecular basis for the synergistic effects of heparin on Nrp-mediated signaling.

CWVK is a Leukemia and Lymphoma Society Fellow. This work was supported by NIH grant CA90466.

**SP014 Crystal Structure of a Sulfur Carrying Protein Complex Found in the Cysteine Biosynthetic Pathway of *Mycobacterium tuberculosis*.** Christopher Jurgenson, Kristin Burns, Tadhg Begley, Steven Ealick, Chemistry and Chemical Biology, Cornell Univ., Baker Lab., Ithaca, NY.

The protein complex structure of the  $\beta$ -replacement enzyme CysM (Rv1336) and the sulfur transfer protein CysO (Rv1335) found in the H37Rv strain of *Mycobacterium tuberculosis* for the biosynthesis of cysteine has been solved to a resolution of 1.6 Å using single anomalous dispersion data and molecular replacement. The protein complex crystallized in the asymmetric CysM:CysO ratio of 2:1. Additionally, the structure of CysM without its binding partner CysO has been solved by molecular replacement to 2.8 Å. CysO is a ubiquitin like protein with a four stranded  $\beta$ -sheet and a long  $\alpha$ -helix spanning strands  $\beta$ 1 and  $\beta$ 2. The C-terminus of CysO consists of two glycine residues and is thiocarboxylated *in vivo* to deliver a sulfur atom to the  $\alpha$ -aminoacrylate intermediate generated by the catalytic reaction between O-acetylserine and the pyridoxyl 5-phosphate cofactor of CysM. The product of the reaction is a CysO molecule with an additional cysteine residue at the C-terminus attached by a peptide bond. Free cysteine is released through a hydrolysis reaction catalyzed by the protease Mec<sup>+</sup> (Rv1334) which regenerates the native CysO molecule. The CysO-CysM complex is the first structural example of a sulfur transfer protein mechanism utilized in the biosynthesis of an amino acid.



**MP015 Crystal Structure of NeuroD/E47 in Complex with DNA: Insight of E-box Recognition by a Heterodimeric bHLH.** A. Longo\*, G. Guanga, R. Rose, Dept. of Molecular and Structural Biochemistry, NCSU, Raleigh, NC, \*also at CCS-CSM, ORNL, Oak Ridge, TN.

NeuroD/Beta2 is a transcription factor belonging to the basic helix-loop-helix (bHLH) family, and plays an essential role in the development and function of the pancreas and the nervous system (1). Mutations in the human *neuroD* gene lead to diabetes, ataxia, deafness (1). Tissue specific NeuroD forms heterodimers with the ubiquitously expressed bHLH E47. We determined the crystal structure of the bHLH NeuroD/E47 heterodimer bound to a DNA containing the insulin promoter E-box. Data were collected on frozen crystals at the SER-CAT beamline at the APS. The structure was solved at 2.5 Å resolution by molecular replacement using the MyoD bHLH structure (2) as a search model. Comparison of the NeuroD/E47 bHLH structure to other bHLH/DNA complex structures indicates a conserved overall structure but unique interactions between protein and DNA. This structure will give an insight into selection of heterodimer partners and DNA binding specificity.

[1] Chae *et al.*, *Mol. Cells*, 2004, **18**, pp 271-288

[2] Ma *et al.*, *Cell*, 1994, **77**, pp 451-459

**SP016 Conformation Changes of Y-family Polymerase Dpo4 from the Apo-enzyme to Substrate Bound Forms.** Jimson H.Y. Wong, Hong Ling, Dept. of Biochemistry, Univ. of Western Ontario, London, ON N6A 5C1, Canada.

Translesion synthesis (TLS) is a fundamental process used by cells to survive DNA damage. In TLS, cells employ low-fidelity Y-family polymerases to replicate past DNA lesions. However, these low-fidelity polymerases produce errors in DNA replication, which can contribute to the development of diseases such as cancer. DNA poly-

merase IV (Dpo4), an archaeal Y-family DNA polymerase, is a representative member of the Y-family. Dpo4 consists of four domains: a classic three-domain polymerase core made of the palm, finger, and thumb domains, and an additional domain called the little finger (LF) domain. We solved the crystal structures of the apo-enzyme Dpo4 at 1.9Å resolution and a Dpo4-DNA binary complex at 2.1Å resolution. The domain organization and orientation of the polymerase core were unchanged across all Dpo4 structures. However, there was a dramatic alteration in the position of the LF domain in the apo-Dpo4 structure. The LF domain is positioned adjacent to the thumb domain, rather than being close to the finger domain as seen in all Dpo4-DNA-dNTP ternary Dpo4 structures. Dpo4 in the binary complex remains in the same conformation as in the ternary complexes. Subtle changes were observed in metal ion coordination and in the side chain conformations of the conserved nucleotide-binding residues upon incoming nucleotide binding. These structural observations suggest that the overall conformation of the Y-family polymerase remains rigid after DNA binding. The subsequent nucleotide incorporation step only involves subtle conformation changes within the active site. These results highlight the differences in DNA replication mechanisms between the low-fidelity Y-family polymerases and their high-fidelity DNA polymerase counterparts.

**SP017 Crystallographic Studies of Pyruvate-formate Lyase Activase.** J. Vey\*<sup>1</sup>, M. Li<sup>2</sup>, J. Yang<sup>2</sup>, J. Broderick<sup>2</sup>, C. Drennan<sup>1</sup>, <sup>1</sup>Dept. of Chemistry, MIT, Cambridge, MA, <sup>2</sup>Dept. of Chemistry and Biochemistry, Montana State Univ., Bozeman, MT.

One newly discovered and exciting role for iron-sulfur clusters in biology is in the initiation of protein-mediated radical chemistry. The SAM Radical protein superfamily uses an iron-sulfur cluster and S-adenosylmethionine (SAM) to generate substrate- or protein-bound radicals via a 5'-deoxyadenosyl radical. As the reactions that follow this initial step are highly diverse, this family is thought to be a metabolically and evolutionarily important group of proteins.

PflAE catalyzes the SAM-dependent activation of pyruvate-formate lyase (PFL) by formation of a catalytic glycy radical on G734 of PFL. We are continuing our studies<sup>1,2</sup> of the SAM Radical superfamily with PflAE with the hope of adding to our understanding of formation and control of the 5'-deoxyadenosyl radical by these enzymes for reaction with highly diverse substrates.

The structure of [4Fe4S]-PflAE was solved in space groups P3<sub>1</sub> and P3<sub>1</sub>21. Difficulties encountered during the refinement led to the investigation of possible problems such as twinning and alternate space groups. The structure of PflAE with the cluster, SAM and a peptide substrate mimic was also solved, allowing identification of conformational changes associated with substrate binding. Current progress towards refinement of the x-ray crystal structures will be presented.

[1] Berkovitch *et al.* *Science* (2004) **303** (5654): 76-9.

[2] Nicolet Y and Drennan CL. *Nuc Acid Res* (2004) **32** (13): 4015-25.

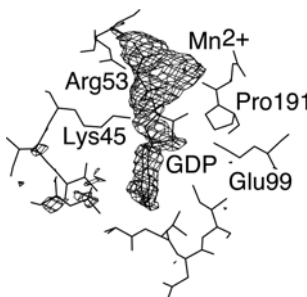
**MP018 Structure of *Thermus aquaticus* Succinyl-CoA Synthetase in Complex with Mn<sup>2+</sup>-GDP.** Marie Fraser, Koto Hayakawa, Edward Brownie, Dept. of Biological Sciences, Univ. of Calgary, Calgary, AB, Canada.

Succinyl-CoA synthetase (SCS) catalyzes the reversible reaction succinyl-CoA + NDP + Pi  $\leftrightarrow$  succinate + CoA + NTP, where N denotes adenosine or guanosine. In the forward direction as written here, SCS catalyzes the substrate-level phosphorylation step of the citric acid cycle. The enzyme from the thermophile, *T. aquaticus*, can use either nucleotide, but in contrast to *E. coli* SCS, *T. aquaticus* SCS prefers

GDP/GTP. To understand the determinants of nucleotide and temperature preference, we determined the structure of *T. aquaticus* SCS in complex with  $Mn^{2+}$ -GDP. The enzyme is an  $\alpha_2\beta_2$ -heterotetramer of 141 kDa. The first crystal form of *T. aquaticus* SCS diffracted to 2.2 Å, but did not show electron density for the nucleotide nor for the carboxy-terminal domain of the  $\beta$ -subunit. These crystals belong to the space group I222 with unit cell dimensions  $a = 100.9$  Å,  $b = 114.2$  Å,  $c = 121.6$  Å,  $\alpha = \beta = \gamma = 90^\circ$  and contain one  $\alpha\beta$ -dimer in the asymmetric unit. We learned that the protein was being cleaved during the crystallization and the best diffracting crystals were from the cleaved protein. We did get crystals of the full-length protein by frequently adding protease inhibitors during the purification of the protein and by modifying the crystallization conditions. Crystals of the full-length protein were grown with  $Mn^{2+}$ -GDP and were rectangular plates, the best growing to a thickness of only 0.04 mm. This crystal form belongs to the space group C2 with unit cell dimensions  $a = 261.7$  Å,  $b = 126.8$  Å,  $c = 110.6$  Å,  $\alpha = \gamma = 90^\circ$ ,  $\beta = 112.8^\circ$ . There are 4  $\alpha$ -subunits and 4  $\beta$ -subunits in the asymmetric unit and each of the  $\beta$ -subunits binds one  $Mn^{2+}$  ion and one molecule of GDP.

**MP019 Mutagenic Bypass of a Major Benzo[a]pyrene Adduct by a Y-Family DNA Polymerase through Strand Misalignment.** Hong Ling<sup>1</sup>, Jacob Bauer<sup>1</sup>, Guangxin Xing<sup>1</sup>, Haruhiko Yagi<sup>2</sup>, Jane M. Sayer<sup>2</sup>, Donald M. Jerina<sup>2</sup>, <sup>1</sup>Dept. of Biochemistry, Univ. of Western Ontario, London, ON, Canada, <sup>2</sup>Lab. of Bioorganic Chemistry, National Inst. of Diabetes and Digestive and Kidney Diseases, National Inst. of Health, DHHS, Bethesda, MD.

Replication of damaged DNA by DNA polymerases leads to elevated mutagenesis. To understand molecular basis of DNA damage-induced mutagenesis, we have determined the X-ray structures of a Y-family polymerase in complex with a DNA substrate containing a bulky DNA lesion and incoming nucleotides. The DNA lesion is derived from a most ubiquitous carcinogenic polycyclic aromatic hydrocarbon, Benzo[a]pyrene (BP). The major BP adduct, BP diol epoxide-N<sup>2</sup>-deoxyguanosine (BP-dG), is at the template-primer junction. Three ternary complexes reveal replication blockage, extension past a mismatched lesion, and -1 frameshift mutation. The nonproductive complex observed accounts for poor efficiency of primer extension past the BP-dG adduct. In the productive structures, the bulky adduct is flipped/looped out of the DNA helix into a unique structural gap between the little finger and core domains. Sequestration of the hydrophobic adduct in the additional substrate binding site permits DNA to exhibit normal geometry for primer extension. Loop out of the adduct by template misalignment leads base 5' to the adduct serving as a template. Subsequent realignment of looped out lesion produces a mismatched base against the lesion. The additional substrate binding site that stabilizes the extrahelical base supports base substitutions and frameshift mutations.



**SP020 Structure of  $\alpha$ -Glycerophosphate Oxidase from *Streptococcus* sp.: A Structural Template for the Mitochondrial  $\alpha$ -Glycerophosphate Dehydrogenase.** Timothy Colussi<sup>1</sup>, Derek Parsonage<sup>1</sup>, Takeshi Matsuoka<sup>2</sup>, P. Andrew Karplus<sup>3</sup>, T. Conn Mallett<sup>1</sup>, Al Claiborne<sup>1</sup>, <sup>1</sup>Center for Structural Biology, Wake Forest Univ. School of Medicine, Winston-Salem, NC, <sup>2</sup>Diagnostics Dept., Asahi Kasei Pharma, Shizuoka, JP, <sup>3</sup>Dept. of Biochemistry and Biophysics, Oregon State Univ., Corvallis, OR.

The soluble flavoprotein  $\alpha$ -glycerophosphate oxidase (GlpO) from *Streptococcus* sp. catalyzes the oxidation of  $\alpha$ -glycerophosphate (Glp) to dihydroxyacetone phosphate (DHAP) with concomitant reduction of  $O_2$  to  $H_2O_2$ . The closest homologues to GlpO, based on sequence, are bacterial and mitochondrial Glp dehydrogenases (GlpD), which lack a 50-residue insert found in GlpO. We have solved the structure of a deletion mutant (GlpO $\Delta$ ) lacking this insert. This structure was then used as a molecular replacement search model to solve the intact GlpO structure. The two structures have been refined to 2.3 Å and 2.4 Å, respectively. The first two domains of the GlpO fold are most closely related to that of *B. subtilis* glycine oxidase (ThiO) and function in FAD-binding and in the homodimer interface, respectively; the GlpO C-terminal domain consists of nine  $\alpha$ -helices and is unique to this flavoprotein structure. An active-site overlay with the ThiO-N-acetylglycine complex implicates GlpO Arg346 as a strong candidate for interaction with the substrate Glp-phosphate, and a docking model of the GlpO $\Delta$ -Glp complex is presented. Overlays of the GlpO and GlpO $\Delta$  active sites show conformational changes in both the isoalloxazine ring of the cofactor and His65. These conformations may correspond to distinct forms of the resting oxidized enzyme identified in earlier kinetic analyses. A structural interpretation of the mitochondrial GlpD based on the GlpO structures will be presented.



**MP021 The Mechanism of Double-Stranded RNA Processing by Ribonuclease III.** J.H. Gan, G. Shaw, J.E. Tropea, D.S. Waugh, D.L. Court, X. Ji, Center for Cancer Research, National Cancer Inst., National Inst. of Health, Frederick, MD.

Members of the Ribonuclease III (RNase III) family are  $Mg^{2+}$  dependent, double-stranded (ds) RNA-specific endoribonucleases, represented by bacterial RNase III and eukaryotic Rnt1p, Drosha and Dicer. RNase III-catalyzed dsRNA processing is important in antiviral defense, is critical in RNA maturation and degradation, and is essential in post-transcriptional gene expression control such as RNA interference. While Dicer is currently the focus of intense interest, the structurally simpler bacterial RNase III serves as a paradigm for the entire family. Previously, we have shown how RNase III uses two catalytic sites to create a 2-nucleotide (nt) 3' overhang in its product (Gan, Tropea, Waugh, Court, and Ji, *Cell* 124:355-366). Here, we present crystal structures of a bacterial RNase III, showing that  $Mg^{2+}$  is essential for the formation of a catalytically competent protein-RNA complex and that two  $Mg^{2+}$  ions are required for the hydrolysis of each phosphodiester bond. Moreover, we show the catalytic site arrangement immediately after phosphoryl transfer, suggesting a model trajectory for the RNase III-catalyzed phosphoryl transfer reaction.

**SP022 Structural Analyses of Proteins Involved in Pilius Assembly in *Streptococcus pyogenes*.** HaeJoo Kang<sup>a</sup>, Fasseli Coulibaly<sup>a</sup>, Thomas Proft<sup>b</sup>, Edward N. Baker<sup>a</sup>, <sup>a</sup>School of Biological Sciences, <sup>b</sup>Dept. of Molecular Medicine and Pathology, Univ. of Auckland, New Zealand.

Bacterial pili are filamentous appendages that are critically involved in adhesion to host cells, leading to colonization of host tissues and establishment of infections. While pili of Gram-negative bacteria such as *E. coli* have been extensively studied, relatively little is known about pili of Gram-positive bacteria such as *Streptococcus pyogenes* (group A Streptococcus; GAS). M protein serotype 1 (M1) of GAS is

the strain most strongly associated with highly invasive GAS infections and we have determined crystal structures of a sortase, SrtC1, and the major backbone protein of pili, Lancefield T1 antigen, which are critically involved in pilus assembly of GAS serotype M1.

Pili of M1 strain are composed of Lancefield T1 antigen and two ancillary proteins, Spy0130 and Cpa (collagen-binding protein of group A streptococci). The subunit proteins contain cell-wall sorting signals at their C-termini, which are cleaved by sortases during covalent polymerization of pili. The cell-wall sorting signal of Lancefield T1 antigen is thought to be cleaved by SrtC1, a sortase that is strictly required for the polymerization. The overall structure of SrtC1 is similar to three other known sortase structures, containing a  $\beta$ -barrel core with outer  $\alpha$ -helices. The crystal structure of T1 antigen reveals a fold that is somewhat different from known folds. The structure also identifies novel intra-molecular isopeptide bonds between side chains of specific amino acid residues, which could play important roles in structural stability of pili.

**SP023 Substrate Recognition in Puromycin Sensitive Aminopeptidase.** S. Sampath, A. Daily, L.B. Hersh, D.W. Rodgers, Dept. of Molecular and Cellular Biochemistry, Center for Structural Biology, Univ. of Lexington, KY.

Biopeptides modulate vital functions in the physiological system and are metabolized by a group of enzymes referred to as neuro-peptidases. Neuropeptidases often recognize substrates with varying sequences, while still maintaining specificity for their target sites. Our goal is to understand the mechanism that allows for this broad substrate specificity. One of our model systems is the puromycin sensitive aminopeptidase (PSA), an exopeptidase belonging to the M1 family of zinc metallopeptidases, which contains the HEXXH(Xn)E active site motif. Work on other neuropeptidases suggests that broad sequence recognition of substrates is mediated by varied interactions with a multifunctional surface of the enzyme. It is our hypothesis that this mechanism also accounts for the broad substrate preference shown by PSA. Structure of wild type PSA is being determined to 2.3 Å. Overall, PSA is U-shaped, and the metallopeptidase domain is contained within the longer of the two limbs. There is an extensive interaction surface between the two domains at the base of the U, consistent with the reported contribution of the C-terminal domain, which makes up the other limb, to the overall stability of the fold. The elongated active site groove is lined with aromatic and hydrophobic residues that may play a role in substrate recognition. Further a conserved sequence that is implicated in recognition of substrate N-terminal residues is found adjacent to the active site. PSA complexed with peptide mimics will allow us to directly visualize the key binding interactions and develop a detailed understanding of substrate recognition.

**MP024 Catabolism of Hyaluronan Polysaccharide: Crystal Structure of Human Hyaluronidase 1.** Kinlin Chao, Lavanya Muthukumar, Osnat Herzberg, Center for Advanced Research in Biotechnology, Univ. of Maryland Biotechnology Inst., Rockville, MD.

Human hyaluronidases (Glycoside Hydrolases family 56, EC 3.2.1.35) hydrolyze hyaluronan, a glycosaminoglycan polymer found in all tissues and body fluids with diverse physiological roles. Human hyaluronidase 1 is responsible for normal cellular hyaluronan turnover by hydrolyzing long polymers into small fragments. Human hyaluronidase 1 is implicated in prostate and bladder cancer proliferation, angiogenesis and inflammatory diseases, and is a potential cancer marker.

The crystal structure of Human hyaluronidase 1 has been determined

at 2.25Å by molecular replacement, revealing a molecule comprised of two closely associated domains. The catalytic domain adopts a distorted ( $\beta/\alpha$ )<sub>8</sub> barrel similar to that of Bee venom hyaluronidase. The C-terminal domain adopts a novel epidermal growth factor (EGF)-like fold, whose presence indicates involvement in protein-protein interactions, signal transduction and regulatory processes. The new structure also shed light on the structural consequences of Human hyaluronidase alternative splicing. Five alternatively spliced variants of Human hyaluronidase 1 are expressed at different levels in normal and bladder cancer cells. The structure of hyaluronidase 1 suggests that the EGF-like domain of four of the alternatively spliced variants remain intact. Thus, the biological function of these spliced variants may be to compete with the full-length protein for the putative partner and regulate its enzymatic activity.

**SP025 Structures of EphrinA3 Receptor Tyrosine Kinase Reveal Aspects of Mechanism and Regulation.** Tara L. Davis<sup>1,2</sup>, John R. Walker<sup>2</sup>, Abdellah Hassani<sup>2</sup>, Christine Butler-Cole<sup>2</sup>, Sirano Dhe-Paganon<sup>1,2</sup>, Dept. of Physiology<sup>1</sup> and Structural Genomics Consortium<sup>2</sup>, Univ. of Toronto, Toronto ON, Canada.

The Ephrin family of receptor tyrosine kinases (RTKs) plays a major role in development, directing axon guidance, angiogenesis, and limb development. Although not significantly present in normal adult tissues, Eph receptors are overexpressed during tumorigenesis, making them attractive therapeutic targets. The architecture of Eph RTKs consists of extracellular ligand binding and transmembrane domains and the intracellular juxtamembrane, kinase, and sterile- $\alpha$ -motif domains. Ephrins, the ligands of the ephrin receptors, are also membrane anchored and are expressed on cells other than those that express receptors. Interaction between Eph- and ephrin-presenting cells leads to intracellular signaling in both cell types, leading either to stabilization of cell-cell contacts or repulsion between cells. The kinase domains of Eph receptors appear to be repressed by their juxtamembrane region, which contains two autophosphorylation sites. To provide additional details of the auto-regulatory mechanism in Eph kinases, we conducted structure-function studies of EphA3. We characterized the effects of the juxtamembrane region on the catalytic kinase domain, as well as mutational changes of residues in the juxtamembrane region and the activation loop. These data elucidate a novel regulatory mechanism involving non-juxtamembrane residues. In addition, we have recently identified an optimized peptide substrate sequence for EphA3, validated the peptide as a substrate for EphA3, and then determined the co-crystal structure of activated EphA3 in complex with this peptide. The substrate complex provides novel insight into the mechanism of action for this medically relevant enzyme.

**SP026 Crystal Structures of Human 2-oxoglutarate Dependent Hydroxylases.** Rasheduzzaman Chowdhury, Michael A. McDonough, Christopher J. Schofield, Dept. of Chemistry, Univ. of Oxford, Mansfield Road, Oxford, UK.

Oxygen homeostasis in multicellular organisms is mediated through transcription of a gene array encoded by the cellular  $\alpha/\beta$ -heterodimeric hypoxia-inducible factor (HIF). In normoxic cells, a family of 2-oxoglutarate dependent prolyl hydroxylases (PHD 1, 2 and 3) signal for the proteosomal degradation of the constitutively expressed HIF-1 $\alpha$  subunit by post-translational hydroxylation of Pro-564 and Pro-402 that are located within two separate oxygen-dependent degradation domains (ODDDs). The PHD enzymes require dioxygen and 2-oxoglutarate (2OG) as co-substrates, and ferrous iron as a co-factor, to generate the predicted highly reactive ferryl-oxo intermediate involved in proton abstraction of the substrate proline C4 alkane

CH2 followed by hydroxylation. The absolute requirement of molecular oxygen for oxidative hydroxylation marks a direct link between changes in cellular dioxygen levels and the transcriptional regulation by HIF. Thus, PHDs act as the oxygen-sensing component in the HIF signalling pathway. Inhibition of PHDs by 2OG analogues has been shown to activate HIF in animal models raising the possibility of treating ischemic/hypoxic diseases. A second oxidative modification of HIF-



1 $\alpha$  is catalyzed by Factor Inhibiting HIF (FIH). FIH catalyze the hydroxylation at Asn-803, a modification that blocks the interaction of HIF with the transcriptional coactivator p300/CBP. Recent crystallographic studies of both substrate and inhibitor complexes of the PHD and FIH hydroxylases will be described. A discussion of how the structures relate to the oxygen sensing system will be presented as well as a comparison of the HIF hydroxylases with other human 2-oxoglutarate oxygenases.

**SP027 Structural Analysis of an Antibiotic Resistant C-O lyase from *Staphylococcus aureus*.** Magdalena Korczynska<sup>1</sup>, Tariq A. Mukhtar<sup>3</sup>, Gerard D. Wright<sup>3</sup>, Albert M. Berghuis<sup>1,2</sup>, <sup>1</sup>Depts. of Biochemistry and <sup>2</sup>Microbiology and Immunology, McGill Univ., Montreal, QC, Canada, <sup>3</sup>Dept. of Biochemistry & Biomedical Sciences, McMaster Univ., Hamilton, ON, Canada, magda.korczynska@mcmill.ca.

The streptogramin family of antibiotics has been used as a last resort treatment for bacterial infections. This family is comprised of Group A and Group B compounds, which bind to the P-site as well as impede the entrance to the peptide exit tunnel of the ribosome. Independently these antibiotics inhibit protein synthesis in Gram-positive bacteria however in combination they have synergistic effects and exhibit bactericidal properties. Unfortunately, resistance to streptogramins has been observed. One such resistance factor is streptogramin B lyase (Vgb). This enzyme inactivates Group B streptogramins by degrading the ring structure of these peptide drugs. In combination with kinetic analysis and site directed mutagenesis we are expanding the understanding of the enzymatic mechanism, which will allow for future development of potent chemical adjuvants.

Previously high-resolution data sets were collected for both the native and L-Seleno-Methionine substituted Vgb. However difficulties were encountered in obtaining crystals of the ternary complex and we will present how mutagenesis efforts were applied to obtain crystals. We will also present the final piece of the puzzle, the structure of Vgb from *Staphylococcus aureus* in complex with Mg<sup>2+</sup> and a Group B streptogramin substrate and propose a novel catalytic mechanism for the C-O intramolecular lyase.

**MP028 Structure of a Heparin-dependent Complex of Hedgehog and Ihog.** Jason S. McLellan<sup>1</sup>, Shenqin Yao<sup>1,2</sup>, Xiaoyan Zheng<sup>1,2</sup>, Brian V. Geisbrecht<sup>1</sup>, Rodolfo Ghirlando<sup>3</sup>, Philip A. Beachy<sup>1,2</sup>, Daniel J. Leahy<sup>1</sup>, <sup>1</sup>Johns Hopkins Univ. School of Medicine, Baltimore, MD, <sup>2</sup>Howard Hughes Medical Inst., <sup>3</sup>Lab. of Molecular Biology, National Inst. of Diabetes and Digestive and Kidney Diseases, National Inst. of Health, Bethesda, MD.

Hedgehog (Hh) signaling molecules mediate key tissue patterning events during animal development, and inappropriate activation of Hh signaling in adults has been associated with human cancers. Recently, a conserved family of Type I integral membrane proteins

required for normal response to the Hh signal was discovered. One member of this family, Ihog (interference hedgehog), functions upstream or at the level of Patched (Ptc), but how Ihog participates in Hh signaling remains unclear. Here we show that heparin binding induces Ihog dimerization and is required to mediate high affinity interactions between Ihog and Hh. We also present crystal structures of a Hh-binding fragment of Ihog both alone and complexed with Hh. Heparin is not well-ordered in these structures, but a basic cleft in the first FNIII domain of Ihog (IhogFn1) is shown by mutagenesis to mediate heparin binding. These results establish that Hh directly binds Ihog and provide the first demonstration of a specific role for heparin in Hh responsiveness.

**MP029 Crystal Structure of Methyltransferase that Modifies P-site Guanine 966 of the 16S rRNA.** J. Osipiuk<sup>1</sup>, D.V. Lesnyak<sup>2</sup>, T. Skarina<sup>3</sup>, P.V. Sergiev<sup>2</sup>, A.A. Bogdanov<sup>2</sup>, A. Edwards<sup>3</sup>, A. Savchenko<sup>3</sup>, O.A. Dontsova<sup>2</sup>, A. Joachimiak<sup>1</sup>, <sup>1</sup>Biosciences Div., Midwest Center for Structural Genomics and Structural Biology Center, Argonne National Lab., Argonne, IL, <sup>2</sup>Dept. of Chemistry and A.N. Belozersky Inst. of Physico-Chemical Biology, Moscow State Univ., Moscow, Russia, <sup>3</sup>Univ. of Toronto, Structural Genomics Consortium, Toronto, Canada.

The crystal structure of *Escherichia coli* predicted methyltransferase, coded by yhhF gene, was determined from 2.05 Å diffraction data by single wavelength anomalous dispersion (SAD) method. The protein with 198 residues crystallizes in space group C2 with cell dimensions of a = 70.504 Å, b = 96.912 Å, c = 193.961 Å  $\alpha = \gamma = 90^\circ$ ,  $\beta = 92.21^\circ$ .

We found yhhF to be a gene encoding for m2G966 specific 16S rRNA methyltransferase. Disruption of yhhF gene by kanamycin resistance marker leads to a loss of modification at G966. The modification could be rescued by expression of recombinant protein from the plasmid carrying yhhF gene. Moreover, purified m2G966 methyltransferase, in the presence of S-adenosylmethionine (SAM), is able to methylate 30S ribosomal subunits that were purified from yhhF knockout strain in vitro. The methylation is specific for G966 base of the 16S rRNA.

The structure of m2G966 methyltransferase closely resembles another rRNA methyltransferase, m2G1207 RsmC. Structural comparisons and analysis of the enzyme active site suggest modes for binding SAM and rRNA to m2G966 methyltransferase. A model for interaction of RsmD with ribosome has been proposed.

This work was supported by National Institutes of Health Grant GM074942 and by the U.S. Department of Energy, Office of Biological and Environmental Research, under contract DE-AC02-06CH11357.

**MP030 Crystallization and Preliminary X-ray Analysis of the GST –  $\alpha$ -Synuclein Fusion Protein.** Beena Narayanan, Daniel Hennessy, Ruth G. Perez<sup>1</sup>, John Rosenberg, Dept. of Biological Sciences, <sup>1</sup>Dept. of Neurology, Univ. of Pittsburgh, Pittsburgh, PA.

$\alpha$ -Synuclein is a 140-amino acid protein that is enriched in neurons. It is believed to play a role in protein trafficking; and deposits of  $\alpha$ -synuclein accumulate in several neurodegenerative diseases known as synucleinopathies (e.g. in Lewy bodies in Parkinson's disease). A central role of  $\alpha$ -synuclein in neurodegeneration was demonstrated by the discovery of missense mutations and duplications or triplications in hereditary forms of Parkinson's disease. The specific mechanism by which  $\alpha$ -synuclein contributes to disease is unclear for multiple reasons, including a lack of knowledge about the protein's structure. The latter is particularly challenging because  $\alpha$ -synuclein is an intrinsically unfolded protein, meaning it is unstructured in iso-

lation and only folds into a stable structure in association with a suitable molecular partner. We report here the crystal structure of the glutathione-S-transferase (GST)- $\alpha$ -synuclein fusion protein, which was expressed in *E. coli*, purified to homogeneity and crystallized using vapor-diffusion technique. The crystals belong to the monoclinic space group  $P2_1$ , with unit-cell parameters  $a=57.88\text{\AA}$ ,  $b=94.09\text{\AA}$ ,  $c=94.19\text{\AA}$ ,  $\alpha=90.0^\circ$ ,  $\beta=89.91^\circ$ ,  $\gamma=90.0^\circ$  and diffracts to  $2.1\text{\AA}$  resolution. Assuming the presence of two molecules in the asymmetric unit, the Matthews coefficient ( $V_M$ ) of approximately  $3.0\text{\AA}^3 \text{Da}^{-1}$ , corresponding to a solvent content of about 58%. Structure determination proceeded by Molecular Replacement using the structure of GST as the probe followed by Fourier synthesis to reveal the  $\alpha$ -synuclein component. A detailed structure description will be presented.

**SP031 Functional Diversity from a Simple Protein Fold.** Y.Z. Guo, B.A. Robertson, W.H. Johnson<sup>†</sup>, C.P. Whitman<sup>†</sup>, M.L. Hackert, Dept. of Chemistry and Biochemistry, <sup>†</sup>College of Pharmacy, The Univ. of TX, Austin, TX.

The tautomerase superfamily is represented by 4-Oxalocrotonate tautomerase (4-OT), 5-(carboxymethyl)-2-hydroxyruconate isomerase (CHMI), and macrophage migration inhibitory factor (MIF). 4-OT and many other proteins in this family are hexameric, while other members are trimeric or dimeric. However, all members of this enzyme superfamily share a simple folding unit represented by the 4-OT monomer that is remarkable for its small size (62 a.a.) and simple ( $\beta$ - $\alpha$ - $\beta$ ) fold. Some subunits, like those of CHMI and MIF, are nearly twice as large as the 4-OT subunit and probably arose by gene duplication. Members of this superfamily also share a key mechanistic feature - an active site amino-terminal proline, which sometimes has an unusually low  $pK_a$ , as the general base in keto-enol tautomerization.

Several members of the 4-OT family have been identified and representative structures determined, although the function of many of these proteins still remains unknown. Within the superfamily, dehalogenase and decarboxylase activities are now known in addition to the tautomerase, isomerase and MIF activities noted previously. The functional diversity in the 4-OT superfamily suggests that nature used these short sequences as building blocks to create new structures and activities.

CgX, an unknown gene product from the soil bacterium *Corynebacterium g.*, has been identified as a member of the 4-OT family with multiple activities found in CaaD, Cis-Caad, MSAD, PPT. To understand the structural basis of its multiple activities, crystal structures of both native and inhibitor protein complexes have been determined. A summary of these results will be presented.

This work is supported by a grant from The Welch Foundation (F 1219).

**MP032 The Structure of an N-acetyl- $\beta$ -D-glucosaminidase from *Streptococcus gordonii*.** David B. Langley<sup>1</sup>, Derek W.S. Harty<sup>2</sup>, Jill Trehwella<sup>1</sup>, J. Mitchell Guss<sup>1</sup>, Charles Collyer<sup>1</sup>, <sup>1</sup>School of Molecular and Microbial Biosciences, Sydney Univ., Australia, <sup>2</sup>Inst. of Dental Research, Millennium Inst., Westmead Centre for Oral Health, Westmead, Australia.

*Streptococcus gordonii* is a primary coloniser of the oral cavity and contributes to the maintenance of a healthy oral microflora. However, should it gain access to the bloodstream it can also colonise damaged heart valve tissue resulting in infective endocarditis which in spite of antibiotic therapy is still often fatal. Survival and growth of the bacterium on the endocardium is believed to be facilitated by the production of numerous glycosidases which may degrade the glycan moiety of mammalian glycoproteins. A screen for such activity led

to the cloning of an N-acetyl- $\beta$ -D-glucosaminidase (GCNA), from this organism.

Se-methionine GCNA was crystallized and the structure solved by the MAD method. The protein crystallizes as a dimer and has a canonical TIM-barrel fold. Two crystal forms of the enzyme have been refined. Only one of these has the putative catalytic residues orientated towards what is postulated to be the active site pocket, suggesting that dynamic substrate capture might be a feature of catalysis. The catalytic mechanism of this "family 20" glycosidase, whereby the substrate rather than the enzyme provides the cleavage-inducing nucleophile, has been confirmed by co-crystallizing the protein with a putative reaction intermediate analogue. A mercury-soaked crystal reveals how the enzyme is poisoned by this and other heavy atoms.

**MP033 Crystal Structure of Adenosine Kinase from *M. tuberculosis* and Structural Basis for Specific Activation of Antimicrobial Nucleoside Analogs.** R. Li, Y. Wang, Z. Qu, V. Escuyer, J.A. Maddy, W.B. Parker, Southern Research Inst., Birmingham, AL.

Adenosine kinase (AK) is a key enzyme in the purine salvage pathway of *Mycobacterium tuberculosis*, an intracellular pathogen that causes tuberculosis (TB). *Mtb* AK, a unique bacterial adenosine kinase catalyzes the phosphorylation of adenosine to adenosine monophosphate and is involved in the bioactivation of some nucleoside analogs that have demonstrated selective activity against *M. tuberculosis*. The mechanism of action of these adenosine analogs is likely to be different from those of current TB treatments; therefore, specific activation of nucleoside analogs by *Mtb* AK may prove to be a novel therapeutic intervention for TB, particularly for multi-drug resistant TB. Specific inhibition of this key enzyme in the purine salvage pathway may also be exploited for therapeutic development. The crystal structure of the enzyme in complex with adenosine or 2-methyladenosine has been determined at  $1.9\text{-\AA}$  resolution with  $R$  factor of 0.19 and  $R_{\text{free}}$  of 0.25. The structure reveals a tightly associated homo-dimer, which is different from the known human and *T. gondii* AK, but rather resembles the structure of ribokinases. The monomer consists of a small domain that is responsible for the dimer formation and a large catalytic domain. The active sites reveal the protein-ligand interaction and significant structural differences between the human and *Mtb* AK. The structural information provides the structural basis for the specific activation of nucleoside analogs by *Mtb* AK and should aid in the design of more potent and selective antimycobacterial agents.

We thank SBC-CAT and NE-CAT at APS for access to beam lines 19-BM and 8-BM. This research is supported in part by two NIH grants, AI55344 to RL and AI43241 to WBP.

**MP034 Crystal Structure of Bovine Lipoyltransferase with Lipoyl-AMP.** Makoto Matsuda<sup>1</sup>, Kazuko Fujiwara<sup>2</sup>, Harumi Hosaka<sup>1</sup>, Kazuko Okamura-Ikeda<sup>2</sup>, Yutaro Motokawa<sup>2</sup>, Mamoru Suzuki, Hisaaki Taniguchi<sup>2</sup>, Atsushi Nakagawa<sup>1</sup>, <sup>1</sup>Inst. for Protein Research, Osaka Univ., Osaka, Japan, <sup>2</sup>Inst. for Enzyme Research, The Univ. of Tokushima, Tokushima, Japan.

Lipoic acid is an essential cofactor of the  $\alpha$ -ketoacid dehydrogenase complexes and the glycine cleavage system. It is covalently attached to a specific lysine residue. The bovine lipoyltransferase (bLT) catalyzes lipoic acid attachment reaction using lipoyl-AMP as a substrate, forming a lipoylated protein and AMP. Crystal of bLT was obtained by hanging drop vapor diffusion method using PEG6000 as precipitant. Diffraction data were collected at BL44XU of SPring-8 (Hyogo, Japan) and NW12 of PF-AR (Inbaraki, Japan). The crystal belonged to space group of  $P3_121$  with its cell dimensions of

$a=b=81.44$  Å,  $c=120.53$  Å. Initial structure of bLT was solved by the single-wavelength anomalous diffraction (SAD) method at 2.85 Å resolution using Hg derivative, then the structure was refined at 2.1 Å using native data. The final  $R$ -factor and  $R_{\text{free}}$ -factor are 0.219 and 0.263, respectively. The structure of bLT consisted of two domains (N-terminal and C-terminal domains), and endogenous Lipoyl-AMP is bound to the active site in the N-terminal domain, adopting a U-shaped conformation. The lipoyl-AMP is tightly bound to the deep pocket of bLT, but the C10 atom of the lipoyl-AMP in bLT was exposed to the surface of bLT, and the C10 atom of the lipoyl-AMP can directly be accessed from the outside of the molecule. Thus, the lipoyl-AMP bound form of bLT is ready for lipoylation of the partners, such as H-protein in the glycine cleavage system.

**SP035 Structure of the Conserved Transcriptional Repressor erh (Enhancer of Rudimentary Homolog).** Cheng Wan, Wolfram Tempel, James Liu, Bi-Cheng Wang, Robert B. Rose, Biochemistry Dept., North Carolina State Univ., Raleigh, NC.

Erh (Enhancer of Rudimentary Homolog) is a ubiquitously expressed transcription co-regulator that is highly conserved among eukaryotes, from humans to plants to protozoa. Functions attributed to erh include enhancement of pyrimidine biosynthesis, a role in cell cycle regulation, and repression of the cell-specific transcription factor HNF-1 (Hepatocyte Nuclear Factor-1) through binding the coactivator DCoH (Dimerization Cofactor of HNF1). No homologous sequences have been identified and little is known about the interactions of erh. We report the 2.0 Å crystal structure of erh. The erh structure is a novel alpha+beta fold consisting of a four-stranded anti-parallel beta sheet with 3 amphipathic alpha helices situated on one face of the beta sheet. Structure-based searches of the protein data base, like sequence based searches, failed to identify evolutionarily-related homologs. We present structural and biochemical evidence that erh functions as a dimer. The dimer interface consists of an 8-stranded anti-parallel beta barrel. Many of the surface residues of erh are conserved, including patches of hydrophobic and charged residues, suggesting protein-protein interaction interfaces. Two putative CKII phosphorylation sites are highly ordered in the structure, and may disrupt dimerization and protein-protein interactions, based on the distribution of surface charge.

**SP036 Crystal Structure of the Human Prostacyclin Synthase.** Chia-Wang Chiang<sup>1</sup>, Hui-Chun Yeh<sup>2</sup>, Lee-Ho Wang<sup>2\*</sup>, Nei-Li Chan<sup>1\*</sup>, <sup>1</sup>Inst. of Biochemistry, College of Life Sciences, National Chung Hsing Univ., Taichung City, Taiwan, <sup>2</sup>Div. of Hematology, Dept. of Internal Medicine, Univ. of Texas Health Science Center at Houston, Houston, TX.

Prostacyclin synthase (PGIS) catalyzes an isomerization of prostaglandin H<sub>2</sub> to prostacyclin, a potent mediator of vasodilation and anti-platelet aggregation. Here we report the crystal structure of human PGIS at 2.15 Å resolution, which represents the first three-dimensional structure of a Class III cytochrome P450. While notable sequence divergence has been recognized between PGIS and other P450s, PGIS exhibits the typical triangular prism-shaped P450 fold with only moderate structural differences. The conserved acid-alcohol pair in the I helix of P450s is replaced by residues G286 and N287 in PGIS, but the distinctive disruption of I helix and the presence of a nearby water channel remain conserved. The side chain of N287 appears to be positioned to facilitate the peroxide bond cleavage, suggesting a functional conservation of this residue in activating oxygen. A combination of bent I helix and tilted B' helix creates a channel extending from the heme distal pocket, which seemingly allows binding of various ligands; however, residue W282, placed in

this channel at a distance of 8.4 Å from the iron with its indole side chain lying parallel to the porphyrin plane, may serve as a threshold to exclude most ligands from binding. Although the primary sequence of the PGIS cysteine ligand loop diverges significantly from consensus, conserved tertiary structure and hydrogen bonding pattern are observed for this region.

**SP037 Crystal Structure of Enoyl-ACP Reductase from *F. tularensis*.** Y. Wang<sup>1</sup>, T. Wang<sup>1</sup>, Marianne Cuff<sup>2</sup>, V. Escuyer<sup>1</sup>, R. Li<sup>1</sup>, <sup>1</sup>Southern Research Inst., Birmingham, AL, <sup>2</sup>Structural Biology Center, Argonne National Lab., Argonne, IL.

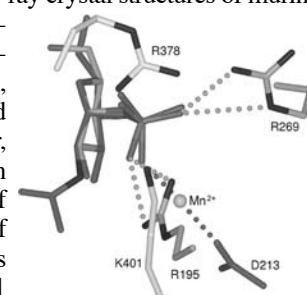
*Francisella tularensis*, a facultative intracellular bacterial pathogen causing tularemia, is considered as a major biological warfare agent, mainly because it is very infectious and can cause life threatening illness in humans that has a high mortality rate without treatment. Treatment of human tularemia relies upon antibiotic therapies but relapse is frequent. Therefore, there is a crucial need for new treatments against tularemia, especially in a biological warfare setting. Enoyl-acyl carrier protein reductase from *F. tularensis*, the *fabI*-gene product (*Ft* FabI), is a key enzyme of a type-II pathway in the fatty acid synthesis that is absent in human, and is a validated antimicrobial drug target. We report here the crystal structure of *Ft* FabI in complex with NADH and triclosan, a potent inhibitor of the enzyme. The structure was solved at 2.0-Å resolution with  $R$  factor of 0.19 and  $R_{\text{free}}$  of 0.24, and revealed a 222-tetramer in the asymmetric unit of the protein crystal in space group  $P2_12_12_1$  and with cell dimensions  $a=71.2$ ,  $b=113.2$  and  $c=126.0$  Å. The tetramer is formed through intermolecular helical bundle interaction and extended  $\beta$ -sheet interaction. The refined structure of the complex revealed the binding site of NADH and triclosan. The active site conformation is highly conserved compared with that of *E. coli* FabI; however, several residues on the surface close to the active site may contribute to the low inhibition activity of triclosan to the *Ft* FabI.



We thank SBC-CAT at APS for access to beam line 19-BM.

**SP038 X-ray Crystal Structure Determination of the Mammalian Glycosyltransferase C2GnT-L.** John E. Pak, Pascal Arnoux, Sihong Zhou, Prashanth Sivarajah, Malathy Satkunarajah, Xuekun Xing, James M. Rini, Dept. of Molecular and Medical Genetics, Univ. of Toronto, Toronto, ON, Canada.

Leukocyte type core 2  $\beta$ 1,6-*N*-acetylglucosaminyltransferase (C2GnT-L) is a key enzyme in the biosynthesis of branched O-glycans. It is a type II Golgi resident membrane protein which catalyzes the formation of the core 2 O-glycan (Gal $\beta$ 1-3[GlcNAc $\beta$ 1-6]GalNAc-*O*-Ser/Thr) from its donor and acceptor substrates UDP-GlcNAc and the core 1 O-glycan (Gal $\beta$ 1-3GalNAc-*O*-Ser/Thr), respectively. Reported here are the x-ray crystal structures of murine C2GnT-L in the absence and presence of the acceptor substrate Gal $\beta$ 1-3GalNAc at 2.0 and 2.7 Å resolution, respectively. C2GnT-L was found to possess the GT-A fold; however, it lacks the characteristic metal ion binding DXD motif. Comparison of the C2GnT-L structure with that of other GT-A fold glycosyltransferases suggests that Arg-378 and Lys-401



serve to electrostatically stabilize the nucleoside diphosphate leaving group, a role normally played by metal ion in GT-A structures. The use of basic amino acid side chains in this way is strikingly similar to that seen in a number of metal ion-independent GT-B fold glycosyltransferases and suggests a convergence of catalytic mechanism shared by both GT-A and GT-B fold glycosyltransferases.

**SP039 Structure to Function Correlations for Adeno-associated Virus Serotype 1.** L. Govindasamy<sup>1</sup>, E.B. Miller<sup>1</sup>, B. Gurda-Whitaker<sup>1</sup>, R. McKenna<sup>1</sup>, S. Zolotukhin<sup>2</sup>, N. Muzyczka<sup>3</sup>, M. Agbandje-McKenna<sup>1</sup>, <sup>1</sup>Dept. of Biochemistry and Molecular Biology, <sup>2</sup>Dept. of Pediatrics, <sup>3</sup>Dept. of Molecular Genetics and Microbiology, College of Medicine, Univ. of Florida, Gainesville, FL.

Adeno-associated viruses (AAVs) are small, nonpathogenic viruses belonging to the *Dependovirus* genus of the *Parvoviridae* family. They have a non-enveloped T=1 icosahedral capsid of ~260 Å in diameter that encapsidate a ssDNA genome of 4.7 kb. These viruses are being extensively researched as a potential vector for gene therapy due to their ability to package and deliver foreign genes into a variety of tissues and organs. The different serotypes that have been identified exhibit dramatic differences in cell tropism and *in vivo* tissue transduction dictated by capsid viral protein (VP) amino acid differences. For example, AAV1 is able to transduce muscle cells much more efficiently than AAV2 and several of the other serotypes. The sequence identity between AAV serotypes are high, with variations distributed in their overlapping VP likely playing a role in the recognition of different cell-surface binding receptors (heparin sulfate, sialic acid etc). For example, AAV2 utilizes heparin sulfate as a primary receptor for cellular transduction, while AAV1 infection is facilitated by binding to terminal sialic acid. To identify the structural features of AAV1 responsible its cell tropism and transduction phenotype, we have determined its capsid structure by X-ray crystallography. A comparison of this structure to that available for AAV2 (Xie *et al.*, PNAS 2002), plus our crystal structures of AAV4 (Govindasamy *et al.*, JV 2006), AAV5 and AAV8 (our unpublished data) clearly shows structural variations in capsid surface loops that have been identified by mutagenesis and biochemical assays as being important for AAV receptor binding, transduction efficiency and antibody recognition. The AAV1 structure determination and comparative analysis will be presented.

**MP040 Structural Studies of the NKX2.5 Homeoprotein.** H.-J. Nam<sup>1</sup>, P. Scone<sup>1</sup>, H. Kasahara<sup>2</sup>, <sup>1</sup>Depts. of Biochemistry and Molecular Biology, <sup>2</sup>Dept. of Physiology and Functional Genomics, Univ. of Florida Gainesville, FL.

Congenital heart disease is a leading non-infectious cause of mortality in newborns. The causes of congenital heart diseases are not clear, however genetic and environmental factors have been implicated. Heart development is a complex process requiring sequential and timely events from early developmental stages to birth, presumably through expression of specific proteins at a specific amount in a specific heart region, most likely regulated by cardiac transcription factors. Indeed, recent genetic analyses revealed that mutations in cardiac transcription factors, such as homeoprotein NKX2.5 cause congenital heart disease. To elucidate the molecular basis for the pathological mechanisms of the NKX2.5 mutations, structural studies of the NKX2.5 protein using X-ray crystallography are in progress. Here we report the purification, crystallization and preliminary X-ray crystallographic analyses of the NKX 2.5 homeodomain (HD) and the NKX2.5 protein including the homeodomain and the N-terminal regulatory domain (ND-HD) in complex with specific DNA elements. The HD and DNA complex crystals diffract X-rays

to 3.5 Å resolution, and belong to the space group  $P2_12_12_1$ , with unit cell parameters  $a = 36$ ,  $b=65$ ,  $c =136$  Å. Based on the volume calculation, one set of dimeric NKX2.5 homeodomain and a double-stranded DNA complex is expected in an asymmetric unit with a solvent content of 52%. The crystals of ND-HD and DNA complex belong to the P1 space group with unit cell dimensions of  $a = 60$ ,  $b=49$ ,  $c=68$  Å,  $\alpha=90^\circ$ ,  $\beta=105^\circ$ ,  $\gamma=90^\circ$ . One set of dimeric protein and double-stranded DNA complex is also expected in an asymmetric unit of the ND-HD and DNA complex crystals.

This research is supported by American Heart Association award #0535161B.

**SP041 The Structure and Function of the Prephenate Dehydratase from *Staphylococcus aureus*.** Kemin Tan, Hui Li, Rongguang Zhang, Minyi Gu, Andrzej Joachimiak, Midwest Center for Structural Genomics and Structural Biology Center, Biosciences Div., Argonne National Lab., Argonne, IL.

The enzyme prephenate dehydratase (PDT) catalyzes the conversion of prephenate to phenylpyruvate in the biosynthesis of L-Phe in bacteria, archaea and plants. PDT is allosterically regulated by L-Phe and other aromatic amino acids. The crystal structure of *Staphylococcus aureus* PDT (Sa-PDT) reveals an intervened catalytic PDT domain and a closely associated regulatory ACT domain. A cleft between two PDT subdomains is proposed to be the PDT catalytic site where highly conserved catalytic residues (including T168 R169 F170) are located. Functional Sa-PDT forms a tetramer, a dimer-of-dimer in the crystal and in solution. Two symmetry-related catalytic clefts of a PDT dimer are aligned to form an extended active site. The ACT dimer in an open conformation also forms a pocket that is

**Table 1: Peptide residues, and the revised alignment of Gag.**

peptide	sequence
HIV-1 p6 <sup>Gag</sup> A	<sup>32</sup> DKELYPLASLRSLFG <sub>46</sub>
HIV-1 p6 <sup>Gag</sup> T	<sup>32</sup> DKELYPLTSLRSLFG <sub>46</sub>
EIAV p9 <sup>Gag</sup>	<sup>19</sup> TQONLYPD---LSEIKK <sub>31</sub>

largely hydrophobic at the ACT dimer interface and between ACT and PDT domains. Most of the residues associated with the pocket are highly conserved and has been shown to influence L-Phe binding. This pocket is proposed to be the L-Phe regulatory binding site. Sa-PDT is the first crystal structure of PDT that provides a prototypic architecture for the structural and functional exploration of members of the enzyme family.

This work was supported by National Institutes of Health Grant GM074942 and by the U.S. Department of Energy, Office of Biological and Environmental Research, under contract DE-AC02-06CH11357.

**SP042 YPxL Motif with ALIX.** Qianting Zhai, Rob Fisher, Dept. of Biochemistry, Univ. of Utah, Salt Lake City, UT.

HIV hijacks cellular machinery, such as multi-vesicular bodies (MVBs), to bud from cells. The MVB pathway is composed of three protein complexes--ESCRT-I, ESCRT-II and ESCRT-III (Endosomal Sorting Complex Required for Transport). Gag protein from HIV and other viruses is required for virus budding and for recruiting host cellular factors through its late domains, such as PTAP motif and YPxL motif. In some other viruses, like EIAV, only YPxL exists. ALG-2-interacting Protein X (ALIX), which was shown to bind ESCRT-I and ESCRT-III. Interaction between YPxL and ALIX is required for virus release, in the absence of PTAP motif.

ALIX is composed of an N-terminal Bro1 domain, a central helical "V" domain and a C-terminal praline-rich region (PRR). Our study focuses on the structure of ALIX and how YPxL motifs interact with

ALIX to facilitate virus budding.

We crystallized the HIV-1 p6<sup>Gag</sup>A, HIV-1 p6<sup>Gag</sup>T and EIAV p9<sup>Gag</sup> peptides individually with ALIX<sub>Bro1-V</sub> (containing Bro1 and “V” domain with K268Y, K269Y mutations, residues 1-698), in addition to the apo structure. There is no large scale conformational change. All three late domain peptides bind to a highly conserved hydrophobic groove on arm2 of the ALIX “V” domain. The side chain of Y36/Y23, the Y in the YPxL motif, sticks into the groove forming a hydrogen bond with the conserved D506 from the bottom of the hydrophobic pocket. It provides the specificity for ALIX by the Gag protein. The two HIV-1 p6<sup>Gag</sup> peptides are closely superimposable throughout, but the HIV-1 p6<sup>Gag</sup> and EIAV p9<sup>Gag</sup> peptide conformation and interactions are different for residues following the LYP tripeptide. Therefore, we revised sequence alignment of the p6<sup>Gag</sup> and p9<sup>Gag</sup> YPxL motif based on the structure.

#### Reference:

Robert D. Fisher, Hyo-Young Chung, Qianting Zhai, Howard Robinson, Wesley I. Sundquist, and Christopher P. Hill. Structural and Biochemical Studies of ALIX/AIP1 and its Role in Retrovirus Budding. *Cell* (in press).

**MP043 Structure of EF0647 from *Enterococcus faecalis*, a Putative HxlR Family Transcriptional Regulator.** Y. Kim, R. Wu, J. Osipiuk, S. Moy, A. Joachimiak, Structural Biology Center and Midwest Center for Structural Genomics, Biosciences, Argonne National Lab., Argonne, IL.

The crystal structure of the putative transcriptional regulator EF0647 of the HxlR-like helix-turn-helix protein from *E. faecalis* V583 has been determined to 2.2 Å. The HxlR-type HTH domain, named after *Bacillus subtilis* HxlR, is a domain of ~90-100 amino acids in many putative transcription regulators with a winged helix-turn-helix (wHTH) structure found in eubacteria as well as in archaea. The sequence and structure of hxlR-type proteins are similar to those of the wHTH-containing protein family MarR. The three dimensional structure of EF0647 is compared with structures of a number of HxlR and MarR family proteins and analyzed in detail.

This work was supported by the grants from the NIH (GM62414 and GM074942) and the U.S. Department of Energy, OBER under Contract W-31-109-ENG-38.

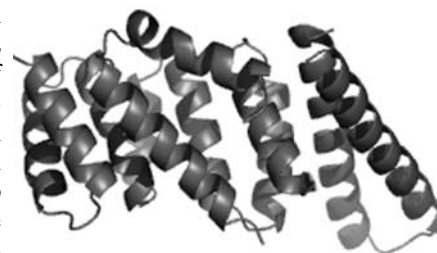
**MP044 Structural and Transcriptional Analyses of a Purine Nucleotide-Binding Protein from *Pyrococcus furiosus*.** M. Gary Newton<sup>1</sup>, Brian Gerwe<sup>1</sup>, Laura-Lee Clancy Kelley<sup>1</sup>, Bret D. Dillard<sup>1</sup>, Thomas Lai<sup>1</sup>, Zhi-Jie Liu<sup>1</sup>, Wolfram Tempel<sup>1</sup>, Lirong Chen<sup>1</sup>, Jeff Habel<sup>1</sup>, Doowon Lee<sup>1</sup>, Francis E. Jenney Jr.<sup>1</sup>, Frank J. Sugar<sup>1</sup>, Jane S. Richardson<sup>2</sup>, David C. Richardson<sup>2</sup>, Bi-Cheng Wang<sup>1</sup>, Michael W.W. Adams<sup>1</sup>, John P. Rose<sup>1</sup>, <sup>1</sup>Southeast Collaboratory for Structural Genomics (SECSG), Dept. of Biochemistry and Molecular Biology, Univ. of Georgia, Athens, GA, <sup>2</sup>Dept. of Biochemistry, Duke Univ., Durham, NC.

The open-reading frame PF0895 in the genome of the hyperthermophile, *Pyrococcus furiosus*, encodes a 206-residue protein. The structure of the recombinant protein was solved by single isomorphous replacement with anomalous scattering (SIRAS) using a mercury derivative. It has been refined to 1.70 Å with a crystallographic R<sub>f</sub> of 19.7%. The PF0895 structure is similar to the ATP binding cassettes observed in the ABC transporter family. However, bioinformatics and molecular analyses indicate that PF0895 is not part of the expected five-gene operon that encodes a typical prokaryotic solute-binding ABC transporter. Rather, transcriptional profiling data show that PF0895 is part of a novel four-gene operon (PF0895-PF0896-PF0897-PF0897.1) where only PF0895 has homologs in other organisms. From the structural studies it can be concluded that one of the subunits of this novel membrane complex, PF0895 likely binds

a purine nucleotide. PF0895 is therefore predicted to be part of a membrane-bound multiprotein complex unrelated to ABC transporters that is so far unique to *P. furiosus*. It may play a role in the stress response, as its expression is down-regulated when the organism is subjected to cold-shock, where cells are transferred from 95° C, near the optimal growth temperature, to 72° C, near the minimal growth temperature.

**SP045 Structural Characterization of a Type III Secretion System Needle Protein YscF in Complex with its Chaperones YscE/YscG.** Ping Sun, Brian P. Austin, Joseph E. Tropea, David S. Waugh, Macromolecular Crystallography Lab., Center for Cancer Research, National Cancer Inst. at Frederick, Frederick, MD.

*Yersinia pestis*, the plague-causing Gram-negative bacterium, utilizes a Type III Secretion System to deliver effector proteins into eukaryotic host cells, where they interfere with signal transduction pathways that mediate phagocytosis and the inflammatory response. Effector proteins are injected through a hollow needle structure composed of the protein YscF. YscG and YscE are “chaperones” of YscF that prevent premature polymerization of YscF in the cytosol of the bacterium prior to assembly of the needle structure. Here, we report the crystal structure of the YscE-YscF-YscG protein complex at 1.8 Å resolution. Unexpectedly, the structure reveals that YscG is a member of the tetratricopeptide repeat family of proteins. Together with YscE, YscG binds tightly to YscF, thereby maintaining it in a monomeric conformation.



**SP046 Crystal Structure of Vestitone Reductase from Alfalfa (*Medicago sativa* L.)** Hui Shao, Richard A. Dixon, Xiaoqiang Wang, Plant Biology Div., Samuel Roberts Noble Foundation, Ardmore, OK, hshao@noble.org.

Isoflavonoids are commonly found in leguminous plants, where they play important roles in plant defense and also have significant health benefits for animals and humans. Medicago sativa is the major antimicrobial isoflavonoid phytoalexin in alfalfa (*Medicago sativa*) responding to fungal pathogen attack. Vestitone reductase (VR) is the central enzyme in a branch pathway for the conversion of non-enantiomeric isoflavones to enantiomeric pterocarpans, and is specifically involved in the biosynthesis of medicarpin in alfalfa. Vestitone reductase catalyzes the NADPH-dependent reduction of the 2-hydroxyisoflavanone (3R)-vestitone to 7,2'-dihydroxy-4'-methoxy-isoflavanol, which is further converted to medicarpin by 7,2'-dihydroxy-4'-methoxy-isoflavanol dehydratase. VR is highly stereochemically specific, and only recognizes the 3R conformation of vestitone, not (3S)-vestitone.

The crystal structure of alfalfa (*Medicago sativa* L.) vestitone reductase has been determined at 1.4 Å resolution using the MAD method. The structure contains a classic Rossmann fold domain in the N-terminus and a small C-terminal domain. Sequence and structural analysis showed that vestitone reductase is a member of the short-chain dehydrogenase/reductase (SDR) superfamily despite the low sequence identities and the prominent structural differences from other SDR enzymes with known structures. The putative binding sites for the co-factor NADPH and the substrate (3R)-vestitone were defined and located in a large cleft formed between the N- and C-terminal domains of enzyme. Potential key residues for enzyme

activity were also identified, including the catalytic triad Ser129-Tyr164-Lys168. A molecular docking study showed that (3*R*)-vestitone, but not the (3*S*) isomer, forms favored interactions with the co-factor and catalytic triad, thus providing an explanation for the enzyme's strict substrate stereo-specificity.

**SP047 Structural Basis for Stem Cell Factor-KIT Signaling and Activation of Class III Receptor Tyrosine Kinases.** He X, Liu H, Chen X, Focia PJ, Dept. of Molecular Pharmacology and Biological Chemistry, Northwestern Univ. Feinberg School of Medicine, Chicago, IL.

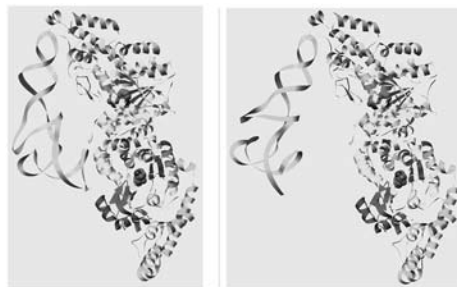
Stem cell factor (SCF) binds to and activates the KIT receptor, a class III receptor tyrosine kinase (RTK), to stimulate diverse processes including melanogenesis, gametogenesis and hematopoiesis. Dysregulation of SCF-KIT signaling and gain-of-function KIT mutations contribute to the genesis of many cancers. Here we reported a 2.5 Å crystal structure of the functional core of SCF bound to the extracellular ligand-binding domains of KIT. The structure reveals a 'wrapping' SCF-recognition mode by KIT, in which KIT adopts a bent conformation to facilitate each of its first three immunoglobulin (Ig)-like domains to interact with SCF. Three surface epitopes on SCF, an extended loop, the B and C helices, and the N-terminal segment, contact distinct KIT domains, with two of the epitopes undergoing large conformational changes upon receptor binding. In the architecture of the 2:2 SCF/KIT complex, SCF remains the head-to-head dimerization mode as in its free state, while two KIT molecules are tethered together entirely through SCF dimerization. Each KIT interacts with only one SCF, and no KIT-to-KIT interaction is observed. The SCF/KIT complex reveals a unique RTK dimerization assembly, and a novel recognition mode between four-helix bundle cytokines and Ig-family receptors. As the first complex structure in the field of the class III RTKs, it also serves as a framework for understanding the activation mechanisms of this class of receptors.

**MP048 Functional Structure of the Periplasmic Component of Bacterial Multidrug Efflux Transporter.** Shunfu Piao, Seulki Kim, Yongbin Xu, Nam-Chul Ha, College of Pharmacy, Pusan National Univ., Jangjeon Dong, Geumjeong Gu, Busan, Korea.

Periplasmic membrane fusion proteins (MFPs) are an essential components of the type I protein secretion system and drug efflux pump in Gram-negative bacteria. They play a crucial role in bridging between the outer membrane porin and innermembrane transporter proteins. Although two crystal structures were reported revealing that MFP consists of  $\alpha$ -helical hairpin, lipoyl, and  $\beta$ -barrel domains, the functional form of MFP is not fully understood. MFP MacA is associated with the resistant to macrolides through MacA-MacB-TdeA efflux pump in *Actinobacillus Actinomycetemcomitans*. Here, we report the crystal structure of MacA from *A. actinomycetemcomitans*, in which MacA forms a hexameric oligomer with a central wide tunnel lined with the  $\alpha$ -helical hairpin domains. Furthermore, the crystal structure suggests a molecular mechanism on how MFPs connect between the other components.

**MP049 Two Conformations of a Crystalline Human tRNA Synthetase—tRNA Complex: Implications for Protein Synthesis.** Xiang-Lei Yang<sup>1</sup>, Francella J. Otero<sup>1</sup>, Karla L. Ewalt<sup>1</sup>, Jianming Liu<sup>1</sup>, Manal A. Swairjo<sup>1</sup>, Caroline Köhrer<sup>2</sup>, Uttam L. RajBhandary<sup>2</sup>, Robert J. Skene<sup>3</sup>, Duncan E. McRee<sup>3,4</sup>, Paul Schimmel<sup>1</sup>, <sup>1</sup>The Scripps Research Inst., La Jolla, CA, <sup>2</sup>Massachusetts Inst. of Technology, Dept. of Biology, Cambridge, MA, <sup>3</sup>Syrrx, Inc., San Diego, CA, <sup>4</sup>Current Address: ActiveSight, San Diego, CA.

Aminoacylation of tRNA is the first step of protein synthesis. Here we report the co-crystal structure of human tryptophanyl-tRNA synthetase and tRNA<sup>Trp</sup> at 2.8 Å resolution. This enzyme is reported to interact



directly with elongation factor 1 $\alpha$ , which carries charged tRNA to the ribosome. Crystals were generated from a 50%/50% mixture of charged and uncharged tRNA<sup>Trp</sup>. These crystals captured two conformations of the complex, which are nearly identical with respect to the protein and a bound tryptophan. They are distinguished by the way tRNA is bound. In one, uncharged tRNA is bound across the dimer, with anticodon and acceptor stem interacting with separate subunits. In this cross-dimer tRNA complex, the class I enzyme has a class II-like tRNA binding mode. This structure accounts for biochemical investigations of human TrpRS, including species-specific charging. In the other conformation, presumptive aminoacylated tRNA is bound only by the anticodon, the acceptor stem being free and having space to interact precisely with EF-1 $\alpha$ , suggesting that the product of aminoacylation can be directly handed off to EF-1 $\alpha$  for the next step of protein synthesis.

Data collection was performed at ALS, which is supported by the US Department of Energy under contract DE-AC03-76SF00098.

**SP050 Crystal Structure of the Tandemly Repeated PTP-like *myo*-inositol Hexaphosphatase (Phytase) Expressed by *Mitsuokella multacida*.** R.J. Gruninger<sup>1</sup>, L.B. Selinger<sup>2</sup>, S.C. Mosimann<sup>1</sup>, <sup>1</sup>Dept. of Chemistry and Biochemistry, <sup>2</sup>Dept. of Biological Sciences, Univ. of Lethbridge, Alberta, Canada.

Inositol phosphatases are involved in a variety of eukaryotic and prokaryotic cellular functions. Phytases are a phosphatase class that preferentially hydrolyzes *myo*-inositol hexakisphosphate (IP6) to lower phosphorylated *myo*-inositols. IP6 is the most abundant inositol phosphate in the cell and has been implicated in important cellular processes including DNA repair, mRNA export, cellular signaling, endocytosis and vesicular trafficking. The phytase expressed by *Mitsuokella multacida* (PhyAmm) is composed of tandemly repeated domains each possessing a PTP active site signature sequence. The N-terminal repeat is inactive despite the presence of all the catalytic residues. Full length PhyAmm (640 aa) crystallizes as a dimer in space group P2<sub>1</sub> with the cell dimensions a=73 b=74 c=160,  $\beta$ =94. MAD data was collected on a WO<sub>4</sub> soaked crystal at the W LIII edge on BL8.3.1 at the Advanced Light Source. SOLVE identified four heavy atom sites (FOM = 0.51) that were used to obtain phases. RE-SOLVE and ARP/wARP were used to trace the model. All of the protein was visible except for the first 40 N-terminal residues which are assumed to be disordered. The structure of the *M. multacida* PTP-like phytase has provided a rationale for the lack of activity in the N-terminal repeat and provides us with a further understanding of this unique class of phytase.

**SP051 Crystal Structure of KPC-2: Insights into Carbapenemase Activity in Class A  $\beta$ -lactamases.** W. Ke<sup>1</sup>, C.R. Bethel<sup>2</sup>, J.M. Thomson<sup>3</sup>, R.A. Bonomo<sup>2,3</sup>, F. van den Akker<sup>1</sup>, <sup>1</sup>Dept. of Biochemistry and Pharmacology, <sup>2</sup>Research Service, Louis Stokes Cleveland Veterans Affairs Medical Center, Cleveland, OH, <sup>3</sup>Case Western Reserve Univ., Cleveland, OH.

The emergence of KPC-type carbapenemases raises an additional threat to our antibiotic therapy because they represent the oncoming of the plasmid-encoded class-A carbapenemases. Their rapid spread in New York and other areas as well has alarmed health care officials. To understand the molecular basis of their carbapenemase activity, we reported the crystal structure of KPC-2 determined at 1.85 Å. The structure was solved by molecular replacement. Twinning was observed during refinement and detwinning operations were added resulting a final R/R<sub>free</sub> 14.9%/19.0%. Although KPC-2 structure shares the overall fold with normal Class-A beta-lactamases, it revealed a number of carbapenemase specific changes. These changes include an outward shift of the catalytic S70 residue so that the active sites of the carbapenemases are more shallow likely allowing easier access of the bulkier carbapenem substrates. Further space is likely provided by shifts in N132 and N170 in addition to concerted movements in the postulated carboxyl-binding pocket that might allow the substrates to bind in a slightly different angle to accommodate the carbapenem specific substituents. In addition, the concomitant shifts of N132 and other key residues likely facilitate efficient deacylation by avoiding getting trapped in long-lived intermediates as was observed for the non-carbapenemase TEM-1. The structure of KPC-2 thus provides key insights into the carbapenemase activity of emerging Class A β-lactamases.

**SP052 Structural Basis for Induction of Plant Disease Resistance in Flax By Flax Rust Avrulence Proteins.** Anderson C.I. Wang<sup>1</sup>, G. Guncar<sup>1,2</sup>, J.K. Forwood<sup>1,2</sup>, A.-M. Catanzariti<sup>3</sup>, J. Mackay<sup>4</sup>, J.G. Ellis<sup>3</sup>, P.N. Dodds<sup>3</sup>, B.n Kobe<sup>1,2</sup>, <sup>1</sup>School of Molecular and Microbial Sciences and <sup>2</sup>Inst. of Molecular Bioscience, Univ. of Queensland, <sup>3</sup>Div. of Plant Industry, Commonwealth Science and Industrial Research Org., Canberra, <sup>4</sup>School of Molecular and Microbial Sciences, Univ. of Sydney, NSW, Australia.

One of the major plant defense mechanisms against pathogens involves the recognition of avirulence (Avr) proteins, produced by pathogens, by plant resistance (R) proteins. This interaction leads to a hypersensitive response (HR) which results in programmed plant cell death at the infected site preventing further spread of the infection.

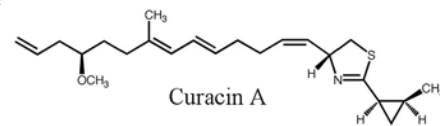
The aim of this project is to investigate the interaction of the Avr and R proteins at the molecular level. We have chosen the AvrL567 protein family from flax rust fungus, whose members have been shown to activate the HR in flax containing R proteins L5, L6 and L7 with varying specificities. In this system, the available evidence suggests a direct recognition between the Avr and R proteins. The Avr proteins were expressed in bacteria and purified using affinity and size exclusion chromatography. The proteins were further characterised by mass spectrometry and circular dichroism. We obtained crystals of AvrL567-A and AvrL567-D proteins. The structure of AvrL567-A was solved using single wavelength anomalous dispersion (SAD) on in-house copper anode x-ray generator at 2.0 Å, and the structure refined at 1.4 Å resolution. The structure of AvrL567-D was determined at 2.3 Å by molecular replacement, using AvrL567-A as the search model.

The structures of AvrL567 proteins have a novel beta-barrel-like fold. Based on the structure of AvrL567 proteins and mutagenesis results, we propose a model for their interaction with the L6 resistance protein, and propose possible interaction sites to explain the specificity of recognition of flax R proteins. The structure analysis also reveals a putative role in gene regulation through DNA binding and possibly promotes the virulence effect in susceptible flax species. The knowledge of the Avr-R interaction may be used to engineer flax rust resistant plants.

**SP053 Structure-Function Studies of the CurF Decarboxylase from *Lyngbya majuscula* Involved in Curacin A Biosynthesis.** Todd W. Geders<sup>§†</sup>, Liangcai Gu<sup>†</sup>, Jonathan C. Mowers<sup>†</sup>, David H. Sherman<sup>†</sup>, Janet L. Smith<sup>†</sup>, <sup>†</sup>Life Sciences Inst., Univ. of Michigan, Ann Arbor, MI, <sup>§</sup>Dept of Biological Sciences, Purdue Univ., West Lafayette, IN.

We have determined the 1.85 Å crystal structure of the wild-type decarboxylase domain of CurF from *Lyngbya majuscula*, a marine cyanobacterium that produces the natural product curacin A. Curacin A is a mixed polyketide/non-ribosomal peptide possessing potent anti-proliferative activity against colon, renal, and breast cancer-derived cell lines due to inhibition of tubulin polymerization [1,2].

The N-terminal domain of CurF catalyzes the decarboxylation of 3-methylglutaconyl-acyl carrier protein (ACP) to 3-methylcrotonyl-ACP, the postulated precursor of the cyclopropane ring of curacin A [3]. The structure revealed that CurF decarboxylase domain is a member of the crotonase superfamily, with Ala78 and Gly118 forming the oxyanion hole responsible for stabilizing the enolate anion intermediate. Structural alignment with other related crotonase family members allowed for modeling of the substrate and identification of residues potentially involved in catalysis. Site-directed mutagenesis of the potential catalytic residues Tyr82, Lys86, Asp95, and His240 was performed and tested in an *in vitro* decarboxylation assay using an ACP-linked substrate. Assay results identified the residues important for catalysis, and have helped formulate a hypothesis on how this decarboxylase produces the correct unsaturated product.



[1] Chang Z, Sitachitta N, Rossi JV, Roberts MA, Flatt PM, Jia J, Sherman DH, Gerwick WH. *J Nat Prod.* 2004 **67**:1356-1367

[2] Gerwick WH, Proteau PJ, Nagle DG, Hamel E, Blokhin A, Slate D. *J Org Chem.* 1994 **59**:1243-1245

[3] Gu L, Jia J, Liu H, Håkansson K, Gerwick WH, Sherman DH. *J Am Chem Soc.* 2006 **128**:9014-9015

**MP054 Crystal Structure of Sialyltransferase PM0188 from *P. multocida* in Complex with Donor Sugar Analogue and Acceptor Sugar.** Dong-Uk Kim<sup>a,b</sup>, Ji-Ho Yoo<sup>a,b</sup>, Kwan Soo Kim<sup>c</sup>, Yong Joo Lee<sup>c</sup>, Hyun-Soo Cho<sup>a</sup>, <sup>a</sup>Dept. of Biology, <sup>b</sup>Protein Network Research Center, and <sup>c</sup>Dept. of Chemistry, Yonsei Univ., Seoul, South Korea.

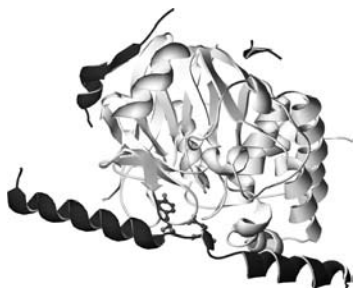
PM0188 is a newly identified sialyltransferase from *P. multocida* which transfers Neu5Ac from CMP-Neu5Ac to acceptor sugar. Although sialyltransferases have very important biological roles, little is investigated about their structure and mechanism. Here, we report the x-ray structures of CMP-GTases with PM0188 in the presence or absence of accept sugar as well as donor sugar analogue. PM0188 consists of two 'Rossmann fold' separated by deep cleft and the donor sugar binding site is located and buried in C-terminal domain, which is shown to have a conformational change of about 50° rotation toward N-terminal domain caused by substrate binding. Moreover, to precisely explain of the Neu5Ac transferring mechanism in the PM0188, we also determined the acceptor sugar binding site with lactose. The site directed mutagenesis assay data reveals that His311, Lys309, Arg313, Ser335, Ser336, Glu338, and Ser356 are important in its activity and Asp141 may act as general base. This is the first work showing the crystal structures of sialyltransferase complexed with not only donor sugar analogue but also acceptor sugar at the same time. Therefore, these complex structures provide insight for understanding the mechanism of other sialyltransferase and various GTases and for structure-based designing of specific inhibitors.

**MP055 The Complex Crystal Structure of Plant Telomere Binding Protein, NgTRF1 and Telomere DNA.** Hyun-Soo Cho, Sung-Hoon Jun, Jung-Sue Byun, Heeyoung Park, Hansol Bae, Woo Taek Kim, Weontae Lee, Dept. of Biology, Dept. of Biochemistry, Yonsei Univ., Seoul1, Korea.

Telomeres, the sequences at the ends of linear chromosomes, are essential for eukaryotic genome stability. During the last decade, telomere has been paid intense attention to because of its relationship with cancer and aging. Shortened telomere length during replication is recovered by telomerase, a reverse-transcriptase that synthesizes telomere with its own RNA template. The addition of telomere by telomerase is regulated by many telomere binding proteins. NgTRF1, a tobacco telomere binding protein, has been isolated as a double strand telomeric DNA binding protein. Its expression is regulated tightly in correlation with cell division and cell cycle. The role of NgTRF1 in telomere length regulation has also been addressed before. Here we report the complex structure of NgTRF1 DNA binding domain and telomere DNA. The DNA binding domain of NgTRF1 are composed of 4  $\alpha$ -helices and helix-turn-helix motif recognizes telomeric DNA sequences in major groove and N-terminal region interacts with DNA in minor groove. From this structure, we tried to show the uniqueness of plant telomere binding proteins in the mode of DNA binding as well as the similarity with the telomere binding proteins in other organisms. To our knowledge, this is the first report of the complex structure of telomere binding protein and telomere DNA in plant.

**MP056 Structural Basis for Regulation of Protein Phosphatase 1 by Inhibitor-2.** T.D. Hurley, J. Yang, L. Zhang, K.D. Goodwin, Q. Zou, M. Cortese, A.K. Dunker, A.A. DePaoli-Roach, Dept. of Biochemistry and Molecular Biology, Indiana Univ. School of Medicine, Indianapolis, IN.

Covalent phosphorylation is mediated by the coordinated action of protein kinases and phosphatases. The functional specificity of type 1 protein phosphatases (PP1) depends on its association with regulatory/targeting and inhibitory subunits. The formation of the complex between PP1 and inhibitor-2 (I-2) results in rapid inhibition of phosphatase activity, followed by a slower inactivation phase. Numerous biochemical, biophysical and computational analyses classify I-2 as an intrinsically disorder protein, yet it is capable of forming a highly specific and high affinity ( $K_d \sim 2$  nM) complex with PP1. To gain insights into the mechanism of PP1 regulation by I-2 we solved the crystal structure of the complex between rat PP1 $\gamma$  and mouse I-2 to 2.5Å resolution ( $R_{free}/R_{cryst} = 0.235/0.194$ ). Our studies show that I-2 acquires three regions of ordered structure in this complex representing only 59 of its 205 amino acids: residues 12-17 bind adjacent to a region recognized by many PP1 regulators, amino acids 44-56 interact along the canonical RVxF binding groove through a surprisingly non-canonical sequence, KSQKW, and residues 130-169, form  $\alpha$ -helical regions that lie across the substrate binding cleft. Specifically, residues 148-151 interact at the catalytic center, displacing essential metal ions, accounting for both rapid inhibition and slower inactivation of PP1 $\gamma$ . This structure provides novel insights into the mechanism of PP1 inhibition and subsequent reactivation and highlights common inhibitory interactions among PPP-family members.



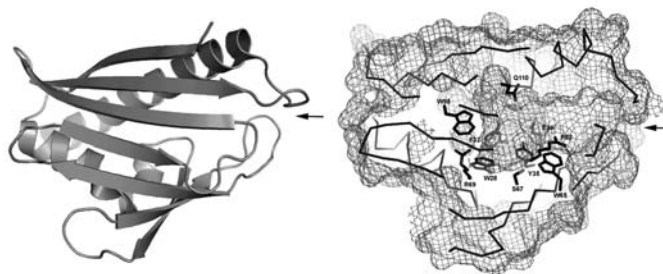
We wish to thank SBC-CAT for access to beamline 19-ID. This work supported by DK063285.

104

American Crystallographic Assn. ©

**MP057 Structure and Functional Analysis of Tetracenomycin Aromatase/cyclase.** B.D. Ames<sup>1</sup>, W.J. Zhang<sup>2</sup>, T.P. Korman<sup>1</sup>, P. Smith<sup>1</sup>, T.N. Vu<sup>1</sup>, Y. Tang<sup>2</sup>, S-C. Tsai<sup>1</sup>, <sup>1</sup>Dept. of Molecular Biology and Biochemistry, Univ. of California, Irvine, CA, <sup>2</sup>Dept. of Chemical and Biomolecular Engineering, Univ. of California, Los Angeles, CA.

Many aromatic polyketide natural products have important pharmacological activity, including the antibiotic activity of the tetracycline's, and the anticancer activity of the anthracycline's. Aromatic polyketides are produced by the type II polyketide synthases (PKSs). Critical to the formation of aromatic rings during biosynthesis are the PKS aromatase/cyclases (ARO/CYC)s. Here we present the crystal structure of tetracenomycin (tcm) ARO/CYC solved by MAD to 1.9 Å resolution. Tcm ARO/CYC is involved in the biosynthesis of the polyketide antibiotic tetracenomycin C from *Streptomyces glaucescens*, catalyzing the regiospecific cyclization, and subsequent aromatization, of the nascent polyketide chain to yield Tcm F2. The structure of tcm ARO/CYC reveals that the enzyme possesses a helix-grip fold and contains a large interior cavity consisting



of conserved hydrophobic, polar, and charged residues. The role of conserved pocket residues in substrate specificity and catalysis was tested *in vivo* by heterologous expression of mutant tcm ARO/CYC with the tcm minimal PKS. Product analysis revealed that mutations R69A (crystal structure shows WT conformation) and Y35A inactivate the enzyme, and N136A results in the increased production of a truncated product. The results provide evidence that the interior pocket of polyketide ARO/CYCs is important for cyclization specificity and catalysis, and may play a role in modulation of polyketide chain length.

We thank the Advanced Light Source for access to beamlines 5.0.1 and 5.0.2. The work was supported in part by the PEW Foundation, and the American Heart Association.

**SP058 Cyclin Box Structure of the P-TEFb Subunit Cyclin T1 Derived from a Fusion Complex with EIAV Tat.** Kanchan Anand, Antje Schulte, Klaus Scheffzek, Matthias Geyer, EMBL Heidelberg, Structural and Computational Biology Programme, Heidelberg, Germany.

The positive transcription elongation factor b (P-TEFb) is an essential regulator of viral gene expression during the life cycle of HIV-1. Its Cyclin T1 subunit forms a ternary complex with the viral Tat protein and the TAR RNA element thereby activating cyclin dependent kinase 9 (Cdk9), which stimulates transcription at the level of chain elongation. We report the structure of the cyclin box domain of human Cyclin T1 at a resolution of 2.67 Å. The structure was obtained by crystallographic analysis of a fusion protein composed of Cyclin T1 linked to the transactivator protein Tat from equine infectious anemia virus (EIAV), which is functionally and structurally related to HIV-1 Tat. The conserved cyclin box domain of Cyclin T1 exhibits structural features for interaction with physiological binding partners such as Cdk9. A recognition site for Cdk/Cyclin substrates is partly covered by a Cyclin T-specific insert, suggesting specific interactions with regulatory factors. The previously identified Tat/TAR recognition motif (TRM) forms a C-terminal helix that is partly occluded in

the cyclin box repeat interface, while cysteine 261 is accessible to form an intermolecular zinc finger with Tat. The EIAV Tat protein instead appeared undefined from the electron density map suggesting that it is highly disordered. Functional experiments confirmed the TAR binding properties of the fusion protein and suggested residues on the second cyclin box repeat to contribute to Tat stimulated transcription.

We thank the staff of ESRF Grenoble, France for access to beamline ID29. This work was supported by an EMBO long term fellowship to K.A. and a DFG grant (GE-976/2) to M.G.

**MP059 From Orphan to Structure: Genetic Control by a Metal-Sensing Riboswitch.** Charles E. Dann III, Catherine A. Wakeman, Cecelia L. Sieling, Wade C. Winkler, Dept. of Biochemistry, Univ. of Texas Southwestern Medical Center, Dallas Texas.

Interest in RNA has expanded tremendously over the last decade due to numerous discoveries of new roles for noncoding RNAs in cellular processes. One class of noncoding RNAs, termed riboswitches, is responsible for cis-regulatory genetic control of transcripts via diverse mechanisms including transcription attenuation, ribosomal binding site sequestration, or transcript degradation. Riboswitches are widespread in bacterial transcripts and have also been identified in plants. For example, in *B. subtilis* ~2.2 % of transcripts are regulated by metabolite binding riboswitches while proteins are known to regulate only half of this number. Riboswitches can act as molecular on or off switches in the absence of protein factors and to date have been shown to function by binding key metabolites including guanine, adenine, glycine, lysine, flavin mononucleotide, *S*-adenosylmethionine, thiamine pyrophosphate, adenosylcobalamin, and glucosamine-6-phosphate for this purpose. We have studied an orphan riboswitch from *B. subtilis* and have shown via genetic, biochemical, and structural means that this class of riboswitch extends the repertoire of riboswitch ligands to include metal ions. These data, including a ligand-bound RNA structure refined to 2.6 Å will be presented.

Data collected at APS SBC-CAT beamline 19ID. CD is funded by the Sara and Frank McKnight Fund for Biochemical Research.

**SP060 Activation of the Human Nuclear Xenobiotic Receptor PXR by the RT-Targeted Anti-HIV Drug PNU-142721.** Yuan Cheng, Matthew R. Redinbo, Depts. of Chemistry, and Biochemistry and Biophysics, Univ. of North Carolina at Chapel Hill, Chapel Hill, NC.

The human pregnane X receptor (PXR), a member of the nuclear receptor superfamily of ligand-regulated transcription factors, detects a wide variety of endogenous and xenobiotic compounds and plays a central role in controlling the expression of drug metabolism pathways. PNU-142721, a potent non-nucleoside human immunodeficiency virus reverse transcriptase (HIV RT) inhibitor, is an established PXR activator, an effect that can generate dangerous drug-drug interactions during chemotherapy. We present the 2.8 Å resolution crystal structure of the human PXR ligand binding domain in complex with PNU-142721. The drug interacts with the PXR ligand binding pocket in a single orientation using a series of hydrogen bonds and non-polar contacts, as well as both edge-to-face and planar face-to-face aromatic stacking interactions. Taken together, these structural data may facilitate the design of novel PNU-142721 analogues that remain potent RT inhibitors but do not activate human PXR. Such compounds would be expected to be more effective than PNU-142721 in the anti-HIV cocktails used widely to treat AIDS and AIDS-related conditions.

**MP061 Structure of Puf4 Bound to RNA Reveals Insights into Binding Specificity.** M. Miller, J. Higgin, T. Hall, Lab. of Structural Biology, National Inst. of Environmental Health, Sciences, National Inst. of Health, Research Triangle Park, NC.

RNA binding proteins are found throughout nature and are largely involved in post-transcriptional gene regulation. The RNA binding Puf family of proteins are found in a wide range of eukaryotic organisms and halt translation by binding to a specific sequence in the 3' untranslated region of mRNA transcripts. Puf proteins are characterized by Pumilio repeats, comprising three helices, with each repeat selectively binding a specific RNA base. These repeats are stacked together to form a protein that recognizes a specific RNA sequence. Previous biochemical and structural work on human Pumilio1 protein revealed that RNA base recognition is facilitated by two side chains in each three helix repeat with one repeat recognizing one RNA base.

The Puf3, Puf4 and Puf5 proteins from *Saccharomyces cerevisiae* contain eight Pumilio repeats and like the *Drosophila* and human homologs are involved in post-transcriptional gene regulation. Each of the yeast Puf proteins bind to the RNA sequence UGUAX2-4UA. Although the yeast, human and fly proteins have a high degree of sequence similarity there are also differences in RNA recognition specificity that remain to be examined, including understanding how 2-4 bases are inserted between two highly conserved recognition regions. The determination of the structures of the Puf proteins would further our understanding of how this class of proteins recognize their RNA targets by directly observing the protein-RNA interface.

We have solved the crystal structure of apo Puf4 to 2.7 Å resolution and to 3.0 Å bound to an 11 base pair RNA oligonucleotide with the Puf4 recognition sequence, UGUUAUUA. This RNA includes a 3 base insertion between the UGUA and UA conserved regions. This structure is an example of how a highly conserved protein scaffold can be modified by subtle changes to key side chain residues to alter specificity. This work will guide further experiments to probe how the protein-RNA interface is affected by modifications to the RNA sequence and protein sidechains. If these interactions are better understood they could potentially be used to engineer Pumilio repeat proteins with new RNA specificity to suppress the translation of proteins that impact human health.

**SP062 Structural Insights into the 3' - 5' Exonucleases - mTrex1 & hTREX2.** Udesch de Silva, Sumana Choudhury, Suzanna L. Bailey, Scott Harvey, Fred W. Perrino, Thomas Hollis, Wake Forest Univ., Winston Salem, NC.

The TREX1 enzyme processes DNA ends as the major 3'-5' exonuclease activity in human cells. Mutations in the TREX1 gene are an underlying cause of the neurological brain disease Aicardi-Goutieres syndrome and Familial Chilblain Lupus implicating TREX1 dysfunction in an aberrant immune response. TREX1 action during apoptosis likely prevents autoimmune reaction to DNA that would otherwise persist. To understand the impact of TREX1 mutations identified in patients with Aicardi-Goutieres syndrome on structure and activity we determined the X-ray crystal structure of the dimeric mouse TREX1 protein in substrate and product complexes containing single-stranded DNA and deoxyadenosine monophosphate, respectively. The structures show the specific interactions between the bound nucleotides and the residues lining the binding pocket of the 3' terminal nucleotide within the enzyme active site that account for specificity, and provide the molecular basis for understanding mutations that lead to disease. Three mutant forms of TREX1 protein identified in patients with Aicardi-Goutieres syndrome were prepared and the measured activities show that these specific mutations

reduce enzyme activity by 4- to 35,000-fold. The structure also reveals an 8 amino acid polyproline II helix within the TREX1 enzyme that suggests a mechanism for interactions of this exonuclease with other protein complexes.

**SP063 Cloning and Crystallization of *Drosophila* Tgo (bHLH-PAS) Protein.** Dongli Wang, Robert Rose, Biochemistry Dept., North Carolina State Univ., Raleigh, NC.

PAS (Per-Arnt-Sim) proteins constitute a large and diverse array of molecules. In prokaryotes, PAS domain proteins are important signaling modules that monitor changes in light, redox potential, oxygen, small ligands and overall energy levels of a cell. In eukaryotes, PAS proteins regulate diverse processes like developmental regulation, circadian rhythms, oxygen metabolism, and dioxin metabolism. bHLH-PAS proteins contain two PAS domains adjacent to a bHLH domain, and the PAS domain selects between dimerization partners.

To characterize the functional role of heterodimer formation between PAS proteins, we have chosen a subset of bHLH-PAS family members which heterodimerize with one another and activate transcription of gene groups in turn. *Drosophila* Tgo, and its mammalian ortholog, Arnt are ubiquitously expressed proteins that dimerize with other bHLH-PAS proteins. In *Drosophila*, Tgo heterodimerizes with Sim, Trh, Sima and Ss, while each of these bind only Tgo and not one another. It is shown that Tgo can form homodimers *in vitro* as well.

Work has been done from other groups to define the structure of PAS proteins. The structure of Per homodimers and a partial structure of Hif2 $\alpha$ -Arnt heterodimers has been described, whereas no crystal structure demonstrating the interaction between bHLH-PAS heterodimers has been described to date. The structural basis for selection of binding partners for PAS proteins is not well understood either.

Our goal is to crystallize Tgo homodimer and Tgo heterodimers to determine how bHLH-PAS proteins select dimerization partners, and how the PAS domain might affect DNA binding. So far in our lab, we have cloned and purified *Drosophila* Tgo (bHLH-PAS). And from crystal trials using the robot at Hauptman-Woodward Institute, we have obtained promising initial crystals of Tgo. We are currently optimizing these conditions.

**SP064 Current Status of the JAXA-GCF Project.** M. Sato<sup>a</sup>, H. Tanaka<sup>b</sup>, K. Inaka<sup>c</sup>, S. Shinozaki<sup>d</sup>, S. Takahashi<sup>b</sup>, M. Yamanaka<sup>b</sup>, E. Hirota<sup>b</sup>, S. Sano<sup>a</sup>, T. Kobayashi<sup>a</sup>, T. Tanaka<sup>a</sup>, <sup>a</sup>Japan Aerospace Exploration Agency, Ibaraki, Japan, <sup>b</sup>Confocal Science Inc., Tokyo, Japan, <sup>c</sup>Maruwa Foods and Biosciences, Inc., Nara, Japan, <sup>d</sup>Japan Space Forum, Tokyo, Japan.

Japan Aerospace Exploration Agency (JAXA) conducted JAXA-GCF project to develop technologies for obtaining high-quality protein crystals in space. In the project, six space experimental opportunities were provided to crystallographers, using Russian flight opportunities, twice a year, from 2003 to 2006. The rate of successful crystallization, that is mostly the improvement of the maximum resolution, has been significantly increased to about 70% of protein that was highly purified and succeeded in the optimization of the crystallization condition. The most remarkable was improvement of maximum resolution even if the ground-grown crystal showed excellent resolution around 1 Å.

Based on the findings from the project, JAXA has started JAXA-New-GCF (JAXA-NGCF) experiment. Three flight opportunities are scheduled, once in every six months. The first flight was launched

on Jan. 18, 2007 and will be landed in April. The purposes of JAXA-NGCF are to obtain atomic-resolution crystals for precise structural analysis, to cooperate with national project, and to transfer technology to private companies for commercial use.

We thank ESA and the Belgium government for Odissea mission and the usage of GCF, the Federal Space Agency and RSC Energia for the usage of the Russian Service Module, and NASA for the usage of the incubator in the US module. We are grateful to Professor Garcia-Ruiz and the members of his laboratory in CSIC-University of Granada for their helpful advices. We thank Protein 3000 Project (Riken and eight universities), NIAS, PCProt, and other users for providing protein samples.

**SP065 Estimation Method of Diffusion Coefficient of Precipitant.** H. Tanaka<sup>a</sup>, N. Furubayashi<sup>b</sup>, K. Inaka<sup>b</sup>, S. Takahashi<sup>a</sup>, M. Yamanaka<sup>a</sup>, M. Sato<sup>c</sup>, S. Sano<sup>c</sup>, T. Kobayashi<sup>c</sup>, A. Nakagawa<sup>d</sup>, T. Tanaka<sup>c</sup>, <sup>a</sup>Confocal Science Inc., Tokyo, Japan, <sup>b</sup>Maruwa Foods and Biosciences, Inc., Nara, Japan, <sup>c</sup>Japan Aerospace Exploration Agency, Ibaraki, Japan, <sup>d</sup>Osaka Univ., Osaka, Japan.

For a successful crystallization in a counter-diffusion method <sup>[1]</sup> including Gel-Tube method <sup>[2]</sup> which is quite convenient for crystallization not only in microgravity but also in terrestrial environment, it is important to figure out the diffusion of precipitant molecules as a function of time. Generally, the diffusion coefficient of established value was used to estimate the diffusion of the molecules. However, not all of the diffusion coefficients of the precipitant have been reported. In addition, the diffusion of the precipitant molecules sometimes may depend on the composition of the crystallization solution. Therefore it is preferable to perform the estimation of the diffusion coefficient in the mixed precipitant solution if it is not difficult.

Here we developed the measuring method of the concentration change of the precipitant molecules as a function of time, using refractometer and simple device made of capillaries and silicone tubing. After the measurement, we applied the least-squares method to estimate the diffusion coefficient. We measured the concentration change of precipitant in distilled water and the estimated diffusion coefficient was matched to the established value. This method is easy to prepare and almost all the crystallization reagent, even mixed solutions, can be applied.

[1] Garcia-Ruiz, JM., Moreno, A., *Acta Cryst.*, 1994, D54, 484-490.

[2] Tanaka, H. *et al.*, *J. Synchrotron Rad.*, 2004, 11, 45-48.

**SP066 Mellitic Acid-Promoted Crystallization of Bovine Trypsin.** Steven B. Larson, John S. Day, Alexander McPherson, Dept. of Molecular Biology and Biochemistry, Univ. of California, Irvine, CA, Robert Cudney, Hampton Research, Aliso Viejo, CA.

During the investigation of the effect that small molecules have on the crystallization of macromolecules, pancreatic bovine trypsin was crystallized from PEG 3350 and a "cocktail" of small organic acids, i.e. mellitic acid, pyromellitic acid, trimesic acid and terephthalic acid. The resulting crystals belonged to space group P3<sub>1</sub>21 having cell dimensions a=b=138.4 Å and c=150.5 Å, a previously unobserved crystal form. The structure was solved by molecular replacement. A single dominant orientation was found in the cross rotation search. However, the translation search yielded eight independent solutions having the same orientation. These independent solutions have a *pseudo*-face centered arrangement, explaining why the data is so weak. The average I/ $\sigma$ (I) is only 4.0 for all data processed to 1.50 Å, despite a redundancy of 12.9.

There are also eight mellitic acid molecules in the asymmetric unit. Each mellitic acid molecule is directly hydrogen bonded to

Lys156 and Thr21 of one bovine trypsin molecule and to Ser217, Gly219 and Lys224 of a neighboring trypsin molecule, while also maintaining several water-mediated interactions. In addition, each trypsin molecule has a molecule of the inhibitor, benzamidine, in the active site.

Larson, Day, Cudney & McPherson. *Acta Cryst. D* **63**, 310-318 (2007).  
McPherson & Cudney. *J. Struct. Biol.* 156, 387-406 (2006).

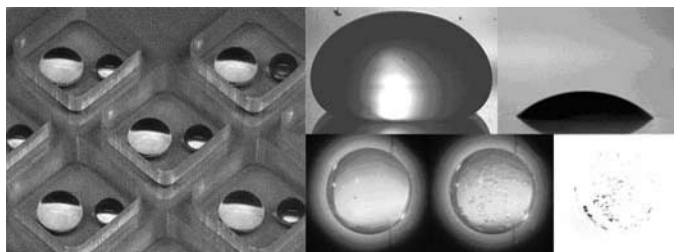
**SP067 Strategies in High Throughput Protein Crystallization: Cryoprotectants as Solubility Enhancers.** Rajendrakumar Gosavi<sup>1</sup>, Timothy Mueser<sup>2</sup>, Constance Schall<sup>1</sup>, <sup>1</sup>Dept. of Chemical and Environmental Engineering, <sup>2</sup>Dept. of Chemistry, Univ. of Toledo, Toledo, OH.

Abstract: Screening of hundreds of different salt/buffer conditions are often made in biomolecular crystallization with high throughput methods relying heavily on trial and error methods employing different commercially available screens. We present here our developing strategy to improve the number of conditions that yield crystals in high throughput crystallization. Earlier studies by our group (Izaac, 2006) have shown that increasing the solubility of protein by optimizing the buffer improved crystal hits during high throughput crystallization compared to crystal hits obtained in a standard 50 mM TRIS HCl pH 7.5, 100 mM NaCl buffer. Optimizing buffer conditions essentially means selecting a combination of salt and buffer in which protein has greater solubility. An increase in protein solubility can lower the barrier for crystallization. Following up on these initial studies, we have used 5 common cryoprotectants (glycerol, ethylene glycol, Na malonate, glucose and 2-methyl-2, 4-pentane diol) some of which are known to improve solubility in the standard buffer. We have evaluated the resultant solubility and number of conditions providing crystals. The effect of these cryoprotectants on the solubility of 10 model proteins and the increase or decrease in crystal hits will be discussed.

Izaac, A.; Schall, C. A. & Mueser, T. (2006) *Acta Crystallogr D* **62**, 833-842.

**SP068 Macromolecular Crystallization Device Based on Contact Line Pinning.** Yevgeniy Kalinin, Viatcheslav Berejnov, Robert E. Thorne, Physics Dept., Cornell Univ., Ithaca, NY.

We describe a macromolecular crystallization plate compatible with automated drop dispensing robots in which drops held in place by microfabricated patterns. Surface micropatterning produces drops with well-defined positions, boundaries and shapes. The drops show excellent stability against vibrations, and arrays of large drops can be rotated 90 degrees to the vertical plane or inverted to the hanging drop configuration with no motion of the drop contact lines. A single micropatterning process strongly pins drops of a wide range of liquids including protein, surfactant and salt solutions. The drop contact line remains pinned as the drop evaporates, resulting in greatly improved reproducibility of evaporation and crystallization kinetics. Because drop shape is reproducible and well defined, automated image analysis to identify crystals is greatly simplified. Supporting the drops on a patterned, optically and X-ray transparent film allows *in situ* X-ray examination. This improved crystallization plate is well



suitable to both high-throughput and manual crystallization experiments, and should provide a very cost-effective alternative to microfluidic crystallization devices.

This research is supported by the NIH (R01 GM65981).

**SP069 Cryoprotectant Requirements for Flash Cooling Protein Crystals based on Measured Thermal Properties and Heat Transfer Analysis – A Prediction.** C.A. Schall\*, B.N. Shah\*, K.J. DeWitt\*, B.L. Hanson\*, S.J. Tomanicek\*, <sup>\*</sup>Dept of Chemical and Env't. Eng., <sup>\*</sup>Chemistry, Univ. of Toledo, Toledo, OH.

X-ray diffraction data is routinely collected on protein crystals at cryogenic temperature. Ice formation at cryogenic temperature is avoided by mixing cryoprotectants with crystallizing solutions. The cryoprotectant reduces the ice nucleation window and its concentration must be optimized to achieve both vitreous state and retain protein crystal integrity for X-ray diffraction. Finding a minimum cryoprotectant concentration to avoid ice formation is a trial and error procedure and often valuable crystals are lost in this exercise. A theoretical basis for prediction of cryoprotectant concentration for successful flash cooling was developed.

The thermal transition temperatures such as glass transition temperature and melting temperature are measured using a differential scanning calorimeter along with temperature dependent heat capacity of cryoprotectant solutions. These properties affect flash cooling of protein crystals. A model is developed to predict the glass transition temperature (transition from vitreous state to crystalline or liquid state) for multi-component mixtures. This model in combination with the heat transfer analysis and temperature dependent heat capacity serves as a guide to predict a conservative estimate for predicting cryoprotection requirements during flash cooling. Cryoprotectant concentration can be predicted for different size protein crystals. This was verified for crystals of Ape FEN 1 using deuterated solutions crystals.

**SP070 A Method for Controlling the Vapor Pressure of Water in Crystallization Experiments using CsCl.** Daniel Hennesy, Lisa Bajpayee, Beena Narayanan, John Rosenberg, Dept. of Biological Sciences, Univ. of Pittsburgh, Pittsburgh, PA.

Much of the experimental effort in vapor diffusion crystallization experiments is effectively altering the vapor pressure of water in the experimental chambers. However, control of the vapor pressure is very indirect. The method reported here consists of a two stage process to directly measure and control the vapor pressure. In the first stage, the vapor pressure is measured by including a small droplet of a simple solution containing only water and a solute, such as CsCl or sucrose, which has a known concentration dependence on its index of refraction (that can be measured in a laboratory refractometer). This first stage determines the vapor pressure at the point of interest (e.g., crystallization). In the second stage, the protein droplets are prepared as usual, i.e. by mixing ratios of stock protein and screening solutions, but the reservoir is a solution of CsCl or sucrose at a concentration near the point of interest, effectively driving the vapor pressure to a controlled value. The advantage of this method is to separate the control of the vapor pressure from the complex set of issues associated with the chemical composition of the protein test solutions using readily available materials. Furthermore, it allows for the expansion of the range of tested conditions by allowing identical initial protein solution compositions to be tested against a variety of vapor pressure conditions (in replica experiments). It also allows for controlled dehydration of crystals by making suitable transfers after the crystals are grown.

**SP071 The X-ray Structures of Monoclinic and Orthorhombic Taka-amylase A; The Crystals Grown in Microgravity Environment.** Akifumi Higashiura<sup>1</sup>, Hiroaki Tanaka<sup>2</sup>, Sachiko Takahashi<sup>2</sup>, Mari Yamanaka<sup>2</sup>, Masaru Sato<sup>3</sup>, Satoshi Sano<sup>3</sup>, Tomoyuki Kobayashi<sup>3</sup>, Tetsuo Tanaka<sup>3</sup>, Koji Inaka<sup>4</sup>, Shigeru Sugiyama<sup>4</sup>, Mamoru Suzuki<sup>1</sup>, Atsushi Nakagawa<sup>1</sup>, <sup>1</sup>IPR, Osaka Univ., <sup>2</sup>Confocul Science Inc., <sup>3</sup>JAXA, <sup>4</sup>Maruwa Food and Biosciences, Inc.

High brilliance and small divergence synchrotron beamlines, cryogenic experiments and technical advances in crystallographic analysis have significantly improved the resolution of X-ray crystallography. Crystallization in microgravity environment sometimes result improvement of resolution limit of X-ray diffraction. We recently succeeded to obtain high-resolution crystals of a Taka-amylase A, a glycoprotein derived from *Aspergillus oryzae*, under microgravity. The space crystals were produced in the JAXA-GCF (Japan Aerospace Exploration Agency – Granada Crystallization Facility) project. Data collections were performed using synchrotron radiation from SPring-8 beamline BL12B2, BL44XU and Photon Factory beamline NW12. High-resolution diffraction data of monoclinic Taka-amylase A were observed up to 0.95Å and orthorhombic Taka-amylase A were 0.94Å. These high-resolution structure was providing us with a more reliable picture of the geometric and conformational properties of proteins and implied the necessity to improve bond length and angle restraints.

**SP072 A Microfluidic Chip for Protein Crystallization and In Situ Diffraction Data Collection.** K. Hamada<sup>a</sup>, T. Hasegawa<sup>a</sup>, M. Sato<sup>b</sup>, M. Motohara<sup>b</sup>, S. Sano<sup>b</sup>, T. Kobayashi<sup>b</sup>, T. Tanaka<sup>b</sup>, Y. Katsube<sup>a</sup>, <sup>a</sup>PharmAxess, Inc., Osaka, Japan, <sup>b</sup>Japan Aerospace Exploration Agency “JAXA”, Ibaraki, Japan.

Microfluidic technologies are available for development of viable devices for protein crystallization screening. Although screening in nanoliter volume free interface diffusion is more useful than conventional screening, crystals grown from nanoliter volume are sufficient size for diffraction studies and it is difficult to mount. We have developed new microfluidic chip, “Micro Chip”, designed to perform liquid-gel-liquid counter-diffusion crystallization method. Protein channel and precipitant cell in Micro Chip produced from PDMS were separated by agarose gel channel. Micro Chip containing protein crystals grown is easily able to mount on X-ray diffractometer and in situ diffraction data were collected for X-ray analysis. Crystals grown in the protein channel are easily accessed by loop so as to mount them. Proteins including membrane proteins were successively crystallized using Micro Chips on the ground, and crystallizations of them under microgravity environment in the JAXA-New-GCF (JAXA-NGCF) project are in progress.

We thank Prof. A. Nakagawa, Prof. Y. Higuchi, Prof. S.Y. Park, Dr. T. Kumasaka, Dr. T. Odahara, Prof. S. Harada, Prof. K. Kita, Dr. K. Inaka and Prof. N. Shimizu for providing protein samples. We are grateful to Dr. T. Yoshida and Dr. K. Takasugi in Fluidware Technologies Inc. for development of device. We thank Ms. M. Yamana and Mr. H. Tanaka for simulation of crystallization conditions.

**SP073 Automated Liquid Dispensing with Precision and Accuracy for Protein Crystallization Using the Alchemist™ II.** Jian Xu, Matt Lundy, Michael Willis, Rigaku Automation, Carlsbad, CA.

Crystallization of macromolecules requires chemical stock solutions of diverse physical and chemical properties, such as viscosity, volatility, and ionic strength, to be dispensed consistently in various volume ranges. The Alchemist II, a robotic liquid handling system from Rigaku, offers a solution that automates the tedious and time-consuming process of producing liquid formulations, enabling crystallographers to quickly and reliably screen a broader selection

of conditions. The applications of positive pressure displacement pipetting and the unique Tapper technology make it capable of dispensing a wide range of volumes (1µL to 10mL) and liquid types, including viscous, aqueous and volatile solutions, with precision and accuracy. The patent pending BirdFeeder™ technology eliminates the usage of tubing and tips and provides an automated pipetting solution without cross contamination. We report here an achievement of high liquid dispensing precision and pH consistency from studies conducted on representative chemical stock solutions showing, for instance, an average coefficient of variation (CV) of less than 2% dispensing 50% PEG 8K with volumes ranging between 1µl and 10µl and an average CV of less than 0.2% with pH values ranging between pH7.0 and pH9.0 using Tris hydrochloride as a buffer system. An example of successful crystallization of HSP90 protein using Alchemist II as a screen making system will also be illustrated.

We thank Dan Bensen, Isaac Hoffman, Kirk Nelson, Dr. Les Tari, and Dr. Duncan McRee at Active Sight for providing the HSP90 protein sample, the chemical stocks and the collaboration.

**SP074 The Current SER Approach.** David Cooper<sup>1</sup>, W.-C. Choi<sup>1</sup>, U. Derewenda<sup>1</sup>, L. Goldschmidt<sup>2</sup>, N. Olekhnovitch<sup>1</sup>, M. Zheng<sup>1</sup>, D. Eisenberg<sup>2</sup>, Z. Derewenda<sup>1</sup>, <sup>1</sup>Mol Physiology and Biol Physics, Univ of Virginia, Charlottesville, VA, <sup>2</sup>Chem and Biochem, UCLA, Los Angeles, CA, <sup>1&2</sup>The Integrated Center for Structure and Function Innovation.

One goal of the ISFI is to develop methods for the structural community. The Surface Entropy Reduction (SER) method has proven to be an effective means of producing crystals for “stubborn crystallizers”. Herein, we report our progress on developing a low- to medium-throughput approach that increases the chance of crystallizing proteins that meet SER criteria.

SER is not a “catch all” for leaks in the high throughput pipeline, nor is it applicable for every difficult protein. We present the analysis and experiments that must be performed before a protein can be considered a SER candidate and outline a strategy from mutation selection to SER structure solution. We have aimed to make our process of protein expression and production as low-tech and affordable as possible, making this approach within the reach of most laboratories, yet scalable for use as an efficient salvage pathway for high-throughput pipelines.

We have developed a variety of tools to assist the structural community effectively implement the SER approach, including the SERp Server (<http://nihserver.mbi.ucla.edu/SER>), which evaluates a sequence and suggests possible SER variants. We will discuss our process of target selection, including a process by which the structural community can request we target a protein. Our crystallization screening and optimization process has been designed with economy, efficiency, and adaptability in mind. We also discuss recent successes of our pipeline and present an indication of the technique’s success rate.

The work of the entire ISFI is acknowledged. The ISFI is supported by NIH Protein Structure Initiative grant U54 GM074946.

**SP075 Strategies of Improving the Crystallization Success Rate.** M. Zhou, L. Bigelow, E. Duggan, C. Hatzos, G. Joachimiak, H. Li, R. Mulligan, L. Volkart, R. Wu, Q. Zhang, G. Babnigg, Y.-C. Kim, R.-G. Zhang, A. Joachimiak, Midwest Center for Structural Genomics and Structural Biology Center, Biosciences, Argonne National Lab., Argonne, IL.

The Midwest Center of Structure Genomics (MCSG) uses high-throughput molecular biology and crystallography approaches in protein purification and crystallization. During second phase of the Protein Structure Initiative the MCSG protein target set has changed

and therefore different methodology was needed to maintain and increase the overall success rate. In the protein structure determination pipeline crystallization shows the highest attrition and choice of strategy can have significant impact. For each MCSG target we use a larger set of orthologues and protein constructs. We vary N- and C-terminal boundaries of family sequence motifs based on secondary structure prediction and other protein parameters and we purify larger set of protein constructs for crystallization. We will present results of analysis of protein expression, solubility, crystallization success rate, and crystal diffraction quality as a function of the protein boundary change. Based on our experimental data we will show how various strategies of designing protein target and a choice of crystallization screening conditions can influence the crystallization success rate.

This work was supported by NIH Grant GM074942 and by the U.S. Department of Energy, OBER, under contract DE-AC02-06CH11357.

**SP076 Purification, Characterization, and Crystallization of a Metal Dependent PI-PLC from *Streptomyces Antibioticus*.** Michael R. Jackson, Thomas L. Selby, Univ. of Central Florida, Orlando, FL.

Phosphatidylinositol (PI) specific phospholipase Cs (PI-PLCs) are ubiquitous enzymes involved in transferring chemical signals from cell surfaces via hydrolysis of P-O bonds through a transesterification mechanism. PI-PLCs function as virulence factors in bacteria and signal transduction enzymes in eukaryotes, and differ in their ability to utilize  $\text{Ca}^{+2}$  as a cofactor. The smaller bacterial enzymes use arginine for charge stabilization during the reaction, and the eukaryotic forms are regulated by  $\text{Ca}^{+2}$ . Identification of a  $\text{Ca}^{+2}$  dependent PI-PLC from *Streptomyces antibioticus* (SaPLC) prompted us to investigate this enzyme to understand the structural similarities and differences required for  $\text{Ca}^{+2}$  regulation in a bacterial PI-PLC. Towards this aim, SaPLC was purified, characterized—using circular dichroism, dynamic light scattering, gel filtration chromatography, and fluorescence spectroscopy (in the presence and absence of  $\text{Ca}^{+2}$ )—and crystallized. Two crystal morphologies are observed from three different crystal conditions that appear to correlate with the purification steps used to prepare the protein for crystallization. Differences in the type and concentration of salts used throughout the process have an effect on crystal growth quality even though the final buffer conditions are identical. This may indicate that membrane lipids are co-purified with the enzyme. The best crystal form produced diffraction data to 2.1 Å in space group I4 with unit cell dimensions; 182.5 Å x 182.5 Å x 102.1 Å and methods of phase determination using molecular replacement, heavy atoms soaks, and selenomethionine crystal growth are underway. Biophysical measurements suggest that  $\text{Ca}^{+2}$  may play a role in regulating enzyme activity as well as promoting structural stability.

**MP077 A New Experimental Station for Long Wavelength Crystallography.** Q. Hao, U. English, A. Kazimirov, E. Fontes, D.H. Bilderback, S.M. Gruner, C.U. Kim, Cornell High Energy Synchrotron Source (CHESS), Cornell Univ., Ithaca, NY.

The Cornell High Energy Synchrotron Source (CHESS) plans to develop a new experimental station for long-wavelength macromolecular crystallography based on novel narrow bandwidth multilayer optics. A recent study at the CHESS F3 bending-magnet station demonstrated the utility of a narrow-bandwidth (0.22%) synthetic multilayer monochromator. The resulting images were processed with standard crystallography programs and were successfully compared to data of the same protein taken with a Si(111) monochromator. The results proved that the new multilayer optics provided a 5-fold gain in X-ray flux while still allowing the use of standard data collection

procedures and crystallography software<sup>[1]</sup>. Adding both vertical and horizontal beam focusing could reduce exposure times by another factor of 5 to 10, which would then make bending-magnet lines competitive with many insertion device beamlines for protein crystallography. We propose to convert the CHESS F3 station to the world's first macromolecular crystallography station utilizing such optics. This project will expand biocrystallography capabilities at CHESS. It will also provide a model for a rapid, cost-effective expansion of capabilities at other sources.

It has recently been demonstrated that pressure-cryocooled crystals can be amenable to phasing using native sulfur SAD<sup>[2]</sup>. Not coincidentally, CHESS scientists have been involved in a number of SAD phasing programs available in the CCP4 open software suite. Accordingly, we propose to further develop SAD in long-wavelength applications.

[1] English, U., A. Kazimirov, Q. Shen, D. H. Bilderback, S. M. Gruner & Q. Hao (2005). *J. Synchrotron Rad.* **12**, 345-348.

[2] Kim, C.U., Q. Hao & S.M. Gruner (2007), *Acta Cryst. D*. submitted.

**MP078 The Use of Longer X-ray Wavelengths in Macromolecular Crystallography.** Manfred S. Weiss, Christoph Mueller-Dieckmann, Santosh Panjikar, Paul A. Tucker, EMBL Hamburg Outstation, c/o DESY, Hamburg, Germany.

The use of longer X-ray wavelengths ( $\lambda = 1.5\text{-}3.0$  Å) in macromolecular crystallography has over the past few years almost become a routine tool for phase determination using the anomalous signal derived from the natively present sulfur and/or phosphorus atoms. In order to extract the maximum possible information contained in the data, it is essential, however, to apply a proper scaling protocol to the data. The best protocols in this respect take absorption into account implicitly. Nevertheless, there seems to be an optimal wavelength at which the anomalous signal-to-noise ratio is highest. In an extensive examination of 75 diffraction data sets collected at different wavelengths from ten different protein and DNA crystal systems, it was found that irrespective of the anomalously scattering substructure present, this optimal wavelength was around 2.0-2.1 Å<sup>[1]</sup>.

Next to being used for phase determination based on the anomalous signal from the light atoms (P, S, Cl, K, Ca), a well measured and processed long wavelength data set may also be utilized for the unequivocal definition of the anomalously scattering substructure. Although a large percentage of proteins are crystallized in the presence of ions derived e.g. from NaCl, KCl,  $\text{Na}_2\text{SO}_4$  and  $\text{Na}_3\text{PO}_4$  only about 10-15% of all PDB entries contain such ions as part of the structure coordinates.

[1] C. Mueller-Dieckmann *et al.* (2005). *Acta Cryst. D* **61**, 1263-1272, C. Mueller-Dieckmann *et al.* (2007); *Acta Cryst. D* **63**, 366-380.

**MP079 Higher Signal, Lower Noise: How to Get the Best Data from Your Crystals.** Martin Adam<sup>a</sup>, Anita Coetzee<sup>a</sup>, Bram Schierbeek<sup>a</sup>, Cary Bauer<sup>b</sup>, Rob Hooft<sup>a</sup>, <sup>a</sup>Bruker AXS B.V., Delft, The Netherlands, <sup>b</sup>Bruker AXS Inc., Madison, WI, USA

In a macromolecular crystallography, where crystals are small and often weakly diffracting, it is imperative to obtain data with as high a signal-to-noise ratio as possible. Improving the signal usually involves using a more powerful source, since obtaining samples with larger diffraction volume is often not possible.

The contribution of the noise should not be underestimated. Especially when looking at weak reflections or small differences in anomalous signal (e.g. doing S SAD phasing on native proteins) one has to take great care to minimize the experimental noise as much as possible. This can be done by careful sample handling,

minimizing the effect of background scatter from the cryo protectant and loop as well as in setting up the data collection experiment. Examples of more efficient data collection methods will be presented which can lead to a dramatic increase in signal to noise ratio, with the same amount of X-ray photons falling on the crystal. If all precautions have been taken to lower the noise of the experiment, then there is only one way to get a higher a signal-to-noise ratio: increasing the amount of X-rays on your sample. The MICROSTAR ULTRA, the next generation of the MICROSTAR series of generators, is substantially brighter than any other X-ray home source available today. With its revolutionary HyperCool™ anode cooling technology the MICROSTAR ULTRA is more intense and yet easier to maintain than other rotating anode generators.



Measurements show that this source compares with many second generation beam lines. Results of crystal data will be presented.

**MP080 Cryopreservation of Protein Crystals: From Art to Science.** Robert E. Thorne, Matthew Warkentin, Viatcheslav Berejnov, Naji Husseini, Physics Dept., Cornell Univ., Ithaca NY.

There are two limiting approaches to cryopreservation. One is to cool slowly in the presence of large cryoprotectant concentrations, allowing full relaxation and equilibration of sample constituents so as to achieve a homogeneous low-temperature state. The other is to cool so quickly that the high temperature state is frozen in. Previous studies have shown that cooling rates achieved in cryopreservation of protein crystals are  $10^3$  K/s or less, in neither of these favorable limits. We describe experiments showing that, for plunge cooling in liquid nitrogen and propane and for sample volumes less than 0.1 ml - i.e., for the sample volume range of interest in protein crystallography - most cooling occurs in the cold gas layer above the liquid cryogen, before the sample ever reaches the liquid [1]. By removing this cold gas layer, cooling rates are increased to  $>1.5 \times 10^4$  K/s, with even larger cooling rates possible with smaller samples. Glycerol concentrations required to eliminate ice crystallization in protein-free aqueous mixtures drop from ~28% to less than 5%. We report diffraction results for crystals of several proteins, and discuss factors relevant to optimizing diffraction outcomes.

Protein at the concentrations present in protein crystals should itself be a very effective cryoprotectant. We find that for lysozyme, trypsin and thaumatin crystals, cooling at rates of less than 10 K/s yields no ice rings in X-ray diffraction, provided that the external protein-poor solvent is removed. This suggests that ice rings arise primarily from crystallization of external solvent, and that the beneficial effects of penetrating cryoprotectants are not primarily associated with inhibition of crystallization of internal solvent.

[1] M. Warkentin *et al.*, *J. Appl. Cryst.* **39**, 805-811 (2006).

**MP081 Flash Cooling in Capillaries: Cooling Rates and Critical Glycerol Concentrations.** Matthew Warkentin<sup>1</sup>, Valentina Stanislavskaja<sup>1</sup>, Katherine Hammes<sup>2</sup>, Robert E. Thorne<sup>1</sup>, <sup>1</sup>Physics Dept., Cornell Univ., Ithaca NY, <sup>2</sup>Chemical and Environmental Engineering Dept., Illinois Inst. of Technology, Chicago, IL.

Protein crystallization in thin-walled plastic or glass capillaries is being considered as an alternative to plate or chip-based high-throughput crystallization because it can allow *in situ* X-ray examination and

structure determination. But can crystals be reliably flash cooled in capillaries for cryocrystallography? We have evaluated cooling rates and critical glycerol concentrations for plunge cooling in liquid nitrogen and liquid propane in capillaries with diameters from 150  $\mu\text{m}$  to 3.3 mm. For the smallest diameter considered, the glycerol concentrations required to achieve vitreous ice in protein-free solutions are 30 % w/v for nitrogen and 20 % w/v for propane, corresponding to cooling rates of ~800 K/s and ~7000 K/s, respectively. These cooling rates are one to two orders of magnitude smaller than can be achieved using standard cryocrystallographic mounting methods and our "hyperquenching" protocol. By comparing cooling rates and critical glycerol concentrations for each size of tubing, the critical cooling rate required for vitrification can be determined as a function of cryoprotectant concentration. This relation is of fundamental importance in cryopreservation.

This work was funded by the National Institute of Health (R01 GM65981).

**MP082 Trash to Treasure: Changing a Poorly Diffracting Frozen Crystal to a High Resolution Data Set.** Kris F. Tesh, A.L. Dowell, Joseph D. Ferrara, J.W. Pflugrath, Rigaku, The Woodlands, TX, Tel: (281) 363-1033, Fax: (281) 364-3628, www.Rigaku.com

One of the primary concerns in modern crystallography laboratories is to develop protocols for improving poorly diffracting crystals. Crystals are optimized by changing a number of parameters during crystallization (salt, buffer concentration, pH, additives, etc.). Additionally, post-crystallization techniques include replacing water with additives (PEG, sugars, salts), dehydrating in air or under oil, and cryo-annealing. Much of what is done today is not reproducible and lacks the ability to improve a very poor quality, mounted crystal. In the case of "bad" diffraction, the usual thought is to cut your losses and mount a new crystal; in the worst case, you go back and attempt to grow better crystals. But, this may not need to happen. If there is evidence of better diffraction from previous crystals, or if there are few options due to little available protein, you may wish to "heal" a crystal. The Free Mounting System (FMS) is used to carefully regulate and adjust the relative humidity about a mounted crystal, which changes the water content within the crystal. Previously flash-cooled crystals of very poor quality will be shown to improve as a result of FMS rescue and rehabilitation, even to the point of usable data.

**MP083 The Structural Biology Center User Program at the Advanced Photon Source, Argonne National Laboratory.** S. L. Ginell, R.W. Alkire, C. Chang, M.E. Cuff, N.E.C. Duke, G. Kazimierz, K. Tan, Y-C. Kim, K. Lazarski, J. Osipiuk, G. Rosenbaum, F.J. Rotella, R-G. Zhang, A. Joachimiak, Structural Biology Center, Biosciences, Argonne National Lab., Argonne, IL.

The Argonne's Structural Biology Center (SBC) operates a national user facility for macromolecular crystallography at sector 19 of the Advanced Photon Source. Both the 19ID and 19BM beamlines are equipped with high-resolution optics, Kappa goniostat, a low noise, large area CCD detectors, advanced software for data analysis, processing and structure determination, cryogenic sample cooling to a temperature of 10K and other equipment to enable the collection of best diffraction data on the most challenging projects. Presentation will highlight advances to the SBC beamlines including point and click sample alignment, auto-loop alignment, new fluorescence scanning, auto energy changes, crystal mounting robotics and advances found in HKL3000 our program for data processing through structure solution and model building in near real time. Some important and interesting highlights from the sector 19 xxx PDB and yyy publications during the past year will

be presented. Information on the user program and the sector 19 beamlines will be provided and can also be obtained from the SBC website ([www.sbc.aps.gov](http://www.sbc.aps.gov)).

This work is supported by the U.S. Department of Energy, Office of Biological and Environmental Research, under Contract DE-AC02-06CH11357.

**MP084 Advanced Crystal Imaging with the DETECT-X Microscope.** Peter Nollert<sup>1</sup>, Yiping Xia<sup>1</sup>, Werner Kaminsky<sup>2</sup>, Mark Mixon<sup>1</sup>, <sup>1</sup>Emerald BioSystems, Inc., Bainbridge Island, WA, <sup>2</sup>Dept. of Chemistry, Univ. of Washington, Seattle, WA.

We will show images that demonstrate the unique protein crystal imaging capabilities of the DETECT-X microscope, an automated polarization microscope that has white light trans-illumination and UV epi-illumination options. In its birefringence microscopy mode the DETECT-X microscope produces quantitative images of crystals depicting the orientation of the slow optical axis of protein crystals and their orientation-independent, quantitative birefringence. While low-birefringent plastic trays work particularly well for quantitative birefringence imaging, the DETECT-X imaging of protein crystallization trials may also be carried out in traditional plasticware devices.

The combination of oblique angle illumination, quantitative birefringence imaging and UV fluorescence microscopy allows the enhanced imaging of protein crystals with strong contrast originating from crystal facets as well as the interior body of the crystal. Colorless, transparent protein crystals appear colored with DETECT-X imaging. This enhanced contrast allows researchers to (i) observe protein crystals through a layer of precipitate, (ii) discern between amorphous precipitate and non-faceted sphaerulites or micro-crystalline matter, (iii) identify crystal twins, and (iv) distinguish between protein and salt crystals.

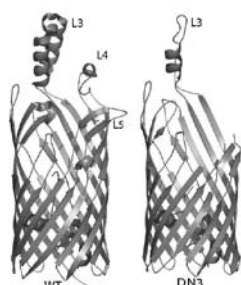
The basic DETECT-X (Difference Extinction for the Detection of Crystals) operation and image processing algorithms will be described together with the aforementioned imaging examples. It is anticipated that DETECT-X microscopy improved efficiencies in optical screening of protein crystallization trials.

This work was supported in part by the NIGMS-NCRR co-sponsored PSI-2 Specialized Center Grant for ATCG3D U54 GM074961, and an SBIR grant 1R43GM071183-02.

**SP085 Insights into Transport of Long Chain Fatty Acids Across the Outer Membrane by FadL.** Dimki R. Patel, Bert van den Berg, Univ. of Massachusetts Medical School, Program in Molecular Medicine, Worcester, MA.

Members of the FadL family are the only known proteins that transport hydrophobic compounds across the outer membrane (OM) of gram-negative bacteria. *E. coli* FadL is essential for the uptake of long-chain fatty acids (LCFAs). A model for LCFA transport across the OM was proposed based on crystal structures of *E. coli* FadL<sup>[1]</sup>. To test and further characterize the transport model, we generated several site-directed mutants of FadL, with the main focus on the proposed low and high affinity binding sites and the hatch domain<sup>[1]</sup>. We have successfully determined crystal structures of several mutant FadL proteins to resolutions of 3.0-3.6 Å ( $R_{\text{free}}$  values of ~29-34%), by molecular replacement with wild type FadL.

Two mutants with three and eight residue deletions in the N-terminus (DN3, DN8) have segments of missing density



for loops L4 (residues 236 to 266) and L5 (residues 300 to 322) (Figure). These loops comprise large parts of the low and high affinity LCFA binding sites in FadL. The results indicate that the LCFA binding sites become disordered upon deletion of the N-terminus, providing support for the hypothesis that conformational changes within the N-terminus of FadL lead to substrate release from the high affinity binding site<sup>[1]</sup>. Other mutants will be analyzed to elucidate the transport process in more detail.

[1] B. van den Berg, P. N. Black, W.M. Clemons, Jr., T.A. Rapoport. (2004) Crystal structure of the long-chain fatty acid transporter FadL. *Science* **304**, 1506-1509.

We thank staff at beamline X6A at the National Synchrotron Light Source for the collection of diffraction data. This research is supported by the National Institute of Health under award number RO1 GM074824-01.

**TP086 Structural Studies of Human Plasma Platelet Activating Factor Acetylhydrolase and Implication to its LDL-binding.** Uttamkumar Samanta, Brian J. Bahnson, Dept. of Chemistry and Biochemistry, Univ. of Delaware, Newark, DE, E-mail: [usamanta@udel.edu](mailto:usamanta@udel.edu), [bahnson@udel.edu](mailto:bahnson@udel.edu).

The plasma form of human platelet activating factor acetylhydrolase (pPAF-AH) functions by reducing PAF levels as a general anti-inflammatory scavenger and is linked to anaphylactic shock, asthma and allergic reactions. In addition to the role in reducing PAF levels, enzyme has also been implicated in hydrolytic activities of other pro-inflammatory agents, such as oxidized lipids. Physiologically, this enzyme is found associated to LDL particles and is considered an interfacial enzyme. Moreover, pPAFAH has been shown to be reactive with organophosphate insecticides and nerve agents. pPAFAH belongs to a subfamily of phospholipase A2 that removes the acetyl group at *sn*-2 position of phospholipids. Here we present the crystal structure of pPAFAH of molecular mass 42 KDa, a truncation of the 47 KDa form. The structure of this enzyme has been solved from data collected to resolution of 1.4 Å after SAD-phasing from the Hg-derivative data to 2.7 Å. It has a typical  $\alpha/\beta$  hydrolase fold and consists of a trypsin-like catalytic triad (S273, D296 and H351). C-terminus region is negatively charged due to the presence of an acidic patch and believed to be the potential force of binding to the LDL interface in human blood plasma, which drives catalytic activity of this enzyme. Complex structures of this enzyme after covalent modification of the active site Ser residue by organophosphates (para-oxon, sarin, soman and tabun) will also be discussed.

**TP087 Remediation of the PDB Archive.** J. Westbrook<sup>1</sup>, H.M. Berman<sup>1</sup>, L. Chen<sup>1</sup>, D. Dimitropoulos<sup>2</sup>, J. Doreleijers<sup>4</sup>, S. Dutta<sup>1</sup>, Z. Feng<sup>1</sup>, J. Flippen-Anderson<sup>1</sup>, O. Haq<sup>1</sup>, K. Henrick<sup>2</sup>, J. Ionides<sup>2</sup>, T. Kosada<sup>3</sup>, A. Kouranov<sup>1</sup>, C. Lawson<sup>1</sup>, J. Markley, H. Nakamura<sup>3</sup>, J. Ory<sup>1</sup>, H. Sun<sup>1</sup>, E.L. Ulrich<sup>4</sup>, S. Velankar<sup>2</sup>, W. Vranken<sup>4</sup>, H. Yang<sup>1</sup>, M. Yousufuddin<sup>1</sup>, Worldwide PDB (wwPDB), <sup>1</sup>RCSB PDB, Piscataway, NJ, USA, <sup>2</sup>MSD-EBI, Hinxton, UK, <sup>3</sup>PDBj, Osaka, Japan, <sup>4</sup>BMRB, Madison, WI, USA.

Members of the wwPDB – the RCSB PDB, MSD-EBI, and PDBj – have worked together to ensure the uniformity of entries archived in the PDB. The entire archive has been reviewed and remediated with the objectives of improving the detailed chemical description of non-polymer and monomer chemical components; standardizing atom nomenclature; updating sequence database references and taxonomies; resolving any remaining differences between chemical the macromolecular sequences; improving the representation of viruses; and verifying primary citation assignments.

Improvements in chemical description and nomenclature changes are documented in a revised Chemical Components Dictionary (formerly known as the “HET” dictionary). The major new features

of this dictionary include: addition of model and idealized coordinates; chemical descriptors (*e.g.* SMILES and InChI) and systematic names; stereochemical assignments; IUPAC nomenclature for standard amino acid and nucleotides; more conventional atom labeling; and removal of redundant ligands.

A complete release of remediated data files will occur in 2007 with a version number that separates it from the original data files.

We thank the funding agencies that support the wwPDB members ([www.wwpdb.org](http://www.wwpdb.org)): RCSB PDB (NSF, NIGMS, DOE, NLM, NCI, NCRR, NIBIB, NINDS); MSD-EBI (Wellcome Trust, EU, CCP4, BBSRC, MRC and EMBL); PDBj (BIRD-JST and MEXT); BMRB (NIH).

**TP088 Gene Duplication in the  $(\beta/\alpha)_8$  Barrel Family.** W.L. Duax, R. Huether, V. Pletnev, T. Umland, Q. Mao, S. Connare, C.M. Weeks, Hauptman-Woodward Medical Research Inst., Buffalo, NY, SUNY Buffalo, NY.

On the basis of crystal structure and protein sequence analysis of an enzyme involved in histidine biosynthesis (HisF) it was concluded that the  $(\beta/\alpha)_8$  barrel arose from the duplication and fusion of ancient half barrels. We have found that the HisF  $(\beta/\alpha)_8$  barrels appear to have evolved *via* sequential introduction of twelve amino acids (one at a time) at a single locus between the two halves of the duplicated  $\beta$ -barrel leading to the existence of 12 subgroups that differ in species distribution. We examined the genes of the 400  $(\beta/\alpha)_8$  barrels for the presence of alternate full-length open reading frames (ORFs). We found 23 genes with sense/antisense overlapping ORFs and eight genes with triple ORFs. When we compared the sequences of the two halves of the  $(\beta/\alpha)_8$  barrels with genes having multiple ORFs, an average of 22 amino acids aligned with no insertions, and an average of 17 of these had conserved wobble-base identity supporting the gene duplication hypothesis. Examination of these 31 genes revealed a GC codon and amino-acid triple bias similar to the bias that we previously found in short chain oxidoreductase enzymes and heat shock proteins. In one of these genes, the bias was so extreme that AT-only triples were completely absent, 96% of the coding was due to just 26 codons (all of which end in G or C), and 95% of the entire protein was composed of just 15 amino acids. The rare occurrence of certain amino acids (MYQCW) is consistent with the frequency of occurrence of these residues in the proteins of *Streptomyces coelicolor*. Further analysis of gene duplication in families of ancient proteins may make it possible to trace the evolution of the genetic code to its origin.

This work is supported by NIH Grant No. DK26546

**TP089 Towards a Statistical Framework for Structure Comparison.** T.R. Schneider<sup>1,2</sup>, B. Brannetti<sup>2</sup>, R. Mosca<sup>1,2</sup>, <sup>1</sup>EMBL Hamburg, Hamburg, Germany; <sup>2</sup>FIRC Inst. of Molecular Oncology, Milan, Italy.

The comparison of structures is a central step in extracting information from structural models. As the coordinate uncertainties in macromolecular structures can vary from 0.01 Å for a well-defined atom in a high-resolution structure to more than 1 Å for a mobile atom in a low-resolution structure, the similarity of models should be measured taking coordinate uncertainties into account.

We suggest to use the fraction of distances that remain identical within experimental uncertainty in an ensemble as a criterion for structural similarity. We define a conformational similarity index 'C.S.I.' as  $C.S.I. = n_{id} / n_{all}$  (where  $n_{id}$  and  $n_{all}$  are the number of equivalent distances that are identical within error and the total number of equivalent distances, respectively). The C.S.I. uses a crude error model based on Cruickshank's DPI<sup>[1]</sup> and can be used (1) to evaluate

the overall similarity of structures and (2) as a criterion to find subsets of atoms that are rigid within experimental uncertainty.

We demonstrate the approach by analyzing the ensemble consisting of crystal structures of protein kinase A as available from the protein data bank. This ensemble contains more than 40 models of the enzyme crystallized in different space groups, with different ligands etc. and shows estimated mean coordinate uncertainties ranging from less than 0.05 Å to more than 0.5 Å. C.S.I.-driven clustering of the models followed by an analysis in terms of rigid bodies divides the protein into the two well-known domains plus some smaller rigid regions and provides an objective basis for superposition and further detailed analysis. A computer program implementing the ideas presented is available from TRS.

[1] D. Cruickshank, *Acta Cryst*, D55, 583 (1999).

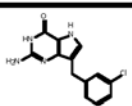
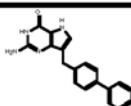
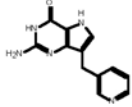
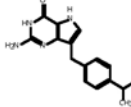
**TP090 Defining the Protein Structure: Mining the Redundant Structure Database.** B. Stec, Y. Zhang, B.V.L.S. Prasad, A. Godzik, The Burnham Inst. for Medical Research, La Jolla, CA.

Rapid increase of structural information allows for rigorous studies of structural context of function. In order to define natural variations in a single crystal structure and differences between protein architectures we have constructed a redundant data-base by clustering the available structures from the PDB at 100% sequence identity. As the first task we analyzed the sequence preferences in the elements that have incomplete representation in the atom records called by us Dual Personality sequences. We show that such fragments have distinctive features that differentiate them both from regularly folded and intrinsically disordered fragments. We showed, that such fragments are often targets of regulation, either by allostery or post-translational modifications. In association with sequence preferences we show that as protein sequence grows longer the structural state that is uniquely associated with it is less and less defined. We find significant variations in a single protein architecture that shows several convergent basins. We are studying the association of the structural variations with functional states like binding of substrates or exposing signaling surfaces. We will review the natural variability of structure and its consequences for defining functional states and their presence as associated with different protein architectures.

**SP091 Structure-activity Relationships and Mechanism Studies for a Series of Inhibitors of Purine Nucleoside Phosphorylase from *Schistosoma mansoni*.** Matheus P. Postigo, Marcela F. Terni, Glaucius Oliva, Adriano D. Andricopulo, Center for Molecular Structural Biotechnology, Inst. of Physics of São Carlos IFSC-USP.

Schistosomiasis is a tropical disease which affects about 300 million people around the World. The lack of effective treatments for schistosomiasis has been stimulating the search for new attractive biological targets as well as promising molecules for drug research. Parasite enzymes are attractive targets for drug discovery. The enzyme purine nucleoside phosphorylase (PNP, EC 2.4.2.1) from *Schistosoma mansoni* is an important target for the development of new chemotherapeutic agents. In presented work, we describe the results of the development of structure-activity relationships (SAR) for a set of inhibitors of *S. mansoni* PNP. The set of PNP inhibitors examined is 9-substituted-9-deazaguanines.  $IC_{50}$  values were measured employing inosine as substrate and a UV spectrophotometric assay. Table 1 shows 4 PNP inhibitors and the respective potency values. Inhibition mechanism was established by plotting  $1/v_0$  vs.  $1/[S]$ , revealing competitive mechanism for all compounds. A molecular modeling study was carried out using the

**Table 1:** Biologic potency of SmPNP inhibitors.

Inhibitor	IC <sub>50</sub> (nM)	Inhibitor	IC <sub>50</sub> (nM)
	498		100
	797		150

docking programs GOLD and FlexX, and shows the interactions between ligand and active site.

Studies of potency and mechanism of the compounds reveal a promising set of drug candidates for schistosomiasis chemotherapy. Molecular modeling provides the understanding of interactions between enzyme and ligand. This information, allied to QSAR models should be useful for design of new structurally related SmPNP inhibitors, more potent and selective.

**TP092 Clustering Proteins Based on Substrate Identification Loops.** Robert Huether, David Parish, Qilong Mao, William Duax, Hauptman-Woodward Inst., Buffalo, NY, SUNY Buffalo, NY.

Short chain oxidoreductase enzymes play a critical role in the body to maintain key metabolic processes for sugars and steroids. There are over 10,000 identified within the GenBank and 65 identified within the human genome alone. Their similar Rossmann type fold easily identifies the proteins but the substrates that bind the proteins are unknown. Two proteins in this family that bind the same substrate can have very low sequence homology between them. This makes substrate identification by homology very difficult. We have identified 3 hypervariable loops that are mainly responsible for substrate interaction and identification. Using a clustering algorithm focused on the loops of the enzymes that identify the substrate, we have been able to group proteins with similar substrates that were previously unable to group based on sequence alone.

The work is supported by NIH Grant No. DK26546.

**TP093 Purification, Crystallization and Preliminary X-ray Analysis of an *Arabidopsis* Chloroplastic Glutaredoxin.** Lenong Li<sup>1</sup>, Ninghui Cheng<sup>2</sup>, Xiaoqiang Wang<sup>1</sup>, <sup>1</sup>Plant Biology Div., Samuel Roberts Noble Foundation, Ardmore, OK, <sup>2</sup>Plant Physiology Group, USDA/ARS Children's Nutrition Research Center, Dept. of Pediatrics, Baylor College of Medicine, Houston, TX.

Glutaredoxins (Grxs) are ubiquitous small heat-stable disulfide oxidoreductases and catalyze the reduction of protein disulfides and of glutathione (GSH)-protein mixed disulfides via a dithiol or monothiol mechanism. Grxs are involved in many cellular processes and play important roles in protecting cells against oxidative stresses. In plants, there are a large Grx gene family, but only a few have been studied. AtGRXcp from *Arabidopsis thaliana* was identified as a member of the monothiol Grxs, contains a conserved putative active motif "CGFS", and may protect plant cells against protein oxidative damage. The AtGRXcp gene was cloned into pET-41a (+) vector and expressed in *E. coli* strain BL21 (DE3). The protein was purified to homogeneity using a GraviTrap affinity column and superdex 75 column, and the GST tag was cleaved by incubation with enterokinase. Crystallization screens were carried out by hanging-drop vapor diffusion method at 20°C, and crystals were obtained in 0.1 M MES pH 6.5, 1.6 M ammonium sulfate, and 10% dioxane. X-ray analysis and structural determination are in progress. The structural study of

AtGRXcp may provide a basis to understand the structure-function relationships within this class of enzymes, and elucidate the mechanism of protecting protein oxidation during plant stress conditions.

**TP094 Gene Composer for Gene Design and Pcr-based Gene Synthesis.** Mark Mixon, Laurelin Ward, Don Lorimer, John Walchli, Kai Post, Alex Burgin, Rena Grice, Adrian Metz, Lance Stewart, Peter Nollert, deCODE biostructures, Inc., Bainbridge Island, WA.

With the goal of improving success rates for eukaryotic protein expression and crystallization, we are developing Gene Composer software to facilitate the information-rich design of protein constructs, their respective nucleic acid coding sequences and expression vectors. The Protein Design Module distills protein structure information from PDB files and comparative sequence information into an interactive alignment viewer. This graphical user interface allows the researcher to simultaneously visualize sequence conservation in the context of known protein secondary structure, ligand contacts, water contacts, crystal contacts, B-factors, solvent accessible area, residue property type and several other property views. The Gene Design Module automates the back-translation of a protein amino acid sequence into a codon-optimized nucleic acid sequence, which can be handed off to be synthesized. The Construct Design Module allows the user to define termini, make insertions or deletions, change residues, add tags, define cloning sites and finally permute those constructs and virtually clone them into one or multiple expression vectors of choice. Using this procedure, Gene Composer will generate all primers and mutagenic oligonucleotides necessary to perform all corresponding wet-lab procedures.

We will present each of the Gene Composer modules and a detailed protocol for PCR-based gene synthesis from designed oligonucleotides.

This work is supported in part by the NIGMS-NCRR co-sponsored PSI-2 Specialized Center Grant for ATCG3D U54 GM074961, and Johnson & Johnson Pharmaceutical Research & Development LLC.

**TP095 Inference of Experimental Structure Determination from Protein Characteristics: Searching for Predictors in Sequence Space.** O. Kirillova, M. Grabowski, W. Minor, Dept. of Molecular Physiology and Biological Physics, Univ. of Virginia, Charlottesville, VA.

In recent years, genome sequencing techniques have vastly increased the number of known protein sequences and families. Currently, there are close to 4 million sequences in the SwissProt/TrEMBL databases and almost 9000 protein families in the Pfam-A database. On the other hand, the Protein Data Bank (PDB) contains representative structures from about 3800 Pfam families. One of the aims of the second phase of Protein Structural Initiatives is to extend the structural coverage of Pfam families. We investigated correlations between properties of Pfam protein families and the presence or absence of a structural representative in each family. In particular, we examined distributions of short fragments in sequence data taken from the Pfam and PDB databases. We have found that fragments, consisting of repeats of all polar or all non-polar as well as all aliphatic residues are more common in Pfam families for which the structure has not been determined than for families represented in PDB. Hence, an over-representation of fragments of contiguous polar and aliphatic residues could be considered as a negative predictor for success in experimental structure determination.

This research is supported by NIH PSI grant GM074942.

**SP096 Structure - Function Study of the Finger Domain of Y Family DNA Polymerases in Translesion DNA Synthesis.**

Kevin Kirouac, Hong Ling, Dept. of Biochemistry, Univ. of Western Ontario, London, ON, Canada.

Human DNA polymerase eta and iota are both Y family polymerases that specialize in bypassing DNA lesions with vast differences in specificity and nucleotide incorporation. The finger domain of these polymerases contains a loop region, which contacts the incoming nucleotide and the template DNA. This region is highly variable between Y family polymerases and has virtually no sequence conservation, hinting at a possible role in the different enzymatic properties of these polymerases. Chimeric finger domain proteins were created using PCR to investigate the role of this domain in lesion specificity and nucleotide incorporation. The finger domain of Y family polymerase Dpo4 from archaea was replaced with the finger domain from human polymerase eta and iota. Functional and structural comparisons of the chimeric proteins with their native counterparts will be examined to determine the role of the finger domain. Primer extension assays revealed that the chimeric Dpo4-Iota protein adopted the nucleotide incorporation pattern of human polymerase iota on undamaged DNA. The same was not observed for the chimeric Dpo4-eta protein, which retained the same incorporation trend as Dpo4. Both chimeric proteins did not adopt the lesion specificity of the human polymerases or the nucleotide incorporation on damaged DNA. This suggests that the finger domain plays different roles in Y family polymerases and likely co-ordinates with other domains to determine the nucleotide incorporation on damaged DNA. Structural comparison of these proteins is currently underway.

**TP097 Crystal Structure of the Proteasome Activator Blm10 with 20S Proteasome from Yeast.**

Kianoush Sadre-Bazaz, Frank Whitby, Katherine Ferrell, Howard Robinson\*, Timothy Formosa, Christopher Hill, Dept. of Biochemistry, Univ. of Utah, \*National Synchrotron Light Source, Brookhaven NY.

Three classes of proteasome activators regulate its function: ATP-dependent proteasome activators unfold their protein substrates and passage them into the catalytic core of the 20S protease. ATP-independent activators include the 11S family and PA200, which allow passage of small peptides. Co-crystal structure of the yeast (*S. cerevisiae*) homologue of PA200, Blm10, with 20S proteasome will be presented at medium resolution

Several crystal forms of Blm10/20S have been obtained and the structure was solved by molecular replacement using yeast 20S proteasome as a model. Blm10 is a single polypeptide chain of 2143 residues. The structure shows that Blm10 binds to 20S proteasome in a two to one molar ratio with each Blm10 molecule occupying each cap of the core protease. Blm10 occupies a unique position when bound to the 20S proteasome. This is also evident of the fact that eukaryotic proteasomes have pseudo seven fold symmetries. The structure is consistent with the 18Å cryo-EM reconstruction of the complex, where the orientation of the 20S was determined in the Blm10-bound state. Blm10 is composed of a series of repetitive helix-turn-helix motifs known as HEAT repeats. HEAT repeats consensus are typically forty residues, however in Blm10, numerous repeats are atypical with varying length of loops and helices. Overall, these motifs are folded to form an alpha solenoid resembling the shape of a dome with a hollow core. A challenging task has been assigning sequence to Blm10 at medium resolution. Heavy atom markers, especially those of mercury, have been helpful in accomplishing this task. Biochemical data supports an open gated 20S proteasome in the bound state with Blm10, however the crystal structure supports a closed gate. This can be explained by the fact that Blm10/20S crystals take as long as months to grow and the complex can be shown to

114

loose activity with time. More will be speculated about the possible function of Blm10 and what the structural information predicts.

**TP098 The Bases for the cCF10 and iCF10 Functional Differences.**

Ke Shi<sup>1</sup>, Heather A. Haemig<sup>2</sup>, Gary M. Dunny<sup>2</sup>, Douglas H. Ohlendorf<sup>1</sup>, Cathleen A. Earhart<sup>1</sup>, <sup>1</sup>Dept. of Biochemistry, Molecular Biology and Biophysics and <sup>2</sup>Dept. of Microbiology, Univ. of Minnesota, Minneapolis MN.

PrgX, a key player in controlling conjugation induced by the peptide pheromone cCF10 in *Enterococcus faecalis*, is the cytoplasmic receptor for the cCF10 peptide pheromone and has been shown to bind to two sequences in the intergenic region of pCF10 between *prgX* and *prgQ* (the *prgQ* operon encodes the conjugative transfer functions of pCF10). cCF10 and iCF10 have very similar chemical composites (both are heptapeptides), but have complete different biological function. The structure of the PrgX/cCF10 complex reveals that pheromone binds in the cleft of the central dimerization domain, causes the C-terminal regulatory domain rotates about 120°. The amino acids 296-298 form a short  $\beta$ -strand interacting with cCF10. Amino acids 304-317 in either the PrgX or PrgX/cCF10 structures are mobile and invisible. iCF10 is a plasmid-encoded peptide competitor of cCF10. iCF10 binds in the pheromone-binding pocket the same way as cCF10. The C-terminal domain in PrgX/iCF10 complex keeps the same conformation as in uncomplexed PrgX. Amino acids 304-315 have clear electron density in the PrgX/iCF10 complex and amino acids 302-304 form a short  $\beta$ -strand interacting with iCF10. cCF10 (LVTLVFV) and iCF10 (AITLIFI), having complete opposite biological functions, have four amino acids that are different. However, their hydrogen bonding interactions with PrgX are very similar. We systematically mutate the cCF10 to study the key amino acid(s) differentiating iCF10 from cCF10. The results will be presented.

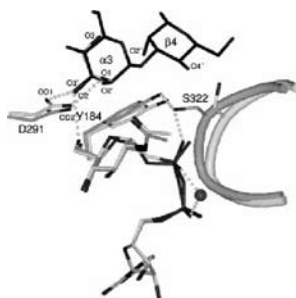
**SP099 Mechanism of the Enzymatic Production and Degradation of Cyclic ADP-ribose by Human CD38.**

Qun Liu<sup>1</sup>, Quan Hao<sup>1</sup>, Irina A. Kriksunov<sup>1</sup>, Richard Graeff<sup>2</sup>, Cyrus Munshi<sup>2</sup>, Hon Cheung Lee<sup>2,3</sup>, <sup>1</sup>MacCHESS, Cornell High Energy Synchrotron Source, Cornell Univ., Ithaca, NY, <sup>2</sup>Dept. of Pharmacology, Univ. of Minnesota, Minneapolis, MN, <sup>3</sup>Dept. of Physiology, Univ. of Hong Kong, Hong Kong, China.

Cyclic ADP-ribose (cADPR) is a calcium mobilization messenger important for mediating a wide range of cellular and physiological functions. The endogenous levels of cADPR in mammalian tissues are primarily controlled by CD38, a multifunctional enzyme capable of synthesizing and hydrolyzing cADPR. To structurally understand how this single enzyme works toward the generation and degradation of cADPR, we determined crystal structures for the enzyme complexed with cADPR and its analogs. The results indicate that both the enzyme and cADPR undergo catalysis associated conformational changes, providing the first direct evidence of conformational changes at the active site during cADPR catalysis. From the enzyme side, dipeptide Glu146-Asp147, residues Arg127 and Trp125 work collaboratively to facilitate the formation of the Michealis complex. From the substrate side, cADPR is found to first bind to an intermediate site 6.12 Å from Glu226, and then dynamically changes its conformation to fit into the active site until it reaches the catalytic residue. The binary CD38/cADPR model described in our study represents the most detailed characterization of CD38 controlled cADPR catalysis. Structural details obtained from these complexes provide a step-by-step description of the catalytic processes in the synthesis and hydrolysis of cADPR. Our structural model should provide insights into the design of effective cADPR analogs as clinical tools.

**TP100 X-ray Crystal Structures of Rabbit N-acetylglucosaminyltransferase I (GnT I) in Complex with Donor Substrate Analogues.** Roni D. Gordon, Prashanth Sivarajah, Malathy Satkunarajah, Dengbo Ma, Chris A. Tarling, Dragos Vizitiu, Stephen G. Withers, James M. Rini, Dept. of Biochemistry, Univ. of Toronto, Toronto, ON, Canada.

The Golgi-resident glycosyltransferase, UDP-*N*-acetyl-D-glucosamine:α-3-D-mannoside β-1,2-N-acetylglucosaminyltransferase I (GnT I), initiates the conversion of high-mannose oligosaccharides to complex and hybrid structures in the biosynthesis of N-linked glycans. Reported here are the X-ray crystal structures of GnT I in complex with UDP-CH<sub>2</sub>-GlcNAc (a non-hydrolyzable C-glycosidic phosphonate), UDP-2-deoxy-2-fluoro-glucose, UDP-glucose and UDP. Collectively, these structures provide evidence for the importance of the GlcNAc moiety and its *N*-acetyl group in donor substrate binding, as well as insight into the role played by the flexible 318-330 loop in substrate binding and product release. In addition, the UDP-CH<sub>2</sub>-GlcNAc complex reveals a well-defined glycerol molecule poised for nucleophilic attack on the C1 atom of the donor substrate analogue. The position and orientation of this glycerol molecule have allowed us to model the binding of the Manα1,3Manβ1 moiety of the acceptor substrate and, based on the model, to suggest a rationalization for the main determinants of GnT I acceptor specificity.



**TP101 The Enolase in the Methionine Salvage Pathway in *Geobacillus kaustophilus*: Crystal Structure and Function.** A. Fedorov<sup>1</sup>, H. Imker<sup>2</sup>, E. Fedorov<sup>1</sup>, J. Gerlt<sup>2</sup>, S. Almo<sup>1</sup>. <sup>1</sup>Dept. of Biochemistry, Albert Einstein College of Medicine, Bronx, NY, <sup>2</sup>Depts. of Biochemistry and Chemistry, Univ. of Illinois at Urbana-Champaign, Urbana, IL.

D-Ribulose 1,5-biphosphate carboxylase/oxygenase (RuBisCO), the most abundant enzyme, is the paradigm member of the recently recognized mechanistically diverse RuBisCO superfamily. The heterofunctional homologue of RuBisCO found in *Geobacillus kaustophilus* catalyze the enolization of 2,3-diketo-5-methylthiopentane 1-phosphate in the methionine salvage pathway. Because the RuBisCO and the enolase – catalyzed reactions differ we sought to establish structure-function relationships for the enolase reaction. The crystal structures of the activated enolase (carboxylated on Lys 173) and enolase liganded with Mg and 2,3-diketo-hexane, a stable alternate substrate, were determined. The stereochemical course of the reaction catalyzed by the enolase was determined using stereospecifically deuterated samples of an alternate substrate. On the basis of these experiments we conclude that the enolase, the functionally divergent member of the RuBisCO superfamily uses the same structural strategy as RuBisCO for stabilizing the enolate anion intermediate, but the proton abstraction is catalyzed by a different general base.

**TP102 High Throughput Screening of Crude Natural Product Extracts: The Search for Novel Human Alpha-Amylase Inhibitors.** G.D. Brayer, C.A. Tarling, R. Zhang, H.C. Brastianos, R.A. Keyzers, C. Li, K. Woods, R.J. Andersen, S.G. Withers, Departments of Biochemistry and Molecular Biology, and Chemistry, Univ. of British Columbia, Vancouver, Canada.

The incidence of diabetes and obesity is increasing at an alarming

rate. Beyond the reduced quality of life and life expectancy experienced by these patients, is a worrisome list of additional health risks associated with these chronic diseases. Human pancreatic alpha-amylase (HPA) provides a unique opportunity for the development of potential therapeutics for both of these conditions. This enzyme is central to the process of starch digestion in foodstuffs and physiologically correlated to post-prandial blood glucose levels, the control of which is an important factor in diabetes and obesity. Although much sought after, identification of HPA inhibitors has proven an elusive goal and those currently available bind non-specifically to a wide range of glucosidases, limiting their effectiveness and leading to undesirable side effects. Recently, we have developed a new high throughput screening approach for the discovery and subsequent structural elucidation of oligosaccharide-based inhibitors for HPA, based upon auto-glycosylation. To widen our search for novel HPA inhibitors we have applied this high throughput screening approach to natural product methanol extracts collected from plants and marine organisms from around the world. To this point nearly 48,000 crude extracts have been analyzed, leading to the discovery of novel classes of HPA inhibitors that are being identified and characterized using a combination of biochemical and X-ray crystallographic approaches.

Supported by the Canadian Institutes of Health Research.

**SP103 Crystal Structures of Fms1 in Complex with Polyamine Analogues.** Q. Huang, Q. Hao, MacCHESS, Cornell High Energy Synchrotron Source, Cornell Univ., Ithaca, NY.

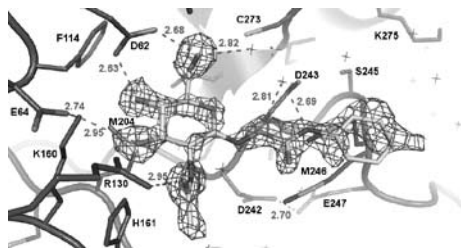
Polyamine oxidase is involved in the metabolism of polyamines which are regulators of essential processes such as cell growth, proliferation and differentiation. Moreover, H<sub>2</sub>O<sub>2</sub>, one product of the oxidation of polyamine catalyzed by polyamine oxidase, is also involved in many important biological processes. Therefore, selective inhibitors of polyamine oxidase are starting points for the development of novel drugs such as antineoplastic drugs. Studying the interaction between polyamine oxidase and polyamine analogues is helpful in design and discovery of selective inhibitors of polyamine oxidase. Here, we report the crystal structures of Fms1 (a polyamine oxidase from yeast) in complex with several polyamine analogues, 1,8-diaminooctane, MDL72527 and bis(hexamethylene)triamine. To our surprise, the polyamine analogue bis(hexamethylene)triamine, a possible inhibitor of Fms1 suggested by the crystal structure of Fms1 in complex with its native substrate spermine<sup>[1]</sup>, is in fact a good substrate. Comparison the structures of Fms1-spermine complex and Fms1-bis(hexamethylene)triamine complex shows that the active site of Fms1 is a very long channel, and spermine locates at the entry of the channel while bis(hexamethylene)triamine locates at the exit of the channel. In the channel, spermine and bis(hexamethylene)triamine have only a little overlap near the catalytic site of FAD.

[1] Q. Huang, Q. Liu & Q. Hao (2005) *J. Mol. Biol.* **348**, 951-959.

**SP104 Structural Analysis of the *Vibrio Cholerae* β-glucosaminidase NagZ in Complex with PUGNAc.** M. Balcewich<sup>‡</sup>, K. Stubbs<sup>‡</sup>, D. Vocadlo<sup>‡</sup>, B. Mark<sup>‡</sup>, <sup>‡</sup>Dept. of Microbiology, Univ. of Manitoba, Winnipeg, MB, Canada, <sup>†</sup>Dept. of Chemistry, Simon Fraser Univ., Burnaby, BC, Canada.

NagZ is a family 3 β-glucosaminidase that is involved in remodeling of the bacterial cell wall. It is a cytosolic enzyme that removes terminal N-acetylglucosamine residues from internalized cell wall degradation intermediates, producing a pool of 1,6-anhydroMurNAc-oligopeptides that are subsequently recycled into UDP-MurNAc pentapeptides and reincorporated into the cell wall. In the presence of β-lactams, destabilization of the cell wall causes a flood of cell wall intermediates into the cytosol where NagZ quickly over-

produces 1,6-anhydroMurNAc-oligo-peptides capable of inducing the expression of the  $\beta$ -lactamase gene *ampC*. We have determined the three-dimensional structure of *Vibrio cholerae* NagZ in complex with PUGNAc by molecular replacement (using PDB 1TR9 as a search model). PUGNAc is a potent (Ki 0.048  $\mu$ M) and fairly selective NagZ inhibitor. The MR solution revealed Fo-Fc electron density that could only be ascribed to PUGNAc bound within the active site. From this crystal structure, we noted that beneath the 2-acetamido methyl group of the inhibitor there exists a large open pocket. This pocket contrasts with the active site architecture of human family 20 hexosaminidases that remove terminal hexosamine residues from GM2-gangliosides. The family 20 enzymes instead form a tight envelope around the 2-acetamido group, holding it in a strained position to participate as a nucleophile during substrate-assisted catalysis. This structural difference suggests that extensions off the 2-acetamido group of PUGNAc would confer high inhibitor selectivity toward family 3  $\beta$ -glucosaminidases over those functionally related enzymes from other families.



**TP105 The Effect of a Polarized Medium on Hydrogen Bond Energies in Myoglobin.** R.F. See, Thomas A. Baker, C. Evans, M.L. Goodbread and S.M. McCollister, Dept. of Chemistry, Indiana Univ. of Pennsylvania, Indiana, PA.

The effects of a polar medium on the energies of hydrogen bonds between imidazole and a ligand-metalloporphyrin complex were investigated by molecular orbital calculations at the B3LYP/LACVP\* level. A hydrogen bond from imidazole to Fe-bound  $O_2$  may be an important factor in the stabilization of  $O_2$ , relative to  $CO$ , in the active site of myoglobin. The gas-phase hydrogen bond energy in the complex  $im \cdots Fe(por)(im)(L)$  was calculated to be 37 kJ/mol when  $L = O_2$ , and about 18 kJ/mol when  $L = CO$ ; this difference in gas-phase hydrogen bond stabilization energy ( $\sim 19$  kJ/mol) is too large for the observed effect of the protein on ligand binding. However, gas-phase calculations may not be entirely realistic for the active site of a protein. SCI-PCM is a technique that allows the effect of a polar medium to be included in a molecular orbital calculation. Since SCI-PCM calculations are not feasible for metal-containing species, stand-in molecules for the ligand-Fe-heme system were used, such as water, urea and SO. These calculations indicate that the hydrogen bond energy decreases with increasing background polarity, the magnitude of this reduction ranging from 20-45% for a background medium with a dielectric value of 10. The implications of these results for ligand stabilization in myoglobin will also be discussed.

**TP106 Crystal Structure of a Spontaneously Damaged Protein: Succinimide Residue Formation in Thiamin Pyrophosphokinase.** I. Vorontsov, G. Minasov, O. Kiryukhina, L. Shuvalova, W.F. Anderson, Dept. of Molecular Pharmacology and Biological Chemistry, Northwestern Univ., Feinberg School of Medicine, Chicago, IL.

Proteins can undergo a number of reactions that result in chemically modified forms with damaged activity or function. One of these modifications is Aspartyl dehydration and Asparagine deamidation that occur through nucleophilic attack of the side chain by the main

chain nitrogen atom. These reactions represent a major type of covalent damage in proteins. The reaction results in formation of the L-Succinimidyl (L-Suc) intermediate that can be followed by its spontaneous hydrolysis back to a normal L-Asp or to an abnormal L-IsoAsp residue. Aspartyl isomerization may affect the activity of an enzyme and seriously complicates its degradation. We present a crystal structure of *Bacteroides thetaiotaomicron* Thiamin Pyrophosphokinase (TPK) which contains an L-Suc residue at the position of Asp38. TPK catalyzes the direct pyrophosphorylation of thiamin with ATP to form Thiamin Pyrophosphate (TPP) – a crucial cofactor in the energy yielding catabolic pathways that produce ATP, NADH and NADPH. The observed L-Suc damage in TPK occurs in the active center of the enzyme. Yeast, mouse and human TPKs contain the same structurally and sequentially preserved active site and might suffer the same damage. Isoaspartyl damage of TPK could play a role in the TPP production deficiency detected in Alzheimer's disease. The possibility exists for the same type of covalent damage in critical TPP-dependent enzymes such as Transketolase and  $\alpha$ -Ketoglutarate dehydrogenase.



We thank LS-CAT and DND-CAT for access to beamlines 21 and 5. This research is supported by National Institute of Health through Midwest Center for Structural Genomics.

**TP107 Cross-reactivity of TCR A6 on Haptenated HTLV-1 Tax<sub>11-19</sub> Peptides Presented by HLA-A2.** Oleg Y. Borbulevych, Brian M. Baker, Dept. of Chemistry and Biochemistry, Univ. of Notre Dame, Notre Dame, IN.

Antigen recognition by the T cell receptor (TCR) is initiated by molecular contact between the TCR and the peptide/MHC complex, which leads to an intracellular signaling cascade resulting in a functional response by the T cell. Although antigen specificity is a distinct feature of the adaptive immune response, a growing number of evidences indicates that TCRs can bind and respond to structurally diverse antigens. Particularly, it has been found that the HTLV-1 Tax<sub>11-19</sub>-specific TCR A6 can cross-reactively recognize several haptenated Tax<sub>11-19</sub> peptides presented by the class I MHC molecule. In these haptenated peptides Tyr5 is substituted by lysine covalently attached to 3-indolyl-butyric acid (IBA) or 3-indolyl-carbonic acid (ICA). However the exact molecular mechanism underlying the cross-reactivity of A6 TCR has not been understood.

To unravel the structural details underlying molecular recognition of the haptenated peptide, we determined the crystal structures of MHC/Tax(Y5K-hapten) and their complexes with TCR A6. The recognition involves cooperative conformational changes for both the peptide and TCR A6. Particularly, the IBA moiety of the haptenated peptide, which is highly flexible and disordered in the unbound state, becomes ordered in the complex and adopts a "folded" conformation allowing this side chain to occupy the same pocket in the A6 interface as occupied by Tyr5 in the native structure. Interestingly, the carbonyl-amide moiety of Lys5-IBA is highly complementary to the Arg95-Gly97 region of the A6 CDR3 $\beta$  loop, which might play an essential role in recognition. Furthermore, an accommodation of the bulk Lys5-IBA side chain also requires a considerable rearrangement of the CDR3 $\beta$  loop as well as a slight shift of V $\alpha$ /V $\beta$  domains of TCR A6.

**TP108 Crystal Structure of the >470 myo Common Ancestor to the Mineralocorticoid - Glucocorticoid Receptor: Evolution by Architectural Epistasis.** Eric A Ortlund<sup>1</sup>, Jamie T Bridgham<sup>2</sup>, Doug M Ormoff<sup>1</sup>, Jason Bischof<sup>1</sup>, Matthew R Redinbo<sup>1</sup>, Joe W. Thornton<sup>2</sup>, <sup>1</sup>Dept. of Chemistry, Univ. of North Carolina - Chapel Hill, Chapel Hill, NC, <sup>2</sup>Center for Ecology and Evolutionary Biology, Univ. of Oregon, Eugene, OR.

Changes in gene sequence drive the evolution of protein function by modifying three-dimensional structure. Understanding of the structural basis for the evolution of protein functions has been limited; however, because ancestral structures have not been available. As a result, most insights have been circumstantial, inferred from comparisons of extant protein structures or predictions based on homology models that use extant structures as backbones. Here we report the first crystal structures of a resurrected ancestral protein, the common ancestor of all present-day glucocorticoid receptors, in complex with aldosterone, cortisol, and 11-deoxycortisol. This common ancestor existed before the divergence of the aldosterone-insensitive GR of bony vertebrates from the aldosterone-sensitive GR of cartilaginous fishes. By combining phylogenetic, functional, and crystallographic analysis, we identify strong epistatic interactions between sites in the sequence, such that the functional effect of a substitution depends on the background at other sites; we show that evolution proceeded by permissive combinations of mutations, and the structural cause of this epistasis is architectural: substitution at one site radically repositions another, setting the stage for functional shifts caused by a mutation at the second site.

**SP109 Metallosubstrate Oxidation and Oxygen Reduction Mechanism in the Multicopper Oxidase CueO.** Satish Singh<sup>1</sup>, Sylvia Franke<sup>2</sup>, Andrzej Weichsel<sup>1</sup>, Sue A. Roberts<sup>1</sup>, Christopher Rensing<sup>2</sup>, William R. Montfort<sup>1</sup>, Depts. of <sup>1</sup>Biochemistry and Molecular Biophysics, and <sup>2</sup>Soil, Water, and Environmental Science, Univ. of Arizona, Tucson, AZ.

Multicopper oxidases (MCO) couple the oxidation of a variety of substrates to the reduction of dioxygen to water ( $O_2 + 4e^- + 4H^+ \rightarrow 2H_2O$ ). Substrates bind near a T1 copper and transfer electrons through the T1 copper on to the trinuclear center formed by two T3 and one T2 copper, where oxygen binds and is reduced to water. The structures of the catalytic cycle intermediates are not known but are key to understanding the mechanism of oxygen reduction. We have expressed and solved the crystal structure of CueO, a MCO that confers tolerance to copper toxicity in *E. coli*. CueO crystals diffract to resolutions greater than 2Å and are catalytically active making it possible to trap functional states in the crystal and solve their structures. We have solved the structures of the resting oxidized and the fully reduced forms of CueO, the two functional states of CueO other than the two oxygen reduction intermediates.

The *in-vivo* substrate and the mechanism by which CueO protects against copper toxicity are not known. We have steady state kinetic measurements establishing Cu(I) as the best substrate for CueO. CueO crystal soaked in Cu(I) led to a 2Å structure clearly displaying three Cu(I) binding near the active site along the methionine rich helix. One of these Cu(I) ions occupies the previously identified regulatory copper site while the other two Cu(I) ions bind along the methionine rich helix using thioether ligation. The metallosubstrate binding site undergoes a change in coordination environment upon Cu(I) substrate oxidation to Cu(II) product. These data suggest that the functional role of CueO includes removal of toxic Cu(I).

**TP110 Crystallographic Pitfalls in Structure Based Drug Design.** A. Heine, H. Steuber, B. Stengl, V. Honndorf, G. Klebe, Dept. of Pharmaceutical Chemistry, Philipps-Univ. Marburg, Marburg, Germany.

Protein structure determination by X-ray crystallography is a fundamental tool in structure based drug design. Here, crystallographic studies are the basis for further design strategies of novel leads and are also used to validate *in silico* approaches. Therefore, crystal structures obtained are often considered the ultimate truth when investigating detailed protein-ligand binding interactions without taking experimental details into consideration. However, different crystallization or ligand soaking conditions can reveal unexpected structural changes such as different binding modes for the same ligand, space group transitions or additional novel metal binding sites as observed in aldose reductase, t-RNA-guanine transglycosylase (TGT) or carbonic anhydrase II. Here, some of these recent examples from our laboratory will be discussed.

**TP111 A Comparison of the Ligand Binding Domain of Two Nuclear Hormone Receptors, Both in the Absence of Ligands.** Ross Reynolds<sup>1,2</sup>, Schoen Kruse<sup>1</sup>, Jennifer Kretschmer<sup>3</sup>, Eric Xu<sup>1</sup>, <sup>1</sup>Van Andel Inst., <sup>2</sup>Grand Valley State Univ., <sup>3</sup>Michigan State Univ. Medical School.

COUP-TFII (Chick ovalbumin upstream promoter transcription factor) is one of the class of orphan receptors, a subset of the Nuclear Hormone Receptor (NHR) class of proteins. The orphan receptors have no known ligands but act, as the other members of the NHR's to promote or restrict transcription when bound to DNA. The members of the family often are active as homo or heterodimers and generally require binding of a co-activator as well as a ligand. The structure of COUP II in the pure apo form has been determined via x-ray diffraction. Data were collected at APS on the native, several heavy atom derivatives, and at multiple wavelengths on both a seleno-methionine and iodine derivative. Data sets varied in resolution between 1.5 and 2.3 Angstroms, with most better than 1.9 Angstroms. Rotation/translation methods using RXR as a search molecule provided phases sufficient to determine about 70% of the structure. Molecular model building using Quanta and O was able to place most of the remaining molecule. This comparison between the COUPII-TF ligand binding domain and that of the previously determined RXR show significant differences between the primarily helical structures. These differences involve the blocking of the co-factor binding site by the repositioning of the AF-2 helix and the closing of the ligand binding pocket by a repositioned portion of helix 10. For the COUP structure, the crystallographic dimer interface shows interaction between upper helix 10, helix 9 and the loop region between helices 8 and 9.

**TP112 Structural Analysis of Newly Designed HIV-1 Protease Inhibitors Based on (R)-(hydroxyethylamino)sulfonamide Isostere.** M.N.L. Nalam<sup>1</sup>, A. Ali<sup>1</sup>, K.K. Reddy<sup>1</sup>, H. Cao<sup>1</sup>, T.M. Rana<sup>1</sup>, M.D. Altman<sup>2</sup>, B. Tidor<sup>2</sup>, S. Chellappan<sup>3</sup>, M. Gilson<sup>3</sup>, C. Schiffer<sup>1</sup>, <sup>1</sup>Dept. of Biochemistry and Molecular Pharmacology, U. Mass Medical School, Worcester, MA, <sup>2</sup>Dept. of Biological Engineering and Computer Science, MIT, Cambridge, MA, <sup>3</sup>CARB, Univ. of Maryland Biotechnology Inst., Rockville, MD.

The development of HIV-1 protease inhibitors is considered a major success of structure-based drug design since they have dramatically reduced the mortality and morbidity rate in AIDS patients. However, this success has not ended the need for new protease inhibitors because the existing inhibitors have become ineffective against rapidly emerging, drug-resistant HIV-1 mutants. All the current HIV-1 pro-

tease inhibitors were designed to inhibit primarily a single variant of HIV-1 protease. Therefore, new inhibitors need to be designed with a broad specificity not only against existing drug-resistant variants of HIV-1 but also against future resistant mutants that may emerge.

Structural analysis of various complexes of protease with drugs and the substrates show that most primary active site mutations do not extensively contact substrates, but are critical to inhibitor binding. It is proposed that the inhibitors that lie within substrate envelope are less prone to develop resistance. To test this model, inhibitors were designed and synthesized to fit within substrate envelope. The binding affinities were measured for all the designed inhibitors and the inhibitors with the best binding affinities were crystallized with the wild-type protease. The inhibitors that fit within the substrate envelope show a flatter resistance profile to various mutants of HIV protease compared to the inhibitors that protrude out of the envelope validating the substrate envelope hypothesis.

**TP113 Crystal Structure of HIV-1 CRF01\_AE Protease in Complex with the Substrate p1-p6.** Rajintha M. Bandaranayake<sup>1</sup>, Moses Prabu-Jeyabalan<sup>1</sup>, Junko Kakizawa<sup>2</sup>, Wataru Sugiura<sup>2</sup>, Celia A. Schiffer<sup>1</sup>. <sup>1</sup>Dept. of Biochemistry and Molecular Pharmacology, Univ. of Massachusetts Medical School, Worcester, MA, <sup>2</sup>Lab. of Therapeutic Research and Clinical Science, AIDS Research Center, National Inst. of Infectious Diseases, Tokyo, Japan.

The homo-dimeric aspartyl protease of human immunodeficiency virus-1 (HIV-1) is a key target in anti-HIV drug development as it is essential for the processing of Gag and Gag-Pol polyproteins in the viral maturation process. At present nine HIV-1 clades and numerous Circulating Recombinant Forms (CRFs) have been identified with clade B being the most widely studied clade as well as the target for inhibitor design. The protease sequences of HIV-1 clades and CRF's differ by ~5-10 % and Non-B clade HIV-1 proteases carry several polymorphisms that have been implicated in protease inhibitor (PI) resistance in clade B and thus have given rise to questions on the efficacy of currently available PIs against non-B proteases. At present no structural information is available on non-B clade proteases and as a result very little is known on how substrate and inhibitor binding takes place. Here we report a crystal structure of inactive HIV-1 CRF01\_AE protease in complex with the p1-p6 substrate determined to a resolution of 2.8 Å. This structure shows a significant change in the flap hinge region of the protease when compared to subtype B p1-p6 structure and forms a unique interaction between two polymorphic residues, Arg20 and Asp35, which is not seen in the subtype B structure. Such an interaction may affect protease stability, activity as well as inhibitor binding and is currently under investigation.

**TP114 From Macromolecular Crystal Structure to Reliable Electrostatic Interactions.** Philip Coppens, Paulina M. Dominiak<sup>[1]</sup>, Anatoliy Volkov, Marc Messerschmidt, Dept. of Chemistry, State Univ. of New York at Buffalo, NY.

The theoretical databank of transferable aspherical pseudoatoms consists of 112 unique C, N, O an H atom types, representing all light atoms in natural amino acid residues and other biological molecules, as well as 3P, 3S and one chlorine atom.<sup>[2]</sup> Each atom type results from averaging over a family of chemically unique pseudoatoms, taking into account both first and second neighbors. A spawning procedure is used to ensure close transferability. Application of the databank is two-fold: a) The corresponding aspherical-atom scattering factors can be applied in the program suit XD<sup>[3]</sup> to improve the refinement of low-resolution X-ray data and eliminate bias in positional and temperature parameters due to approximations in the scattering factor model,<sup>[4]</sup> and b) For very large molecules a molecu-

118

lar electron density can be synthesized given the known structure, allowing evaluation of electrostatic interactions, such as occur in enzyme-drug complexes. Applications to the syntenin PDZ2 domain complexed with four-residue peptides, to the PDZ2 dimer,<sup>[2]</sup> and to a series of *Influenza* neuraminidase-inhibitor complexes<sup>[5]</sup> will be described. The databank and an auxiliary program LSDB are available at harker.chem.buffalo.edu.

Research supported by the National Institute of Health (GM56829) and the National Science Foundation (CHE0236317).

[1] Current address: Chemistry Department, Warsaw University, ul. Zwirki i Wigury 101, 02-089 Warszawa, Poland.

[2] Dominiak, Volkov, Li, Messerschmidt, Coppens, *J. Chem. Theory Comput.* 2007, 3, 232-247

[3] <http://xd.chem.buffalo.edu/>

[4] Volkov, Messerschmidt, Coppens, *Acta Cryst.* 2007. D63, 160-170

[5] Dominiak, Volkov, Dominiak, Coppens, to be published

**TP115 Two Periplasmic Sensor Domains with c-type Heme from Chemotaxis Proteins of *G. sulfurreducens* show PAS Fold and Form Helix-swapped Dimers.** P.R. Pokkuluri, Y.Y. Londer, N.E.C. Duke, S.J. Wood, M. Schiffer, Biosciences Div., Argonne National Lab., Argonne, IL.

We report the first structures of two periplasmic sensor domains containing one c-type heme with PAS fold. Periplasmic sensor domains of about 135 residues from two proteins annotated as methyl-accepting chemotaxis proteins from *Geobacter sulfurreducens* (encoded by genes GSU0935 and GSU0582) were expressed in *E. coli*. The sensor domains were isolated, purified and crystallized. Their structures were determined using the anomalous dispersion of the Fe atom of their hemes using data collected at the SBC 19BM beamline at APS. As predicted by the program 3D-PSSM, these domains had the PAS fold. Both sensor domains were found to form helix-swapped dimers in the crystal. The swapped segment consists of two helices of about 45 amino acids at the N-terminus with the hemes located between the two monomers. In case of GSU0935, the dimer is a non-crystallographic dimer. The heme of each monomer differs in its coordination; heme of monomer-1 has His – Met ligation with the axial ligands contributed by both monomers, whereas heme of monomer-2 has His – Water coordination. In case of the sensor domain from GSU0582, the dimer is a crystallographic dimer and the heme has His – Water coordination as observed for heme of monomer-2 of the GSU0935 sensor. Although it is not known what these domains are sensing *in vivo*, the two sensor domains *in vitro* show similar heme-binding characteristics; they bind CO and NO in solution. The two sensor domain structures will be compared with each other and with cytoplasmic PAS sensor domains containing a b-type heme.

This research is supported by DOE OBER GTL program; use of SBC beamlines and APS are supported by DOE under contract No. DE-AC02-06CH11357.

**TP116 Crystal Structure of the DNA-binding Domain of PhoP, a Response Regulator from *Mycobacterium tuberculosis*.** Shuishu Wang, Public Health Research Inst., New Jersey Medical School, UMDNJ, Newark, NJ.

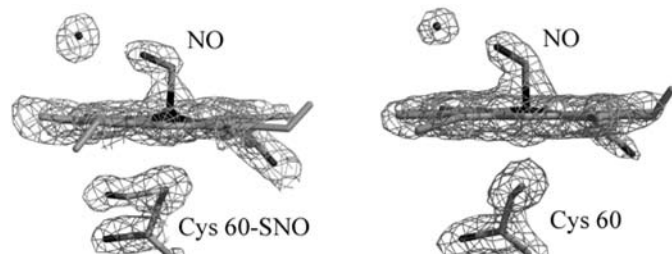
The PhoP-PhoR two-component signaling system from *M. tuberculosis* is essential for the virulence of the TB bacillus. The response regulator, PhoP, regulates expression of over 110 genes. We have determined the crystal structure of the DNA-binding domain of PhoP (PhoPC) to 1.75 Å. PhoPC exhibits a typical fold of the winged helix-turn-helix subfamily of response regulators. The structure starts with a four-stranded anti-parallel β-sheet at the N-terminus, followed by a three-helical bundle of α-helices, and then a C-terminal β-hairpin, which together with a short β-strand between the first and second helices forms a three-stranded anti-parallel β-sheet. The molecular

surface around the third  $\alpha$ -helix has positive electrostatic potential, confirming the role of this helix in DNA sequence recognition. The crystal packing of PhoPC gives a ring of hexamer, with neighboring molecules interacting in a head to tail fashion. This packing interface suggests that PhoP binds DNA as a tandem dimer. Detailed structural analysis and the implications with respect to DNA binding will be presented.

We thank Dr. Vivian Stojanoff, Dr. Fabiano Yokaichiya, and other staff members at the beamline X6A of the National Synchrotron Light Source (NSLS) for assistance in data collection.

**TP117 Exploring the Mechanism of Nitric Oxide Binding to Cimex Nitrophorin, a Heme-Thiolate Protein from the Bedbug.** A. Weichsel, H. Badgandi, R.E. Berry, J.T. Hazzard, F.A. Walker, G. Tollin, W.R. Montfort, Depts. of Biochemistry and Molecular Biophysics, and Chemistry, Univ. of Arizona, Tucson, AZ.

Cimex nitrophorin (cNP) is a ferric heme-thiolate protein from the saliva of a blood-feeding insect *Cimex lectularius* commonly called bedbug. In the slightly acidic environment of the insect's salivary glands the protein is bound to nitric oxide (NO), a strong vasodilator and inhibitor of blood coagulation. During a blood meal, the protein is delivered with the insect's saliva to the feeding site, where dilution and higher pH lead to release of NO to increase efficiency of blood intake. We found *in vitro* that ferric cNP exposed to sub-millimolar concentrations of NO binds two NO molecules: one to the heme iron, and one to the thiolate group of Cys 60, the heme ligand at the proximal position (left figure). Such binding of NO is accomplished through a remarkable heme-assisted nitrosation of the proximal thiolate, which requires hemolytic cleavage of the covalent bond between iron and sulfur of Cys 60. This unique mechanism was probed in a series of crystallographic and spectroscopic experiments



with chemically reduced protein. The reaction of the ferrous cNP with NO also resulted in 5-coordinate nitrosyl-heme and unmodified proximal thiol group (right figure). The ferrous cNP complexes with H<sub>2</sub>O and CO revealed a very long Fe – S bond and spectroscopic evidence of protonation of the proximal thiolate. These results suggest that the apparent instability of the Fe – S bond in the cNP-NO complex originates from a structural constraint caused by an unusual orientation of the proximal cysteine with respect to heme, while the pH-dependent character of NO binding to ferric cNP is attributed to protonation of the proximal thiolate.

**TP118 High Resolution Structure of *P. abyssi* aRrp41-aRrp42 Complex: A Closer View to the Archaeal Exosome RNA Processing Mechanism.** Beatriz G. Guimarães<sup>1</sup>, Marcos V.A.S. Navarro<sup>1</sup>, Nilson I.T. Zanchin<sup>1</sup>, Carla C. Oliveira<sup>2</sup>, <sup>1</sup>Center for Structural Molecular Biology, Brazilian Synchrotron Light Lab., Campinas, Brazil, <sup>2</sup>Dept. of Biochemistry, Inst. of Chemistry, Univ. of São Paulo, São Paulo, Brazil.

Initially identified in yeast, the RNA exosome has emerged as the central component of the RNA maturation and degradation machinery both in archaea and in eukaryotes. An increasing number of stud-

ies has contributed to understand exosome architecture and activity. However, important issues concerning how the RNA is progressively degraded remain unclear. The archaeal exosome core is formed by dimers of the RNase PH proteins aRrp41 and aRrp42 which assemble into a hexameric ring. Analysis of a series of high-resolution crystal structures of the exosome core from *Pyrococcus abyssi* enabled us to significantly enlarge the picture of the archaeal exosome RNA processing mechanism. We describe a structure with three 10-mer RNA strands assembled within the catalytic chamber. The five inner-most 3'-end bases of each 10-mer occupy a particular cleft in the catalytic chamber, while the remaining nucleotides extend towards the top entry of the core chamber. Residues from all three aRrp41-aRrp42 heterodimers participate in the processing of a single RNA molecule. Interestingly, an ADP-bound structure revealed a rearrangement of nucleotide interactions, placing the phosphate group on the region postulated to be the exit channel after catalysis.

Financial Support: FAPESP, LNLS

**TP119 Structural Insights into the Bactericidal Mechanism of Human Peptidoglycan Recognition Proteins.** S. Cho, Q. Wang, C.P. Swaminathan, R.A. Mariuzza, Center for Advanced Research in Biotechnology, W.M. Keck Lab. for Structural Biology, Univ. of Maryland Biotechnology Inst., Rockville, MD.

Peptidoglycan recognition proteins (PGRPs) are a family of highly conserved pattern recognition molecules in the innate immune system that bind bacterial cell wall peptidoglycans (PGNs), which are polymers of alternating *N*-acetylglucosamine (NAG) and *N*-acetylmuramic acid (NAM) cross-linked by short peptide stems. Human PGRPs are bactericidal against pathogenic and non-pathogenic Gram-positive bacteria, but not normal flora bacteria. Like certain glycopeptide antibiotics (*e.g.* vancomycin), PGRPs kill bacteria by directly interacting with their cell wall PGN, thereby interfering with PGN maturation. To better understand the bactericidal mechanism of human PGRPs, we determined the crystal structure of the C-terminal PGN-binding domain of human PGRP-I $\beta$  in complex with NAG-NAM-L-Ala- $\gamma$ -D-Glu-L-Lys-D-Ala-D-Ala, a synthetic glycopeptide comprising a complete PGN repeat. This structure, in conjunction with the previously reported NMR structure of a dimeric PGN fragment, permitted identification of major conformational differences between free and PGRP-bound PGN with respect to the relative orientation of saccharide and peptide moieties. These differences suggest a bactericidal mechanism whereby PGRPs disrupt cell wall maturation not only by sterically encumbering access of the biosynthetic enzymes to the nascent PGN chains, but also by locking PGN into a conformation that disfavors formation of cross-links between peptide stems in the growing cell wall.

**TP120 Conformational Flexibility Influences on Activity: Structures of *Pneumocystis carinii* Dihydrofolate Reductase Inhibitor Complexes.** V. Cody<sup>1</sup>, J.B. Pace<sup>1</sup>, A. Rosowsky<sup>2</sup>, <sup>1</sup>Hauptman-Woodward Medical Research Inst., Buffalo, NY, <sup>2</sup>Dana-Farber Cancer Inst., Boston, MA.

To understand the properties that confer selectivity and specificity of antifolate binding to dihydrofolate reductase (DHFR), a series of 2,4-diamino-5-methylpyrido[2,3-*d*]pyrimidines modified with 5-[2'-methoxy-5'-( $\omega$ -carboxyalkoxy)]benzyl substituents at the 6-position were tested. These substituents significantly enhanced selectivity in a series of 2,4-diamino-5-benzylpyrimidines. Unlike the pyrimidine series, these compounds showed poor inhibition and selectivity. Structural data are reported for a series of ternary complexes of *Pneumocystis carinii* DHFR with NADPH and pyridopyrimidine inhibitors in which the side chain length varied (5'-O-(CH<sub>2</sub>)*n*-COOH,

where  $n = 3-5$  and  $X = \text{H}$  or ethyl). Data for the  $n = 4$  and  $X = \text{ethyl}$  analogue reveal multiple binding modes in which the 5'-[2'-methoxy-5'-( $\omega$ -carboxyalkoxy)benzyl ester adopts two orientations; one that places the 2'-methoxy near the nicotinamide ribose ring of NADPH, and the other that shifts this group deeper in the binding pocket, similar to the *p*-aminobenzoyl ring of folates. In one orientation the carboxy ester contacts the conserved Arg 75, as observed in other DHFR structures and the other places the side chain in contact with Phe69 in pcDHFR, but not with Arg75. In the structure of the  $n=5$  and  $X=\text{H}$  analogue, the side chain folds itself such that the carboxylate makes favorable interactions with the conserved Arg75, similar to the potent pyridopyrimidine analogue with the  $\omega$ -side chain  $n=3$  and  $X=\text{H}$ . Changes in the bridge torsion angles that help orient the side chain to interact with Arg75 also place the 2'-methoxy near the cofactor, and may play a role in their weak inhibitory activity.

Supported by GM51670 (VC) and AI29904 (AR).

**SP121 Is Dimerization Required for the Catalytic Activity of Bacterial Biotin Carboxylase?** Yang Shen<sup>1</sup>, Chi-Yuan Chou<sup>2</sup>, Gu-Gang Chang<sup>2</sup>, Liang Tong<sup>1</sup>, <sup>1</sup>Dept. of Biological Sciences, Columbia Univ., New York, NY, USA, <sup>2</sup>Faculty of Life Sciences, National Yang-Ming Univ., Taipei, Taiwan.

Acetyl-coenzyme A carboxylases (ACCs) have crucial roles in fatty acid metabolism. The biotin carboxylase (BC) subunit of *Escherichia coli* ACC is believed to be active only as a dimer, although the crystal structure shows that the active site of each monomer is 25 Å from the dimer interface. It is currently believed that *E. coli* BC is active only as a dimer, while monomers of the enzyme are presumed to be inactive catalytically. We report here biochemical, biophysical, and structural characterizations of BC carrying single-site mutations in the dimer interface. Our studies demonstrate that two of the mutants, R19E and E23R, are monomeric in solution but have only a 3-fold loss in catalytic activity. The crystal structures of the E23R and F363A mutants show that they can still form the correct dimer at high concentrations. Our data suggest that dimerization is not an absolute requirement for the catalytic activity of the *E. coli* BC subunit, and we propose a new model for the molecular mechanism of action for BC in multisubunit and multidomain ACCs.

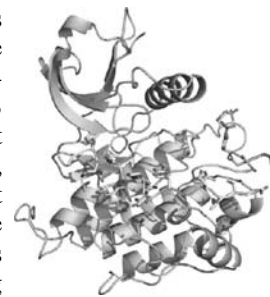
This research is supported in part by a grant from the National Institutes of Health (DK67238) to L.T.

Reference: Shen Y, Chou CY, Chang GG and Tong L. Is dimerization required for the catalytic activity of bacterial biotin carboxylase? *Mol Cell*. 2006 Jun 23;22(6):807-18.

**TP122 Structural Basis for Recruitment of Insulin Receptor Substrate-2 to the Insulin Receptor.** Jinhua Wu, Chongfeng Xu, Thomas A. Neubert, Stevan R. Hubbard, Skirball Inst. of Biomolecular Medicine, New York Univ. School of Medicine, New York, NY.

Insulin receptor substrate-1 (IRS1) and IRS2 play critical roles in mediating the metabolic effects of insulin. IRS1 and IRS2 are recruited to the insulin receptor (IR) through binding of their phosphotyrosine-binding (PTB) domains to pTyr972 in the juxtamembrane region of the receptor. Previous yeast two-hybrid studies had demonstrated that IRS2, but not IRS1, possesses a second region, downstream of the PTB domain, that interacts with the tyrosine kinase domain of the IR (IRK). This region is known as kinase regulatory-loop binding (KRLB). To elucidate the binding mechanism of KRLB to the IR, we co-crystallized a 15-residue peptide from KRLB, which had been shown previously to be critical for binding to the IR, with phosphorylated IRK. The structure reveals that Tyr628 in KRLB binds in the active site of the kinase, and numer-

ous contacts are made between residues of the peptide and the kinase, far more than for a typical substrate-IRK interaction. We found that Tyr628 in KRLB can be phosphorylated by IRK, but  $K_m(\text{ATP})$  for this event is very high,  $\sim 2 \text{ mM}$ , compared to  $\sim 50 \mu\text{M}$  for most IRK substrates. The crystal structure suggests that Tyr621 in KRLB competes with the adenine ring of ATP for binding in the ATP binding pocket, resulting in the aberrantly high  $K_m(\text{ATP})$ . Mutagenesis in this 15-residue region of KRLB demonstrates that many of the residues proximal to Tyr628 are important for the interaction with IRK. *In vitro* kinase assays performed with monomeric and dimeric IRK suggest that the Tyr628 region of KRLB serves as an anchor in one kinase domain to facilitate tyrosine phosphorylation *in trans* of downstream YMXM sites by the second kinase domain within the IR.



**SP123 Activities and Structure of  $\beta$  Hemolysin.** Medora Huseby<sup>1</sup>, Ke Shi<sup>1</sup>, Patrick M. Schlievert<sup>1</sup>, Douglas H. Ohlendorf<sup>1</sup>, Cathleen A Earhart<sup>1</sup>, <sup>1</sup>Univ. of Minnesota, Minneapolis, MN.

$\beta$  hemolysin is a virulence factor of *Staphylococcus aureus* that catalyzes the cleavage of sphingomyelin in biological membranes to ceramide and phosphorylcholine causing lysis of erythrocytes.  $\beta$  hemolysin belongs to the neutral sphingomyelinase C family and shares homology to mammalian neutral sphingomyelinase C enzymes which are important in sphingolipid signaling and metabolism. Crystals of  $\beta$  hemolysin were found to be fully merohedrally twinned. Diffraction data were collected at the Molecular Biology Consortium facilities on beam line 4.2.2 at the Advanced Light Source. The structure was solved via molecular replacement using SmeL (sphingomyelinase C from *Listeria ivanovii*) as the search model and refined to 2.4 Å resolution.  $\beta$  hemolysin belongs to  $\alpha/\beta$  protein family and is arranged in a 4-layer sandwich (CATH class 3.60.10) adopting a similar fold to that of DNase I. Assays of native and structure suggested site-directed mutants of  $\beta$  hemolysin demonstrate that the lysing of sheep erythrocytes and the killing of proliferating human lymphocytes is linked to the sphingomyelinase activity of  $\beta$  hemolysin. These data are the first to show a direct effect upon human tissue and provide a rationale for the importance of  $\beta$  hemolysin in virulence. A C-terminal  $\beta$  hairpin has been proposed to penetrate the lipid bilayer and aid in substrate binding and positioning. Our analysis shows this involved in the observed twinning. The structure of a deletion mutant,  $\Delta 274-279$ , was solved via molecular replacement and refined to 2.8 Å resolution. The crystals were not twinned, and the data were collected on beam line 14BMC at the Advanced Photon Source. This deletion did not significantly perturb the structure nor the function of  $\beta$  hemolysin. Further mutations are testing the function of the C-terminal  $\beta$  hairpin.

[1] www.cdc.gov/ [2] Openshaw *et al.* *JBC*, 2005.

**TP124 Identification of Functional Motifs and Binding Site Properties in Potential Drug Targets from Tropical Parasites.** T.L. Arakaki<sup>1,2</sup>, I. Le Trong<sup>1,2</sup>, E.T. Larson<sup>1,2</sup>, H. Neely<sup>1,2</sup>, E. Boni<sup>1,2</sup>, N. Mueller<sup>1,2</sup>, A. Napuli<sup>1,2</sup>, A. Kelley<sup>1,2</sup>, B.E. Krumm<sup>1,2</sup>, L. Xiao<sup>1,2</sup>, S. Shibata<sup>1,2</sup>, Z. Zhang<sup>1,2</sup>, W. Deng<sup>1,2</sup>, F. Zucker<sup>1,2</sup>, E. Fan<sup>1,2</sup>, F.S. Buckner<sup>2,3</sup>, W.C.E. Van Voorhis<sup>2,3</sup>, C.L.M.J. Verlinde<sup>1,2</sup>, W.G.J. Hol<sup>2</sup>, E.A. Merritt<sup>1,2</sup>, Depts of <sup>1</sup>Biochemistry and <sup>3</sup>Medicine, Univ. of Washington, Seattle, <sup>2</sup>Medical Structural Genomics of Pathogenic Protozoa Consortium.

The assignment of accurate functional annotations to proteins is one

of many interesting challenges facing structural genomics. An intriguing example from the eukaryotic parasite *Plasmodium vivax* is the Raf kinase inhibitor protein (PvRKIP). PvRKIP is a member of the phosphatidylethanolamine-binding protein (PEBP) sequence family consisting of more than 500 sequences with diverse functions. While a handful of these sequences have been functionally characterized and are involved in membrane biogenesis or cell proliferation and differentiation, other PEBP family members have distinctly different functions. Some mammalian PEBPs bind to Raf-1 and inhibit Raf-1's ability to phosphorylate MEK1. Recent studies of the homologous *P. falciparum* RKIP suggest an analogous regulatory role involving *P. falciparum* Ca-dependent protein kinase (PfCDPK1). To learn more about PvRKIP's function, its structure was determined to 1.3 Å resolution. Structural analysis reveals a distinctive left-handed helix located at one edge of the putative phospholipid-binding region. Since left-handed helices are rare and often appear on the protein surface at ligand-binding sites, protein-protein interfaces or other functional sites, the left-handed helix may be important for PvRKIP's function. This unusual structural motif may be characteristic of a subfamily of the PEBP sequence family.



**TP125 Sequence, Structure, Function: Understanding Roles of Specific Residues and Predicting Substrates Within the Short-Chain Oxidoreductase Superfamily.** T.C. Umland<sup>1,2</sup>, Q. Mao<sup>1</sup>, R. Huether<sup>1,2</sup>, V.Z. Pletnev<sup>1</sup>, W.L. Duax<sup>1,2</sup>, J. Thomas<sup>3</sup>, L. Gambino<sup>1</sup>, <sup>1</sup>Hauptman Woodward Medical Research Inst., <sup>2</sup>State Univ. of New York at Buffalo, NY, <sup>3</sup>Mercer Univ., Macon, GA.

The Short-Chain Oxidoreductase (SCOR) superfamily is an ancient protein family currently represented by over 13,500 verified and putative members. A characteristic of this superfamily is the presence of the Rossmann fold and NAD(H) or NADP(H) dependent catalytic activity. Despite the common fold, this superfamily exhibits vast diversity, including the lack of a single completely conserved residue and the presence of SCOR representatives in all kingdoms. This diversity is further exemplified by the different substrate types (e.g., steroids, alcohols, prostaglandins, xenobiotics, etc.) acted upon by discrete SCOR subfamilies. Previously, we have identified and assigned specific functional roles (fold, cofactor-binding, etc.) to a subset of the most highly conserved residues. Recently, we have begun to identify sets of residues which define substrate preference. These substrate defining residues are hypervariable in the context of the entire superfamily and thus are often neglected in sequence only analyses. We are targeting individual SCOR proteins for structure-function analysis to both test and expand the *fingerprints* that we are uncovering for the accurate classification of SCOR proteins into functional subfamilies. Results of these experiments will be presented, including the 1.8 Å resolution crystal structure of *Aquifex aeolicus* FabG, a putative β-ketoacyl-acyl-carrier protein reductase and component of fatty acid synthase II, which exhibits naturally occurring variations to the functional fingerprints previously identified.

**TP126 Recent Structures Solved at the Center for Eukaryotic Structural Genomics.** J.G. McCoy, E. Bitto, C.A. Bingman, G.E. Wesenberg, G.N. Phillips, Jr., Univ. of Wisconsin-Madison, Madison, WI.

The Center for Eukaryotic Structural Genomics (CESG) is one of six specialized centers funded through the National Institute of General Medical Sciences Protein Structure Initiative. CESG has solved over 100 eukaryotic structures and is committed to the development of

new methods and technology for improving the efficiency of protein production, purification, and structure determination.

CESG has a tripartite target selection strategy, drawing from sequence-structure, medical relevance and outside request categories. Sequence-structure targets are chosen based on sequence dissimilarity to known structures. The pallet of sequence-structure targets is pan-eukaryotic: including human, mouse, zebrafish, rice and *Arabidopsis* proteins. Most recently, CESG has evaluated two unicellular acido-thermophilic eukaryotes as a source of sequence-structure targets. Workgroups consisting of 192 targets from *Galdieria sulphuraria* and *Cyanidioschizon merolae* are in process. Results are nearly complete. These organisms have proven to be effective sources of targets for structural genomics research.

In addition to sequence-structure targets, CESG has also solved the structures of a large number of medically-relevant proteins, and eukaryotic targets requested by the general biological community. Traditional literature searches for medically-relevant targets are supplemented by a procedure for automatically parsing the Mendelian Inheritance of Man database.

Here we present a number of recently solved eukaryotic protein structures, which either have strong medical relevance or are from thermophilic eukaryotes. The work of the entire CESG staff is acknowledged.

Supported by NIH Protein Structure Initiative grants P50 GM64598 and U54 GM074901 (J. L. Markley, PI)

**SP127 Structural and Biophysical Characterization of hRecQL4, a Double Ring DNA Helicase Responsible for Rothmund-Thomson Syndrome.** Megan Guelker, Yousif Shamoo, Rice Univ., Houston, TX.

Mutations to the human DNA helicase, hRecQL4, give rise to genomic instability that in turn is responsible for a group of autosomal recessive conditions including Rothmund-Thomson Syndrome, RAPADILINO and the majority of cases of Baller-Gerold Syndrome. The symptoms and severity of the syndrome are correlated to mutations that broadly map to the helicase and C-terminal regions of hRecQL4 and their effects are poorly understood. hRecQL4 is classified as a RecQ family helicase that also includes the Werner's (WRN) and Bloom's (BLM) Syndrome helicases which function during DNA repair and replication restart. Recent work from our lab and that of our collaborators (A. Venkitaraman, Cambridge U.) suggest that although there are some similarities to WRN and BLM, hRecQL4 plays an essential role in the initiation of DNA replication and has a quaternary structure unlike WRN and BLM. Since over 50% of the hRecQL4 primary sequence shows no significant homology to any known protein, we used a structural genomics approach to design a number of expression constructs. Our EM studies show that hRecQL4 constructs containing the conserved helicase domain assemble into a double ring similar to the SV40 large T-antigen origin binding protein and not like other RecQ family proteins. This suggests that hRecQL4 may act as a 'DNA pump' that extrudes ssDNA from the helicase domain. The constructs that form a double ring elute as a single peak at a molecular weight range of 443-2000 kD consistent with the size expected for the double ring observed by EM and are able to hydrolyze ATP. These data together with the unique clinical phenotypes associated with mutation of hRecQL4 suggest a distinct biochemical function for hRecQL4.

Funding: NIGMS Training Grant (T32 GM008280), Welch Foundation (YS) C1584

**TP128 The Structure of NP\_294789.1 from *Deinococcus radiodurans* Suggests a Possible Function in DNA Damage Regulation.** C. Rife, M. Miller, A. Deacon, Structure Determination Core, The Joint Center for Structural Genomics, Stanford Synchrotron Radiation Lab., Menlo Park, CA.

The Joint Center for Structural Genomics (JCSG) has built a high-throughput pipeline, which automates all of the major experimental steps in the structure determination process from target selection through submission to the PDB. The x-ray crystal structure of NP\_294789.1 from *Deinococcus radiodurans*, a polyextremophile capable of resisting heat, cold, dehydration, and high levels of radiation, was solved at 1.80Å using the automated JCSG pipeline. NP\_294789.1 is the first member of PFAM family PF04978 to be structurally characterized.

Size-exclusion chromatography indicates that NP\_294789.1 exists as a dimer in solution, although it crystallizes as a monomer. Each monomer contains a four-helix bundle at its core. This helical bundle is unusual in that it does not follow a typical up and down topology; instead, each helix is connected by long loops. Helices two and four contribute residues to a metal binding site in which nickel is coordinated.

NP\_294789.1 is classified in PFAM family PF04978 as a protein of unknown function (DUF664), however, sequence and structural similarity searches suggest that NP\_294789.1 may in fact be related to PFAM PF05163, which is a family of DNA damage inducible genes which are part of a global regulatory network. Additionally, other possible functional roles will be examined.

The JCSG is funded by the Protein Structure Initiative of the National Institutes of Health, National Institute of General Medical Sciences. SSRL operations is funded by DOE BES, and the SSRL Structural Molecular Biology program by DOE BER, NIH NCRR BTP and NIH NIGMS.

**TP129 Crystal Structure of *Mycoplasma arthritis*-derived Mitogen Reveals a 3D-domain Swapped Dimer.** Hongmin Li<sup>1,2</sup>, Yi Guo<sup>1</sup>, Zhong Li<sup>1</sup>, Sandra J. VanVranken<sup>1</sup>, <sup>1</sup>Wadsworth Center, New York State Dept. of Health, and <sup>2</sup>Dept. of Biomedical Sciences, School of Public Health, Univ. at Albany, NY.

*Mycoplasma arthritis*-derived mitogen (MAM) is a superantigen (SAg) that can activate large fractions of T cells bearing particular Vβ elements of T-cell receptor (TCR). We previously determined the 3D structure of MAM complexed with a human class II MHC molecule and with both TCR and MHC molecules. The ligand-bound MAM structure showed a novel SAg fold that is completely different from other bacterial SAGs. Here we report the crystal structure of the MAM wild-type (wt) and two mutants (L50A and K201A). Functional studies indicated that both K201A and L50A MAM mutants are biologically active. The MAM wt and L50A mutant were crystallized isomorphously in a monoclinic space group  $P2_1$  with 10 homodimers in the asymmetric unit. The K201A mutant was crystallized in a cubic space group  $P4_132$ , with one homodimer per asymmetric unit. The structures of the MAM<sub>K201A</sub>, MAM<sub>L50A</sub>, and MAM<sub>wt</sub> were determined using molecular replacement method. The final  $R_{\text{factors}}$  for the MAM<sub>K201A</sub>, MAM<sub>L50A</sub>, and MAM<sub>wt</sub> were 25.3%, 37%, 40.8% at 2.8Å, 3.6Å, and 4.0Å resolution, respectively. Strikingly and unexpectedly, the unliganded MAM and MAM mutants form 3D-domain swapped dimer. The MAM monomers have exchanged more than half of their C-terminal domains, so that the fold of each domain is intimately intertwined, resulting in a highly twisted "knot" at the center of the elongated dimer. Interestingly, the unliganded MAM monomer re-constructed from the swapped dimer displays large structural differences from the liganded MAM.

We thank the New York Structural Biology Center for access to beamline X4A at NSLS. This research is supported by NIH grant AI50628.

122

**SP130 Crystallographic Studies of the C-terminal Domain of DNA Gyrase.** Tung-Ju Hsieh<sup>1</sup>, Hsun-Tang Chang<sup>1</sup>, Te-Sheng Lin<sup>1</sup>, Shu-Yun Huang<sup>1</sup>, Lynn Farh<sup>2</sup>, and Nei-Li Chan<sup>1</sup>, <sup>1</sup>Inst. of Biochemistry, National Chung Hsing Univ., Taichung City, Taiwan, <sup>2</sup>Dept. of Applied Chemistry and Life Science, National Ping Tung Univ. of Education, Ping Tung, Taiwan.

Most bacteria harbor two essential Type IIA DNA topoisomerases, DNA gyrase and topoisomerase IV (TopoIV). While these two enzymes are homologous, they exhibit distinct activities. DNA gyrase supports transcription and replication with its unique capability of introducing (–) supercoils, whereas Topo IV preferentially relaxes (+) supercoils and serves as the main decatenating enzyme during chromosome segregation. Based on crystal structures of the C-terminal domains (CTDs) from *Borrelia burgdorferi* gyrase (BbGyrA-CTD) and *Bacillus stearothermophilus* TopoIV (BsTopoIV-CTD), it was proposed previously that the divergence of enzyme function can be attributed to differences in the overall shaping of these two domains. However, recently determined CTD of *Escherichia coli* gyrase (EcGyrA-CTD) closely resembles BsTopoIV-CTD, rather than its functionally equivalent partner BbGyrA-CTD. To understand the molecular basis of this functional divergence in greater detail, we have now determined the crystal structures of *Xanthomonas campestris* gyrase CTD (XcGyrA-CTD) and EcGyrA-CTD in a new crystal form. Detailed structural analysis and functional implication of our findings will be presented during the meeting.

**TP131 Targeting Metabolic Enzymes for Antibiotic Development.** Ronald E. Viola, Dept. of Chemistry, Univ. of Toledo, Toledo, OH.

The dramatic increase in the number of multidrug resistant microorganisms has provided renewed urgency in the search for new antibiotics. Clearly new tools and new approaches must be developed that are directed against novel targets to control these infectious organisms. The biosynthetic pathway derived from aspartate is unique to plants and microorganisms, producing four of the amino acids required for protein synthesis. In addition, products from this pathway are involved in general methylation reactions, bacterial cell wall cross-linking, sporulation in Gram-positive bacteria, and quorum sensing in Gram-negative bacteria. Disruption of this pathway will have potentially devastating consequences for the survival of a microorganism. We have determined high-resolution structures of a key enzyme in this pathway, ASA dehydrogenase from several Gram-negative and Gram-positive infectious organisms, including structures of enzyme-substrate, enzyme-inhibitor, enzyme-intermediate, and mutant enzyme complexes. Despite a wide range of sequence homologies, the key active site functional groups are conserved in this enzyme from archaea to plants. However, differences in the mode of coenzyme binding and intersubunit communication provide attractive targets for the potential development of species specific antibiotics.

**TP132 Mutation of Lys170 Affects Structural and Proton Shuttle Properties of Human Carbonic Anhydrase II.** J.F. Dominic<sup>1</sup>, W. Williams<sup>1</sup>, A. Aspesi<sup>1</sup>, S.Z. Fisher<sup>1</sup>, M.B. Sines<sup>1</sup>, C.K. Tu<sup>2</sup>, L. Govindasamy<sup>1</sup>, M. Agbandje-McKenna<sup>1</sup>, D.N. Silverman<sup>2</sup>, R. McKenna<sup>1</sup>, <sup>1</sup>Dept. of Biochemistry and Molecular Biology and <sup>2</sup>Dept. of Pharmacology and Therapeutics, College of Medicine, Univ. of Florida, Gainesville, FL.

Human carbonic anhydrase II (HCAII) is a zinc metalloenzyme that catalyzes the reversible hydration and dehydration of carbon dioxide and bicarbonate, respectively. It has been well established that the rate-limiting step in catalysis is the intramolecular transfer of a

proton between the zinc-bound solvent ( $H_2O/OH$ ) to a proton-shuttling residue His64, and onto the bulk solvent. Situated near His64 on the rim of active site is residue Lys170. To investigate the role of this basic surface residue on the conformation of His64 and its effect on proton transfer, we have structurally and kinetically characterized four mutants Lys170 to Ala, Asp, Glu, and His. We have determined the crystal structures of all four mutants to  $\sim 1.8\text{\AA}$  resolution and correlated the conformation of His64 with kinetic data that shows up to a 9-fold increase in the catalytic rate. These observed changes in the rate of proton transfer are most likely a consequence of the observed single conformer of His64 and a change in the  $\Delta pK_a$  between the Zn bound solvent and His64.

**TP133 X-ray Crystallographic and Inhibition Studies on Carbonic Anhydrase IX Mimic Drug Complexes.** C. Genis<sup>1</sup>, N. Case<sup>2</sup>, L. Govindasamy<sup>1</sup>, C. Tu<sup>2</sup>, D. N. Silverman<sup>1,2</sup>, M. Agbandje-McKenna<sup>1</sup>, R. McKenna<sup>1</sup>, <sup>1</sup>Dept. of Biochemistry and Molecular Biology and <sup>2</sup>Dept. of Pharmacology and Therapeutics, College of Medicine, Univ. of Florida, Gainesville, FL.

The inhibition of carbonic anhydrase IX (CAIX) shows promising prognosis in controlling hypoxic tumor metastasis. Hypoxic tumors are common in many cell lines and the clinical challenge with these tumors is their resistant to radiotherapy and chemotherapy. Tumor cells adapt to their hypoxic microenvironments with the up-regulation of hypoxia-inducible factor-1 (HIF-1) and the transmembrane CAIX<sup>[1]</sup>. The importance of CAIX in aiding hypoxic tumor metastasis is due to the high catalytic activity of the enzyme to hydrate carbon dioxide to produce bicarbonate and a proton. The production of protons facilitates the acidification of the microenvironment of tumors<sup>[2]</sup>. Additionally the increased proton gradient prevents the uptake of weakly basic anti-cancer drugs therefore the inhibition of CAIX represents a two-fold approach to anticancer therapies<sup>[3]</sup>. In this structural study we present a mimic of the CAIX active site, using a double mutant A65S N67Q of CAII, in complex with classical carbonic anhydrase inhibitors acetazolamide, methazolamide, and chlorzotamide to 1.8 Å resolution. This study correlates the inhibition of these inhibitors to structure and provides information on what key amino acids are important for drug binding and isozyme specificity.

<sup>1</sup>Wykoff, C. C., Beasley, N. J., Watson, P. H., Turner, K. J., Pastorek, J., & Sibtain, A., *et al.* (2000). Hypoxia-inducible expression of tumor-associated carbonic anhydrases. *Cancer research*, **60**(24), 7075-7083.

<sup>2</sup>Thiry, A., Dogne, J. M., Masereel, B., & Supuran, C. T. (2006). Targeting tumor-associated carbonic anhydrase IX in cancer therapy. *Trends in pharmacological sciences*, **27**(11), 566-573.

**TP134 Structure and Catalytic Effects of an E401K Mutation in the *E. coli* Pyruvate Dehydrogenase E1 Component Complex.** P. Arjunan<sup>1,2</sup>, K. Chandrasekhar<sup>1,2</sup>, S. Kale<sup>3</sup>, N. Nemeria<sup>3</sup>, F. Jordan<sup>3</sup>, W. Furey<sup>1,2</sup>, <sup>1</sup>Biocrystallography Lab., VA Pittsburgh Healthcare System, Pittsburgh, PA, <sup>2</sup>Dept. of Pharmacology, Univ. of Pittsburgh, School of Medicine, Pittsburgh, PA, <sup>3</sup>Dept. of Chemistry, Rutgers Univ., Newark, NJ.

Glu401 is present in the loop residues 401-413 and is part of the active site channel situated at the dimer interface of the thiamin diphosphate (ThDP) dependent E1 component from the *E. coli* pyruvate dehydrogenase multienzyme complex (PDHc). The crystal structure of the reaction intermediate analogue  $\alpha$ -phosphonolactylthiamin diphosphate (PLThDP) in complex with the native E1 indicated that the loop region 401-413 has an important function for the catalytic activity of the E1 enzyme in the multienzyme complex. We have now determined the crystal structures of variant E401K complex with

both the cofactor ThDP and reaction intermediate analogue PLThDP in the active site. Results from this study, and structural comparison with the native E1 structure will be presented.

**TP135 Structural Studies of Uridine Diphosphate Glycosyltransferases from *Medicago truncatula*.** Xiaoqiang Wang, Hui Shao, Lenong Li, Luis L. Escamilla-Trevino, Zhenzhan Chang, Luzia Modolo, Jack W. Blount, Xianzhi He, Lahoucine Achnine, Richard A. Dixon, Plant Biology Div., Samuel Roberts Noble Foundation, Ardmore, OK.

Glycosylation reactions are quantitatively the most important biochemical reactions on earth. The glycosylation of small molecules is catalyzed by uridine diphosphate glycosyltransferases (UGTs), and play key roles in many biological processes, including biosynthesis of various bioactive compounds, regulation of hormone activity, and metabolism of toxins. Plants contain a very large number of UGTs to catalyze the full range of biological glycosylation reactions for huge variety of plant natural products, and control their bioactivity, function, and storage in plants. We determined crystal structures of three UGTs from *Medicago truncatula*. These structures revealed that the UGT fold is conservative, and the structures consist of two N- and C-terminal domains with similar Rossmann-type folds, and the two domains pack very tightly and form a deep cleft which is the binding pocket for substrates. Structural analyses and comparison revealed that the key residues for binding with sugar donor are highly conserved, residues for recognizing acceptor substrates are extremely varied, and substrate binding may involve some conformational changes. The structural study suggested a histidine residue (His22 for UGT71G1) as the catalytic base and an aspartate (Asp121 for UGT71G1) as a key residue which may assist deprotonation of the acceptor substrate by interacting with the catalytic base. Mutagenesis study confirmed the roles of these key residues in donor substrate binding and enzyme activity and explored the possibility for manipulating substrate specificity and product regio-selectivity and enhancing the enzymatic activity.

**SP136 Structural Insights into Thiopurine Pharmacogenetics.** Y. Peng<sup>1</sup>, D. Wilk<sup>1</sup>, Q. Feng<sup>2</sup>, A.A. Adjei<sup>2</sup>, O.E. Salavagione<sup>2</sup>, R.M. Weinshilboum<sup>2</sup>, and V.C. Yee<sup>1</sup>, <sup>1</sup>Dept. of Biochemistry, Case Western Reserve Univ., Cleveland, OH, <sup>2</sup>Dept. of Molecular Pharmacology and Experimental Therapeutics, Mayo Clinic College of Medicine-Mayo Clinic, Rochester, MN.

Thiopurine S-methyltransferase (TPMT) is an S-adenosylmethionine (SAM)-dependent methyltransferase responsible for the methylation of thiopurine drugs used for cancer therapy. Genetic polymorphisms of TPMT have been found to be associated with interindividual variation in the metabolism, therapeutic efficacy and toxicity of thiopurine drugs, and were discovered to control the level of TPMT activity. In order to obtain structural information to understand thiopurine pharmacogenetics, we have determined an ensemble of TPMT crystal structures, of wild-type and variant TPMTs, as binary and ternary substrate complexes. The structures are consistent with substrate binding modes that confirm the  $S_N2$ -like mechanism found in other SAM-dependent methyltransferases. The structures also reveal differences in substrate binding and conformation between wild-type and variant proteins, and provide an explanation for the reduced activity of the variant TPMT.

**SP137 Structural Determinants of Regulatory Cysteine-Sulfinic Acid Formation in Human DJ-1.** M.A. Wilson, M. Lakshminarasimhan, A.C. Witt, A. Raza, Dept. of Biochemistry and Redox Biology Center, Univ. of Nebraska, Lincoln, NE.

Human DJ-1 is a ubiquitously expressed protein that protects cells from oxidative stress and is involved in both Parkinsonism and certain types of cancer. Some of the cytoprotective functions of DJ-1 are positively regulated by the oxidation of a conserved cysteine residue (Cys106) to a cysteine-sulfinic acid. Atomic resolution X-ray crystallography shows that the specific oxidation of Cys106 to Cys106-sulfinic acid in DJ-1 is initiated by an oxygen-containing species bound near the reactive cysteine. The addition of a second oxygen to Cys106 is stabilized by a short hydrogen bond (2.47 Å) that is donated by a proximal and constitutively protonated glutamic acid (Glu18). Site directed mutagenesis of Glu18 to a variety of other residues results in variably diminished oxidation of Cys106 and loss of stability for the oxidized protein as assayed using differential scanning calorimetry. Structural analysis of these substitutions indicates that the short hydrogen bond donated to Cys106-sulfinic acid by Glu18 plays a complex and important role in stabilizing the formation of regulatory cysteine-sulfinic acid modification in human DJ-1.

**SP138 A Study of Differing Oligomeric Forms of Protocatechuate 3,4-dioxygenase.** Rebecca D. Hoeft, Jeff Digre, Ke Shi, David L. Burk, Zu-Yi Gu, C. Kent Brown, Cathleen A. Earhart, Douglas H. Ohlendorf, Univ. of Minnesota, Minneapolis, MN.

Protocatechuate 3,4-dioxygenase is a nonheme, iron containing enzyme that catalyzes the intradiol oxidative cleavage of 3,4-dihydroxybenzoic acid to  $\beta$ -carboxy-*cis,cis*-muconic acid via incorporation of molecular oxygen into the aromatic ring of the substrate. The functional unit of this enzyme is a heterodimer  $\alpha\beta\text{Fe}^{3+}$  with the active site lying on the interface of the alpha and beta subunits with the iron coordinating residues being contributed entirely by the beta. The number of these heterodimers in the isolated aggregate varies among species from 2 to 12. The enzyme from *Brevibacterium fuscum*, a gram-positive soil bacterium, exists as a hexamer ( $\alpha\beta\text{Fe}^{3+}$ )<sub>6</sub> and is especially interesting due to its unique sharp EPR spectral characteristics. The structure of the enzyme from *B. fuscum* has been solved to a resolution of 2.0 Å in space group P1 (a=96.5, b=97.6, c=119.2,  $\alpha$ =114.1,  $\beta$ =90.5,  $\gamma$ =117.9). The gene for the *B. fuscum* enzyme has recently been cloned and sequenced allowing the structure to be refined to  $R_{\text{work}}$  and  $R_{\text{free}}$  values of 16.5 and 22%, respectively. A detailed structural and functional comparison of this enzyme with the archetypal enzyme from *Pseudomonas putida* ( $\alpha\beta\text{Fe}^{3+}$ )<sub>12</sub> will be presented.

**SP139 A Structure-based Hypothesis for Cleavage of Protease Inhibitors by the Inhibitor-resistant Serine Protease Mesotrypsin.** Evette S. Radisky, Mohammed Salameh, Alexei S. Soares<sup>†</sup>, Alexandra S. Hockla; Dept. of Cancer Biology, Mayo Clinic Cancer Center, Jacksonville, FL, <sup>†</sup>National Synchrotron Light Source, Brookhaven, NY.

The canonical protein inhibitors of serine proteases fulfill a paradoxical function, binding to proteases in a manner that mimics substrates ideally positioned for catalysis, yet acting instead as inhibitors, being cleaved and released only very slowly<sup>1</sup>. Human mesotrypsin is a serine protease that demonstrates remarkable resistance to inhibition by canonical trypsin inhibitors, and has been reported to cleave some of these inhibitors at an accelerated rate<sup>2</sup>. An unusual Gly to Arg substitution at active site residue 193 is responsible for the inhibitor resistance of mesotrypsin<sup>2</sup>, and modeling based on the crystal structure of mesotrypsin identifies potential steric and electrostatic

clashes between mesotrypsin Arg-193 and canonical inhibitors<sup>3</sup>. Here, we present the crystal structure of mesotrypsin in complex with bovine pancreatic trypsin inhibitor (BPTI), revealing the conformational changes that accommodate canonical inhibitor binding. This structure, in combination with biochemical studies on the interaction between mesotrypsin and BPTI, leads us to propose a novel mechanistic model for mesotrypsin-catalyzed proteolysis of BPTI and other canonical inhibitors.

[1] Radisky, E. S. & Koshland, D. E., Jr. *Proc Natl Acad Sci USA* **99**, 10316-21 (2002).

[2] Szmola, R., Kukor, Z. & Sahin-Toth, M. *J Biol Chem* **278**, 48580-9 (2003).

[3] Katona, G., Berglund, G. I., Hajdu, J., Graf, L. & Szilagy, L. *J Mol Biol* **315**, 1209-18 (2002).

**TP140 Determining the Function of Novel *Treponema Lipoproteins* Via a Small-Scale Structural Genomics Project.** D.R. Tomchick\*, M. Machius\*, C.A. Brautigam\*, R.K. Deka\*, F.L. Tomson†, S.B. Lumpkins\*, P. Ward\*, X.F. Yang†, J.S. Blevins†, L. Neil†, K.E. Hagman†, M.V. Norgard†, Depts. of \*Biochemistry and †Microbiology, Univ. of Texas Southwestern Medical Center, Dallas, TX.

Syphilis is a chronic, complex sexually transmitted disease of humans caused by the noncultivable spirochete *Treponema pallidum*. Despite the availability of effective antimicrobials, syphilis remains a significant threat to global health, and can facilitate the transmission of HIV. Humans are the only known reservoir for *T. pallidum* and, although syphilis is one of the oldest recognized sexually transmitted diseases, it remains very poorly understood. This knowledge-gap is largely a consequence of the fact that *T. pallidum* cannot be cultivated continuously *in vitro*, thereby hampering studies on treponemal virulence and syphilis pathogenesis. Approaches for discerning *T. pallidum*'s membrane biology, which could reveal key aspects of the bacterium's enigmatic parasitic strategy, thus have been substantially limited. As an alternative approach to investigating the peculiar membrane biology of *T. pallidum*, we have adopted a structure-to-function approach to formulate new testable hypotheses regarding the potential function(s) of a number of the treponemal lipoproteins. That a structural biology approach for analyzing *T. pallidum* lipoproteins is a fruitful avenue of investigation is exemplified by at least four recent structure-function studies from our lab on the novel penicillin-binding protein Tp47, the L-methionine-binding protein Tp32, the purine nucleoside receptor PnrA and the metal-bound lactoferrin-binding protein Tp34. An overview of the results of these studies and the prospect for future insight into the membrane biology of *T. pallidum* will be presented.

**TP141 Hydroxymandelate Synthase and Hydroxyphenylpyruvate Dioxygenase: Minor Changes in Structure, Altered Catalytic Outcomes.** J.M. Brownlee, P. He, D.H.T. Harrison, G.R. Moran, Rosalind Franklin, Univ. of Medicine and Science, North Chicago, IL, Univ. of Wisconsin-Milwaukee, Milwaukee, WI.

We have determined the structure of hydroxymandelate synthase (HMS) to a resolution of 2.3 Å in order to compare its active site to that of hydroxyphenylpyruvate dioxygenase (HPPD). Enzymes accelerate biologically important chemical transformations with surprising fidelity to the exclusion of competing side reactions. HMS and HPPD are both examples of  $\alpha$ -keto acid dependent ferrous dioxygenases. Both enzymes use hydroxyphenylpyruvate as the source of the  $\alpha$ -keto acid and as the object of dioxygenation, but HPPD yields only homogentisate, while HMS yields only hydroxymandelate. The sequences of these two enzymes are highly similar, showing as high as 35% identity. Several structures of example HPPD's are available. Model building of the HMS active site based on the known

HPPD structures has shown that residues within 10 Å of the metal center are over 50% conserved, and, when not strictly conserved tend to be similar. The modeled structures have given inadequate insight into why these two enzymes catalyze the formation of different products. In order to better address this question of how the two active sites differ, we have crystallized HMS from *A. orientalis*. Crystals were grown of the Fe-depleted enzyme in the presence of Co<sup>++</sup> and hydroxyphenylpyruvate with the goal of capturing either a substrate-like or intermediate-like complex due to the inactivity of the cobaltous protein. X-ray data were collected at the cobalt edge, and phases derived from the cobalt anomalous signal (SAD) were used as a starting point for successful refinement. This structure reveals the basis for substrate specificity for both enzymes and provides insights into pathway selectivity.

**TP142 N- and C-terminal Helices are Involved in Light-Induced Signal Transduction in the Blue Light Sensor LOV2 Domain from *Avena sativa* Phototropin1.** A.S. Halavaty, J. Wojcik, K. Moffat, Dept. of Biochemistry and Molecular Biology, Univ. of Chicago, Chicago, IL.

Phototropins are flavin-photoreceptors that regulate phototropism, chloroplast movement, stomatal opening, and leaf expansion in plants. *Avena sativa* phototropin1 is composed of two N-terminal light, oxygen, voltage LOV1 and LOV2 domains, and a C-terminal serine/threonine kinase domain. Light absorption by LOV domains that bind the flavin mononucleotide (FMN) results in formation of a covalent bond between a conserved cysteine and the C4a atom of the FMN. This process initiates structural changes in the FMN-binding pocket, which are presumed to propagate through LOV domain to the kinase domain. We focus on a light-driven signal transduction mechanism in the LOV2 domain. High-resolution dark and light crystal structures of the LOV2 (404-546) construct have been determined at 105K and room temperature. LOV2 (404-546) possess the typical Per-ARNT-Sim (PAS) fold, which is flanked by a newly determined conserved N-terminal turn-helix-turn motif and a C-terminal amphipathic  $\alpha$  helix. These regions dock on the LOV2 core domain and bury certain hydrophobic residues that would otherwise be exposed to solvent. Light structures of LOV2 (404-546) reveal that formation of the covalent bond between Cys450 and the C4a atom of the FMN results in local rearrangement of the hydrogen-bonding network among residues in the FMN-binding pocket. These rearrangements are also associated with disruption of the Asn414-Asp515 hydrogen bond on the surface of the protein and displacement of the N- and C-terminal flanking regions of LOV2 (404-546), both of which constitute a structural signal.

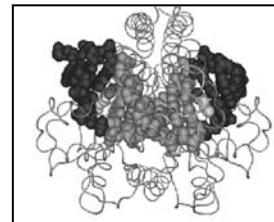
**TP143 Differential P<sub>1</sub> Arginine and Lysine Recognition in the Prototypical Proprotein Convertase Kex2.** Todd Holyoak, Joshual L. Wheatley, Dept. of Biochemistry and Molecular Biology, The Univ. of Kansas Medical Center, Kansas City, KS.

The high-resolution crystal structure of Kex2 in complex with a peptidyl-chloromethylketone inhibitor containing a non-cognate lysine at the P<sub>1</sub> position provides the structural basis for the differential lysine/arginine selectivity that defines the PC family. By comparison with the previous structures of Kex2 and furin, this structure of the acylated enzyme provides a basis for the observed decrease in the acylation rate with substrates containing a lysine at P<sub>1</sub> and the absence of an effect upon the deacylation rate without involving mobility of the S<sub>1</sub>-lid. The structure of the complex shows that a secondary subsite in the S<sub>1</sub> pocket is present and that this site recognizes and binds the P<sub>1</sub> lysine in a more shallow fashion than arginine. This results in a displacement of the bound peptide away from the S385 nucleophile

relative to substrates containing a P<sub>1</sub> arginine. It is concluded that this alternate binding site and resultant displacement of the scissile bond in the active site results in the observed decrease in the acylation rate. Studies of the inactivation kinetics of Kex2 by two peptidyl chloromethylketone inhibitors demonstrates that the selectivity between lysine and arginine at the P<sub>1</sub> position arises at the acylation step consistent with what was observed with peptidyl substrates (Rockwell, N. C. & Fuller, R. S. (2001) *J Biol Chem* 276, 38394-9).

**TP144 Alteration of Sequence Specificity of a Type II Restriction Endonuclease via an Indirect Readout Mechanism.** N. C. Horton, Dept. of Biochemistry and Molecular Biophysics, Univ. of Arizona, Tucson, AZ.

HincII is a sequence specific DNA endonuclease which cleaves duplex DNA at sequences GTYRAC (where Y=C or T and R=A or G). The x-ray crystal structure shows that HincII makes direct contacts to all bases of the recognition sequence, with the exception of the base at the Y position. The DNA bound to HincII is also highly distorted at the center YR step, suggesting that HincII may be using indirect readout of the DNA sequence as part of DNA sequence recognition. Modeling suggests a connection between DNA intercalation by the side chain Q138 and the DNA distortion at the YR sequence 3 base pairs away. We prepared the mutant HincII, Q138F, in order to test the connection between DNA intercalation and indirect readout of the DNA sequence. Multiple turnover kinetic studies indicated that Q138F HincII did possess an altered specificity at the YR sequence. However, binding studies showed no effect by the mutation on affinity for the different DNA sequences. Single turnover DNA cleavage measurements did show a 4 four fold greater preference for TA over CG, relative to the wild type enzyme by Q138F HincII. X-ray crystal structures of the mutant enzyme with the different DNA sequences show that the origin of the altered preference derives from the different base stacking energies of AA vs. GG.



**TP145 Introducing Mutations in *Methanococcus jannaschii* Aspartate Transcarbamoylase.** Nermina Covic, Jacqueline Vitali, Cleveland State Univ., Cleveland, OH.

The catalytic trimer of *Methanococcus jannaschii* aspartate transcarbamoylase is extremely heat stable, maintaining 75% of its activity after heat treatment for 60 min at 75° C. The structural analysis of a C2 crystal form with two catalytic trimers per asymmetric unit showed that the two crystallographically independent trimers associate into a stable staggered complex with an inter-trimer distance of 33.8 Å. In addition, each trimer has a sulfate in its central channel at the center of an extensive ion pair network.

We are carrying two types of mutations in order to understand their effect on the thermostability of this system. The first is in the residues that are part of the extensive ion pair network in the central channel. The second is in the residues at the interface of the two trimers. Our progress will be discussed in the presentation.

**TP146 Crystal Structure of a Signaling-competent Reelin Fragment.** Terukazu Nogi<sup>1</sup>, Norihisa Yasui<sup>1</sup>, Tomoe Kitao<sup>1</sup>, Kenji Iwasaki<sup>1,2</sup>, Junichi Takagi<sup>1</sup>, <sup>1</sup>Research Center for Structural and Functional Proteomics, Inst. for Protein Research, Osaka Univ., <sup>2</sup>Core Research for Evolution and Technology (CREST).

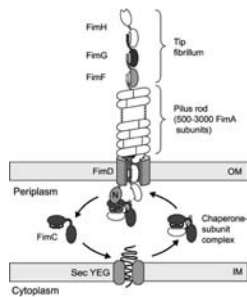
Reelin, a gigantic extracellular glycoprotein produced by Cajal-

Retzius and other neurons in the cortex, plays a central role in cortical layer formation during mammalian brain development. It is now accepted that reelin binds to the lipoprotein receptors ApoER2 or VLDLR and initiates a signaling cascade involving phosphorylation of the adaptor molecule Dab-1. Biochemical basis for the reelin-receptor interaction, however, remained poorly understood due to lack of structural information. Reelin consists of eight tandem repeats, termed reelin repeat, which has a central EGF motif flanked by two homologous subrepeats. Although the two subrepeats show a weak sequence similarity to each other, they fail to show any sequence similarity to other known protein domains. In this study, we first tried to obtain the 3D structural data on the reelin repeat. We designed and tested a series of deletion constructs of reelin to find a fragment suitable for structural study. As a result, the third repeat, R3, showed the highest expression level, and was subjected to crystallization. The R3 fragment was produced in the mammalian expression system, and the structure has been solved by the Se-SAD method. The resulting structure had a horseshoe-like globular structure with some similarities to carbohydrate binding modules. Next, we carried out functional analysis on the reelin-receptor interaction, and succeeded in narrowing down the receptor-binding unit to a two-repeat fragment. In this presentation, we will present the crystal structure of the minimum signaling-competent unit of reelin and discuss the interaction mode between reelin and its receptor at an atomic level.

**SP147 Structural Insights into Type 1 Pilus Assembly.** Oliv Eidam<sup>1</sup>, Mireille Nishiyama<sup>2</sup>, Michael Vetsch<sup>2</sup>, Chasper Puorger<sup>2</sup>, Florian Dworkowski<sup>2</sup>, Denis Erilov<sup>2</sup>, Franck Tarendeau<sup>3</sup>, Diego Sanchez<sup>1</sup>, Darren J. Hart<sup>3</sup>, Rudi Glockshuber<sup>2</sup>, Guido Capitani<sup>1</sup>, Markus G. Grutter<sup>1</sup>, <sup>1</sup>Dept. of Biochemistry, Univ. of Zurich, Switzerland, <sup>2</sup>Inst. of Molecular Biology, ETH Zurich, Switzerland, <sup>3</sup>European Molecular Biology Lab. (EMBL), Grenoble, France.

Type 1 pili enable uropathogenic *E. coli* to bind to epithelial cells of the urinary tract and are therefore a main virulence factor for cystitis (bladder infection).

Type 1 pili are heterooligomeric protein complexes composed of several thousand protein subunits (FimH, FimG, FimF and FimA) which are assembled by the chaperone-usher pathway (see schematic figure). In this pathway (which is conserved among many pathogenic bacteria) a periplasmic chaperone (FimC) binds pilus subunits and delivers them to the "usher" (FimD), where binary chaperone-subunit complexes are recognized by the N-terminal domain of the assembly platform (FimD<sub>N</sub>).

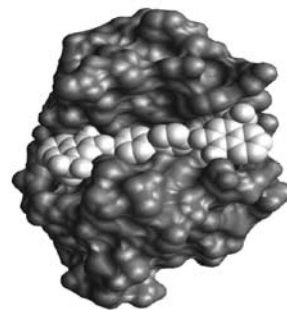


To gain a deeper understanding of the entire pilus assembly process, we have determined several protein-protein complexes of the type 1 pilus system. For example, the X-ray structure of the ternary complex of FimD<sub>N</sub> bound to the chaperone-subunit complex FimC-FimH<sub>p</sub> provides the first atomic resolution insights into a key event of pilus assembly: substrate binding by the usher. An overview of our crystallographic, biochemical and bioinformatic work is presented.

**TP148 Further Computational Studies at the Micromolecule / Macromolecule Interface.** D.A. Straka<sup>1,2</sup>, M.M. Siorek<sup>3</sup>, W.B. Gleason<sup>1,4,5</sup> Depts. of Chemistry<sup>1</sup>, Computer Science<sup>2</sup>, Physics<sup>3</sup>, Lab. Medicine & Pathology<sup>4</sup>, Biomedical Engineering Inst.<sup>5</sup>, Univ. of Minnesota, Minneapolis, MN.

*In silico* lead development is of continuing interest for the development of new therapeutic agents. When an experimental structure of **126**

the macromolecule is available, docking techniques are particularly popular for high throughput small molecule categorization. Using Autodock 3.05, we have investigated several clinically relevant systems including the EGFR receptor kinase domain, HIV protease, and lysozyme. The EGFR kinase domain has been docked with a series of compounds to investigate the conservation of ligand binding interactions. Docking of the HIV protease with several classes of inhibitors including azo dyes, monosulfates, and disulfates has also been studied. In preparation for continuing crystallization experiments, models have been developed for the binding of Congo Red to lysozyme. In addition to docking studies, results of molecular dynamics simulations will be presented.



CR-Lysozyme Complex  
PDB = 2LYZ

We thank the Minnesota Supercomputer Institute and the Undergraduate Research Opportunities Program (UROP) at Minnesota for support.

**TP149 High Resolution Protein Crystallography and Electrostatic Interaction Energy Computation.** B. Fournier, A. Lagoutte, E. Bendeif, B. Guillot, V. Pichon-Pesme, C. Jelsch, C. Lecomte, LCM3B, UHP Nancy I, Vandoeuvre-les Nancy, France.

The PDB shows that the number of (ultra-)high resolution biological macromolecules X-ray structures is increasing very rapidly. Feasibility of multipolar refinement [Hansen and Coppens, 1978] of such structures has been proved [Jelsch *et al.*, PNAS 2000 97: 3171-3176], assuming sufficiently low thermal motion. This model gives an analytical representation of the charge density. It enables the experimental estimation of electrostatic potential [Muzet *et al.*, PNAS 2003 100: 8742-8747] and electrostatic interaction energy. As these properties are of major importance in many biological processes (catalysis, molecular recognition, ligand binding), computing intermolecular electrostatic interaction energy is a necessary step in analyzing the structure-function relationships, providing informations related to biological macromolecules activity.

We will present the advancement of the crystallographic software suite MoPro & VMoPro [Jelsch, J. *et al.*, *J. Appl. Cryst.* 2005 38: 38-54] for the estimation of protein-ligand interaction energy. The energy computation, developed in our software, is a numerical integration of the product of the ligand charge density times the protein electrostatic potential, both obtained from the VMoPro software. The protein electron density parameters may be either refined or transferred from our charge density database [Zarychta, *Acta. Cryst.* A63 2007]. The software allows computing the total electrostatic energy and the van der Waals energetic contribution.

This new development is applied to the human aldose reductase (hAR), a protein involved in diabetic diseases. To illustrate our method, the interaction energy between the hAR and a new inhibitor, Fidarestat, will be presented.

**TP150 Twin Refinement of C-terminal Domain HCN Channel Protein.** B. Sankaran<sup>a\*</sup>, P.H. Zwart<sup>a</sup>, G. E. Flynn<sup>b</sup>, K. D. Black<sup>b</sup>, W.N. Zagotta<sup>b</sup>, P.D. Adams<sup>a</sup>, <sup>a</sup>Lawrence Berkeley National Lab., Physical Biosciences Div., Berkeley, CA, <sup>b</sup>Dept. of Physiology and Biophysics, Howard Hughes Medical Inst., Univ. of Washington, Seattle, WA.

Twinning detected in a recent <sup>[1]</sup> structure of a C-terminal domain of a hyperpolarization-activated, cyclic nucleotide-modulated (HCN) channel protein led to the discovery that two related <sup>[2]</sup> crystal struc-

tures are twinned as well. A re-refinement of these structures with *phenix.refine*<sup>[3,4,5]</sup> resulted in lower R values. The twinning in these structures is obscured by the presence of a non crystallographic symmetry axis parallel to the twin law.

A significant decrease in R-value was observed for one of the structures when least-squares twin refinement was combined with the refinement of a TLS model. A detailed comparison of the structures and electron density maps refined with and without inclusion of the assumption of twinning will be presented.

[1] G.E. Flynn, K.D. Black, L.D. Islas, B. Sankaran & W.N. Zagotta. *Submitted*.

[2] W.N. Zagotta, N.B. Olivier, K.D. Black, E.C. Young, R. Olson, & E. Gouaux, (2003) *Nature*, **425**, 200-205.

[3] P.D. Adams, R.W. Grosse-Kunstleve, L.-W. Hung, T.R. Ioerger, A.J. McCoy, N.W. Moriarty, R.J. Read, J.C. Sacchettini, N.K. Sauter and T.C. Terwilliger. (2002) *Acta Cryst.* **D58**, 1948-1954.

[4] P. Afonine, R.W. Grosse-Kunstleve & P.D. Adams (2005), *CCP4 newsletter* **42**.

[5] P.H. Zwart, R.W. Grosse-Kunstleve, P.Afonine & P.D. Adams, *to be published*.

**TP151 Parallelization of SHELXD to Quickly Solve Heavy-atom Partial Structures on High-performance Computers.** Zheng-Qing Fu<sup>1,2</sup>, John Chrzas<sup>1,2</sup>, George M. Sheldrick<sup>3</sup>, John Rose<sup>1</sup>, Bi-Cheng Wang<sup>1</sup>, <sup>1</sup>Dept. of Biochemistry and Molecular Biology, Univ. of Georgia, Athens, GA, <sup>2</sup>SER-CAT, APS, Argonne National Lab., Argonne, IL, <sup>3</sup> Dept. Structural Chemistry, Univ. of Göttingen, Göttingen, Germany.

A parallel algorithm and computer program is developed for SHELXD to quickly solve the heavy-atom partial structures of protein crystals. Tests on the 32-cpu Linux cluster at SER-CAT, APS, Argonne National Laboratory show that the parallelization dramatically speeds up the process by a factor of roughly the number of CPUs applied, leading to reliable and instant heavy-atom sites solution, which provides the opportunity to practically bring the heavy-atom search up as an alternative tool for anomalous scattering data quality evaluation during SAD/MAD data collection at synchrotron beamlines. The program also runs on multiple-CPU Linux PCs or workstations, and is available by sending an email to fuzq@anl.gov. The parallelization algorithm described in this work can be adapted to parallel any other direct-method-based programs or programs having the similar nature that search or derive the solution by starting with initial sets of parameters.

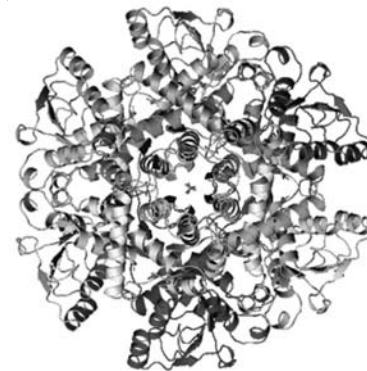
**TP152 Use of the All-atom Force Field OPLS in PrimeX to Restrain Protein Refinement at Moderate Resolution.** Jeffrey A. Bell, Yixiang Cao, Schrödinger LLC, New York, NY.

The first release of PrimeX provides a graphical and computational environment for the complete refinement of molecular replacement structures. It features automated real-space loop building of up to forty residues and Glide-based ligand placement that is well-suited to the analysis of binding in the presence of ambiguous electron density. PrimeX uses the all-atom force field OPLS for geometric restraints with a maximum likelihood target function for X-ray refinement. The requirement for at least transient positioning of all hydrogens in the structure for calculation of the geometric gradients, and the consequences for reciprocal-space refinement of using this all-atom force field will be discussed. The benefits of the use of this force field will be analyzed with respect to crystallographic and structural metrics typically used for validation of protein crystal structures. The hybrid refinement of all atoms under the influence of the force field and of non-hydrogens according to the maximum likelihood target help produce a high-quality model that is well optimized for use in computational chemistry operations such as ligand docking.

**TP153 Structure of the Catalytic Trimer of *Methanococcus jannaschii* Aspartate Transcarbamoylase.** Jacqueline Vitali<sup>1</sup>, Michael Colaneri<sup>2</sup>, Evan Kantrowitz<sup>3</sup>, <sup>1</sup>Cleveland State Univ., Cleveland, OH, <sup>2</sup>SUNY College at Old Westbury, Old Westbury, NY, <sup>3</sup>Boston College, Chestnut Hill, MA.

The catalytic trimer of *Methanococcus jannaschii* aspartate transcarbamoylase is extremely heat stable, maintaining 75% of its activity after heat treatment for 60 min at 75° C. We undertook its structural analysis in order to understand the molecular basis of its thermostability. The crystals are monoclinic C2 with cell constants  $a = 139.90$ ,  $b = 91.89$ ,  $c = 154.20$  Å and  $\beta = 98.30^\circ$ , two catalytic trimers per asymmetric unit, and diffract to 2.8 Å. The structure was determined by molecular replacement using a model derived from the *E. coli* catalytic trimer. Model building was facilitated with NCS averaged maps over all six monomers.

The refinement was carried out with CNS using NCS restraints for most of the six monomers Final R and Rfree are 0.199 and 0.257. Several structural elements potentially contributing to thermostability were identified. These include: (i) changes in the amino acid composition such as a decrease in the thermolabile residues Gln and Asn, an increase in the charged residues Lys and Glu, an increase in Tyr and a decrease in Ala residues; (ii) a larger number of salt bridges, in particular, the improvement of ion-pair networks; (iii) shortening of the N-terminus and shortening of three loops. An interesting feature of the crystal structure is the association of two crystallographically independent catalytic subunits into a staggered complex with an inter-trimer distance of 33.8 Å which is illustrated in the Figure.



**TP154 Structures of Human MutS $\alpha$  DNA Lesion Recognition Complexes: Phasing a Large Complex Structure at Moderate Resolution.** J.J. Warren<sup>1</sup>, T.J. Pohlhaus<sup>1</sup>, A. Changela<sup>1</sup>, P.L. Modrich<sup>1,2</sup>, L.S. Beese<sup>1</sup>, <sup>1</sup>Dept. of Biochemistry, <sup>2</sup>Howard Hughes Medical Inst., Duke Univ. Medical Center, Durham, NC.

The DNA mismatch repair (MMR) pathway ensures the fidelity of DNA replication, initiates the cellular response to certain classes of DNA damage, and has been implicated in the generation of immune diversity. Each of these functions requires the activity of MutS $\alpha$  (a heterodimer of MSH2•MSH6). Inactivation of this protein complex is responsible for tumor development in about half of known hereditary nonpolyposis colorectal cancer kindreds, and also occurs in ~15% of all sporadic tumors in a variety of tissues. The ~230 kDa human MutS $\alpha$ -ADP-DNA mismatch ternary complex crystallizes in the cubic spacegroup P4<sub>3</sub>32. A variation on SIRAS with a Ta<sub>6</sub>Br<sub>12</sub> heavy atom cluster derivative followed by selenomethionine MAD phasing yielded initial phases to ~4.25Å, and the final model was refined to 2.75Å. Additional structures of MutS $\alpha$  with were solved by fourier synthesis from the initial, experimentally-determined model. Together these comprise a series of crystal structures of human MutS $\alpha$  bound to DNA substrates representing different classes of recognition events for the diverse functions of MMR. These different lesions are recognized in a similar manner, indicating that diversity of MutS $\alpha$ -dependent responses to DNA lesions is generated downstream of lesion recognition events. This study also allows rigorous mapping of cancer-causing mutations. Results of TLS refinement of these complexes suggest pathways for allosteric communication between different structural elements within the heterodimer.

**TP155 Closed TrpRS Structures Require a Covalent Bond Between Ligands Occupying Two of the Three Subsites.**

P. Laowanapiban, C.W. Carter, Jr., Dept. of Biochemistry and Biophysics, Univ. of North Carolina Chapel Hill, NC.

We have never verified experimentally the circumstantial evidence that the closed conformations of tryptophanyl-tRNA synthetase (TrpRS) are maintained by covalent bonds between AMP and either PPI (PreTS) or tryptophan (Products). We show here that the TrpRS crystal structure complexed with the three fragments, tryptophan, AMP, and PPI solved at 2.7 Å using a combination of molecular replacement, SeMet anomalous scattering and density modification, resembles the substrate-binding open structures. Three native and 3 MAD datasets were collected using synchrotron radiation at SERCAT Beamline 22-ID, APS, ANL. Autoindexing using HKL2000 revealed that the SeMet and native protein complexes possessed different crystal packing. The native dataset was indexed in space group C2 with unit cell dimension of  $a=223.60$ ,  $b=91.98$ ,  $c=158.32$ ,  $\beta=134.01^\circ$  while one SeMet derivative dataset was indexed with lower symmetry in P1 with unit cell dimensions  $a=122.45$ ,  $b=122.86$ ,  $c=122.81$ ,  $\alpha=79.91^\circ$ ,  $\beta=80.62^\circ$ ,  $\gamma=79.87^\circ$ . Molecular replacement using the AD dimer of the open, Trp-complex TrpRS structure (1MB2) placed 9 dimers into the SeMet unit cell in group of three with nearly rhombohedral centering. The anomalous difference Fourier map calculated using the SeMet peak wavelength dataset and phases calculated from the MR solution revealed 167 out of 180 peaks above  $5\sigma$ , all corresponding to methionine sulfur positions. Selenium positional parameters were refined (SHARP) and the remaining 13 sites were identified in the residual map. The phase ambiguity was resolved by density modification using SOLOMON. Protein-bound ligands in the electron density map will be identified and built for further protein-ligand interaction analysis.

Supported by NIH GM 48519.

**TP156 Expanding Structural Genomics High-throughput Protein Structure Determination Pipeline to Challenging Targets.**

R.-G. Zhang<sup>1</sup>, A. Binkowski<sup>1</sup>, C.-S. Chang<sup>1</sup>, M. Cuff<sup>1</sup>, M. Cymborowski<sup>2</sup>, N. Duke<sup>1</sup>, Y.-C. Kim<sup>1</sup>, B. Nocek<sup>1</sup>, J. Osipiuk<sup>1</sup>, F. Rotella<sup>1</sup>, K. Tan<sup>1</sup>, Z. Otwinowski<sup>3</sup>, W. Minor<sup>2</sup>, A. Joachimiak<sup>1</sup>, <sup>1</sup>Midwest Center for Structural Genomics and Structural Biology Center, Biosciences, Argonne National Lab., Argonne, IL, <sup>2</sup>Univ. of Virginia, Charlottesville, VA, <sup>3</sup>Univ. of Texas, Southwestern Medical Center, Dallas, TX.

The Midwest Center for Structural Genomics (MCSG) has established a protein structure determination pipeline using x-ray crystallography and synchrotron radiation and applies this pipeline to a wide range of proteins including biomedical and community proposed targets. Using this pipeline the MCSG has determined and deposited to PDB 312 structures in PSI2 and 592 total. However, a number of projects present difficult problems at various stages of the process and challenge the limits of current high-throughput methods. Cases in which initial structure determination attempts fail are being evaluated and based on the analysis different approaches are being applied. These include: optimization of crystals and their quality, cocrystallization with ligands and additives, improving crystal cryo-protection, improving low resolution data coverage and increasing data redundancy, checking for twinning, verifying space group, searching for non-crystallographic symmetry, improving phases, model building and refinement parameters. The MCSG pipeline is being adjusted with newly gained expertise. In some special cases a combination of manual and semi-automated methods are used for model improvement and refinement. All the MCSG structures and their analysis are made available to the public.

This work was supported by NIH Grant GM074942 and by the U.S. Department of Energy, OBER, under contract DE-AC02-06CH11357.

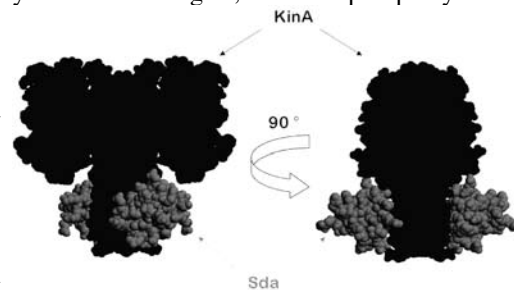
**MP157 Investigation of the Structural Basis for the Inhibition of Histidine Kinase A by Sda in *Bacillus subtilis*.**

David A. Jacques<sup>1</sup>, David B. Langley<sup>1</sup>, Andrew E. Whitten<sup>2</sup>, Boualem Ham-mouda<sup>3</sup>, Tracey L. Hanley<sup>2</sup>, Glenn F. King<sup>4</sup>, J. Mitchell Guss<sup>1</sup>, Jill Trehwella<sup>1</sup>, <sup>1</sup>Univ. of Sydney, NSW, Australia, <sup>2</sup>Bragg Inst., Lucas Heights, NSW, Australia, <sup>3</sup>National Inst. for Standards and Technology, Gaithersburg, MD, USA, <sup>4</sup>Univ. of Connecticut Health Center, Farmington, CT, USA.

The *Bacillus subtilis* histidine kinase A (KinA) regulates the activation of the transcription factor, Spo0A, that governs sporulation. In response to an as yet unidentified signal, KinA autophosphorylates at a conserved histidine residue.

The phosphate is relayed via two other proteins to Spo0A, which becomes activated. The D N A - d a m - a g e checkpoint inhibitor, Sda, halts the sporulation pathway by binding to KinA and inhibiting the autokinase reaction. The structure of Sda has been solved by NMR methods, and while the structure of KinA is unknown, there are homologous structures that provide a basis for modelling. It had been proposed that Sda sterically blocks the catalytic domains of KinA from accessing the target histidine. Small-angle X-ray scattering (SAXS) revealed low-resolution structural information on the KinA, Sda, and KinA<sub>2</sub>:Sda<sub>2</sub> complex in solution.

Small-angle neutron scattering (SANS) with contrast variation was used to obtain details of the interaction between KinA and Sda. The scattering data show that upon Sda binding, KinA undergoes a conformational change, which results in a compaction of the structure. The SANS data revealed that two monomers of Sda bind KinA, and that the centres of these monomers are separated by a distance of ~45 Å. SANS also revealed that the centres of mass of KinA and Sda were separated by ~27 Å. Using these constraints and the available structural models for the components, we used a rigid body refinement method to model the KinA<sub>2</sub>:Sda<sub>2</sub> complex.

**MP158 Protein Organization in Lipid Membranes.** Thomas M. Weiss, SSRL, Stanford Univ., Menlo Park, CA.

Using the technique of grazing incidence X-ray scattering on highly aligned, substrate supported membranes to investigate the organization of small proteins embedded in the lipid bilayer. By changing the hydration level of the membrane matrix, interactions between the proteins within one membrane layer as well as across neighboring layers within the stack can be induced. These interactions lead to partial ordering of the proteins within the membranes as signified by higher order reflections in the measured scattering intensity.

**MP159 Small-Angle X-ray Scattering Study of the Ligand-Induced Conformational Changes in the N-terminal Region of the Inositol Triphosphate Receptor.**

A.E. Whitten<sup>1,2</sup>, J. Chan<sup>3</sup>, I. Bosanac<sup>3</sup>, T.K. Mal<sup>3</sup>, J. Ito<sup>3</sup>, C.M. Jeffries<sup>2</sup>, J. Trehwella<sup>2</sup>, T. Michikawa<sup>4</sup>, K. Mikoshiba<sup>4</sup>, M. Ikura<sup>3</sup>, <sup>1</sup>Bragg Inst., ANSTO, <sup>2</sup>School of Molecular and Microbial Biosciences, Univ. of Sydney, <sup>3</sup>Div. of Signalling Biology, Ontario Cancer Inst., Dept. of Medical Biophysics, Univ. of Toronto, <sup>4</sup>Div. of Molecular Neurobiology, The Inst. of Medical Science, Univ. of Tokyo.

Intracellular second messengers, such as Ca<sup>2+</sup> and inositol 1,4,5-triphosphate (IP<sub>3</sub>), play critical roles in the regulation of protein func-

tions and signal transduction. Of specific interest is how  $\text{Ca}^{2+}$  and  $\text{IP}_3$  modulate the calcium channel function of the  $\text{IP}_3$  receptor ( $\text{IP}_3\text{R}$ ) as part of a mammalian cell's response to external signals. The receptor contains four functionally different regions, and one of these is a 604 residue N-terminal cytoplasmic region ( $\text{IP}_3\text{R}_\text{N}$ ).  $\text{IP}_3\text{R}_\text{N}$  contains the  $\text{IP}_3$ -binding core (that binds  $\text{IP}_3$  in the cleft between the  $\beta$ -trefoil and  $\alpha$ -helical domains) and the suppressor domain (that brings  $\text{IP}_3$  binding into the physiologically relevant range). There are crystal structures for both domains separately<sup>[1]</sup>, but there is no crystal structure of the entire  $\text{IP}_3\text{R}_\text{N}$  domain. To study the domain interactions within  $\text{IP}_3\text{R}_\text{N}$  and to understand how these might regulate  $\text{Ca}^{2+}$  flow, we have undertaken small-angle X-ray scattering (SAXS) experiments. SAXS is sensitive to domain rearrangements, such as those that occur upon ligand binding, hence, data collected on the protein in the presence and absence of both  $\text{IP}_3$  and  $\text{Ca}^{2+}$ , should yield insight into how  $\text{IP}_3\text{R}_\text{N}$  modulates calcium channel function.

[1] I. Bosanac, *et al.*, *Nature*, **420** (2002), pp 696 – 700; I. Bosanac, *et al.*, *Molecular Cell*, **17** (2005), pp 193-203.

**MP160 In-situ X-ray Scattering and Brewster-angle Microscopy Studies of 2D Streptavidin Crystals Bound to a Lipid Monolayer at the Solution/vapor Interface.** Suntao Wang, Lin Yang, Benjamin Ocko, Masfumi Fukuto, National Synchrotron Light Source, Brookhaven National Lab., Upton, NY.

Adsorption and two-dimensional (2D) crystallization of soluble protein streptavidin on a biotinylated lipid monolayer at an aqueous solution/vapor interface have been studied using *in-situ* x-ray and optical methods. For a given subphase and lipid condition, surface normal and in-plane structures at molecular length scales were elucidated via synchrotron x-ray reflectivity (XR) and grazing-incidence diffraction (GID) measurements, respectively, at the solution/vapor interface. For GID, CCD was used for fast data collection while a microfocusing mirror was used to enhance the lateral resolution by reducing the illuminated footprint area. The 2D crystalline structures thus revealed were correlated with the morphologies of growing 2D crystal domains observed optically by carrying out Brewster-angle microscopy (BAM) under exactly the same lipid, protein, and sub-phase conditions. The results show that at high salt concentration (0.5 M NaCl) and moderate biotin surface density (130 or 650  $\text{\AA}^2/\text{biotin}$ ), streptavidin nearly always forms 2D crystals, but both the unit cell structures and the crystal domain shapes are different at low, intermediate and high subphase pH values (3.2, 5.5, and 8.2).

**MP161 Small-angle X-ray Scattering Study of Photosystem I-Detergent Complexes.** Volker S. Urban, Hugh O'Neill, William T. Heller, Katherine E. Helton, Elias Greenbaum, Chemical Sciences Div. and Center for Structural Molecular Biology, Oak Ridge National Lab., Oak Ridge, TN.

Small-angle X-ray scattering (SAXS) was used to investigate the structure of isolated Photosystem I (PSI) complexes in detergent solution. PSI prepared by solubilizing thylakoid membranes with Triton X-100 and purified by density gradient centrifugation exhibits large scattering objects that can be described as sheets with  $\sim 68\text{\AA}$  thickness and a virtually infinite lateral extension. Conversely, PSI preparations further purified by anion exchange chromatography result in functional complexes consisting of single PSI units with attached surfactant as evidenced by the particle volume and gyration radius extracted from SAXS. Several approaches to model the solution conformation of the complex found extended structures with dimensions not consistent with the PSI crystal structure. The SAXS data also rule out a model using the crystal structure embedded in a disk of detergent. Considering the possibility of partially unfolded

protein, the data were modeled using a "beads-on-a-string" approach that describes detergent micelles associated with the unfolded polypeptide chains. This model reproduces characteristic features of the SAXS data at short length scales, but is not consistent with the data at larger length scales. We conclude that the polypeptide subunits at the periphery of the PSI complex were partially unfolded and associated with detergent micelles while the catalytically active core of the PSI complex remained structurally intact.

Work supported by the Offices of Basic Energy Sciences and Biological and Environmental Research, U. S. Department of Energy, under contract no. DE-AC05-00OR22725 with Oak Ridge National Laboratory, managed and operated by UT-Battelle, LLC.

**MP162 Mechanism of the Self Assembly of Amyloid Congeners into Supramolecular Structures.** S.V. Pingali<sup>1</sup>, Y. Liang<sup>2</sup>, P. Liu<sup>2</sup>, S.W. Childers<sup>2</sup>, K. Lu<sup>2</sup>, D.G. Lynn<sup>2</sup>, P. Thiyagarajan<sup>1</sup>, <sup>1</sup>IPNS, Argonne National Lab., IL, <sup>2</sup>Emory Univ., Atlanta, GA.

Amyloid peptide's unique amphiphilic character allows the peptide to self-assemble in aqueous media into well-organized fibrillar structures. A smaller variant K<sup>16</sup>L<sup>16</sup>V<sup>16</sup>F<sup>16</sup>A<sup>22</sup> was studied using SAXS and WAXS to probe the self-assembly mechanism of the amyloid peptides. The effect of hydrophobic and side-chain interactions on the self-assembly was studied by different substitutions at the 17<sup>th</sup> and 18<sup>th</sup> positions. Wildtype peptide forms nanotubes of diameter (d) $\sim 53\text{nm}$  and a shell thickness (t) $\sim 4.5\text{nm}$  in acidic pH, but forms rectangular fibrils of thickness  $\sim 3.3\text{nm}$  at neutral pH. Our studies show that a bulkier and more hydrophobic terleucine at the 18<sup>th</sup> position forms larger nanotubes with d $\sim 68\text{nm}$  and t $\sim 5.5\text{nm}$  in acidic pH and interestingly, in contrast to wildtype, at neutral pH forms nanotubes with d $\sim 60\text{nm}$  and t $\sim 4.5\text{nm}$ . On the other hand, substitutions at the 17<sup>th</sup> position with L2-aminobutyric acid (a short linear chain, lower hydrophobicity) results in nanotubes with d $\sim 43\text{nm}$  and t $\sim 5\text{nm}$  in acidic pH and at neutral pH forms larger nanotubes with d $\sim 70\text{nm}$  and t $\sim 4.5\text{nm}$ . However, nanotube formation is disrupted by the substitutions: terleucine at 17<sup>th</sup> position and L2-aminobutyric acid at 18<sup>th</sup> position. All the samples exhibited the classic cross-beta diffraction pattern and the nanotubes exhibited more pronounced  $\sim 10\text{\AA}$  peaks. The dramatic difference in the supramolecular structure we propose to be due to the variation in the interfacial curvature caused by the interplay between the hydrophobic interaction between the laminates and the charge at the termini.

Work benefited from the use of IPNS and APS funded by DOE, BES under contract DE-AC02-06CH11357 to the UChicago Argonne, LLC and funding from DOE ER15377 to DGL.

**MP163 Use of Ligand- and Fragment-based Cocktail Crystallography to Identify Binding Sites in Potential Drug Targets From Tropical Parasites.** E.T. Larson<sup>1,2</sup>, T.L. Arakaki<sup>1,2</sup>, I. Le Trong<sup>1,2</sup>, J. Bosch<sup>1</sup>, H. Neely<sup>1,2</sup>, E. Boni<sup>1,2</sup>, N. Mueller<sup>1,2</sup>, A. Napuli<sup>1,2</sup>, A. Kelley<sup>1,2</sup>, B.E. Krumm<sup>1,2</sup>, L. Xiao<sup>1,2</sup>, S. Shibata<sup>1,2</sup>, Z. Zhang<sup>1,2</sup>, W. Deng<sup>1,2</sup>, F. Zucker<sup>1,2</sup>, E. Fan<sup>1,2</sup>, F.S. Buckner<sup>1,3</sup>, W.C.E. Van Voorhis<sup>1,3</sup>, C.L.M.J. Verlinde<sup>1,2</sup>, W.G.J. Hol<sup>1,2</sup>, E.A. Merritt<sup>1,2</sup>, <sup>1</sup>Medical Structural Genomics of Pathogenic Protozoa Consortium, Depts. of <sup>2</sup>Biochemistry and <sup>3</sup>Medicine, Univ. of Washington, Seattle, WA.

Diseases caused by eukaryotic pathogens such as *Plasmodium spp.*, *Trypanosoma spp.*, *Leishmania spp.*, *Toxoplasma gondii*, *Entamoeba histolytica*, *Giardia lamblia* and *Cryptosporidium parvum* have a devastating effect on billions of people around the world. Current drugs generally have major side effects and are being overcome by increased resistance. Design of new drugs to fight and prevent these diseases is clearly needed. The Medical Structural Genomics of Pathogenic Protozoa Consortium is investigating druggable target

enzymes from essential pathways in these pathogens. We use a combination of virtual and biophysical screening with ligand- and fragment-based cocktail crystallography to determine potential lead compounds for structure-based drug design. Several structures of protein-ligand complexes will be presented, including *L. major* coproporphyrinogen III oxidase in the porphyrin metabolic pathway, *T. cruzi* spermidine synthase in the arginine metabolic pathway, *T. brucei* riboflavin kinase in the riboflavin metabolic pathway, *L. donovani* dihydroorotate dehydrogenase in the pyrimidine biosynthetic pathway, and *P. vivax* adenosine deaminase and *T. brucei* nucleoside phosphorylase in the purine scavenging pathway. These structures lay the foundation for future studies in molecular modeling, biochemical, and structure-based drug design.



**MP164 Structure of YraM, a Protein Essential for the Growth of *Haemophilus influenzae*.** M.A. Saper, J. Vijayalakshmi, B.J. Akerley\*, Biophysics Research Div. and Dept of Biological Chemistry, Univ. of Michigan, Ann Arbor, MI, \*Dept of Molecular Genetics and Microbiology, Univ. of Massachusetts Medical School, Worcester, MA.

Nontypeable *Haemophilus influenzae* is an obligate human parasite that causes children's ear infections and exacerbates chronic obstructive pulmonary disorder, the fourth leading cause of death in the U.S. The 575-residue lipoprotein YraM (gene *HII655*) was identified as essential for growth of *H. influenzae*, but its function is unknown. The crystal structure of the N-terminal module (YraM-N, 33–253), solved by M.I.R. (2 Å resolution,  $R_{\text{work/free}} = 0.24/0.28$ ), is all helical containing several TPR-like motifs. Its crescent shape resembles the structure of PilF, yet YraM-N shows no sequence similarity to other proteins other than its homologs. Data from crystals of the C-terminal module (YraM-C, 257–575) were phased by MAD and refined to 1.35 Å ( $R_{\text{work/free}} = 0.21/0.23$ ). Despite low sequence identity, the two-domain structure of YraM-C adopts a fold identical to that observed for the open, unliganded forms of periplasmic binding proteins (PBPs). Sequence alignments with YraM homologs from other Gram-negative species showed that the most conserved residues are in YraM-C and cluster between the two domains in the location where other PBPs bind their cognate ligand. Modeling of YraM-C in the 'closed' form shows a putative binding pocket larger than the Leu-binding site in LIV-binding protein (LIVBP). The pocket has both polar and nonpolar surfaces; the latter analogous to a similar region in LIVBP that interacts with the Leu side chain. Efforts are underway to elucidate the function and putative ligand of this novel fusion protein.

Supported by Philip Morris (M.A.S.), NIH (B.J.A.) and AHA (B.J.A.).

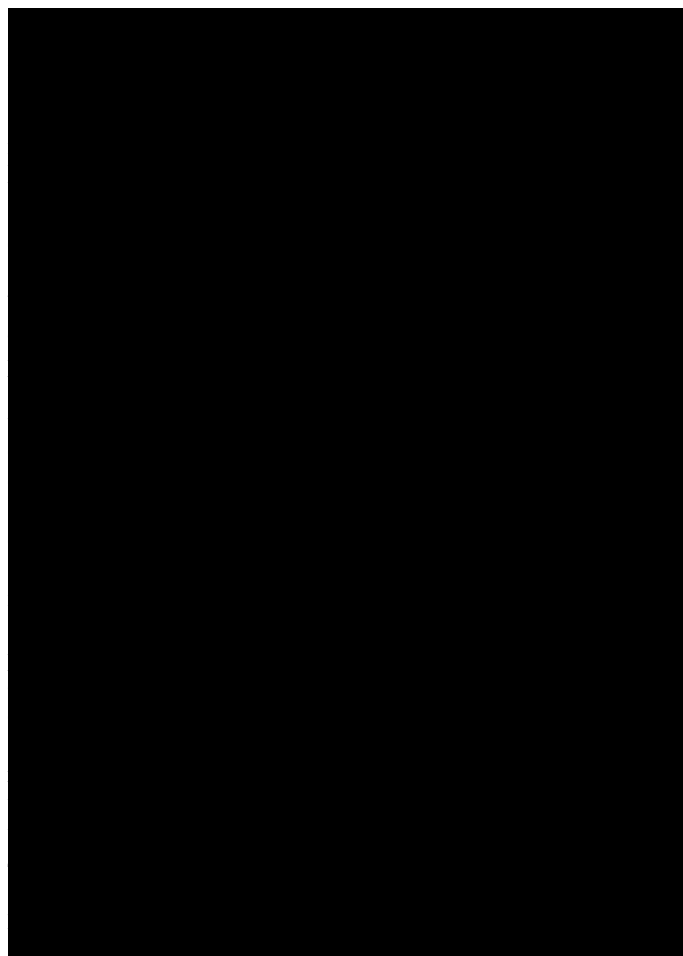
**MP165 The Invasion Machinery of the Malaria Parasite.** J. Bosch<sup>1</sup>, S. Turley<sup>1</sup>, C. Roach<sup>1</sup>, B. Krumm<sup>1</sup>, C. Buscaglia<sup>2</sup>, V. Nussenzweig<sup>2</sup>, A.B. Vaidya<sup>3</sup>, L.W. Bergman<sup>3</sup>, W.G.J. Hol<sup>1</sup>, <sup>1</sup>Dept. of Biochemistry, Univ. of Washington, Seattle, WA, <sup>2</sup>Dept. of Pathology, New York Univ. School of Medicine, New York, <sup>3</sup>Dept. of Microbiology and Immunology, Drexel Univ., Philadelphia, PA.

The causative agents of malaria mainly *Plasmodium falciparum* and *P. vivax* have developed a sophisticated machinery for entering multiple cell types in the human and insect hosts. In this machinery critical interactions occur between a "chain" of proteins, including the unusual myosin motor MyoA and the MyoA-tail Interacting Pro-

tein (MTIP) and Aldolase and TRAP (Thrombospondin Anonymous Repeat Protein) within the parasite. Blocking crucial interactions between proteins belonging to this machinery at multiple life stages of the parasite could lead to a new approach in drug development, replacing current commercially available drugs in areas of increased resistance.

We present two complexes obtained of the Malaria parasite invasion machinery namely the Aldolase:TRAP complex at 2.4Å and the MTIP:MyoA complex at 2.4Å (*P. knowlesi*) and 1.6Å (*P. falciparum*). TRAP is bound in a most unusual manner to Aldolase. The indole ring of the critical penultimate Trp-residue of TRAP fits snugly into a newly formed hydrophobic pocket delimited by only hydrophilic residues: two arginines, one glutamate and one glutamine.

Even more dramatic changes are observed in the MTIP:MyoA complex of the Malaria invasion machinery. The high plasticity has been captured crystallographically in four conformations, revealing major conformational changes in the C-terminal domain of MTIP upon binding the MyoA-tail helix thereby creating several hydrophobic pockets in MTIP, which are the recipients of key hydrophobic side chains of MyoA. The complex of MTIP:MyoA undergoes a large pH-dependent change from an extended to a closed conformation bound to MyoA-tail.



**MP167 Structure-based Pathogen Design – Extending the Host Range of *Listeria monocytogenes*.** T. Wollert<sup>1</sup>, B. Pasche<sup>2</sup>, M. Rochon<sup>3</sup>, A. D. Gruber<sup>4</sup>, J. van den Heuvel<sup>3</sup>, D. W. Heinz<sup>3</sup>, A. Lengeling<sup>2</sup>, W.-D. Schubert<sup>1</sup>, <sup>1</sup>Molecular Host-Pathogen Interactions, Div. of Structural Biology, <sup>2</sup>Infection Genetics, Div. of Microbiology, <sup>3</sup>Div. of Structural Biology, Helmholtz Centre for Infection Research, Braunschweig, Germany, <sup>4</sup>Dept. of Veterinary Pathology, Free Univ. of Berlin, Berlin, Germany.

The food-borne pathogen *Listeria monocytogenes* has co-evolved with and adapted to humans such that it specifically recognizes human E-cadherin through its invasion protein Internalin (InlA). Individual amino acid substitutions in murine E-cadherin are sufficient to avoid recognition by InlA, effectively preventing mice from being infected by the oral route. We have extended the host range of *L. monocytogenes* by structure-based re-engineering of InlA. Based on the crystal structure of the InlA / human E-cadherin complex, we have identified regions of poor complementarity between both proteins. Two rationally chosen point mutations improve complementarity and enhance binding affinity of InlA for human E-cadherin 6700-fold allowing murine E-cadherin to be recognized with a binding affinity similar to that of wild-type InlA for human E-cadherin.

As murine E-cadherin is not recognized by wild-type InlA, *L. monocytogenes* do not cause a lethal infection in a majority of orally infected mice. By contrast, a mutant strain of *L. monocytogenes* that carries both mutations infects mice  $\sim 10^4$ -fold more efficient. Our results indicate that subtle atomic changes in protein interfaces can increase binding affinity and in turn influence entire biological systems, namely the host specificity of *L. monocytogenes*.

Reference: Wollert, T. *et al.* Extending the host range of *Listeria monocytogenes* by rational protein design. *Cell*, in press

**SP168 A Study at 150K and 295K of the Disorder in the Polymorphic System p-methylbenzylidene-p-methylaniline.** A.G. Beasley, T.R. Welberry, Research School of Chemistry, Australian National Univ., Canberra, ACT, Australia.

We are applying diffuse scattering methods to polymorphic molecules with conformational degrees of freedom in order to elucidate the disorder in such systems. The determination of crystal structures beyond the average structures available from Bragg data provides information on intermolecular interactions, which may contribute to solving the problem of polymorph prediction and control.

The molecule p-methylbenzylidene-p-methylaniline (MeMe) has three polymorphs, all of which exhibit strong diffuse scattering indicating substantial disorder. Two of the polymorphs, MeMe1 and MeMe3, have two and four orientations of the molecule, respectively, and it is known that in MeMe3 the molecule interconverts between orientations by a "pedalling" motion of the  $-C=N-$  bridge. Most remarkable is the MeMe2 form which is nominally perfectly ordered and yet its diffraction pattern shows highly structured diffuse scattering indicating the presence of highly correlated displacive disorder. We have produced models of the three polymorphs which reproduce the major features in their room-temperature diffraction patterns. We have recently collected low-temperature (150K) data from all three polymorphs in order to disentangle the static and dynamic components of the disorder.

**MP169 Diffuse Scattering in Octakis(trivinylsilyl)octasilicate.** C. Slebodnick<sup>1</sup>, R. J. Angel<sup>1</sup>, B. E. Hanson<sup>1</sup>, P. Agaskar<sup>2</sup>, T. Soler<sup>3</sup>, L.R. Falvello<sup>3</sup>, <sup>1</sup>Depts. of Chemistry and Geosciences, Virginia Tech, Blacksburg, VA, <sup>2</sup>Spherosils LLC, Princeton, NJ, <sup>3</sup>Dept. of Inorganic Chemistry, Univ. of Zaragoza, Spain.

Octakis(trivinylsilyl)octasilicate was prepared by capping octaspherosilicate cubes,  $(Si_8O_{12})^{8-}$ , with trivinylsilyl groups in methanol solution. Crystals grown from carbon tetrachloride crystallize in the tetragonal space group I4<sub>1</sub> ( $a = 21.170(2) \text{ \AA}$ ,  $c = 16.060(1) \text{ \AA}$ ,  $V = 7197 \text{ \AA}^3$ ). Crystals grown from toluene give a diffraction pattern consisting of sharp peaks that can be indexed on the  $\sim 7200 \text{ \AA}^3$  unit cell with  $h + k$  even, and  $l$  even. The  $l = \text{odd}$  layers exhibit diffuse sheets of intensity which arise from well ordered rods of molecules parallel

to  $c$ . Within the sheets, the intensity is not uniform; there are higher intensity streaks perpendicular to the  $\{110\}$  planes that cross and form maxima at the  $h+k$  odd Bragg positions. These streaks indicate short-range ordering of the rods along  $\langle 110 \rangle$  to form ordered  $\{110\}$  finite layers of rods and that the ordered domains are displaced from one another by random  $00\frac{1}{2}$  fault vectors. This paper describes how the diffuse scattering pattern was used to predict the stacking disorder relative to the ordered structure and how the resulting disordered structural model was fit to the Bragg reflections of the diffuse-scattering sample.

**MP170 Motions of Biological Molecules in Crystals and their Diffuse Scattering.** Demian Riccardi, George N. Phillips, Jr., Biochemistry, Univ. of Wisconsin at Madison, Madison, WI.

The structure of a given biological macromolecule is an ensemble of states. The dynamic transitions between states, due to correlated motions of a subset of atoms, facilitates complex functionality. A typical Bragg experiment yields the average electron density throughout the crystal, and as a result, the diversity of the ensemble is lost. Fortunately, much of information related to various correlated motions can be regained by studying the diffuse scattering, which is a measure of the variance of the Fourier components of the electron density throughout the crystal. The distinct patterns of diffuse scattering due to various correlated motions in a simple two-dimensional, toy system is presented. These concepts are then applied to the experimental scattering of a few biological molecules.

**TP171 Selenium Derivatization of Nucleic Acids for Phasing and Crystallization.** Zhen Huang, Jiansheng Jiang, Jia Sheng, Nicolas Carrasco, Dept. of Chemistry, Georgia State Univ., Atlanta, GA, Huang@gsu.edu.

X-ray crystallography is a powerful tool for structure determination of RNA structure, RNA-protein and DNA-protein complexes with high resolution. Derivatization with heavy atoms for phase determination, however, has largely slowed down structural determination of nucleic acids with novel folds. Recently we have developed a novel strategy to derivatize RNA and DNA by directly replacing oxygen with selenium [1-3]. We find that the Se-derivatized DNA structures have virtually identical structures to the corresponding native structures, while the conventional Br-derivatization caused severe perturbations on the local backbone and hydration [1]. Furthermore, we found that the Se-derivatization can facilitate crystallization and the diffraction quality is high. Our results suggest that the Se derivatization is a better alternative to the conventional Br derivatization. This Se derivatization strategy *via* the atom-specific substitution will significantly facilitate crystal structure studies of nucleic acids and their protein complexes.

This work is supported by NIH (GM069703) and NSF (MCB-0517092).

[1] Jiang, Sheng, Carrasco, Huang\*, "Selenium Derivatization of Nucleic Acids for Crystallography", *Nucleic Acids Research*, 2007, 35, 477-485.

[2] Jia Sheng, Jiansheng Jiang, Jozef Salon, and Zhen Huang\*, "Synthesis of a 2'-Se-Thymidine Phosphoramidite and Its Incorporation into Oligonucleotides for Crystal Structure Study", *Organic Letter*, 2007, 9, 749-752.

[3] Carrasco, Canton-Williams, Brandt, Wang, Huang\*, "Efficient Enzymatic Synthesis of Phosphoroselenoate RNA Using Adenosine 5'-( $\alpha$ -P-seleno)triphosphate, *Angewandte Chemie*, 2006, 45, 94-97.

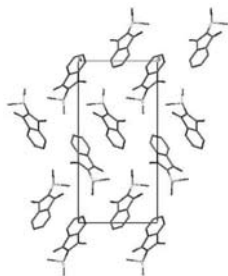
**TP172 SBEVSL: Communicating Scripts Between Molecular Visualization Programs.** C. Westin, B. Hanson, H.J. Bernstein, I. Awuah Asiamah, D. Boycheva, G. Darakev, N. Darakev, J. Jemilawon, N. Jia, P. Kamburov, G. Todorov, P.A. Craig, S. Mottarella, Dept. of Biological Sciences, Rochester Inst. of Technology, Rochester, NY.

Structural biologists and molecular scientists in many other disciplines need to communicate effectively about biological macromolecules. The number and complexity of available structures are both increasingly dramatically. There are many free molecular visualization programs that facilitate macromolecular structure analysis and experimental design. Each program has distinct features and limitations, often leading researchers to utilize multiple programs to successfully investigate all qualities of a macromolecular structure. To alleviate this problem, we are creating a common ontology called the Structural Biology Extensible Visualization Scripting Language (SBEVSL) that will serve as a central resource for communicating scripts between different visualization programs. As a first step, we have prepared a list of individual commands that are used in PyMOL, as well as groups of commands which we are calling "features" to serve as input to SBEVSL. We have also created a plug-in for PyMOL that can take information from the central ontology by reading files line by line, find the associated commands, and output them to another script file. Future steps will lead to script interchange between PyMOL, Rasmol, Jmol and Chime using the SBEVSL ontology as the intermediary in the communication. The completion of this project will allow researchers to move easily between these programs and quickly reproduce the same view in each program, giving them more time to spend on analysis of the macromolecular structure instead of script manipulation.

Work supported in part by grants from NSF ATE 0402408, NIGMS 1R15GM078077-01

**TP173 Comparative Analysis of the Monoclinic and Orthorhombic Polymorphs of YLID and a Comment on the Unit Cell Parameter Precision of the Latter.** Ilia A. Guzei<sup>a</sup>, Galina A. Bikzhanova<sup>a</sup>, Tatiana V. Timofeeva<sup>b</sup>, Tiffany L. Kinnibrugh<sup>b</sup>, Charles F. Campana<sup>c</sup>, <sup>a</sup>Dept. of Chemistry, Univ. of Wisconsin-Madison, Madison, WI, <sup>b</sup>Dept. of Natural Sciences, New Mexico Highlands Univ., Las Vegas, NM, <sup>c</sup>Bruker AXS Inc., Madison, WI.

The centrosymmetric monoclinic ( $P2_1/c$ ) form of YLID (2-dimethylsulfuranylidene-1,3-indanedione), is  $\sim 2.77$  kcal/mol less stable than its non-centrosymmetric orthorhombic ( $P2_12_12_1$ ) form. Excellent agreement is observed among the corresponding molecular parameters in the monoclinic and orthorhombic polymorphs and with those from the theoretically optimized (DFT) molecular structure of YLID. Spherically ground orthorhombic crystals of YLID have been used as test crystals for diffractometry alignment since 1969, and we report how and why YLID was chosen. A statistical analysis of 49 complete room temperature datasets acquired on the orthorhombic YLID test crystals on CCD-equipped diffractometers yields average cell constants of  $a = 5.961(3)$  Å,  $b = 9.037(4)$  Å,  $c = 18.390(9)$  Å, and  $V = 990.6(14)$  Å<sup>3</sup>. The relationship among the axial lengths of the orthorhombic form is 1:1.51613(19):3.0853(7), while the estimated precision of the unit cell lengths determined with a CCD detector equipped diffractometer is  $\sim 5$  parts in  $10^4$ .



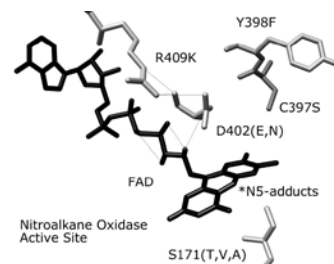
**TP174 Support for Maps in RasMol.** H.J. Bernstein, I. Awuah Asiamah, G. Darakev, J. Jemilawon, P. Kamburov, Dowling College, Oakdale, NY.

RasMol is a popular molecular graphics program, but it lacks support for display of electron density maps. In the past, this omission was a necessary consequence of the need to keep RasMol sufficiently "light weight" to allow it to run efficiently on small computers with limited memory. Many low-end computers now have enough memory to allow for efficient storage and manipulation of maps without disk thrashing. DINO, CCP4MG and PyMOL provide good models for superimposing externally loaded maps onto macromolecular structures. We are combining recent work on compressed map support within CBFLib with cross-fertilization of scripting between PyMol and RasMol in the Structural Biology Extensible Visualization Scripting Language (SBEVSL)<sup>[1]</sup> to provide map manipulation in RasMol. imgCIF has long supported two-dimensional compressed and uncompressed images. Extensions have now been proposed to support three-dimensional maps using similar compression techniques, and the CBFLib API for imgCIF has been augmented to support these extensions. The SBEVSL project is establishing a common scripting language for multiple molecular graphics programs thereby providing the necessary infrastructure to move PyMol map support into RasMol.

Work supported in part by grants from NIGMS (1R15GM078077-01), DOE and NSF. [1] C. Westin, B. Hanson, H. J. Bernstein, I. Awuah Asiamah, D. Boycheva, G. Darakev, N. Darakev, J. Jemilawon, N. Jia, P. Kamburov, G. Todorov, P. A. Craig, S. Mottarella, "SBEVSL: Communicating scripts between molecular visualization programs," abstract submitted to ACA 2007.

**TP175 Mechanistic Insights into Nitroalkane Oxidases from Structures of Trapped Reaction Intermediates and Active Site Mutants.** Annie Héroux, Allen M. Orville, Akanksha Nagpal, Michael P. Valley, Paul F. Fitzpatrick. Biology Dept., Brookhaven National Lab., Upton, NY.

Nitroalkane oxidase (NAO) from *Fusarium oxysporum* catalyzes the oxidation of the neutral nitroalkanes to the corresponding aldehydes or ketones with production of H<sub>2</sub>O<sub>2</sub> and nitrite. The flavoenzyme is a member of the acyl-CoA dehydrogenase (ACAD) superfamily, but it does not react with acyl-CoA substrates. We recently reported crystal structures of oxidized NAO and the enzyme trapped during turnover of nitroethane as a covalent N5-nitrobutyl FAD adduct<sup>[1]</sup>. These structures reveal a hydrophobic channel that extends from the exterior of the protein and terminates at Asp402 and the N5 position on the *re*-face of the FAD. Thus, Asp402 is in the correct position to serve as the active site base, where it is proposed to abstract the  $\alpha$ -proton from neutral nitroalkane substrates. Several residues forming the active site cavity as illustrated in the figure have been mutated and studied by crystallographic and kinetic analysis. The inactive D402N mutant isoform affords the opportunity to crystallize several enzyme-nitrosubstrate complexes. Our ongoing results correlate with the carbanion-based mechanism for the NAO reductive half-reaction. This differentiates NAO from the hydride-transfer reaction mechanism proposed for ACAD family members, and the hydroxylation reaction catalyzed by the structurally homologous *p*-hydroxyphenylacetate 3-hydroxylase from *Acinetobacter baumannii*. Thus individual members of this superfamily catalyze remarkably diverse reactions, but with relatively conserved active site architectures.



[1] Nagpal, A., Valley, M. P., Fitzpatrick, P. F., and Orville, A. M. (2006) *Biochemistry* 45, 1138-1150.

**TP176 Insight into Autoproteolytic Activation of Cephalosporin Acylase: A Mutant with Three Proteolytic Chemistries.**

Jin Kwang Kim<sup>†</sup>, Ki Joon Cho<sup>†</sup>, Hye Jeong Shin, In Seok Yang, Ji-Hye Lee, Kyung Hyun Kim, J.K.K. and K.J.C. contributed equally to this work.

Cephalosporin acylase (CA), a member of the N-terminal nucleophile hydrolase family, is activated through two sequential steps of intramolecular autoproteolysis, the first of which is mediated by a serine residue, and the second by a glutamate. We have determined the sequential intermediate crystal structures of a slow-processing mutant, which show additional self-cleavage. Its double mutant structures provide evidence that the side chain of a threonine residue is involved in this self-cleavage, suggesting that the mutant may harbor three distinct proteolytic chemistries within a single polypeptide. They also provide detailed structural evidence regarding these diverse autoproteolytic activation mechanisms. CA may have evolved separate self-cleaving mechanisms driven by structural constraints, which could be regarded as a minimal requirement for autoproteolysis.

**MP177 Microscale Vapour Diffusion Protein Crystallization Using a New Crystallization Plate.**

Joby Jenkins<sup>1</sup>, A. Marek Brzozowski<sup>2</sup>, <sup>1</sup>TTP LabTech Ltd, Melbourn Science Park, Herts, UK, e-mail: joby.jenkins@ttplabtech.com, <sup>2</sup>Structural Biology Lab., Dept. of Chemistry, Univ. of York, York, UK.

The development of crystallization technologies for high-throughput research has delivered a plethora of crystallization plates suitable for robot driven and manual setups. However, practically all these plates (except microfluidic channel chips) are based on a very similar design and well volume: drop ratios. Therefore we have developed and tested a new type of crystallization plate ( $\mu$ plate) that still employs classical vapour diffusion technique but minimizes the precipitant well volume to 1.2 $\mu$ L. This enables (i) a very significant saving on the total bulk of screens, and (ii) allows the introduction and use of rate and chemically expensive solutions to the automated screening procedures. Due to the very low drop to well volume ration the new  $\mu$ plate can significantly accelerate equilibrium time necessary for crystal nucleation and growth, shortening in many cases the high-throughput crystallisation screening process to a few hours.

**MP178 Structure-based Fragment Screening: Finding Hits for Novel Lead Compound Design.**

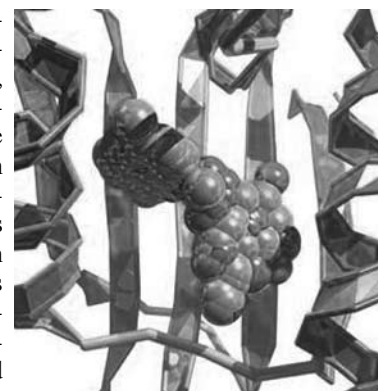
Robin Rosenfeld, John Badger, Paul Collins, Vicki Nienabar, Duncan McRee, ActiveSight, San Diego, CA, www.active-sight.com.

Fragment-based screening is a method for developing novel lead compounds. The goal is to identify small, low molecular weight fragments that bind with high efficiency in an active site. Small fragments have "room to grow" - they can be linked together or built upon in order to generate novel high affinity compounds within the size constraints of a typical drug molecule.

Here, we present a complete home laboratory system for rapid structure-based fragment screening. We created a library containing 384 small molecular weight fragments organized into a kit of shape diverse mixtures of four. We screened our library against several proteins, including Hsp90.

For our pilot project, we soak apo Hsp90 protein crystals in solutions containing four fragments and used an automated data collection system to determine structures. Our pilot project with Hsp90 resulted in a 3.3% hit rate. In this work, we have identified general strategies for structure-based fragment screening. We streamlined the process by creating a fragment library kit generally suitable for screening against many protein targets.

Our fragment screening laboratory consists of the ActiveSight Fragment Library, the ACTOR robot crystallizing system, FR-E home X-ray source, and Saturn CCD detector. The Molecular Images software suite was used to go from diffraction data to refined structure files ready for viewing and analysis in MIFit. This work validates our fragment library and demonstrates that structure based fragment screening can be achieved rapidly and successfully in a home laboratory.



Superposition of HSP90 Hits

**MP179 Crystal Creator Feeds Protein Structure Pipeline.**

Armando Villaseñor, April Wong, Manjiri Ghate, Seth Harris, Andreas Kuglstatler, Michelle Browner, Biophysics and Protein Crystallography, Roche Palo Alto, CA.

Today's drug discovery programs demand structure information of dozens of small molecules bound to therapeutic targets. This poster describes how we use the Crystal Creator liquid dispenser to deliver hundreds of crystals to feed our structure pipeline. The Crystal Creator delivers 48 crystallization experiments per minute with minimal protein excess requirements. The instrument features accurate liquid dispensing with plastic tips that wash thoroughly in seconds and a rotating deck with ten standard SBS stations, each fully accessible by peripheral instrumentation such as plate stackers, plate sealers, incubators etc.

**TP180 On Retrosynthetic Diamond Growth in Hypercritical Water.**

Boris Udovic, Sezana, Slovenia, boris.udovic@email.si.

The synthesis of diamonds from aqueous solutions bursts the limits of classical procedures within experienced reactive media. Over magmatic temperatures up to 1600 °C, the Keesom free energy of angle-averaged dipole-dipole interactions between water molecules loses its predominance in the operative range of highest pressures, towards several GPa, beyond the critical temperature of 374 °C and critical pressure of 22.1 MPa. Noticeably, as soon as the relative permittivity  $\epsilon_r$  of scH<sub>2</sub>O drops into lower targeted range  $2 < \epsilon_r < 20$  the extent of solvated carbon monoxide CO ( $\epsilon_r \sim 1$ ) abruptly rises to highest saturation values. The simultaneous presence of scCO<sub>2</sub> as co-solvent or nutrient of carbon atoms through stepped reactions of the type CO<sub>2</sub>  $\rightarrow$  CO + 1/2O<sub>2</sub> is unnecessary, a more reductive environment is achieved. As the graphitic carbon atoms are promptly and reversibly gasified in the form of soft base CO species from readily solubilized nutrient source (asphalt  $\epsilon_r \sim 2.7$ ) the water gas shift reaction (WGS) can be reverted by temperature decrements driving a mediated backward deposition of carbon atoms: C + H<sub>2</sub>O  $\leftarrow$  CO + H<sub>2</sub>.

In this highly reductive environment the catalytic presence of Fe and Th reduced species must constitute active CO uptake centres being subsequently transformed into paramagnetic carbide forms owing partially occupied orbitals at higher energy levels. The cubic symmetry of interstitial carbon sublattice propagates throughout the solid carbide surface and redirects the clustering processes of incoming carbon atoms into the growing process of diamond phase ( $\epsilon_r \sim 5.5$ ). As the earliest linked M-C pairs are produced in essentially carbenic form, the epitaxially entering carbon atoms can accumulate themselves taking place because of their unique capability to bind the multicenter attractors as carbenic bidentate fragments.

The crystalline diamonds (hexoctahedral symmetry) as well as the glassy carbon mesophase are allowed phases by 3D *head-tail* sewing-connecting combination between isolobal fragments into pyramidal *sp*<sup>3</sup> clustering networks. Remarkably, the carbene units also experience insertion reactions into carbo-olefinic  $\pi$  bonds with the result that the occurring graphitic phase is promptly destroyed.

**TP181 A Rietveld and Pair-distribution Function Analysis of Aged U-Nb Alloys.** H.M. Volz<sup>1</sup>, Th. Proffen<sup>1</sup>, R.E. Hackenberg<sup>1</sup>, A.M. Kelly<sup>1</sup>, W.L. Hults<sup>1</sup>, A.C. Lawson<sup>1</sup>, R.D. Field<sup>1</sup>, D.F. Teter<sup>1</sup>, D.J. Thoma<sup>1</sup>, M.A. Rodriguez<sup>2</sup>, <sup>1</sup>Los Alamos National Lab., Los Alamos, NM, <sup>2</sup>Sandia National Lab., Albuquerque, NM.

The uranium-niobium alloy system is complex, exhibiting many different stable and metastable phases including martensite and shape-memory behavior. It is desirable to understand any long-term changes in the structure of these materials in order to improve predictions of materials properties over time, but changes may be subtle. Therefore, we collected powder diffraction patterns on aged polycrystalline U-Nb samples. Compositionally homogeneous U-5.6 Nb and U-7.7 Nb (wt%) experimental specimens have been artificially aged by isothermal treatments at temperatures of 373K, 473K, 523K, and 573K for times ranging from 10 to 100,000 minutes. Pair-distribution function analysis and full pattern Rietveld analysis with GSAS were performed on data collected at NPDF at the Lujan Neutron Scattering Center at LANSCE. Sealed tube X-ray powder diffraction data were also collected and will be discussed and compared. As multiple metastable and equilibrium phases are possible in the range of 0 to 10 wt% niobium, Rietveld analysis and interpretation were quite challenging. PDFs were therefore investigated in order to look for evidence of ordering. We will present observations of aging-induced changes (or lack thereof) in lattice parameters, atomic positions, occupancies, and thermal parameters, as well as present insights obtained from PDFs. Finally, speculation on aging mechanisms involved will be discussed.

**TP182 Concept on Petrogenesis of Crystal Growth of Olivine Coronas in Troctolites, Eastern Desert, Egypt.** Hussein A. Hegazy, Geology Dept., Faculty of Science, Assiut Univ., Egypt, hegazy512000@yahoo.com

Olivine minerals as a Gem stone exhibit partly or completely corona microstructures surrounding olivine crystals. The texture occurs in olivine gabbros and troctolites in which the primary mineral phases are represented by varying proportions of cumulus and intercumulus olivine (Fo<sub>80-83</sub>), orthopyroxene (En<sub>65-70</sub>), clinopyroxene (Wo<sub>40-41</sub>En<sub>49-50</sub>Fs<sub>8-9</sub>), plagioclase (An<sub>62-72</sub>Ab<sub>27-37</sub>Or<sub>0.10-0.12</sub>), amphibole, magnetite and Al-rich spinel. Coronas may develop around olivine of any composition, where three types of coronas have been recognized. The inner shells are composed of orthopyroxenes with little tremolite-actinolite, while the outer shells are made of colorless clinopyroxene and brown-green amphiboles mainly in vermicular intergrowth. Spinel symplectite intergrowth commonly associates with the outer rim. Clinopyroxene in symplectites is commonly in optical continuity with the surrounding free-pyroxene rim.

Textural observations and chemical features support the magmatic cooling hypothesis. The chemical similarity between orthomagmatic mineral phases and the coronitic minerals suggest crystallization under similar PTX conditions during late magmatic stages.

Thermodynamic calibrations showed that the mineral assemblage in the studied coronas could not grow simultaneously, in concomitant with solid-state diffusion origin but due to reaction between the cumulus phases and the coexisting melt. The equilibrium curve for

olivine-plagioclase reaction have a positive slope ( $dP/dT > 0$ ) suggesting reaction during cooling.

**TP183 First Results of Spin Density Measurements of a Low Spin Bis(imidazole)(meso-tetraphenylporphinato)iron(II) Chloride.** Brenda Dougan<sup>2</sup>, Christina Hoffmann<sup>1</sup>, Ziling Xue<sup>2</sup>, Garry Mcintyre<sup>3</sup>, <sup>1</sup>Neutron Scattering Sciences Div., Oak Ridge National Lab., Oak Ridge, TN, <sup>2</sup>Dept. of Chemistry, Univ. of Tennessee, Knoxville, TN, <sup>3</sup>Inst. Laue-Langevin, Grenoble, France.

[Fe(TPP)(HIm)<sub>2</sub>]Cl is a low spin Fe-complex with a centro-symmetric planar tetraphenylporphinato ligand and imidazole axial ligands. Two molecules are in the unit cell and were reported to exhibit distinctly different bondlength and orientation with respect to the phenyl rings of the planar ligand. The torsion angle of the axial ligands is considered to be determined by the steric hindrance introduced by the planar tetraphenylporphinato ligands<sup>[1]</sup>. The unit cell parameters were reported as space group = P 1, Z = 2,  $a = 13.331(2)$  Å,  $b = 17.688(3)$  Å,  $c = 11.213(2)$  Å,  $\alpha = 107.99(1)^\circ$ ,  $\beta = 94.70(1)^\circ$ , and  $\gamma = 69.68(1)^\circ$  at 292 K<sup>[1,2]</sup>. The cause and consequences of the two different orientations and torsion angles are still unknown and might have significant influence on magnetic properties.

We investigated the spin density distribution of [Fe(TPP)(HIm)<sub>2</sub>]Cl with polarized single crystal neutron diffraction, measuring a total of 145 non-equivalent reflections / flipping ratios. The data collection was carried out at the hot single crystal neutron diffractometer D3 at the Institute Laue-Langevin (ILL). The sample was in a magnetic holding field of 9 T between 2 – 4.89 K at two different orientations. We will present the first results of this study.

ORNL/SNS is managed by UT-Battelle, LLC, for the U.S. Department of Energy under contract DE-AC05-00OR22725.

[1] Collins, D. M.; Countryman, R.; Hoard, J. L. *J. Am. Chem. Soc.* 1972, Vol. 94, 2066-2072.

[2] Scheidt, W. R.; Osvath, S.R., Lee, Y.J., *J. Am. Chem. Soc.* 1987, Vol. 109, 1958-1963.

**TP184 Magnetic Structure Investigation of Two Ferromagnetic Spinel GeM<sub>2</sub>O<sub>4</sub> (M = Co, Ni) Measured at the IPNS-SCD Using a Polarized Neutron Beam.** C. Hoffmann<sup>1</sup>, G. Ehlers<sup>1</sup>, G.L. Jones<sup>2</sup>, W.C. Chen<sup>3</sup>, T.R. Gentile<sup>3</sup>, P.M.B. Piccoli<sup>4</sup>, M.E. Miller<sup>4</sup>, A.J. Schultz<sup>4</sup>, W.T. Lee<sup>1</sup>, H.Y. Yan<sup>5</sup>, X. Tong<sup>5</sup>, M. Snow<sup>5</sup>, <sup>1</sup>Oak Ridge National Lab., Oak Ridge, TN, <sup>2</sup>Hamilton College, Clinton, NY, <sup>3</sup>NIST Center for Neutron Research, Gaithersburg, MD, <sup>4</sup>Intense Pulsed Neutron Source, Argonne, IL, <sup>5</sup>IUCF, Indiana Univ., Bloomington, IN.

Spinel of GeM<sub>2</sub>O<sub>4</sub>, M=Ni, Co, have been synthesized as single crystals and displayed distinguished magnetic behavior in magnetic susceptibility measurements. The magnetic states of Ni<sup>+2</sup> and Co<sup>+2</sup> undergo ordering when passing the Neel temperature of the material. The exact ordering parameter is still unknown. The Co-spinel undergoes a single Neel transition at 20.6 K whereas the nickelate passes through two Neel transitions at 12.13 and 11.46, respectively<sup>[1,2]</sup>. Only the Co compound undergoes at phase transition from cubic to tetragonal.

We investigated how closely the nuclear phase transition is related to the change in the magnetic ordering parameter. We measured the nuclear structure parallel to flipping ratio measurements to analyze the spin density of the ferromagnetic low temperature phase. The experiment was carried out at the IPNS-SCD using a compact <sup>3</sup>He-based neutron spin filter for polarized single crystal neutron diffraction of a polychromatic beam<sup>[3,4]</sup>. The compact polarizer provides continuous optical pumping of the <sup>3</sup>He for long term stability in a very small package and includes an (AFP) NMR flipper<sup>[5]</sup>.

We will report the results of the magnetic structure investigation.

The authors want to thank M. Crawford (DuPont) and J. Gardner (NIST) for providing the sample and sample details and discussions.

ORNL/SNS is managed by UT-Battelle, LLC, for the U.S. Department of Energy under contract DE-AC05-00OR22725.

[1] S. Hara *et al.*, *J. PHYS. SOC. JAPAN* 73 2959-2962 2004

[2] M. Crawford, *et al.*, *PHYS. REV. B* 68 220408 2003

[3] G.L. Jones *et al.*, *Nucl. Instrum. Meth. A* 440,772 (2000).

[4] D.R. Rich *et al.*, *Nucl. Instrum. Meth. A*, 481, 431 (2002).

[5] G.L. Jones *et al.*, *Physica B*, (PNCMI04 Conf. Proceedings)

**TP185 Determination of Detailed Envelopes of SIR D/H Amino Acid Substructures at Less than Inter-atomic Resolution.** David A. Langa, Hongliang Xu, Herbert A. Hauptman, Dept. of Structural Biology, Hauptman-Woodward Medical Research Inst., Buffalo, NY.

Neutron crystallographers have envisioned using selectively hydrogenated, perdeuterated (D/H) macromolecules crystallized from deuterated buffers as a means of forming suitable SIR derivatives for structure determination. The most logical approaches consist of (1) inserting exchangeable D/H binding ligands or (2) expressing perdeuterated proteins in the presence of an excess of some chosen D/H amino acid to affect only those residue sites.

These ligand/residue-based D/H derivatives will contain many geminal and vicinal related D/H atomic substitution sites separated by 1.7Å and 2.4Å respectively. Traditional methods to determine the substructure from the difference amplitude data will thus require data to at least 1.5Å in order to resolve these sites from one another. We here report that SnB procedures can be adapted to produce solution maps of these substructures at 2.5Å even though a resolvable peak representation of the D/H sites is not in principal possible. Atomic sites can be unambiguously determined to within ~ 0.1Å by fitting the known substructural motifs to these low-resolution SnB maps.

Research support from the Human Frontier Scientific Program is gratefully acknowledged.

**TP186 Recent Results from the New Laue Diffractometer, LADI-III.** M.P. Blakeley, Inst. Grenoble, France, blakeley@ill.fr.

As a first step in a broader project that aims to 1) make neutron protein crystallography more accessible to the structural biology community, 2) extend the size and complexity of systems that can be studied and 3) maintain our competitiveness with diffractometers coming on-line at spallation sources, an upgraded neutron Laue diffractometer - LADI-III - has been designed, constructed and installed at the ILL. LADI-III is dedicated to neutron protein crystallography at high-resolution (1.5-2.5 Å) and is used to study key hydrogen atoms and water structure in protein single crystal structures. Improvements to the detector design and readout system have been incorporated into the miniaturized reading head located inside the drum source image-plate. The transferral of the image-plates and readout system internally provides a 3-fold gain in neutron detection compared to the original LADI instrument. In order to help reduce the background scatter per pixel and the number of spatially overlapped reflections, the dimensions of the drum have been increased. Furthermore, the entire detector height can be adjusted to allow for relocation to a higher intensity beam, promising yet further gains in the future. Current projects aim to address questions concerning enzymatic mechanism, ligand-binding interactions, solvent effects, structure dynamics and their implications. Thanks to the ILL/EMBL deuteration laboratory, the production in *E. Coli* and purification of fully deuterated proteins has become routine so that we can use much smaller crystal volumes (~0.2 mm<sup>3</sup>) and/or address much larger unit-cell projects (>150Å) than were previously possible. Some examples of recent results from LADI-III will be presented.

**SP187 Mechanistic Insights from a Structural Comparison of Hydrogenated and Perdeuterated Haloalkane Dehalogenase.** Xuying Liu<sup>1</sup>, Leif Hanson<sup>1</sup>, Paul A. Langan<sup>2</sup>, Ronald E. Viola<sup>1</sup>, <sup>1</sup>Dept. of Chemistry, Univ. of Toledo, Toledo, OH, <sup>2</sup>Los Alamos National Lab., Los Alamos, NM.

Haloalkane dehalogenase from *Xanthobacter autotrophicus* (*XaDhl*) is a key enzyme in the degradation of a broad range of haloalkanes. This enzyme is composed of a central domain with the typical  $\alpha/\beta$ -hydrolase fold and an  $\alpha$ -helical cap domain, with the active site buried between these two domains. Both crystallographic and biochemical studies of *XaDhl* have contributed to our understanding of its action. However, uncertainties remain about the details of hydrogen transfer during catalysis, the mode of halide binding and the origin of acid inhibition. As the first step towards neutron crystallographic studies that will address these issues in the mechanism of *XaDhl*, a comparison of the x-ray crystal structures of hydrogenated *XaDhl* (h-*XaDhl*) and perdeuterated enzyme (d-*XaDhl*) was conducted. Significant differences are observed in the surface of h-*XaDhl* and d-*XaDhl* that can be related to the differences in properties between C-H and C-D bonds. Unexpectedly, the active site of d-*XaDhl* is crucially different; the primary nucleophile Asp124 swings away from its position in h-*XaDhl* and rotates towards His289 to form the strong hydrogen bond, excluding a critical nucleophilic water from the active site. This new arrangement corresponds to the observation *for the first time* of a natural inhibited state of the catalytic reaction, and provides a structural explanation for the termination of the catalytic reaction of *XaDhl*. It also suggests a possible way of altering the environment of catalytic sites to conditions beyond what is possible with hydrogenous protein crystals. This work was supported by a grant from the NSF.

**TP188 New Structures in the SrMnO<sub>x</sub> System: Sr<sub>N</sub>Mn<sub>N-2</sub>O<sub>3N-2</sub> (N=5 & 7). A Neutron and X-ray Diffraction Study.** L. Suescun<sup>1,2</sup>, B. Dabrowski<sup>2</sup>, J.D. Jorgensen<sup>1</sup>, <sup>1</sup>Argonne National Lab., Argonne, IL, <sup>2</sup>Northern Illinois Univ., DeKalb, IL.

Perovskite manganites have been extensively studied during last several decades due to a wide range of functional properties like CMR, mixed conductivity, and large magnetocaloric effect. Combining neutron and synchrotron x-ray powder diffraction we have been able to determine the crystal structures of two oxygen vacancy-ordered phases of the newly identified homologous series *Sr<sub>N</sub>Mn<sub>N-2</sub>O<sub>3N-2</sub>*: *Sr<sub>5</sub>Mn<sub>5</sub>O<sub>13</sub>* (N=5) and *Sr<sub>7</sub>Mn<sub>7</sub>O<sub>19</sub>* (N=7)<sup>[1]</sup>. This homologous series includes also the previously known *Sr<sub>2</sub>Mn<sub>2</sub>O<sub>5</sub>* phase<sup>[2]</sup>, which is indeed the N=4 (*Sr<sub>4</sub>Mn<sub>4</sub>O<sub>10</sub>*) member of the new series. Starting with the N=4 member of the series, containing pyramidally coordinated Jahn-Teller *Mn<sup>3+</sup>*, a basic building block for the homologous series is built based on four pyramids lying on the 001 plane. The Nth member of the series is built by adding N-4 octahedrally coordinated *Mn<sup>4+</sup>* to the four pyramids while keeping the symmetry of the original block. The existence of N=7 and absence of N=6 and 8 members of the series is discussed based on the uniqueness and multiplicity of the 3D network and possible distortions of blocks made of pyramids and octahedra. Similar oxygen-vacancy arrangements observed in *LaCuO<sub>x</sub>*<sup>[3]</sup> system have been found to confirm the structural trends of this new homologous series.

[1] Suescun L. *et al.* (2007) Submitted to *J. Sol. State Chem.* [2] Caignaert V. *et al.* (1985) *Mater. Res. Bull.*, 20, 479-484. [3] Bringley J.F. *et al.* (1990) *Nature*, 347, 263-265.

*Acknowledgements:* Work at NIU was funded by NSF Grant No. DMR-0302617, the U.S.-DO Education and the U.S.-DOT. At Argonne, this work was supported by the U.S. Department of Energy, Office of Science, under contract No. DE-AC02-06CH11357.

**TP189 Crystal Structure Solution of a Newly Isolated Natural Product by High Resolution X-ray Powder Diffraction and Global Optimization Methods.** S. Pagola<sup>1</sup>, M.I. Tracanna<sup>2</sup>, S.M. Amani<sup>2</sup>, A.M. González<sup>2</sup>, A.B. Raschi<sup>2</sup>, E. Romano<sup>2</sup>, A.M. Benavente<sup>2</sup>, P.W. Stephens<sup>3</sup>, M. Kelley<sup>1</sup>, <sup>1</sup>Applied Research Center, Newport News, VA, USA, <sup>2</sup>Fac. of Biochemistry, Chemistry and Pharmacy, Nat. Univ. of Tucumán, Tucumán, Argentina, <sup>3</sup>Dept. of Physics and Astronomy, SUNY, Stony Brook, NY, USA.

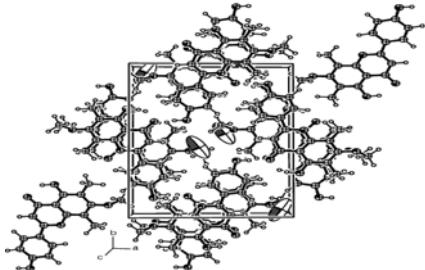
Sideroxylin (4*H*-1-Benzopyran-4-one,5-hydroxy-2-(4-hydroxyphenyl)-7-methoxy-6,8-dimethyl) is a recently isolated natural product from *Miconia ioneura* leaves (northwest argentinian flora), which showed bactericide and fungicide activity. The molecular structure was elucidated with the aid of NMR (<sup>1</sup>H y <sup>13</sup>C) and UV spectroscopy. The high resolution X-ray powder diffraction pattern of sideroxylin was collected at the X16C powder diffraction beamline, N.S.L.S., Brookhaven National Laboratory. The pattern was indexed to a monoclinic unit cell with the program ITO (M=25.9). The molecular geometry of sideroxylin was optimized with semiempirical methods and the AM1 Hamiltonian. The crystal structure solution was found with the simulated annealing method and the program PSSP, in the space group P2<sub>1</sub>/a, Z=4. The material is a monohydrate. After the Rietveld refinement the unit cell parameters are a=12.3328(6) Å, b=17.0373(6) Å, c=7.4335(2) Å, α=90°, β=94.587(4)°, γ=90°, V=1556.9(1) Å<sup>3</sup>. The agreement factors R<sub>wp</sub>=5.51%, R<sub>i</sub>=6.67% and χ<sup>2</sup>=1.51 were obtained. The crystal structure view from [001] is shown in the figure.

Research carried out in part at X16C beamline, N.S.L.S., Brookhaven National Laboratory.

**TP190 Small Angle X-ray Scattering from Transition Metal Oxide Aerogels.** T. Willey<sup>1</sup>, C. Saw<sup>1</sup>, J. Kinney<sup>1</sup>, J. Stolken<sup>1</sup>, T. Baumann<sup>1</sup>, J. Satcher<sup>1</sup>, J. Ilavsky<sup>2</sup>, T. van Buuren<sup>1</sup>, <sup>1</sup>Lawrence Livermore National Lab., Livermore, CA, <sup>2</sup>Advanced Photon Source, Argonne National Lab., Argonne, IL

Although a great amount of study has been devoted to the physical properties of porous structures, it is not clear whether the theoretical models developed to date can be extended to nanoscopic length scales. Our goal is to quantify the microstructure of highly porous materials, and to determine how processing of the porous material relates to the structure and ultimately to the mechanical behavior. We will quantify structural changes with a combination of small angle x-ray scattering (SAXS) and high-resolution x-ray tomography. Finite element modeling, using the structures determined above, will be used to study the effects of mechanical loading on the cell structures, and to map out relationships between processing, density, and strength.

USAXS data shows that there are significant changes to the cell structure of tantalum oxide foams as a function of decreasing density. We find that radius of gyration associated the smallest particles which define the strut width in the aerogel does not change with density. However the correlation length decreases suggesting that strut length also decreases with increased density. In the USANS we see evidence for large voids (> 500 nm) in the aerogels with the lowest density. From these measurements, stochastic lattices will be generated for finite element simulations. Simulations will then provide the elastic constants of the material. In addition to providing the elastic constants of



the foam, finite element simulation will be used to study thermo-elastic deformation.

This work is supported by the US-DOE, under contract W-7405-ENG-48, LLNL, APS is supported by the U.S. DOE, BES, Office of Science under contract No. W-31-109-ENG-38.

**SP191 X-ray Diffraction Study of Two Compounds Isolated from *Verbesina turbacensis* H.B.K.** J. Bruno-Colmenárez,<sup>a</sup> G. Díaz de Delgado<sup>a</sup>, P. Delgado<sup>b</sup>, I. Ramirez<sup>b</sup>, and J.M. Amaro-Luis<sup>b</sup>, <sup>a</sup>Lab. de Cristalografía-LNDRX, <sup>b</sup>Lab. de Productos Naturales, Dept. de Química, Facultad de Ciencias, Univ. de Los Andes, Mérida, Venezuela.

As part of a continuous effort to characterize species commonly found in the Venezuelan Andes, two compounds isolated from the aerial parts of *Verbesina turbacensis* H.B.K, are reported in this work. Species of the genus *Verbesina* (family: Compositae; Helintheae) and derivatives have great importance as promoters of vegetal growth and germination. Additionally, many species have antibacterial, fungicidal, antiviral, and antitumoral activity. The compounds reported here are structural isomers with formula C<sub>24</sub>H<sub>32</sub>O<sub>4</sub> and crystallize in the orthorhombic system, space group P2<sub>1</sub>2<sub>1</sub>2<sub>1</sub>. 3β-Hydroxiverbesindiol-6β-o-cinnamate (1) has unit cell parameters a = 12.378(2), b = 18.813(4) and c = 9.647(2) Å, V = 2246.3(8) Å<sup>3</sup>. Its packing arrangement is governed by two intermolecular hydrogen bonds and six intramolecular hydrogen bonds. On the other hand, eudesman-15-oic-6-cinnamate acid (2) has cell parameters a = 8.8177 (18), b = 14.266(3), c = 17.310(4) Å, V = 2177.5(8) Å<sup>3</sup>. The packing arrangement is also governed by two intermolecular hydrogen bonds and six intramolecular hydrogen bonds. A detailed description of these compounds will be presented.

This work was possible thanks to grants LAB-98000821 from FONACIT- Venezuela.

**MP192 A Crystallographic Study of Methoxyflavone Inhibitors of Cytochrome P450.** Cheryl L. Klein Stevens, Naijue Zhu, Dept., of Chemistry, Xavier Univ. of Louisiana, New Orleans, LA.

Cytochrome P450 enzymes oxidize both endogenous compounds (steroids, fatty acids, and vitamins) and xenobiotic compounds (drugs, environmental pollutants, and procarcinogens). These enzymes protect the body from foreign substances through this oxidation mechanism allowing the oxidation products to be more readily eliminated. It has been shown that some flavones function as substrates of some of the P450 enzymes (specifically P450 1A1 and 1B1) and may also function as enzyme inhibitors. In this study, the X-ray crystal structures of four methoxyflavone analogs have been determined. These include 2'-methoxyflavone, 3'-methoxyflavone, 4'-methoxyflavone, and 3',4'-methoxyflavone. All four molecules crystallized with a methoxy substituted phenyl ring which is nearly coplanar with the fused ring system. Preliminary studies show that all four of these compounds function as inhibitors in P450 1A1, P450 1A2, P450 2A6, and P450 2B1 enzymes.

Support from the NIH/MBRS-SCORE grant is gratefully acknowledged S06 GM08008.

**MP193 Crystal Structure Refinements and Cation Ordering in Kutnahorite, Ideally CaMn(CO<sub>3</sub>)<sub>2</sub>.** Sytle M. Antao<sup>1</sup>, Ishmael Hassan<sup>2</sup>, <sup>1</sup>Advanced Photon Source, Argonne National Lab., Argonne IL, USA, <sup>2</sup>Dept. of Chemistry, Univ. of the West Indies, Mona, Jamaica.

The crystal structure of two kutnahorite crystals from Franklin, New

Jersey, and one crystal from Sterling Hill, NJ have been refined using single-crystal X-ray diffraction data. In addition, a Rietveld refinement using powder synchrotron X-ray diffraction (XRD) was performed on the same Franklin kutnahorite sample as that used in the single-crystal work. Although the bulk composition of the samples are close to ideal, particularly for the Franklin sample, the Ca-Mn distribution is different for samples from different localities, and even for different crystal fragments from the same specimen. Nevertheless, all the hexagonal cell parameters are similar to each other. Different Ca-Mn distributions give rise to different octahedral A-O and B-O distances, from which cation ordering in kutnahorite can be deduced. The mixing of cations on the A site is close to ideal, while that on the B site is less than ideal.

**MP194 Transannular N ... N Interaction in Energetic  $\beta$ -HMX.** Elizabeth A. Zhurova, Vladimir V. Zhurov, A. Alan Pinkerton, Dept. of Chemistry, Univ. of Toledo, Toledo, OH.

Chemical bonding in the  $\beta$ -phase of the 1,3,5,7-tetranitro-1,3,5,7-tetraazacyclooctane (HMX) crystal based on the experimental electron density obtained from X-ray diffraction data at 20K, and solid state theoretical calculations has been analyzed in terms of the Quantum Theory of Atoms in Molecules. Features of the intra- and intermolecular bond critical points and the oxygen atom lone-pair locations are discussed. An unusual N ... N bonding interaction across the 8-membered ring has been discovered and characterized. Hydrogen bonding, O ... O and O ... C intermolecular interactions are reported. Atomic charges and features of the electrostatic potential are discussed.

**MP195 Functional Microporous Metal-Organic Frameworks for Gas Storage, Catalysis and Chiral Separation.** Bao-Qing Ma,<sup>ab\*</sup> Karen L. Mulfort,<sup>b</sup> So-Hye Cho,<sup>b</sup> SonBinh T. Nguyen<sup>b</sup>, Joseph T. Hupp<sup>b</sup>, <sup>a</sup>Pharmaceutical Research and Development, Bristol-Myers Squibbs, Wallingford, CT, <sup>b</sup>Dept. of Chemistry, Northwestern Univ., Evanston, IL.

Microporous metal-organic frameworks (MOFs), emerging promising materials, have numerous advantages over traditional zeolites and find a variety of applications in gas storage, sensing, separation and catalysis. A series of isorecticular MOFs featuring 3D paddle-wheel networks built from mixed dicarboxylic acids and bipyridine-like pillars with tunable channel sizes have been prepared. They exhibit high thermal stability and retain their original frameworks after excluding the embedded solvents. Nitrogen isothermal absorption demonstrates that the permanent porosity of these MOFs with high internal surface area, which even keeps intact after the pyridine pillars have been reduced. Salen-supported MOFs exhibit high catalytic activity, which is comparable to corresponding homogeneous counterpart.

We gratefully acknowledge the Office of Science, U.S. Department of Energy (Grant No. DE-FG02-01ER15244) and the Materials Research Center at Northwestern University for financial support of our research.

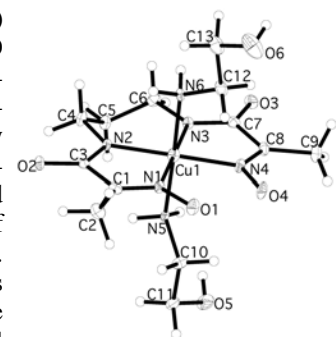
**MP196 Molecular Structure of Novel Cobalt(III) Complexes with a Tetradentate Oxime Open-chain Ligand.** S. Tomyn<sup>a</sup>, M. Haukka<sup>b</sup>, I. O. Fritsky<sup>a</sup>, <sup>a</sup>Dept. of Chemistry, Kiev National Taras Shevchenko Univ., Kiev, Ukraine, <sup>b</sup>Dept. of Chemistry, Univ. of Joensuu, Joensuu, Finland.

The reaction of cobalt(II) perchlorate with the open-chain oxime-and-amide ligand, *N,N*8-bis(2-hydroxyiminopropionyl)-propane-1,3-diamine (L) and imidazole (1) or 2-aminoethanol (2) in methanol solution produced the mononuclear complexes

[Co(L-3H)Im<sub>2</sub>] $\cdot$ 2CH<sub>3</sub>OH (1)

and [Co(L-3H)mea<sub>2</sub>] $\cdot$ 1.5H<sub>2</sub>O (2).

This reaction is accompanied by the spontaneous oxidation of Co(II) to Co(III) by aerial oxygen at ambient conditions, the products were isolated and characterized by means of single crystal X-ray analysis. The compound (1) crystallizes in monoclinic system with the space group C2/c; the unit cell parameters are  $a = 15.0998(5)$ ,  $b = 8.8794(3)$ ,  $c = 16.6915(5)$  Å,  $\alpha = 90^\circ$ ,  $\beta = 91.658(2)^\circ$ ,  $\gamma = 90^\circ$ ;  $Z = 4$ ,  $V = 2237.01(16)$  Å<sup>3</sup>. Another complex [Co(L-3H)mea<sub>2</sub>] crystallizes in triclinic system with the space group P-1; the unit cell parameters are  $a = 8.9134(2)$ ,  $b = 14.5197(3)$ ,  $c = 16.5354(3)$  Å,  $\alpha = 68.5380(10)^\circ$ ,  $\beta = 86.5642(10)^\circ$ ,  $\gamma = 75.0823(10)^\circ$ ;  $Z = 2$ ,  $V = 1923.10(7)$  Å<sup>3</sup>. In both compounds the central atoms are octahedrally surrounded by the tetradentate N4-coordinated L with two molecules of imidazole (1) or 2-aminoethanol (2) in the axial positions. (L-3H) residues form the short intramolecular H-bonds between the oxygen atoms of the oxime groups stabilize a closed pseudo-macrocyclic environment of the central atom.



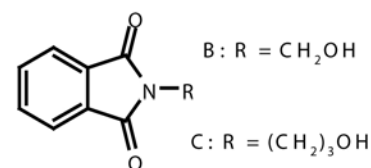
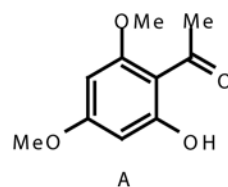
**MP197 Testing Etter's Rule with 6-membered Hydrogen-bonded Rings.** C.H. Schwalbe, H. Wang, C.J. Bache, School of Life and Health Sciences, Aston Univ., Birmingham, UK.

Margaret Etter proposed an empirical rule<sup>[1]</sup> that "Six-membered-ring intramolecular hydrogen bonds (HB) form in preference to intermolecular hydrogen bonds." We report three compounds which could satisfy this rule. Molecule A features three electron-donating substituents, *o*-OH, *o*-OMe, and *p*-OMe, which feed electron density into the ring and thence to the carbonyl O atom, strengthening it as HB acceptor. Molecule B can take some electron density from the imide nitrogen atom and divide it between the carbonyl O atoms, one of which must be the acceptor in a putative 6-membered hydrogen bonded ring. In C a 6-membered ring with C<sub>3</sub>H<sub>6</sub>OH as HB donor must have the imide nitrogen atom as the (weakened) hydrogen bond acceptor.

Geometrical parameters relevant to hydrogen bonds are tabulated below.

Compound	Atoms	Graph	d(X...O)/Å	d(H...O)/Å	X-H...O/ $^\circ$
A (mol. 1)	O-H...O	S(6)	2.500(2)	1.77	147
A (mol. 2)	O-H...O	S(6)	2.490(2)	1.76	147
B	O-H...O	C(6)	2.844(1)	2.03	177
B	C-H...O	R <sub>2</sub> <sup>2</sup> (10)	3.313(1)	2.49	143
C (mol. 1)	O-H...O	C(10)	2.851(3)	2.04	171
C (mol. 2)	O-H...O	C(10)	2.832(3)	2.02	173

A and C have  $Z' = 2$  with similar HB for both molecules, but B has  $Z' = 1$ . A forms strong O-H...O=C intramolecular HB from phenolic OH to carbonyl O. Of 34 single-ring 2-hydroxyacetophenones, 32 form intramolecular HB, all "strong" [2] with normalized  $d(H...O) \leq 2.3$  Å. Molecule B forms chains via O-H...O HB, along with a dimeric R<sub>2</sub><sup>2</sup>(10) ring by C-H...O HB to the same O atom. Only 16 of 91 similar candidates in the CSD



C: R = (CH<sub>2</sub>)<sub>3</sub>OH

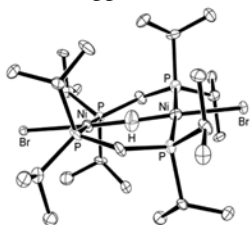
form S(6) rings within the sum of van der Waals radii, 10 with strong HB. Molecule C uses neither N atom; no similar structure of 23 in the CSD has HB to an imine N atom.

[1] Etter, M. (1990), *Acc. Chem. Res.* 23: 120-126.

[2] Bilton, C., Allen, F.H., Shields, G.P. and Howard, J.A.K. (2000) *Acta Cryst.* B56: 849-856.

**MP198 Neutron Diffraction Studies of Linear M-H-M Bonding in Dinuclear Nickel Complexes.** A. J. Schultz<sup>a</sup>, J. A. Cowan<sup>a</sup>, P.M.B. Piccoli<sup>a</sup>, D.A. Vivic<sup>b</sup>, T.J. Anderson<sup>b</sup>, W.S. Tyree<sup>b</sup>, <sup>a</sup>IPNS, Argonne National Lab., Argonne, IL, <sup>b</sup>Dept. of Chemistry, Univ. of Arkansas, Fayetteville, AR.

Neutron diffraction studies on transition metal hydrides have suggested that the M-H-M linkage is inherently bent. Here we report two dinuclear nickel complexes, each containing a single bridging hydride, that are found to lie co-linearly with the two metal centers and shows no disorder in the neutron diffraction studies. Single crystal neutron diffraction structures of [(dippm)<sub>2</sub>Ni<sub>2</sub>Br<sub>2</sub>]( $\mu$ -H) (1, see figure) and [(dippm)<sub>2</sub>Ni<sub>2</sub>Cl<sub>2</sub>]( $\mu$ -H) (2, dippm = bis(di-*i*-propylphosphino)methane) were obtained and exhibit the first examples of linear M-H-M bonding in simple dinuclear metal complexes [1,2]. Data were obtained using the neutron time-of-flight Laue SCD instrument at the Argonne Intense Pulsed Neutron Source. Based on simple molecular orbital arguments, we had anticipated that the replacements of Br in 1 by Cl in 2 might result in a bent bond. The linear bonds observed in both 1 and 2 indicate the dominance of steric factors in determining the geometry. In addition, intramolecular isopropyl CH-to-halide interactions appear to stabilize the linear X-Ni-H-Ni-X moiety, in comparison to cyclohexyl derivatives which adopt A-frame structures as determined from X-ray diffraction data.



Work at Argonne was supported by the DOE Office of Science-BES under contract DE-AC02-06CH11357.

[1] D. A. Vivic, T. J. Anderson, J. A. Cowan and A. J. Schultz (2004). *J. Am. Chem. Soc.* 126, 8132-8133.

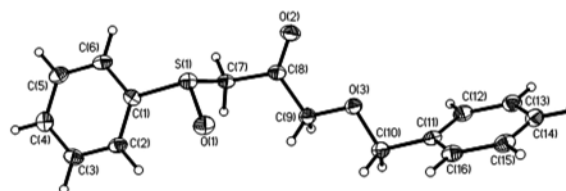
[2] W. S. Tyree, D. A. Vivic, P. M. B. Piccoli and A. J. Schultz (2006). *Inorg. Chem.* 45, 8853-8855.

**SP199 Crystal Structure of [1, 2, 3-<sup>13</sup>C]-1-Phenylsulfinyl-3-Benzyloxyacetone and Related Labeled Compounds as Precursors for Isotopically Labeled Materials.** E. Asani, R.A. Martinez, V.N. Khrustalev, T.V. Timofeeva. Dept. of Natural Sciences, New Mexico Highlands Univ., Las Vegas, NM.

Several <sup>13</sup>C labeled sulfurorganic material, sulfoxides, sulfones and sulfides have been synthesized and structurally characterized. Most of these materials are precursors for synthesis of isotopically labeled chiral small molecules for labeling of biomolecules, including proteins, to follow metabolic processes. For instance, [1,2,3-<sup>13</sup>C]-1-(phenylsulfinyl)-3-benzyloxyacetone has been synthesized and its crystal structure has been determined. The above compound has been used by Rodolfo *et al.* (*J. Am. Chem. Soc.*, 2006, 128, 14325-14336) to synthesize stereochemically differentiated glycerol which was further used in feeding experiments to show labeling of the C-2 of the glycolate units from [2-<sup>13</sup>C]-glycerol in Soraphen A and leucomycin, and C-1 from [1(3)-<sup>13</sup>C] glycerol in concanamycin. X-ray diffraction study revealed that this compound crystallizes in the monoclinic crystal system in the acentric space group *Pc*, with cell constants at *T* = 100 K: *a* = 16.073(5) Å, *b* = 5.5079(16) Å, *c* = 7.949(2) Å,  $\beta$  = 100.221(4)°, *V* = 692.6(3) Å<sup>3</sup>, *Z* = 2, *d*<sub>calc</sub> = 1.383 g/cm<sup>3</sup>. This compound contains the chiral tetravalent three-coordinated sulfur atom, which has a distorted tetrahedral configuration

138

American Crystallographic Assn. ©



with a lone electron pair occupying one of the tetrahedron vertices. In the crystal, the molecules are packed in stacks along the *b* axis; the stacks consist of the molecules of the same chirality. Furthermore, the stacks of the molecules of the opposite chirality alternate along the *c* axis. The molecules in neighboring stacks are arranged by head-to-tail orientations. The molecular structure of this material is shown.

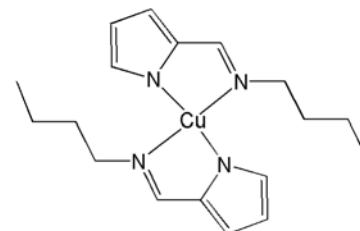
**SP200 Crystal Structures of Pharmacological Activity of Enaminones.** Carlito Lariucci<sup>1</sup>, José R. Sabino<sup>1</sup>, Rafael S. Nunes<sup>1</sup>, Ivo Vencato<sup>1,2</sup>, Silvio Cunha<sup>3</sup>, Jailton Ferreira<sup>3</sup>, <sup>1</sup>Inst. de Física - UFG, <sup>2</sup>Ciências Exatas e Tecnológicas - UEG, <sup>3</sup>Inst. de Química - UFBA.

Enaminones form a class of organic compounds with a broad spectrum of activities in several biological systems such as antibacterial, antimicrobial and anticonvulsive. These compounds are easily synthesized at a low cost. They are potentially active when H-bond donors and acceptors are present. Our goal on the synthesis of such compounds is to evaluate their pharmacological activity. In this work, we describe the results concerning the x-rays structural analysis of three such enaminones potentially active. Diffraction data collections of the samples were performed in a CAD4 diffractometer using Cu-K $\alpha$  radiation at room temperature. The structures solution, refinements and other calculations were carried out using the SHELX and WINGX suite of programs. (1) C<sub>14</sub>H<sub>15</sub>N<sub>1</sub>O<sub>4</sub>; *a* = 10.455(4), *b* = 11.172(5), *c* = 11.995(3) Å,  $\alpha$  = 99.27(3)°,  $\beta$  = 99.72(3)°,  $\gamma$  = 100.82(4)°, triclinic system, space group *P*-1, *R* = 0.0851; (2) C<sub>16</sub>H<sub>15</sub>N<sub>1</sub>O<sub>4</sub>; *a* = 7.261(3), *b* = 8.677(2), *c* = 21.894(2) Å,  $\beta$  = 93.52(2)°, monoclinic system, space group *P*<sub>2</sub><sub>1</sub>/*c*, *R* = 0.0514; (3) C<sub>13</sub>H<sub>15</sub>N<sub>1</sub>O<sub>6</sub>; *a* = 8.9605(8), *b* = 19.066(1), *c* = 7.951(2) Å,  $\beta$  = 94.47(1)°, monoclinic system, space group *P*<sub>2</sub><sub>1</sub>/*c*, *R* = 0.0877. The correlation between observed hydrogen bonds in the three structures and their pharmacological activity assays will be investigated.

This work was partially financed by CNPq, PrP/UEG and FUNAPE/UFG.

**SP201 Twin Upgrades by Temperature Control.** Frank R. Fronczek<sup>1</sup>, Stephen Fox<sup>2</sup>, <sup>1</sup>Dept. of Chemistry, Louisiana State Univ., Baton Rouge, LA, <sup>2</sup>Dept. of Chemistry, Univ. of Louisiana at Monroe, LA.

In favorable cases, non-merohedral twins can be converted to pseudo-merohedral by adjusting the temperature. This results in less troublesome refinement, because overlap of reflections is complete, and triage of the diffraction data is not necessary. If, as is normally the case, cell dimensions vary anisotropically with temperature, then axes which are approximately equal might be coaxed to be exactly equal, approximate 90° angles coaxed to be exactly 90°, and diffraction patterns with partial overlap coaxed to overlap exactly, by judicious choice of *T*. Application to orthorhombic twins with *a* ≈ *b* and monoclinic twins with  $\beta$  ≈ 90° will be discussed. Choosing the appropriate *T* can be done visually, by periodically taking images during *T* ramping.



Annual Program and Abstract Book 2007

An example of success of this technique is the structure of the Cu complex shown. It is orthorhombic ( $P2_12_12_1$ ) with two of its axes differing by 0.8% at  $T=90\text{K}$ , and non-merohedrally twinned with a very messy diffraction pattern. The structure could be solved using these data, but a satisfactory refinement was not obtained. As  $T$  is increased, the two axes converge in length, so the diffraction pattern shows closer overlap. By  $T=170\text{K}$ , the two axes are equal, and the diffraction pattern is clean. Refinement using one TWIN and one BASF command leads to  $R=0.035$ .

**TP202 Comparative Crystal Structures of "Infinite" Helical Coordination Compounds.** Kenneth L. Martin<sup>1</sup>, Carolyn S. Anderson<sup>1</sup>, Abigail V. Hunter<sup>1</sup>, S. Russell Seidel<sup>2</sup>, Russell G. Baughman<sup>3</sup>, <sup>1</sup>Berry College, Mt. Berry, GA, <sup>2</sup>Dowling College, Oakdale, NY, <sup>3</sup>Truman State Univ., Kirksville, MO.

Three coordination compounds having the general formula  $M(\text{hfac})_2(\text{dtdp})$  (where hfac = hexafluoroacetylacetonate, dtdp = 4,4'-dithiodipyridine, and  $M = \text{Mn, Cu, or Zn}$ ) have been synthesized and crystals have been grown.  $\text{Mn}(\text{hfac})_2(\text{dtdp})$  is yellow,  $\text{Cu}(\text{hfac})_2(\text{dtdp})$  is green, and  $\text{Zn}(\text{hfac})_2(\text{dtdp})$  is colorless. X-ray diffraction data sets collected at room temperature on a Bruker P4 single-crystal diffractometer revealed that all three compounds crystallize in the  $P2_1/c$  space group having four "molecules" per unit cell. The compounds have the following unit cell dimensions: for  $\text{Mn}(\text{hfac})_2(\text{dtdp})$ ,  $a = 7.902(2)\text{ \AA}$ ,  $b = 16.253(3)\text{ \AA}$ ,  $c = 20.902(4)\text{ \AA}$ ,  $\beta = 91.47(3)^\circ$ , and  $V = 2684(2)\text{ \AA}^3$ ; for  $\text{Cu}(\text{hfac})_2(\text{dtdp})$ ,  $a = 7.935(2)\text{ \AA}$ ,  $b = 16.034(3)\text{ \AA}$ ,  $c = 20.374(4)\text{ \AA}$ ,  $\beta = 91.30(3)^\circ$ , and  $V = 2591(2)\text{ \AA}^3$ ; and for  $\text{Zn}(\text{hfac})_2(\text{dtdp})$ ,  $a = 7.835(2)\text{ \AA}$ ,  $b = 16.368(3)\text{ \AA}$ ,  $c = 20.642(4)\text{ \AA}$ ,  $\beta = 91.46(3)^\circ$ , and  $V = 2646(2)\text{ \AA}^3$ . The unit cell data help explain why the crystal of one compound may act as a "seed crystal" in the solution of another compound, thus forming zonal systems. Each of these compounds exists in the solid as a racemate of right- and left-handed helices, in which the  $M(\text{hfac})_2$  units are bridged by a dtdp having a C—S—S—C torsion angle of  $\sim 90^\circ$ . It is interesting to note that as the ionic radius of the metal increases, the C—S—S—C torsion angle decreases from  $91.96(2)^\circ$  (in the copper structure) to  $90.61(2)^\circ$  (in the zinc structure) to  $90.05(1)^\circ$  (in the manganese structure).

**TP203 Crystal Structure of Novel Cu<sup>II</sup>Cr<sup>III</sup> Thiocyanato-bridged Heterometallic Complexes with Ethylenediamine.** V. Nikitina<sup>1</sup>, D. Shevchenko<sup>1</sup>, V. Kokozay<sup>1</sup>, V. Dyakonenko<sup>2</sup>, O. Shishkin<sup>2</sup>, <sup>1</sup>Kyiv National Taras Shevchenko Univ., Kyiv, Ukraine, <sup>2</sup>STC "Inst. for Single Crystals", National Academy of Sciences of Ukraine, Kharkiv, Ukraine.

In recent years, great interest has been enjoyed by heterometallic systems obtained on the bases of relatively inert anionic complexes with potentially bridging ligands, which have been widely employed to design heterospin systems with interesting magnetic properties. The present work is focussed on the fascinating anionic block – the anion of the Reineckes salt,  $[\text{Cr}(\text{NCS})_4(\text{NH}_3)_2]^-$ , which can form bridges with different metal ions *via* the thiocyanato groups. We are investigating the possibility of this anion as a precursor of thiocyanato-bridged heteronuclear species. In this study, two different complexes –  $[\text{Cu}(\text{en})_2\text{Cr}(\text{NCS})_4(\text{NH}_3)_2]_n[\text{Cr}(\text{NCS})_4(\text{NH}_3)_2]_{n-3n\text{DMF}}$  (1) (crystallizes in triclinic system with the space group P-1; the unit cell parameters are  $a = 11.040(2)$ ,  $b = 11.720(2)$ ,  $c = 12.945(13)\text{ \AA}$ ,  $\alpha = 73.2(4)$ ,  $\beta = 84.1(4)$ ,  $\gamma = 72.4(4)^\circ$ ;  $Z = 1$ ,  $V = 1528(16)\text{ \AA}^3$ ) and  $\{[\text{Cu}(\text{en})_2]_3\{[\text{Cr}(\text{NCS})_4(\text{NH}_3)_2]_2(\text{NCS})_2\}[\text{NCS}]_2\}$  (2) (crystallizes in triclinic system with the space group P-1; the unit cell parameters are  $a = 7.650(3)$ ,  $b = 13.621(4)$ ,  $c =$

$14.536(4)\text{ \AA}$ ,  $\alpha = 71.19(2)$ ,  $\beta = 81.62(3)$ ,  $\gamma = 86.05(3)^\circ$ ;  $Z = 2$ ,  $V = 1418.1(8)\text{ \AA}^3$ ) – have been synthesized by the reaction of copper powder and Reineckes salt by the use of the different reagent ratio in nonaqueous solution of ethylenediamine (en) in air. Their crystal structure will be presented.

**SP204 Novel Cu/Fe Heterometallic Complex Comprising a Unique  $[\text{Cu}_2\text{Fe}_2(\text{dipy})_6(\text{NCS})_2(\text{CN})_4]^{+}$  Squares.** O.V. Vreshch<sup>1</sup>, O.V. Nesterova<sup>1</sup>, V.N. Kokozay<sup>1</sup>, B.W. Skelton<sup>2</sup>, <sup>1</sup>Chemistry Dept., Kyiv National Taras Shevchenko Univ., Kyiv, Ukraine, <sup>2</sup>Chemistry, Univ. of Western Australia, Crawley, Australia.

Copper powder reacts with sodium nitroprusside and ammonia thiocyanate in  $\text{CH}_3\text{CN}$  solution of 2,2'-dipyridine (dipy) affording novel heterometallic complex  $[\text{Cu}_2\text{Fe}_2(\text{dipy})_6(\text{NCS})_2(\text{CN})_4]_2[\text{Fe}(\text{CN})_5(\text{NO})] \cdot 2(\text{NCS}) \cdot 6\text{H}_2\text{O}$ . The crystal structure has been determined by X-ray crystallography (Bruker SMART CCD, MoK $\alpha$ ,  $\omega$  rotation scans with narrow frames), solved by direct methods and refined by full-matrix least-squares methods on  $F^2$  using XTAL 3.7.

The compound crystallizes in the  $P\bar{1}$  triclinic space group and the cell dimensions are:  $a = 13.4540(10)$ ,  $b = 13.6360(10)$ ,  $c = 21.026(2)\text{ \AA}$ ,  $\alpha = 86.149(2)$ ,  $\beta = 77.439(2)$ ,  $\gamma = 66.486(2)^\circ$ ;  $Z = 1$ ,  $V = 3451.6(5)\text{ \AA}^3$  and  $d = 1.555\text{ g/cm}^3$ . The final  $R_I$  value is 0.057 for 979 parameters. The  $[\text{Fe}(\text{CN})_5(\text{NO})]^{2-}$  block is disordered on a crystallographic inversion centre. A tetranuclear  $[\text{Cu}_2\text{Fe}_2(\text{dipy})_6(\text{NCS})_2(\text{CN})_4]^{+}$  square is comprised of  $[\text{Cu}(\text{dipy})\text{NCS}]^{+}$  and  $[\text{Fe}(\text{dipy})_2]^{2+}$  corners and CN edges, with a Cu...Fe, Cu...Cu and Fe...Fe separations of 5.12, 6.72 and 7.73  $\text{\AA}$ , respectively. Both copper atoms have a trigonal-bipyramidal geometry and  $\text{N}_6$  donor set formed by one NCS, two CN and dipy ligand. Each iron atom in the cationic square has  $\text{N}_4\text{C}_2$  surroundings and coordinates by two chelating dipy ligands and two CN groups. The uncoordinated SCN anion is disordered over two positions with site occupancy set equal to 0.5. Residual peaks in the difference maps were modelled as disordered water molecules, each assigned site occupancies of 0.5.

**TP205 Structural Versatility of Copper(II) and Nickel(II) Complexes with Novel Polydentate Oxime-containing Schiff Base Ligands.** I.S. Moroz<sup>a</sup>, M. Haukka<sup>b</sup>, I.O. Fritsky<sup>a</sup>, <sup>a</sup>Dept. of Chemistry, Kiev National Taras Shevchenko Univ., Kiev, Ukraine, <sup>b</sup>Dept. of Chemistry, Univ. of Joensuu, Joensuu, Finland.

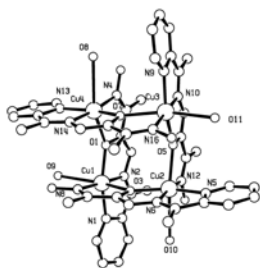
A series of 3d-metal complexes with two novel polyfunctional Schiff base ligands (2E)-2-(hydroxyimino)-N<sup>-</sup>-(1-(pyridin-2-yl)ethylidene)propanehydrazide (POP) and (2E)-2-(hydroxyimino)-N<sup>-</sup>-(pyridin-2-ylmethylene)propanehydrazide (POP<sub>a</sub>) containing several donor functions (oximic, hydrazide, hydrazone and pyridine cycle) has been synthesized and characterized by a variety of spectral methods; four complexes of different composition:  $[\text{Cu}_4(\text{POP-2H})_4(\text{H}_2\text{O})_4]$  (1),  $[\text{Cu}_4(\text{POP-2H})_4(\text{HCOOH})_4]$  (2),  $[\text{Ni}_4(\text{POP-H})_4(\text{HCOO})_4]$  (3) and  $[\text{Cu}_2(\text{POPa-2H})_2(\text{H}_2\text{O})]$  (4) were studied by X-ray single crystal analysis. The complexes 1-3 indicate  $[2 \times 2]$  grid structure (Figure) and comprise of tetranuclear six-coordinated metal clusters. The coordination of the ligand is realized in a tetradentate mode via the pyridine, azomethine and oximic nitrogen atoms and the bridging amide oxygen atom. In the nickel complex two types of chromophores are realized ( $\text{NiN}_2\text{O}_4$  and  $\text{NiN}_4\text{O}_2$ ). On the other hand, for the copper complexes there is only one type of chromophore ( $\text{CuN}_3\text{O}_3$ ). The average distances between the metal ions is close to 4  $\text{\AA}$ , the M-O-M' angles fall in the range 137-139° for 3 and 139-142° for 1, 2. In 4 POP<sub>a</sub> ligand exhibit quite different from POP coordination mode. The coordination of POP<sub>a</sub> is realized in tetradentate mode via the pyridine, amide and oxime nitrogen atoms and oxime oxygen atom with formation of a five-membered and a six-membered chelate rings.

**SP206 Co-crystals: A New Approach in the Development of Active Pharmaceutical Ingredients.** Safiyyah Forbes, Christer B. Aakeröy, John Desper, Dept. of Chemistry, Kansas State Univ., Manhattan, KS.

Crystal engineering have recently being used as a way of tailoring the physicochemical properties of active pharmaceutical ingredients (API's). The majority of API's exist in a variety of crystalline forms (polymorphs, salts, solvates) because of the inherent physico-chemical stability of crystalline materials. However, some API's display unwanted physical properties such as poor solubility/dissolution rate or thermal stability. With the use of pharmaceutical co-crystals a given API can be incorporated with another pharmaceutically acceptable molecule in the crystal lattice, which may improve the solubility, melting point and physical stability of the drug. Syntheses and crystal structures of several co-crystals of a family of anti-tumor API's prepared with acceptable carboxylic acids, amides, oximes and alcohols, are presented in this contribution. Intermolecular interaction-preferences are identified and rationalized based upon simple electrostatic principles of molecular recognition.

**SP207 Modified Cavittands: Expanding the Boundary.** Arbin Rajbanshi, Christer B. Aakeröy, John Desper, Dept. of Chemistry, Kansas State Univ., Manhattan, KS.

The ever exciting world of cavittand chemistry is further probed to modify the functionalities on the structure to better accommodate different types of guests. The structures were so designed that the binding sites are rightly oriented to form homo as well as heterodimeric capsules. This broadened the potential of functionalized cavittands to be used in different fields ranging from localized drug delivery to the ability to bring together otherwise unreactive moieties in close contact for a reaction. Various synthetic techniques were carried out to modify the binding sites of C-pentyltetra-bromocavittand. These assemblies incorporated ligands with H-bonding potential like acetamidopyridine and acetamidopyrazine into the upper rim of cavittand. The hierarchy of competing intermolecular forces in binding of guest molecule to the cavittand as well as in closing of the capsule was studied. In order to establish the potential of cavittand as heterodimeric capsule, cocrystallization was carried out with various carboxylic acids, oximes, haloarenes, and halogen substituted benzoic acids. The structures were characterized by <sup>1</sup>HNMR, <sup>13</sup>CNMR spectroscopy, mass spectroscopy, IR spectroscopy, and single crystal x-ray analysis.



**TP208 Triply Interpenetrated Pore Network in the Solvated Coordination Polymer Zinc Aminotriazolate Carbonate Hydroxide (7:8:2:2).** Urs Geiser, John A. Schlueter, Russell J. Funk, Materials Science Div., Argonne National Lab., Argonne, IL.

The title compound contains three translationally equivalent, intricate three-dimensional network of tunnel-like pores that interpenetrate without being connected to each other. Three distinct pore segments are discerned: (1) Infinite zigzag channels along the *c*-direction, (2) infinite zigzag channels along the *a+c* direction, and (3) finite straight segments along the *b*-direction connecting (1) and (2). The open tunnel cross section varies in diameter from ca. 3 to 5 Å, hence it is expected that the dry material has interesting gas storage and transport properties.

The crystal structure contains a Zn<sub>3</sub>(AmTAZ)<sub>6</sub> (AmTAZ = 3-amino-1,2,4-triazolate) trimer with an octahedrally coordinated Zn atom at

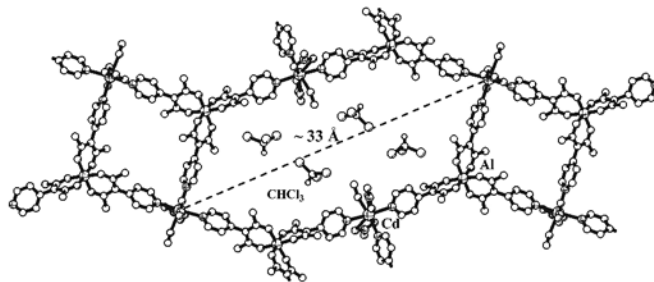
the center and tetrahedral Zn atoms on the outside, all of which bind to the 1- and 2-nitrogen atoms of AmTAZ. In addition, hydroxy- and carbonate-bridge dimers (one each) of tetrahedral zinc atoms bind to the 4-nitrogen atoms of AmTAZ. The two dimers are also connected to the trimer via carbonate- and hydroxy-bridges, respectively.

Crystal data: *a* = 26.356(2) Å, *b* = 22.914(2) Å, *c* = 16.545(2) Å, β = 97.263(6)°, *V* = 9912(2) Å<sup>3</sup>, *Z* = 8, *T* = 298 K, space group *C2/c*.

This work was supported by the U.S. Department of Energy, Office of Science, Basic Energy Sciences, at Argonne National Laboratory, a U.S. Department of Energy Office of Science laboratory, operated by UChicago Argonne, LLC, under contract DE-AC02-06CH11357. The U.S. Government retains for itself and others acting on its behalf a nonexclusive, royalty-free license in this contribution, with the rights to reproduce, to prepare derivative works, and to display publicly.

**SP209 Two-step Construction of Heterometallic Coordination Frameworks.** V.D. Vreshch, K.V. Domasevitch, Dept. of Inorganic Chemistry, Kyiv National Taras Shevchenko Univ., Kyiv, Ukraine.

Design and synthesis of new bimetallic coordination polymers is attractive area of supramolecular chemistry. In spite of significant interest in view of potential properties, synthesis in such the systems remains quite difficult and uncontrollable. To improve this we propose a methodology of step-by-step utilization of the ligand functionality. A series of ligands combining two most characteristic and typical ligand functions - β-diketonate and pyridine have been synthesized. The bifunctional ligand 3-(4-pyridyl)-2,4-pentanedione (HL) was exploited for the synthesis of molecular complexes

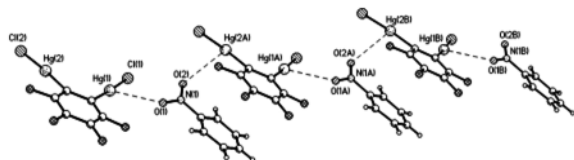


[BeL<sub>2</sub>], [AlL<sub>3</sub>], [FeL<sub>3</sub>] and [ZrL<sub>4</sub>], employing the diketonate group, as a first step. The beryllium complex was used for generation of Be/(Cd,Zn,Co,Cu) alternating superstructures utilizing the pyridyl donor sites. Coordination compounds adopt either molecular [M{BeL<sub>2</sub>}<sub>2</sub>Cl<sub>2</sub>] (M = Cd,Co) and one- [CdX<sub>2</sub>{BeL<sub>2</sub>}] (X = Br, J) [Cu<sub>2</sub>X<sub>2</sub>{BeL<sub>2</sub>}<sub>2</sub>]; (X = Cl,Br) or two-dimensional [Cd(SCN)<sub>2</sub>{BeL<sub>2</sub>}], [Co{BeL<sub>2</sub>}(CH<sub>3</sub>OH)<sub>2</sub>SO<sub>4</sub>], [Cu<sub>2</sub>Br<sub>2</sub>{BeL<sub>2</sub>}<sub>2</sub>] polymeric patterns.

The tris-diketonate complexes of 3-(4pyridine) and a suitable molecular model (phenyl, biphenyl substituent) are appreciably distorted through the "molecular collapse" effect. Such effect plays an important role in the designing bimetallic (Al,Fe)/(Zn,Cd,Co) superstructure and it predetermines the formation of dense bimetallic squares, which is a future of most crystal structures. Compounds [Cd{AlL<sub>3</sub>}(CH<sub>3</sub>OH){NO<sub>3</sub>}<sub>2</sub>]-2CHCl<sub>3</sub> and [Cd{AlL<sub>3</sub>}(CH<sub>3</sub>OH)Br]-2CHCl<sub>3</sub>·2CH<sub>3</sub>OH (Figure) have the unprecedented 2D structure based upon plane tiling by a set of heterobimetallic squares and octagons, while [Cd{FeL<sub>3</sub>}<sub>2</sub>(NO<sub>3</sub>)<sub>3</sub>] and [Co{AlL<sub>3</sub>}<sub>2</sub>Cl<sub>2</sub>] are 1D polymers and exist as chains of heterobimetallic squares sharing opposite vertices.

**TP210 Crystal Structure of Complexes 1,2-Bis-(chloro-mercurio) Tetrafluorobenzene with Natural Bidentate Lewis Bases.** Andrey A. Yakovenko, Jose H. Gallegos, Mikhail Yu. Antipin, Tatiana V. Timofeeva, Dept. of Natural Sciences, New Mexico Highlands Univ., Las Vegas, NM.

Over the two last decades, there has been a rapid progress in supramolecular chemistry of multidentate Lewis acids. It was found that the bidentate Lewis acid, 1,2-bis(chloromercurio) tetrafluorobenzene  $p\text{-}(\text{C}_6\text{F}_4)(\text{HgCl})_2$  (1) forms complexes with monodentate Lewis bases such as dimethylsulfoxide (DMSO), dimethylformamide (DMF), acetone, dimethyl methylphosphonate (DMMP), benzaldehyde, acetonitrile, THF and propylene oxide. However, for now we

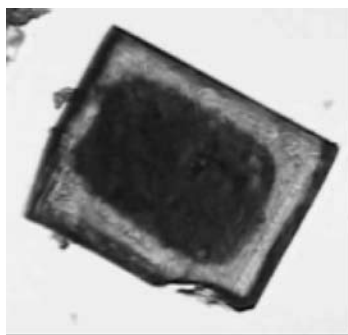


did not find in the literature complexes of 1 with bidentate Lewis bases. It is known that such bases are very important in organic synthesis and catalysis. In our project complexes of 1 with a series of neutral bifunctional Lewis bases have been prepared and structurally characterized. For example, in the case of nitrobenzene, the resulting complex  $\{[p\text{-}(\text{C}_6\text{F}_4)(\text{HgCl})_2(\text{PhNO}_2)]_n\}$  (2) contains one molecule of a Lewis base per one molecule of 1. Complex 2 have chiral supramolecular structure (space group  $P2_1$ ), were each oxygen atom of nitro group is coordinated with one mercury atom of 2. Also it is interesting to mention that in this case acentric crystal is built of non-chiral molecules.

The authors are grateful for NSF support via the NM EPSCoR program and DMR/NSF grant No. 0420863.

**SP211 Crystal Growth and Design of Composite and Mixed Crystals Using the Terpy Embrace Motif.** G. Soriano-Giles<sup>a</sup>, M. L. Marín-García<sup>a</sup>, A. Moreno-Carcano<sup>a</sup>, M. Rivera-Hernández<sup>b</sup>, J. Valdés-Martínez<sup>a</sup>, <sup>a</sup>Inst. de Química, <sup>b</sup>Inst. de Física, Univ. Nacional Autónoma de México, México.

Using the embracing motif observed in terpyridine complexes of formula  $[\text{M}(\text{terpy})_2](\text{ClO}_4)_2$  we have designed mixed crystals (crystalline molecular alloys) in which mixtures of  $[\text{Co}(\text{terpy})_2](\text{ClO}_4)_2$  and  $[\text{Cu}(\text{terpy})_2](\text{ClO}_4)_2$  complexes are incorporated in the same crystals. We have made alloys with different relative molar ratios coincident with the molar ratios present in solution. We have also been able to engineer composite crystals by the epitaxial growth of crystals from  $[\text{M}(\text{terpy})_2](\text{ClO}_4)_2$ ,  $\text{M} = \text{Co}(\text{II}), \text{Cu}(\text{II})$  on the surface of a seed crystal that contains a second  $[\text{M}'(\text{terpy})_2](\text{ClO}_4)_2$ ,  $\text{M}' = \text{Cu}(\text{II}), \text{Co}(\text{II})$ . In these, the different metal complexes are located in specific regions of the crystal. The design strategy as well as AFM, SEM and SEM-EDS studies on both mixed and composite crystals will be presented.



**SP212 Guest Intercalation into  $\text{SnI}_2$  Inorganic-organic Layered Perovskite Hybrid Solids.** Nilantha Bandara, Alicia M. Beatty, Dept. of Chemistry, Mississippi State Univ., Mississippi State, MS.

Inorganic-organic hybrid perovskites make up an important class of materials to study due to their unique electronic and optical properties.<sup>[1,2]</sup> We are interested in making layered perovskites using  $\text{SnI}_2$  with mono-substituted and di-substituted organic amine components, which contain aromatic and halide functional groups. In the past, small molecules have been incorporated into perovskite lattices

using co-crystallization techniques,<sup>[3]</sup> and we are investigating the ability to *remove* and *reincorporate* these guests into the solid framework by sonication. Therefore, the ability to intercalate guest molecules depending on the arrangement of close-packing structure was tested and will be discussed. The products are mainly characterized by thermogravimetric analysis (TGA), differential scanning calorimetry (DSC), single crystal X-ray diffraction, powder X-ray (PXRD) and melting point analysis.

[1] Mitzi, D.B.; Chondroudis, K.; Kagan, C. R., *IBM J. Res.& Dev.* 2001, **45**, 29.

[2] Mitzi, D.B., *J. Mater. Chem.* 2004, **14**, 2355.

[3] Mitzi, D.B.; Dimitrakopoulos, C.D.; Kosbar, L.L., *Chem. Mater.* 2001, **13**, 3728.

**SP213 Transmission Electron Microscopy Studies of Hydrogen-bonded “Clay Mimics”.** Christina Costin-Hogan, A.M. Beatty, Dept. of Chemistry, Mississippi State Univ., Mississippi State, MS.

Hydrogen-bonded “clay mimics” are 2-D crystalline materials made from organic or inorganic molecular components. For this TEM study, we are interested in examining our inorganic/organic hybrid “clay mimics”. Intercalation of guest molecules by sonication has been performed, and a noticeable change in the solids before and after intercalation has been observed visually. To obtain a better picture of the solids before and after sonication we must employ the use of a transmission electron microscope. Using TEM, bright field images (BFI) will be obtained in order to obtain the grain size and shape of the materials before and after sonication. Theoretical calculations will also be performed in order to determine expected changes in d spacing before and after sonication. Finally, diffraction patterns (DP), and kikuchi patterns will be obtained, resulting in experimental d spacing, for the starting material and intercalated guest molecule samples.

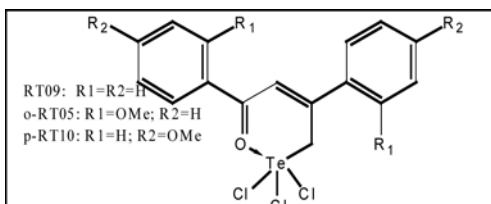
**TP214 Polar Organic Molecule Intercalation into Clay Mimics.** Austin Pickett, Alicia M. Beatty, Dept. of Chemistry, Mississippi State Univ., Mississippi State, MS.

To test intercalation ability of hydrogen-bonded **organic** clay mimics, a layered solid will be constructed of 3,5-Pyridinedicarboxylic acid and a long-chained diamine. The two diamines used are 1,10-Diaminodecane and 1,12-Diaminododecane. Attempts will be made to intercalate several polar organic molecules will be intercalated into the clay mimics by sonication of the solid in a hydrocarbon solvent that will not dissolve the hydrogen-bonded solid. Thermogravimetric Analysis (TGA), Differential Scanning Calorimetry (DSC), and NMR will be used to determine if intercalation occurred. The results of these tests for several guest molecules will be discussed. Further studies will involve the synthesis of an amine-containing ether, to replace the diamines used. Oxygen atoms in the carbon chain provide more possible sites for hydrogen bonding, which will better secure the intercalated guests.

**TP215 Crystal Structure, Supramolecular Arrangement and Docking Studies in Cathepsin B of Some Dipones.** Julio Zukerman-Schpector<sup>1</sup>, M. Vega-Tejido<sup>1</sup>, Iñez Caracelli<sup>2</sup>, R.L.O.R. Cunha<sup>3</sup>, J.V. Comasseto<sup>4</sup>, <sup>1</sup>LaCrEMM, Dept. de Química, C.P. 676-13560-905- UFScar, São Carlos-SP, Brazil, <sup>2</sup>Dept. de Física, Fac. de Ciências, UNESP, Bauru, Brazil, <sup>3</sup>Dept. de Biofísica, UNIFESP, São Paulo, Brazil, <sup>4</sup>Inst. de Química, USP, São Paulo, Brazil, julio@power.ufscar.br.

In all cases the Te(IV) makes two secondary interactions, one intra and one intermolecular, thus displaying a  $\psi$ -pentagonal bipyramidal coordination, if the lone pair is considered. The molecules

are arranged in centrosymmetric dimmers through a  $\text{Te}\cdots\text{Cl}$  secondary bond in I and II, and a  $\text{Te}\cdots\text{O}$  in III. The supramolecular arrangements being different in each case: in I the dimmers are linked through a  $\text{C}\cdots\text{H}\cdots\text{Cl}$  hydrogen bond, in II the packing is through a  $\pi\cdots\pi$  interaction and in III through a  $\text{C}_{\text{Me}}\cdots\text{H}\cdots\pi$  interaction. These results show that the self-assembly of the molecules is quite sensible to the type of substituents on the aryl moieties. As compound II was shown to be a strong inhibitor of cathepsin B [1], in order to gain more insight of the inhibition mechanism, a flexible docking study, using GOLD, of I, II and III in human cathepsin B (PDB: 1gmy) was undertaken. In all calculations the Cys29 was considered as a Cys, and the histidines were protonated as Hid, as it was postulated [1] that the inactivation by organotellurium (IV) compounds can be due to the high nucleophilic character of the thiol residue at the active site combined with the electrophilic character of the Te atom. The results suggest that there has to be a breaking of the intramolecular  $\text{Te}\cdots\text{O}$  secondary bond so the Te can get close to the S atom of Cys29 and that, in order to form a covalent bond, a Cl should be released.



[1] *Bioorg. Med. Chem. Letters* 15(2005)755  
FAPESP, CNPq, CAPES, FUNDUNESP

**SP216 Orientating Assembly from Transversal to Longitudinal Arrays of Metallomacrocycles.** Shaohua Gou, Zaolian Chu, Haibin Zhu, Huaze Dong, State Key Lab. of Coordination Chemistry, Nanjing Univ., Nanjing, P. R. China.

By varying non-coordinated R groups of the ligand, 1,6-di(triazole-1-yl-methyl)-4-R-phenol (dtp: R=*t*-Bu, dtmp: R=Me), the resulting [2+2] metallomacrocycles, derived from the construction of the ligand with  $\text{Cd}(\text{SCN})_2$  under the same condition, have been orientated from transversal to longitudinal arrays. Reaction of dtp with  $\text{Cd}(\text{SCN})_2$  produced a coordination polymer (1), in which macrocyclic units were connected side by side via metal knots forming a 1D looped chain with  $\text{NCS}^-$  groups on terminal positions. Substitution of dtmp for dtp with  $\text{Cd}(\text{SCN})_2$  yielded a new coordination polymer (2), where metallomacrocycles were connected via metal knots in a face-to-face mode to produce a 1D molecular ladder with macrocyclic platforms. The rungs of the ladder are made up of  $\text{M}_2\text{L}_2$  ring units, and the side rails are made of double-stranded chain of  $[\text{Cd}(\text{SCN})_2]_\infty$ .

This research is supported by the National Natural Science Foundation of China (Project 20271026). H. Zhu is grateful to China Postdoctoral Foundation for a research grant.

**TP217 Reaction of Itaconic Acid with Ba and Ca Carbonates Under Hydrothermal Conditions Gives  $\text{Ba}_3[(\text{Citraconate})_2(2,3\text{-dimethylfumarate})]$  and  $\text{Ca}(\text{citramalate})$ .** G. Díaz de Delgado<sup>a</sup>, J. Contreras<sup>a</sup>, B. Alí Bahsas<sup>b</sup>, J.M. Delgado<sup>a</sup>, <sup>a</sup>Lab. de Cristalografía-LNDRX, <sup>b</sup>Lab. de Resonancia Magnética Nuclear, Dept. de Química, Facultad de Ciencias, Univ. de Los Andes, Mérida, Venezuela.

Hydrothermal and solvothermal conditions of synthesis have proven useful to obtain new metal coordination polymers with hybrid organic-inorganic frameworks. One shortcoming of the use of organic reagents such as carboxylic acids, under these harsh conditions is that they may suffer rearrangements, decomposition, and/or reactions during the process. For example, reaction of  $\text{BaCO}_3$  and ita-

conic acid (methylenesuccinic acid) at 160 °C for 48 hours, in a stainless steel autoclave, resulted in a complex with two 2-methylmaleate ligands (citraconates) and one 2,3-dimethylfumarate ligand. The crystals are triclinic, P-1, with  $a=7.3221(4)$ ,  $b=10.6580(6)$ ,  $c=11.6713(7)$  Å,  $\alpha=77.402(2)^\circ$ ,  $\beta=81.354(2)^\circ$ ,  $\gamma=75.480(1)^\circ$ ,  $Z=5$ . Solution NMR experiments of the solid resulting from the reaction indicated the presence of residual citraconate, mesaconate, itaconate, 2-(hydroxymethyl)-succinate, and traces of citramalate anions. Under similar conditions, the reaction of itaconic acid with  $\text{CaCO}_3$  results in crystals of  $\text{Ca}(\text{citramalate})$  (C2/c,  $a=23.128(6)$ ,  $b=10.666(3)$ ,  $c=6.0037(15)$  Å,  $\beta=92.408(8)^\circ$ ,  $Z=8$ ). The solid material recovered from the reaction contains not only citraconate, mesaconate, itaconate, 2-(hydroxymethyl)-succinate anions, but also 2,3-dimethylfumarate and 5-oxotetrahydrofuran-3-carboxylate.

This work was possible thanks to grant LAB-98000821 from FONACIT- Venezuela.

**SP218 Structural Studies of  $[\text{Re}_6\text{Se}_8]^{2+}$  Core-containing Compounds.** Gary S. Nichol, Peter J. Orto, Xiaoyan Tu, Zhiping Zheng, Dept. of Chemistry, Univ. of Arizona, Tucson, AZ.

Part of our research interests in Arizona focus on the synthesis and characterization of thermally and atmospherically stable transition metal cluster compounds. We have been interested in compounds containing a  $[\text{Re}_6\text{Se}_8]^{2+}$  core for some time now [1] focusing on their electrochemical properties [2] and their use in the design and synthesis of supramolecular arrays. [3]

The nature of these compounds means that X-ray crystallography is essentially the only possible technique that can be used to characterize structurally these compounds. The structures are often fraught with problems. Crystallographic work on some new carbonyl-containing clusters will be discussed, along with examples of the use of the cluster in crystal engineering.

[1] Selby, H. D. & Zheng, Z. (2005). *Comments Inorg. Chem.* **26**, 75–102.3

[2] Roland, B. K., Flora, W. H., Selby, H. D., Armstrong, N. R. & Zheng, Z. (2006). *J. Am. Chem. Soc.* **128**, 6620–6625.

[3] Roland, B. K., Selby, H. D., Cole, J. R. & Zheng, Z. (2003). *Dalton Trans.* **22**, 4307–4312; Selby, H. D., Roland, B. K. & Zheng, Z. (2003). *Acc. Chem. Res.* **36**, 933–944.

**SP219 Metal-organic Frameworks with Co, Cu, Zn, and Cd Based on the Polyfunctional Ligand 3-Pyrid-4-ylbenzoic Acid.** T.L. Kinnibrugh<sup>1</sup>, J.Luo<sup>2</sup>, V. N. Khrustalev<sup>1</sup>, T.V. Timofeeva<sup>1</sup>, <sup>1</sup>Dept. of Natural Sciences, New Mexico Highlands Univ., Las Vegas, NM, <sup>2</sup>Los Alamos National Lab., Los Alamos, NM.

3-Pyrid-4-ylbenzoic acid was used as a linker to synthesize several metal organic frameworks (MOFs), containing Co, Cu, Ni, and Cd. MOFs are nanoporous crystalline materials with potential application as gas storage for fuel or waste and as sensors. Understanding their structural chemistry is important for the development of their applications. X-ray diffraction analysis was used to characterize four MOFs structure and pores. The MOF containing Cu is connected with four linkers by O and N, resulting in an octahedral coordination (Figure 1) while the MOF with Co has both octahedral and tetrahedral coordination. The variation in metals and synthetic conditions resulted in a variety of metal frameworks and different metal coordination which affects the pore size therefore the potential applications.

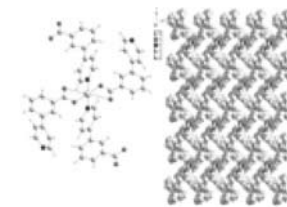
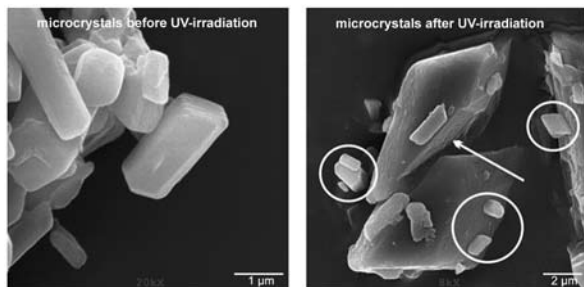


Figure 1. A view of the molecular structure and the space-filling model for the MOF containing Cu.

**TP220 Preparation and Single-crystal-to-single-crystal Reactivity of Nanosized Cocrystals Formed by Sonocrystallization.** Dejan-Krešimir Bučar, Leonard R. MacGillivray, Dept. of Chemistry, Univ. of Iowa, Iowa City, IA.

A recent report by Nakanishi *et al.* (*J. Am. Chem. Soc.*, 2002, 124, 10944.) describes a method to achieve single-crystal-to-single-crystal (SCSC) within organic crystalline solids by reducing the crystal size to nanodimensions using a precipitation method. Having considered this study, we anticipated that a SCSC [2+2] photoreaction of supramolecular hydrogen-bonded assemblies within molecular cocrystals could be achieved *via* decrease of crystal size.



In this contribution, we demonstrate the application of low-intensity ultrasonic radiation to cocrystals of composition 2(resorcinol)-2(4,4'-bpe) [where 4,4'-bpe = *trans*-1,2-bis(4-pyridyl)ethylene] through sonocrystallization produces nano- and submicron-sized cocrystals that are shown to exhibit SCSC reactivity, in contrast to macroscopic cocrystals obtained by conventional cocrystallization methods (*J. Am. Chem. Soc.*, 2007, 129, 32.). We also demonstrate that that the sonochemical treatment succeeds where sole precipitation fails. The SCSC reactivity of these assemblies was studied by proton nuclear magnetic resonance (<sup>1</sup>H-NMR) and X-ray diffraction (XRPD) while the morphology of the crystalline samples was observed by scanning electron microscopy (SEM).

**TP221 Crystal Chemistry and Crystallography of the Type-II Clathrate, Cs<sub>8</sub>Na<sub>16</sub>Ge<sub>136-x</sub>Ag<sub>x</sub>, and a Novel Phase, Na<sub>1-x</sub>Ge<sub>3+2z</sub>.** W. Wong-Ng<sup>1</sup>, M. Beekman<sup>2</sup>, G. Nolas<sup>2</sup>, J.A. Kaduk<sup>3</sup>, Q. Huang<sup>1</sup>, Z. Yang<sup>1</sup>, A. Shapiro<sup>1</sup>; <sup>1</sup>MSEL, National Inst. of Standards and Technology, Gaithersburg, MD, <sup>2</sup> Physics Dept., Univ. of South Florida, Tampa, FL, <sup>3</sup>INEOS Technologies, Naperville IL.

Type-II semiconducting clathrates have great potential as effective thermoelectric materials for power conversion and cooling applications. In this paper we will discuss two structures related to the type-II clathrates. Since doping of the framework Si or Ge sites with different elements could lead to enhancement of their thermoelectric properties, we have prepared a series of Ag-doped Cs<sub>8</sub>Na<sub>16</sub>Ge<sub>136</sub> phases. During the process of synthesizing the type II clathrate Na<sub>x</sub>Ge<sub>136</sub> using a vacuum decomposition technique, an unknown phase of Na-Ge was obtained. Two samples prepared using slightly different procedures were investigated using synchrotron, conventional x-ray, and neutron scattering (room-temperature as well as at 4K) techniques. This new phase was confirmed to have a zeolite-type framework that has open channels running through the structure. The general chemical formula can be written as Na<sub>1-x</sub>Ge<sub>3+2z</sub>. The structure of the Ag-doped Cs<sub>8</sub>Na<sub>16</sub>Ge<sub>136-x</sub>Ag<sub>x</sub> phases obtained using single crystal x-ray diffraction method and the features of the structure of the novel Na<sub>1-x</sub>Ge<sub>3+2z</sub> phase will be summarized.

**TP222 Automation at SER-CAT: A New Robot Implementation.** James Fait<sup>1</sup>, John Chrzas<sup>1</sup>, Andy Howard<sup>3</sup>, John Gonczy<sup>1</sup>, Zheng-Qing (Albert) Fu<sup>1</sup>, Zhongmin Jin<sup>1</sup>, John Rose<sup>2</sup>, B.C. Wang<sup>2</sup>, <sup>1</sup>SER-CAT, APS, ANL, Argonne, IL, <sup>2</sup>Dept. of Biochemistry and

Molecular Biology, The Univ. of Georgia, Athens, GA, <sup>3</sup>Biological, Chemical, and Physical Sciences Dept., Illinois Inst. of Technology, Chicago, IL.

A new sample mounting robot has been designed and implemented on the SER-CAT insertion device beamline, 22-ID. This robot realizes concepts and improvements based on the SER-CAT version of the ALS robot on 22-BM, which has been operational for over a year. This new design includes improvements in sample capacity, dewar design, gripper design, thermal behavior, alignment facilities and other features. Advances in automation software have also been developed, including automatic loop centering, automatic strategy collection and determination, screening functions, and other sample manipulations. Performance data from the installation and commissioning will be presented.

**TP223 NorthEastern Collaborative Access Team (NE-CAT) Beam Lines at the Advanced Photon Source.** Igor Kourinov, Steven E. Ealick, Malcolm Capel, Ed Lynch, Kanagalaghatta Rajashankar, Narayanasami Sukumar, John P. Unik, James Withrow, NE-CAT, Argonne, IL, Dept. of Chemistry and Chemical Biology, Cornell Univ., Ithaca, NY.

The Northeastern Collaborative Access Team (NE-CAT) facility at the Advanced Photon Source (APS) will consist of four beamlines. Three of the beamlines are based upon use of a novel canted undulator source, which consists of two undulators in a single straight section. A bending magnet beamline completes the set of four beamlines. At the present time, there are two operational undulator beamlines: 24ID-C is fully tunable in the energy range from 5 to 25keV with a focused beam size of 20x60 microns and 24ID-E - fixed energy at ~12.66keV or 14.84 keV (with small variability to cover selenium and bromine edges). The operational undulator beamline (24ID-C) is currently open to general APS users. 24ID-E will be open to general users later this year. A third, bending magnet beamline is scheduled for commissioning early next year.

NE-CAT is a consortium of scientists organized to design, construct and operate a structural biology sector at the APS. This facility will be used to focus on structural studies involving technically challenging crystallographic projects. In order to meet these needs, an ALS robot for screening a large number of sample crystals is now being commissioned, a microfocus diffractometer MD-2 is currently being commissioned on 24ID-E beamline, and several novel hardware and software tools are being implemented.

Funding for NE-CAT is provided through P41 grant from the National Center for Research Resources of the NIH and from the NE-CAT member institutions.

**SP224 Automated Sample Alignment at the Structural Biology Center Beamlines.** A. Joachimiak, K. Lazarski, S. Ginell, K.J. Gofron, M. Molitsky, Structural Biology Center and Biosciences, Argonne National Lab., Argonne, IL.

At synchrotron facilities majority of diffraction data are collected from crystals mounted in cryoloops. To minimize errors in recording diffraction peaks and improve detection of weak anomalous signal the crystal sample must be aligned with the x-ray beam to assure that equal crystal volume is exposed to x-rays during crystal rotation. Traditionally at synchrotron facilities crystals were mounted and aligned manually. This is time consuming and inefficient. Moreover, use of crystal mounting robots, need for rapid screening to find the best crystal and development of remote data collection capabilities requires automated sample alignment. We have developed and implemented at SBC robust and efficient cryoloop auto-centering protocols (SBCcollect). The automatic cryoloop alignment is using

specific crystal illumination and camera viewing conditions along with advanced and reliable image recognition to calculate displacement in 3-D between the cryoloop and the x-ray beam. The procedure allows automated alignment of loop with x-ray beam for initial crystal screening. The alignment can be improved using point-and-click. The procedure has been tested on a large number of samples. We will also report our progress on crystal alignment approaches.

This work was supported by the U.S. Department of Energy, OBER, under contract DE-AC02-06CH11357 and by NIH Grant GM074942.

**TP225 Crystal Centering for High Throughput Crystallography.** A. Jain<sup>1</sup>, V. Stojanoff<sup>2</sup>, <sup>1</sup>Massachusetts Inst. of Technology, MA, <sup>2</sup>Brookhaven National Lab.

Crystal centering is a time-consuming process in macromolecular X-ray crystallography experiments, taking 5-20 minutes per sample. In many experiments - especially ones those requiring crystal screening - the time spent by a researcher centering samples exceeds time spent on data collection. A new method using image processing and machine vision techniques in conjunction with a sample automounter and a computer-controlled goniostat allows for fully automatic centering of small crystals in the X-ray beam. This method positions crystals even when the loop cannot initially be seen in the camera's field of view and adapts the length of its procedure to the difficulty of the centering process. It has been tested on many diverse crystals with a 93% success rate when compared to manual centering and has been used in a screening experiment.

Acknowledgements: The NIGMS East Coast Structural Biology Research Facility team, the National Synchrotron Light Source staff, the DOE Science Undergraduate Laboratory Internship (SULI), GM0080 and DE-AC0298CH10886.

**SP226 Structure and Function of the Surrogate Light Chain Variable Domain.** Lucia Morstadt, Andrew Bohm, Deniz Yuksel, David Stollar, Jim Baleja, TUFTS Sackler School, Boston, MA.

B cell development in the bone marrow, divisible into different stages, results in circulating, mature B cells that express antibodies on their plasma membrane and are capable of interacting with antigens. Precursor cells differentiate successively into pro-B, pre-B and immature B cells, a process linked to development of the immunoglobulin repertoire by heavy (H) and light (L) chain gene rearrangements. During development, H chains are made before L chains. In the pro-B cell to pre-B cell transition, successfully rearranged H chains are co-expressed with the surrogate light chain (SLC) in place of L chain. There is only one SLC to pair with the whole pool of H chains generated by gene rearrangement in different cells. The proposed function of the SLC is to test a  $\mu$ H chain for its ability to bind later in development to a conventional L chain. We wish to characterize features of the V-domain of the SLC that allow pairing with all H chains. The binding of a construct representing the SLC V-domain, VpreBJ, to an H chain V domain (VH) was demonstrated by surface plasmon resonance spectroscopy. We then solved the structure of VpreBJ with X-ray crystallography to a resolution of 2.0 Angstroms using isomorphous replacement. VpreBJ strongly resembles a mature L chain immunoglobulin V-domain (VL), with two  $\beta$ -pleated sheets of 4 and 5 strands each, packed face-to-face and covalently connected by a disulfide bond. The 5 strand interface interacts with the VH chain and this interaction is mimicked by a crystallographic dimer of SLC domains. Analytical ultracentrifugation verified the presence of dimers in solution. We identified the residues of VpreBJ that likely mediate the SLC-VH interaction, and found some that are not conserved with other VL chains. The difference also lies in a longer CDR2 loop in VpreBJ, which, unlike most VL domain classes

has 11 amino acids and reaches further into the interface with the VH chain. Thus this work has provided important insight into the mechanism by which the SLC is able to recognize VH chain, and thus allow progression in the development of B cells.

This work was supported by NIH grant AI064433.

**MP227 Are Your Crystals too Small or Weakly Diffracting for Your Home Laboratory Diffractometer?** S.J. Teat<sup>\*</sup>, K.N. Raymond<sup>\*</sup>, <sup>\*</sup>Advanced Light Source, Lawrence Berkeley National Lab., Berkeley, CA, <sup>\*</sup>Dept. of Chemistry, Univ. of California, Berkeley, CA.

One of the challenges facing chemical crystallographers: how to collect good data. This is especially challenging on the more complex structures chemists are making and even some of the relatively simple compounds, since both can produce small and weakly diffracting crystals. If these crystals produce little or no diffraction on a laboratory diffractometer with long exposures, what can be done to get the structure? One answer would be to combine a much higher X-ray flux and a focused beam better matching the crystal size. Station 11.3.1 on the Advance Light Source combines the high flux from a synchrotron,  $10^{10}$  photons per second, with a focused beam of  $90 \times 200$  microns. This allows high quality data to be rapidly collected from small and weakly diffracting crystals, that otherwise show little or no diffraction using a laboratory source. And unlike a laboratory source, the synchrotron wavelength can be tuned from 2.0 to 0.7Å. This ability permits anomalous dispersion based studies, making it possible to discriminate isoelectronic species. Examples of recently collected data will be presented, including those of actinide compounds.

The Advanced Light Source is supported by the Director, Office of Science, Office of Basic Energy Sciences, of the U.S. Department of Energy under Contract No. DE-AC02-05CH11231.

**MP228 Generating High Brilliance X-ray Beams for X-ray Diffraction and Scattering Applications.** Brett Kraabel, Pascal Boulée, Dan Cenda, Peter Høghøj, Lykourgos Spanos, Vincent Roger, Xenocs SA, Sassenage, France, E-mail info@xenocs.com.

Today a large fraction of the X-ray analytical systems used in two-dimensional diffraction and scattering applications are still equipped with non-optimized beam-generating schemes that combine high power sealed tubes or rotating anodes with large source-sizes with inefficient optical schemes. With the advent of single reflection graded multilayer optics and efficient, low power micro-focus sealed tubes, it has become advantageous and cost-effective to replace these high power systems with this more efficient and robust technology.

The key to this new technology are Xenocs' high performance, single reflection X-ray optics that couple optimally to small x-ray sources. The relative figure-of-merit for X-ray beams is the brilliance, which typically is expressed as photons/mrad<sup>2</sup>/mm<sup>2</sup>/s in the relevant part of the spectrum (i.e. Cu K-alpha), and which can never exceed the brilliance of the source (Liouville's Theorem). Xenocs' single reflection optics optimally conserve the brilliance of these sources, resulting in extremely bright X-ray beams.

The GeniX product line from Xenocs combines a micro-focus X-ray tube with high-efficiency Xenocs X-ray optics, and offers a high performance solution with clearly defined characteristics (beam size, divergence, spectral purity, flux...). Compared to high power sealed tubes, the Genix solution offers superior brilliance enabling faster data collection in a package with a small footprint, low power consumption, and low facility requirements. The low maintenance requirements of this solution also make it appealing as a replacement for traditional rotating anodes.

In addition to presenting the GeniX product platform we present data obtained with the GeniX to demonstrate its performance and its value as an efficient, cost-effective X-ray beam delivery solution for a variety of applications including single crystal and protein crystallography, high pressure diffraction, and SAXS.

**MP229 X06DA: A Production Beamline for Protein Crystallography at SLS.** Meitian Wang, Roman Schneider, Claude Pradervand, Mauro Roccamante, Wayne Gletting, Takashi Tomizaki, Ezequiel Panepucci, Andreas Isenegger, Herbert Kalt, Hubert Baechli, Qianhong Chen, Clemens Schulze-Briese, Swiss Light Source at Paul Scherrer Inst., Villigen, Switzerland.

The new protein crystallography beamline X06DA (PXIII) receives light from a 2.9 T super bending magnet in the 2.4 GeV, 400 mA electron storage ring at the Swiss Light Source (SLS). The general design concepts are optimized for simplicity without compromising the performance. Some notable features are: (1) A Bartels monochromator offering fast wavelength changes and a true fixed beam position. (2) An innovative goniometer (PRIGO) for alternative data collection protocols. (3) An IRELEC automatic sample changing system with possibilities of both cryogenic sample mounting and crystallization plate screening. (4) A mini-hutch design improving the efficiency of manual sample mounting. Special attention will be paid in integrating automatic data processing and structure solution into data collection protocols for further improving the productivity of the beamline. The beamline is funded by a partnership between the Paul Scherrer Institut and Swiss and international pharmaceutical companies (Actelion, Boehringer Ingelheim, Novartis, and Proteros Biostructures). The beamline is currently under construction, and the first user experiments are expected by the end of 2007. Approximately 50 percent of beamtime will be available to the international user community from spring 2008.

**MP230 Automation Program for Macromolecular Crystallography at the NSLS.** Alexei S. Soares, Mary Carlucci-Dayton, Howard Robinson, Robert Sweet, Dieter Schneider, Biology Dept., Brookhaven National Lab., Upton, NY.

An automation program that facilitates a high degree of experimental design flexibility has been implemented for macromolecular crystallography at the National Synchrotron Light Source (NSLS). The central piece in this program is a cryogenic robotic specimen mounting system based on the hybrid pneumatic/stepper motor system developed at the Lawrence Berkeley National Laboratory (LBNL). This design was selected for its minimal footprint, inherent safety, and reliable random access to a large selection of specimens. An overview of the mechanical and software capabilities is presented, along with a summary of reliability and usage statistics. The focus will be on a detailed description of user access modes, with complimentary training material and an opportunity for hands-on familiarization and demonstration of parts and tools needed to participate in our programs.

**MP231 Q-Crystallography at the NSLS/PXRR.** Howard Robinson, John Skinner, Rick Buono, Matt Cowan, Grace McCarthy, Bob Sweet, Alex Soares, Dieter Schneider, Biology Dept./PXRR, Brookhaven National Lab., Upton, NY.

The Queueing Crystallography Program is tailored for NSLS industry proprietary users who want daily access to synchrotron beamtime, but would prefer to maintain a normal work schedule at their home base.

Proprietary users identify the crystals in their pucks via our web-ac-

cessed database, PXDB and ship them to the NSLS/PXRR. The user also loads a queue (to-do list) in the PXDB for the crystals in each puck. The PXRR staff put the pucks in the auto-mounter and feed the user's queue into our beamline data-collection program, CBASS. The crystals are auto-mounted, auto-centered with C3D and auto-evaluated with DNA (diffraction quality analysis). On completion, a notice is sent to the user to examine the crystal assessments from within PXDB. If the user would like a screen to be centered elsewhere on the crystal, they click on the crystal image at that new center and a new request is added to the queue. This new queue is then executed when beamtime is available, thus repeating the cycle. The user can also queue a collection when they are satisfied with the screens. The user can download the diffraction images via the PXDB for analysis at their home. In this way, the PXRR staff supports the beamline and collection queue, but is not involved with the crystals or diffraction images (a requirement for proprietary work).

A side benefit of the new system is that on-site visiting researchers can queue up their collections and go to dinner. In the Queueing Crystallography Program the user is responsible for the experiment and analysis. This is distinct from our Mail-in program where the home user and synchrotron scientist both contribute to the project.

**MP232 FedEx Crystallography the Next Generation: Combining Mail-in Crystallography Program with Remote Data Collection Capability at SER-CAT.** Zhongmin Jin, John Chrzas, James Fait, John Gonczy, Zheng-Qing (Albert) Fu, John Rose, B.C. Wang, Southeast Regional Collaborative Access Team, Advanced Photon Source, Argonne National Lab., Dept. of Biochemistry and Molecular Biology, Univ. of Georgia, Athens GA.

SER-CAT implemented a mail-in Crystallography program in 2003 to provide its members with high quality data and to maximize data collection efficiency by collecting data during times where users could not be scheduled. Most SER-CAT member institutes have participated in the program. Since 2003, the mail-in program has used 500 hours beam time, screened 512 crystals and collected 255 data sets (including native, SAD and MAD). Beginning in 2005, with the implementation of reliable robotic sample mounting system and secure remote data collection capability on 22BM over a third of SER-CAT member institutions have now participated in remote data collection activities. SER-CAT is now finishing the installation of an improved robotic sample mounting system on its undulator beamline 22ID and will soon offer remote data collection capabilities on both its beamlines. Details of mail-in program and remote data collection capability will be presented.

**SP233 Automatic Crystal Centering and Crystal Optimisation on the SRS.** Mylrajan Muthusamy, John Cowan, Steve Kinder, Steve Buffey, Colin Nave, Daresbury Lab., Warrington, UK.

To fully utilise sample changing robots for protein crystallography, a reliable means of centring the crystal in the x-ray beam is required. We have implemented two different programs for alignment C3D search from EMBL Grenoble and XREC from EMBL Hamburg. A java interface was used to run these programs as external processes. A pre-alignment of the loop position is first carried out at a low zoom level followed by full alignment with various angles and a higher zoom level. A weighted average of the outputs of both programs was used. The system has been integrated into the control software at the SRS. Crystals with various dimensions were used for centring and analysis of the images showed excellent centring. Performance enhancement using grid system will be described.

For very small crystals, surrounded by large amounts of solvent, the crystal can be obscured or refraction effects can distort its apparent position. Use of an x-ray centring method, based on the characteristics of the diffraction pattern as the crystal is translated, will also be described. An integrated approach for crystal centring will be discussed.

The Proteros Free Mounting System (FMS) humidity control system is used to optimize the crystals with respect to their diffraction characteristics via control of crystal water content. Advantages are improved resolution, mosaicity, anisotropy, improved cryo-protocols, reduced background. The FMS has been installed on the SRS station 9.6 with a graphical user interface and the information analysed with LABELIT.

The work was funded by the EU BIOXHIT project.

**MP234 Recent Advances in IP and CCD Technology.** Joseph D. Ferrara<sup>1</sup>, Lee M. Daniels<sup>1</sup>, Hugh Garvey<sup>2</sup>, James W. Pflugrath<sup>1</sup>, Katsunari Sasaki<sup>3</sup>, Cheng Yang<sup>1</sup>, <sup>1</sup>Rigaku Americas Corporation, The Woodlands, TX, <sup>2</sup>Rigaku Innovative Technologies, Tucson, AZ, <sup>3</sup>Rigaku Corporation, Tokyo, Japan.

Imaging plate (IP) and charge-coupled device (CCD) detectors have both benefited from improvements in their underlying technologies as well as improvements in electronic technology in general. We will review some of those improvements as well as explore the cutting edge applications that result from those improvements from macromolecular phasing to fragment-based screening to charge density studies.

**MP235 Synthesis and Structure of  $\text{Li}_6\text{Y}(\text{BO}_3)_3$  as a Neutron Scintillator.** C.J. Rawn<sup>1,2</sup>, E.A. Sheats<sup>1</sup>, P.A. Cutler<sup>1</sup>, J.P. Hodges<sup>3</sup>, M.L. Crow<sup>4</sup>, B.C. Chakoumakos<sup>3</sup>, <sup>1</sup>Dept. of Materials Science and Engineering, Univ. of Tennessee, Knoxville, TN, <sup>2</sup>Materials Science and Technology Div., <sup>3</sup>Neutron Scattering Science Div., <sup>4</sup>Neutron Facilities Development Div., Oak Ridge National Lab., Oak Ridge, TN.

$\text{Li}_6\text{Y}(\text{BO}_3)_3:\text{Ce}^{3+}$  is a fast bright scintillator intrinsically sensitive to neutrons. This material is a promising candidate for use in detectors at a pulsed spallation neutron facility where microsecond time resolution is desired. Single phase  $\text{Li}_6\text{Y}(\text{BO}_3)_3$  has been synthesized by melting stoichiometric amounts of  $\text{Li}_2\text{CO}_3$ ,  $\text{Y}_2\text{O}_3$ , and  $\text{H}_3\text{BO}_3$  at 1100 °C for 10 minutes and quenching. Samples of  $\text{Li}_6\text{Y}_{1-x}\text{A}_x(\text{BO}_3)_3$  where A = Ce, Sc, Ca, La, Sr, and Gd and x = 0.15 have been synthesized as well as  $\text{Li}_6\text{Y}_{1-x}\text{A}_x\text{Ce}_y(\text{BO}_3)_3$  where A = Sc, Ca, La, Sr, and Gd and x and y are 0.15. X-ray powder diffraction data show all samples are mostly single-phase with minor amounts of secondary phases indicating a large solid solubility range. Lattice parameters determined from the Rietveld refinement of data collected on  $\text{Li}_6\text{Y}_{0.85}\text{La}_{0.15}(\text{BO}_3)_3$  using the monoclinic space group  $P12_1/c1$  are  $a = 7.190(2)$  Å,  $b = 16.456(3)$  Å,  $c = 6.645(2)$  Å, and  $\beta = 105.314(6)$  and result in a unit cell volume of  $758.3(6)$  Å<sup>3</sup>, a little more than 1% larger than the volume reported for  $\text{Li}_6\text{Y}(\text{BO}_3)_3$  reported by Tu *et al.* [1].

[1] C.Y. Tu, A.D. Jiang, Z.-D. Luo, *Jiegong Huaxue*, 8, 215-219 (1989).

Oak Ridge National Laboratory is managed by UT-Battelle, LLC, for the U.S. Department of Energy under Contract DE-AC05-00OR22725.

**MP236 First Results of the ÅXIOM 200, a New High-Speed Photon-Counting X-ray Detector.** M. Benning<sup>1</sup>, R. Durst<sup>1</sup>, B. Schierbeek<sup>2</sup>, Y. Diawara<sup>1</sup>, D. Khazins<sup>1</sup>, <sup>1</sup>Bruker AXS Inc., Madison, WI, <sup>2</sup>Bruker AXS B.V., Delft, The Netherlands.

Photon-counting detectors were once widely used for macromolecu-

lar crystallography. Due to a lower counting rate, smaller detecting area and limited spatial resolution, they have been replaced by analog detectors (e.g., Image Plates and CCDs) for most single crystal data collection. The ÅXIOM 200 is a new digital photon-counting detector based on microgap technology which combines a large 200 mm diameter active area with superior noise performance, dynamic range and sensitivity compared to traditional analog detectors. Unlike conventional detectors, the ÅXIOM has no dead time between frames for faster, more accurate data acquisition. Detector characteristics as well as data examples will be presented.

**MP237 Improvement of Crystallographic Data Near Corners in Mosaic CCD Detectors.** A.S. Arvai<sup>1</sup>, S. Brockhauser<sup>2</sup>, G. Cioci<sup>3</sup>, G.A. Leonard<sup>3</sup>, A. McCarthy<sup>2</sup>, S. McSweeney<sup>3</sup>, C. Müller-Diekmann<sup>3</sup>, C. Nielsen<sup>1</sup>, D. Nurizzo<sup>3</sup>, R.B.G. Ravelli<sup>2</sup>, Ng. H. Xuong<sup>1</sup>, <sup>1</sup>Area Detector Systems Corp, Poway, CA, <sup>2</sup>EMBL, Grenoble, France, <sup>3</sup>ESRF, Grenoble, France.

Large area fast-readout CCDs have become the detector of choice for modern Macromolecular Crystallography synchrotron beam lines. These mosaic detectors are flat-field corrected in order to give a uniform response over the whole surface area. Nevertheless, it has been observed that crystalline diffraction intensities are often underestimated when recorded near the corners of a CCD module. We believe that this effect is primarily due to a variation of the point spread function from the center to the corner of each module. The location of these corners on 3x3 and 4x4 CCD detectors often has significant negative impact on structure solution when important medium resolution reflections are measured in these areas. A method to construct and apply a correction for this effect is presented along with some examples showing improvement in R-factors, anomalous signal, and the ability to solve a structure.

**TP239 The Present and the Future of Protein Microcrystallography at SPring-8.** N. Shimizu<sup>a</sup>, M. Kawamoto<sup>a</sup>, K. Hasegawa<sup>a</sup>, A. Nisawa<sup>b</sup>, G. Ueno<sup>b</sup>, K. Hirata<sup>b</sup>, T. Kumasaka<sup>a</sup>, M. Yamamoto<sup>a,b</sup>, <sup>a</sup>Structural Biology Group, JASRI/SPring-8, <sup>b</sup>Div. of Synchrotron Radiation Instrumentation, RIKEN SPring-8 Center, Hyogo Japan.

BL41XU is an undulator beamline at Japanese third-generation synchrotron facility SPring-8. This beamline has been improved for obtaining high quality data from protein micro crystals (~ 25 µm) using a micro beam (~ 25 µm). The new K/B mirror system was installed at the autumn of 2006, and the monochromatized beam is focused to V70 × H100 µm (F.W.H.M.) at sample position. The final beam size at sample position is defined from 25 × 25 to 70 × 100 µm<sup>2</sup> (F.W.H.M.) by using two set of quadrant slits. Photon flux and flux density of the 25 × 25 µm<sup>2</sup> beam at 1 Å are  $3.0 \times 10^{11}$  photons/sec and  $4.8 \times 10^{14}$  photons/sec/mm<sup>2</sup>, respectively.

It is essential for the data collection to control the radiation dose since micro crystals will be received remarkable radiation damage. The data collection software installed to BL41XU can change the beam irradiation position automatically to suppress the effect of radiation damage by using multiple positions on a crystal and multiple crystals. SAD measurements of Se-methionine samples with the crystal size from 15 to 50 µm were performed by using this tool, and we successfully obtain the initial phase at the resolution from 2.7 to 3.9 Å.

A new micro focus beamline in order to utilize the real micro beam; target beam size is  $1 \times 1$  µm<sup>2</sup>, is planned at SPring-8. We present the present status of protein microcrystallography at BL41XU and the future plan of the real micro beam beamline.

**TP240 The Quest for Higher Resolution In-house Data.**  
Ina Dix, Lehrstuhl für Strukturchemie, Univ. Göttingen, Germany.

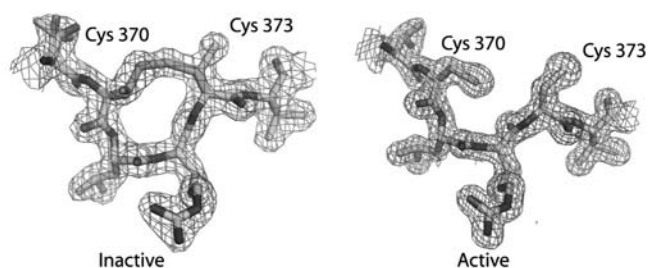
The combination of an Incoatec I $\mu$ S microsource and a Bruker Axiom-200 detector has a number of advantages - focused beam, zero readout time, no cooling required, small footprint and a very sensitive (quantum counting) detector that make it predestined for screening small crystals in the crystallization lab. However the zero noise of the detector - the energy filtering even removes the cosmic ray background - gives it a unique advantage over virtually all other detector technologies, namely the ability to make long exposures without accumulating any background and so measure reflections that would otherwise be lost in the noise. I will present comparisons using the same test crystals with different sources and detectors to establish how much gain in resolution can be obtained in practice

**MP241 The Bench Top X-ray Diffractometer as an Effective Teaching Tool.** Ronald E. Benson, Rigaku Americas Corporation, The Woodlands, TX.

A small bench top x-ray diffractometer was recently developed that features simplified hardware and almost fully automated software. These advances in technology ensure that the user spends less time on maintaining hardware or learning the nuances of complicated software and more time teaching students. The simplified hardware makes it easy for undergraduates to learn to mount and center crystals. The automated software allows students to dedicate more time learning the fundamental concepts of diffraction theory, structure solution, and structure refinement. The Rigaku SCXmini presents these hardware and software advances in a compact area that fits easily into any research or teaching laboratory.

**SP242 Crystal Structure and Possible Redox Regulation of S-nitrosogluthione Reductase from Arabidopsis Thaliana.** Justin Crotty, Matthew Grieving, Guenter Wildner, Ung Lee, Susanne Brettschneider, Jacqueline L. Brailey, Andrzej Weichsel, Elizabeth Vierling, William R. Montfort, Depts. of Biochemistry and Molecular Biophysics, and Chemistry, Univ. of Arizona, Tucson, AZ.

The number of proteins that have been shown to be S-nitrosated in vivo is increasing steadily, highlighting the importance of this redox based post translational modification. S-nitrosogluthione reductase (GSNOR) reduces S-nitrosogluthione (GSNO) to GSNHOH, removing GSNO from the cytosol. GSNOR has been linked to asthma in humans and plays a role in disease resistance and in the model plant *Arabidopsis thaliana*. We became interested in *Arabidopsis* GSNOR after discovering an apparent genetic link between it and heat shock response. We expressed and purified recombinant *Arabidopsis thaliana* GSNOR from *E. coli* and determined its crystal structure to 1.4 Å resolution. While searching for an inhibitor of the enzyme as part of a drug discovery program, we discovered that it can be oxidized to an inactive state, through disulfide linkage of Cys370 and Cys373 (below). Subsequent reduction of this disulfide bond with DTT restores the enzyme to an active state. Mutation of Cys370 and Cys373 to alanine leaves a functional enzyme that cannot be oxidized to an



inactive form. The  $K_m$  and  $k_{cat}$  for GSNO are 26(6)  $\mu$ M and 188(10)  $sec^{-1}$  for wild type and 28(5)  $\mu$ M and 176(8)  $sec^{-1}$  for the mutant. We will present structures of this enzyme in both the oxidized (1.7 Å) and reduced (1.4 Å) forms.

**MP243 Crystal Structure of the Core Domain of Human Coactivator-associated Arginine Methyltransferase 1 (CARM-1).** John S. Sack<sup>a</sup>, Gerald J. Duke<sup>b</sup>, Dianlin Xie<sup>b</sup>, Herbert E. Klei<sup>a</sup>, Kevin F. Kish<sup>a</sup>, <sup>a</sup>Depts of Macromolecular Crystallography and <sup>b</sup>Gene Expression and Protein Biochemistry, Bristol-Myers Squibb Research & Development, Princeton, NJ.

Coactivator-associated arginine methyltransferase 1 (CARM-1) is a member of the protein arginine methyl transferase (PRMTs) family that catalyze the transfer of methyl groups from S-Adenosyl-L-Methionine (SAM) to the sidechain of specific arginine residues of activator proteins. The over-expression of CARM-1 has been seen in tumor tissue samples and has been suggested as a possible target for the treatment of tumors related to nuclear hormone receptor and p53 signaling pathways. The de novo structure of the core domain of CARM-1 in complex with S-Adenosyl-homocysteine (SAH) has been determined using MAD phasing techniques at 2.1 Å resolution and refined to an R-factor of 20.6%. The two-domain protein has an N-terminal mixed  $\alpha\beta$  Rossmann fold domain and a C-terminal  $\beta$ -barrel, similar to that of the related cores of PRMT1 and PRMT3. The structure shows many of the key features previously seen in the previously reported PRMT structures but differs in relative orientation of the two domains and of the two monomers that form the CARM-1 dimer. It also has an extended dimer "antenna" and a C-terminal extension. The organization of the proposed arginine binding site is compared to that seen in the other PRMTs. The precise knowledge of the arrangement of the protein in this region will be instrumental in the structure-based design of small molecule inhibitors of this enzyme.

**SP244 Chemistry Under the Microscope.** Julie Harris, James Maynard, John W. Moore, Elizabeth Moore, UW-Madison, Dept. of Chemistry and Journal of Chemical Education, Madison, WI.

A Nikon SMZ microscope camera in combination with Nikon ACT-2U software is used to photograph various chemical reactions under the microscope. Small scale chemical reactions between a single crystal and one to two drops of solutions are photographed. Many reactions reveal chemical structures and characteristics that are not distinguished in a large scale reaction, such. Brilliant colors, interesting crystal structures and interesting effects are produced in these reactions. The stages of precipitation are observed in a reaction between potassium iodide and lead nitrate. Gold's characteristic cranberry color is shown with the simultaneous oxidation of tin by gold chloride in a sun-ray type effect. Silver dendrites are shown as they grow off of a thin copper wire during a reaction between copper wire and silver nitrate. All colors involved in the Prussian Blue reaction are shown within a single drop. The final products are observed and photographed for unique as well as characteristic features.

These pictures and videos have a dual purpose, first, to shown small scale effects that are not normally seen, and secondly, to combine art and chemistry.

Pictures have been featured in the Journal of Chemical Education as well as a variety of their publications including Chemistry Comes Alive! Volume 8. For more information and photographs please reference the previous publications.

**TP245 Structural Basis for Conserved Complement Factor-like Function in the Antimalarial Protein TEPI.** Richard Baxter, Chung-I Chang, Yogarany Chelliah, Stephanie Blandin, Elena Levashin, Johann Deisenhofer, Biochemistry, Univ. of Texas Southwestern Medical Center, Dallas, TX.

Thioester-containing proteins (TEPs) are a major component of the innate immune response of insects to invasion by bacteria and protozoa. TEPs form a distinct clade of a superfamily that includes the pan-protease inhibitors alpha2-macroglobulins and vertebrate complement factors. The essential feature of these proteins is a sequestered thioester bond that, following cleavage in a protease-sensitive region of the protein, is activated and covalently binds to its target.

Recently, thioester-containing protein 1 (TEP1) from the malarial vector *Anopheles gambiae* was shown to mediate recognition and killing of ookinetes from the malarial parasite *Plasmodium berghei*, a model for the human malarial parasite *P. falciparum*. Here we present the crystal structure of the TEP1 isoform TEP1r. While the overall protein fold of TEP1r resembles that of complement factor C3, the TEP1r domains are repositioned to stabilize the inactive conformation of the molecule (containing an intact thioester) in the absence of the anaphylotoxin domain, a central component of complement factors. The structure of TEP1r provides a molecular basis for the differences between TEP1 alleles TEP1r and TEP1s, which correlate with resistance of *A. gambiae* to infection by *P. berghei*.

**SP246 The RNA (UGGGGU)4 Quadruplex Revisited: Alternate Crystal Packings and Density Basin Structure.** A. Fyfe, P. Dunten, M.M. Martick, W.G. Scott, Scott Lab, UCSC, Sinsheimer Labs, Santa Cruz, CA.

The capacity of guanine residues to associate into quadruplexes, stacked, four-membered, planar units linked by Hoogsteen hydrogen bonds, provides a well-known structure for linking nucleic acid strands. A variety of quadruplex topologies are possible, depending in part on whether one, two or four molecules are involved and these structures have been reported in diverse biological contexts<sup>[1]</sup>. The structure of quadruplexes in the telomere region of chromosomes and their association with telomerase is an active area of cancer research. Here the structure of guanine quadruplexes is studied in a tetramolecular complex of UGGGGU RNA oligonucleotides.

The complexes, assembled from four parallel strands, crystallize readily and, similarly to their DNA counterparts<sup>[2]</sup>, diffract to high-resolution<sup>[3]</sup>. We report two alternate crystal packings, one in a tetragonal lattice but with different cell dimensions than previously published<sup>[3]</sup>, the other in an orthorhombic lattice.

Interestingly, standard molecular replacement algorithms failed to yield a solution for these packings and the structures were solved by iterative cycles of rigid-body placement and refinement.

The sub-Angstrom resolution yielded high-quality electron density maps. To further investigate the structure of the maps we partitioned the density in the quadruplex region into aspherical atomic basins bounded by zero-flux surfaces. Results from two partitioning algorithms<sup>[4],[5]</sup> are compared and the effects of different levels of critical point coalescing are presented.

[1] Burge, S. *et al.*, *NAR*, 2006, **34**(19), 5402

[2] Phillips, K. *et al.*, *JMB* 1997, **273**, 171

[3] Deng, J. *et al.*, *PNAS* 2001, **98**(24), 13665

[4] Henkelman, G. *et al.*, *Comp. Mat. Sci.*, 2006, **36**, 354

[5] Gyulassy, A. *et al.*, *IEEE Trans. Vis. and Comp. Graph.*, 2006 **12**(4), 474

**MP247 Structure of PF04013 Member APC86534.1.** N.E.C. Duke<sup>a</sup>, M. Zhou<sup>b</sup>, M. Gu<sup>b</sup>, A. Joachimiak<sup>a,b</sup>, <sup>a</sup>Structural Biology Center, <sup>b</sup>Midwest Center for Structural Genomics, Biosciences Div., Argonne National Lab., Argonne IL.

PF04013 (DUF358, BIG\_123.1) composes a family of proteins which are members of the "alpha/beta knot superfamily", but which are of unknown function. Usually approximately 200 residues in length, no representative structure has previously been available for this family. APC86534.1, from *Archaeoglobus fulgidus*, is a 194 residue protein belonging to this Pfam. The structure reveals a knot, as well as clear electron density for a bound small-molecule moiety. The crystal structure will be compared to other, closely related proteins, highlighting similarities and differences between these protein structures.

This work was supported by the U.S. Department of Energy, Office of Biological and Environmental Research and Office of Basic Energy Sciences, under Contract W-31-109-ENG-38.

**SP248 Crystal Structure of a Phenylacetic Acid Degradation Protein from *R. eutropha* JMP134 at 2.2Å Resolution.** D. Das, Q. Xu, M. Miller, A. Deacon, The Joint Center for Structural Genomics, Stanford Synchrotron Radiation Lab., Menlo Park, CA.

Aromatic compound catabolism via the phenylacetate pathway is mediated by a gene cluster and is used as an energy source by a wide variety of microbes. For example, in *E. coli*, a 14 gene cluster comprised of *paalABCDEFGHIJKXYZ* is involved in this process. The functions and substrates of many of the proteins encoded by these genes remain largely unknown.

The *R. eutropha* JMP134 gene gi73538604 encodes a 140 amino acid protein with the annotation of phenylacetic acid degradation related protein of the thioesterase superfamily. However, there are no crystal structures of this protein or any of its close sequence homologs. *R. eutropha* plays an important role in bioremediation<sup>1</sup>, which includes this pathway for the degradation of aromatic compounds. We present the crystal structure of this protein and explore its structural attributes.

The structure reveals that the protein possesses the classic "Hot Dog" thioesterase fold with a high structural similarity (despite the low sequence identity of ~25%) to the PaaI proteins from *E. coli* and *T. thermophilus*, whose structures have been recently solved. Three out of five catalytic residues from the *E. coli* PaaI structure<sup>2</sup> are identical in this protein. This opens up the possibility of further structure-based biochemical studies of this protein involved in breakdown of aromatic pollutants and may provide an avenue for the exploitation of this functionality in microbial bioremediation.

[1] Pohlmann A, *et al.* Genome sequence of the bioplastic-producing "Knallgas" bacterium *Ralstonia eutropha* H16. *Nat Biotechnol.* 2006, **24**(10):1257-62.

[2] Song F, *et al.* Structure, function, and mechanism of the phenylacetate pathway hot dog-fold thioesterase PaaI. *J Biol Chem.* 2006, **281**(16):11028-38.

The JCSG is funded by the Protein Structure Initiative of the National Institutes of Health, National Institute of General Medical Sciences. SSRL operations is funded by DOE BES, and the SSRL Structural Molecular Biology program by DOE BER, NIH NCRR BTP and NIH NIGMS.

**TP249 PriB-ssDNA Structure and Suggests a Novel Single-stranded DNA Binding Mode.** C.-D. Hsiao, C.-Y. Huang, C.-H. Hsu, Y.J. Sun, H.N. Wu, Inst. of Molecular Biology, Academia Sinica, Taipei, Taiwan, ROC.

PriB is one of the *E. coli* pre-primosome proteins which is required for assembly of the primosome, the multisubunit protein complex involved in the initiation of DNA replication of bacteriophage  $\phi$ X174.

Recent studies suggest that the  $\phi$ X174-type primosome is involved not only in DNA replication but also in recombination and repair when encountering DNA damage. Prior to the present study, little is known about the quantitative aspects such as stoichiometry of the PriB-ssDNA complex, cooperativity of the binding process, and the binding modes of PriB. In this study, we report the crystal structure of PriB in complex with 15-mer oligodeoxythymidylate (dT15) at 2.7 Å resolution (Huang *et al.*). In the PriB-dT15 complex crystal, the PriB dimers form a long chain along the ssDNA. This arrangement of PriB-ssDNA complex is consistent with the morphology observed by electron microscopy. This ssDNA binding mode of PriB is significantly differs from *E. coli* single-stranded DNA-binding protein (*EcoSSB*). Therefore, the structure present here may provide a novel implication for possible roles of PriB in *E. coli* DNA replication.

Huang, C.-Y., Hsu, C.-H., Sun, Y.-J., Wu, H.-N., Hsiao, C.-D., *Nucleic Acids Res.* **34**, 3878 (2006)

### MP250 Small Angle Scattering Studies of LacI Repressor.

Marc Taraban<sup>1</sup>, Hongli Zhan<sup>2</sup>, Kathleen Matthews<sup>2</sup>, Liskin Swint-Kruse<sup>3</sup>, Jill Trehwella<sup>1,4</sup> <sup>1</sup>Univ. of Utah, Salt Lake City, UT, <sup>2</sup>Rice Univ., Houston, TX, <sup>3</sup>The Univ. of Kansas Medical Center, Kansas City, KS, <sup>4</sup>Univ. of Sydney, Sydney, Australia.

Small-angle X-ray scattering (SAXS) gives information on shape and size of macromolecules in solution. It is particularly powerful for characterization of domain and subunit organization within the supramolecular structures formed when proteins and polynucleotides associate. The gene regulatory protein LacI repressor is a dimer of homodimers in the crystal structure of its complex with DNA. LacI-DNA interactions are regulated allosterically by the binding of small effector molecules to LacI. We have carried out SAXS experiments on LacI repressor, and on various LacI mutants. A deletion mutant of LacI in which the first 11 residues of the wild type are deleted is shown to exist as a tetramer in solution, but the association is a distinctive end-to-end association of two homodimers, rather than the side-by-side association of homodimers that is observed in wild type crystal structure. Our studies also include examination of LacI mutants that are predominately homodimers in solution, their complexes with DNA, and the effects of the binding of effector molecules.

### TP251 Caffeine Co-crystals Composed of Two Supramolecular Heterosynthons.

Dejan-Krešimir Bučar, Rodger F. Henry, Xiaochun Lou, Richard W. Duerst, Thomas B. Borchardt, Leonard R. MacGillivray, Geoff G.Z. Zhang, Global Pharmaceutical R&D, Abbott Labs., North Chicago, IL, Dept. of Chemistry, Univ. of Iowa, Iowa City, IA.

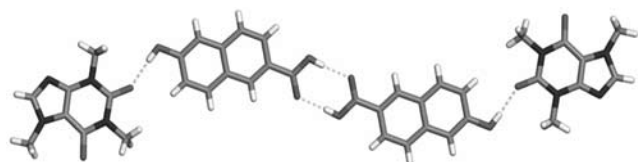
Pharmaceutical co-crystals are emerging as useful means to improve properties of pharmaceutical agents. Caffeine, a pharmaceutical model compound, generally forms molecular complexes with carboxylic acids in which the carboxylic acid group interacts with the N-atom of the caffeine imidazole ring *via* an O-H...N hydrogen bond. To examine the possibility of introducing new synthons to the caffeine-carboxylic acid system, a group of carboxylic acids with an additional hydrogen-bond donating functional group (*i.e.* hydroxy group) along their periphery was screened for cocrystal formation with caffeine. A new screening method was utilized, based on thermodynamically driven solution-mediated phase transforma-

tion. Structural analysis of the co-crystals thus identified revealed the presence of cocrystals composed of two caffeine-carboxylic acid heterosynthons. Additionally, an unusual case in which a carboxylic acid dimer forms in the presence of a heterosynthon was observed.

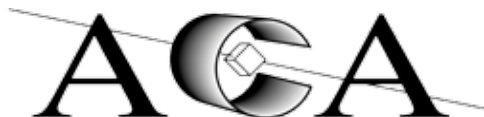
### SP252 Crystal Structures of Murine Thrombin in Complex with the Extracellular Fragment of Murine PAR<sub>3</sub> and PAR<sub>4</sub>.

Alaji Bah, Zhiwei Chen, Leslie A. Bush-Pelc, F. Scott Mathews, Enrico Di Cera, Dept. of Biochemistry and Molecular Biophysics, Washington Univ. School of Medicine, St. Louis, MO.

It has been suggested that the cleaved form of PAR<sub>3</sub> acts as a cofactor for thrombin cleavage and activation of PAR<sub>4</sub> on murine platelets. X-ray crystal structures of murine thrombin bound to extracellular fragments of the murine receptors PAR<sub>3</sub> (<sup>38</sup>SFNG-GPQNTFEEFPLSDIE<sup>56</sup>) and PAR<sub>4</sub> (<sup>51</sup>KSSDKPNPR↓GYPGKFCANDSDTLELPASSQA<sup>81</sup>, ↓=site of cleavage) have been solved at 2.0 and 3.5 Å resolution, respectively. The cleaved form of PAR<sub>3</sub>, traced in the electron density maps from Gln-44 to Glu-56, makes extensive hydrophobic and electrostatic contacts with exosite I of thrombin via the fragment <sup>47</sup>FEEFPLSDIE<sup>56</sup>. Occupancy of exosite I by PAR<sub>3</sub> allosterically changes the conformation of the 60-loop and shifts the position of Trp-60d ~10 Å with a resulting widening of the access to the active site. The PAR<sub>4</sub> fragment, traced entirely in the electron density maps except for five C-terminal residues, clamps Trp-60d, Tyr-60a and the aryl binding site of thrombin with Pro-56 and Pro-58 at the P2 and P4 positions and engages the primary specificity pocket with Arg-59. The fragment then leaves the active site with Gly-60 and folds in a short helical turn from Pro-62 to Cys-66 that redirects the backbone away from exosite I and over the autolysis loop. The structures demonstrate that thrombin activation of PAR<sub>4</sub> may occur with exosite I available to bind cofactor molecules, like the cleaved form of PAR<sub>3</sub>, that allosterically enhance accessibility of the active site.







---

## Program

Chair: Jill Trehwella

Committee: Robert Bau  
Alicia Beatty  
Simon Billinge  
Bryan Chakoumakos  
Aina Cohen  
Lachlan Cranswick  
Anna Gardberg  
James Holton  
Robert Huether

Katherine Kantardjieff  
Charles Kissinger  
Jeanette Krause  
Paul Langan  
David Londono  
Peter Müller  
Bruce Noll  
Craig Ogata  
Allen Oliver

Joseph Orgel  
Thomas Proffen  
Claudia Rawn  
William Royer  
Robert Scavetta  
Gerald Stubbs  
Ian Swainson  
Volker Urban  
Xiaoping Wang

## Local

Chairs:  
Chris Hill  
Heidi Schubert

---

## Meeting Sponsors

ActiveSight  
American Chemical Society-PRF  
Anton Paar USA  
Area Detector Systems Corp.  
Array BioPharma, Inc.  
Art Robbins Instruments  
AstraZeneca AB  
Axygen Biosciences  
BioCryst Pharmaceuticals, Inc.  
Boehringer Ingelheim Pharmaceuticals  
Bristol-Myers Squibb Pharmaceutical  
Research Institute

Bruker AXS  
Cambridge Crystallographic Data Centre  
Cell Press  
Charles Supper Company  
CrystEngComm  
Eli Lilly & Co.  
Genentech  
Hampton Research  
Hindawi Publishing Corporation  
Hoffmann-La Roche Inc.

International Centre for Diffraction Data  
International Union of Crystallography  
Matthews, David and Carolyn  
Merck Research Laboratories  
Oxford University Press  
Pfizer, Inc.  
Rigaku Americas Corp.  
SSCI, An Aptuit Company  
TransForm Pharmaceuticals  
Wyatt Technology  
Wyeth Research

---

## Exhibitors

Area Detector Systems Corp.  
Art Robbins Instruments  
Axygen Biosciences  
Blake Industries, Inc.  
Brandel, Inc.  
Bruker AXS  
Cambridge Crystallographic Data Centre  
CCP4  
CRYO Industries of America  
CyBio US, Inc.  
Douglas Instruments Ltd.  
Emerald Biosystems  
Fluidigm Corp.

Formulatrix, Inc.  
GE Healthcare  
Genomic Solutions  
Greiner Bio-One  
Hampton Research  
Incoatec GmbH  
International Centre for Diffraction Data  
International Union of Crystallography  
Jena Bioscience GmbH  
Korima, Inc.  
Mar USA  
Marresearch GmbH  
Micro Photonics/STOE

Mitegen, LLC  
Oak Ridge National Laboratory  
Oxford Cryosystems, Inc.  
Oxford Diffraction Ltd.  
QIAGEN, Inc.  
RCSB Protein Data Bank  
Rigaku Americas Corp.  
Southeast Regional Collaborative  
Access Team  
Thermo Fisher Scientific  
TTP LabTech Ltd.  
Wyatt Technology  
XENOCs

---

## Corporate Members

ActiveSight  
Area Detector Systems Corp.  
Art Robbins Instruments  
ATPS, Inc.  
Axxora, LLC  
Axygen Biosciences  
Bibliothek Technische Hochschule  
Blake Industries, Inc.  
Bruker AXS  
Cambridge Crystallographic Data Centre  
Charles Supper Company  
Corning, Inc.  
CRYO Industries of America, Inc.

Crystal Logic, Inc.  
CyBio US, Inc.  
Douglas Instruments Ltd.  
Emerald Biosystems  
Fluidigm Corp.  
Genomic Solutions  
Hampton Research  
Jena Bioscience GmbH  
Korima, Inc.  
Malvern Instruments  
Mar USA  
MARRResearch GmbH  
Mitegen, LLC  
Molecular Dimensions Inc

Neuro Probe, Inc.  
Oxford Cryosystems, Inc.  
Oxford Diffraction Ltd.  
RCSB Protein Data Bank  
Rigaku Americas Corp. Select  
Biosciences Ltd.  
Taylor & Francis  
Thermo Fischer Scientific  
Tri Tek, Corp.  
UOV/Biblioteca Universitaria  
Viscotek Corp.  
Wyatt Technology  
Xenocs SA

# Saturday, July 21

Meeting Registration Desk .....7:30a -7:30pm ..... North Lobby

Opening Reception & Exhibit Show.....7:30p -10:30pm ..... Exhibit Hall 2/3  
(name tag required for entry)

## WK.01 SHELX

Peter Müller, Presiding

255B

09:00-09:35 WK.01.01  
Introduction to SHELXL Refinement: Restraints, Constraints and Esds. George M. Sheldrick.

09:35-10:10 WK.01.02  
Refinement of Disorder with SHELXL. Peter Müller.

10:10-10:45 WK.01.03  
Twinning. R. Herbst-Irmer.

10:45-11:15 Coffee Break.

11:15-11:55 WK.01.04  
Protein Refinement at Atomic Resolution. Thomas Schneider.

11:55-12:10 WK.01.05  
SHELXPRO. George Sheldrick.

12:10-12:35 WK.01.06  
Preparing CIFs for Publication. Useful Programs and Common Errors. Ilia A. Guzei.

12:35-01:00 WK.01.07  
Crystal Structure Validation with PLATON. A.L. Spek.

01:00-02:00 Lunch Break.

02:00-02:35 WK.01.08  
SHELXD for Large Small Molecules and SHELXC/D for Macromolecular Substructures. George M. Sheldrick.

02:35-03:10 WK.01.09  
HKL2MAP. Thomas Schneider.

03:10-03:45 WK.01.10  
Practical Aspects of SAD and MAD. Judit E. Debreczeni.

03:45-04:15 Coffee Break.

04:15-05:00 WK.01.11  
SHELXE: From Substructure to Structure. George M. Sheldrick.

05:00-05:30 WK.01.12  
Coot for SHELXL Users. Paul Emsley.

05:30-06:00 Panel Discussion on the Future of Software for Crystal Structure Determination. Peter Müller.

## WK.02 Standards for Publication of Macromolecular NMR Structures

Howard Einspahr, Presiding

255C

08:00-08:30 WK.02.01  
Introduction. The Purpose of Publication Standards. Howard Einspahr.

08:30-09:00 WK.02.02  
The NMR Task Force of the World-wide PDB. Robert Kaptein.

09:00-09:30 WK.02.03  
BioMagResBank (BMRB) Data Deposition and Entry Annotation Requirements. Eldon Ulrich, Jurgen Dorelejers, Jundong Lin, Steve Mading, Dimitri Maziuk, Christopher Schulte, David Tolmie, Hongyang Yao, John Markley.

09:30-10:00 WK.02.04  
Standards for Crystallographic Publishing. Manfred Weiss.

10:00-10:30 Coffee Break.

10:30-11:00 WK.02.05  
Evaluating Protein Structures Determined by Structural Genomics Consortia. Gaetano T. Montelione, Aneerban Bhattacharya, Roberto Tejero.

11:00-12:00 Discussions and Breakout Assignments.

12:00-01:00 Lunch Break.

01:00-02:45 Breakouts: Discussions and Drafting Recommendations.

02:45-03:15 Coffee Break.

03:15-05:00 Presentations of Draft Recommendations and Discussions.

Opening Ceremony and Welcome Sunday, July 22

8:00am

Room 255B

A. Alan Pinkerton, ACA President Presiding

Meeting Registration Desk..... 7:30am-5:30pm.....North Lobby	Fluidigm Luncheon..... 12:00pm .....TBA
Speaker Ready Room ..... 7:30am-5:30pm.....260	General Interest Meeting ..... 5:00pm.....255B
Council Meeting Room..... 7:30am-5:30pm.....257	Fiber Diffraction SIG Meeting ..... 5:00pm.....255F
Opening Ceremony..... 8:00am.....255B	Poster Session I ..... 5:30-7:30pm .....Exhibit Hall 2/3
Exhibit Show..... 10:00am-7:30pm.....Exhibit Hall 2/3	

**01.01 New Structures**

*Acknowledgement is made to Hampton Research & Wyatt Technology for partial support of this session.*

**C. Correll, 255B**  
**J. Horton, Presiding**

08:30-09:00 01.01.01  
Structure of a Eukaryotic Repressor:mRNA Complex: IRP1:IRE Ferritin H. Karl Volz, Anna Selezneva, Elizabeth Theil, William Walden.

09:00-09:20 01.01.02  
The Crystal Structure of Cytochrome P460 of *Nitrosomonas europaea* Reveals a Novel Cytochrome Fold and Heme-protein Cross-link. Carrie Wilmot, Arwen Pearson, Bradley Elmore, Cheng Yang, Joseph Ferrara, Alan Hooper.

09:20-09:50 01.01.03  
The Structural Basis for Ribozyme-Catalyzed RNA Assembly and its Implications for a Pre-Biotic RNA World. William Scott, Michael Robertson.

09:50-10:10 01.01.04  
The Structure of the TraI C-terminal Domain Reveals a Novel Fold: Implications for Assembly of the Multi-protein Relaxosome Conjugative DNA Transfer Complex. Laura Guogas, Matthew Redinbo.

10:10-10:30 Coffee Break.

10:30-11:00 01.01.05  
Crystal Structure of Rhomboid Intramembrane Protease GlpG. Ya Ha, Yongcheng Wang, Yingjiu Zhang.

11:00-11:20 01.01.06  
Mechanistic Insights into Flavoenzyme Oxidases from Structures of Trapped Reaction Intermediates. Allen Orville, Annie Hèroux, George Lountos, Paul Fitzpatrick, Fan Fan, Giovanni Gadda, Rajeev Prabhakar, Djamaladdin Musaev, Keiji Morokuma.

11:20-11:50 01.01.07  
Recognition and Catalysis of Ribosomal Protein L11 by the Protein Trimethyltransferase PrmA. Gerwald Jogl, Steven T. Gregory, Albert E. Dahlberg, Hasan Demirci.

11:50-12:10 01.01.08  
Structure of Mammalian DNA Methyltransferase Dnmt3a Catalytic Domain in Complex with its Regulator DNMT3L. Da Jia, Xiaodong Cheng.

**05.01 Non-Ambient Crystallography**  
**A. Payzant, Presiding 255C**

08:30-09:00 05.01.01  
*In-situ* Diffraction Study of the High Temperature Behavior of Ni-Al-Pt-Hf Alloys.

Scott Speakman, Sumer Singh, Linn Hobbs, Anthony Garratt-Reed, Liza Plotnikov, Bruce Pint.

09:00-09:30 05.01.02  
*In situ* Simultaneous Raman and High-Resolution X-ray Powder Diffraction Study of Transformations Occurring in Materials at Non-Ambient Conditions. Davide Viterbo, E. Boccaleri, M. Milanese, F. Carniato, G. Croce, W. van Beek, H. Emerich.

09:30-10:00 05.01.03  
Photocrystallography: Application to the Phase Transitions Occuring in Magnetic Molecular Materials: Domain Formation and Electron Density Studies. Claude Lecomte, Sébastien Pillet, William Nicolazzi.

10:00-10:30 Coffee Break.

10:30-11:00 05.01.04  
Thermally Induced Disorder of Cu Ions in [(C<sub>6</sub>H<sub>5</sub>)<sub>3</sub>CH<sub>3</sub>P]Cu<sub>3</sub>Br<sub>4</sub>. Roger Willett, Salim Haddad, Brendan Twamley.

11:00-11:30 05.01.05  
Variable Temperature Neutron and X-ray Diffraction Studies of the A<sup>2+</sup>A<sup>2+</sup>W<sub>3</sub>O<sub>12</sub> Family. Amy Gindhart, Cora Lind.

11:30-12:00 05.01.06  
Small Molecule Laue Diffraction for Time Resolved Experiments. Milan Gembicky, Mateusz Pitak, Marc Messerschmidt, Philip Coppens, Shin-Ichi Adachi, Shin-Ya Koshihara.

**10.01 Important Science from Small Molecule Structures**  
**A. Oliver, Presiding 255E**

*In Memory of F. Albert Cotton*

08:30-08:50 10.01.01  
New Building Blocks for the Construction and Deconstruction of Ternary Supermolecules. Michelle Smith, Christer Aakeroy, John Desper.

08:50-09:10 10.01.02  
Snapshots of a Solid State Reaction: Photolysis of Coordinated Azide in Chromium(III) Complexes. Marilyn Olmstead, Lauren Bria.

09:10-09:30 10.01.03  
Porphyrin-Based Framework Coordination Polymers Tailored with Lanthanide Bridging Reagents. Israel Goldberg, Sophia Lipstman, Sumod George, Sankar Muniappan.

09:30-10:00 10.01.04  
High Throughput Single Crystal Neutron Diffraction - New Opportunities in Molecular Structure. Chick Wilson.

10:00-10:30 Coffee Break.

10:30-11:00 10.01.05  
The Combined use of X-ray Diffraction, Neutron Scattering and (PGSE) NMR Measurements in Coordination Chemistry. Alberto Albinati.

11:00-11:20 10.01.06  
Structure Determination and Glass Transition Behaviour of Cyclohexene. R.M. Ibberson, M.T.F. Telling, S. Parsons.

11:20-11:40 10.01.07  
The Role of Protonated Water Aggregates (H<sub>2n+1</sub>,On)<sup>+</sup> in the World of Crystalline Hy-peracid Salts. Michael Galella, Jack Gougoutas, John DiMarco, Mary Malley.

11:40-12:00 10.01.08  
Problem Structures: Attempts to Rationalize their Description and Refinement. A. David Rae.

*Session continues at 01:30.*

**13.01 Advances in Data Collection**  
**S. Ginell, 255F**  
**A. Cohen, Presiding**

08:30-09:10 13.01.01  
Tackling Large Proteins: Lessons Learned from a Decade of RNA Polymerase II Crystallography. David Bushnell, Roger Kornberg, Dong Wang, Guillermo Calero, Henrik Spahr, Ken Westover.

09:10-09:40 13.01.02  
Data Collection Strategies for Ultra-high Resolution X-rays at 15K and Neutron Diffraction at 293K: The Fully Deuterated h-Adose Reductase Case. Andre Mitschler, S. Ginell, A. Joachimiak, M. Blakeley, F. Meilleur, I. Hazemann, D. Myles, A. Podjarny.

09:40-10:10 13.01.03  
Breakthrough in Amyloid-like Segment Structure Determination by using ESRF Microfocus Beamline. Magdalena Ivanova. M. Sawaya, S. Sambashivan, R. Nelson, S. Sievers, M. Apostol, M. Thompson, M. Balbirnie, J. Wiltzius, H. McFarlane, A. Madson, C. Riek, D. Eisenberg.

10:10-10:30 Coffee Break.

10:30-11:00 13.01.04  
Phasing Macromolecular Structures with UV-induced Structural Changes. Max Nanao, Raimond Ravelli.

11:00-11:30 13.01.05  
Optimizing the Success Rate of Structure Determination. James M. Holton, George Meigs.

11:30-12:00 13.01.06  
High Pressure Cryocooling for Capillary Sample Cryoprotection and Diffraction Phasing at Long Wavelengths. Chae Un Kim, Quan Hao, Sol M. Gruner.

**SP.01 Undergraduate****Research Showcase****K. Kantardjieff, Presiding****255B**01:30-01:35 Opening Remarks.  
Katherine Kantardjieff.01:35-02:05 SP.01.01  
Teaching Crystallography to Undergraduates Through Distance Learning and Remote Access. K.A. Kantardjieff, A.R. Johnson, X. Ouyang.02:05-02:35 SP.01.02  
Passing the Torch: The Challenge of Teaching Biologists Protein Crystallography in an Increasingly Automated Environment. Gary D. Brayer.02:35-03:05 SP.01.03  
Comparison of Crystal Structures of the Tetramethylammonium and Sodium Salts of 3-Nitrophenolate. Stephanie E. Bettis, Kenneth L. Martin, Edwin D. Stevens.

03:05-03:30 Coffee Break.

03:30-04:00 SP.01.04  
Characterizing the Catalytic Boost Provided by an Alternative Anion in Human Pancreatic Alpha-Amylase. Leslie Williams, Robert Maurus, Anjuman Begum, Stephen Withers, Gary Brayer.04:00-04:30 SP.01.05  
Characterization of Anti-cooperative Substrate and Metal Cofactor Binding. Christa Panizales, Kimberly A. Stieglitz, Mary F. Roberts.04:30-05:00 SP.01.06  
ProMOL, Simplification and Increased Functionality of PyMOL. Brett Hanson, Charles Westin, Len Slate, Paul Craig.05:00 Closing Remarks.  
Katherine Kantardjieff.**01.02 Strategies for Crystallization Challenged Macromolecules****R. Judge,****255C****J. Newman, Presiding**01:30-02:00 01.02.01  
Fluorescence-detection Size Exclusion Chromatography for Pre-crystallization Screening of Integral Membrane Proteins. Toshimitsu Kawate, Jaysankar Jasti, Michael Rosconi, Paul Shaffer, Alexander Sobolevsky, Tanja Homrichhausen, Eric Gouaux.02:00-02:30 01.02.02  
Advances Towards the Design of a 'Universal' Nucleant for Protein Crystallization. Naomi Chayen.02:30-03:00 01.02.03  
Uroporphyrinogen Decarboxylase-substrate Complex - Coping with an Unusual, Oxygen-sensitive Substrate. Frank Whitby, John Phillips, Hector Bergonia, Christy Warby, James Kushner, Christopher Hill.

03:00-03:30 Coffee Break.

03:30-04:00 01.02.04  
Microfluidic Platforms for Membrane Protein Crystallization. Paul Kenis, Sarah Perry, Josh Tice, Griffin Roberts.04:00-04:30 01.02.05  
High-Throughput Crystallization Pipeline at the Center for Eukaryotic Structural Genomics. Craig Bingman, Cody Robson, Louise Meske, Xioakang Pan, Gary Wesenberg, Jason McCoy, Zsolt Zolnai, George Phillips.04:30-05:00 01.02.06  
Role of the Purification Tag in Crystal Lattice Interactions. Ludmilla Shuvalova, George Minasov, Ivan Vorontsov, Joseph Brunzelle, Wayne Anderson.**10.01 Important Science from Small Molecule Structures****L. Falvello,****255E****A. Oliver, Presiding***In Memory of F. Albert Cotton*01:30-01:50 10.01.09  
Crystal Structures of Seven Chalcones with Pharmacological Activity. Hamilton Napolitano, Ademir Camargo, Ivo Vencato, Carlito Lariucci, Wender Silva, Carlos Andrade.01:50-02:10 10.01.10  
Neutron Diffraction Characterization of Hydrogen in Transition Metal Complexes. Paula Piccoli, John Cowan, Arthur Schultz, Thomas Koetzle, Christina Hoffmann.02:10-02:40 10.01.11  
New Chemistry and New Magnets from Small-Molecule Structure. Joel Miller.02:40-03:00 10.01.16  
Finding Chiral Crystals in Racemic Mixtures - A Reflection on How to Get the Most from X-ray Crystallography in the Laboratory of Molecular Structure and Bonding at Texas A&M University. Xiaoping Wang.

03:00-03:30 Coffee Break.

03:30-03:50 10.01.12  
F. Albert Cotton (1930-2007) and the Development and use of Chemical Crystallography. Larry R. Falvello03:50-04:10 10.01.13  
Electronic Structure from Changes in Metal-Metal Bond Distances Using Variable Temperature Crystallography. Carlos Murillo.04:10-04:30 10.01.14  
Non-traditional Bonding Interactions via Experimental Charge Density. Lee Daniels, Stanley Cameron, Joseph Ferrara.04:30-05:00 10.01.15  
Small Molecule Crystallography - Way more than Structure Determination. Alan Pinkerton.**13.02 Detectors****T. Earnest,****255F****C. Nielsen, Presiding**01:30-02:00 13.02.01  
Recent Advances in X-ray Pixel Array Detectors. Mark Tate.02:00-02:30 13.02.02  
3DX: An X-ray Pixel Array Detector with Active Edges. Edwin Westbrook, Christopher Kenney, Albert Thompson, Sherwood Parker.02:30-03:00 13.02.03  
Diffraction Data Collection with Continuous Rotation Method using CMOS Flat Panel Detector. Masaki Yamamoto, Kazuya Hasegawa, Kunio Hirata.

03:00-03:30 Coffee Break.

03:30-04:00 13.02.04  
Obtaining Better Data from Existing CCD Detectors. Gerard Bricogne, Thomas Womack, Christopher Nielsen.

Rigaku Fun Run	7:00am	Memory Grove Park	Industrial SIG Meeting	5:00pm	255E
Meeting Registration Desk	7:30am-5:30pm	North Lobby	Small Molecule SIG Meeting	5:00pm	255C
Speaker Ready Room	7:30am-5:30pm	260	Neutron/Powder/Materials joint SIG	5:00pm	255B
Council Meeting Room	7:30am-5:30pm	257	Poster Session II	5:30-7:30pm	Exhibit Hall 2/3
Exhibit Show	10:00am-7:30pm	Exhibit Hall 2/3	MarUSA Event (tickets available at Mar booth)	7:30pm	
BioMac SIG Meeting	12:00pm	255C	Mentor/Mentee Dinner (ticket required)	8:00pm	Salt Lake City Brew Pub - Squatters
Bruker Luncheon (by invitation only)	12:00pm	Radisson Hotel			

**TR.01 TRANSACTIONS SYMPOSIUM Diffuse Scattering for the Masses: Local Structural Correlations in Molecular, Macromolecular and Inorganic Crystals**

*Acknowledgement is made to the Donors of the American Chemical Petroleum Research Fund for partial support of this session.*

**J. Britten, Presiding - Part 1 255B**

08:25-08:30 Opening Remarks.  
Branton Campbell.

08:30-09:05 TR.01.01  
Diffuse Scattering as a Probe of Nanoscale Structure and Function. T.R. Welberry, D.J. Goossens, A.G. Beasley, A.P. Heerdegen.

09:05-09:30 TR.01.02  
The Quest for Quantitative Three-Dimensional Defect Structures. Branton J. Campbell.

09:30-10:00 TR.01.03  
Interpreting Diffuse X-ray Scattering Patterns from Crystals of Macromolecules. George Phillips.

10:00-10:30 Coffee Break.

**G. Phillips, Presiding - Part II**

10:30-11:00 TR.01.04  
A Brief History of Variations in Regimented States of Living and Inanimate Matter Reflected in Reciprocal Space. Donald L.D. Caspar.

11:00-11:30 TR.01.05  
From Diffuse Features to Precise Motions: An MD Approach. Lars Meinhold, Jeremy C. Smith.

11:30-12:00 TR.01.06  
Crystallography without Crystals: Determining the Structure of Individual Biological Molecules. Abbas Ourmazd, Dilano Saldin, Valentin Shneerson.

*Session continues at 01:30.*

**01.03 Experimental Phasing with Longer Wavelength X-rays**

**M. Weiss, Presiding - Part I 255C**

08:30-09:00 01.03.01  
Progress Towards Routine Soft X-ray Structure Determination at UGA and SER-CAT. John Rose, John Ruble, John Chrzas, John Gonczy, James Swindell II, Lirong Chen, James Fait, Zheng-Uing Fu, Zhongmin Jin, Bi-Cheng Wang.

09:00-09:20 01.03.02  
On the use of a New Crystal Mounting

Method for the Longer X-ray S-SAD Phasing. Nobuhisa Watanabe.

09:20-09:40 01.03.03  
Determination of a Protein's Anomalous Scattering Substructure using Longer X-ray Wavelengths. Christoph Mueller-Dieckmann, Santosh Panjikar, Paul A. Tucker, M. S. Weiss.

09:40-10:00 01.03.04  
Taking the Edge Off: The Softer Side of In-house SAD Phasing. Cheng Yang, James W. Pflugrath, Joseph D. Ferrara.

10:00-10:30 Coffee Break.

**B.C. Wang, Presiding - Part II**

10:30-11:00 01.03.05  
Is Long Wavelength More Damaging? Zbigniew Dauter.

11:00-11:20 01.03.06  
New Computational Algorithms for Density Modification. George M. Sheldrick.

11:20-11:40 01.03.07  
A Sulfur SAD Story: Effects of Resolution Cutoffs and Data Quality on Successful Phasing. Ganapathy Sarma, P. Andrew Karplus.

11:40-12:00 01.03.08  
Practical Aspects of Sulfur Phasing using Chromium Anodes. Aiping Dong.

**04.01 Impact of Crystallography in Industry**

**R. Bott, Presiding 255E**

08:30-08:50 04.01.01  
Impact of Structure-based Drug Design on the Development of a Selective Chk1 Inhibitor for the Treatment of Cancer. Ping Chen.

08:50-09:10 04.01.02  
Fragment Screening and Structure-guided Fragment Optimisation. John Barker.

09:10-09:30 04.01.03  
Fragments of Life™ (FOL) for Lead Identification and Optimization. Doug Davies, L. Stewart, B. Mamat, J. Singh, R. Mishra, B. Pease, D. Connor, H. Kim, A. Burgin, M. Gurney, V. Sandanayaka, E. Hanse, J. Wingler, T. Anreso, D. Zembower.

09:30-09:50 04.01.04  
The Benefits of Protein Crystallography to Monsanto's Ag Biotech R&D. Timothy Rydel.

09:50-10:10 04.01.05  
The Importance of Single Crystal Studies

of Process Relevant Pharmaceutical Crystal Forms. John DiMarco, Jack Gougoutas, Raymond Scaringe, Michael Galella, Carolyn Pommier.

10:10-10:30 Coffee Break.

10:30-10:50 04.01.06  
From Images to Co-crystal Structures in a Single Automated Process. John Badger, Paul Collins, Robin Rosenfeld, Bradley Smith, Russ Athay, Duncan McRee.

10:50-11:10 04.01.07  
The Value of Tertiary Structure in Intellectual Property. Richard Bott, K. MacKnight.

11:10-11:30 04.01.08  
Industrial Macromolecular Crystallography in the 21st Century: One Technique, Multiple Roles. Giovanna Scapin.

11:30-12:00 Round Table Discussion.

**13.03 Biomacromolecular Assemblies and Biomembranes**

**W. Heller, T. Weiss, Presiding 255F**

08:20-08:45 13.03.01  
Biological Relevance of Protein Structures, Assemblies and Conformational Mobility Probed with Solution X-ray Scattering. J.G. Grossmann, A. Large, P. Lund, J. Viney, N. Hunter, A. Gutierrez, G. Roberts.

08:45-09:10 13.03.02  
Signal Transduction and Transcription Activation by Bacterial Enhancer Binding Proteins. B. Tracy Nixon, B. Chen, M. Doucleff, S. De Carlo, H. Huang, D. Wemmer, E. Nogales, T. Hoover, E. Kondrashkina, L. Guo.

09:10-09:35 13.03.03  
Membrane Protein-Detergent Interactions and Protein-Detergent Complex Structure Studied by Small-Angle X-ray Scattering. Jan Lipfert, Linda Columbus, Scott A. Lesley, Sebastian Doniach.

09:35-10:00 13.03.04  
Monitoring Structural Ordering in Two-dimensional Assemblies of Proteins and Viruses. Lin Yang, Masafumi Fukuto, S. Wang.

10:00-10:30 Coffee Break.

10:30-10:55 13.03.05  
Structure Modeling of Intrinsically Disordered Proteins using SANS and Computational Methods. Susan Krueger, J. Curtis.

*session continues on next page*

10:55-11:20 13.03.06  
Small-angle X-ray Scattering and Neutron Contrast Variation Reveal the Arrangement of Synaptic Proteins Implicated in Autism. Jill Trehwella, Davide Comoletti, Alexander Grishaev, Andrew Whitten, Igor Tsigelny, Palmer Taylor.

11:20-11:45 13.03.07  
Neutrons in Biology: SAS Solutions in Protein Structural Analysis. Joanna Krueger, (fnu) Ashish.

11:45-12:10 13.03.08  
The Center for Structural Molecular Biology (CSMB) at Oak Ridge National Laboratory. William Heller, Gary Lynn, Aravinda Raghavan, Volker Urban, Kevin Weiss, Yiming Mo, Dean Myles.

**TR.01 TRANSACTIONS  
SYMPOSIUM Diffuse Scattering  
for the Masses: Local Structural  
Correlations in Molecular, Macromolecular and Inorganic Crystals**  
**B. Campbell, Presiding, Part I 255B**

01:30-02:05 TR.01.07  
Disorder Diffuse Scattering - from Elementary to Exotic. Friedrich Frey.

02:05-02:30 TR.01.08  
Probing Nanoscale Correlations in Crystal-line Materials using Single Crystal Diffuse Scattering. Stephan Rosenkranz.

02:30-03:00 TR.01.09  
Local Structures from Powders: Recent Advances in Atomic Pair Distribution Function Methods and Modeling. Simon Billinge.

03:00-03:30 Coffee Break.  
**T. Proffen, Presiding - Part II**

03:30-04:00 TR.01.10  
Explorations of Reciprocal Space - Routine Observations of Diffuse Scattering. Jim Britten, Weiguang Guan.

04:00-04:30 TR.01.11  
X-ray Diffuse Scattering. Ross Angel, Carla Slebodnick, Jing Zhao, Boriana Mihailova, Ulli Bismayer, G. Diego Gatta, Tiziana Boffa-Ballaran, Leigh Rees, Steve Jacobsen.

04:30-05:00 TR.01.12  
Liquid Crystal Elastomers: Display and Analyses of Diffuse, 3D X-ray Scattering. John Konnert, J. Deschamps, C. Spillmann, J. Naciri, B. Ratna.

**10.02 Tricks of the Trade: Interpretation of Structural Results**  
**P. Piccoli, Presiding 255C**

01:30-02:00 10.02.01  
Is Small Molecule Crystallography Still Science? Phillip Fanwick.

02:00-02:30 10.02.02  
On the Correct Use of Incorrect Space Groups and Unit Cells. Larry R. Falvello.

02:30-03:00 10.02.03  
Multiple Component Twins: The Challenges of the Refinement of Problematic Data. Victor Young.

03:00-03:30 Coffee Break.

03:30-04:00 10.02.04  
PLATON, A Set of Tools for the Interpretation of Structural Results. Anthony Spek.

04:00-04:20 10.02.05  
Elucidation of Disorder in a Crystal Structure. Xiaoping Wang.

04:20-04:40 10.02.06  
Guest-induced Changes in Long-range and Local Order in Crystals of p-tert-butylcalix[4]arene. Gary Enright, Darren Brouwer, Igor Moudrakovski, Konstantin Udachin, John Ripmeester.

04:40-05:00 10.02.07  
Optimal use of Measured Data to Determine the Absolute Configuration of Pharmaceutically Interesting Molecules. Rob Hooft, Leo Straver, Anthony Spek.

**13.05 Structural Mechanisms of Infectious Diseases**

*Acknowledgement is made to ActiveSight, Area Detector Systems, Corp., David & Carolyn Matthews, and BioCryst Pharmaceuticals, Inc., for partial support of this session.*

**T. Jardetzky, 255E  
D. Matthews, Presiding**

01:30-02:00 13.05.01  
The Structural Basis of Translation Initiation by a Viral Internal Ribosome Entry Site RNA. Jeffrey Kieft, David Costantino, Amanda Keel, Jennifer Pfingsten.

02:00-02:30 13.05.02  
The Influenza Virus Nucleoprotein. Yizhi Jane Tao, Qiaozhen Ye, Robert Krug.

02:30-03:00 13.05.03  
Negative Strand RNA Virus Nucleocapsid Structure and Function. Winfried Weissenhorn, A. Albertini, A. Wernimont, T. Muziol, R. Ravelli, B. Hartlieb, S. Becker, G. Schoehn, R. Ruigrok.

03:00-03:30 Coffee Break.

03:30-04:00 13.05.04  
Structural Aspects of SNARE - Botulinum Neurotoxin Interactions. Axel T. Brunger, Mark Breidenbach, Rongsheng Jin, Thomas Binz, Andreas Rummel.

04:00-04:30 13.05.05  
Receptor Binding, Membrane Fusion and Virus Entry Mediated by the Paramyxovirus HN and F Proteins. Theodore Jardetzky,

Hsien-sheng Yin, Xiaolin Wen, Ping Yuan, Reay Paterson, Robert Lamb.

04:30-05:00 13.05.06  
HIV-1 Mechanisms for Evading Antibody-Mediated Neutralization. Peter Kwong, P. Acharya, L. Chen, L. Kong, Y.D. Kwon, S. Majeed, G. Ofek, M. Pancera, T. Zhou, A. Shah, J. Stuckey.

**13.07 Nanostructures**  
**K. Littrell, 255F  
J. Wang, Presiding**

01:30-02:00 13.07.01  
Structure and Dynamics of Nanocrystal Superlattices. Xiao-Min Lin.

02:00-02:20 13.07.02  
Surfactant Assisted Assembly of Nanocrystals. Youli Li, N. Belman, Y. Golan, J. Irwin, C.R. Safinya, J.N. Israelachvili.

02:20-02:40 13.07.03  
Strategy for Better Ordering of Polymer Phase in Diblock Copolymer Based Nanocomposites. Pappannan Thiyagarajan, Chieh-Tsung Lo, Byeongdu Lee, Nancy Dietz Rago, Randall Winans.

02:40-03:00 13.07.04  
Conformation of Oligo(ethylene glycol) Grafted Polystyrene in Aqueous Solutions. Gang Cheng, Yuri Melnichenko, George Wignall, Kunlun Hong, Fengjun Hua, Jimmy Mays.

03:00-03:30 Coffee Break.

03:30-04:00 13.07.05  
Calixarene-Encapsulated Nanoparticles: Self-Assembly into Functional Nanomaterials. Alexander Wei, B. Kim, S. Tripp, R. Balasubramanian, B. Decker, J. Mattay, R. Dunin-Borkowski, T. Kasama.

04:00-04:30 13.07.06  
New Methodologies for Formulation and Characterization of Polymer Nanocomposites. Marie Kissinger-Kane.

04:30-04:50 13.07.07  
*In-situ* Investigation of Nucleation and Grain Growth of Sol-gel Derived BiFeO<sub>3</sub> Thin Films. Tao Sun, Xuefa Li, Jin Wang, Vinayak Dravid.

04:50-05:10 13.07.08  
Local Atomic Structure of Gold Nanoparticles on Oxide Support. Wojtek Dmowski, Takeshi Egami, Sheng Dai, Steven Overbury.

05:10-05:30 13.07.09  
Magnetic Structure of Co/CoO Core-Shell Nanoparticles: Implications for Exchange Bias. Meigan Aronson, Sue Inderhees, Julie Borchers, K. Green, K. Sun, G. Strycker.

Meeting Registration Desk..... 7:30am-5:30pm .....North Lobby	IUCR Journals Committee Mtg..... 12:00pm ..... 259
Speaker Ready Room ..... 7:30am-5:30pm .....260	SAS SIG Meeting ..... 5:00pm ..... 255F
Council Meeting Room..... 7:30am-5:00pm .....257	Service SIG Meeting ..... 5:00pm ..... 255B
Exhibit Show ..... 10:00am-7:30pm .....Exhibit Hall 2/3	Poster Session III ..... 5:30-7:30pm..... Exhibit Hall 2/3
Synchrotron SIG Meeting ..... 12:15pm .....255E	Young Scientist SIG Mixer (ticket required).....8:00pm..... Salt Lake City
Canadian Division Meeting ..... 12:15pm .....255C	Public Library

**AW.01 Trueblood Award Symposium**

*Acknowledgement is made to AstraZeneca AB, Hoffmann-La Roche, Inc. and Cambridge Crystallographic Data Centre for partial support of this session.*

**C. Brock, Presiding - Part I 255B**

**Presentation of Award to Angelo Gavezzotti.** Alan Pinkerton, ACA President.

08:30-09:30 AW.01.01  
Forty Years of Struggle With Computers Over Crystallography and Intermolecular Interactions. A. Gavezzotti.

09:30-10:00 AW.01.02  
*Ab initio* Prediction of Crystal Structures - Blind Tests and Recent Applications. Graeme M. Day.

10:00-10:30 Coffee Break.

**J. Bernstein, Presiding - Part II**

10:30-11:00 AW.01.03  
Fluorine - Odd Man Out. Jack D. Dunitz

11:00-11:30 AW.01.04  
Thermodynamics of Molecular Crystals Under High Pressure from Quantum Chemistry: The Solid-Solid Phase Transitions of  $\text{Co}_2(\text{CO})_6(\text{XPh}_3)_2$  (X=P, As). Piero Macchi, Nicola Casati, Angelo Sironi.

11:30-12:00 AW.01.05  
Is There a Mechanism for Crystal Growth and Dissolution? J. Michael McBride, Joshua H. Baraban, Thomas J. Gniadek.

**01.04 New Membrane Protein Structures**

**H. Luecke, 255C**  
**B. Van Den Berg, Presiding**

08:30-09:00 01.04.01  
Cleaning Up the Mess: Transport of Xenobiotics Across the Bacterial Outer Membrane During Biodegradation. Bert van den Berg.

09:00-09:30 01.04.02  
Structure Determination of Colicin I Receptor Alone and in Complex with Colicin Ia: Transport of Large Proteins Across Bacterial Outer Membranes. Susan K. Buchanan, Petra Lukacik, Sylvestre Grizot, Rodolfo Ghirlando, Maruf Ali, Travis J. Barnard, Karen S. Jakes, Paul S. Kienker, Lothar Esser.

09:30-10:00 01.04.03  
A Mechanism of Phosphate Specific Transport Across the Outer Membrane of *Pseudomonas aeruginosa*: The Crystal Structure of OprP. Trevor Moraes, Manjeet Bains, Robert Hancock, Natalie Strynadka.

10:00-10:30 Coffee Break.

10:30-11:00 01.04.04  
Robert Stroud.

11:00-11:30 01.04.05  
The Crystal Structure of Human Very-long-chain acyl-CoA Dehydrogenase. Ryan McAndrew, Yudong Wang, Al-Walid A. Mohsen, Miao He, Jerry Vockley, Jung-Ja Kim.

**06.01 Neutron Macromolecular Crystallography**

**P. Langan, Presiding - Part I 255E**

08:30-08:35 Welcome.

08:35-09:15 06.01.01  
Neutron Structure of DFPase: Insights into the Phosphotriesterase Mechanism. Julian Chen, Marc-Michael Blum, Benno Schoenborn, Paul Langan.

09:15-09:40 06.01.02  
Joint X-ray and Neutron Study of Aldose Reductase: Observation of Enzymatic Proton Networks. Pavel Afonine, M. Blakeley, F. Ruiz, R. Cachau, I. Hazemann, F. Meilleur, A. Mitschler, S. Ginell, O. Ventura, A. Cousido, M. Haertlein, A. Joachimiak, D. Myles, P.D. Adams, A. Podjarny.

09:40-10:00 06.01.03  
Structural Studies of the Short Hydrogen Bonds in Photoactive Yellow Protein (PYP). Suzanne Fisher, S. Anderson, R. Henning, K. Moffat, P. Thiyagarajan, P. Langan, A. Schultz.

10:00-10:30 Coffee Break.

**P. Thiyagarajan, Presiding - Part II**

10:30-11:00 06.01.04  
A Neutron Crystallographic Analysis of a Cubic Insulin at pD 6.6 and Ribonuclease A. Nobuo Niimura.

11:00-11:20 06.01.05  
X-ray and Neutron Structure of Low pH, Polyamine-free, Z-DNA. Marat Mustykimov, Sean Seaver, Leif Hanson, Paul Langan, Leighton Coates.

11:20-11:40 06.01.06  
The Enzymatic Mechanism of Xylose Isomerase Revealed by Neutron Protein Crystallography. Flora Meilleur, Zhong Ren, Edward Snell, Mark van der Woerd, Russel Judge, Dean Myles.

11:40-12:00 06.01.07  
Joint Refinement of Neutron and Room Temperature X-ray Diffraction Data from Endothiapepsin. Leighton Coates, Paul Langan, Jon Cooper.

**13.06 Energy Storage and Conversion**

**J. Huot, Presiding 255F**

08:30-09:00 13.06.01  
Some Applications of INS and DFT in Hydrogen Containing Materials, Thermodynamics Study of the Structural and Dynamical Properties. Anibal Ramirez-Cuesta.

09:00-09:30 13.06.02  
Nanostructured and Catalysed  $\text{MgH}_2$  Powders for Fast Reactions. Nataliya Skryabina, Jean Charbonnier, Patricia de Rango, Daniel Fruchart, Gregory Girard, Salvatore Miraglia.

09:30-10:00 13.06.03  
Impact on the Crystallization Process of Shape Memory Alloys upon Hydrogen Insertion. Daniel Fruchart, Laurent Cagnon, Nataliya Skryabina, Aleksander Selyakov.

10:00-10:30 Coffee Break.

10:30-11:00 13.06.04  
Neutron Diffraction Study of the Dormant Form of a Catalyst for Ammonia Borane Dehydrogenation. Thomas F. Koetzle, D. Michael Heinekey, Paula M.B. Piccoli, Arthur J. Schultz.

11:00-11:30 13.06.05  
Synthesis and Structural Characterization of New Metal Hydrides and Borohydrides. Ewa Ronnebro.

11:30-12:00 13.06.06  
*In situ* Powder Diffraction Studies of Metal Hydrides for Hydrogen Storage. Yumiko Nakamura, Etsuo Akiba.

**AW.02 Fankuchen Award Symposium**

*Acknowledgement is made to SSCI, an Aptuit Company and Oxford University Press for partial support of this session.*

**C. Brock, Presiding - Part 1****255B**

**Presentation of Award to Frank H. Herbstein.** Alan Pinkerton, ACA President.

01:30-02:30 AW.02.01

What Can We Learn From the Multiple Crystal Structures Reported for Pentacene, and for the Anthracene and Tetracyanoquinodimethane (TCNQ) Molecules in Their Various Guises? Frank H. Herbstein, Moshe Kapon.

02:30-03:00 AW.02.02

Kinetic and Thermodynamic Crystals. Interactions and Close Packing. Gautam R. Desiraju.

03:00-03:30 Coffee Break.

**J. Bernstein, Presiding - Part II**

03:30-04:00 AW.02.03

Detailed Studies of the Low-Temperature Phase Transitions in  $[\text{Ni}(\text{H}_2\text{O})_6](\text{NO}_3)_2 \cdot (15\text{-crown-5}) \cdot n\text{H}_2\text{O}$ ,  $n = 1$  and 2. Carolyn P. Brock, Maxime A. Siegler, Sean Parkin.

04:00-04:30 AW.02.04

Phase Transitions, Polymorphism and Parametric Powder Diffraction. William David.

04:30-05:00 AW.02.05

Eligio Perucca First Observed Induced Optical Activity in 1919. Bart Kahr.

**01.05 Informatics in Structural Biology****K. Henrick,****255C****J. Westbrook, Presiding**

01:30-02:00 01.05.01

Detecting Register Shifts in Protein Structures and Recognising Ligand Conformations. Gerard J. Kleywegt, Marian Novotny, Mark Harris, Henrik Hanson, Helena Strombergsson.

02:00-02:30 01.05.02

Assessing the Impact of Structural Genomics. John-Marc Chandonia.

02:30-03:00 01.05.03

Validation of Ligand Geometries and Protein-Ligand Interactions by Automated Data Mining of Crystallographic Databases. Robin Taylor.

03:00-03:30 Coffee Break.

03:30-04:00 01.05.04

Identifying Protein Structural Domains: Progress, Challenges and Insights. Stella Veretnik, Timothy Holland, Ilya Shindyalov, Philip Bourne.

04:00-04:30 01.05.05

Anchor-Point Registration for Multi-Resolution Modeling of Biomolecular Assemblies. Stefan Birmanns, Willy Wriggers.

04:30-05:00 01.05.06

Mechanisms of Conformational Transitions in Cell Signaling Proteins. Matthew Young.

**12.01 FLYS - Fun Lectures for Young Scientists****B. Dillard,****255E****B. Huether, Presiding**

01:30-02:10

Vitamin C and Other Essentials for Being a Successful Scientist. Cora Lind.

02:10-02:35

5 Easy Steps for Structure Deposition. Jasmine Young.

02:35-03:00

Experiences in Crystallographic Research. Jenny Glusker.

03:00-03:30 Coffee Break.

03:30-03:50

Getting Your First Postdoc Position. Peter Horanyi.

03:50-04:30

From Industry to Academics: Evolution of a Structural Biologist. William Lanzilotta.

**13.04 Time and Field Dependent Responses in Scattering Experiments**

*Acknowledgement is made to Anton Paar USA for partial support of this session.*

**L. Porcard, C. Rawn****255F****V. Urban, Presiding**

01:30-02:00 13.04.01

Small Angle Neutron Scattering (SANS) Studies of the Vortex Lattice in Type II Superconductors. Charles Dewhurst, Robert Cubitt.

02:00-02:30 13.04.02

Quenched SANS for Studies of Polymer Relaxation. Wim Pyckhout-Hintzen, Louisa Dahbi, Dieter Richter, Ekkehard Straube.

02:30-03:00 13.04.03

Shear-Induced Disaggregation of Droplets in Attractive Nanoemulsions Probed by Rheo-SANS. T.G. Mason, J.N. Wilking, C. B. Chang, L. Porcar.

03:00-03:30 Coffee Break.

03:30-04:00 13.04.04

*In situ* Time-resolved X-ray Diffraction (TR-XRD) as a Tool for Characterizing Catalysts and Active Sites. Jonathan Hanson, Xianqin Wang, Wen Wen, Jose Rodriguez, Peter Chupas.

04:00-04:30 13.04.05

*In situ* X-ray Diffraction Studies of the Magnetic Field Induced Structural Transformations. Vitalij Pecharsky.

04:30-05:00 13.04.06

Time Resolved Neutron Diffraction Studies of Defect Structure formation in Lithium Imide during Hydrogenation and De-hydrogenation. Ashfia Huq, Luke Heroux, James W. Richardson, Evan R. Maxey, Mark S. Bailey, Dhanesh Chandra.

Meeting Registration Desk..... 7:30am-5:30pm..... North Lobby	Young Scientist SIG Meeting..... 12:15pm..... 255C
Speaker Ready Room ..... 7:30am-5:30pm..... 260	All Member Business Meeting..... 5:00pm..... 255A
Council Meeting Room..... 7:30am-5:30pm..... 257	<b>Awards Banquet</b> ..... Radisson
Exhibit Show..... 10:00am-1:30pm..... Exhibit Hall 2/3	Cash Bar 6:30pm Dinner 7:30pm (ticket required) Hotel

**Remove Posters before 1:30pm**

**01.06 Function from Structure**  
**S.-H. Kim, Presiding - Part I** **255C**

**Part I: Methods**

08:30-08:55 01.06.01  
 Functional Prediction of Proteins with Neither Sequence nor Structure Homologues of Known Function. Sung-Hou Kim, Jingtong Hou, Se-Ran Jun, Gregory Sims, In-Geol Choi.

08:55-09:20 01.06.02  
 Structure to Function from a Structural Genomics Perspective. James Watson, Roman Laskowski, Janet Thornton.

09:20-09:45 01.06.03  
 Functional Insights from the PSI-2 Funded NYSGXRC Activities. Stephen Burley, Steven Almo, Andras Fiser, Jeff Bonanno, S. Swaminthan, Andrej Sali, Mark Chance.

09:45-10:10 01.06.04  
 Functional Insights from Structure at the Joint Center for Structural Genomics. Ashley Deacon, Herbert Axelrod, Krishna Subramanian, Dana Weekes, Adam Godzik, Scott Lesley, Ian Wilson.

10:10-10:40 Coffee Break.

**O. Herzberg, Presiding - Part II**

**Part II: Examples**

10:40-11:05 01.06.05  
 Structure2Function of Prokaryotic and Eukaryotic Proteins. Osnat Herzberg, Gary Gilliland, John Orban, Andrew Howard, John Moulton.

11:05-11:30 01.06.06  
 Functional Assignments Through Structural Genomics and Bioinformatics. Farhad Frouhar, G. Liu, J. Cort, M. Kennedy, T. Acton, B. Rost, T. Szyperski, J. Hunt, L. Tong, G. Montelione, M. Abashidze, J. Seetharaman, R. Xiao, J. Liu, Y. Chen.

11:30-11:55 01.06.07  
 The Utility of Protein Surfaces for Functional Site Annotation. T. Andrew Binkowski, Andrzej Joachimiak.

**03.01 General Interest I**  
**B. Noll, Presiding** **255B**

08:30-08:50 03.01.01  
 The Structure of the *Halothiobacillus neapolitanus* Carboxysome Shell Protein CsoS1A. Yingssu Tsai, Michael R. Sawaya, Gordon C. Cannon, Fei Cai, Eric B. Williams, Sabine Heinhorst, Cheryl A. Kerfeld, Todd O. Yeates.

08:50-09:10 03.01.02  
 Structural Basis of NO and CO Activation

of Soluble Guanylyl Cyclase. Xiaolei Ma, Nazish Sayed, Annie Beuve, Focco van den Akker.

09:10-09:30 03.01.03  
 A Revolutionary Instrument for Protein Recognition: The Korima PRS-1000 Protein Review Station. Gil Ravich, Vu Tran.

09:30-10:00 03.01.04  
 PURY: Database and Server of Geometric Restraints of Hetero Compounds. Dusan Turk, Miha Andrejasic.

10:00-10:30 Coffee Break.

10:30-11:00 03.01.05  
 Microfocusing X-ray Equipment for the Lab Diffractometer. Joerg Wiesmann, Jorgen Graf, Christian Hoffmann, Carsten Michaelsen.

11:00-11:30 03.01.06  
 True Walk-Away Automation in Chemical Crystallography. Michael Ruf, Joerg Kaercher, Arah Leonard, Stephen Leo.

11:30-12:00 03.01.07  
 The Humble Web Browser as a Responsive Interface to Remote Instruments and Data. Peter Turner, Ian Atkinson, Douglas du Boulay, Clinton Chee, Kenneth Chiu, Tristan King, Donald McMullen, Roman Quilici, Nigel Sim, Mathew Wyatt.

**10.03 Supramolecular Chemistry**

*Acknowledgement is made to CrystEngComm, Eli Lilly & Co., Hindawi Publishing Corp. and TransForm Pharmaceuticals, for partial support of this session.*

**K. Wheeler, Presiding** **255E**

08:30-09:10 10.03.01  
 Solid-state Transformations of Metal Carboxylates. Bruce M. Foxman, Benjamin M. Heyman, Jeremy B. Heyman.

09:10-09:30 10.03.02  
 Coordination and Hydrogen-Bonded Frameworks for Anion Binding and Separation. Radu Custelcean, Vincent Sellin, Bruce Moyer.

09:30-10:00 10.03.03  
 Synthetic Protocols for the Assembly of Molecular Co-crystals. Christer Aakeroy.

10:00-10:30 Coffee Break.

10:30-11:10 10.03.04  
 Phase- and Shape-Selective Synthesis and Crystallization of Solid-State Materials. Kenneth Doxsee.

11:10-11:30 10.03.05  
 The Ability of Lower Peptides to Form Co-crystals: Inclusion Compounds of the Tripeptide L-Leucyl-L-Leucyl-L-Leucine. Tara Burchell, Dima Soldatov, Gary Enright, John Ripmeester.

11:30-12:00 10.03.06  
 Insights into the Intercalation of Small Molecules into Hydrogen-bonded "Clay Mimics". Alicia Beatty, Nilantha Bandara, Greg Hogen, Austin Pickett.

*Session continues at 01:30.*

**13.08 Micro-crystals, Micro-beams, and Multiple Crystals**  
**R. Gillilan,** **255F**  
**G. Rosenbaum Presiding**

08:15-08:30  
 Introduction and Overview of Beamlines with Microcrystal Capability. Gerd Rosenbaum.

08:30-09:00 13.08.01  
 Towards Understanding the Atomic Basis of Prion Amyloid. Marcin Apostol, Michael Sawaya, Lukasz Goldshmidt, Michael Thompson, Anders Madsen, Christian Riekel, David Eisenberg.

09:00-09:30 13.08.02  
 Protein Micro-crystallography at the Swiss Light Source. Clemens Schulze-Briese, Elaine Chiu, Fasseli Coulibaly, Sascha Gutmann, Peter W. Haelber, Peter Metcalf, Hajime Mori, Claude Pradervand, Roman Schneider, Takashi Tomizaki.

09:30-10:00 13.08.03  
 Mini-beam for Macromolecules on GM/CA-CAT Beamlines at APS. Ruslan Sanishvili, Venugopalan Nagarajan, Shenglan Xu, Michael Becker, Derek Yoder, Janet Smith, Robert Fischetti.

10:00-10:30 Coffee Break.

10:30-11:00 13.08.04  
 Implementation of Microdiffraction Techniques at NorthEastern Collaborative Access Team APS Beamlines. Malcolm Capel, Steven Ealick, Kanagalaghatta Rajashankar.

11:00-11:30 13.08.05  
 ID23-2 - The New MX-dedicated Microfocus Beamline at the ESRF. David Flot, T. Mairs, E. Mitchell, M. Guijarro, V. Rey, D. Nurizzo, S. McSweeney.

11:30-12:00 13.08.06  
 Microcrystals and Microbeams at MacCHESS. Richard Gillilan, Mike Cook, Sterling Cornaby, Detlef Smlgies, Thomas Szebenyi, Don Bilderback.

## Wednesday, July 25

**AW.03 Etter Early Career Award Symposium**

P. Horanyi, Presiding

255B

**Presentation of Award to Cora Lind.** Alan Pinkerton, ACA President.

01:30-02:00 AW.03.01

Negative Thermal Expansion Materials: X-ray and Neutron Diffraction Adventures under Non-ambient Conditions. Cora Lind, Stacy Gates, Amy Gindhart.

02:00-02:20 AW.03.02

Single-Crystal-to-Single-Crystal E/Z Isomerization Studies of Molecules Embedded in Supramolecular Solids. Shao-Liang Zheng, Milan Gembicky, Cris Vande Velde, Oanh Pham, Philip Coppens.

02:20-02:40 AW.03.03

Bis-pyrazole Based Ligands...Versatile Tools for Supramolecular Synthesis. Benjamin Scott, Christer Aakeröy, John Desper.

02:40-03:00 AW.03.04

When Chemistry Meets Charge Density, and Chemistry Wins..... Christophe M.L. Vande Velde, Anil Cetin, William S. Durfee, Christopher J. Ziegler, Philip Coppens.

03:00-03:30 Coffee Break.

03:30-03:50 AW.03.05

Structure-Guided Design of a Protein-Based Therapeutic for Nerve Agent Exposure. Andrew Hemmert, Chris Fleming, Doug Cerasoli, Phil Potter, Matt Redinbo.

03:50-04:10 AW.03.06

Structural Insights into an Enzyme Interacting with its Substrate: Golgi alpha-mannosidase II & GnMan<sub>5</sub>Gn<sub>2</sub>. Niket Shah, David R Rose, D.A. Kuntz.

04:10-04:30 AW.03.07

Crystallographic Analyses of Coenzyme A-Disulfide Reductase in Complex with Pyridine Nucleotides. Jamie Wallen, Carleitta Paige, T. Conn Mallett, Al Claiborne.

04:30-04:45 AW.03.08

4-Chlorobenzoate CoA Ligase/Synthetase Utilizes a 140° C-terminal Domain Rotation to Perform Two Unique Half-Reactions. Albert S. Reger, Rui Wu, Debra Dunaway-Mariano, Andrew Gulick.

04:45-05:00 AW.03.09

Photochemical Reactions in Inclusion Compounds. Tali Lavy, Menahem Kafroy.

**01.07 Computational Methods**

P. Adams,

255C

E. Merritt, Presiding

01:30-02:00 01.07.01

Use of Molecular Envelopes in Phasing. Quan Hao.

02:00-02:30 01.07.02

The Complimentary use of Small Angle X-ray Scattering with Crystallography in the Determination of Biological Macromolecular Structures. Greg Hura.

02:30-03:00 01.07.03

Crystallography and CryoEM Studies of STIV; A Virus that Thrives in Boiling Acid. John E. Johnson, Reza Khayat, Liang Tang, Mark Young.

03:00-03:30 Coffee Break.

03:30-03:55 01.07.04

Analysis of Ensemble Refinement as a Method for Describing Protein Dynamics. Elena Levin, Dmitry Kondrashov, Gary Wengen, George Phillips Jr.

03:55-04:20 01.07.05

The Primrose Path of Multi-Copy Refinement. Ronald Stenkamp, Ethan Merritt.

04:20-04:45 01.07.06

*Ab initio* Phasing by *ab initio* Folding. Rhiju Das, Bin Qian, Divya Bhat, Airlie Mccoy, Randy Read, David Baker.

04:45-05:10 01.07.07

Twinning and PHENIX. Peter Zwart, Ralf Grosse-Kunstleve, Pavel Afonine, Paul Adams.

**09.01 USANS/USAXS**

J. Ilavsky,

255F

K. Littrell, Presiding

01:30-01:45 09.01.01

USAXS Facility at Advanced Photon Source for Complex Microstructure Studies in Materials Science. Jan Ilavsky, Peter Jemian, Andrew Allen, Gabrielle Long, Fan Zhang.

01:45-02:00 09.01.02

Riching the Theoretical Limit of Sensitivity for the Bonse-Hart Ultra-small-angle Neutron Scattering (USANS) Technique. Michael Agamalian, Jack Carpenter, Ken Littrell, Jim Richardson.

02:00-02:20 09.01.03

Morphological Considerations in the Design of Temperature-Responsive Encapsulants. Dale W. Schaefer, Kevin A. Heitfeld.

02:20-02:40 09.01.04

Void Distributions in Temperature-Cycled Insensitive High Explosives. Trevor Willey, Tony van Buuren, Jon Lee, Jan Ilavsky, George Overturf, John Kinney, Jeff Handy, Brandon Weeks.

02:40-03:00 09.01.05

Microstructural Characterization of Ferritic-Martensitic Steels using SANS/USANS/USAXS Techniques. Govindarajan Muralidharan, Michael Agamalian, Ron Klueh, Weiju Ren, John Shingledecker, Michael Santella, Man-Ho Kim, Jan Ilavsky, Pete Jemian.

03:00-03:30 Coffee Break.

03:30-03:50 09.01.06

Application of Ultra-Small-Angle Scattering Methods in Biomedical Materials Research. Andrew J. Allen, Vincent A. Hackley, Kristen S. Wilson, Jan Ilavsky.

03:50-04:10 09.01.07

Small-angle Scattering Studies on the Hierarchical Structure of Reinforcing Fillers. Doug Kohls, Dale Schaefer.

04:10-04:25 09.01.08

Large-Scale Structure of Block Polyelectrolyte Micelles: Analogies to Attractive Colloids. Surita R. Bhatia.

04:25-04:40 09.01.09

Quantitative Characterization of Contrast Mechanism in Ultra-Small-Angle X-ray Imaging. Fan Zhang, Gabrielle Long, Jan Ilavsky, Pete Jemian, Lyle Levine.

04:40-04:55 09.01.10

Coarsening Studies in Controlled Waspaloy Microstructures Based on SEM and USAXS Observations. V. Siva Kumar G. Kelekanjeri, Lewis Moss, Rosario Gerhardt.

**10.03 Supramolecular Chemistry**  
**K. Wheeler, Presiding** **255E**

01:30-02:10 10.03.07  
 Amphidynamic Materials: Steps Towards Controllable Inertial Motions in Crystalline Solids. Miguel A. Garcia-Garibay, Steven D. Karlen, Jose E. Nuñez, Zachary O'Brien.

02:10-02:30 10.03.08  
 Tuning Intermolecular Interactions in H-bonded Coordination Compound Networks. Jesus Valdes-Martinez, Juan Manuel German-Acacio, Simon Hernandez-Ortega, Christer B. Aakeroy, John Desper.

02:30-03:00 10.03.09  
 Considerations for the Design of Complex Modular Solids. John MacDonald, Yu Wang, Lisa S. Lee, Mehmet V. Yigit, G. Tayhas R. Palmore, T. -J. Mark Luo, Brian Moulton, Brian S. Luisi.

03:00-03:30 Coffee Break.

03:30-04:10 10.03.10  
 Crystal Porosity: Discovery and Design. Len Barbour, Liliana Dobrzanska, Tia Jacobs.

04:10-04:30 10.03.11  
 Do "Clay Mimics" Mimic Clays? Greg A. Hogan, Alicia M. Beatty.

04:30-05:00 10.03.12  
 Polar Lattices of Aryl Diamines. A New Synthon for Dipolar Alignment of Organic Arylamine Crystals. Silas C. Blackstock, Lester T. Gray, J. Richard Duncan, Laura T. Kyser.

**13.09 Teaching Gadgets and Educational Tools**  
**P. Müller, Presiding** **255A**

01:30-02:00 13.09.01  
 Are Teaching Gadgets Obsolete in Times of Computer Animations? Peter Müller.

02:00-02:30 13.09.02  
 Crystallographic Teaching Tools for Beginners. Jenny Glusker.

02:30-03:00 13.09.03  
 Walking the Reciprocal Space: Beyond Bragg & Co. Joerg Kaercher, James F. Britten, Clemens Boere, Michael Ruf.

03:00-03:30 Coffee Break.

03:30-04:00 13.09.04  
 PowerPoint Presentations as Warm, User-friendly Teachers: New Tricks for an Old Dog. Bruce M. Foxman, Jerry P. Jasinski, Michael J. Vela, Tae H. Cho.

04:00-04:45 13.09.05  
 How to Teach the Phase Problem and the Basics of Direct Methods. Henk Schenk.

**2007 Margaret C. Etter Student Lecturer Awards**

Each Special Interest Group (SIG) within the ACA has the opportunity to select one student to receive an award and to present a lecture in one of the sessions organized by that SIG. Selections are based upon submitted abstracts and are independent of whether the student presenter originally requested an oral or poster presentation. Award winners are determined by the elected officers of the SIGs. Students who are selected receive a monetary award of \$250 and a certificate.

**Congratulations to this year's winners:**

- Biological Macromolecules ..... Ryan McAndrew, Medical College of Wisconsin.....01.04.05
- Materials Science ..... Amy Gindhart, Univ. of Toledo.....05.01.05
- Powder Diffraction ..... Jae-Hyuk Her, State Univ. of New York Stony Brook.....07.01.11
- Small Angle Scattering ..... Jan Lifert, Stanford Univ. ....13.03.03
- Small Molecule ..... Greg Hogan, Mississippi State Univ. ....10.03.11
- Young Scientist ..... Tali Lavy, Technion, Israel.....AW.03.09

Meeting Registration Desk ..... 7:30am-3:30pm ..... North Lobby  
 Speaker Ready Room ..... 7:30am-:30pm ..... 260

Council Meeting Room..... 7:30am-5:00pm..... 257

### SP.02 Plenary Lecture

*A Lecture by Nobel Laureate R. Kornberg, presented by Bruker AXS.*

**C. Hill, Presiding 255BC**

08:30-09:30 SP.02.01  
 Structural Basis of Transcription. Roger Kornberg.

### 01.08 Large and Difficult Structures

*Acknowledgement is made to Area Detector Systems, Corp., Array BioPharma, Inc., Art Robbins Instruments, Boehringer Ingelheim Pharmaceuticals, Inc., Bristol-Myers Squibb Pharmaceutical Research Institute, and Pfizer, Inc. for partial support of this session.*

**C. Hill, L. Tong, Presiding 255BC**

09:30-10:00 01.08.01  
 Architecture of Megadalton Respiratory Proteins from Annelids. William Royer.

10:00-10:30 01.08.02  
 Structure and Function of Eukaryotic RNA Exosomes. Christopher Lima, Quansheng Liu, Jaclyn Greimann.

10:30-11:00 Coffee Break.

11:00-11:20 01.08.03  
 Draft Crystal Structure of the cpMVP Vault at 9 Å Resolution. Daniel Anderson, Valerie Kickhoefer, Stuart Sievers, Leonard Rome, David Eisenberg.

11:20-11:40 01.08.04  
 Crystal Structure of Acostatin, a Dimeric Disintegrin from the Venom of Southern Copperhead. Marc Allaire, Natalia Moiseva, Robert Bau.

11:40-12:30 01.08.05  
 Structures of Functional Complexes of the Ribosome. Venki Ramakrishnan, Christine Dunham, Frank Murphy, Sabine Petry, Maria Selmer, Albert Weixlbaumer.

### 07.01 Structure Determination from Powder Diffraction: Getting Better and Better

**A. Huq, Presiding 255E**

09:30-10:00 07.01.01  
 EXPO2007: A Tool for Crystal Structure Solution and Refinement from Powder Data. Carmelo Giacovazzo, Angela Altomare, Rocco Caliendo, Mercedes Camalli, Corrado Cuocci, Anna Grazia G. Moliterni, Rosanna Rizzi.

10:00-10:30 07.01.02  
 Structure Solution from Powder Diffraction Data - Tackling the Bottlenecks. Kenneth Shankland, William David.

10:30-11:00 Coffee Break.

11:00-11:30 07.01.03  
 Solving Structures from Powder Data Using Density Building Functions and Histogram Matching. Chris Gilmore, Douglas Dorset.

11:30-12:00 07.01.04  
 Aromatic Carboxylates. Trimellitates. James Kaduk.

12:00-12:20 07.01.05  
 Novel Mineral Structure of  $\text{LiNaSiB}_3\text{O}_7(\text{OH})$  from Lab Powder Diffraction Data and *ab-initio* Quantum Optimization. Pamela Whitfield, Y. Le Page, J. Grice, C. Stanley, G. Jones, M. Rumsey, C. Blake, A. Roberts, J. Stirling, G. Carpenter.

*Session continues at 01:30.*

### 09.02 Characterization of Surfaces and Interfaces

**B. Lee, Presiding 255F**

09:40-10:05 09.02.01  
 Water-Barrier Properties of Anticorrosion Coatings Based on Bridged Silanes. Dale W. Schaefer, Yimin Wang, Guirong Pan, Peng Wang.

10:05-10:30 09.02.02  
 Phasing Resonant Anomalous X-ray Reflectivity Data and Fourier Synthesis of Element-specific Density Profiles at Buried Interfaces. Changyong Park, Paul A. Fenter.

10:30-11:00 Coffee Break.

11:00-11:25 09.02.03  
*In situ* GISAXS Studies of Metal Nanocluster Catalysis. Randall Winans, Stefan Vajda, Byeongdu Lee, Soenke Seifert, Sungsik Lee, Joseph Calo.

11:25-11:50 09.02.04  
*In situ* GIXS and GISAXS Studies of the Self-organized Growth of Cobalt Nanostructures. Frederic Leroy, Gilles Renaud, Antoine Letoublon, Remi Lazzari.

11:50-12:15 09.02.05  
 Multidimensional Self-Assembly of Liquid Crystalline Rod-coil Block Copolymers. Rachel Segalman, Bradley Olsen, Yuefei Tao, Xuefa Li, Jin Wang.

12:15-12:40 09.02.06  
 Kinetic Study of Nucleation and Growth of Environmental Nanoparticles at Water-Mineral Interfaces using *in situ* Time-Resolved GISAXS. Young-Shin Jun, Glenn Waychunas, Byeongdu Lee.

### 10.04 Cool Structures

**A. Oliver, Presiding 255A**

09:40-10:00 10.04.01  
 $[\text{Ni}(\text{MeCN})(\text{H}_2\text{O})_2(\text{NO}_3)_2] \cdot (15\text{-crown-5}) \cdot \text{MeCN}$ : Another Uncommon Polymorphic System with an Intermediate High-Z' Phase. Maxime Siegler, Sean Parkin, Carolyn Brock.

10:00-10:20 10.04.02  
 Structures of Amyloid-like Fibrils Suggest Seven Distinct Classes of the Steric Zipper Motif. Michael Sawaya, Shilpa Sambashivan, Magdalena Ivanova, Stuart Sievers, Marcin Apostol, Anders Madsen, Christian Riek, David Eisenberg.

10:20-10:50 Coffee Break.

10:50-11:10 10.04.03  
 Influence of the Asymmetric Binding Modes of the Azido-bridged Cu(II) Compounds in the Crystals Structures. Janaina G. Ferreira, Regina H.A. Santos, Antonio E. Mauro, Fabiana C. Andrade, Alexandre O. Legendre, Sandra R. Ananias.

11:10-11:30 10.04.04  
 A Solid-state Search for Structure-organizing Halogen-nitrile Contacts in "Bridge-flipped" Isomeric Benzylideneanilines. W.H. Ojala, K.M. Lystad, B. Balidemaj, T.K. Deal, J.E. Engebretson.

11:30-11:50 10.04.05  
 Gold Monomers, Dimers and Trimers; All in One Structure! Christine M. Beavers, Marilyn M. Olmstead.

11:50-12:10 10.04.06  
 Control, Prediction and Rationalization of Packing Motifs: Predicted and Observed Structures of Carbamazepine and Some of its Analogues. Francesca Fabbiani, Andrea Johnston, Alastair Florence, Norman Shankland, Kenneth Shankland, Charlotte Leech, Harriott Nowell, Sally Price.

**03.02 General Interest II**

**B. Noll, Presiding 255B**

01:30-02:00 03.02.01  
Non-merohedral Twinning in Small Molecule and Protein Crystallography. Regine Herbst-Irmer, Madhumati Sevvana, Ina Dix, George M. Sheldrick.

02:00-02:30 03.02.02  
Novel Approach to Reconstruct Nuclear/Electron Density Distribution based on Modified Maximum Entropy Method with Monte Carlo Method. Ryoji Kiyonagi, James Richardson.

02:30-03:00 03.02.03  
Journey into the Twilight Zone of Crystallographic Riemann-Finsler Geometry. Carroll Johnson.

03:00-03:30 Coffee Break.

03:30-04:00 03.02.04  
The Quality of Chocolate, the Polymorphism of Cocobutter, and the Mechanism of Fat Bloom. Henk Schenk, Jan Van Mechelen, Rene Peschar.

04:00-04:30 03.02.05  
A Temperature-Dependent Phase Transition in (Nitrosyl)Iron(II) Tetraphenyl Porphyrinate. Bruce C. Noll, Nathan J. Silvermail, Marilyn M. Olmstead, Olga Trofymuk, Charles E. Schulz, W. Robert Scheidt.

**05.02 Mineralogy and Crystallography: Real Crystals, Extreme Conditions**

**L. Groat, Presiding 255D**

01:30-02:00 05.02.01  
Crystallography of Earth Materials at Extreme Conditions from Experimental and Computational Studies. George Lager.

02:00-02:30 05.02.02  
Hydration-Dehydration Reactions under Extreme Conditions: Experimental Methods and Results. Ron Peterson.

02:30-03:00 05.02.03  
High Energy X-ray Diffraction Studies of Str II and Str H Noble Gas Clathrate Hydrates. Chris Tulk, Dennis Klug, Bryan Chakoumakos, Lars Ehm, John Parise.

03:00-03:30 Coffee Break.

03:30-03:50 05.02.04  
The Geometric Effects of  $v\text{Fe}^{2+}$  for  $v\text{Mg}$  Substitution on the Crystal Structures of the Grandidierite-ominelite Series. Lee Groat, Tashia Dzikowski, Edward Grew.

03:50-04:10 05.02.05  
High-P/T Neutron and Synchrotron X-ray Diffraction Study of  $\text{Ni}(\text{OD})_2$ . Hongwu Xu, Yusheng Zhao, Jianzhong Zhang, Yuejian Wang, Donald Hickmott, Luke Daemen, Monika Hartl.

04:10-04:30 05.02.06  
Synthesis and Crystal-structure Refinement of  $\text{Ba}_4\text{Nb}_2\text{O}_9$ . Jana Bezzjak, Boštjan Jančar, Danilo Šuvorov.

04:30-04:50 05.02.07  
The Crystal Chemistry of  $\text{Bi}_6\text{TP}_2\text{O}_{15+x}$ , T = Fe, Ni, Zn. Isomorphism and Polymorphism, Structural Relationship to  $\text{Bi}_6\text{TiP}_2\text{O}_{16}$ . N. Arumugam, V. Lynch, H. Steinfink.

**07.01 Structure Determination from Powder Diffraction: Getting Better and Better**

**A. Huq, Presiding 255E**

01:30-02:00 07.01.06  
Use of Powder Diffraction in Molecular Magnetism. Peter Stephens.

02:00-02:30 07.01.07  
An *in-situ* Crystallographic Study of Crystal Growth and Ion Exchange in Titanium Silicates. Abraham Clearfield, Aaron J. Celestian, Akhilesh Tripathi, Dimitri Medvedev, John B. Parise.

02:30-03:00 07.01.08  
Polymorphic Discoveries Using Power X-Diffraction - Discoveries during Pharmaceutical Development. Eugene Cheung, Matthew Peterson.

03:00-03:20 Coffee Break.

03:20-03:50 07.01.09  
Reaching for High Resolution in Protein Powder Diffraction. Robert Von Dreele.

03:50-04:20 07.01.10  
POWGEN3: A New Neutron Powder Diffractometer Suitable for *ab-initio* Crystal Structure Determination. Jason Hodges, Ashfia Huq.

04:20-04:40 07.01.11  
Maximum Entropy Crystal Structure Reconstruction using X-ray Powder Diffraction Data. Jae-Hyuk Her, Peter Stephens.

04:40-05:00 07.01.12  
Distance Puzzle - Structure Mining from Pair Distribution Function. Pavol Juhas, Phillip M. Duxbury, Simon J.L. Billinge.

**09.03 X-ray Imaging and Resonant Scattering**

**R. Hjelm, J. Kortright Presiding 255A**

01:30-02:00 09.03.01  
Resonant Soft X-ray Magnetic Scattering to Resolve Lateral and In-Depth Structure. Jeff Kortright.

02:00-02:30 09.03.02  
Thin Polymer Film Structure using Resonant Soft X-ray Scattering and Reflectometry. Cynthia Welch, Rex Hjelm, Joseph Mang, Marilyn Hawley, Debra Wroblewski, Bruce Orler, Jeffrey Kortright.

02:30-03:00 09.03.03  
Coherent Diffraction Imaging using Free-Electron Lasers. Sebastien Boutet, M. Bogan, B. Woods, A. Barty, U. Rohner, M. Seibert, S. Marchesini, M. Frank, J. Hajdu, H. Chapman.

03:00-03:15 Coffee Break.

03:15-03:45 09.03.04  
Resonant X-ray Scattering from Novel Ordering in Strongly Correlated Materials. Stuart Wilkins, Thomas Beale, Natasa Stojic, Nadia Bingeli, Peter Hatton, Massimo Altarelli, John Hill, Gerry Lander.

03:45-04:05 09.03.05  
Anomalous Small-Angle X-ray Scattering Characterization of Bulk Block Copolymer/Nanoparticle Composites. Byeongdu Lee, Chieh-Tsung Lo, Nancy L. Dietz Rago, Randall Winans, P. Thiyagarajan.

04:05 Open Discussion of X-ray Imaging and Resonant Scattering Facilities and Plans. Kortright and Hjelm.

**13.10 Radiation Damage**

**J. Holton, Presiding 255F**

01:30-01:52 Introduction.

01:52-02:15 13.10.01  
Radiation Damage in Macromolecular Cryocrystallography. Elspeth Garman.

02:15-02:37 13.10.02  
Crystal Heating in a Third Generation Synchrotron X-ray Beam, a Significant Factor or Not? E.H. Snell, H.D. Bellamy, G. Rosenbaum, M.J. van der Woerd.

02:37-03:00 13.10.03  
A Statistical Measure of Mitigation of Radiation Damage to Protein Crystals. Binal N. Shah, Bradley S. Yaniga, Unmesh N. Chinte, Alan A. Pinkerton, Bryant L. Hanson, Constance A. Schall.

03:00-03:30 Coffee Break.

03:30-03:52 13.10.04  
Martin Weik.

03:52-04:15 13.10.05  
A Quick Soak for Long Life - Practical Radiation Damage Prevention. Andrea Schmidt, Brice Kauffmann, Annette Faust, Manfred Weiss, Victor Lamzin.

04:15-04:37 13.10.06  
Can Radiation Damage to Protein Crystals Be Reduced using Small Molecule Compounds? Jan Kmetko, Matthew Warkentin, Ulrich English, Robert Thorne.

04:37-05:00 13.10.07  
The Effects of Radiation Damage on Anomalous Dispersion Experiments. Ana Gonzalez.

## Exhibitors with Booth Numbers

Area Detector Systems Corp.....	312,314	International Centre for Diffraction Data.....	111
Art Robbins Instruments .....	306,308	International Union of Crystallography .....	112
Axygen Biosciences.....	403	Jena Bioscience GmbH .....	508
Blake Industries, Inc.....	315	Korima, Inc.....	214
Brandel, Inc.....	409	Mar USA .....	413
Bruker AXS .....	503	Marresearch GmbH .....	103
CCDC.....	102,104	Micro Photonics/STOE.....	615
CCP4 .....	110	Mitegen, LLC .....	504
CRYO Industries of America.....	502	Oak Ridge National Laboratory .....	113
CyBio US, Inc. ....	506	Oxford Cryosystems, Inc.....	515
Douglas Instruments, Ltd.....	209	Oxford Diffraction, Ltd. ....	203,205,207
Emerald Biosystems .....	313	QIAGEN, Inc.....	405
Fluidigm Corp. ....	410,412	RCSB Protein Data Bank.....	108
Formulatrix, Inc.....	302,304	Rigaku Americas Corp. ....	303
GE Healthcare.....	405	Southeast Regional Collaborative	
Genomic Solutions .....	215	Access Team (SER-CAT) .....	114
Greiner Bio-One .....	311	Thermo Fisher Scientific.....	511,513
Hampton Research .....	414	TTP LabTech, Ltd.....	605
Incoatec GmbH .....	607	Wyatt Technology .....	603
		XENOCs .....	213

## Show Hours

**Saturday, July 21**

7:30pm - 10:30pm

**Sunday, July 22**

10:00am - 7:30pm

**Monday, July 23**

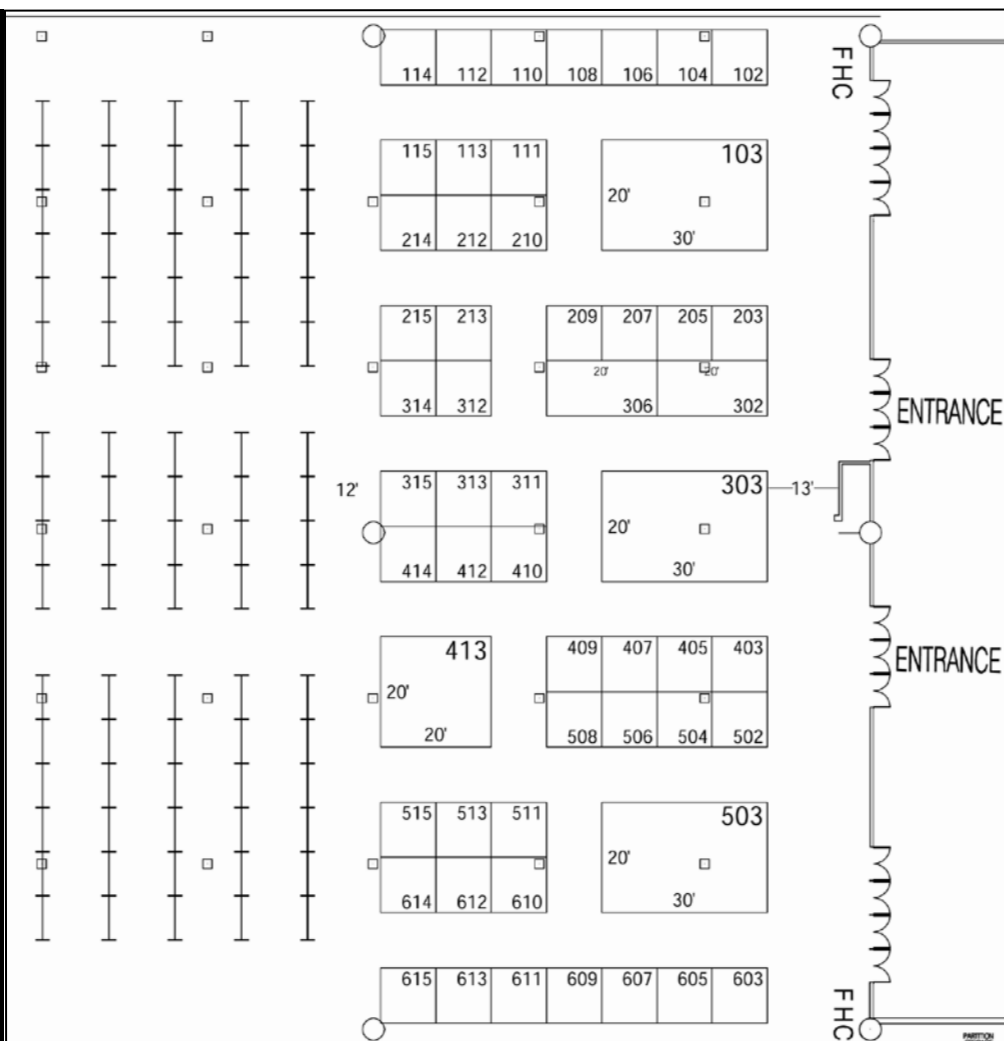
10:00am - 7:30pm

**Tuesday, July 24**

10:00am - 7:30pm

**Wednesday, July 25**

10:00am - 1:30pm



## POSTER SESSIONS

Posters beginning with S will present in Poster Session I, Sunday, July 22, 05:30pm - 07:30pm

Posters beginning with M will present in Poster Session II, Monday, July 23, 05:30pm - 07:30pm

Posters beginning with T will present in Poster Session III, Tuesday, July 24, 05:30pm - 07:30pm

**All posters should be assembled on Sunday before 05:00pm and removed on Wednesday before 01:30pm  
Please be present at your poster during the entire time on the day to which you are assigned.**

SP001

Structural Studies of *T. Acidophilum* Proteasome: Implications for Proteasome Activation and Inhibition. E.I. Masters, A. Förster, C.P. Hill.

SP002

Crystallization of the Dyrk1B Kinase Domain. Helen Rho.

SP003

Structure Based Protein Engineering of Ribosomal Protein Trimethyltransferase. Hasan Demirci, Steven T. Gregory, Albert E. Dahlberg, Gerwald Jogl.

MP004

Structural Investigations into the Role of Human Maltase-glucoamylase in Starch Digestion. Lyann Sim, David Rose.

MP006

The Crystal Structure of Carboxysome Subunit CcmL Reveals a Pentameric Assembly Suggesting its Role as a Vertex in the Bacterial Microcompartment. Shiho Tanaka, Michael R. Sawaya, Cheryl A. Kerfeld, Todd O. Yeates.

MP007

Structures of the Immunogenic Region of A-beta Complexed with Anti-protofibril Antibodies. Anna Gardberg, Lezlee Dice, Susan Ou, Rebecca Rich, Elizabeth Helmbrecht, Jan Ko, Ronald Wetzell, David Myszk, Paul Patterson, Chris Dealwis.

SP008

Crystal Structure of Inositol Polyphosphate Multikinase 2 with Substrate Kinetics Analysis. William Holmes, Gerwald Jogl.

SP009

Elucidation of the First Crystal Structure of HoxA9 and Pbx Homeodomains Bound to an *in vivo* Derived DNA Target. Bill Bauer, Jessica Kocsis, Timothy Umland.

MP010

The Crystal Structure of GTP Cyclohydrolase III with Bound Substrate. Sue A. Roberts, Shane D. Morrison, V. Bandarian.

SP011

Structural Studies on HMG-CoA Reductase from the Pathogenic Bacterium *Enterococcus faecalis*. Sucharita Bose, Calvin Steussy, Matija Hedl, Victor Rodwell, Cynthia Stauffacher.

SP012

Crystal Structure of the Zinc-binding Trans-

port Protein ZnuA from *Escherichia coli* Reveals an Unexpected Variation in Metal Coordination. Hua Li, Gerwald Jogl.

MP013

Structural Basis for Ligand and Heparin Binding to Neuropilin B Domains. Craig Vander Kooi, Manuel Jusino, Benjamin Perman, David Neau, Henry Bellamy, Daniel Leahy.

SP014

Crystal Structure of a Sulfur Carrying Protein Complex Found in the Cysteine Biosynthetic Pathway of *Mycobacterium tuberculosis*. Christopher Jurgenson, Kristin Burns, Tadhg Begley, Steven Ealick.

MP015

Crystal Structure of NeuroD/E47 in Complex with DNA: Insight of E-box Recognition by a Heterodimeric bHLH. Antonella Longo, Gerald Guanga, Robert Rose.

SP016

Conformation Changes of Y-family Polymerase Dpo4 from the apo-enzyme to Substrate Bound Forms. Jimson Wong, Hong Ling.

SP017

Crystallographic Studies of Pyruvate-formate lyase Activase. Jessica Vey, Meng Li, Jian Yang, Joan Broderick, Catherine Drennan.

MP018

Structure of *Thermus aquaticus* Succinyl-CoA Synthetase in Complex with Mn<sup>2+</sup>-GDP. Marie Fraser, Koto Hayakawa, Edward Brownie.

MP019

Mutagenic Bypass of a Major Benzo[a]pyrene Adduct by a Y-Family DNA Polymerase through Strand Misalignment. Hong Ling, Jacob Bauer, Guanxin Xing, Haruhiko Yagi, Jane Sayer, Donald Jerina.

SP020

Structure of  $\alpha$ -Glycerophosphate Oxidase from *Streptococcus* sp.: A Structural Template for the Mitochondrial  $\alpha$ -Glycerophosphate Dehydrogenase. Timothy Colussi, Derek Parsonage, Takeshi Matsuoka, P. Andrew Karplus, T. Conn Mallett, Al Claiborne.

MP021

The Mechanism of Double-Stranded RNA Processing by Ribonuclease III. Jianhua Gan, Gary Shaw, Joseph Tropea, David Waugh, Donald Court, Xinhua Ji.

SP022

Structural Analyses of Proteins Involved in Pilus Assembly in *Streptococcus pyogenes*. HaeJoo Kang, Fasseli Coulibaly, Thomas Proft, Edward N. Baker.

SP023

Substrate Recognition in Puromycin Sensitive Aminopeptidase. Sowmya Sampath, Abigail Daily, Louis Hersh, David Rodgers.

MP024

Catabolism of Hyaluronan Polysaccharide: Crystal Structure of Human Hyaluronidase 1. Kinlin Chao, Lavanya Muthukumar, Osnat Herzberg.

SP025

Structures of EphrinA3 Receptor Tyrosine Kinase Reveal Aspects of Mechanism and Regulation. Tara L. Davis, John R. Walker, Abdallah Hassani, Christine Butler-Cole, Sirano Dhe-Paganon.

SP026

Crystal Structures of Human 2-oxoglutarate Dependent Hydroxylases. Rasheduzzaman Chowdhury, Michael A. McDonough, Christopher J. Schofield.

SP027

Structural Analysis of an Antibiotic Resistant C-O lyase from *Staphylococcus aureus*. Magdalena Korczynska, Tariq A. Mukhtar, Gerard D. Wright, Albert M. Berghuis.

MP028

Structure of a Heparin-dependent Complex of Hedgehog and Ihog. Jason McLellan, Shenqin Yao, Xiaoyan Zheng, Brian Geisbrecht, Rodolfo Ghirlando, Philip Beachy, Daniel Leahy.

MP029

Crystal Structure of Methyltransferase that Modifies P-site Guanine 966 of the 16S rRNA. Jerzy Osipiuk, D.V. Lesnyak, T. Skarina, P.V. Sergiev, A.A. Bogdanov, A. Edwards, A. Savchenko, O.A. Dontsova, A. Joachimiak.

MP030

Crystallization and Preliminary X-ray Analysis of the GST- $\alpha$  Synuclein Fusion Protein. Beena Narayanan, Daniel Hennessy, Ruth G. Perez, John Rosenberg.

SP031

Functional Diversity from a Simple Protein Fold. Youzhong Guo, Hector Serrano, William Johnson, Chris Whitman, Marvin Hackert, B.A. Robertson.

MP032

The Structure of an N-acetyl-,D-glucosaminidase from *Streptococcus gordonii*. David Langley, Derek Harty, Jill Trehwella, Mitchell Guss, Charles Collyer.

MP033

Crystal Structure of Adenosine Kinase from *M. tuberculosis* and Structural Basis for Specific Activation of Antimicrobial Nucleoside Analogs. Rongbao Li, Yimin Wang, Zhican Qu, Vincent Escuyer, Joseph Maddry, William Parker.

MP034

Crystal Structure of Bovine Lipoyltransferase with Lipoyl-AMP. Makoto Matsuda, Kazuko Fujiwara, Harumi Hosaka, Kazuko Okamura-Ikeda, Yutaro Motokawa, Mamoru Suzuki, Hisaaki Taniguchi, Atsushi Nakagawa.

SP035

Structure of the Conserved Transcriptional Repressor *erh* (enhancer of rudimentary homolog). Cheng Wan, Wolfram Tempel, James Liu, Bi-Cheng Wang, Robert Rose.

SP036

Crystal Structure of the Human Prostacyclin Synthase. Chia-Wang Chiang, Hui-Chun Yeh, Lee-Ho Wang, Nei-Li Chan.

SP037

Crystal Structure of Enoyl-ACP Reductase from *F. tularensis*. Yimin Wang, Tan Wang, Marianne Cuff, Vincent Escuyer, Rongbao Li.

SP038

X-ray Crystal Structure Determination of the Mammalian Glycosyltransferase C2GnT-L. John Pak, Pascal Arnoux, Sihong Zhou, Prashanth Sivarajah, Malathy Satkunarajah, Xuekun Xing, James Rini.

SP039

Structure to Function Correlations for Adeno-associated Virus Serotype 1. Govindasamy Lakshmanan, Edward B Miller, Brittney Gurda-Whitaker, Robert McKenna, Sergei Zolotukhin, Nicholas Muzyczka, Mavis Agbandje-McKenna.

MP040

Structural Studies of the NKX2.5 Homeoprotein. Hyun-Joo Nam, Peyton Scone, Hideko Kasahara.

SP041

The Structure and Function of the Prephenate Dehydratase from *Staphylococcus aureus*. Kemin Tan, Hui Li, Rongguang Zhang, Minyi Gu, Andrzej Joachimiak.

SP042

YPxL Motif with ALIX. Qianting Zhai, Rob Fisher.

MP043

Structure of EF0647 from *Enterococcus fae-*

*cali*, a Putative HxlR Family Transcriptional Regulator. Youngchang Kim, Wu Ruiying, Osipiuk Jerzy, Moy Shiu, Joachimiak Andrzej.

MP044

Structural and Transcriptional Analyses of a Purine Nucleotide-Binding Protein from *Pyrococcus furiosus*. M. Gary Newton, B. Gerwe, L.L. Clancy Kelley, B.D. Dillard, T. Lai, Z.-J. Liu, W. Tempel, L. Chen, B.-C. Wang, J.P. Rose, J. Habel, F. Jenny, F. Sugar, D. Lee, J. Richardson, D. Richardson, M. Adams.

SP045

Structural Characterization of a Type III Secretion System Needle Protein YscF in Complex with its Chaperones YscE/YscG. Ping Sun, Brian P. Austin, Joseph E. Tropea, David S. Waugh.

SP046

Crystal Structure of Vestitone Reductase from Alfalfa (*Medicago sativa* L.). Hui Shao, Richard A. Dixon, Xiaoqiang Wang.

SP047

Structural Basis for Stem Cell Factor-KIT Signaling and Activation of Class III Receptor Tyrosine Kinases. Xiaolin He, Heli Liu, Xiaoyan Chen, Pamela Focia.

MP048

Functional Structure of the Periplasmic Component of Bacterial Multidrug Efflux Transporter. Shunfu Piao, Seulki Kim, Yongbin Xu, Nam-Chul Ha.

MP049

Two Conformations of a Crystalline Human tRNA Synthetase-tRNA Complex: Implications for Protein Synthesis. Xiang-Lei Yang, Francella Otero, Karla Ewalt, Jianming Liu, Manal Swairjo, Caroline Kohrer, Uttam Rajbhandary, Robert Skene, Duncan McRee, Paul Schimmel.

SP050

Crystal Structure of the Tandemly Repeated PTP-like Myo-inositol Hexaphosphatase (phytase) Expressed by *Mitsuokella multacida*. Robert J. Gruninger, L. Brent Selinger, Steven Mosimann.

SP051

Crystal Structure of KPC-2: Insights into Carbapenemase Activity in Class A  $\beta$ -lactamases. Wei Ke, Christopher Bethel, Jodi Thomson, Robert Bonomo, Focco van den Akker.

SP052

Structural Basis for Induction of Plant Disease Resistance in Flax by Flax Rust Avirulence Proteins. Anderson Wang, Gregor Guncar, Jade Forwood, Ann-Maree Catanzariti, Joel Mackay, Jeffrey Ellis, Peter Dodds, Bostjan Kobe.

SP053

Structure-Function Studies of the CurF Decarboxylase from *Lyngbya majuscula* Involved in Curacin A Biosynthesis. Todd Geders, Liangcai Gu, Jonathan Mowers, David Sherman, Janet Smith.

MP054

Crystal Structure of Sialyltransferase Pm0188 from *P. multocida* in Complex with Donor Sugar Analogue and Acceptor Sugar. Dong-Uk Kim, Ji-Ho Yoo, Kwan Soo Kim, Yong Joo Lee, Hyun-Soo Cho.

MP055

The Complex Crystal Structure of Plant Telomere Binding Protein, Ngtrf1 and Telomere DNA. Hyun-Soo Cho, Sung-Hoon Jun, Jung-Sue Byun, Heeyoung Park, Hansol Bae, Woo Taek Kim, Weontae Lee.

MP056

Structural Basis for Regulation of Protein Phosphatase 1 by Inhibitor-2. Thomas Hurlley, Jie Yang, Lili Zhang, Kristie Goodwin, Qin Zou, Marc Cortese, A. Keith Dunker, Anna DePaoli-Roach.

MP057

Structure and Functional Analysis of Tetraenomycin Aromatase/cyclase. Brian Ames, Wenjun Zhang, Tyler Korman, Peter Smith, Thanh Vu, Yi Tang, Shiou-Chuan Tsai.

SP058

Cyclin Box Structure of the P-TEFb Subunit Cyclin T1 Derived from a Fusion Complex with EIAV Tat. Kanchan Anand, Antje Schulte, Klaus Scheffzek, Matthias Geyer.

MP059

From Orphan to Structure: Genetic Control by a Metal-Sensing Riboswitch. Charles E. Dann III, Catherine A. Wakeman, Cecelia L. Sieling, Wade C. Winkler.

SP060

Activation of the Human Nuclear Xenobiotic Receptor PXR by the RT-Targeted Anti-HIV Drug PNU-142721. Yuan Cheng, Matthew Redinbo.

MP061

Structure of Puf4 Bound to RNA Reveals Insights into Binding Specificity. Matthew Miller, Joshua Higgin, Traci Hall.

SP062

Structural Insights into the 3' - 5' Exonucleases. Udesch de Silva, Sumana Choudhury, Suzanna Bailey, Scott Harvey, Fred Perrino, Thomas Hollis.

SP063

Cloning and Crystallization of *Drosophila* Tgo (bHLH-PAS) protein. Dongli Wang, Robert Rose.

SP064

Current Status of the JAXA-GCF Project.

Masaru Sato, Hiroaki Tanaka, Koji Inaka, Shinichi Shinozaki, Sachiko Takahashi, Mari Yamanaka, Erika Hirota, Satoshi Sano, Tomoyuki Kobayashi, Tetsuo Tanaka.

SP065

Estimation Method of Diffusion Coefficient of Precipitant. Hiroaki Tanaka, Naoki Furubayashi, Koji Inaka, Sachiko Takahashi, Mari Yamanaka, Masaru Sato, Satoshi Sano, Tomoyuki Kobayashi, Atsushi Nakagawa, Tetsuo Tanaka.

SP066

Mellitic Acid-Promoted Crystallization of Bovine Trypsin. Steven Larson, John Day, Alexander McPherson, Robert Cudney.

SP067

Strategies in High Throughput Protein Crystallization: Cryoprotectants as Solubility Enhancers. Rajendrakumar Gosavi, Timothy Mueser, Constance Schall.

SP068

Macromolecular Crystallization Device Based on Contact Line Pinning. Yevgeniy Kalinin, Viatcheslav Berejnov, Robert Thorne.

SP069

Cryoprotectant Requirements for Flash Cooling Protein Crystals based on Measured Thermal Properties and Heat Transfer Analysis - A Prediction. Constance A. Schall, Binjal N. Shah, Kenneth J. DeWitt, Bryant Leif Hanson, Steve J. Tomanicek.

SP070

A Method for Controlling the Vapor Pressure of Water in Crystallization Experiments using CsCl. Daniel Hennessy, Lisa Bajpayee, Beena Narayanan, John Rosenberg.

SP071

The X-ray Structures of Monoclinic and Orthorhombic Taka-amylase A; The Crystals Grown in Microgravity Environment. Aki-fumi Higashiura, Hiroaki Tanaka, Masaru Sato, Satoshi Sano, Tomoyuki Kobayashi, Tetsuo Tanaka, Koji Inaka, Mamoru Suzuki, Atsushi Nakagawa, Sachiko Takahashi, S Sugiyama, Mari Yamanaka.

SP072

A Microfluidic Chip for Protein Crystallization and *in situ* Diffraction Data Collection. Kensaku Hamada, Tomokazu Hasegawa, Masaru Sato, Moritoshi Motohara, Satoshi Sano, Tomoyuki Kobayashi, Tetsuo Tanaka, Yukiteru Katsube.

SP073

Automated Liquid Dispensing with Precision and Accuracy for Protein Crystallization using the Alchemist™ II. Jian Xu, Matthew Lundy, Michael Willis.

SP074

The Current SER Approach. David Cooper,

Won-Chon Choi, Urszula Derewenda, Lukasz Goldschmidt, Natalya Olekhnovitch, Meiyang Zheng, David Eisenberg, Zygmunt Derewenda.

SP075

Strategies of Improving the Crystallization Success Rate. Min Zhou, Lance Bigelow, Erica Duggan, Cathy Hatzos, Grazyna Joachimiak, Hue Li, Rory Milligan, Lour Volkart, Ruiying Wu, Qizhi Zhang, Y.-c. Babnigg, R.-g. Zhang, A. Joachimiak.

SP076

Purification, Characterization, and Crystallization of a Metal Dependent PI-PLC from *Streptomyces antibioticus*. Michael R. Jackson, Tom L. Selby.

MP077

A New Experimental Station for Long Wavelength Crystallography. Quan Hao, Ulrich Englisch, Alex Kazimirov, Ernie Fontes, Don Bilderback, Sol Gruner, Chae Un Kim.

MP078

The Use of Longer X-ray Wavelengths in Macromolecular Crystallography. Manfred S. Weiss, Christoph Mueller-Dieckmann, Santosh Panjekar, Paul Tucker.

MP079

Higher Signal, Lower Noise: How to Get the Best Data from Your Crystals. Martin Adam, Bram Schierbeek, Anita Coetzee, Cary Bauer, Rob Hooft.

MP080

Cryopreservation of Protein Crystals: From Art to Science. Robert E. Thorne, Matthew Warkentin, Viatcheslav Berejnov, Naji Hussein.

MP081

Flash Cooling in Capillaries: Cooling Rates and Critical Glycerol Concentrations. Matthew Warkentin, Valentina Stanislavskaia, Katherine Hammes, Robert E. Thorne.

MP082

Trash to Treasure: Changing a Poorly Diffracting Frozen Crystal to a High Resolution Data Set. Kris F. Tesh, A.L. Dowell, Joseph D. Ferrara, J.W. Pflugrath.

MP083

The Structural Biology Center User Program at the Advanced Photon Source, Argonne National Laboratory. Stephan L. Ginnell, R. Alkire, C. Chang, M. Cuff, N.E.C. Duke, G. Kazimierz, Y. Kim, K. Lazarski, J. Osipiuk, G. Rosenbaum, F.J. Rotella, K. Tan, R. Zhang, A. Joachimiak.

MP084

Advanced Crystal Imaging with the DETECT-X Microscope. Peter Nollert, Yiping Xia, Werner Kaminsky, Mark Mixon.

SP085

Insights into Transport of Long Chain Fatty Acids Across the Outer Membrane by FadL. Dimki Patel, Bert Van Den Berg.

TP086

Structural Studies of Human Plasma Platelet Activating Factor Acetylhydrolase and Implication to its LDL-binding. Uttamkumar Samanta, Brian Bahnsen.

TP087

Remediation of the PDB Archive. J. Westbrook, H.M. Berman, L. Chen, D. Dimitropoulos, J. Dorelejers, S. Dutta, Z. Feng, J. Flippen-Anderson, O. Haq, K. Henrick, J. Ionides, T. Kosada, A. Kouranov, C. Lawson, J. Markley, H. Nakamura, J. Ory, J. Sun, E.I. Ulrich, S. Velankar, W. Vranken, H. Yang, M. Yousufuddin.

TP088

Gene Duplication in the ( $\beta/\alpha$ )<sub>8</sub> Barrell Family. W.L. Duax, R. Huether, V. Pletnev, T. Umland, Q. Mao, S. Connare, C.M. Weeks.

TP089

Towards a Statistical Framework for Structure Comparison. Thomas R. Schneider, Barbara Brannetti, Roberto Mosca.

TP090

Defining the Protein Structure: Mining the Redundant Structure Database. Boguslaw Stec, Ying Zhang, B.V.L.S. Prasad, Adam Godzik.

SP091

Structure-activity Relationships and Mechanism Studies for a Series of Inhibitors of Purine Nucleoside Phosphorylase from *Schistosoma mansoni*. Matheus Postigo, Marcela Terri, Glaucius Oliva, Adriano Andricopulo.

TP092

Clustering Proteins Based on Substrate Identification Loops. Robert Huether, David Parish, Qilong Mao, William Duax.

TP093

Purification, Crystallization and Preliminary X-ray Analysis of an Arabidopsis Chloroplastic Glutaredoxin. Lenong Li, Ninghui Cheng, Xiaoqiang Wang.

TP094

Gene Composer for Gene Design and PCR-based Gene Synthesis. Mark Mixon, Don Lorimer, Laurelin Ward, John Walchli, Alex Burgin, Rena Grice, Adrian Metz, Lance Stewart, Peter Nollert, Kai Post.

TP095

Inference of Experimental Structure Determination from Protein Characteristics: Searching for Predictors in Sequence Space. Olga Kirillova, Marek Grabowski, Wladek Minor.

- SP096  
Structure - Function Study of the Finger Domain of Y Family DNA Polymerases in Translesion DNA Synthesis. Kevin Kirouac, Hong Ling.
- TP097  
Crystal Structure of the Proteasome Activator B1m10 with 20S Proteasome from Yeast. Kianoush Sadre-Bazzaz, Frank Whitby, Katherine Ferrell, Howard Robinson, Timothy Formosa, Christopher Hill.
- TP098  
The Bases for the cCF10 and iCF10 Functional Differences. Ke Shi, Heather A. Haemig, Gary M. Dunny, Douglas H. Ohlen-dorf, Cathleen A. Earhart.
- SP099  
Mechanism of the Enzymatic Production and Degradation of Cyclic ADP-ribose by Human CD38. Qun Liu, Quan Hao, Irina Kriksunov, Richard Graeff, Cyrus Munshi, Hon Cheung Lee.
- TP100  
X-ray Crystal Structures of Rabbit N-acetylglucosaminyltransferase I (GnT I) in Complex with Donor Substrate Analogues. Roni Gordon, Prashanth Sivarajah, Malathy Satkunarajah, Dengbo Ma, Chris Tarling, Vizitiu Dragos, Withers Stephen, Rini James.
- TP101  
The Enolase in the Methionine Salvage Pathway in *Geobacillus kaustophilus*: Crystal Structure and Function. Alexander Fedorov, Heidi Imker, Elena Fedorov, John Gerlt, Steve Almo.
- TP102  
High Throughput Screening of Crude Natural Product Extracts: The Search for Novel Human Alpha-Amylase Inhibitors. Gary Brayer, Chris Tarling, Ran Zhang, Harry Brastianos, Robert Keyzers, Chunmin Li, Kate Woods, Raymond Andersen, Stephen Withers.
- SP103  
Crystal Structures of Fms1 in Complex with Polyamine Analogues. Qingqiu Huang, Quan Hao.
- SP104  
Structural Analysis of the Vibrio Cholerae  $\beta$ -glucosaminidase NagZ in Complex with PUGNAc. Misty Balcewich, Keith Stubbs, David Vocadlo, Brian Mark.
- TP105  
The Effect of a Polarized Medium on Hydrogen Bond Energies in Myoglobin. Ronald See, Thomas Baker, Colin Evans, Michele Goodbread, Sarah McColester.
- TP106  
Crystal Structure of a Spontaneously Damaged Protein: Succinimide Residue Formation in Thiamin Pyrophosphokinase. Ivan Vorontsov, G. Minasov, O. Kiryukhina, L. Shuvalova, W.F. Anderson.
- TP107  
Cross-reactivity of TCR A6 on Haptenated HTLV-1 Tax<sub>11-19</sub> Peptides Presented by HLA-A2. Oleg Borbulevych, Brian Baker.
- TP108  
Crystal Structure of the >470 myo Common Ancestor to the Mineralocorticoid - Glucocorticoid Receptor: Evolution by Architectural Epistasis. Eric Ortlund, Jamie Bridgman, Doug Ormoff, Jaone Bischof, Matthew Redinbo, Joseph Thornton.
- SP109  
Metallosubstrate Oxidation and Oxygen Reduction Mechanism in the Multicopper Oxidase CueO. Satish Singh, Sylvia Franke, Rebekah Quick, Andrzej Weichsel, Sue A. Roberts, Christopher Rensing, William R. Montfort.
- TP110  
Crystallographic Pitfalls in Structure Based Drug Design. Andreas Heine, Holger Steuber, Bernhard Stengl, Valerie Honndorf, Gerhard Klebe.
- TP111  
A Comparison of the Ligand Binding Domain of two Nuclear Hormone Receptors, both in the Absence of Ligands. Ross Reynolds, Schoen Kruse, Jennifer Kretschmer, Eric Xu.
- TP112  
Structural Analysis of Newly Designed HIV-1 Protease Inhibitors Based on (R)-(hydroxyethylamino)sulfonamide Isostere. Madhavi Nalam, Akbar Ali, Kiran Reddy, Hong Cao, Tariq Rana, Michael Altman, Bruce Tidor, Sripriya Chellappan, Michael Gilson, Celia Schiffer.
- TP113  
Crystal Structure of HIV-1 CRF01\_AE Protease in Complex with the Substrate p1-p6. Rajintha Bandaranayake, Moses Prabu-Jeyabalan, Junko Kakizawa, Wataru Sugiura, Celia Schiffer.
- TP114  
From Macromolecular Crystal Structure to Reliable Electrostatic Interactions. Philip Coppens, Paula Dominiak, Anatoliy Volkov, Marc Messerschmidt.
- TP115  
Two Periplasmic Sensor Domains with c-type Heme from Chemotaxis Proteins of *G. sulfurreducens* Show PAS Fold and Form Helix-swapped Dimers. P. Raj Pokkuluri, Yuri Londer, Norma Duke, Stephen Wood, Marianne Schiffer.
- TP116  
Crystal Structure of the DNA-binding Domain of PhoP, a Response Regulator from *Mycobacterium tuberculosis*. Shuishu Wang.
- TP117  
Exploring the Mechanism of Nitric Oxide Binding to Cimex Nitrophorin, a Heme-Thiolate Protein from the Bedbug. Andrzej Weichsel, Hemant Badgandi, Robert Berry, James Hazzard, Ann Walker, Gordon Tollin, William Montfort.
- TP118  
High Resolution Structure of *P. abyssi* aRrp41-aRrp42 Complex: A Closer View to the Archaeal Exosome RNA Processing Mechanism. Beatriz Guimaraes, Marcos Navarro, Carla Oliveira, Nilson Zanchin.
- TP119  
Structural Insights into the Bactericidal Mechanism of Human Peptidoglycan Recognition Proteins. Sangwoo Cho, Qian Wang, Chitoor Swaminathan, Roy Mariuzza.
- TP120  
Conformational Flexibility Influences on Activity: Structures of *Pneumocystis carinii* Dihydrofolate Reductase Complexes with Quinazolines. Vivian Cody, Jim B. Pace, Andre Rosowsky.
- SP121  
Is Dimerization Required for the Catalytic Activity of Bacterial Biotin Carboxylase? Yang Shen, Chi-Yuan Chou, Gu-Gang Chang, Liang Tong.
- TP122  
Structural Basis for Recruitment of Insulin Receptor Substrate-2 to the Insulin Receptor. Jinhua Wu, ChongFeng Xu, Thomas Neubert, Stevan Hubbard.
- SP123  
Activities and Structure of  $\beta$  Hemolysin. Medora Huseby, Ke Shi, Patrick. M. Schlievert, Doughlas. H. Ohlendorf, Cathleen. A. Earart.
- TP124  
Identification of Functional Motifs and Binding Site Properties in Potential Drug Targets from Tropical Parasites. Tracy Arakaki, Ethan Merritt, Wim Hol, Christophe Verlinde, Erkang Fan, Isolde Le Trong, Eric Larson, Helen Neely, Brian Krumm, Liren Xiao.
- TP125  
Sequence, Structure, Function: Understanding Roles of Specific Residues and Predicting Substrates within the Short-Chain Oxidoreductase Superfamily. T.C. Umland, Q. Mao, R. Huether, V.Z. Pletnev, W.L. Duax, J. Thomas, L. Gambino.
- TP126  
Recent Structures Solved at the Center for

Eukaryotic Structural Genomics. Jason McCoy, Eduard Bitto, Craig Bingman, Gary Wesenberg, George Phillips.

SP127

Structural and Biophysical Characterization of hRecQL4, a Double Ring DNA Helicase Responsible for Rothmund-Thomson Syndrome. Megan Guelker, Yousif Shamoo.

TP128

The Structure of NP\_294789.1 from *Deinococcus radiodurans* Suggests a Possible Function in DNA Damage Regulation. Christopher Rife, Mitchell Miller, Ashley Deacon.

TP129

Crystal Structure of *Mycoplasma arthritidis*-derived Mitogen Reveals a 3D-domain Swapped Dimer. Hongmin Li, Yi Guo, Zhong Li, Sandra J. VanVranken.

SP130

Crystallographic Studies of the C-terminal Domain of DNA Gyrase. Tung-Ju Hsieh, Hsun-Tang Chang, Te-Sheng Lin, Shu-Yun Huang, Lynn Farh, Nei-Li Chan.

TP131

Targeting Metabolic Enzymes for Antibiotic Development. Ronald Viola.

TP132

Mutation of Lys170 Affects Structural and Proton Shuttle Properties of Human Carbonic Anhydrase II. John Domsic, Wilton Williams, Anthony Aspesi, S. Zoe Fisher, Matthew Sines, Chingkuang Tu, Lakshmanan Govindasamy, Mavis Agbandje-McKenna, David Silverman, Robert McKenna.

TP133

X-ray Crystallographic and Inhibition Studies on Carbonic Anhydrase IX Mimic Drug Complexes. C. Genis, N. Case, L. Govindasamy, C. Tu, D. Silverman, M. Agbandje-McKenna, R. McKenna.

TP134

Structure and Catalytic Effects of an E401K Mutation in the *E. coli* Pyruvate Dehydrogenase E1 Component Complex. Palaniappa Arjunan, Krishnamoorthy Chandrasekhar, Sachin Kale, Natalia Nemeria, Frank Jordan, William Furey.

TP135

Structural Studies of Uridine Diphosphate Glycosyltransferases from *Medicago truncatula*. Xiaoqiang Wang, Hui Shao, Lenong Li, Luis L. Escamilla-Trevino, Zhenzhan Chang, Luzia Modolo, Jack Blount, Xianzhi He, Lahoucine Achnine, Richard A. Dixon.

SP136

Structural Insights into Thiopurine Pharmacogenetics. Yi Peng, Dennis Wilk, Qiping Feng, Araba Adjei, Oreste Salavaggione, Richard Weinshilboum, Vivien Yee.

SP137

Structural Determinants of Regulatory Cysteine-Sulfinic Acid Formation in Human DJ-1. Mark Wilson, Mahadevan Lakshminarasimhan, Anna Witt, Ashraf Raza.

SP138

A Study of Differing Oligomeric Forms of Protocatechuate 3,4-dioxygenase. Rebecca Hoeft, Jeff Digre, Ke Shi, David Burk, Zu Yi Gu, C. Kent Brown, Cathleen Earhart, Douglas Ohlendorf.

SP139

A Structure-Based Hypothesis for Cleavage of Protease Inhibitors by the Inhibitor-Resistant Serine Protease Mesotrypsin. Evette Radisky, Mohammed Salameh, Alexei Soares, Alexandra Hockla.

TP140

Determining the Function of Novel *Treponema* Lipoproteins via a Small-Scale Structural Genomics Project. Diana R. Tomchick, M. Machius, C.A. Brautigam, R.K. Deka, F.L. Tomson, S.B. Lumpkins, P. Ward, J. Blevins, K. Hagman, M.V. Norgard, X.F. Yang, L. Neil.

TP141

Hydroxymandelate Synthase and Hydroxyphenylpyruvate Dioxygenase: Minor Changes in Structure, Altered Catalytic Outcomes. June Brownlee, Panqing He, David Harrison, Graham Moran, Rosalind Franklin.

TP142

N- and C-terminal Helices are Involved in Light-Induced Signal Transduction in the Blue Light Sensor LOV2 Domain from *Avicennia sativa* Phototropin1. Andrei Halavaty, John Wojcik, Keith Moffat.

TP143

Differential P<sub>1</sub> Arginine and Lysine Recognition in the Prototypical Proprotein Convertase Kex2. Todd Holyoak, Joshua Wheatley.

TP144

Alteration of the Sequence Specificity of a Type II Restriction Endonuclease via an Indirect Readout Mechanism. Nancy Horton.

TP145

Introducing Mutations in *Methanococcus jannaschii* Aspartate Transcarbamoylase. Nermina Covic, Jacqueline Vitali.

TP146

Crystal Structure of a Signaling-competent Reelin Fragment. Terukazu Nogi, Norihisa Yasui, Tomoe Kitao, Kenji Iwasaki, Junichi Takagi.

SP147

Structural Insights into Type 1 Pilus Assembly. Oliv Eidam, Mireille Nishiyama, Chasper Puorger, Florian Dworkowski, Denis Erilov, Franck Tarendeau, Darren J. Hart,

Rudi Glockshuber, Guido Capitani, Markus G. Grutter, M. Vetsch, D. Sanchez.

TP148

Further Computational Studies at the Molecule/Macromolecule Interface. William Gleason, Derek Straka, Margo Siorek.

TP149

High Resolution Protein Crystallography and Electrostatic Interaction Energy Computation. Bertrand Fournier, Angèlique Lagoutte, El-Eulmi Bendeif, Benót Guillot, Virginie Pichon-Pesme, Christian Jelsch, Claude Lecomte.

TP150

Twin Refinement of C-terminal Domain HCN Channel Protein. Banuamthi Sankaran, Peter Zwart, Galen Flynn, K.D. Black, William Zagotta, Paul Adams.

TP151

Parallelization of SHELXD to Quickly Solve Heavy-Atom Partial Structures on High-Performance Computers. Zheng-Qing Fu, John Chrzas, George Sheldrick, John Rose, Bi-Cheng Wang.

TP152

Use of the All-atom Force Field OPLS in PrimeX to Restrain Protein Refinement at Moderate Resolution. Jeffrey Bell, Yixiang Cao.

TP153

Structure of *Methanococcus jannaschii* Aspartate Transcarbamoylase. Jacqueline Vitali, Michael Colaneri, Evan Kantrowitz.

TP154

Structures of Human MutS $\alpha$  DNA Lesion Recognition Complexes: Phasing a Large Complex Structure at Moderate Resolution. Joshua Warren, Timothy Pohlhaus, Anita Changela, Paul Modrich, Lorena Beese.

TP155

Closed TrpRS Structures Require a Covalent Bond Between Ligands Occupying Two of the Three Subsites. Poramaet Laowanapiban, Charles W. Carter Jr.

TP156

Expanding Structural Genomics High-throughput Protein Structure Determination Pipeline to Challenging Targets. Rongguang Zhang, A. Binkowski, C. Chang, M. Cuff, M. Cymborowski, N. Duke, Y.-C. Kim, B. Nocek, J. Osipiuk, F. Rotella, K. Tan, Z. Otwinowski, W. Minor, A. Joachimiak.

MP157

Investigation of the Structural Basis for the Inhibition of Histidine Kinase A by Sda in *Bacillus subtilis*. David Jacques, David Langley, Andrew Whitten, Boualem Hamouda, Tracey Hanley, Glenn King, Mitchell Guss, Jill Trehwella.

- MP158  
Protein Organization in Lipid Membranes. Thomas M. Weiss.
- MP159  
Small-Angle X-ray Scattering Study of the Ligand-Induced Conformational Changes in the N-terminal Region of the Inositol Triphosphate Receptor. Andrew Whitten, J. Chan, I. Bosanac, T. Mal, J. Ito, C. Jeffries, J. Trehwella, T. Michikawa, K. Mikoshiba, M. Ikura.
- MP160  
*In-situ* X-ray Scattering and Brewster-angle Microscopy Studies of 2D Streptavidin Crystals Bound to a Lipid Monolayer at the Solution/vapor Interface. Suntao Wang, Lin Yang, Benjamin Ocko, Masfaumi Fukuto.
- MP161  
Small-angle X-ray Scattering Study of Photosystem I-Detergent Complexes. Volker S. Urban, Hugh O'Neill, William T. Heller, Katherine E. Helton, Elis Greenbaum.
- MP162  
Mechanism of the Self Assembly of Amyloid Congeners into Supramolecular Structures. Sai Venkatesh Pingali, Yan Liang, Peng Liu, Seth W. Childers, Kun Lu, David G. Lynn, Pappannan Thiyagarajan.
- MP163  
Use of Ligand- and Fragment-based Cocktail Crystallography to Identify Binding Sites in Potential Drug Targets From Tropical Parasites. Eric Larson, Tracy Arakaki, Isolde Le Trong, Juergen Bosch, Erkang Fan, Fred Buckner, Wesley Van Voorhis, Christophe Verlinde, Wim Hol, Ethan Merritt.
- MP164  
Structure of YraM, a Protein Essential for the Growth of *Haemophilus influenzae*. Mark Saper, J. Vijayalakshmi, Brian Akerley.
- MP165  
The Invasion Machinery of the Malaria Parasite. Joergen Bosch, Stewart Turley, Claudia Roach, Brian Krumm, Carlos Buscaglia, Victor Nussenzweig, Akhil Vaidya, Lawrence Bergman, Wim Hol.
- MP166  
Structure Basis of Fcγ<sub>2</sub> Receptor Recognition by Human C-reactive Protein. Jinghua Lu, Lorrain L. Marnell, Carolyn Mold, Terry W. Du Clos, Peter D. Sun.
- MP167  
Structure-based Pathogen Design - Extending the Host Range of *Listeria monocytogenes*. Thomas Wollert, Bastian Pasche, Maike Rochon, Achim Gruber, Joop van den Heuvel, Dirk Heinz, Andreas Lengele, Wolf-Dieter Schubert.
- SP168  
A Study at 150K and 295K of the Disorder in the Polymorphic System p-methylbenzylidene-p-methylaniline. A.G. Beasley, T.R. Welberry.
- MP169  
Diffuse Scattering in Octakis(trivinylsilyl)octasilicate. Carla Slebodnick, Ross J. Angel, Brian E. Hanson, Pradyat Agaskar, Tatiana Soler, Larry R. Falvello.
- MP170  
Motions of Biological Molecules in Crystals and their Diffuse Scattering. Demian Riccardi, George N. Phillips Jr.
- TP171  
Selenium Derivatization of Nucleic Acids for Phasing and Crystallization. Zhen Huang, Jiansheng Jiang, Jia Sheng, Nicolas Carrasco.
- TP172  
SBEVSL: Communicating Scripts Between Molecular Visualization Programs. C. Westin, B. Hanson, H.J. Bernstein, I. Awuah Asiamah, D. Boycheva, G. Darakev, J. Jemilawon, N. Jia, P. Kamburov, G. Todo-rov, P.A. Craig, S. Mottarella, N. Darakev.
- TP173  
Comparative Analysis of the Monoclinic and Orthorhombic Olymorphs of YLID and a Comment on the Unit Cell Parameter Precision of the Latter. Ilia A. Guzei, Galina A. Bikzhanova, Tatiana V. Timofeeva, Tiffany L. Kinnibrugh, Chrales F. Campana.
- TP174  
Support for Maps in RasMol. Herbert J. Bernstein, Isaac Awuah Asiamah, Georgi Darakev, John Jemilawon, Petko Kamburov.
- TP175  
Mechanistic Insights into Nitroalkane Oxidases from Structures of Trapped Reaction Intermediates and Active Site Mutants. Annie Hèroux, Allen Orville, Akanksha Nagpal, Michael P. Valley, Paul F. Fitzpatrick.
- TP176  
Insight into Autoproteolytic Activation of Cephalosporin Acylase: A Mutant with Three Proteolytic Chemistries. Jin Kwang Kim, Ki Joon Cho, Hye Jeong Shin, In Seok Yang, Ji-Hye Lee, Kyung Hyun Kim.
- MP177  
Microscale Vapour Diffusion Protein Crystallization using a New Crystallization Plate. Joby Jenkins, A. Marek Brzozowski.
- MP178  
Structure Based Fragment Screening: Finding Hits for Novel Lead Compound Design. Robin Rosenfeld, John Badger, Vicki Nienaber, Duncan McRee.
- MP179  
Crystal Creator Liquid Dispenser Feeds Protein Structure Pipeline. Armando Villasenor, Manjiri Ghate, April Wong, Seth Harris, Andreas Kuglstatter, Michelle Browner.
- TP180  
On Retrosynthetic Diamond Growth in Hypercritical Water. Boris Udovic.
- TP181  
A Rietveld and Pair-Distribution Function Analysis of Aged U-Nb Alloys. Heather Volz, Thomas Proffen, Robert Hackenberg, Ann Kelly, William Hulst, Andrew Lawson, Robert Field, David Teter, Dan Thoma, Mark Rodriguez.
- TP182  
Cocept on Petrogenesis of Crystal Growth of Olivine Coronas in Troctolites, Eastern Desert, Egypt. Hussein Hegazy.
- TP183  
First Results of Spin Density Measurements of a Low Spin Bis(imidazole)(meso-tetraphenylporphinato)iron(III) Chloride. Brenda Dougan, Christina Hoffmann, Ziling (Ben) Xue, Garry McIntyre.
- TP184  
Magnetic Structure Investigation of Two Ferromagnetic Spinel GeM<sub>2</sub>O<sub>4</sub> (M = Co, Ni) Measured at the IPNS-SCD using a Polarized Neutron Beam. C.M. Hoffmann, G. Ehlers, W.T. Lee, W.C. Chen, T.R. Gentile, P.M.B. Piccoli, M.E. Miller, A.J. Schultz, H.Y. Yan, X. Tong.
- TP185  
Determination of Detailed Envelopes of SIR D/H Amino Acid Substructures at Less Than Inter-Atomic Resolution. David Langs, Hongliang Xu, Herbert Hauptman.
- SP187  
Mechanistic Insights from a Structural Comparison of Hydrogenated and Perdeuterated Haloalkane Dehalogenase. Xuying Liu, Ronald Viola, Leif Hanson, Paul Langan.
- TP188  
New Structures in the SrMn<sub>x</sub>O<sub>3N-2</sub> System: Sr<sub>N</sub>Mn<sub>N</sub>O<sub>3N-2</sub> (N=5 & 7). A Neutron and X-ray Diffraction Study. Leopoldo Suescun, Bogdan Dabrowski, James D. Jorgensen.
- TP189  
Crystal Structure Solution of a Newly Isolated Natural Product by High Resolution X-Ray Powder Diffraction and Global Optimization Methods. S. Pagola, M.I. Tracanna, S.M. Amani, A.M. Gonzalez, A.B. Raschi, E. Romano, A.M. Benavente, P.W. Stephens, M. Kelley.
- TP190  
Small Angle X-ray Scattering from Transition Metal Oxide Aerogels. Trevor Willey, Cheng Saw, John Kinney, Ted Baumann, Joe Satcher, Jan Ilavsky, Tony van Buuren, J. Stolken.

SP191

X-Ray Diffraction Study of Two Compounds Isolated from *Verbesina turbacensis* H.B.K. Julia Bruno Colmenarez, Graciela Díaz de Delgado, Paulino Delgado, Irama Ramirez, Juan Manuel Amaro Luis.

MP192

A Crystallographic Study of Methoxyflavone Inhibitors of Cytochrome P450. Cheryl Klein Stevens, Naijue Zhu.

MP193

Crystal Structure Refinements and Cation Ordering in Kutnahorite, Ideally  $\text{CaMn}(\text{CO}_3)_2$ . Sytle Antao, Ishmael Hassan.

MP194

Transannular N - N Interaction in Energetic  $\beta$ -HMX. Elizabeth Zhurova, Vladimir Zhurov, Alan Pinkerton.

MP195

Functional Microporous Metal-Organic Frameworks for Gas Storage, Catalysis and Chiral Separation. Baoqing Ma, Karen L. Mulfort, So-Hye Cho, SonBinh T. Nguyen, Joseph T. Hupp.

MP196

Molecular Structure of Novel Cobalt(III) Complexes with a Tetradentate Oxime Open-chain Ligand. Stefaniya Tomya, Matti Haukka, Igor Fritsky.

MP197

Testing Etter's Rule with 6-Membered Hydrogen-Bonded Rings. Carl Schwalbe, Honghao Wang, Chris Bache.

MP198

Neutron Diffraction Studies of Linear M-H-M Bonding in Dinuclear Nickel Complexes. Arthur Schultz, John Cowan, Paula Piccoli, David Vicic, Thomas Anderson, William Tyree.

SP199

Crystal Structure of [1, 2, 3-13C3]-1-Phenylsulfonyl-3-Benzyloxyacetone and Related Labeled Compounds as Precursors for Isotopically Labeled Materials. Ernest Asani, Tatiana Timofeeva, Rodolfo Martinez, Victor Khrustalev.

SP200

Crystal Structures of Pharmacological Activity of Enaminones. Carlito Lariucci, J. Ricardo Sabino, Ivo Vencato, Rafael Nunes, Silvio Cunha, Jailton Ferreira.

SP201

Twin Upgrades by Temperature Control. Frank Fronczek, Stephen Fox.

TP202

Comparative Crystal Structure of "Infinite" Helical Coordination Compounds. Kenneth L. Martin, Carolyn Anderson, Abigail Hunter, S. Russell Seidel, Russell Baughman.

TP203

Crystal Structure of Novel  $\text{Cu}^{\text{II}}\text{Cr}^{\text{III}}$  Thiocyanato-Bridged Heterometallic Complexes with Ethylenediamine. Vitalina Nikitina, Deryn Shevchenko, Vladimir Kokozay, Victoria Dyakonenko, Oleg Shishkin.

SP204

Novel Cu/Fe Heterometallic Complex Comprising a Unique  $[\text{Cu}_2\text{Fe}_2(\text{dipy})_6(\text{NCS})_2(\text{CN})_4]^+$  Squares. Olesya Vreshch, Oksana Nestorova, Volodymyr Kokozay, Brian Skelton.

TP205

Structural Versatility of Copper(II) and Nickel(II) Complexes with Novel Polydentate Oxime-containing Schiff Base Ligands. Iurii Moroz, Matti Haukka, Igor Fritsky.

SP206

Co-crystals: A New Approach in the Development of Active Pharmaceutical Ingredients. Safiyah Forbes, Christer Aakeröy, John Desper.

SP207

Modified Cavitands: Expanding the Boundary. Arbin Rajbanshi, Christer Aakeröy, John Desper.

TP208

Triply Interpenetrated Pore Network in the Solvated Coordination Polymer Zinc Aminotriazololate Carbonate Hydroxide (7:8:2:2). Urs Geiser, John A. Schlueter, Russell J. Fink.

SP209

Two-Step Construction of Heterometallic Coordination Frameworks. Volodymyr Vreshch, Konstantin Domasevitch.

TP210

Crystal Structure of Complexes 1,2-Bis(chloromercurio) Tetrafluorobenzene with Neutral Bidentate Lewis Bases. Andrey A. Yakovenko, Jose H. Gallegos, Mikhail Yu. Antipin, Tatiana V. Timofeeva.

SP211

Crystal Growth and Design of Composite and Mixed Crystals using the Terpy Embrace Motif. Gabriela Soriano-Giles, Jesus Valdes-Martinez, Abel Moreno-Carcamo, Maria Liliana Marin-Garcia, Margarita Rivera-Hernandez.

SP212

Guest Intercalation into  $\text{SnI}_2$ , Inorganic-organic Layered Perovskite Hybrid Solids. Nilantha Bandara, Alicia Beatty.

SP213

Transmission Electron Microscopy Studies of Hydrogen-bonded "Clay Mimics". Christina Costin-Hogan, Alicia Beatty.

TP214

Polar Organic Molecule Intercalation into Clay Mimics. Austin Pickett, Alicia Beatty.

TP215

Crystal Structure, Supramolecular Arrangement and Docking Studies in Cathepsin B of Some Dipnones. Julio Zukerman-Schpector, Mauricio Vega-Tejido, Ignez Caracelli, Rodrigo Cunha, Joao Comasseto.

SP216

Orientating Assembly from Transversal to Longitudinal Arrays of Metallomacrocycles. Shaohua Gou, Zhaolian Chu, Haibin Zhu, Huaze Dong.

TP217

Reaction of Itaconic Acid with Ba and Ca Carbonates Under Hydrothermal Conditions Gives  $\text{Ba}_2[(\text{Citraconate})_2(2,3\text{-dimethylfumurate})]$  and  $\text{Ca}(\text{citramalate})$ . Graciela Diaz de Delgado, Jines Contreras, B. Ali Bahsas, Jose Miguel Delgado.

SP218

Structural Studies of  $[\text{Re}_6\text{Se}_8]^{2+}$  Core-Containing Compounds. Gary Nichol, Peter Orto, Xiaoyan Tu, Zhiping Zheng.

SP219

Metal-Organic Frameworks with Co, Cu, Zn, and Cd Based on the Polyfunctional Ligand 3-Pyrid-4-ylbenzoic Acid. Tiffany Kinnibrugh, J. Luo, V. Khrustalev, T. Timofeeva.

TP220

Preparation and Single-crystal-to-single Crystal Reactivity of Nanosized Cocystals Formed by Sonocrystallization. Dejan Kresimir Bucar, Leonard R. MacGillivray.

TP221

Crystal Chemistry and Crystallography of the Type-II Clathrate,  $\text{Cs}_8\text{Na}_{16}\text{Ge}_{136-x}\text{Ag}_x$ , and a Novel Phase,  $\text{Na}_x\text{Ge}_{136-x}$ . Winnie Wong-Ng, M. Beekman, G. Nolas, J.A. Kaduk, Q. Huang, Z. Yang, A. Shapiro.

TP222

Automation at SER-CAT: A New Robot Implementation. James Fait, John Chrzas, Andy Howard, John Gonczyk, Zheng-Qing Fu, Zhongmin Jin, John Rose, B.C. Wang.

TP223

NorthEastern Collaborative Access Team (NE-CAT) Beam Lines at the Advanced Photon Source. Igor Kourinov, Steven E. Ealick, Malcolm Capel, Ed Lynch, Kanagalaghatta Rajashankar, Narayanasami Sukumar, John P. Unik, James Withrow.

SP224

Automated Sample Alignment at the Structural Biology Center Beamlines. Andrzej Joachimiak, Krzysztof Lazarski, Stephen Ginell, Kazimierz Gofron, Mike Molitsky.

TP225

Crystal Centering for High Throughput Crystallography. Anubhav Jain, Vivian Stojanoff.

SP226

Structure and Function of the Surrogate Light Chain Variable Domain. Lucia Morstadt, Andrew Bohm, Deniz Yuksel, David Stollar, Jim Baleja.

MP227

Are Your Crystals Too Small or Weakly Diffracting for Your Home Laboratory Diffractometer? S.J. Teat, K.N. Raymond.

MP228

Generating High Brilliance X-ray Beams for X-ray Diffraction and Scattering Applications. Brett Kraabel, Pascal Boulee, Dan Cenda, Peter Hoghoj, Lykourgos Spanos, Vincent Roger.

MP229

X06DA: A Production Beamline for Protein Crystallography at SLS. Meitian Wang, Roman Schneider, Claude Pradervand, Wayne Glettig, Takashi Tomizaki, Ezequiel Panepucci, Andreas Isenegger, Herbert Kalt, Qianhong Chen, Clemens Schulze-Briese, Mario Roccamante.

MP230

Automation Program for Macromolecular Crystallography at the NSLS. Alexei Soares, Mary Carlucci-Dayton, Howard Robinson, Robert Sweet, Dieter Schneider.

MP231

Q-Crystallography at the NSLS/PXRR. Howard Robinson, John Skinner, Rick Bruno, Matt Cowan, Grace McCarthy, Bob Sweet, Alex Soares, Dieter Schneider.

MP232

FedEx Crystallography the Next Generation: Combining Mail-in Crystallography Program with Remote Data Collection Capability at SER-CAT. Zhongmin Jin, John Chrzas, James Fait, John Gonczyk, Zheng-Qing (Albert) Fu, John Rose, B. C Wang.

SP233

Automatic Crystal Centering and Crystal Optimisation on the SRS. Mylrajan Muthusamy, John Cowan, Steve Kinder, Steve Buffey, Colin Nave.

MP234

Recent Advances in IP and CCD Technology. Joseph Ferrara, Lee Daniels, Hugh Garvey, James Pflugrath, Katsunari Sasaki, Cheng Yang.

MP235

Synthesis and Structure of  $\text{Li}_6\text{Y}(\text{BO}_3)_3$  as a Neutron Scintillator. Claudia Rawn, Emily Sheats, Paul Cutler, Jason Hodges, Lowell Crow, Bryan Chakoumakos.

MP236

First Results of the ÅXIOM 200, a New High-Speed Photon-Counting X-ray Detector. Matthew Benning, Roger Durst, Bram Schierbeek, Yacouba Diawara, David

Khazins.

MP237

The Improvement of Crystallographic Data near Corners in Mosaic CCD Detectors. Andrew Arvai, Sandor Brockhauser, Gordon Leonard, Andrew McCarthy, Sean McSweeney, Christopher Nielsen, Raimond Ravelli, Ng. h. Xuong, C. Muller-Diekmann, G. Cioci, D. Nurizzo.

TP239

The Present and the Future of Protein Microcrystallography at SPring-8. Nobutaka Shimizu, Masahide Kawamoto, Kazuya Hasegawa, Atsushi Nisawa, Go Ueno, Kunio Hirata, Takashi Kumasaka, Masaki Yamamoto.

TP240

The Quest for Higher Resolution In-house Data. Ina Dix.

MP241

The Bench Top X-ray Diffractometer as an Effective Teaching Tool. Ronald Benson, Lee Daniels, Joseph Ferrara.

SP242

Crystal Structure and Possible Redox Regulation of S-nitrosoglutathione Reductase from *Arabidopsis thaliana*. Justin Crotty, Matthew Grieving, Guenter Wildner, Ung Lee, Susanne Brettschneider, Jacquie Brailey, Andrzej Weichsel, Elizabeth Vierling, William Montfort.

MP243

Crystal Structure of the Core Domain of Human Coactivator-Associated Arginine Methyltransferase 1 (CARM-1). John Sack, Gerald Duke, Dianlin Xie, Herbert Klei, Kevin Kish.

SP244

Chemistry Under the Microscope. Julie Harris, James Maynard, John Moore, Elizabeth Moore.

TP245

Structural Basis for Conserved Complement Factor-like Function in the Antimalarial Protein TEP1. Richard Baxter, Chung-I Chang, Yogarany Chelliah, Stephanie Blandin, Elena Levashin, Johann Deisenhofer.

SP246

The RNA (UGGGGU)<sub>4</sub> Quadruplex Revisited: Alternate Crystal Packings and Density Basin Structure. A. Fyfe, P. Dunten, M. M. Martick, W.G. Scott.

MP247

Structure of PF04013 member APC86534.1. Norma Duke, Min Zhou, Minyi Gu, Andrzej Joachimiak.

SP248

Crystal Structure of a Phenylacetic Acid Degradation Protein from *R. eutropha* JMP134

at 2.2Å Resolution. Debanu Das, Qingping Xu, Mitch Miller, Ashley Deacon.

TP249

PriB-ssDNA Structure and Suggests a Novel Single-stranded DNA Binding Mode. Chwan-Deng Hsiao, Cheng-yang Huang, Che-Hsiung Hsu, Yuh-Ju Sun, Huey-Nan Wu.

MP250

Small Angle Scattering Studies of LacI Repressor. Marc Taraban, Hongli Zhan, Kathleen Matthews, Liskin Swint-Kruse, Jill Trewhella.

TP251

Caffeine Co-crystals Composed of two Supramolecular Heterosynthons. Dejan Kresimir Bucar, Rodger F. Henry, Xiaochun Lou, Richard W. Duerst, Thomas B. Borchardt, Leonard R. MacGillivray, Geoff G.Z. Zhang.

SP252

Crystal Structures of Murine Thrombin in Complex with the Extracellular Fragments of Murine PAR<sub>3</sub> and PAR<sub>4</sub>. Alaji Bah, Zhiwei Chen, Leslie A. Bush-Pelc, F. Scott Mathews, Enrico Di Cera.

## POSTER PRIZES

### Pauling, Canadian and IUCR

The Pauling Prize is awarded to not more than six of the best student poster presentations including one poster from a Canadian Lab.

The IUCr Executive Committee is pleased to continue the series of IUCr awards presented at meetings of the regional affiliates and national crystallographic associations.

### Journal of Chemical Crystallography

The best student poster presentation in the area of chemical crystallography or small molecule structure determination and analysis.

### RSCB Protein Data Bank

To recognize a student poster presentation involving macromolecular crystallography.

### Oxford Cryosystems

Awarded to any poster describing work in low temperature crystallography.

**Winners of poster prizes will be announced at the banquet on Wednesday evening.**

**Identify, analyze and interpret your evidence  
with material identification databases from the  
International Centre for Diffraction Data**

**PDF-4/Organics 2007**

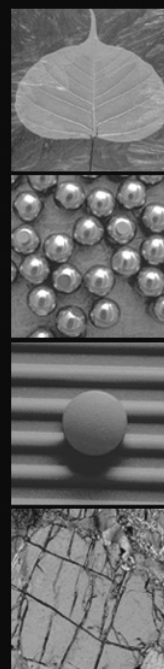
database features 312,355 organic and organometallic phases. It is a practical results-oriented product that includes drug active compounds, excipients, polymers, hydrates, acids, and pharmaceuticals.



**PDF-4+ 2007**

(Available 1 September 2007)

database has comprehensive coverage for inorganic materials. It features 272,232 data sets, digitized patterns, molecular graphics and atomic parameters.



**Visit us at Booth #111**

International Centre for Diffraction Data

Phone: 610.325.9814 Fax: 610.325.9823

marketing@icdd.com www.icdd.com www.dxcicdd.com

